

**SEISMIC BEHAVIOUR OF EXISTING AND REHABILITATED
REINFORCED CONCRETE FRAME CONNECTIONS**

By

ASHRAF MAHMOUD SAMY BIDDAH

A Thesis

Submitted to the School of Graduate Studies

in Partial Fulfilment of the Requirements

for the Degree

Doctor of Philosophy

McMaster University

© Copyright by Ashraf Biddah, July 1997

SEISMIC BEHAVIOUR OF REINFORCED CONCRETE
FRAME CONNECTIONS

McMaster University
Hamilton, Ontario

AUTHOR: Ashraf Mahmoud Samy Biddah, B.Sc. (Ain Shams University)
M.Sc. (Ain Shams University)

NUMBER OF PAGES: xxiv, 326

ABSTRACT

Many multi-story reinforced concrete frame structures were designed before the availability of current seismic design codes. The lateral load resistance of these structures may not be adequate even for a moderate earthquake due to the non-ductile reinforcement details of this type of structures. Recent post-earthquake investigations indicated that extensive damage occurs as a result of excessive shear deformation of the beam-column joints in the non-ductile frames, thus leading to full collapse of structures.

The objectives of this study are to investigate the seismic behaviour of existing reinforced concrete frames under simulated seismic loading; as well as develop a rehabilitation technique for strengthening non-ductile frames. The first major part of the study is an experimental program conducted to: (i) investigate the inelastic behaviour of the non-ductile beam-column connections under cyclic loading; (ii) compare the response of the non-ductile beam-column connections with the response of beam-column connections designed according to the current concrete design code; and (iii) propose a practical method of rehabilitating existing connections and investigate their cyclic behaviour. The tested connections represent one-third scale model of existing connections. Six beam-column connections were tested under cyclic loading. The variables in the test specimens included the amount of joint and column transverse reinforcement and jacketing of the column only or both the column and the beam. Based on the test results, a design procedure is proposed for the rehabilitation of beam-column connections using corrugated steel jackets. The second major part of the study

is to develop a suitable analytical procedure to simulate the behaviour of existing reinforced concrete joints so as to predict the proper behaviour of the non-ductile frames and develop a strategy for rehabilitation of such frames. Two joint elements are developed to represent the joint shear deformation and the beam reinforcing bar bond slip. The two elements are introduced into a non-linear dynamic analysis program which is used to simulate existing and rehabilitated frames.

From the experimental and analytical research findings, recommendations for the design and detailing of the corrugated steel jacketing system for existing reinforced concrete frames are developed. In addition, a rehabilitation strategy is proposed to improve the performance of existing structures. The effects of the rehabilitation system on the confinement of beam-column connections, the provision of adequate development length for the positive bottom beam bars and the provision of full joint shear capacity are assessed and quantified.

Test results indicated that corrugated steel jacketing system was found to be efficient in the rehabilitation of existing structures which do not meet the current seismic code requirements. A method is proposed for the design of the corrugated steel jacket to enhance the shear strength and ductility of the beam-column joint.

ACKNOWLEDGEMENTS

I wish to express my sincere appreciation to my research supervisors, Dr. A. Ghobarah and Dr. T.S. Aziz for their guidance and encouragement throughout the course of this study. I am grateful to their dedication and the number of hours that they spent with me on this research.

I am indebted to my Supervisory Committee members, Dr. M. Dokainish and Dr. W.K. Tso for their valuable comments and suggestions on my research and also their time in reviewing this thesis.

The help of the ADL technicians, Dave Perrett who assisted me in the experiments and Maurice Forget who fabricated the wooden forms is appreciated.

Financial support from McMaster University and the Natural Sciences and Engineering Research Council of Canada are gratefully acknowledged.

Much appreciation is extended to my parents and my brothers for their encouragement and support during the course of this study.

Finally, I would like to thank my wife, Engy for her support, patience and linguistic tips during this study.

To Engy and my parents

TABLE OF CONTENTS

	Page
ABSTRACT	iii
ACKNOWLEDGEMENTS	v
TABLE OF CONTENTS	vii
LIST OF FIGURES	xii
LIST OF TABLES	xxvii
CHAPTER 1	INTRODUCTION AND REVIEW OF PREVIOUS RESEARCH
	1
1.1	INTRODUCTION
	1
1.1.1	Motivation of the study
	3
1.1.2	Objectives
	4
1.1.3	Scope of research
	4
1.2	REVIEW OF PREVIOUS RESEARCH
	6
1.2.1	Rehabilitation of reinforced concrete connections
	7
1.2.2	Modelling of reinforced concrete
	10
CHAPTER 2	EXPERIMENTAL PROGRAM
	19
2.1	INTRODUCTION
	19
2.2	MODELLING CRITERIA
	20
2.3	SPECIMEN DETAILS
	22
2.4	SPECIMEN FABRICATION
	25
2.4.1	Existing joints
	25
2.4.2	Rehabilitated specimens
	26
2.5	TEST SET-UP
	27
2.6	LOADING PROGRAM
	27

Table of contents (cont'd)

	2.7	INSTRUMENTATION	29
	2.8	DATA ACQUISITION	31
CHAPTER 3		OVERALL BEHAVIOUR OF THE SPECIMENS	51
	3.1	INTRODUCTION	51
	3.2	OBSERVED BEHAVIOUR	52
	3.2.1	Specimen J1	52
	3.2.2	Specimen J2	53
	3.2.3	Specimen J3	54
	3.2.4	Specimen J4	55
	3.2.5	Specimen J5	56
	3.2.6	Specimen J6	57
	3.3	LOAD - DISPLACEMENT RELATIONSHIP	59
	3.4	STORY SHEAR	62
	3.5	MOMENT - ROTATION RELATIONSHIP	64
	3.6	STRAIN GAUGE DATA	65
	3.6.1	Stress in the steel reinforcement	65
	3.6.2	Load-strain relationship	65
	3.7	SUMMARY	67
CHAPTER 4		ANALYSIS OF TEST RESULTS	97
	4.1	INTRODUCTION	97
	4.2	LOAD - CARRYING CAPACITY	98
	4.3	RESPONSE ENVELOPES AND STORY SHEAR BEHAVIOUR	99
	4.4	DATA ANALYSIS	100
	4.4.1	Yield moment	100
	4.4.2	Shear in beams	101
	4.4.3	Shear in joints	103
	4.4.4	Shear deformation of joints	104
	4.5	MEMBER CONTRIBUTION TO DRIFT ANGLE	105
	4.6	STIFFNESS	108

Table of contents (cont'd)

4.7	ENERGY DISSIPATION AND EQUIVALENT VISCOUS DAMPING FACTOR	109
4.7.1	Dissipated energy by the specimens	109
4.7.2	Equivalent viscous damping factor	110
4.8	SLIPPAGE BETWEEN STEEL JACKET AND GROUT	112
4.9	LATERAL CONFINEMENT PRESSURE AT JOINT REGION	112
4.10	SUMMARY	113
CHAPTER 5	PROPOSED DESIGN AND CONSTRUCTION OF THE CORRUGATED STEEL JACKET	137
5.1	INTRODUCTION	137
5.2	ADVANTAGES OF CORRUGATED STEEL	138
5.3	PROPOSED DESIGN METHODOLOGY	139
5.3.1	Design of the steel jacket thickness	139
5.3.2	Design of the depth of corrugation	142
5.3.3	Design of column jacket height	143
5.4	NUMERICAL EXAMPLE	144
5.5	PROPOSED CONSTRUCTION CONSIDERATIONS	147
5.5.1	Surface preparation	147
5.5.2	Corrugated steel jacket construction	147
5.5.3	Placing of non-shrink grout	148
5.5.4	Proposed construction of different connections	148
5.6	SUMMARY	149
CHAPTER 6	DEVELOPMENT OF JOINT ELEMENT	157
6.1	INTRODUCTION	157
6.2	COMPUTATIONAL TOOL: SARCF	158
6.3	MODELLING OF SLAB	158
6.4	MODELLING OF JOINT SHEAR	160
6.4.1	Shear-deformation relationship	161
6.4.2	Equilibrium of joint forces	169
6.4.3	Development of computer program "SHEAR"	170

Table of contents (cont'd)

	6.4.4	Model verification	171
	6.4.5	Moment-rotation relationship under cyclic loading	171
	6.4.6	Effect of transverse beams	171
	6.4.7	Slab contribution	173
6.5		MODELLING OF BOND SLIP	174
	6.5.1	Moment-rotation relationship	175
	6.5.2	Moment-rotation relationship under cyclic loading	179
6.6		MODELLING OF LAP-SPLICES IN COLUMN BARS	180
6.7		CORRELATION WITH TEST RESULTS	182
6.8		SUMMARY	183
CHAPTER 7		DYNAMIC ANALYSIS OF MULTI-STORY FRAMES	205
	7.1	INTRODUCTION	205
	7.2	DESIGN OF THE EXISTING FRAME STRUCTURES	206
	7.3	DESIGN OF REHABILITATED FRAME STRUCTURES	208
	7.4	COMPUTER MODELLING	209
	7.5	INPUT GROUND MOTION	211
	7.6	DYNAMIC ANALYSIS	213
		7.6.1 Dynamic characteristics of the frames	213
		7.6.2 Roof displacement time histories	214
		7.6.3 Fundamental period variation with time	216
		7.6.4 Damage index	217
		7.6.5 Location and type of hinges	219
		7.6.6 Envelopes of lateral displacements	220
		7.6.7 Interstory drift	221
		7.6.8 Curvature ductilities	223
		7.6.9 Shear strength envelopes	223
	7.7	APPLICATION OF NBCC 1995 TO EVALUATE EXISTING BUILDINGS	224
	7.8	SUMMARY	225

Table of contents (cont'd)

CHAPTER 8	CONCLUSIONS	286
	8.1 SUMMARY	286
	8.2 CONCLUSIONS	287
	8.3 RECOMMENDATIONS FOR FUTURE RESEARCH	290
APPENDIX A	STRAIN GAUGE DATA	291
	A.1 SPECIMEN J1	291
	A.2 SPECIMEN J2	292
	A.3 SPECIMEN J3	292
	A.4 SPECIMEN J4	293
	A.5 SPECIMEN J5	294
	A.6 SPECIMEN J6	295
APPENDIX B	COMPUTER PROGRAM "SHEAR"	308
	B.1 SOLUTION ALGORITHM	308
	B.2 LISTING OF THE PROGRAM	311
REFERENCES		317

LIST OF FIGURES

Figure	Description	Page
1.1	Motivation of the study	14
1.2	Plan of research program	15
1.3	Strengthening scheme for an exterior beam-column joint (Migliacci et al., 1983)	16
1.4	Details of external steel reinforcement (Corazao and Durrani, 1989)	16
1.5	Strengthening scheme for interior beam-column joint (Estrada, 1990)	17
1.6	Beam-column joint confinement cage (Alcocer and Jirsa, 1991)	17
1.7	Retrofit configuration for an interior beam-column joint (Beres et al., 1992)	18
1.8	Strengthening scheme for an exterior beam-column joint (Beres et al., 1992)	18
2.1	Dimensions of the prototype and the specimen	35
2.2	Concrete dimensions of the specimens	36
2.3a	Details of reinforcement of specimens J1, J3 and J5	37
2.3b	Details of reinforcement of specimen J2	38
2.3c	Details of reinforcement of specimens J4 and J6	39
2.4	Proposed rehabilitation technique	40
2.5	Properties of corrugated steel sections	41
2.6	Wooden form used in casting the specimens	42
2.7	Details of the reinforcement cage	42
2.8	Assembling of beam and column jackets	43
2.9a	Schematic of test set-up	44
2.9b	Test set-up	45

List of Figures (cont'd)

Figure	Description	Page
2.10	Loading routine	46
2.11	Frame deflection due to seismic loads	46
2.12	The drift angle definition	47
2.13	Instrumentation of test specimens	48
2.14	Locations of the strain gauges	49
2.15	Data acquisition and control system	50
3.1	Final crack pattern of specimen J1	69
3.2	Crack pattern of specimen J1 at drift angle of 2%	70
3.3	Crack pattern of specimen J1 at yielding of reinforcement	70
3.4a	Crack pattern of specimen J2 at positive drift angle of 2%	71
3.4b	Crack pattern of specimen J2 at negative drift angle of 2%	71
3.5	Final crack pattern of specimen J2	72
3.6	Specimen J3 at the end of the test (cycle #17)	73
3.7	Damage at the beam-column interface at cycle #17	73
3.8a	Crack pattern of specimen J3 after removing the steel casing	74
3.8b	Crack pattern of specimen J3 after removing the grout	74
3.9	Final crack pattern of specimen J4	75
3.10	Crack pattern of specimen J4 at drift angle of 2%	75
3.11	Crack pattern of specimen J4 at drift angle of 1%	76
3.12	Final crack pattern of specimen J5	77
3.13	Crack pattern of specimen J5 at drift angle of 2%	77
3.14	Specimen J5 after removing the concrete cover and steel casing	78
3.15	Final crack pattern of specimen J6	79
3.16	Crack pattern of specimen J6 at drift angle of 2%	79

List of Figures (cont'd)

Figure	Description	Page
3.17	Forces of anchor bolts	80
3.18	Specimen J6 after removing the steel casing	80
3.19a	Beam tip load-displacement relationship of specimen J1	81
3.19b	Beam tip load-displacement relationship of specimen J2	81
3.19c	Beam tip load-displacement relationship of specimen J3	82
3.19d	Beam tip load-displacement relationship of specimen J4	82
3.19e	Beam tip load-displacement relationship of specimen J5	83
3.19f	Beam tip load-displacement relationship of specimen J6	83
3.20a	Story shear-drift angle relationship of specimen J1	84
3.20b	Story shear-drift angle relationship of specimen J2	84
3.20c	Story shear-drift angle relationship of specimen J3	85
3.20d	Story shear-drift angle relationship of specimen J4	85
3.20e	Story shear-drift angle relationship of specimen J5	86
3.20f	Story shear-drift angle relationship of specimen J6	86
3.21a	Story shear-joint shear deformation of specimen J1	87
3.21b	Story shear-joint shear deformation of specimen J2	87
3.21c	Story shear-joint shear deformation of specimen J3	87
3.21d	Story shear-joint shear deformation of specimen J4	88
3.21e	Story shear-joint shear deformation of specimen J5	88
3.21f	Story shear-joint shear deformation of specimen J6	88
3.22a	Beam moment-rotation at 80 mm from column face of specimen J1	89
3.22b	Beam moment-rotation at 330 mm from column face of specimen J1	89
3.22c	Beam moment-rotation at 580 mm from column face of specimen J1	89
3.23a	Beam moment-rotation at 80 mm from column face of specimen J2	90

List of Figures (cont'd)

Figure	Description	Page
3.23b	Beam moment-rotation at 330 mm from column face of specimen J2	90
3.23c	Beam moment-rotation at 580 mm from column face of specimen J2	90
3.24a	Beam moment-rotation at 80 mm from column face of specimen J3	91
3.24b	Beam moment-rotation at 330 mm from column face of specimen J3	91
3.24c	Beam moment-rotation at 580 mm from column face of specimen J3	91
3.25a	Beam moment-rotation at 80 mm from column face of specimen J4	92
3.25b	Beam moment-rotation at 330 mm from column face of specimen J4	92
3.25c	Beam moment-rotation at 580 mm from column face of specimen J4	92
3.26a	Beam moment-rotation at 80 mm from column face of specimen J5	93
3.26b	Beam moment-rotation at 330 mm from column face of specimen J5	93
3.26c	Beam moment-rotation at 580 mm from column face of specimen J5	93
3.27a	Beam moment-rotation at 80 mm from column face of specimen J6	94
3.27b	Beam moment-rotation at 330 mm from column face of specimen J6	94
3.27c	Beam moment-rotation at 580 mm from column face of specimen J6	94
3.28a	Positive rotation at 80 mm - displacement ductility factor	95
3.28b	Negative rotation at 80 mm - displacement ductility factor	95
3.29	Beam tip load - strain at joint tie for specimen J1	96
3.30	Beam tip load - strain at bottom steel of beam for specimen J2	96
3.31	Beam tip load - strain at beam third stirrup for specimen J3	96
4.1	Comparison of load levels attained by specimens	116
4.2	Comparison of story shear levels attained by specimens	116
4.3	Beam shear force resisted by concrete and transverse reinforcement for J1	117
4.4	Beam shear force resisted by concrete and transverse reinforcement for J2	117

List of Figures (cont'd)

Figure	Description	Page
4.5	Beam shear force resisted by concrete and transverse reinforcement for J3	118
4.6	Beam shear force resisted by concrete and transverse reinforcement for J4	118
4.7	Beam shear force resisted by concrete and transverse reinforcement for J5	119
4.8	Beam shear force resisted by concrete and transverse reinforcement for J6	119
4.9	Joint shear resisted by concrete and transverse reinforcement with drift angle for J1	120
4.10	Joint shear resisted by concrete and transverse reinforcement with drift angle for J2	120
4.11	Joint shear resisted by concrete and transverse reinforcement with drift angle for J3	121
4.12	Joint shear resisted by concrete and transverse reinforcement with drift angle for J4	121
4.13	Joint shear resisted by concrete and transverse reinforcement with drift angle for J5	122
4.14	Joint shear resisted by concrete and transverse reinforcement with drift angle for J6	122
4.15	Joint shear deformation model	123
4.16	Joint shear-joint shear deformation	123
4.17a	Positive drift angle-joint shear deformation	124
4.17b	Negative drift angle-joint shear deformation	124
4.18a	Contribution to story drift angle (positive drift) for specimens J1 and J2	125
4.18b	Contribution to story drift angle (positive drift) for specimens J3 and J4	126
4.18c	Contribution to story drift angle (positive drift) for specimens J5 and J6	127
4.19a	Contribution to story drift angle (negative drift) for specimens J1 and J2	128
4.19b	Contribution to story drift angle (negative drift) for specimens J3 and J4	129

List of Figures (cont'd)

Figure	Description	Page
4.19c	Contribution to story drift angle (negative drift) for specimens J5 and J6130	
4.20	Member contributions to drift angle	131
4.21	Definition of Peak-to-peak stiffness	132
4.22	Comparison of peak-to-peak stiffness of specimens	132
4.23	Stiffness-displacement ductility factor relationship	132
4.24	Cumulative energy dissipated-cycles number relationship	133
4.25	Cumulative energy dissipated-displacement ductility factor relationship	133
4.26	Definition of equivalent viscous damping factor	134
4.27	Equivalent viscous damping factor-displacement ductility factor relationship	134
4.28a	Slip between steel jacket and grout	135
4.28b	Slip between steel and grout-displacement ductility factor relationship	135
4.29	Installation and location of load cells	136
4.30	Confinement stress measured by the load-cells	136
5.1	Behaviour of rehabilitated rectangular column using flat steel jacket (Priestley et al., 1994)	151
5.2	Column and joint dimensions	151
5.3	Proposed rehabilitation technique for columns and joints	152
5.4	Installation technique for column, beam and joint jackets	153
5.5	Installation of anchor bolts	154
5.6	Proposed rehabilitation system for exterior connections with and without slabs and transverse beams	155
5.7	Proposed rehabilitation system for interior connections with and without slabs and transverse beams	156
6.1	Proposed effective slab width for negative moments	186
6.2a	Idealization of the joint shear element in frame analysis	187

List of Figures (cont'd)

Figure	Description	Page
6.2b	Idealization of the joint shear and bond slip elements in frame analysis	187
6.3	Joint geometry	188
6.4	Definitions of stresses and coordinate systems	189
6.5	Stress-strain relationships of concrete	190
6.6	Local stresses at a crack	191
6.7	Effective joint width	192
6.8	Equilibrium of interior beam-column joint	192
6.9	Equilibrium of exterior beam-column joint	193
6.10	Equilibrium of top floor interior beam-column joint	193
6.11	Analytical results compared to current experimental program results	194
6.12	Analytical results compared with the experimental results of Morita and Fujii (1991)	195
6.13	Analytical results compared with the experimental results of Kaku and Asakusa (1991)	196
6.14	Typical moment-rotation relationship for the shear spring	197
6.15	Confinement action due to cracked transverse beams (Kitayama, 1991)	197
6.16	Story drift-joint shear stress relationships (Kitayama, 1991)	198
6.17	Proposed moment-rotation relationship due to bond slip	198
6.18	Stress and strain distribution assumption in the joint	199
6.19	Definition of L_{max} and L_{ymax}	199
6.20	Computational procedure for pinching effect	200
6.21	Bond failure of lapped reinforcement (Priestley and Seible, 1991)	201
6.22	Comparison between experimental and analytical load-deflection curves of the tested specimens	203
6.23	Comparison between experimental and analytical load-deflection envelopes of the tested specimens	204

List of Figures (cont'd)

Figure	Description	Page
7.1	Plan and elevation for the 3 and 9 story building	233
7.2	Member dimensions (mm) for the 3 and 9 story frames	234
7.3	Reinforcement details for the 3 and 9 story frames	234
7.4	Details of the non-ductile reinforced concrete frames	235
7.5	Rehabilitation technique for discontinuity of beam bottom bars (Estrada, 1990)	235
7.6	Acceleration time history and response spectra for the Artificial earthquake scaled to 0.2g	236
7.7a	Acceleration time histories for the selected earthquakes records	237
7.7b	Response spectra for the selected earthquake records	238
7.8	Roof displacement time histories for the 3-story frames due to the El Centro earthquake scaled to PGA of 0.3g	239
7.9	Roof displacement time histories for the 3-story frames due to the Mexico earthquake scaled to PGA of 0.3g	240
7.10	Roof displacement time histories for the 3-story frames due to the Artificial earthquake scaled to PGA of 0.3g	241
7.11	Roof displacement time histories for the 9-story frames due to the El Centro earthquake scaled to PGA of 0.3g	242
7.12	Roof displacement time histories for the 9-story frames due to the Mexico earthquake scaled to PGA of 0.3g	243
7.13	Roof displacement time histories for the 9-story frames due to the Artificial earthquake scaled to PGA of 0.3g	244
7.14	Variation of the fundamental period with time for the 3-story frames when subjected to the El Centro earthquake	245
7.15	Variation of the fundamental period with time for the 3-story frames when subjected to the Mexico earthquake	246
7.16	Variation of the fundamental period with time for the 3-story frames when subjected to the Artificial earthquake	247
7.17	Variation of the fundamental period with time for the 9-story frames when subjected to the El Centro earthquake	248

List of Figures (cont'd)

Figure	Description	Page
7.18	Variation of the fundamental period with time for the 9-story frames when subjected to the Mexico earthquake	249
7.19	Variation of the fundamental period with time for the 9-story frames when subjected to the Artificial earthquake	250
7.20	Summary of hinge type and location for the 3-story frames due to the El Centro earthquake scaled to PGA of 0.1g	251
7.21	Summary of hinge type and location for the 3-story frames due to the El Centro earthquake scaled to PGA of 0.2g	252
7.22	Summary of hinge type and location for the 3-story frames due to the El Centro earthquake scaled to PGA of 0.3g	253
7.23	Summary of hinge type and location for the 3-story frames due to the Mexico earthquake scaled to PGA of 0.1g	254
7.24	Summary of hinge type and location for the 3-story frames due to the Mexico earthquake scaled to PGA of 0.2g	255
7.25	Summary of hinge type and location for the 3-story frames due to the Mexico earthquake scaled to PGA of 0.3g	256
7.26	Summary of hinge type and location for the 3-story frames due to the Artificial earthquake scaled to PGA of 0.1g	257
7.27	Summary of hinge type and location for the 3-story frames due to the Artificial earthquake scaled to PGA of 0.2g	258
7.28	Summary of hinge type and location for the 3-story frames due to the Artificial earthquake scaled to PGA of 0.3g	259
7.29	Summary of hinge type and location for the 3-story frames due to the Nahanni earthquake scaled to PGA of 0.3g	260
7.30	Summary of hinge type and location for the 9-story frames due to the El Centro earthquake scaled to PGA of 0.1g	261
7.31	Summary of hinge type and location for the 9-story frames due to the El Centro earthquake scaled to PGA of 0.2g	262
7.32	Summary of hinge type and location for the 9-story frames due to the El Centro earthquake scaled to PGA of 0.3g	263
7.33	Summary of hinge type and location for the 9-story frames due to the Mexico earthquake scaled to PGA of 0.1g	264

List of Figures (cont'd)

Figure	Description	Page
7.34	Summary of hinge type and location for the 9-story frames due to the Mexico earthquake scaled to PGA of 0.2g	265
7.35	Summary of hinge type and location for the 9-story frames due to the Mexico earthquake scaled to PGA of 0.3g	266
7.36	Summary of hinge type and location for the 9-story frames due to the Artificial earthquake scaled to PGA of 0.1g	267
7.37	Summary of hinge type and location for the 9-story frames due to the Artificial earthquake scaled to PGA of 0.2g	268
7.38	Summary of hinge type and location for the 9-story frames due to the Artificial earthquake scaled to PGA of 0.3g	269
7.39	Summary of hinge type and location for the 9-story frames due to the Nahanni earthquake scaled to PGA of 0.3g	270
7.40	The damaged areas in existing frames and a proposed rehabilitation approach	271
7.41	Maximum displacement and interstory drift for the 3-story frames due to the El Centro earthquake	272
7.42	Maximum displacement and interstory drift for the 3-story frames due to the Mexico earthquake	273
7.43	Maximum displacement and interstory drift for the 3-story frames due to the Artificial earthquake	274
7.44	Maximum displacement and interstory drift for the 3-story frames due to the Nahanni earthquake	275
7.45	Maximum displacement and interstory drift for the 9-story frames due to the El Centro earthquake	276
7.46	Maximum displacement and interstory drift for the 9-story frames due to the Mexico earthquake	277
7.47	Maximum displacement and interstory drift for the 9-story frames due to the Artificial earthquake	278
7.48	Maximum displacement and interstory drift for the 9-story frames due to the Nahanni earthquake	279
7.49	Maximum story shear, beam and column ductilities for the 3-story frames due to the El Centro earthquake	280

List of Figures (cont'd)

Figure	Description	Page
7.50	Maximum story shear, beam and column ductilities for the 3-story frames due to the Mexico earthquake	281
7.51	Maximum story shear, beam and column ductilities for the 3-story frames due to the Artificial earthquake	282
7.52	Maximum story shear, beam and column ductilities for the 9-story frames due to the El Centro earthquake	283
7.53	Maximum story shear, beam and column ductilities for the 9-story frames due to the Mexico earthquake	284
7.54	Maximum story shear, beam and column ductilities for the 9-story frames due to the Artificial earthquake	285
A.1	Beam tip load-strain at bottom steel of beam of specimen J1	296
A.2	Beam tip load-strain at bottom steel of beam of specimen J1	296
A.3	Beam tip load-strain at top steel of beam of specimen J1	296
A.4	Beam tip load-strain at top steel of beam of specimen J1	297
A.5	Beam tip load-strain at top steel of beam of specimen J1	297
A.6	Beam tip load-strain at beam second stirrup of specimen J1	297
A.7	Beam tip load-strain at beam second stirrup of specimen J5	298
A.8	Beam tip load-strain at beam second stirrup of specimen J2	298
A.9	Beam tip load-strain at column main steel above joint of specimen J3	298
A.10	Beam tip load-strain at joint tie of specimen J3	299
A.11	Beam tip load-strain at beam second stirrup of specimen J3	299
A.12	Beam tip load-strain at beam steel jacket (mid point) of specimen J3	299
A.13	Beam tip load-strain at beam steel jacket (bottom side) of specimen J3	300
A.14	Beam tip load-strain at steel jacket at joint of specimen J3	300
A.15	Beam tip load-strain at steel jacket (joint confinement) of specimen J3	300
A.16	Beam tip load-strain at bottom steel of beam of specimen J4	301

List of Figures (cont'd)

Figure	Description	Page
A.17	Beam tip load-strain at column tie below joint of specimen J4	301
A.18	Beam tip load-strain at column tie above joint of specimen J4	301
A.19	Beam tip load-strain at beam second stirrup of specimen J4	302
A.20	Beam tip load-strain at bottom steel of beam of specimen J5	302
A.21	Beam tip load-strain at bottom steel of beam of specimen J5	302
A.22	Beam tip load-strain at column main steel above joint of specimen J5	303
A.23	Beam tip load-strain at column main steel in the joint of specimen J5	303
A.24	Beam tip load-strain at column main steel below joint of specimen J5	303
A.25	Features of column and joint behaviour (Paulay and Priestley, 1992)	304
A.26	Development of tensile strains in column bars participating in truss mechanism of joint shear resistance (Cheung et al., 1993)	304
A.27	Beam tip load-strain at joint tie of specimen J5	305
A.28	Beam tip load-strain at joint tie (joint confinement) of specimen J5	305
A.29	Beam tip load-strain at joint steel jacket of specimen J5	305
A.30	Beam tip load-strain at bottom steel of beam of specimen J6	306
A.31	Beam tip load-strain at column main steel above joint of specimen J6	306
A.32	Beam tip load-strain at column main steel below joint of specimen J6	306
A.33	Beam tip load-strain at column tie above joint of specimen J6	307
A.34	Beam tip load-strain at beam second stirrup of specimen J6	307

LIST OF TABLES

Table	Title	Page
2.1	Features of the beam-column connection specimens in the test program	32
2.2	Scaling factors for modelling under quasi-static loading	33
2.3	Uniaxial compressive and split tensile strength of concrete cylinders	34
2.4	Reinforcing and corrugated steel properties	34
3.1	Displacement ductilities of specimens and modes of failure	68
4.1	Comparison of beam yield moments	114
4.2	Experimental peak-to-peak stiffness K_p (kN/mm)	114
4.3	Energy dissipated in each cycle (kN.m) and the equivalent damping factor	115
5.1	Sectional design profiles for corrugated sheet (Handbook of steel, 1984)	150
5.2	Ultimate load capacity of Hilti bolts (Hilti, 1994)	150
6.1	Parameters of joint shear and bar bond slip elements	185
7.1	Summary of design loads for the existing building	227
7.2	Ratio of sum of column moment capacities to sum of beam moment capacities at connections	227
7.3	Thickness and dimensions of the steel jackets	228
7.4	Characteristics of the selected ground motions	228
7.5	Maximum predicted roof displacement	229
7.6	Maximum predicted story drift	230
7.7	Maximum base shear	231
7.8	Modified response factors (elastic/inelastic)	232

CHAPTER 1

INTRODUCTION AND REVIEW OF PREVIOUS RESEARCH

1.1 INTRODUCTION

As building codes are updated, some existing reinforced concrete structures may not comply with current standards even though they may have been properly designed and constructed according to earlier building standards. If judged in light of today's knowledge of reinforced concrete building performance during earthquakes, many existing structures would be found inadequate and may pose severe life safety hazard during seismic events. Many of these existing structures were designed for gravity loads only. As a result, lateral strength and ductility were minimal. The characteristics typical of buildings constructed during the 1950s through 1970s include flexible columns, non-ductile detailing of reinforcement, strong beam-weak column systems and vulnerable joints.

Recent earthquakes have demonstrated that even if the beams and columns in a reinforced concrete frame remain intact, the beam-column joint failure will undermine the integrity of the whole structure. The vulnerability of existing structures to moderate and severe ground motions have been documented. These structures suffered extensive damage due to excessive shear deformation of the beam-column joints in the non-ductile frames, which contributed to the collapse of many structures.

Rehabilitation is a feasible approach to mitigate the risk posed by hazardous structures and to provide safety to building occupants and protect their investments (Alcocer and Jirsa, 1993). However, rehabilitation is a complex problem since well-understood methods of design for new construction may not apply. Seismic retrofit of existing buildings is particularly challenging because of the interrelated effects of any change to a structural system. For existing structures, the problems of identifying weaknesses, assessing the condition of the structure, designing techniques for correcting deficiencies, and developing economic and rapid construction procedures have not received adequate attention from structural engineers and researchers. Some research effort has been devoted to develop a variety of techniques for seismic retrofit. The most common of these techniques include reinforced concrete or steel jackets, increased number of structural walls and the installation of steel bracing systems. The decision to use any of these systems depends on the condition and the characteristics of the particular structure. Reinforced concrete jackets require intensive labour and more artful detailing than other retrofitting techniques. The use of steel jacketing does not increase the weight of the structure significantly and saves construction time when compared with reinforced concrete jacketing system. The steel elements can be pre-fabricated, and are more rapidly installed and less disruptive to building occupants than other retrofitting techniques.

Most of the non-linear inelastic dynamic frame analysis programs assume the beam-column joint to be rigid regardless of the detailing of the reinforcement. Observations following recent earthquakes and experimental results indicated that slippage of beam bottom positive moment bars which are discontinuous at joints as well as joint distress occur at high

levels of loading. The validity of the conventional rigid joint assumption in modelling existing reinforced concrete frames constructed prior 1970 is questionable.

1.1.1 Motivation of the study

During an earthquake, beam-column connections may experience severe cyclic load reversals. If the joints in a moment resisting frame do not have adequate strength, the overall strength and stiffness of the frame may be adversely affected. At present, there is no effective guidelines for the design of rehabilitation techniques of beam-column connections. Most of the research done on beam-column joints was concerned with the behaviour of typical interior and exterior joints under cyclic loads. Moreover, in the few cases where improving the seismic behaviour was studied, the focus was on the detailing of new joints and not the existing ones. There has been very little experimental investigation of joint rehabilitation techniques. As such, an effective, inexpensive and non-disruptive rehabilitation technique for beam-column joints is needed.

Most of the available non-linear inelastic dynamic analysis programs assume the joint to be rigid. This modelling of the joint is questionable for the unreinforced and the lightly reinforced joints. To analyze properly an existing structure, an accurate, simple and practical model should be developed to represent the flexible behaviour and modes of failure of the joints. The availability of such model allows the assessment of the seismic performance of existing structures. The present study is devoted to respond to the joint modelling and rehabilitation needs as summarized in figure 1.1.

1.1.2 Objectives

The objectives of the present research program are:

- 1- To develop an effective, inexpensive and non-disruptive rehabilitation system for existing deficient joints in non-ductile reinforced concrete frames and to develop an economical jacket design procedure.
- 2- To evaluate the behaviour of existing frames during earthquakes by developing a flexible joint model that takes into account joint failure modes. The joint modelling should be accurate, simple and practical. The joint model is incorporated in a non-linear inelastic dynamic analysis program to properly represent the seismic behaviour of the whole structure.

1.1.3 Scope of research

The plan of the research program is schematically outlined in figure 1.2. To achieve the stated objectives, the scope of the research program consists of the following:

- 1- Conducting an experimental program to study the performance of existing reinforced concrete beam-column connections and those detailed according to the current Canadian seismic code.
- 2- Developing a jacketing technique (corrugated steel jacket) for rehabilitation of deficient connections. The aim is to evaluate the effectiveness of such technique in improving the ductility and the hysteretic behaviour of the joint.
- 3- Studying the constructability of the jacketing technique and developing recommendations for design and construction of the jacketing rehabilitation system.

- 4- Developing a model for the joint element capable of predicting the dynamic behaviour and the failure modes of the joints. The performance of this proposed model would be assessed by comparing the model's predicted response with the experimental results.
- 5- Incorporating the joint model into a non-linear inelastic dynamic analysis program to represent properly the behaviour of frames that include joints of various details.
- 6- Evaluating the behaviour of two existing frames taking into account the effect of the joint behaviour and comparing the results with those obtained assuming rigid joints.
- 7- Performing the analysis of the existing frames after applying the proposed rehabilitation technique in order to evaluate the effectiveness of such technique in improving the dynamic performance of the frames.

From the experimental and analytical research findings, recommendations for the design and detailing of the corrugated steel jacketing rehabilitation system for existing reinforced concrete frames are developed. In addition, a rehabilitation strategy is proposed to improve the performance of existing structures. The effects of the rehabilitation system on the confinement of beam-column connections, the provision of adequate development length for the positive bottom beam bars and the provision of full joint shear capacity are assessed and quantified.

1.2 REVIEW OF PREVIOUS RESEARCH

The behaviour of reinforced concrete frames during earthquakes received considerable attention during the past three decades. Most of the work that was carried out over this period focused on the improvement of design procedures. Studies on the dynamic behaviour of existing non-seismically designed buildings are few. The first extensive monograph on the seismic design of reinforced concrete structures was published by Blume et al. (1961). In the early sixties, studies on the reinforced concrete beam-to-column connection regions were carried out at the Portland Cement Association laboratories by Hanson and Conner (1967). These experiments showed the fundamental benefits of proper seismic detailing. On the basis of this study as well as the work of other investigations (e.g., Wight and Sozen, 1973), the first seismic design recommendations were developed. The principles of seismic design were reflected in the first edition of the ACI-ASCE Committee 352 (1985) recommendations for joints and connections in monolithic concrete structures published in 1976. The recommendations were based on the test series conducted on isolated beam-column joints without transverse beams or slabs.

The first comprehensive and widely accepted explanations of the behaviour of the reinforced concrete beam-to-column joints were given by Park and Paulay (1975) and Paulay et al. (1978). Since then, many complex analytical models were suggested elaborating on important details such as the effect of joint reinforcement and concrete compression struts on the joint shear capacity. Attention of researchers shifted to unexplored areas such as slab contribution and eccentric beams. Small-scale models of multi-story, multi-bay buildings were tested on shake-tables.

Several models have been put forward to describe the effect of transverse reinforcement on improving the strength and ductility. The mechanics of passive confinement by reinforcing steel has been explained successfully by Sheikh and Uzumeri (1980) for square sections with rectilinear hoops. Sheikh (1994) proposed an effective procedure for predicting the required amount of confinement steel for rectangular columns considering the effect of curvature ductility and column axial load.

1.2.1 Rehabilitation of reinforced concrete connections

The first coordination meeting of U.S. researchers involved in seismic repair and rehabilitation studies was held at Salt Lake City, Utah in 1991. Due to the recognized importance of seismic rehabilitation of existing structures, two major organizations began sponsoring research programs in the area. The National Science Foundation, NSF, is dealing with strengthening and repairing of non-ductile reinforced concrete frames using external steel jackets and plates. Meanwhile, the National Center of Earthquake Engineering Research, NCEER, is studying the retrofit of lightly reinforced concrete frames and non-ductile flat plate connections (Liu and Lagorio, 1991).

During the past two decades many experimental studies of the behaviour of typical interior and exterior joints under cyclic loads have been conducted (Uzumeri and Seckin, 1974; Beckingsale et al., 1980; Gavrilovic et al., 1980; Durrani and Wight, 1982; Kanada et al., 1985; Kitayama et al., 1985 and 1987; Ruitong and Park, 1987; Kurose et al., 1988; Ehsani and Alameddine, 1989; Sugano et al., 1990; Pessiki et al., 1990; Winters et al., 1991; Choudhuri et al., 1992; Aycardi et al., 1992). However, there is little experimental testing of

joint strengthening techniques. Data sets for existing and strengthened structures were collected by Phan et al. (1994) for frames, beam-column joints and columns. Seventy sets of data were collected on the behaviour of frames and infill walls. More than half of the data was on the behaviour of various retrofit schemes. In contrast, over one hundred sets of data were collected on the behaviour of beam-column joints, but only few of the tests were on strengthened joints.

Migliacci et al. (1983) reported the behaviour of exterior frame connections jacketed by a steel skeleton made of steel angles at the column edges tied by straps as shown in figure 1.3. To improve the confinement of the beam and column, the straps were prestressed by pre-heating. They concluded that steel jacketing enhanced the strength and energy dissipation capacity, however, prestressing by pre-heating should not be relied on as it is difficult to control in the field.

Corazao and Durrani (1989) proposed to strengthen beam-column connections using reinforced concrete jacketing and external steel encasement as shown in figure 1.4. It was found that specimens strengthened by reinforced concrete and by steel encasement showed increase in the strength, stiffness, and ductility and exhibited desirable failure mechanisms. Strengthening by reinforced concrete jacketing requires more labour than other strengthening techniques. The placement of continuous ties around the column in the joint region can be difficult. Another complication in case of strengthening by external steel reinforcement is that the transfer of stresses at the joints is not properly understood.

Estrada (1990) attached a steel strap with epoxy-resin type anchor bolts to the beams at the beam-column joint. For developing the tensile capacity of the steel strap, a bracket was

welded to the strap and connected to a large threaded rod placed through the column just below the soffit as shown in figure 1.5. The strengthening scheme improved the development conditions for the beam bottom reinforcement so that the bars reached yield even though their splice length within the joint was inadequate. This system increases the flexural capacity of the beams, hence, the shear strength required to develop the improved flexural capacity will be higher. For this reason, the beam shear capacity as well as the strength of the columns should be carefully checked and maintained higher than the strength of the beams.

Following the 1985 Mexico earthquake, Alcocer and Jirsa (1991) tested a few strengthened joints. The proposed scheme required perforating the slab in order to construct a steel and concrete jacket around the joint, column and the beams in some cases. The retrofit scheme includes longitudinal and transverse steel bars around the jacketed columns and beams, as well as welded steel angles and straps intended to confine the concrete in the joint as shown in figure 1.6. It was found that this technique changes the behaviour of the specimens from weak column-strong beam to strong column-weak beam. The technique, however, requires intensive labour and more artful detailing than other strengthening methods.

Beres et al. (1992) investigated the behaviour of two rehabilitation schemes. The first scheme is intended for interior joints in which the retrofit was designed to prevent the pull-out of discontinuous bottom beam reinforcement. This was achieved by bolting steel channel sections onto the bottom surfaces of beams on each side of the joint. The channels were connected by steel rods installed through drilled holes in the columns as shown in figure 1.7. They found this scheme to be successful in preventing pull-out, increasing shear strength and

reducing the rate of strength deterioration. The second scheme is intended for exterior joints in which the retrofit was designed to reduce vertical cracks propagating in the column lap splice zone above the joint. Steel plates above and below the beam were through-bolted to a continuous steel plate on the outside of the joint as shown in figure 1.8. They reported improvements in the behaviour of the specimen as the cover was protected. The strength, initial stiffness and energy dissipation capacity of the connection were increased. However, by comparison to the unstrengthened specimens, significant strength deterioration occurred after reaching the maximum strength value.

Hoffschild et al. (1993) proposed another method of retrofit which consists of encasing the reinforced concrete joint with a circular grouted steel jacket. The casing caused an increase in moment capacity of the section which forced most of the specimens to fail outside the jacket.

1.2.2 Modelling of reinforced concrete

Analytical modelling of reinforced concrete members and frames has been the subject of much research. Several different models have been proposed to simulate the observed hysteretic behaviour of reinforced concrete. Most of these attempts have been met with some success. An accurate evaluation of the early models was not possible due to lack of experimental data. Advances in digital computers have made the modelling of inelastic behaviour and dynamic response of frames more practical.

Clough (1966) developed a bi-linear hysteresis model based on test data of a reinforced concrete frame. This model accounted for stiffness degradation in the concrete.

The model was used to predict the response of a single degree of freedom system and the results showed some similarity between the model and the actual test. The model was simple but did not take into account cracking, strength deterioration, pinching, beam reinforcing bars bond slip nor joint shear deformation.

Takeda et al. (1970) developed a tri-linear hysteresis model which included a cracking point, yield point, and post-yield stiffness in the primary curve. Bond slip was incorporated in the definition of the yield displacement. A set of rules was developed to govern the cycles beyond the primary curve. Stiffness degradation was accounted for by defining a relationship between the unloading stiffness and the yielding stiffness using the maximum deflection in the loading cycle and the yield deflection. This model was based on test results of a single degree of freedom system. Comparisons between the model predictions and the tests indicate agreement for specimens characterized by flexural behaviour. The model did not take into consideration pinching due to high shear, strength deterioration nor joint shear deformation.

Otani (1974) developed a two-component beam element for use in the non-linear analysis of reinforced concrete frames. The element had two parallel line sub-elements (one elastic and the other inelastic). These two sub-elements were connected to non-linear springs at their ends. The springs represented plastic hinges at the beam ends and were assigned a modified Takeda bi-linear hysteretic curve. Rules were developed to govern further load cycling beyond the primary curve. The model incorporated a movable point of contraflexure, stiffness degradation, and bond slip. Comparisons to actual tests showed some agreement. The model did not take into account pinching, strength deterioration nor joint shear deformation.

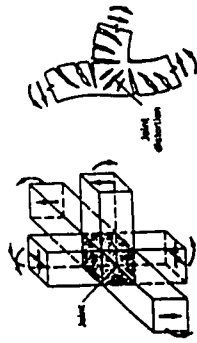
Al-Haddad and Wight (1988) developed a one-component beam element with movable plastic hinge locations and rigid ends to simulate end connections. The non-linear plastic hinge zones were governed by a modified Clough hysteresis model based on test results from beam to column joints. Some correlation between the model and cyclic load reversal tests was observed. As Otani's (1974) model, the model did not take into consideration pinching due to high shear, strength deterioration nor joint shear deformation.

Roufaei and Meyer (1987) developed a model for reinforced concrete members that incorporates a member damage parameter, a global damage parameter, and a plastic hinge of finite length. This model was programmed as a new element for the DRAIN-2D program. The model uses Takeda style rules to govern the hysteretic behaviour. The closing of the cracks and strength degradation are included in the model using empirical values obtained from experimental data. The hysteretic response of the test specimens was predicted using this model. The results showed close agreement between the observed response and that predicted by the model for a wide variety of reinforced concrete specimens. All the specimens had adequate transverse reinforcement in the joints. The model did not consider the joint shear deformation nor the beam reinforcing bars bond slip.

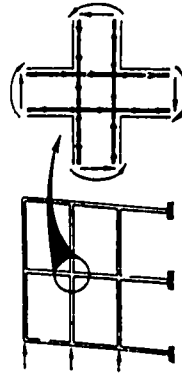
Filippou and Issa (1988) developed a super-element model composed of several sub-elements connected in series. The sub-elements model the basic mechanisms that control the hysteretic behaviour of girders and columns. Correlation between the model and static load reversal testing of beam-column subassemblages was good. The subassemblages had adequate transverse reinforcement in the joint. The model also compared quite favourably with the more common one-component models that were developed previously. The model assumed

rigid joint without joint shear deformation.

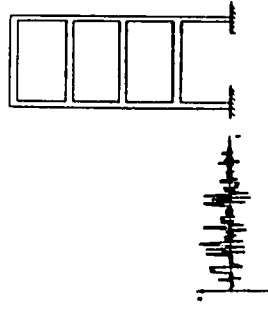
Computerized non-linear dynamic analysis techniques were enhanced since the development of the computer program DRAIN-2D by Kanaan and Powell (1973). Besides the several offsprings of the original code, new software packages like IDARC by Park et al. (1987), its refined version by Valles et al. (1996), DRAIN-2DX by Allahabadi (1987) and Powell and Prakash (1992) were developed. These analytical tools were used by several investigators for the analysis of lightly reinforced concrete frames (Shahrooz and Muvdi, 1991; Hoffmann et al., 1992). However, all of these programs assume infinite rigidity of the beam-column joint which limit their applicability in the case of existing structures with deficient joints.



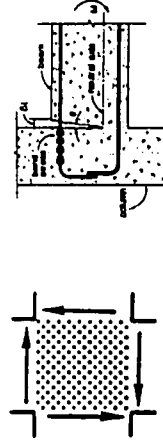
What is the behaviour of the existing reinforced concrete beam-column connections under cyclic loading?



To what extent is the conventional rigid joint assumption valid in the analysis of existing frames?



What is the effect of such connections on the performance of the frame during future earthquakes?



Is there a simple, accurate and practical joint model to represent the dynamic behaviour of existing joints?

?

Is there a simple, economical and effective rehabilitation technique to strengthen this type of connections?

?

Which strategy can be developed to rehabilitate such frames?

Figure 1.1 Motivation of the study

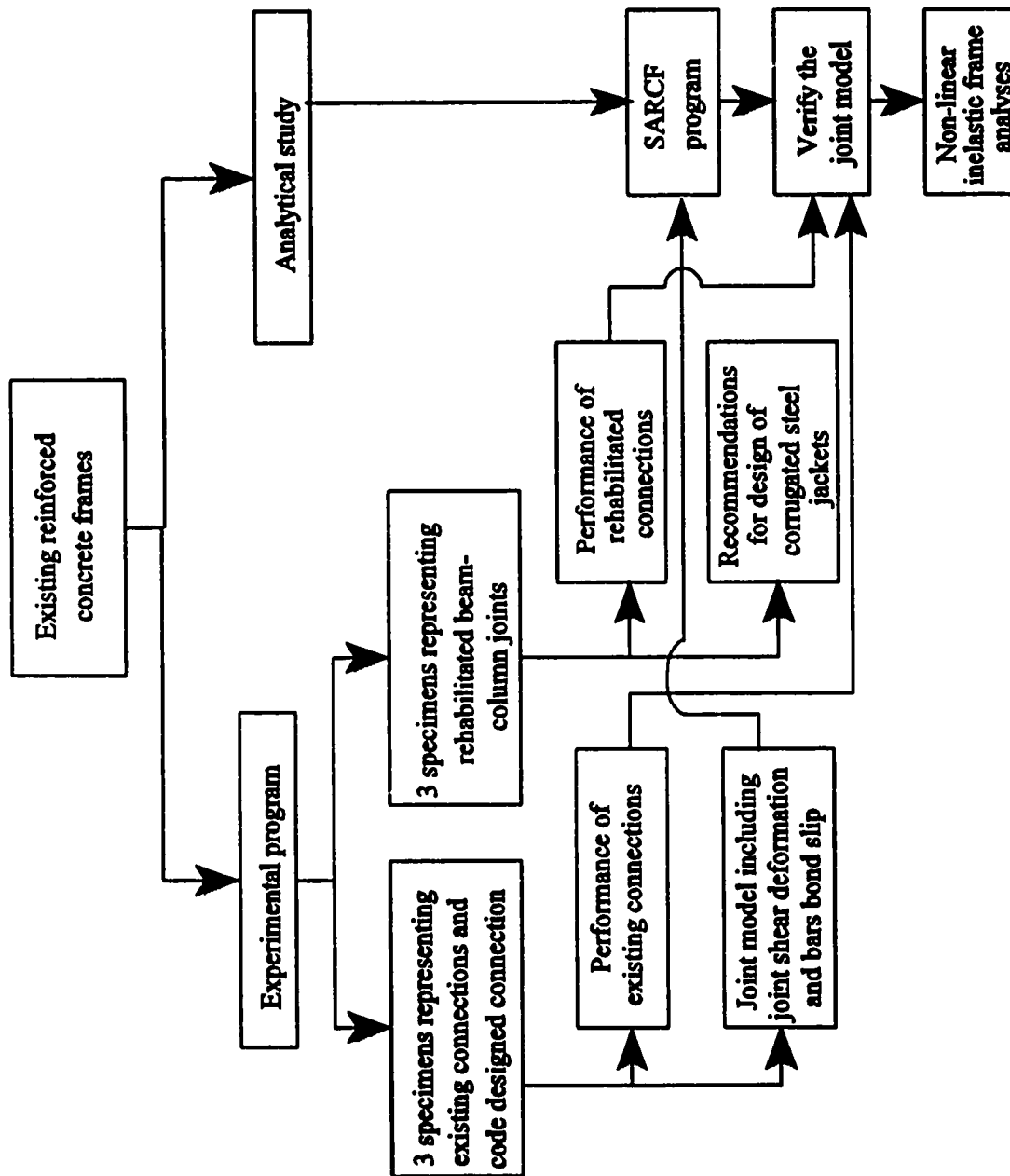


Figure 1.2 Plan of research program

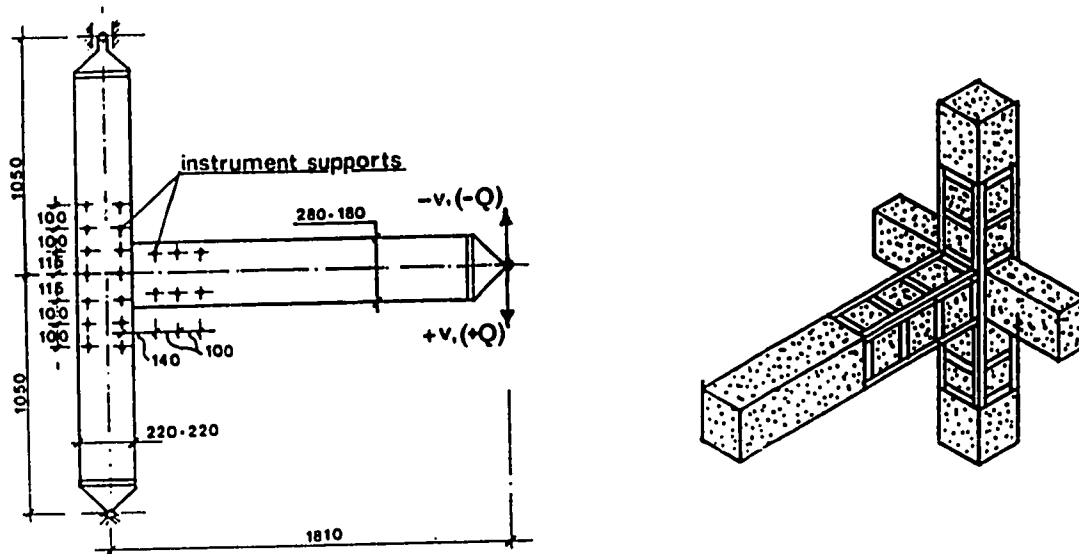


Figure 1.3 Strengthening scheme for an exterior beam-column joint (Migliacci et al., 1983)

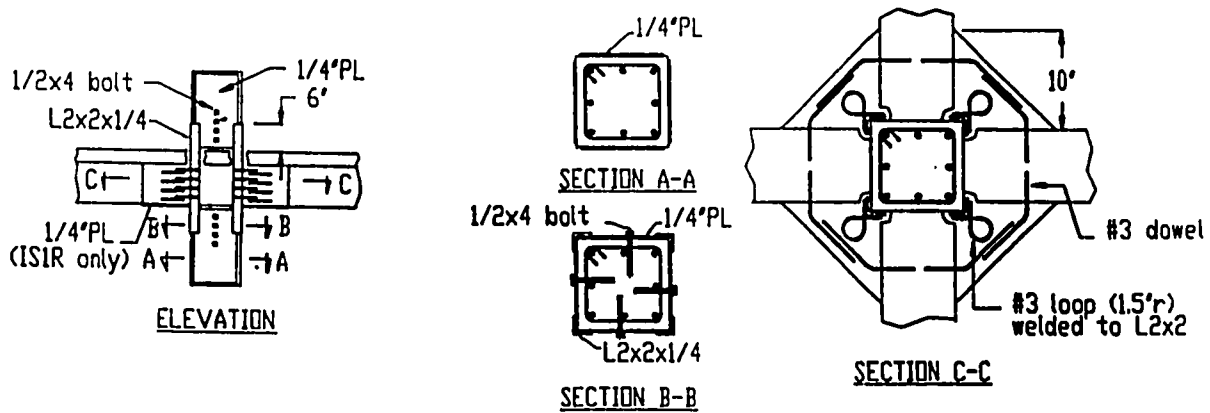


Figure 1.4 Details of external steel reinforcement (Corazao and Durrani, 1989)

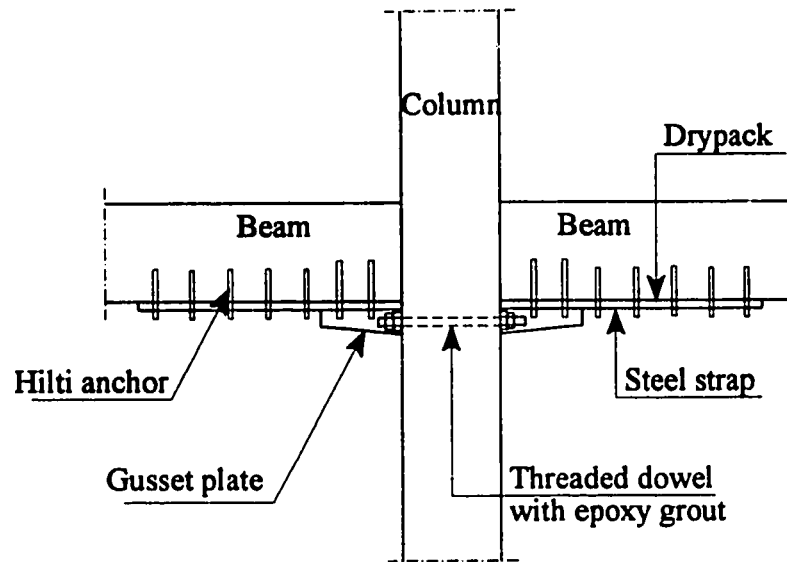


Figure 1.5 Strengthening scheme for interior beam-column joint (Estrada, 1990)

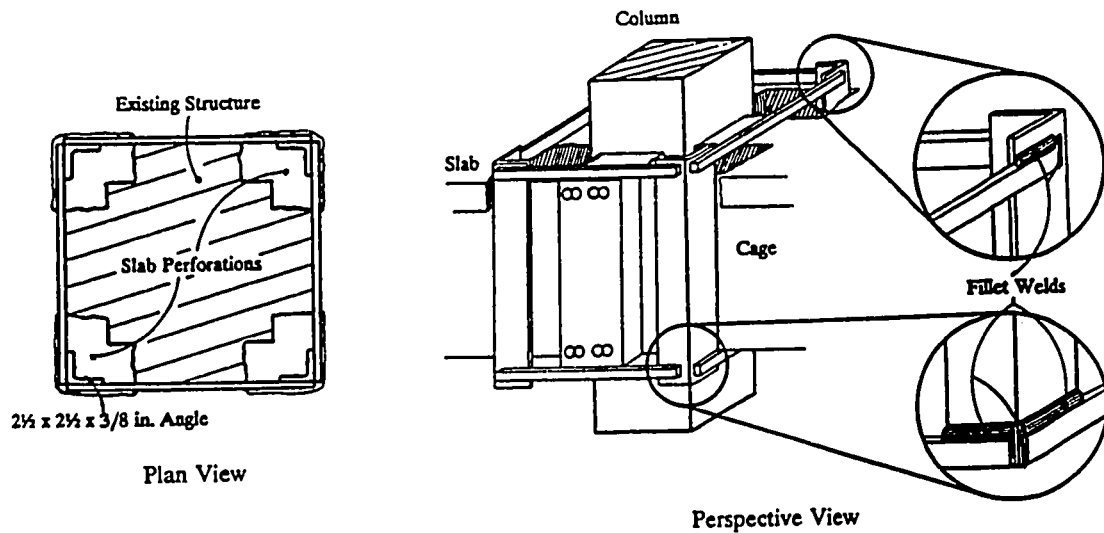


Figure 1.6 Beam-column joint confinement cage (Alcocer and Jirsa, 1991)

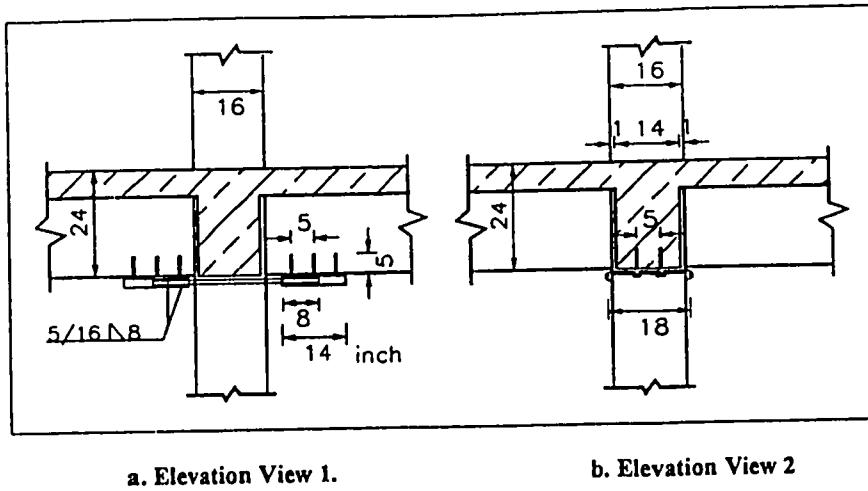


Figure 1.7 Retrofit configuration for an interior beam-column joint (Beres et al., 1992)

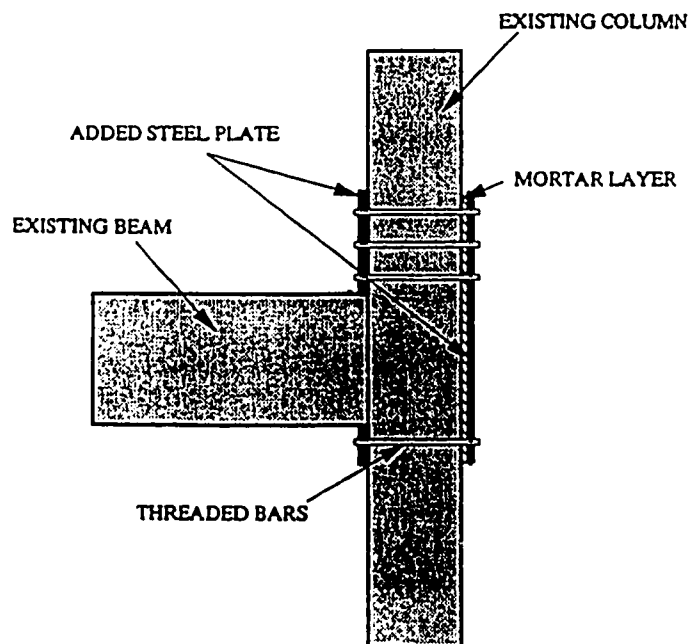


Figure 1.8 Strengthening scheme for an exterior beam-column joint (Beres et al., 1992)

CHAPTER 2

EXPERIMENTAL PROGRAM

2.1 INTRODUCTION

Six large-scale reinforced concrete frame connections were constructed and tested. All the specimens were of identical dimensions. The specimens represent an exterior joint of an existing two story frame supporting the pressure relief duct structure located in Pickering Nuclear Generating Station in Ontario. The frame was designed and constructed in 1969, before the current seismic codes were available. The frame is 21.96 m high and is symmetrical about the vertical axis. The column size is 1524 x 1829 mm. The beam span is 6.71 m from column face to column face. The lower level beam has a square cross-section of dimension 1829 mm. The column longitudinal reinforcement is 28 #11 bars distributed around the section perimeter and is spliced above the foundation level and above the lower beam level at the construction joints. The top and bottom longitudinal reinforcement in the lower beam are 16 #11 bars each. The frame is characterized by flexible columns, weak joints and strong beams with non-ductile reinforcement detailing. The first, third and fifth specimens (J1, J3 and J5) were detailed to represent the steel of the existing reinforced concrete frame. Specimen J2 includes confinement reinforcement that was detailed according to the current Canadian concrete design code (CSA A23.3-94, 1994). Specimen J3 was

encased by a corrugated steel jacket around the column and the beam to enhance its seismic behaviour. Specimen J5 was encased by a corrugated steel jacket around the column only. Specimen J4 was detailed to represent a case of no shear reinforcement in the joint and insufficient positive beam reinforcement development length inside the joint. Specimen J6 was encased by corrugated steel jacket around the column only in addition to two steel plates anchored to the beam and the joint to prevent the pull out of the positive beam reinforcement. The specimens were subjected to severe cyclic loading. The features of the test specimens in the experimental program are summarized in table 2.1.

2.2 MODELLING CRITERIA

Although considerable advances have been made in the use of analytical methods to predict the seismic performance of structures, the prediction of the performance of as built frame components such as beams, columns and joints continues to rely on laboratory testing. The most representative results are those determined from full scale member testing. However, because of equipment capacity limitations, scaled models are a viable alternative. However, if a representative model is to be constructed, it is necessary to satisfy the similitude relationship $\rho_p = (S_\sigma / S_l) \rho_m$; where ρ_p and ρ_m are the densities of prototype and model materials, S_σ is the prototype to model stress scaling factor and S_l is the prototype to model geometrical scaling factor. If the prototype and model are made of the same density of concrete material then $\rho_m = \rho_p$. In this case, the similitude requirement can only be met by a substantial alteration in the stress scaling ratio S_σ , which would require the use of unreasonably weak model materials. If the same density and strength of materials of the

prototype are to be used for the model, one answer to the similitude requirement is to increase the mass of the model by placing additional weights on the model structure. Since the models were subjected to quasi-static cyclic loading then the presence of the additional mass will not affect the results. The scale factors used between the model and prototype are listed in table 2.2. A reliable simulation of the seismic behaviour of existing structures should take the ductility of critical regions and the stiffness and strength distribution into account. To retain the ductility similitude, the following parameters are selected to be equal in both the prototype and the specimen:

- 1- Percentages of longitudinal reinforcements,
- 2- the ratio between the tension and compression reinforcement,
- 3- mechanical volumetric percentage of confining reinforcement,
- 4- normalised axial compression force ($P/A_c f'_c$), where P is the axial load on the column, A_c is the gross cross-sectional area of the column and f'_c is the concrete compressive strength,
- 5- shear ratio ($M/V d$), where M is the moment, V is the shear and d is the depth of the member,
- 6- ratio of ultimate shear force resistance values, corresponding to shear or flexural failure modes.

In a recent research programme at the University of Illinois at Urbana-Champaign, Abrams (1987) constructed eighteen reinforced concrete beam-column assemblies using different scales (approximately one-twelfth, one-quarter, and three-quarter scales). The specimens were subjected to reversals of lateral force to study scale correlations for non-linear hysteretic properties. It was concluded that one-quarter scale is the minimum scale at

which conventional reinforcing bars and concrete aggregate can be used and still maintain the force-deformation behaviour.

Because of the laboratory size and equipment limitations, a full scale test of the beam-column connection is not possible. Instead, one-third-scale was selected for use in the present testing programme. Applying $S_l = 3$ and $S_o = 1$ to the factors given in table 2.2, the scaling of various quantities of interest between the prototype and the specimen were calculated. The dimensions of the prototype and the specimen are shown in figure 2.1.

2.3 SPECIMEN DETAILS

The dimensions of the specimens are shown in figure 2.2. All specimens consisted of a 1270 mm long beam framing into a 3450 mm high column at a distance 1270 mm from the top. The height of the column is taken to model the distance between contraflexure points. The column cross-section is 610 x 510 mm and the beam cross-section is 610 x 610 mm.

The specified compressive strength of concrete f'_c was selected to be similar to that of the existing structure at 20.7 MPa (3000 psi.). The compressive strength and split tensile strength of concrete cylinders at 28 days and at the time of the test are presented in table 2.3. The average compressive strength from the test cylinders was 23.0 MPa (3335 psi). Non-shrink grout was used between the concrete and the steel jackets (M-BED Superflow-high fluidity, premixed cementitious grout). The average compressive strength of the grout was 39 MPa after 7 days and 44 MPa after 28 days. The split test gave tensile strength of 2.6 MPa after 28 days.

Grade 400 MPa steel reinforcement was used as the principal reinforcing bars.

Smooth wire size steel was used for the stirrups in the beam and column ties of all the specimens except the column ties of specimen J2 which were M10, grade 400 MPa steel. The smooth wire sizes used were 6.35 mm diameter round hot rolled A36 bars and 4.7 mm diameter cold finished round bars (AISI C1018/A 108). Steel tensile properties are presented in table 2.4. The average measured value for the yield strength of the M15 steel bars was 440 MPa and that of the wire size stirrups was 448 MPa. Corrugated steel sheets meeting the CSA (1981) Standards (CAN3-G401-M81) were used in the joint confinement jacket with minimum specified yield strength of 230 MPa. The average measured value for the yield strength of the 2.8 mm and the 3.5 mm thick corrugated sheets were 363 MPa and 342 MPa, respectively. Corrugated steel tensile properties are presented in table 2.4.

Grade 400 MPa (60 ksi) steel reinforcement was used in the specimens instead of grade 275 MPa (40 ksi) steel used in the prototype frame. For this reason, lower number of longitudinal steel bars in the beam was needed. The longitudinal bars in the beam were fitted in one row as compared to the prototype beam section with two rows of longitudinal steel. Although the selected wire size for the column transverse steel did not meet the requirement of the ACI 318 (1989) (nor the Canadian Specifications Standard CSA A23.3-94, 1994), the important parameter to maintain in the modelling process is the shear strength of the transverse steel. In the specimens, the clear cover for the reinforcing steel was 30 mm.

The longitudinal steel in the beams and columns of all the specimens was taken to be identical except for specimens J4 and J6 where shorter development length of the bottom beam reinforcement was applied. The main difference between the specimens was in the shear reinforcement of the beam, columns and joint. The transverse reinforcement of specimens J1,

J3 and J5 shown in figure 2.3a, were four legged 6.35 mm diameter stirrups at 120 mm spacing for the beam, while the column and joint ties were two legged 4.7 mm and two legged 6.35 mm diameter ties at 150 mm spacing. The transverse reinforcement of specimen J2 shown in figure 2.3b, was four legged 6.35 mm diameter stirrups at 60 mm spacing for the beam, while the column and joint ties were four legged M10 bars at 96 mm spacing. The transverse reinforcement of specimens J4 and J6 shown in figure 2.3c, were four legged 6.35 mm diameter stirrups at 120 mm spacing for the beam, two legged 4.7 mm and two legged 6.35 mm diameter ties at 150 mm spacing for the column with no ties in the joint.

To confine the critical regions of the joint and the column, a structural corrugated steel casing was welded around the joint and the column for the rehabilitated specimens (J3, J5 and J6) and around the beam for J3 only, as illustrated in figure 2.4. Non-shrink grout was poured between the concrete and the casing. The casing was expected to provide the required strength and confinement of the column and joint. The corrugated steel jackets were fabricated using 2.8 mm thick steel for specimens J3 and J5 and 3.5 mm thick steel for specimen J6.

The properties of the corrugated steel section is shown in figure 2.5. It was selected from commercially available sections. Tomii (1993) suggested the ratio of the pitch to maximum column width to be approximately 0.1 so that half the pitch would be almost equal to the thickness of concrete cover of the main bars in an ordinary reinforced concrete members. The thickness of the non-shrink grout between the concrete and the steel jacket was a minimum of 25 mm.

2.4 SPECIMEN FABRICATION

2.4.1 Existing joints

The specimens were fabricated in a horizontal position. Two sets of wooden forms were constructed for easy assembly and disassembly after casting. The bottom and the sides of the forms consisted of 5/8 in. plywood with the sides stiffened with a 2 inches square border. The gaps between the plywood sheets were sealed with tape to prevent bleeding of the concrete that would occur during pouring. Figure 2.6 shows the assembled forms. Prior to assembling the reinforcing cage, some of the steel bars were instrumented with strain gauges. For the assembly of the reinforcing steel, the column longitudinal bars were positioned using the two end ties after sliding all the column ties inside. The beam longitudinal bars were then positioned perpendicular to the column longitudinal bars using the beam's two end stirrups after sliding all the beam stirrups from the far end of the beam. The column and beam transverse reinforcement were then positioned and tied to the longitudinal reinforcement with a flexible steel wire. The joint ties were then positioned and tied to the longitudinal reinforcement. The assembled reinforcement cage for the specimen is shown in figure 2.7. The wooden forms were coated with a thin film of oil to facilitate stripping of the forms without damage. Chairs made from steel bars were used to maintain the proper cover distance between the form and the reinforcement bars.

The concrete was delivered to the laboratory by ready-mix concrete truck at which time additional water was added to obtain a slump of about 80 mm. The concrete consists of Portland cement (# 10), coarse aggregates (gravel) of maximum size of 20 mm, fine aggregates (sand) and water. The concrete was mechanically vibrated to eliminate voids.

Several hours after casting, the specimens were covered with damp burlap to provide a moist curing condition. Polyethylene sheets were used over the burlap to help retain moisture. The burlap was kept damp by wetting it twice a day. After three days, the forms were stripped. The specimens were moist cured for another seven days and then air cured in the laboratory until the time of testing which was always more than 28 days after casting. Concrete cylinders were cured in the same manner as the specimens. Before testing, the specimens were painted with a flat white paint to aid in locating the cracks.

2.4.2 Rehabilitated specimens

The corrugated steel jackets were built-up using pre-manufactured "U" shape sections fitted to the column or beam and welded at the site as shown in figure 2.8. For the joint region, two steel angles were installed to resist the lateral pressure. These two angles were welded to the "U" shape and anchored to the concrete by expansion anchor bolts as shown in figure 2.8.

To improve the bond between the existing concrete and the grout, concrete surface was roughened. To remove small particles and dust, the specimen surface was brushed with a thick brush and vacuum cleaned. Afterwards, the required holes for anchor bolts were drilled in the beam. The column jacket was then constructed by welding the "U" shape section to close the box around the column. The two angles were fixed to the sides of the beam by two M20 (20 mm diameter Hilti-HSL) anchor bolts for each angle. The beam jacket was then constructed by welding the "U" shape section to close the box around the beam. The bottom of column jacket and the far end of the beam jacket were sealed and grout was injected between the concrete and the steel jacket from top.

2.5 TEST SET-UP

Figures 2.9a and b show the overall test set-up. The specimens were held hinged at both ends of the column while the beam tip was subjected to a cyclic loading pattern using a 1112 kN (250 kips) double acting hydraulic jack (actuator) with a 254 mm stroke. Two 30 mm thick steel plates were placed on the top and the bottom of the beam end which were stiffened with 25 mm thick stiffeners, and were tied together using six 25 mm threaded rods.

The bottom plate had a vertical plate welded to it. The vertical plate was attached to the end of the loading ram through a greased pinned connection. This provided the mechanism for transmitting the reversing jack action to the beam.

To simulate the gravity load on the column, an axial load of 505 kN, which corresponds to 4550 kN on the existing frame, was applied to the column as a constant load.

2.6 LOADING PROGRAM

A cyclic load was applied at the beam tip of the test specimens. The selected load is intended to cause forces that simulate high levels of inelastic deformations that may be experienced by the frame during a severe earthquake ground motion. The selected load history shown in figure 2.10, consists of two phases. The first phase is load-controlled followed by displacement-controlled loading phase.

Load Control

Two cycles at approximately 15 percent of the estimated strength of the specimen (60 kN) were applied to ensure that all data acquisition channels were functioning properly. This was followed by two cycles to the load causing initial cracking of the concrete estimated at

120 kN. The two cracking load cycles were followed by two cycles of loads that caused initial steel yield. This load was measured to be 330 kN. The displacement at initial yield of the steel, δ_y , was recorded and used in the displacement controlled phase of the load.

Displacement Control

After determining the yield displacement from the elastic cycles, the specimens were subjected to an increasing displacement controlled loading history starting from $\delta / \delta_y = 2.0$ using multiples of the displacement recorded at the initial yield of the steel, δ_y . Two cycles were applied at each ductility level to verify the stability of the specimens behaviour (hysteresis loops). The effect of repetitive cyclic load-carrying capacity, stiffness, strength degradation and energy dissipation capacity of the specimens were examined. Testing was continued until the specimen lost its ability to resist an applied load of approximately 25% of the ultimate load.

The deflected shape of a frame structure subjected to lateral loading is shown in figure 2.11. The interstory drift angle, R , is defined as the ratio of the column relative displacement over the column height as shown in figure 2.12a. However, for practical and economic reasons, column ends in the test set-up are often pinned with restricted lateral movement and beam ends are displaced vertically. In this case the drift angle is defined as the ratio of beam tip displacement to the beam length, figure 2.12b.

In comparing the two configurations shown in figures 2.12a and 2.12b, it is noticed that the P- Δ effect due to story drift is unaccounted for in the test setup. Considering equilibrium of the free body diagram shown in figure 2.12a and neglecting the weight of members, the summation of moments about the support point "B" yields:

$$P (\delta_h) + V_{\text{actual}} H = F (L/2 - \delta_h/2) \quad (2.1)$$

Considering the force equilibrium in the test setup as shown in figure 2.12b, and neglecting the weight of members, the summation of the moments about the support point "B" yields:

$$V H = F (L/2) \quad (2.2)$$

From equations 2.1 and 2.2:

$$V / V_{\text{actual}} = (F L/2) / (F \{L/2 - \delta_h/2\} - P \{\delta_h\}) \quad (2.3)$$

Where F is the beam tip force, L/2 is the beam length, H is the column height, δ is the beam tip displacement, P is the column axial load and R is the drift angle.

The significant parameter for the designer is the actual column shear (V_{actual}) rather than the measured column shear from the test (V). Using equation 2.3, it is possible to convert the measured column shear (V) in the test to column shear that should be used by the designer (V_{actual}) (Uzumeri, 1974).

2.7 INSTRUMENTATION

The instrumentation of the specimens was designed to measure the overall response and the load resistance mechanism in the beam-column subassembly. Three types of measuring devices were used: load cells, LVDTs (Linear Variable Differential Transformers) and strain gauges.

The load applied at the beam tip was measured with a load cell mounted on the shaft of the hydraulic actuator. A 1780 kN (400 Kips) hydraulic jack and a similar capacity load cell were used to apply and measure the column axial load. The beam tip displacement was monitored by a 762 mm (30 in.) LVDT. These measurements allowed the calculation of story

shear and drift angle as given by the formulae:

$$V = F (L/2) / H \quad \text{and} \quad R = \delta / (L/2) \quad (2.4)$$

The LVDTs were mounted on 8 mm (5/16 in.) diameter all-threaded rods that were deeply embedded in the concrete in order to avoid loss of readings due to surface spalling. They were installed at locations to enable computation of the contribution of beam, column and joint to the total deformation. Diagonal measurement of displacement provided the shear distortion to the beam and joint. The instrumentation used to determine the joint shear distortion is shown in figure 2.13a. The joint shear distortion γ_{average} was calculated by using the equation

$$\gamma_{\text{average}} = (\Delta_1 + \Delta_2) / D \sin 2\theta \quad (2.5)$$

Where D is the undistorted diagonal distance, $\tan \theta = b/h$ and b and h are the respective horizontal and vertical distances between the points. Equation 2.5 is only valid for uncracked sections, or regions with vertical flexural cracking. The equation does not apply to inclined cracks traversing only one diagonal gauge. Nevertheless, the equation does give an idea of the average shear even after a diagonal crack crossed the instrumented region. Using four LVDTs mounted on a reference frame which was fixed relative to the specimen, joint distortion γ was calculated as the difference between the vertical joint angle α and the horizontal joint angle β , figure 2.13a.

The instrumentation used to determine the beam shear and flexural deformation is shown in Figure 2.13b over the beam plastic hinge zone.

Instrumentation used for beam rotations and column rotations is shown in figures 2.13c and 2.13d. Beam rotations were measured using LVDTs positioned 51 mm (2 in.)

above the beam top and below the beam soffit. Similarly, column rotations were measured. The column and beam deformations included in the rotation measurements, as a result of the position of the LVDTs, were taken into account. After several large loading cycles, the concrete in the vicinity of the LVDT mounting devices sometimes spalled and further measurements were unreliable. The average beam and column curvatures were determined by dividing the measured relative rotation at one section by the length along the member over which they occurred.

The reinforcing steel in the beam, column and joint; and the steel jacket were instrumented with high elongation electrical strain gauges. The locations of the strain gauges in the concrete specimen, as well as in the beam and column jacketing, are shown in figures 2.14a and 2.14b. The purpose of the strain measurement was to monitor the start of yielding in the main and shear reinforcements.

2.8 DATA ACQUISITION

Data from load cells, displacement transducers and strain gauges were recorded using an automatic computer controlled data acquisition system, figure 2.15. The load and displacement readings, the load-displacement plot and top and bottom reinforcement strains were monitored on a microcomputer screen during the test. At each load stage the instrumentation channels were read and a hard copy of the readings was obtained. The software used allowed conversion of test data to engineering units in real time to monitor the test. Measurements were saved on floppy disks for further data compilation and analysis of results.

Table 2.1 Features of the beam-column connection specimens in the test program

Specimen designation	Transverse reinforcement in column and joint	Transverse reinforcement in beam	Beam longitudinal reinforcement development length	Comments
J1	16% of the code requirement	50% of the code requirement	Satisfies code	Existing
J2	Satisfies code	Satisfies code	Satisfies code	Current code design
J3	16% of the code requirement + steel casing	50% of the code requirement + steel casing	Satisfies code	Existing but with column and beam steel jacket
J4	0% of the code requirement + steel casing	50% of the code requirement	Does not satisfy code	Existing but with no shear reinforcement in the joint
J5	16% of the code requirement + steel casing	50% of the code requirement	Satisfies code	Existing but with column steel jacket only
J6	0% of the code requirement + steel casing	50% of the code requirement	Does not satisfy code	As J4 but with bottom steel plates and column steel jacket only

Table 2.2 Scaling factors for modelling under quasi-static loading

Quantity	Dimensions	Scale factor	Practical scale factor ($S_\sigma = 1$)
Concrete stress σ_c	FL^{-2}	S_σ	1
Concrete strain ϵ_c	-	1	1
Modulus of elasticity E_c	FL^{-2}	S_σ	1
Poissons ratio ν_c	-	1	1
Steel stress σ_s	FL^{-2}	S_σ	1
Steel strain ϵ_s	-	1	1
Length l	L	S_l	S_l
Displacement u	L	S_l	S_l
Area A_s	L^2	S_l^2	S_l^2
Concentrated load Q	F	$S_\sigma \cdot S_l^2$	S_l^2
Line load	FL^{-1}	$S_\sigma \cdot S_l$	S_l
Pressure p	FL^{-2}	S_σ	1
Moment M	FL	$S_\sigma \cdot S_l^3$	S_l^3
Shear V	F	$S_\sigma \cdot S_l^2$	S_l^2
Density ρ	FL^{-3}	S_σ / S_l	$1 / S_l$

F: force,

L: length,

$$S_\sigma = \sigma_p / \sigma_m$$

$$S_l = l_p / l_m$$

 σ_p : stress in prototype, σ_m : stress in model, l_p : length in prototype, l_m : length in model.

Table 2.3 Uniaxial compressive and split tensile strength of concrete cylinders

Time	Specimen					
	J1	J2	J3	J4	J5	J6
28 days compressive strength (MPa)	21.5	22.0	21.5	24.0	22.0	24.0
28 days Split tensile strength (MPa)	2.85	2.40	2.85	2.42	2.40	2.42
compressive strength at time of test (MPa)	23.6	22.0	25.0	24.0	23.0	25.5

Table 2.4 Reinforcing and corrugated steel properties

Item	f_y (MPa)	ϵ_u (%)	f_u (MPa)
M10 rebar	500	12.0	750
M15 rebar	440	14.5	697
6.35 mm diameter smooth bar	448	13.8	534
4.7 mm diameter smooth bar	648	5.0	706
2.8 mm corrugated steel sheet	363	2.8	397
3.5 mm corrugated steel sheet	342	2.9	390

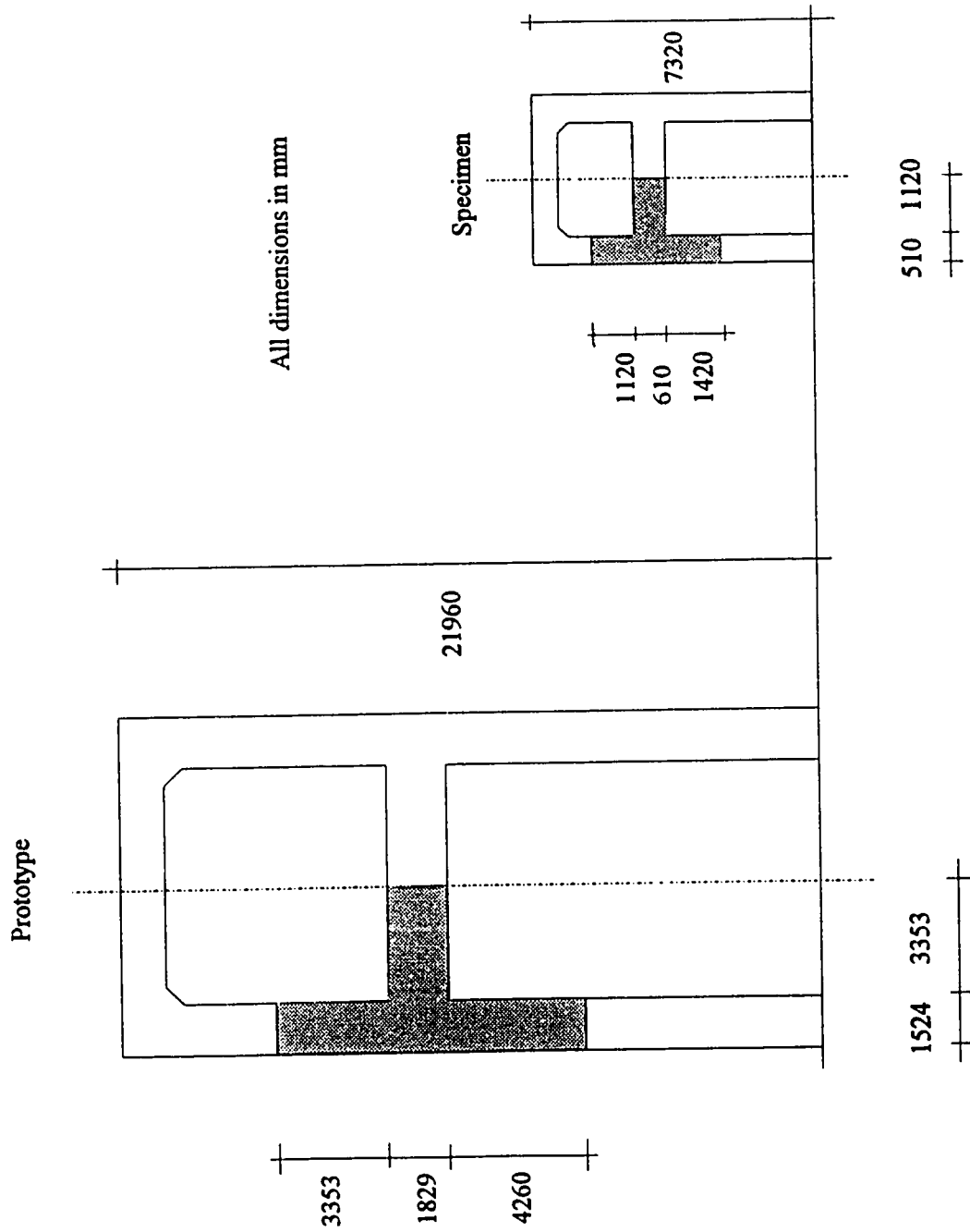


Figure 2.1 Dimensions of the prototype and the specimen.

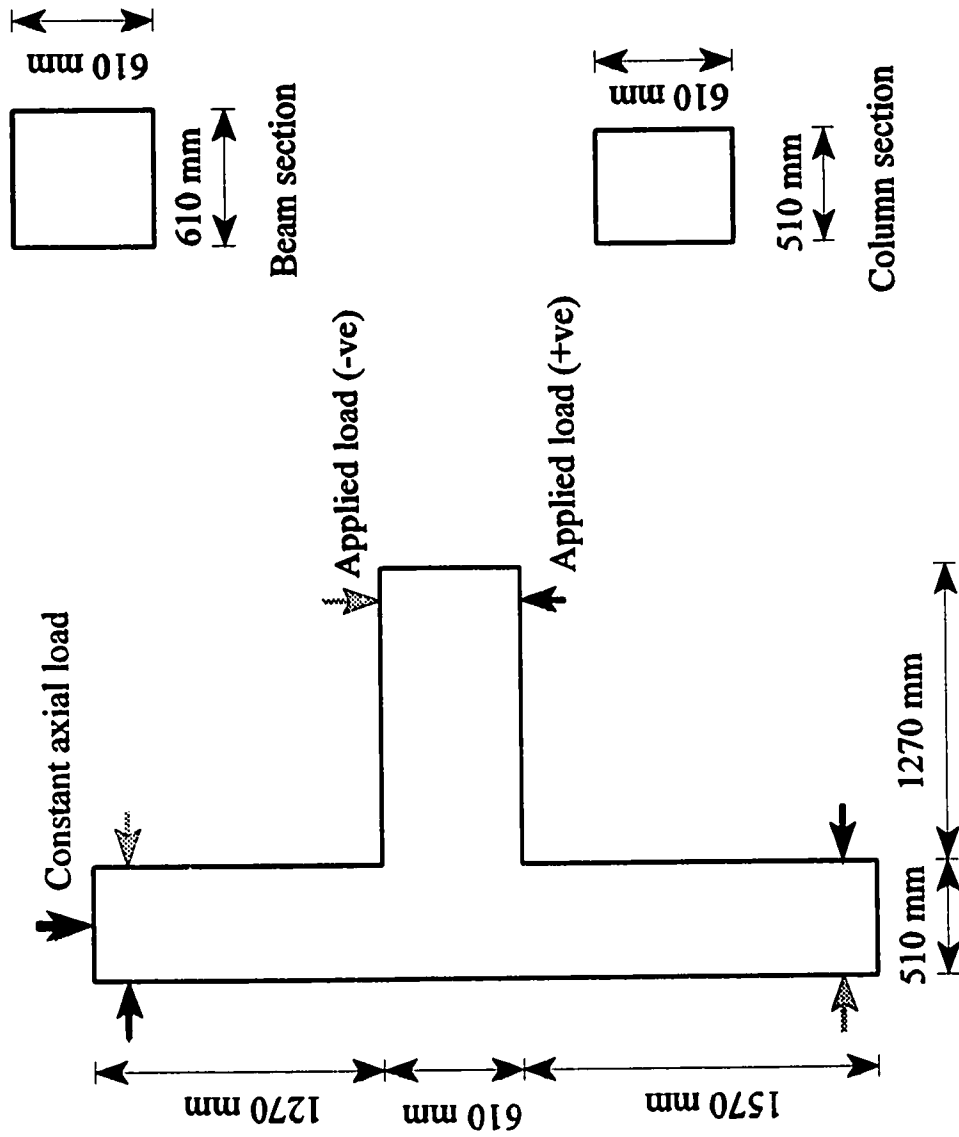


Figure 2.2 Concrete dimensions of the specimens.

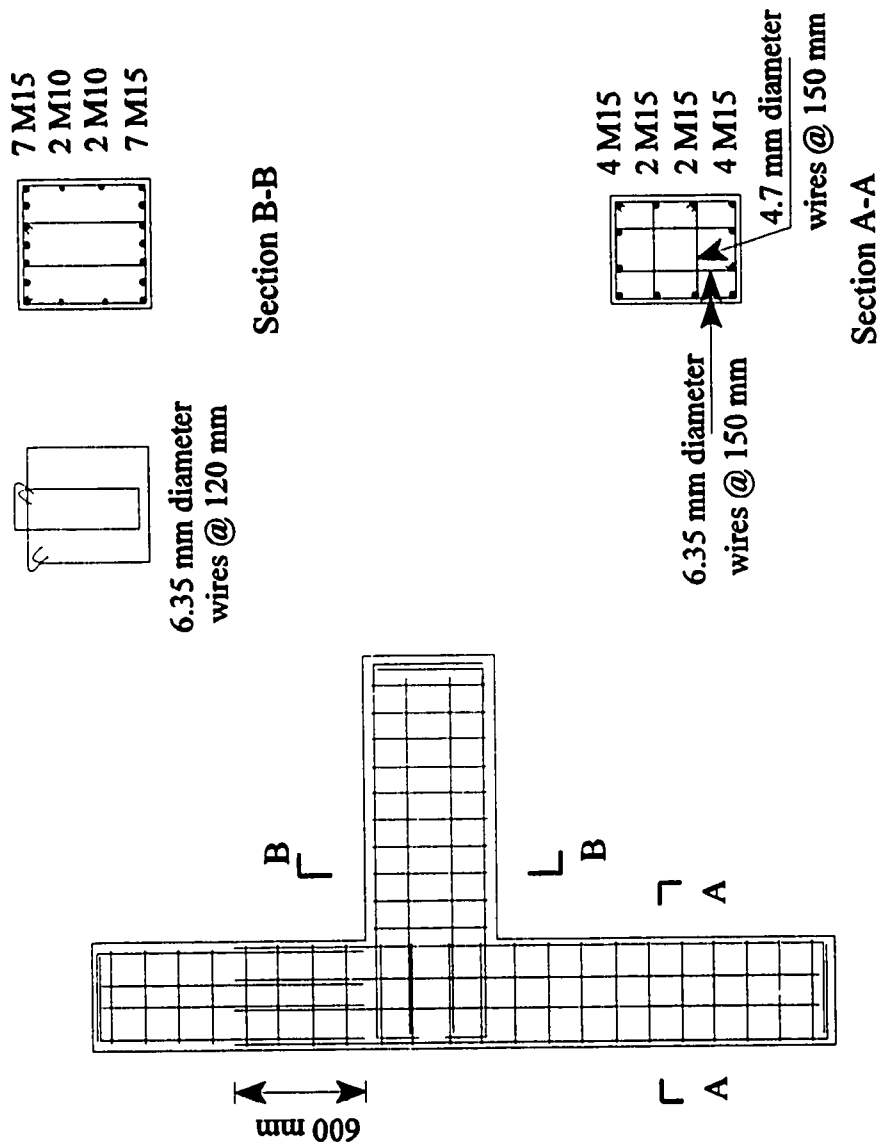


Figure 2.3a Details of reinforcement of specimens J1, J3 and J5

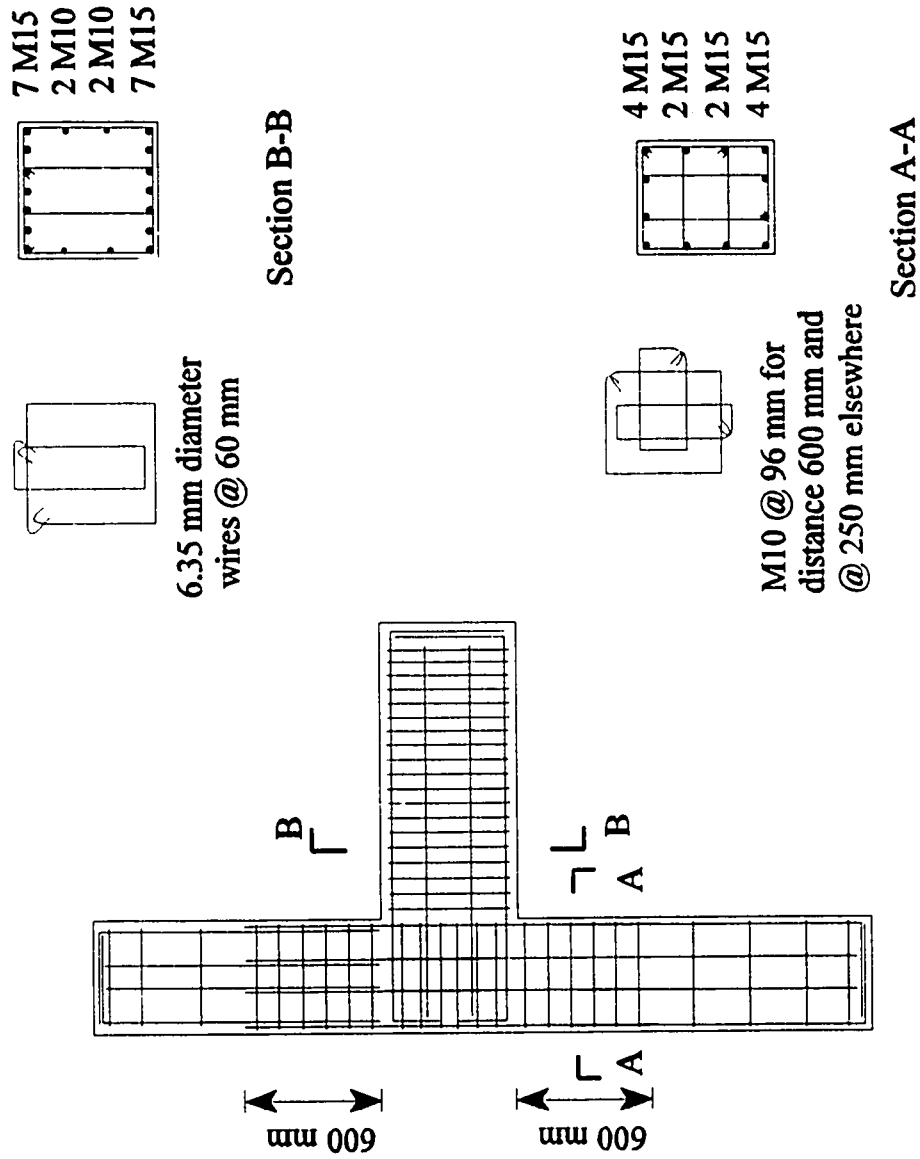


Figure 2.3b Details of reinforcement of specimen J2

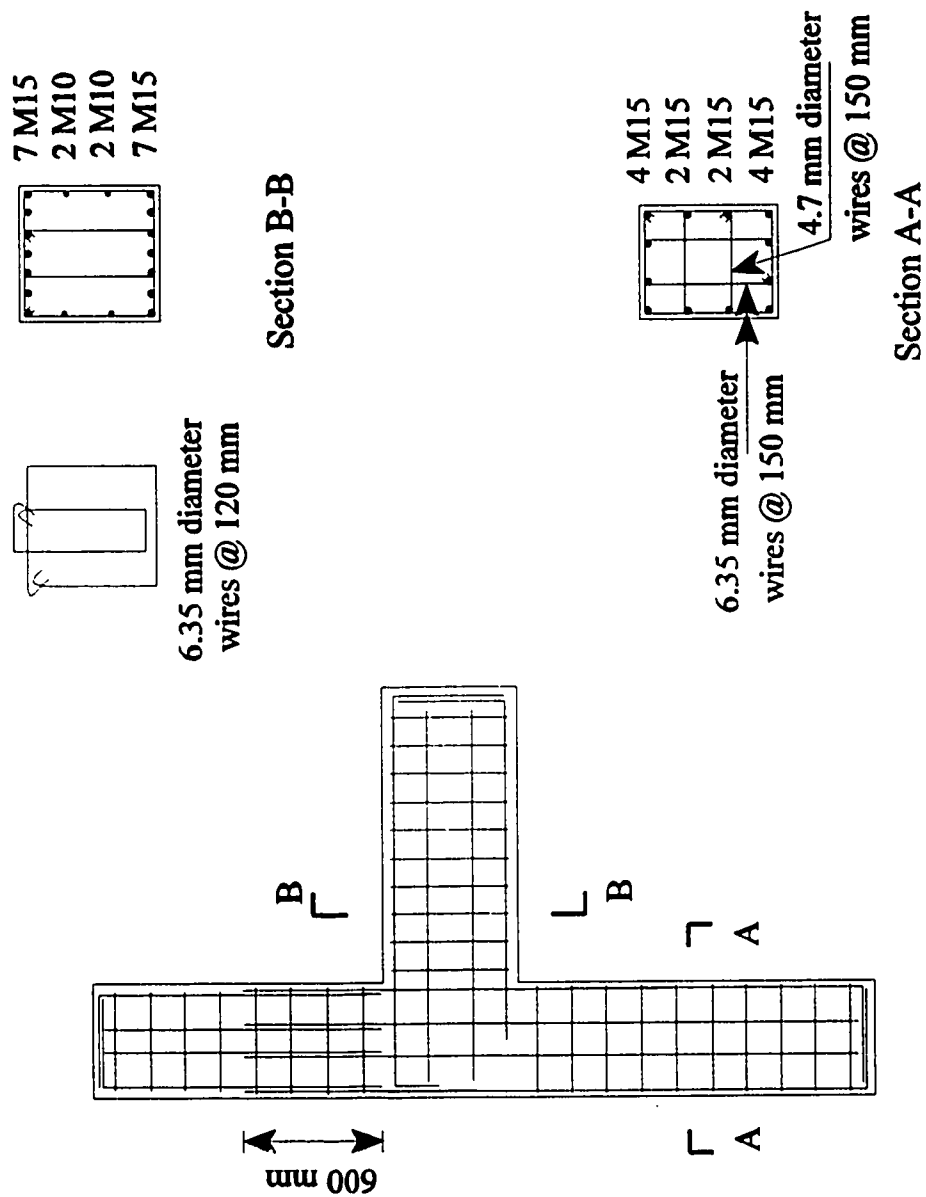
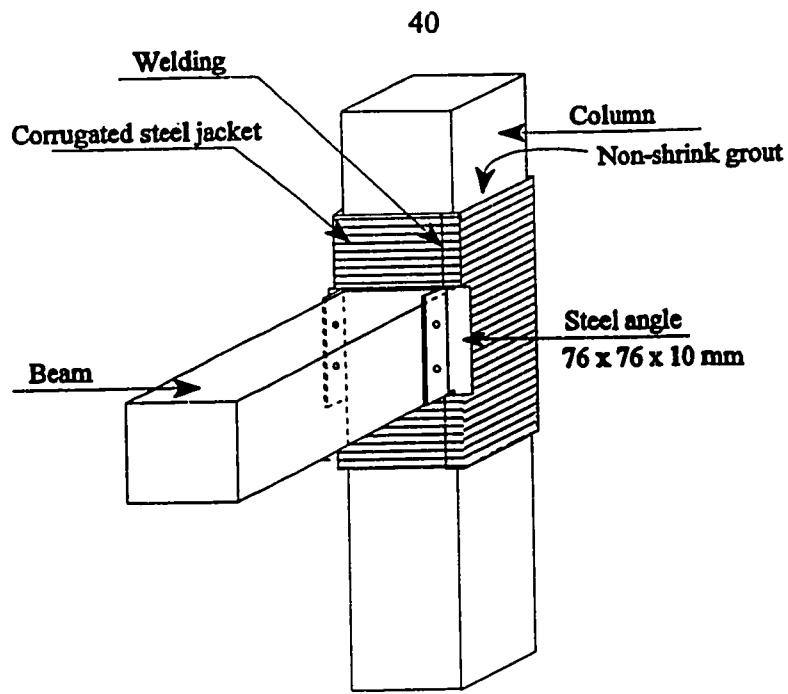
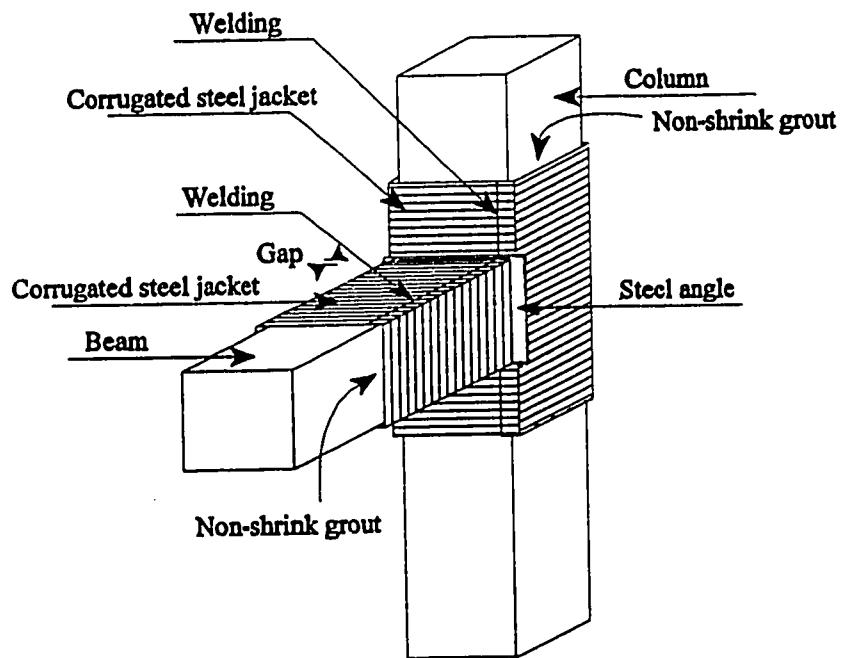


Figure 2.3c Details of reinforcement of specimens J4 and J6



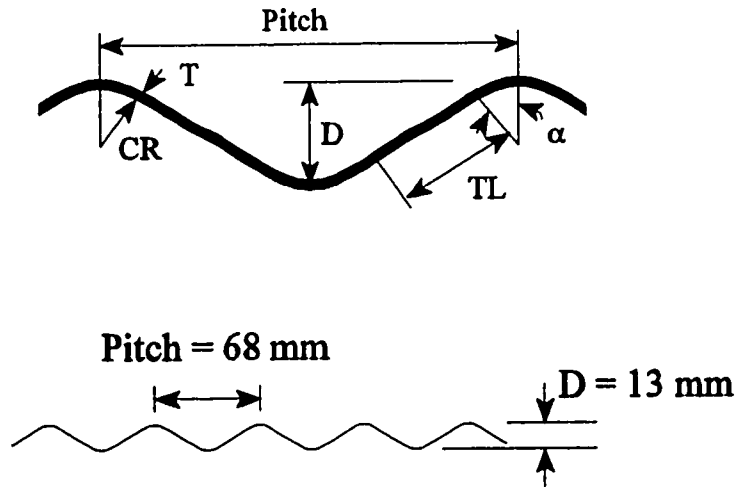
a) Column jacket.



b) Beam and column jacket.

Figure 2.4 Proposed rehabilitation technique.

Corrugation profile 68 x 13 mm



	2.8 mm thick	3.5 mm thick
Depth, D (mm)	13	13
Pitch (mm)	68	68
Corrugation radius, CR (mm)	17.46	17.46
Specified thickness, T (mm)	2.80	3.50
Tangent length, TL (mm)	18.77	18.27
Tangent angle α (degrees)	27.14	27.38
Area (mm ² /mm)	2.85	3.62
Moment of inertia (mm ⁴ /mm)	54.57	70.16
Section modulus (mm ³ /mm)	7.11	8.74

Figure 2.5 Properties of corrugated steel sections.

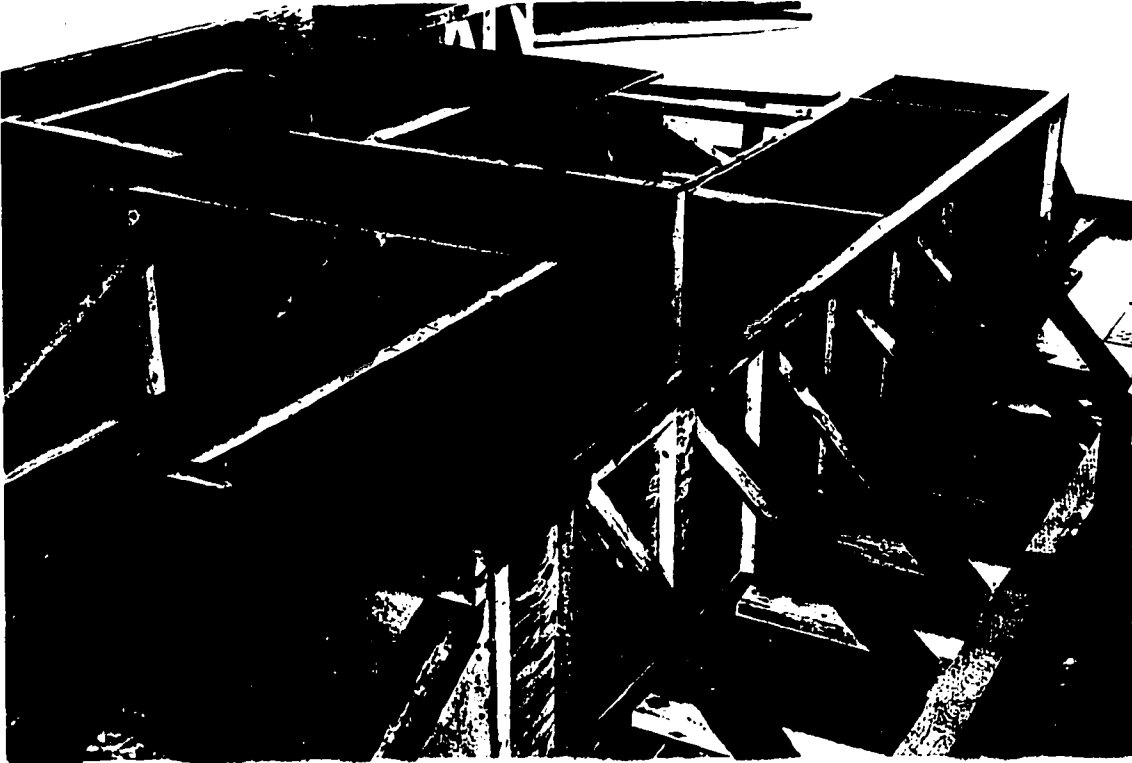


Figure 2.6 Wooden form used in casting the specimens.

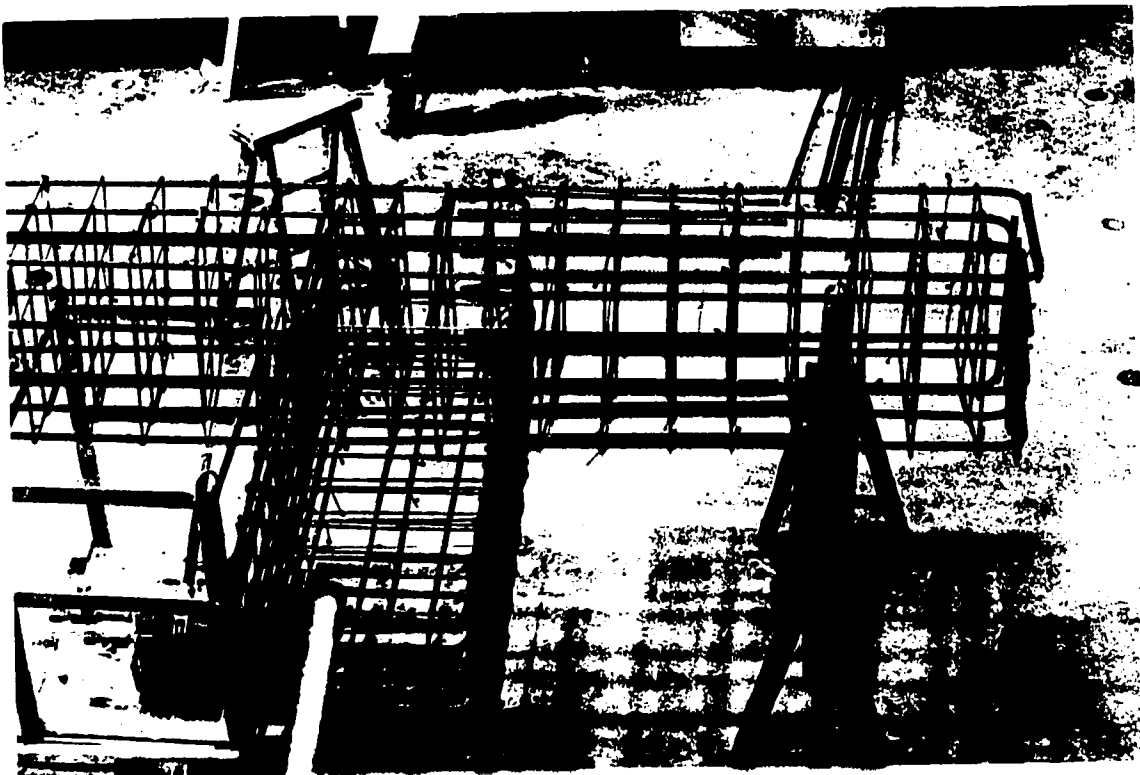
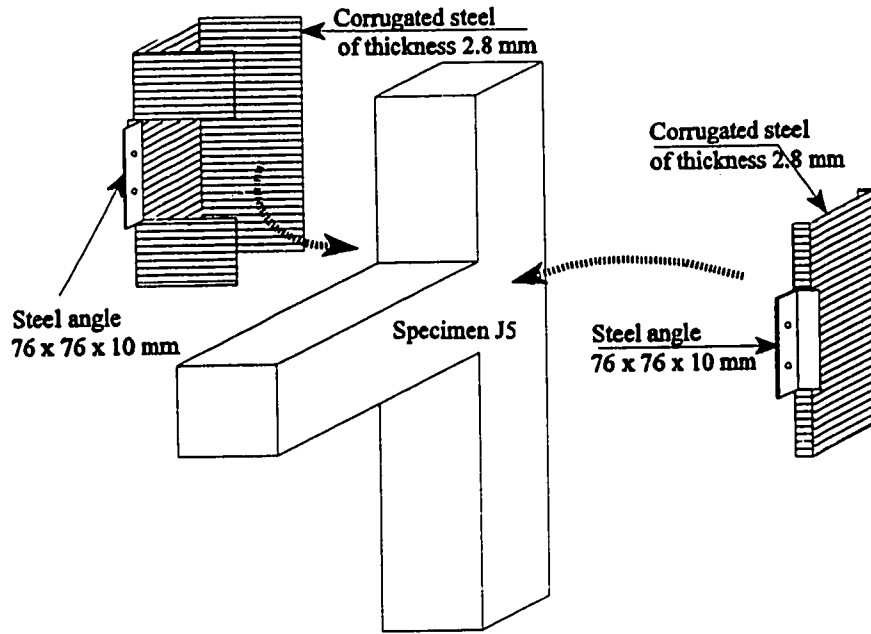
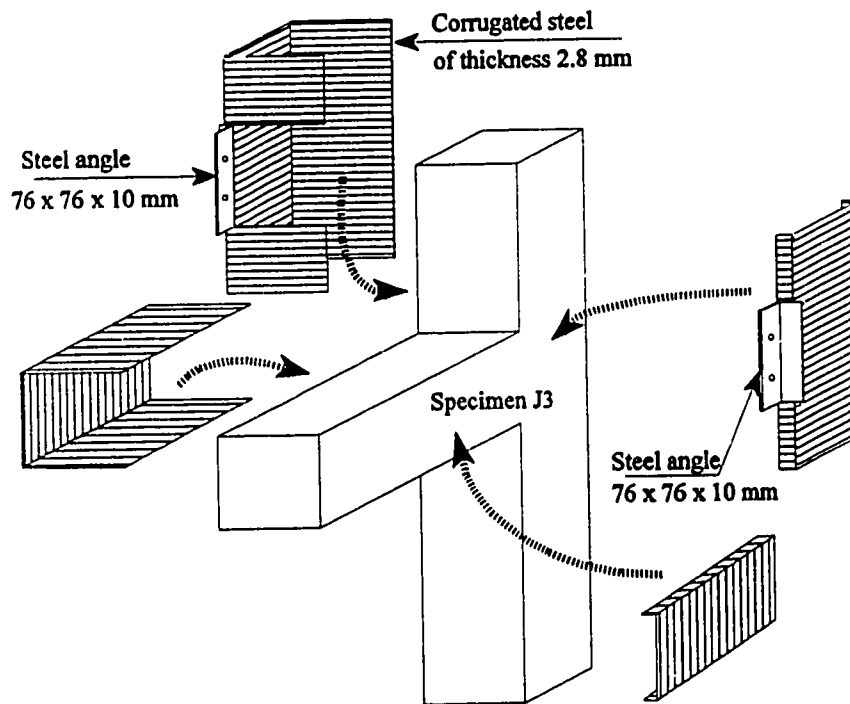


Figure 2.7 Details of the reinforcement cage.



a) Column jacket



b) Beam and column jackets

Figure 2.8 Assembling of beam and column jackets.

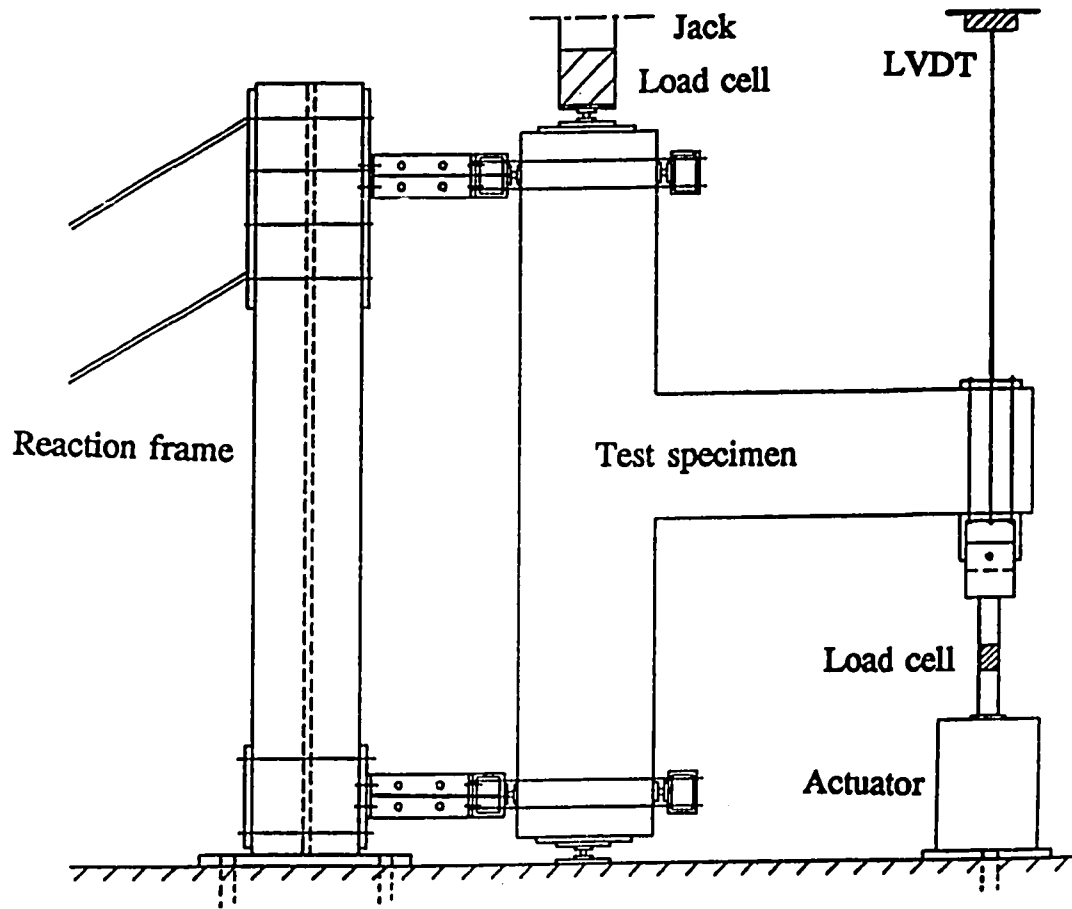


Figure 2.9a Schematic of test set-up.

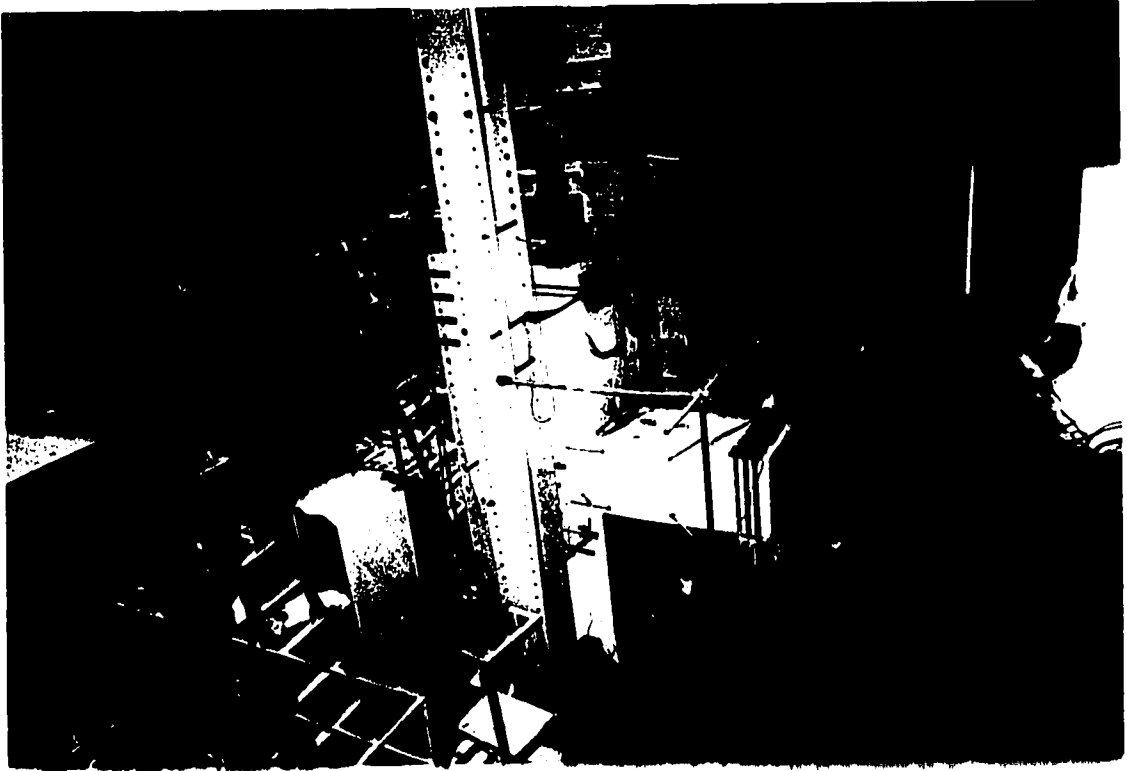


Figure 2.9b Test set-up.

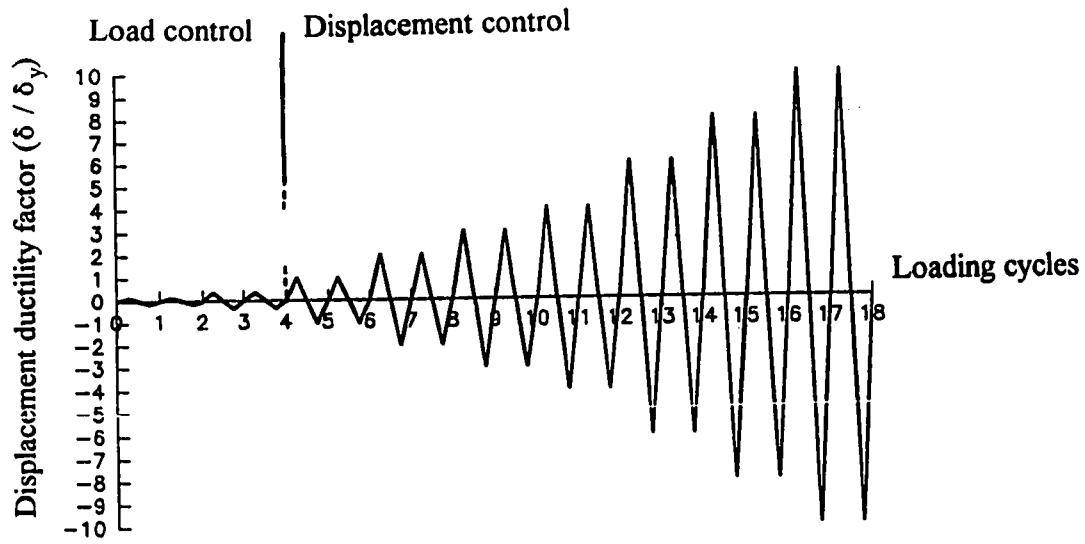


Figure 2.10 Loading routine.

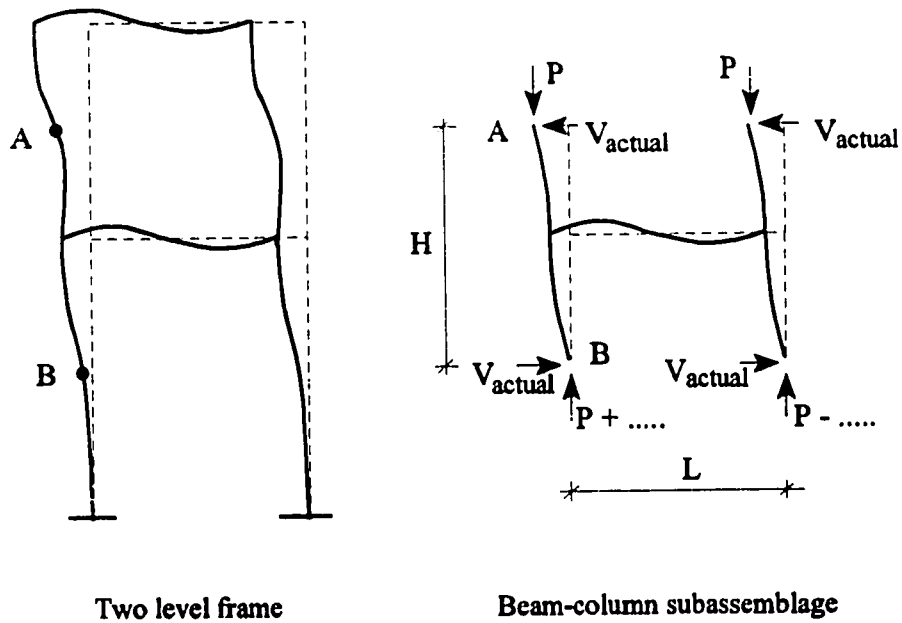
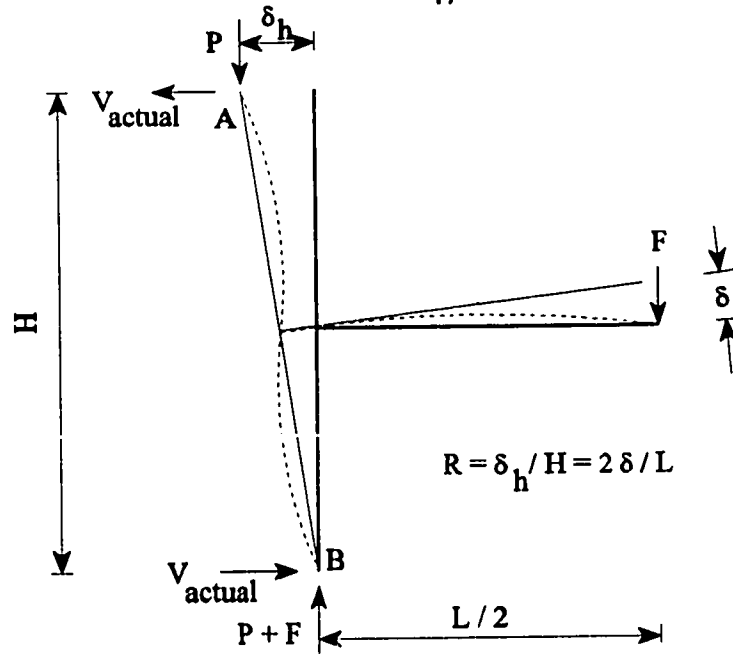
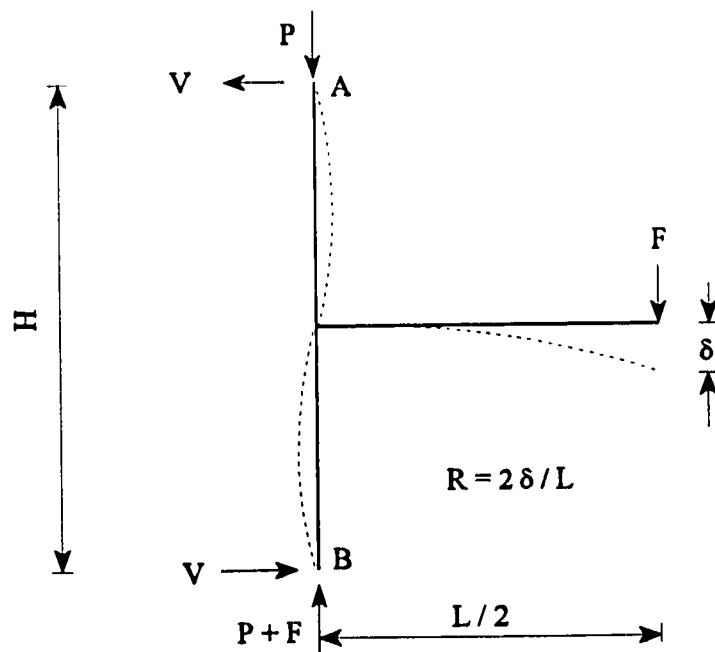


Figure 2.11 Frame deflection due to seismic loads.



a) Free body diagram for joint in an idealized structure



b) Joint in the Laboratory test set-up

Figure 2.12 The drift angle definition

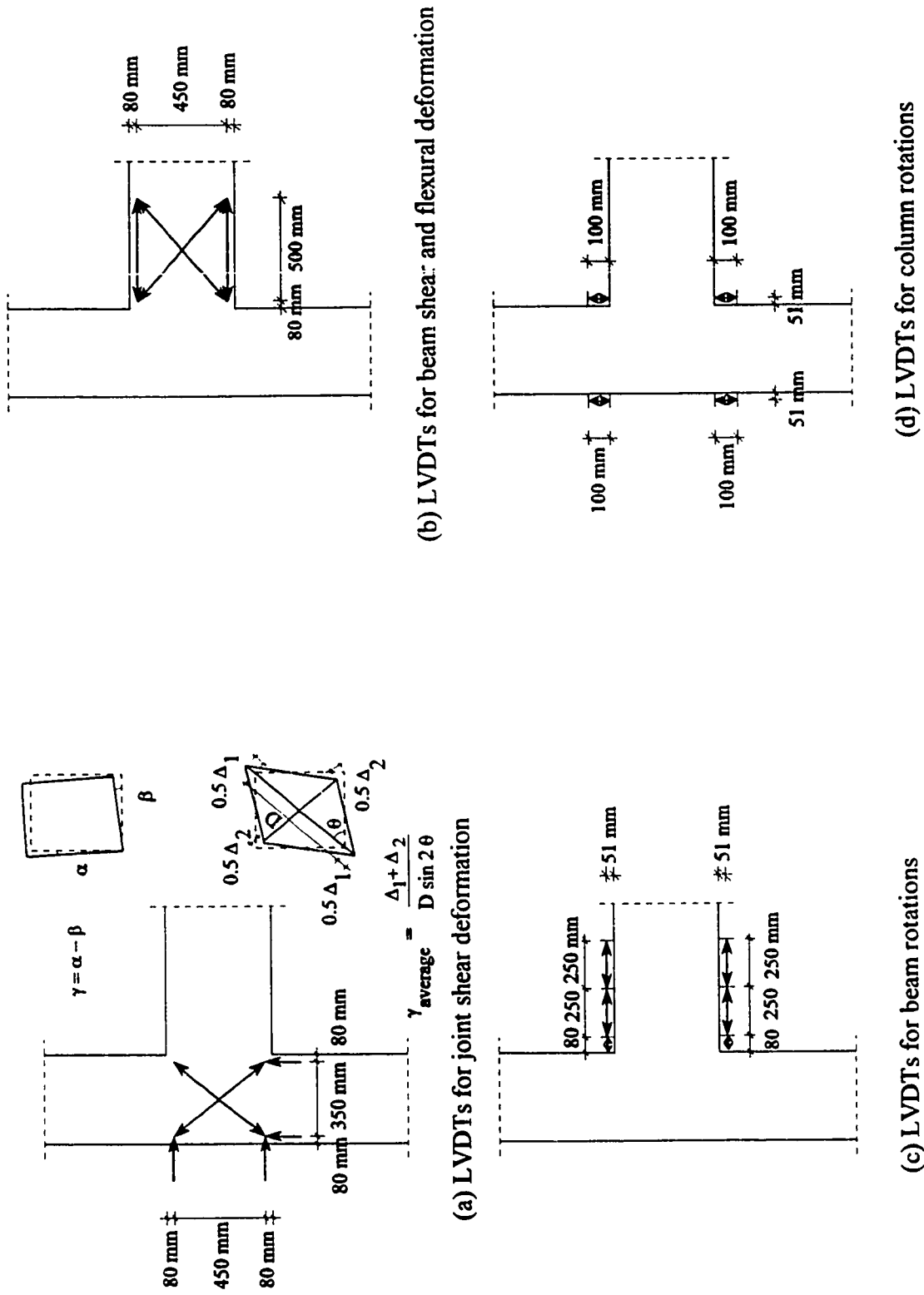
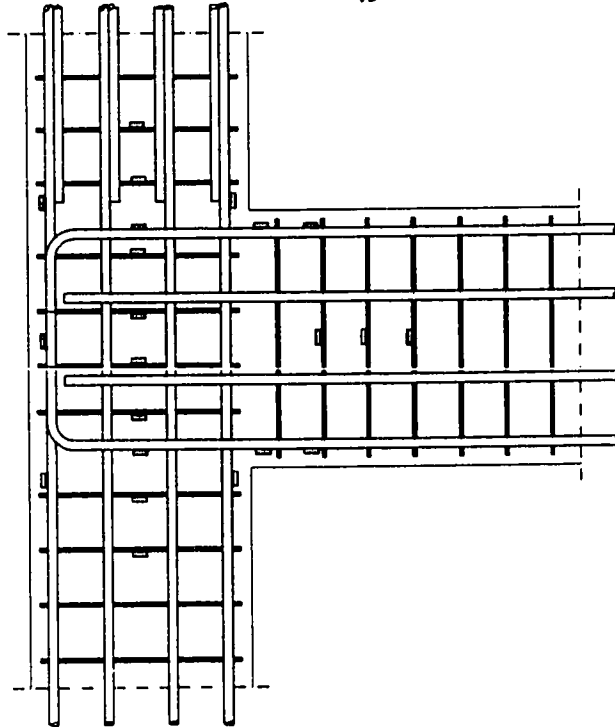
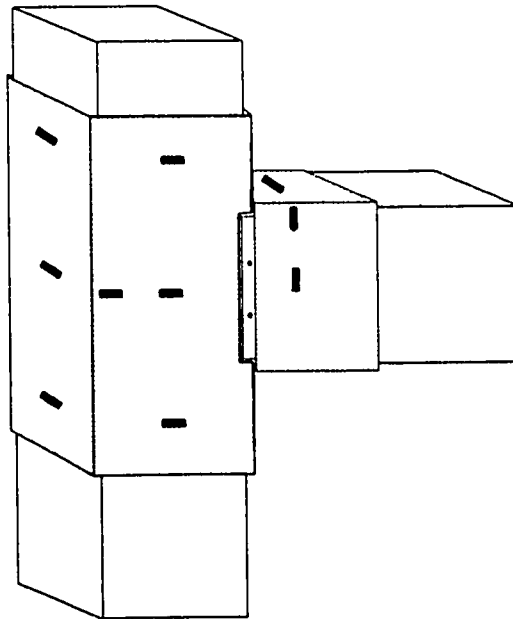


Figure 2.13 Instrumentation of test specimens.



(a) Strain gauges on the reinforcement bars



(b) Strain gauges on the steel jacket

Figure 2.14 Locations of strain gauges.

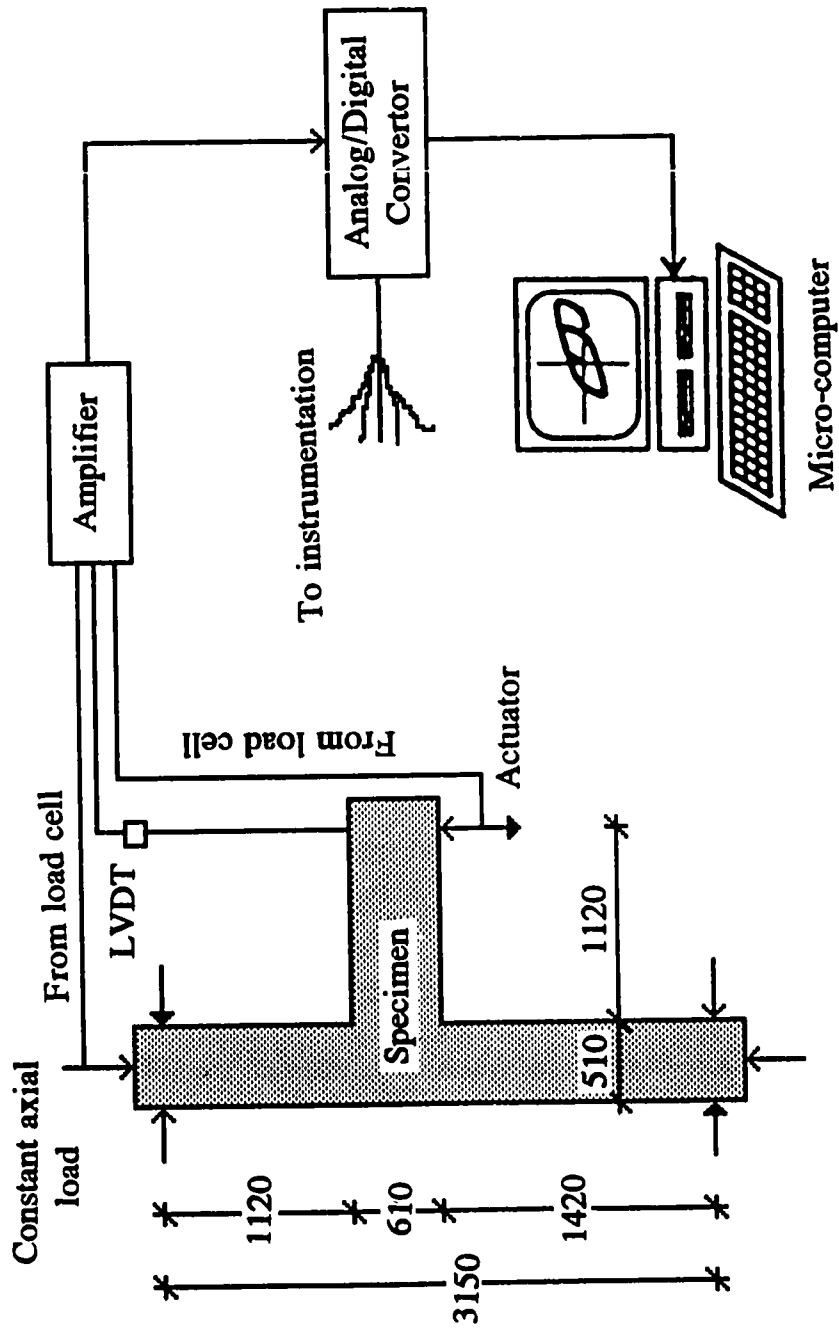


Figure 2.15 Data acquisition and control system

CHAPTER 3

OVERALL BEHAVIOUR OF THE SPECIMENS

3.1 INTRODUCTION

The overall response of the test specimens is discussed in this chapter. For each specimen, the crack pattern was carefully marked and recorded. Crack patterns provide insight into the failure mechanism of each specimen. The load-displacement, the story shear-drift angle, story shear-joint shear distortion and moment-rotation relationships are presented. The behaviour of the specimens J1 and J4 representing existing structures is evaluated. The effectiveness of jacketing as a rehabilitation technique is evaluated by comparing the response of specimen J1 with those of J2 and J3. The response of specimen J5 is compared with that of specimen J3 to investigate the effect of beam jacket around the critical section of the beam at the face of the column. Finally, the responses of specimens J4 and J6 are compared to assess the benefits of using external steel plates to enhance the main reinforcement of the beam and their effect on the seismic performance of beam-column connections. Selected strain gauge data, useful for understanding the behaviour of the members and the possible failure mode, is compiled and discussed.

3.2 OBSERVED BEHAVIOUR

3.2.1 Specimen J1

Specimen J1 is the first of three specimens (J1, J3 and J5) built to represent existing structures. Although the imposed deformation was large for a prototype building subjected to strong ground motions, it provided information on the behaviour of beam-column joints with flexible columns to levels of deformation expected to cause severe damage. The ratio of the factored resistance moment of the columns to the nominal resistance moment of the beam is 1.55 which is higher than the 1.1 ratio specified by the current Canadian concrete design code (CSA A23.3-94, 1994). The final crack pattern is shown in figures 3.1a and b. The crack pattern of the specimen during cycle #7 (2% drift angle), is shown in figure 3.2. The beam of specimen J1 suffered less damage than that of specimens J2 and J5 because the joint shear distortion of specimen J1 dominated the overall deformation. The first crack was in the beam at the face of the column during cycle #3, then very fine flexural and flexural-shear cracks were formed in the beam at cycle #5. Before yielding of the beam reinforcement, diagonal cracks appeared inside the joint then the ties yielded progressively. Yielding of the beam reinforcement occurred at cycle #5 at a load of 320 kN and a displacement of 12.7 mm. In the following cycles, the width of flexural cracks along the beam stopped increasing and major cracks were concentrated in the joint and beam-column interface regions causing the joint core concrete to be sliced in rhombic blocks. Some flexural cracks were recorded in the lower column at drift angle of 2%. At cycle #11 a displacement of 51 mm was applied while the specimen sustained a load of 170 kN. Peak resistance of 380 kN was obtained at displacement ductility of 2 (corresponding to drift angle of 1.85%). Spalling occurred mainly

inside the joint due to lateral strain. The shear sliding between the blocks is resisted by the interlock of the aggregates and dowel action of the reinforcement. With subsequent loading, the interlock and dowel actions deteriorated by progressive fracture and crushing of the blocks. A splitting crack appeared at the longitudinal bottom reinforcement of the beam inside the joint during cycle #5 ($1\delta_y$) which indicate failure of bond for part of the longitudinal beam reinforcement. This was attributed to the inadequate concrete confinement in the joint region even though the anchorage length requirement of the code was satisfied. Further analysis of strain gauge data confirmed that anchorage of the beam's lower corner reinforcement bar was affected by the cracking. The progression of cracks is demonstrated in figure 3.3 for the positive direction of loading. A symmetric crack pattern occurred for the negative loading direction.

Peak strength of the specimen was in cycle #7 ($2\delta_y$), after which severe strength decay was noted. The strength degradation is mainly due to deterioration of joint concrete.

3.2.2 Specimen J2

Specimen J2 was detailed according to the current Canadian concrete design code (CSA A23.3-94, 1994). The specimen was able to withstand 18 cycles of reversed loading and reached displacement ductility of ten. The progress and nature of cracking which the specimen experienced can be visualized by observing the beam hinging zone after 7 cycles of loading as shown in figures 3.4a and 3.4b. The first crack formed in the beam at the face of the column then two more vertical or very steeply inclined cracks occurred at approximately $d/4$ and $d/2$ from the column face. Yielding of the beam reinforcement was reached during

cycle #5 at a load of 340 kN and a displacement of 13 mm. Peak resistance of 400 kN was obtained at displacement ductility of 2 (corresponding to drift angle of 2%). The column behaved in an almost elastic manner. No cracks in the column were observed. At cycle #17, a displacement of 130 mm was achieved while sustaining a load of 150 kN. The crack pattern after 17 cycles of loading is shown in figures 3.5a and 3.5b. The concrete adjacent to the crack at $d/2$ from the column face suffered the greatest deterioration during the course of testing. High shear at the flexural hinge caused rapid deterioration and disintegration of the concrete in the hinge zone. This can be attributed to the high depth to length ratio of the beam. It is recommended that the shear reinforcement in the current Canadian concrete design code (CSA A23.3-94, 1994) in case of beams with high depth to length ratio should be checked experimentally under cyclic loading.

3.2.3 Specimen J3

Specimen J3 has the same dimensions and reinforcement detail as J1 but was rehabilitated using corrugated steel jacket on the column and the beam. The final deformed shape is shown in figure 3.6. A close up for the damage at the gap between the beam and the column is shown in figure 3.7. Flexure cracks were observed in the beam at the column face during cycle #3. Yielding of the beam reinforcement occurred at cycle #5 at a beam tip load of 348 kN and a displacement of 12 mm. At cycle #17 a displacement of 122 mm was applied while the specimen sustained a load of 202 kN. Peak resistance of 466 kN was obtained at displacement ductility factor of 4 (corresponding to drift angle of 3.5%). No cracks in the column were recorded and no indication of concrete delamination between the jacket and the original concrete was found. After failure of the specimen, the steel casing was removed and

the joint was visually examined. Few cracks were observed in the joint with very narrow crack width as shown in figure 3.8a and 3.8b. The presence of the corrugated steel jacket restrained the spalling of concrete in the column and joint and therefore allowing a more gradual degradation of strength.

3.2.4 Specimen J4

Specimen J4, is a gravity design specimen with no ties in the joint and the beam bottom reinforcement extended 250 mm inside the joint (34% of the required development length by the current Canadian concrete design code for straight bars terminated at a joint). The final crack pattern is shown in figure 3.9. The crack pattern of the specimen during cycle #7 (2% drift angle) is shown in figure 3.10. The first crack was in the beam at the face of the column followed by flexural and flexural-shear cracks in the beam. Before yielding of the beam reinforcement, diagonal cracks appeared inside the joint. Yielding of specimen J4 occurred at cycle #5 at a negative load of 321 kN and a displacement of 13.5 mm. No yielding occurred at positive loading. Some flexural cracks were recorded in the lower column at 1% drift angle and some vertical cracks were also observed as shown in figure 3.11. At cycle #11, a displacement of 57 mm was applied while the specimen sustained a load of 190 kN for negative loading and 40 kN for positive loading. Positive peak resistance of 239 kN was obtained at cycle #5 and then the beam bottom longitudinal bars were pulled out from the joint. A negative peak resistance of 378 kN was obtained at cycle #7. After the peak resistance was reached rapid deterioration in the strength was observed.

3.2.5 Specimen J5

Specimen J5 was rehabilitated using corrugated steel jacket on the column as in specimen J3 but there was no jacket on the beam. By comparing the behaviour of specimens J3 and J5, the influence of the beam jacket on the response of the rehabilitated specimen J3 can be assessed. The final crack pattern of specimen J5 is shown in figure 3.12. The crack pattern during cycle #7 (at drift angle of 2%) is shown in figure 3.13. The first crack was in the beam at the face of the column at cycle #3 followed by inclined cracks in the beam at cycle #5 ($1\delta_y$). Yielding of the beam reinforcement occurred during cycle #5 at a load of 325 kN and a displacement of 11.5 mm. During cycle #7, an inclined crack in the beam with large crack width was noticed. Most of the damage was concentrated in the beam away from the column face due to the confinement of the joint by the corrugated steel jacket and the two angles at the face of the column. First concrete crushing was noticed in the beam during cycle #9 ($3\delta_y$). At cycle #13 ($5\delta_y$), a displacement of 92 mm was achieved while sustaining a load of 145 kN. Peak resistance of 430 kN was obtained at displacement ductility factor of 4 (corresponding to drift angle of 3%). The beam curvature was lower during downward loading than upward loading with maximum curvature of about 0.00007 mm^{-1} which was recorded at 2% drift angle. In subsequent cycles, the beam moment-curvature cycles showed stiffness degradation and pinching. No cracks in the column were observed. Failure of the specimen was due to shear failure in the beam plastic hinge. Damage produced during the positive half-cycle affected the strength reached in the negative direction. No evidence of delamination of the column jacket was noted.

After failure of the specimen, the steel casing was removed and the joint was visually examined. Few narrow cracks were observed in the joint as shown in figure 3.14a and 3.14b. The presence of the corrugated steel jacket restrained the spalling of concrete in the column and joint and therefore allowing a more gradual degradation of strength.

3.2.6 Specimen J6

Specimen J6 had the same dimensions and reinforcement details as specimen J4 but was rehabilitated by jacketing the column and adding two steel plates to resist the pull out of the beam bottom reinforcement. The steel plates were fastened to the sides of the beam using three 20 mm diameter Hilti expansion anchors. The final crack pattern is shown in figure 3.15. The crack pattern of the specimen at cycle #7 at drift angle 2% is shown in figure 3.16. The first crack was in the beam at the face of the column during cycle #3. Yielding of the beam top reinforcement occurred at cycle #5 at a load of 329 kN and a displacement of 10 mm. Maximum curvature of 0.00009 mm^{-1} was recorded at 2% drift which is less than that of specimen J4. At cycle #17 a displacement of 100 mm was applied while the specimen sustained a load of 386 kN for negative loading and 46 kN for positive loading. A negative peak resistance of 412 kN was obtained at displacement ductility factor of 3 (corresponding to drift angle of 2.3%) while positive peak resistance of 333 kN was obtained at displacement ductility factor of 2 (corresponding to drift angle of 1.5%). An increase of 9% of the negative peak resistance compared to that of J4 while an increase of 39% of the positive peak resistance compared to that of specimen J4.

Progressive failure of the bolts occurred starting by the far end bolt then the bolt near the column. The failure can be attributed to the following two factors: first, the bolts carried

vertical shear due to the bending stiffness of the plate in addition to horizontal shear due to the horizontal tensile force in the plate acting as bottom reinforcement. The far bolt carried low horizontal shear but high vertical force while the bolt near the column carried low vertical shear but high horizontal shear. It should be noted here that the bolts were designed using horizontal shear only on each bolt and it is believed that the bolts were under designed. Second, the sleeves around the anchors were installed sunk in the concrete and did not assist in resisting the shear. The bolts acted in single shear without the help of the sleeve in resisting the shear. Therefore, it is recommended to install the sleeve in the steel plate. The horizontal and vertical shears on the bolt may be considered in the design as follows, figure 3.17:

$$V_1 : V_2 : V_3 = L_1 : L_2 : L_3 \quad (3.1)$$

$$H_1 : H_2 : H_3 = (L - L_1) : (L - L_2) : (L - L_3) \quad (3.2)$$

Very few narrow cracks appeared in the column as shown in figure 3.18 after removing the steel jacket. The joint deformation remained small compared to J4 with few narrow cracks in the joint as shown in figure 3.18. The presence of the corrugated jacket restrained the spalling of concrete in the column and joint and resisted the joint shear.

3.3 LOAD - DISPLACEMENT RELATIONSHIP

The load-displacement relationships for the six specimens are shown in figures 3.19a to 3.19f. All the figures are plotted using the same scale so that comparisons between the results of different tests can be easily made. The displacement of the specimens at yield

served as a guide in defining the specimen ductility in subsequent cycles. The yield displacement, which was initially calculated using beam theory and later confirmed using strain gauge data, was estimated for each specimen as shown in table 3.1. For each specimen, a specific cycle was selected, when the load carrying capacity has undergone a 20% reduction of the maximum load (Park, 1989). The maximum displacement at the end of that cycle was recorded as the maximum available displacement. For all the specimens, the displacement ductility was defined as the ratio of the maximum available displacement to the yield displacement listed in table 3.1. From the displacement ductility results in table 3.1, the use of corrugated steel jacket (specimens J3, J5 and J6) was found to be effective in improving the displacement ductility of the specimens.

The hysteretic behaviour was evaluated in terms of strength as well as ductility. The horizontal lines marked " F_y " and " F_u " in figures 3.19a to 3.19f indicate the first yielding of the beam longitudinal reinforcement and the theoretical ultimate flexural load-capacity of the unconfined beam section of the specimens. The theoretical ultimate flexural load, F_u , was calculated from the measured material properties and dimensions, using the computer program "RESPONSE" developed by Collins and Mitchell (1991).

The shape of the load-displacement curves can be characterized by three slopes; the slope at point of zero displacement, the reloading and the unloading slopes. The slope at point of zero displacement, when compared with reloading or unloading slopes, provides a measure of the "Pinching" or narrowing of the hysteresis loop at small displacements and also gives a measure of the response of the specimen to loads that produce small displacements. When the displacements increase beyond the pinching region of the loops, but before reaching

levels that produce new damage, the remaining undamaged components of the specimen begin to resist the load and temporarily exhibit an elastic behaviour. This is manifested in the straight part of the hysteresis loop immediately following the pinching region. After reaching the peak displacement, the test subassembly undergoes the unloading process. The first part of the unloading process is generally non-linear for two reasons. First, the strain in the newly damaged concrete under compression is not completely recovered when the load is reduced. Second, the unloading of the yielded reinforcement is non-linear in nature. After this initial region and before the pinched zone is reached, the unloading process is characterized by another quasi-elastic branch that represents the behaviour of the portions that are left undamaged since the previous peak.

The hysteresis loops of specimen J1 for the two loading directions (positive and negative) are nearly symmetrical as plotted in figure 3.19a and show considerable pinching, especially at drift angles more than 2%, and severe stiffness degradation. The loss of stiffness is primarily due to concrete deterioration in and adjacent to the joint and slippage of column and beam longitudinal reinforcement. The pinching of hysteresis loops for cycles beyond yielding is primarily due to the slippage of the beam longitudinal bars, joint shear deformation, yield penetration into the joint area and the unclosed beam flexural cracks near the face of the column. The hysteresis curves are dominated by the response of the most damaged elements, namely the beam and joint. Large joint deformations were measured during the test.

Although specimen J1 almost reached the theoretical ultimate flexural capacity at displacement ductility factor of 2, a rapid strength deterioration and stiffness degradation were observed after displacement ductility factor of 2 due to the joint shear failure. The lack

of adequate joint confining steel probably caused the joint shear failure.

Specimen J2 exceeded the theoretical ultimate flexural capacity as shown in figure 3.19b and was able to maintain high flexural capacity until displacement ductility factor of 4. A specimen detailed according to current seismic codes was expected to sustain higher displacement ductility factors than 4. The limited ductility observed in specimen J2 was attributed to the high shear at the flexural hinge caused rapid deterioration and disintegration of the concrete in the hinge zone due to the high depth to length ratio of the beam.

The hysteresis loops of specimen J3 shown in figure 3.19c are symmetrical and exhibit improved performance in strength and ductility when compared with specimen J1 in figure 3.19a. The specimen exceeded the theoretical ultimate flexural capacity which caused large shear forces on the joint, however, no joint distress was observed. The pinching of hysteresis loops was less than that of specimen J1. This is because of the confining action of the corrugated steel jacket prevented the slippage of the beam longitudinal bars and reduced the joint shear deformation.

The hysteresis loops of specimen J4 are not symmetric as shown in figure 3.19d due to the pull out of the positive longitudinal bars in the beam. The specimen did not reach yield in the positive direction while reaching the theoretical ultimate flexural capacity in the negative direction at displacement ductility factor of 2. A rapid lateral strength deterioration and stiffness degradation were observed after displacement ductility factor of 2 due to the joint shear failure. The lack of joint confining steel probably caused the joint shear failure in the negative loading while the insufficient development length of the positive longitudinal reinforcement in the beam caused the pull out failure.

The hysteretic behaviour of specimen J5 showed higher stiffness, strength and total energy dissipation characteristics as shown in figure 3.19e than that of specimen J1, but not as good as that of the code detailed specimen, J2. This is due to the lack of beam shear reinforcement which cause shear failure in the beam. The theoretical ultimate flexural capacity was exceeded in all cycles of 2% drift angle and up to drift angle of 3.5%.

The hysteresis loops of specimen J6 showed some improvement in the response in the positive direction as shown in figure 3.19f than that of specimen J4. The beam reinforcement reached yielding in the positive direction but at cycle #9 (drift angle of 2.3%) the middle anchor bolt anchoring the plates to the beam failed in shear at the surface of the concrete which cause sudden drop in the load-displacement relationship as shown in figure 3.19f. The negative direction showed improvement in the response as shown in figure 3.19f compared to that of specimen J4 in figure 3.19d. This is attributed to the corrugated steel jacket on the joint and column.

3.4 STORY SHEAR

The story shear-drift angle relationships for the six specimens are presented in figures 3.20a to 3.20f. The story shear was obtained by multiplying the beam tip load by the beam length over the column length taking into account the $P-\Delta$ effect as discussed in Chapter 2. The drift angle was obtained by dividing the beam tip displacement by the beam length.

The maximum story shear occurred during the positive loading segment of cycle #7 (drift angle of 1.8%) for specimen J1 and during cycle #9 (drift angle of 2.7%) for specimen J3. Specimen J2 showed better ductility than J1 due to the joint ties which provided

confinement of the concrete and increased its strength and ductility. The limited ductility of J2 is attributed to the high shear acting on the flexural hinge. Specimen J5 showed good behaviour when compared to J1 as no damage occurred in the joint and the plastic hinge is transferred from the joint to the beam. However, at high drift angle, specimen J5 showed shear failure in the beam at the column face due to insufficient transverse reinforcement in the beam. Specimen J6 showed better ductility than J4 due to the corrugated steel jacket and the steel plates which provided confinement of the concrete and increased its strength and ductility. Specimen J3 showed the best behaviour in terms of strength and ductility. Jacketing of frame elements was demonstrated to improve the seismic behaviour of the existing structure as illustrated by the behaviour of specimens J3, J5 and J6.

The joint behaviour can be studied through the story shear-joint shear distortion relationships shown in figures 3.21a to 3.21f. Joint distortion was measured using two transducers mounted in diagonal directions on the joint panel. The loops of specimen J1 are symmetrical up to cycle #6 (repetition of $1\delta_y$) and show considerable pinching, loss of stiffness and strength deterioration typical of joint distress. From cycle #7 ($2\delta_y$), the joint shear distortion increased faster than the imposed drift angle. The joint distress was evident with the formation of inclined cracks. The joint response of specimens J2 and J3 were almost linear up to cycle #7 ($2\delta_y$). The joint first cracked during cycle #7 ($2\delta_y$). These cracks remain stable and very narrow till the end of the test. The loops of specimen J4 were symmetrical up to cycle #6 similar to those of specimen J1 and showed considerable pinching, loss of stiffness and strength deterioration typical of joint distress. From cycle #7 the joint shear distortion increased faster than the imposed drift angle for one direction and decreased in the

other direction due to the pull-out of the beam bottom reinforcement. The joint response of specimens J5 and J6 were almost linear up to cycle #11. The joint first cracked during cycle #13 (drift angle of 5%). The results indicate that corrugated steel jacket was effective in reducing joint distortion.

3.5 MOMENT - ROTATION RELATIONSHIP

Figures 3.22a to 3.27c show the applied beam moment at column face plotted against the rotation of the section of the beam at distances of 80 mm, 330 mm, and 580 mm from column face with respect to the previous section. The angle of rotation θ was calculated using the expression

$$\theta = (\Delta_1 + \Delta_2) / d \quad (3.3)$$

where Δ_1 is the measured elongation on the tensile face of the beam, Δ_2 is the measured shortening on the compression face of the beam, and d is the vertical distance between the transducers.

A comparison of the beam rotation at a section 80 mm from the column face for the different specimens at various ductilities is shown in figures 3.28a and 3.28b. The rotations of specimen J5 are small compared to J2 and J3. This can be attributed to the shear failure of the beam in a plastic hinge away from the column face. The plastic hinge occurred a distance away from the face due to the confinement of the joint by the corrugated steel jacket and the two angles at the face of the column.

3.6 STRAIN GAUGE DATA

3.6.1 Stress in the steel reinforcement

Strain measurements of the beam steel reinforcement, beam stirrups, column longitudinal reinforcement, column ties and joint ties at selected locations were made using electric strain gauges. Due to the reversing nature of loading, it was necessary to base the computation of stresses in the steel on the full loading history. In cases where the steel has numerous excursions into yield and strain hardening regions, a simple bi-linear model for steel which accounts for cyclic loading effect was assumed and used to represent the stress-strain hysteresis of the steel. Strain reversals were assumed to have a slope defined by the initial elastic modulus. The strain hardening branches envelope the loading-unloading segments. Initial elastic modulus, yield stress, strain hardening slope and rupture strain define the hysteretic law for cyclic behaviour of reinforcing steel. The steel properties, reported in Chapter 2 and used in the stress-strain model, were measured in bar coupons during monotonic tensile tests. Therefore, the calculated stress may be considered as an indicator to qualitatively explain the trends in the response.

3.6.2 Load-strain relationship

Strain gauge data was used to explain and confirm the visually observed response and quantified some critical aspects of behaviour. This is illustrated by the plot of beam tip load versus joint tie strain of specimen J1 shown in figure 3.29. First cracking in the joint occurred between the load points designated as "A" and "B". At some load between these two points, the tensile strength of the concrete was exceeded and the stress carried by the concrete was suddenly transferred to the steel, as shown by the large strain which accompanied the load

increase between points "A" and "B". The strain in the tie reached the yield strain during the test. This indication of inadequate transverse reinforcement is in agreement with visual observations of joint behaviour.

The maximum strains in the centre beam-column joint tie of specimen J1 were significantly larger than the tie's yield strain, as shown in figure 3.29. The overall strain in this tie tended to increase slightly with each loading reversal and strains increased significantly when displacement ductility factor exceeded one (cycle #4 through #10).

Strain gauge data was also important in confirming conclusions which have been based on other data. One example is the plot of beam load versus bar strain in the bottom longitudinal reinforcement in the beam shown in figure 3.30 for specimen J2. The bar yield strain and the load point at which yield was assumed based on load versus displacement curve shape are both indicated in this figure. In this case, the strain gauge data confirms the assumed yield of longitudinal tension reinforcement at load point "A". Because of the higher percentage of joint transverse hoop reinforcement, specimen J2 exhibited less damage in the joint and the main damage was in the beam. The main reinforcement in the beam yielded during cycle #5 at a location close to the face of the column. A typical load versus strain plot for a gauge at this location is shown in figure 3.30. From the curve, this specimen experienced very little slippage in the beam main reinforcement.

The plot of beam load versus beam stirrup strain of specimen J3 is shown in figure 3.31. The approximate load accompanying the first inclined crack to cross this tie can be estimated based on the break in the curve. During repeated loading, the strain in the stirrup never reached yield as an indication of the effectiveness of the corrugated steel jacket in

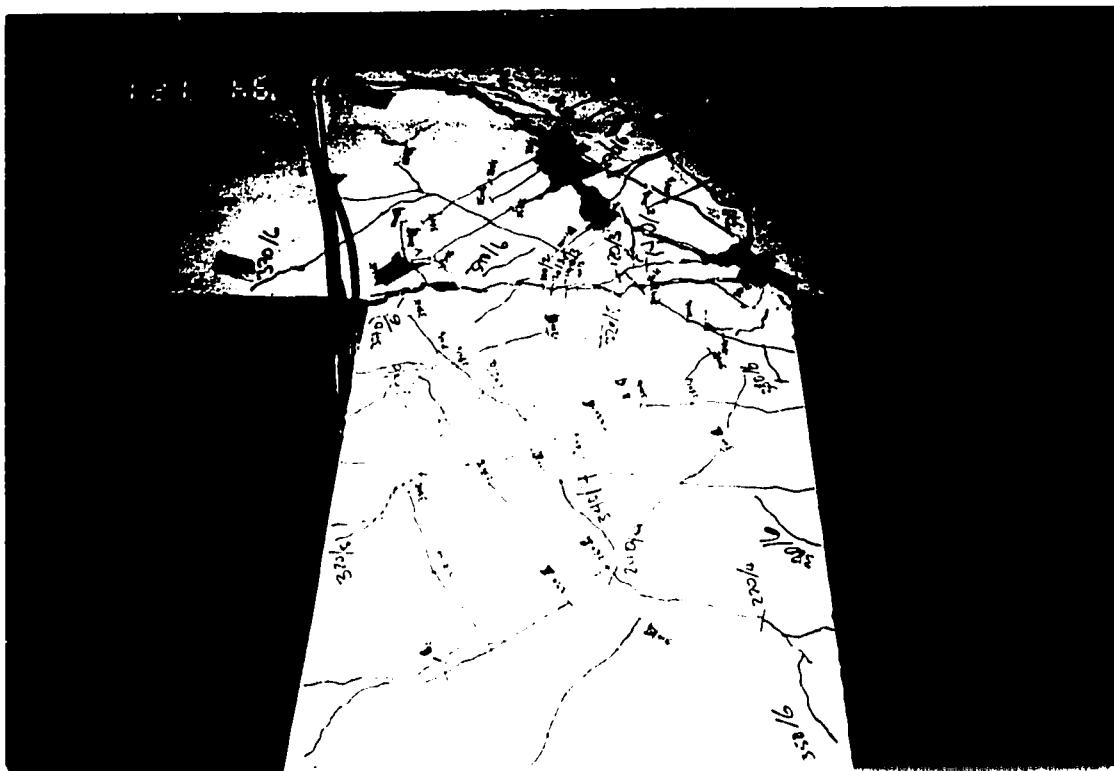
carrying the beam shear. Other more detailed strain gauge data is included in Appendix A.

3.7 SUMMARY

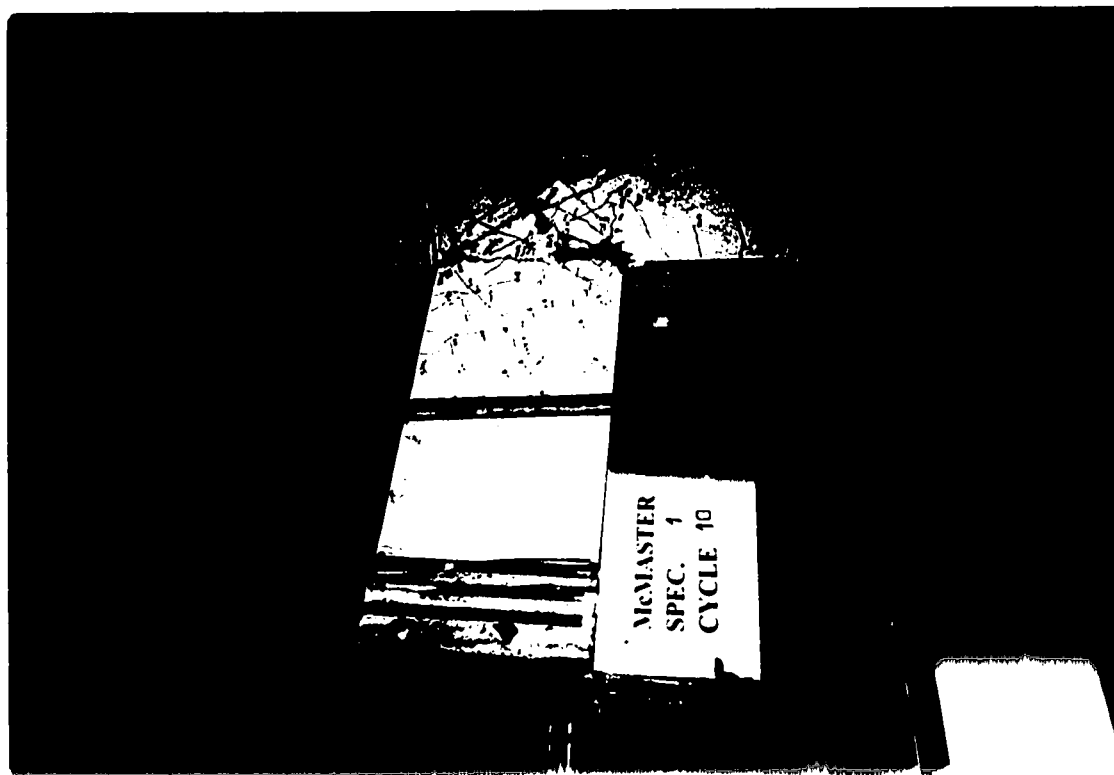
The behaviour of each specimen during the test was presented, crack pattern of the specimens were recorded which provided insight into the specimen failure mechanism. The load-displacement relationships as well as the moment-rotation relationships were presented. The behaviour of the specimens representing existing structures showed similar hysteretic response, characterized by considerable pinching and stiffness degradation. Strength decay was observed at large deformation cyclic levels. All rehabilitated specimens showed beam hinging and a more favourable energy dissipation mechanism as compared with the failure mode of the specimens representing existing structures. The corrugated steel jacket provided lateral confinement, shear resistance and ductility to the connection. It is concluded that corrugated steel jacketing of frame elements improved the ductility and response of deficient beam-column subassemblages representing existing structures. Selected strain gauge data were presented which proved beneficial in understanding the behaviour of the members and the possible failure modes.

Table 3.1 Displacement ductilities of specimens and modes of failure

Specimen	Yield displacement (mm)	Maximum available displacement (mm)	Displacement ductility	Failure Mechanism
J1	12.7	38.5	3.0	Joint shear failure
J2	13.0	78.0	6.0	Beam flexural plastic hinge
J3	12.0	72.0	6.0	Beam flexural plastic hinge
J4	13.5	- 40.0 -ve	- 3.0 -ve	Joint shear failure & bar pull out
J5	11.5	52.0	4.5	Shear failure in beam hinge
J6	10.0	25.0 +ve 100.0 -ve	2.5 +ve 10.0 -ve	Flexural plastic hinge & bar pull out



(b)



(a)

Figure 3.1 Final crack pattern of specimen J1.

A hand-drawn map of a coastline, likely a bay or inlet, with various points labeled with numbers and letters. The labels are as follows:

- 240/a
- 240/b
- 240/c
- 240/d
- 240/e
- 240/f
- 240/g
- 240/h
- 240/i
- 240/j
- 240/k
- 240/l
- 240/m
- 240/n
- 240/o
- 240/p
- 240/q
- 240/r
- 240/s
- 240/t
- 240/u
- 240/v
- 240/w
- 240/x
- 240/y
- 240/z

The map shows a series of points along the coastline, with some points connected by lines, suggesting a path or a specific area of interest. The labels are handwritten and appear to be in a specific code or system.

Figure 3.3 Crack pattern of specimen J1 at yielding of reinforcement.



Figure 3.4a Crack pattern of specimen J2 at positive drift angle of 2%.

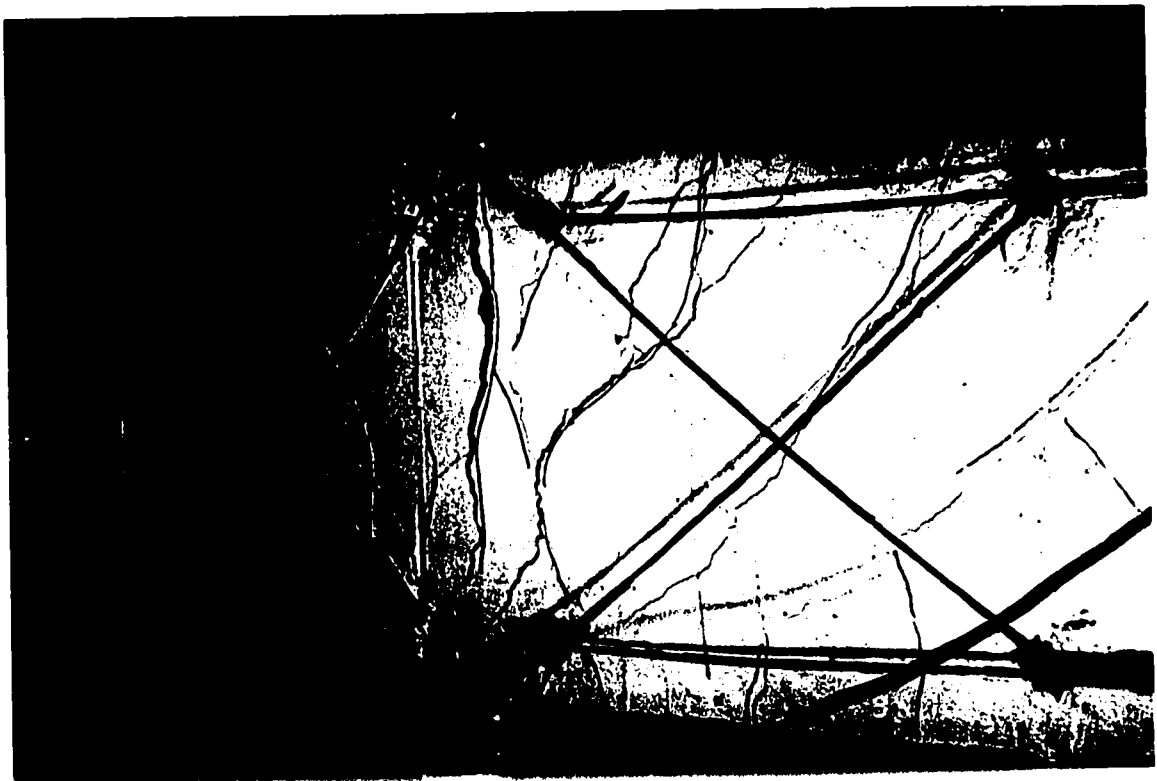
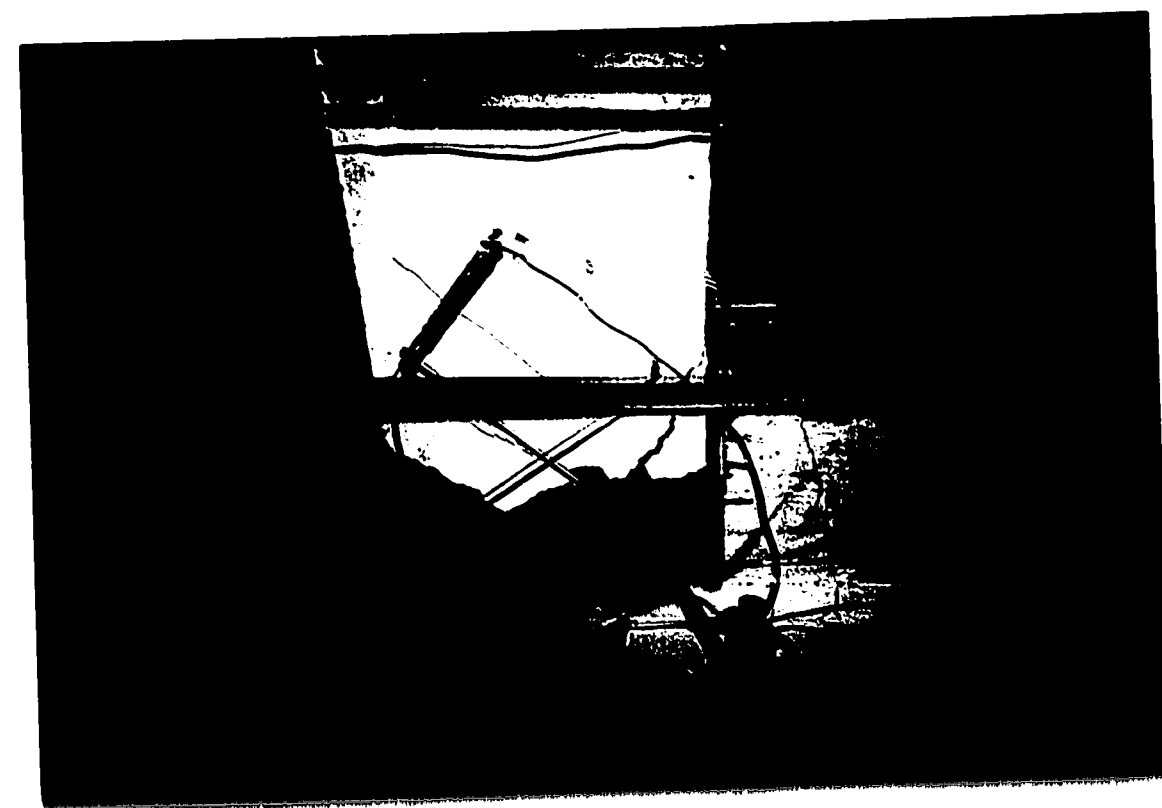


Figure 3.4b Crack pattern of specimen J2 at negative drift angle of 2%.



(a)



(b)

Figure 3.5 Final crack pattern of specimen J2.



Figure 3.7 Damage at the beam-column interface at cycle #17.

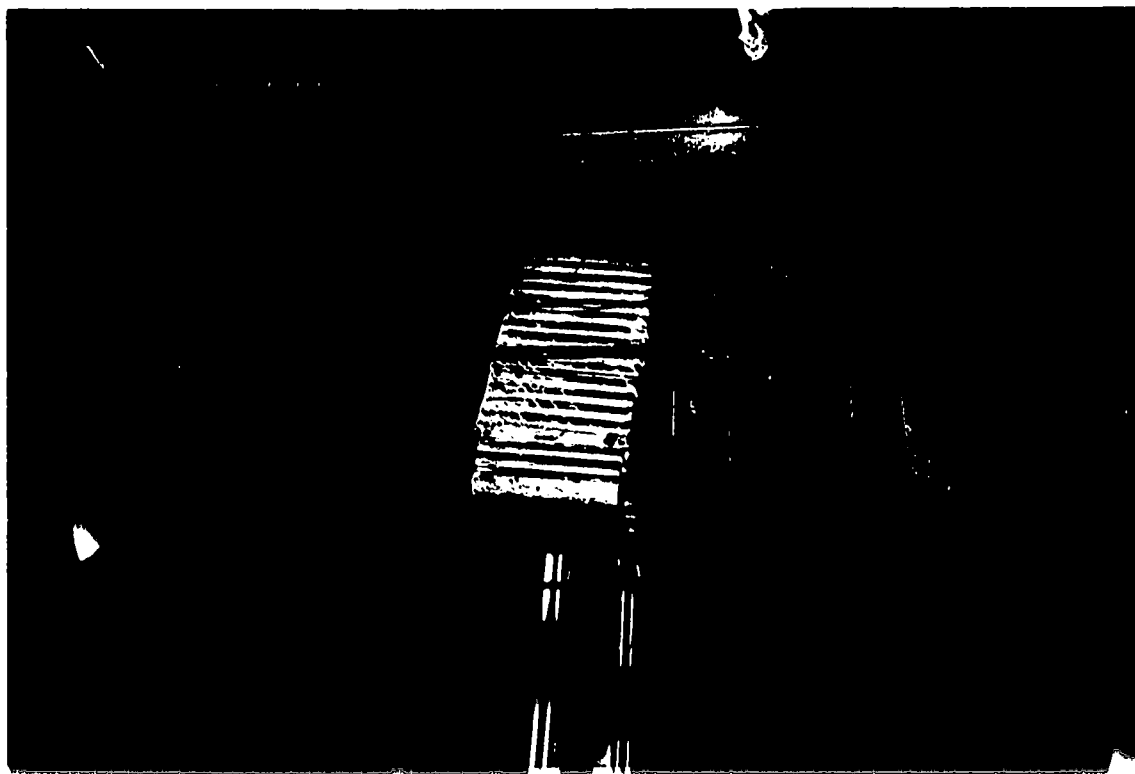


Figure 3.6 Specimen J3 at the end of the test (cycle #17).

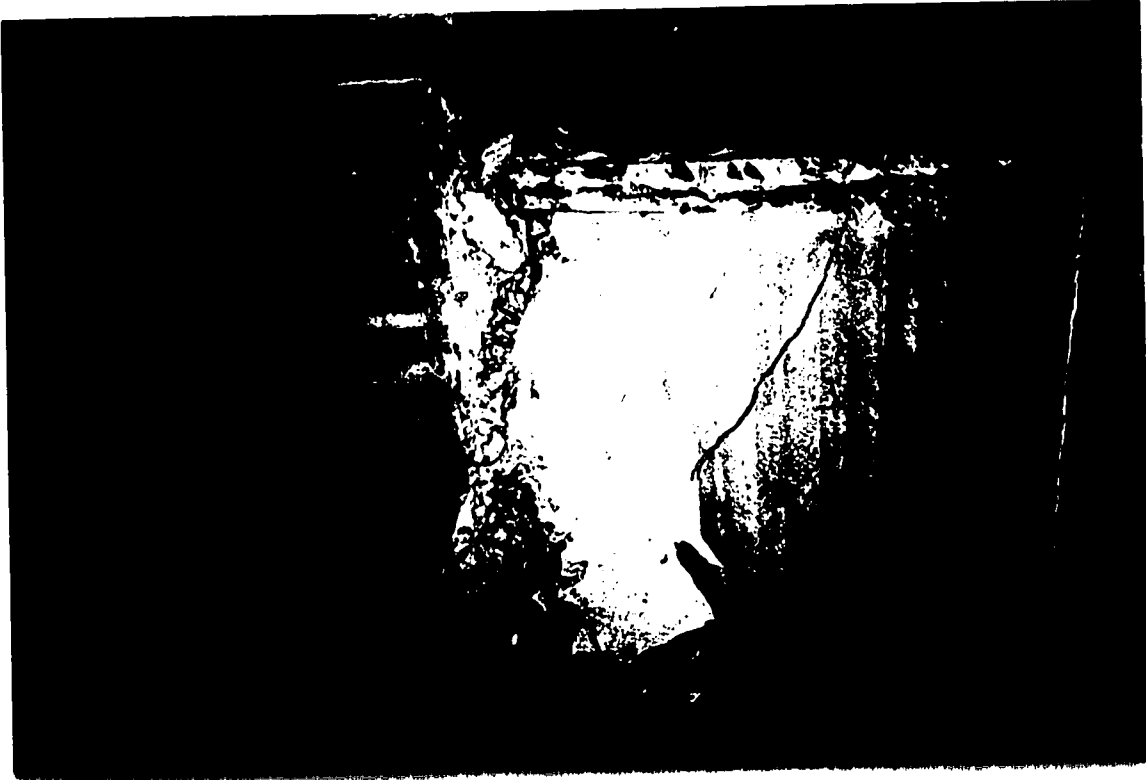


Figure 3.8a Crack pattern of specimen J3 after removing the steel casing.



Figure 3.8b Crack pattern of specimen J3 after removing the grout



Figure 3.10 Crack pattern of specimen J4 at drift angle of 2%.

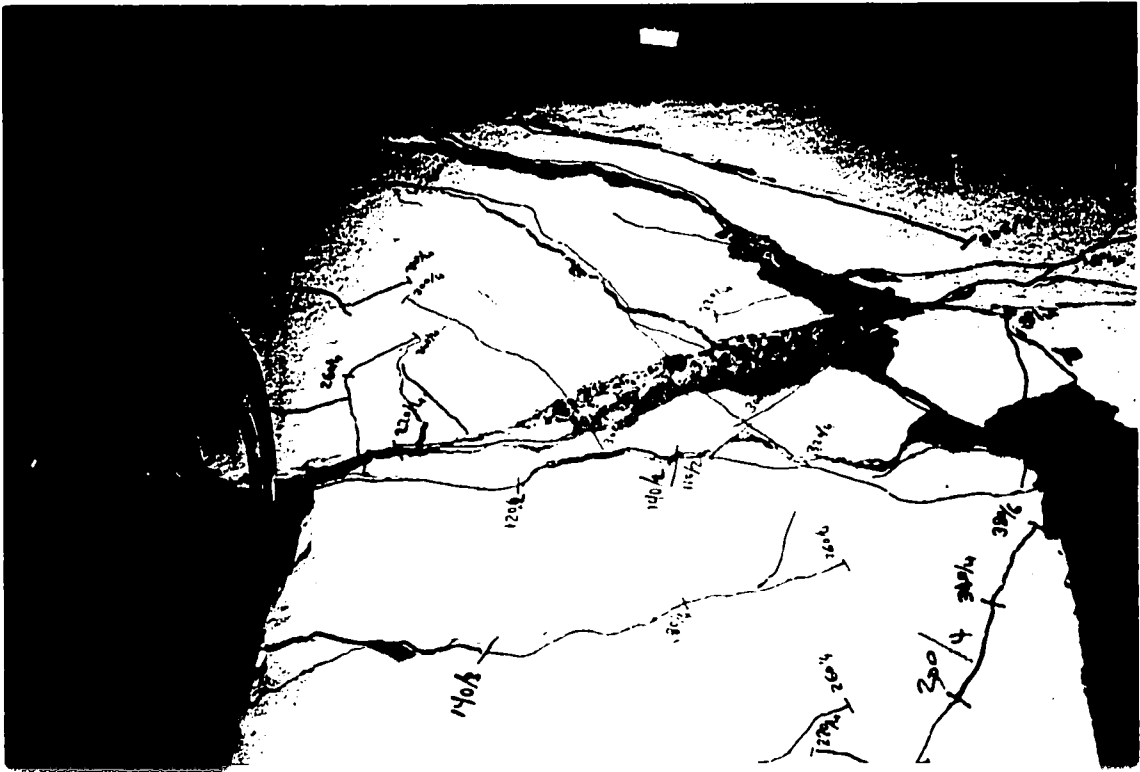


Figure 3.9 Final crack pattern of specimen J4.

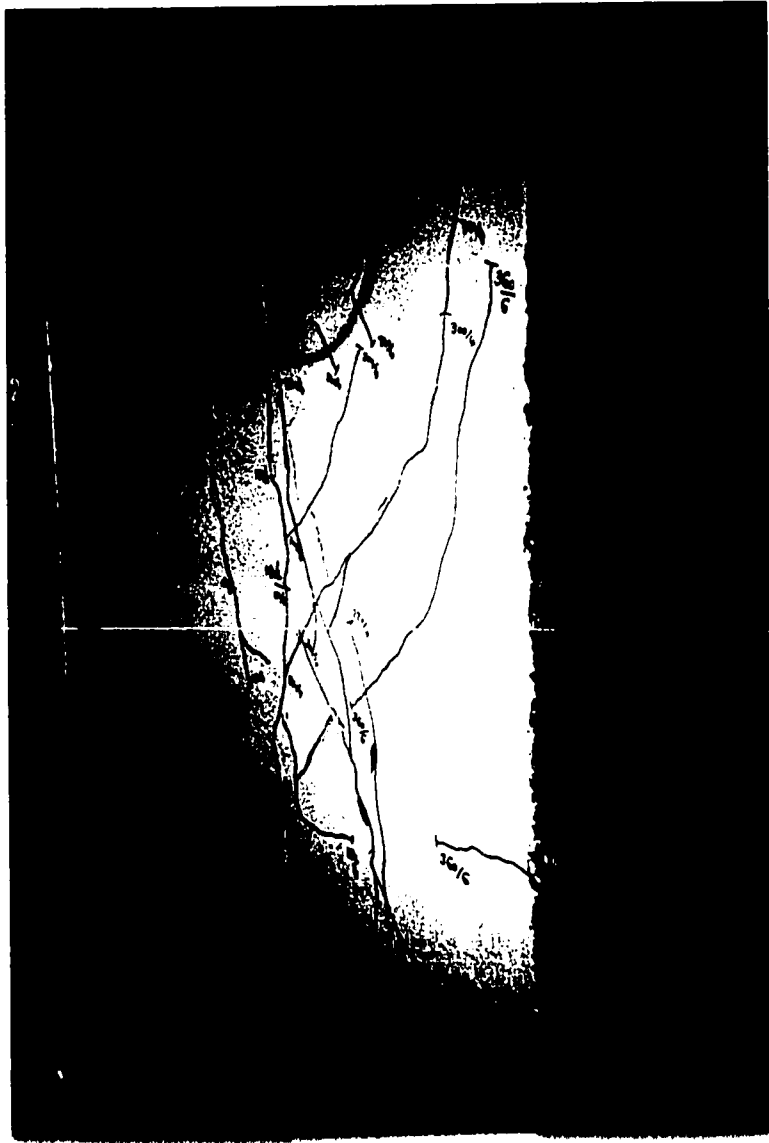


Figure 3.11 Crack pattern of specimen J4 at drift angle of 1%.

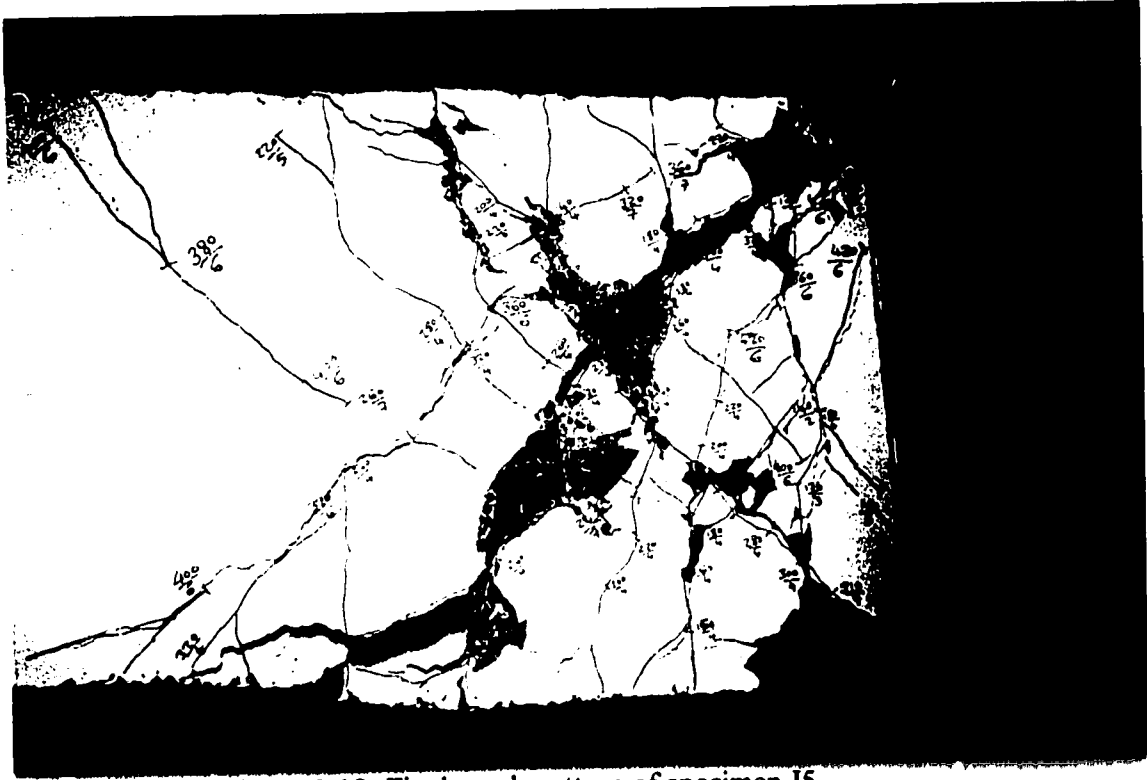


Figure 3.12 Final crack pattern of specimen J5.

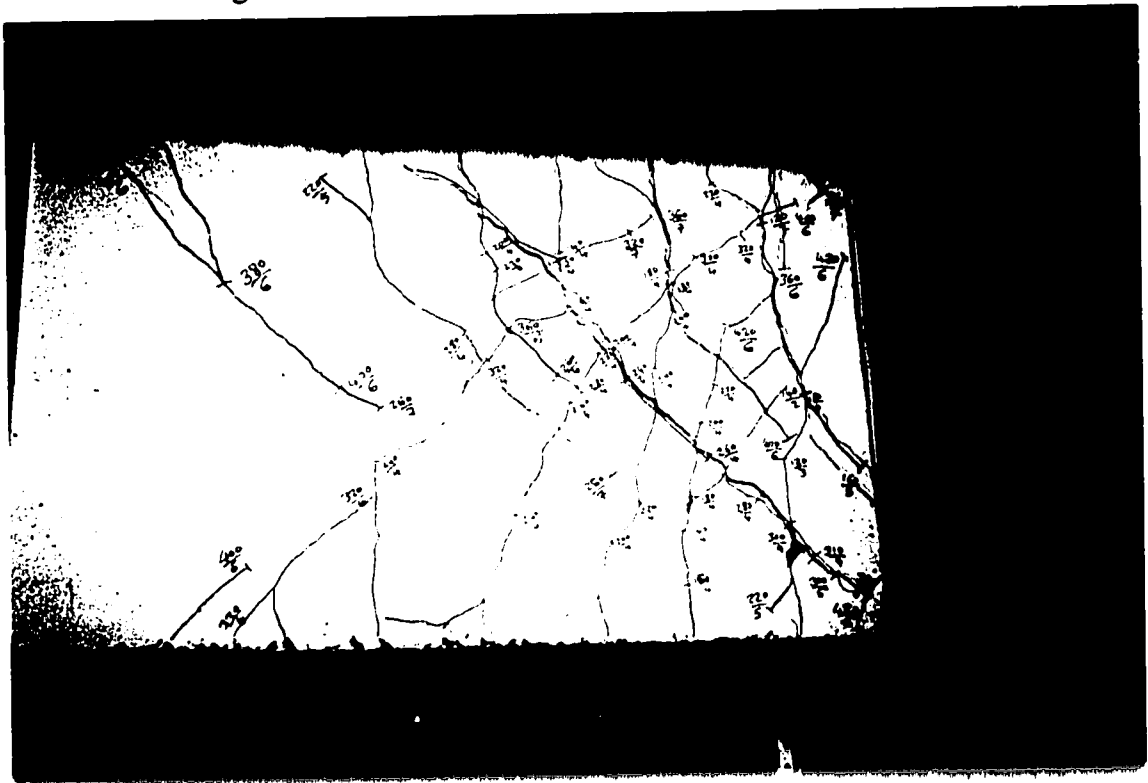
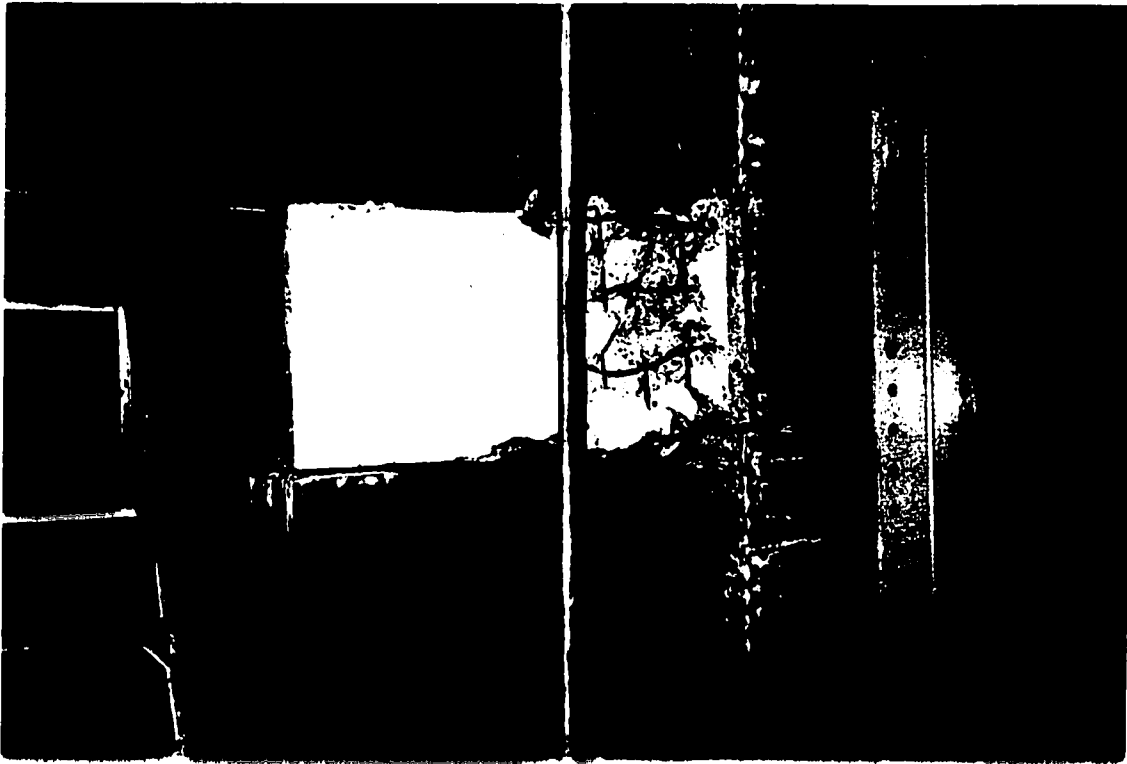


Figure 3.13 Crack pattern of specimen J5 at drift angle of 2%.



(a)



(b)

Figure 3.14 Specimen J5 after removing the concrete cover and steel casing.

A high-contrast, black and white image of a map. The map is covered with a network of thin, dark lines representing roads or boundaries. Numerous handwritten numbers are scattered across the map, including '240/4', '260/4', '280/4', '300/4', '320/4', '340/4', '360/4', '380/4', '400/4', '420/4', '440/4', '460/4', '480/4', '500/4', '520/4', '540/4', '560/4', '580/4', '600/4', '620/4', '640/4', '660/4', '680/4', '700/4', '720/4', '740/4', '760/4', '780/4', '800/4', '820/4', '840/4', '860/4', '880/4', '900/4', '920/4', '940/4', '960/4', '980/4', '1000/4'. A ruler is placed horizontally across the middle of the map, with a pen resting on it. The ruler has markings and numbers, and the pen has a dark, cylindrical body. The overall image is very dark, with the map and ruler/pen standing out against the black background.

Figure 3.16 Crack pattern of specimen J6 at drift angle of 2%.

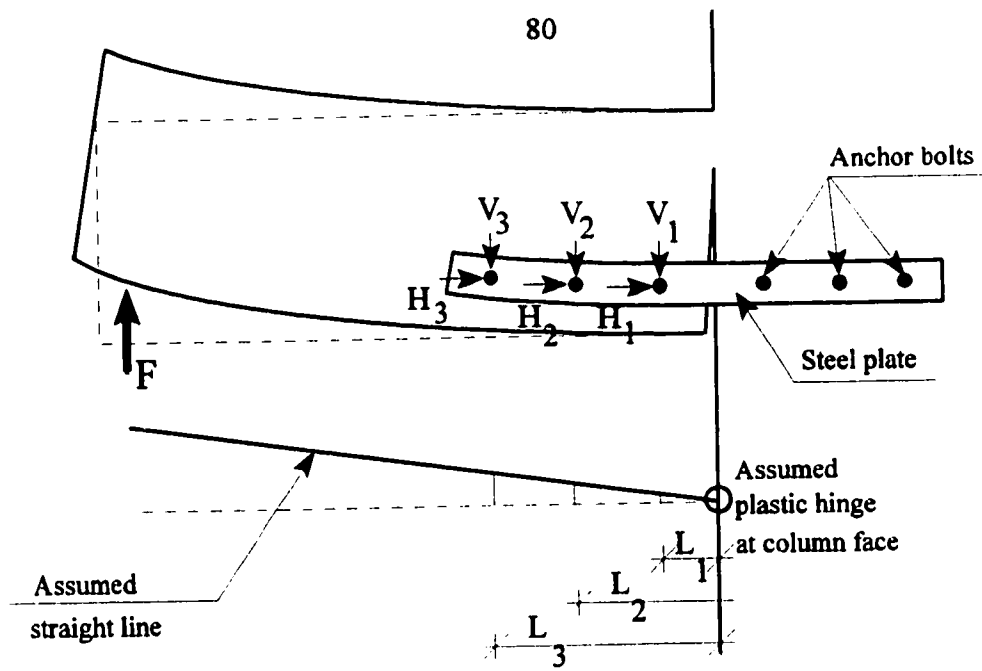


Figure 3.17 Forces on anchor bolts



Figure 3.18 Specimen J6 after removing the steel casing.

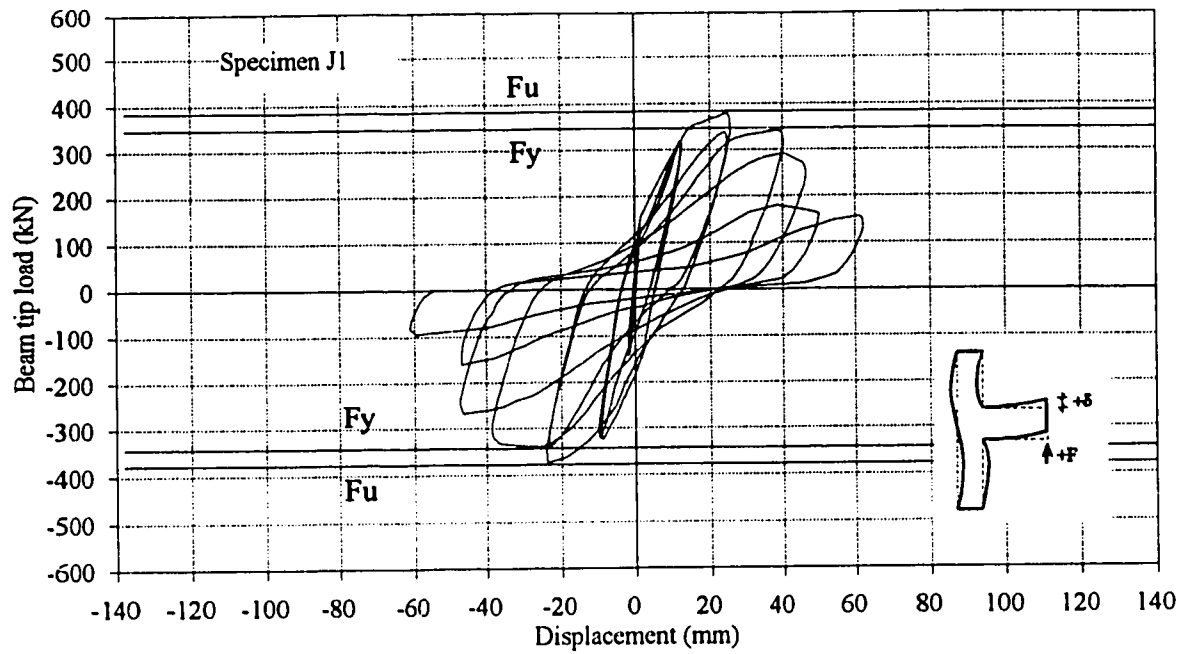


Figure 3.19a Beam tip load-displacement relationship of specimen J1

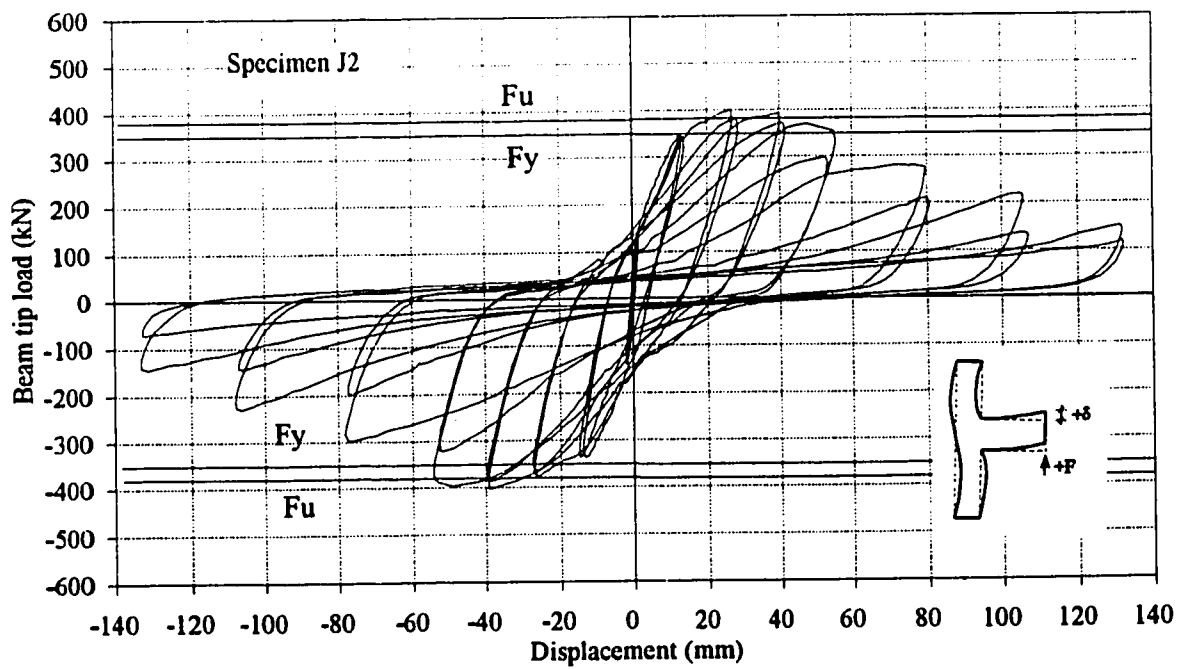


Figure 3.19b Beam tip load-displacement relationship of specimen J2

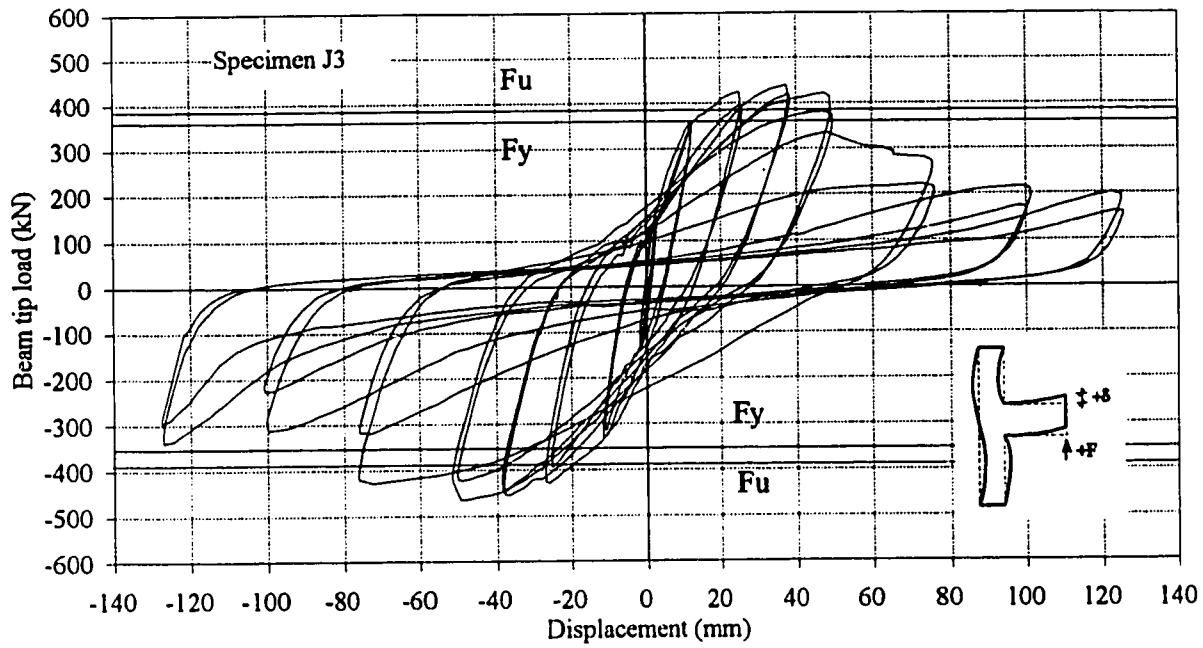


Figure 3.19c Beam tip load-displacement relationship of specimen J3

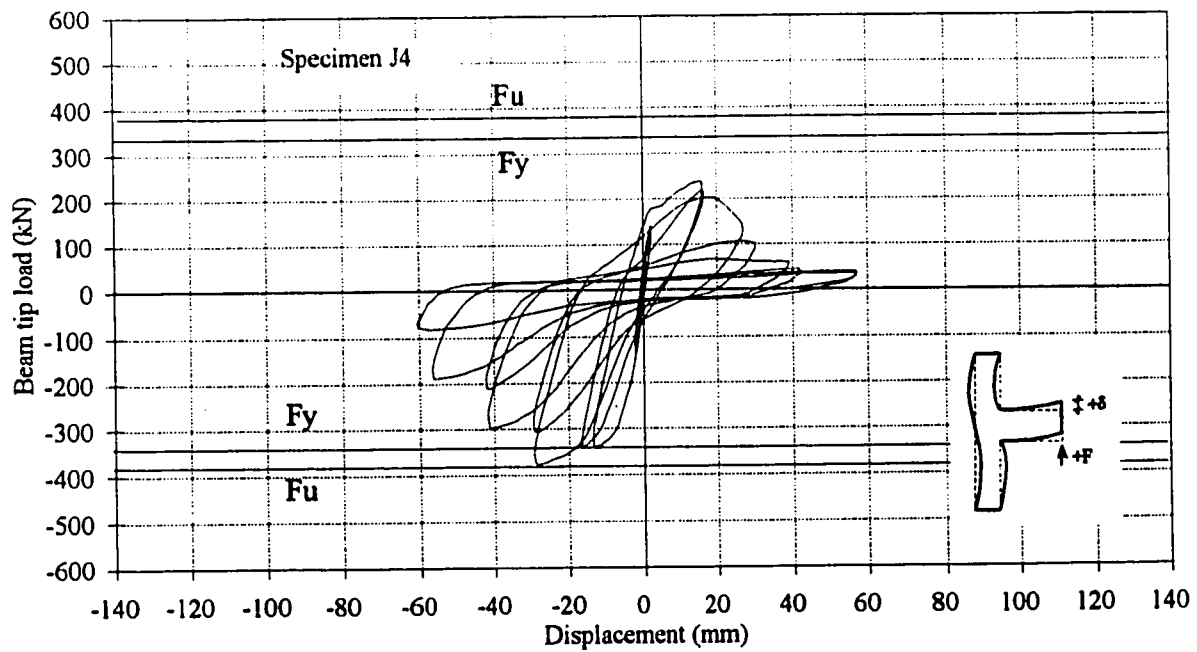


Figure 3.19d Beam tip load-displacement relationship of specimen J4

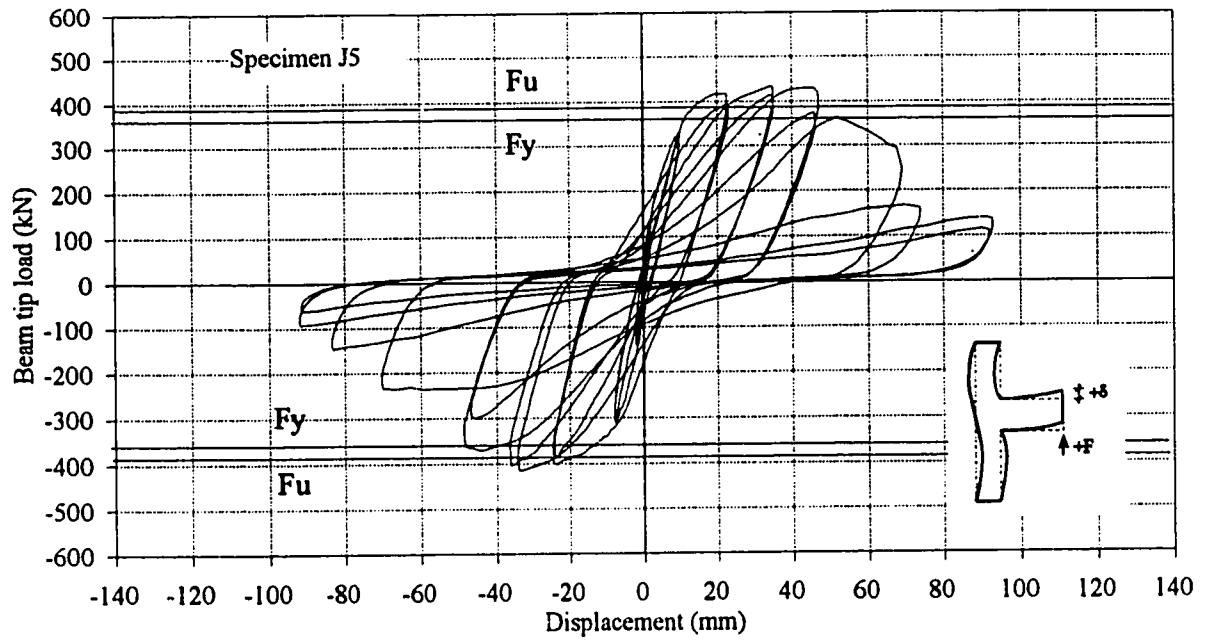


Figure 3.19e Beam tip load-displacement relationship of specimen J5

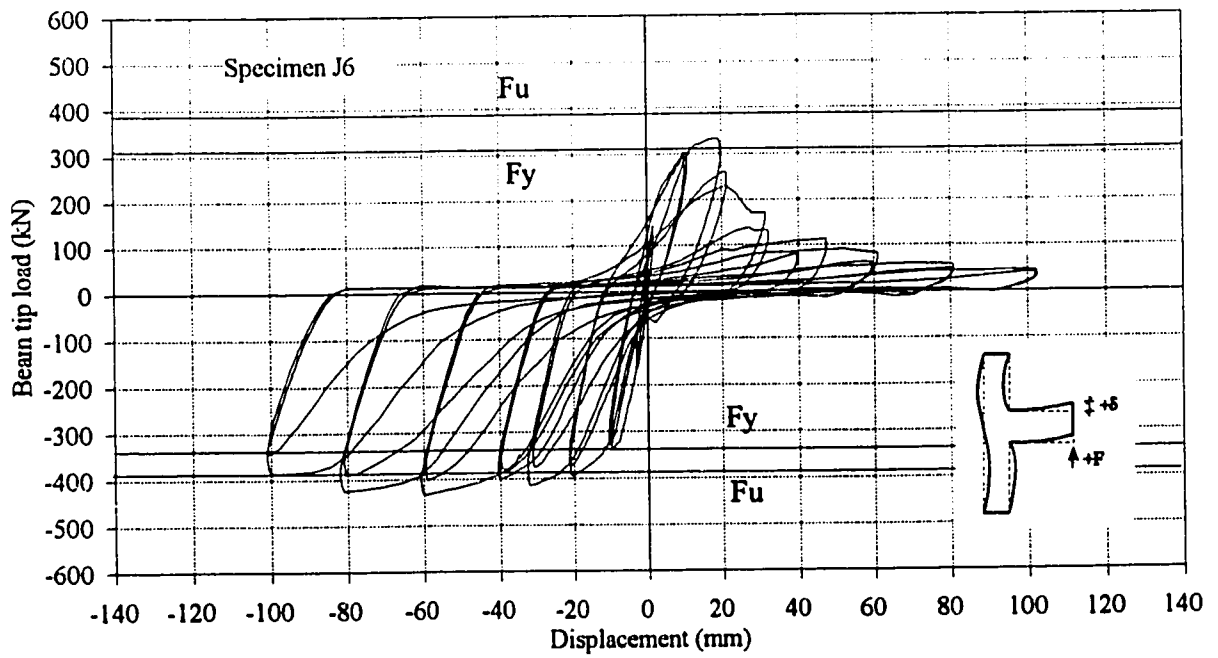


Figure 3.19f Beam tip load-displacement relationship of specimen J6

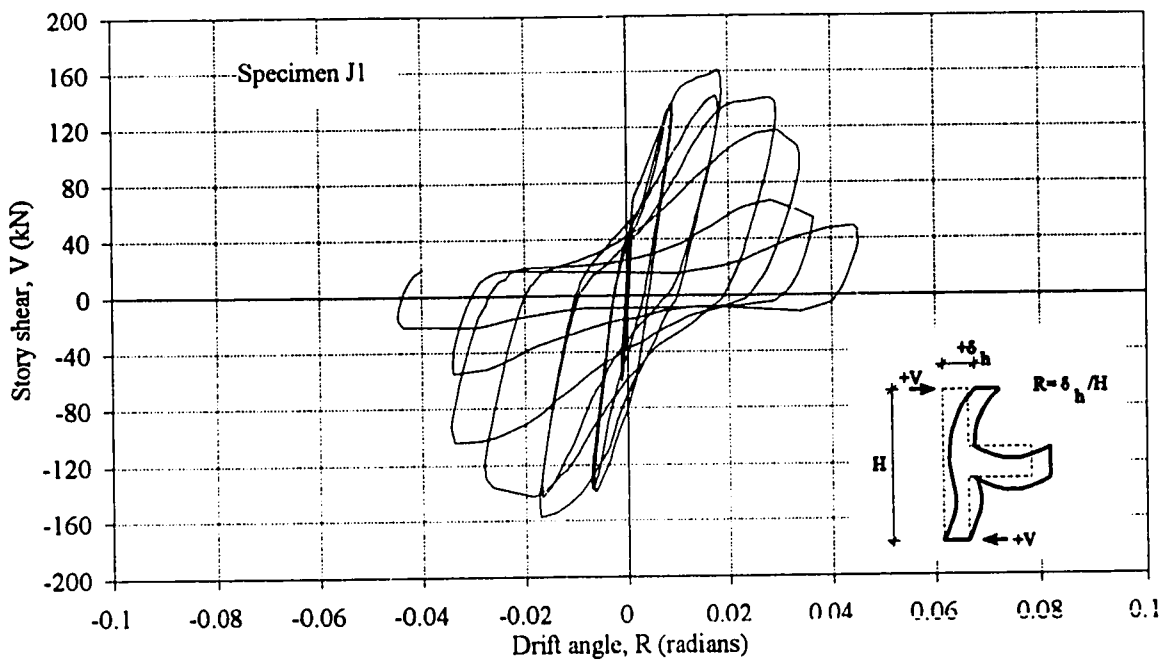


Figure 3.20a Story shear-drift angle relationship of specimen J1

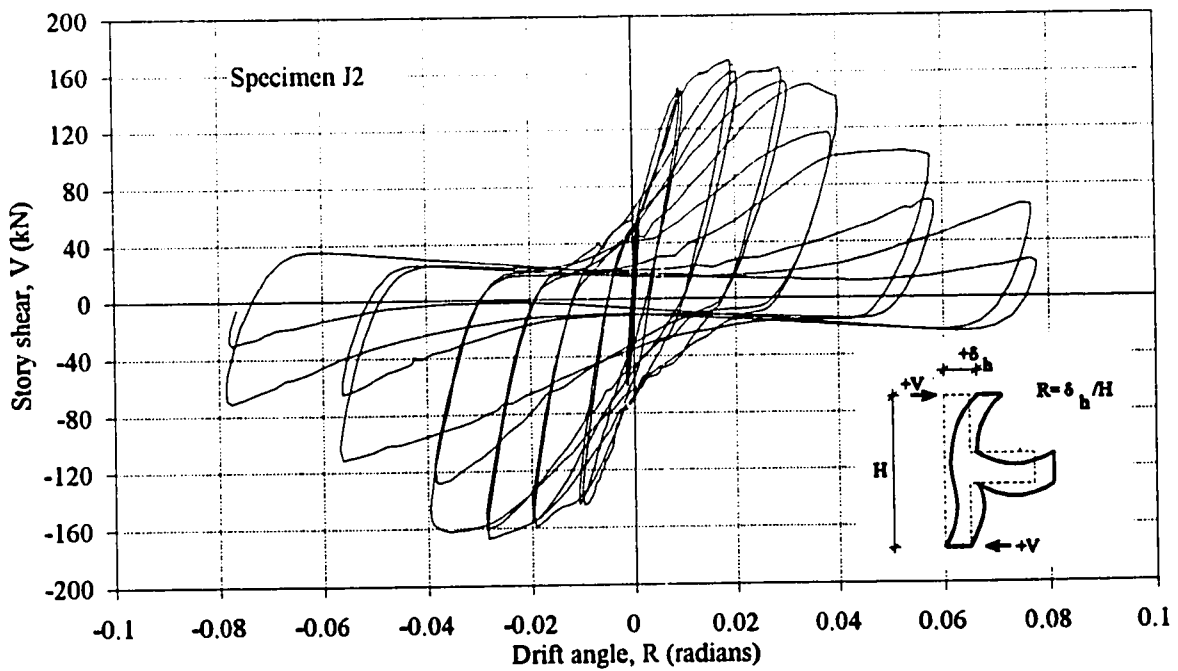


Figure 3.20b Story shear-drift angle relationship of specimen J2

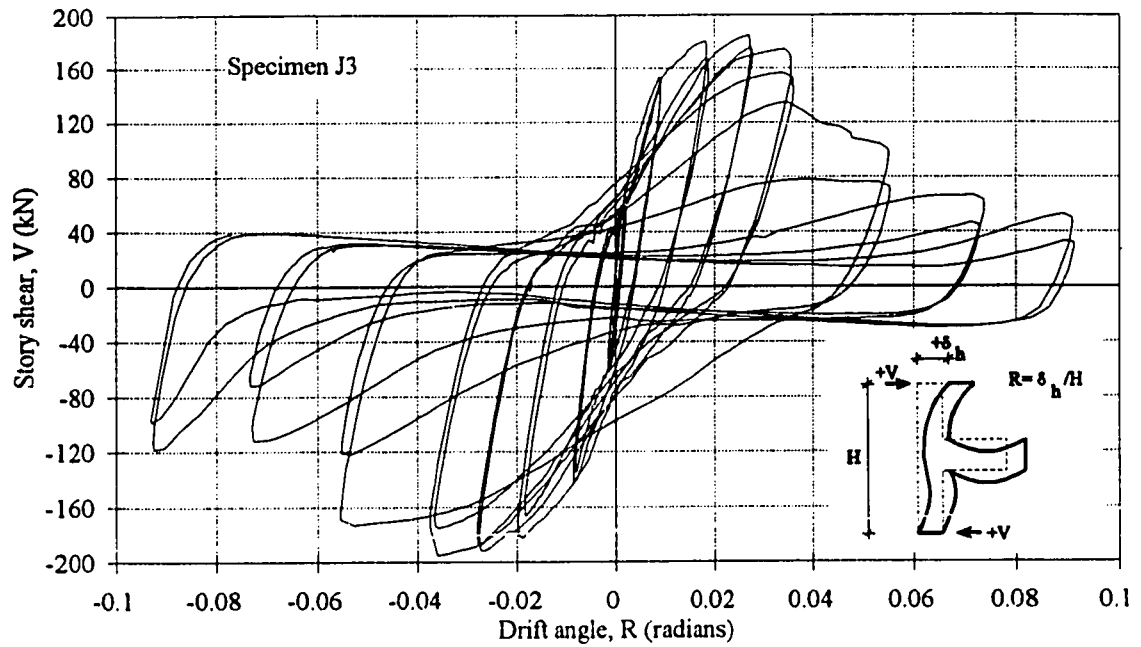


Figure 3.20c Story shear-drift angle relationship of specimen J3

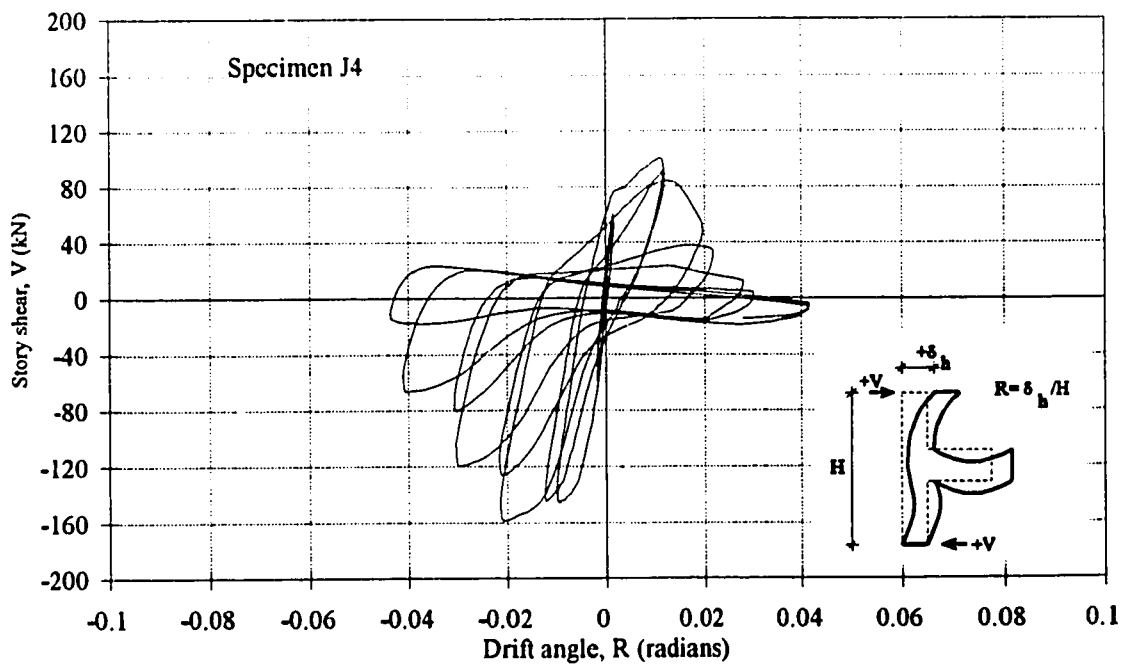


Figure 3.20d Story shear-drift angle relationship of specimen J4

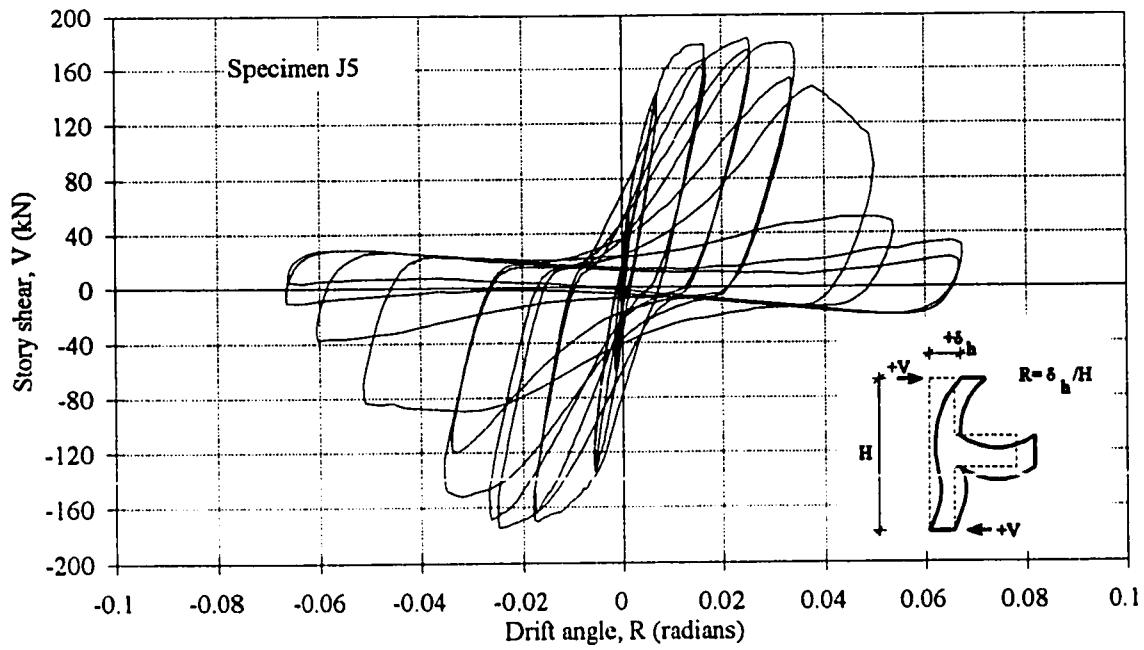


Figure 3.20e Story shear-drift angle relationship of specimen J5

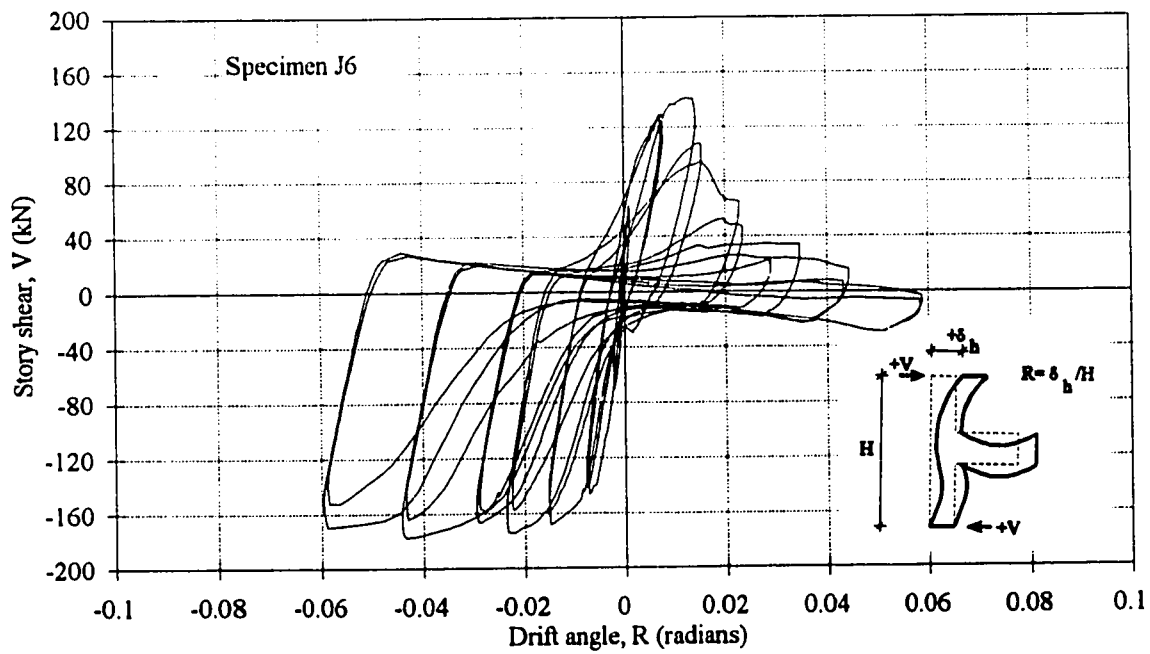


Figure 3.20f Story shear-drift angle relationship of specimen J6

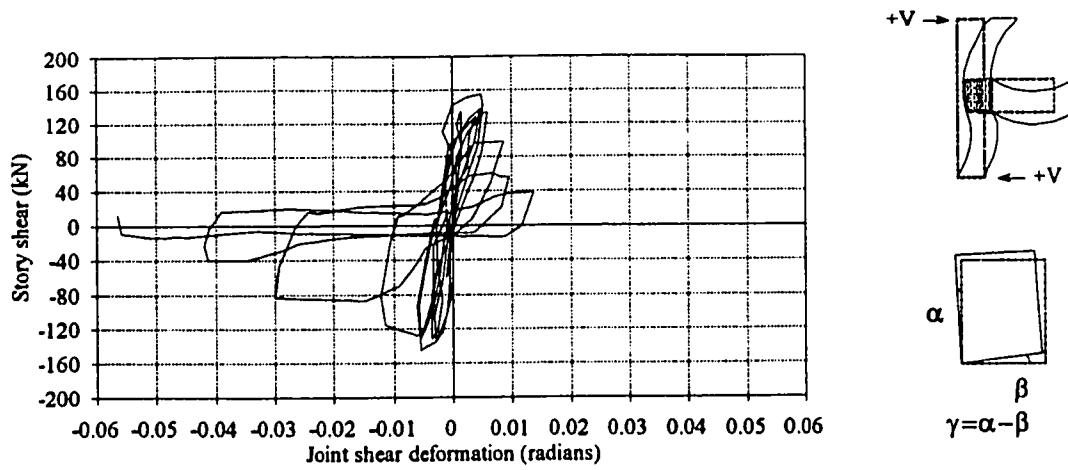


Figure 3.21a Story shear-joint shear deformation of specimen J1

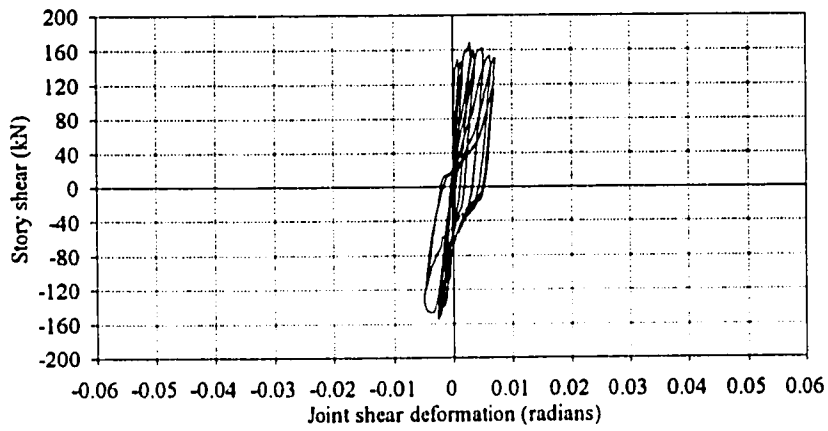


Figure 3.21b Story shear-joint shear deformation of specimen J2

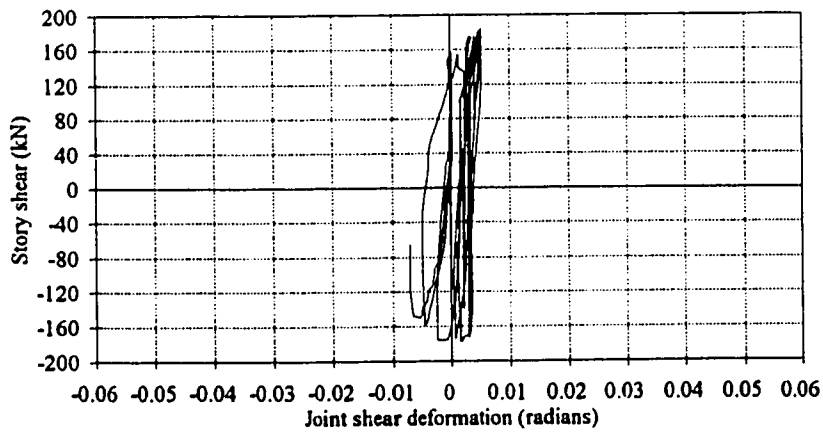


Figure 3.21c Story shear-joint shear deformation of specimen J3

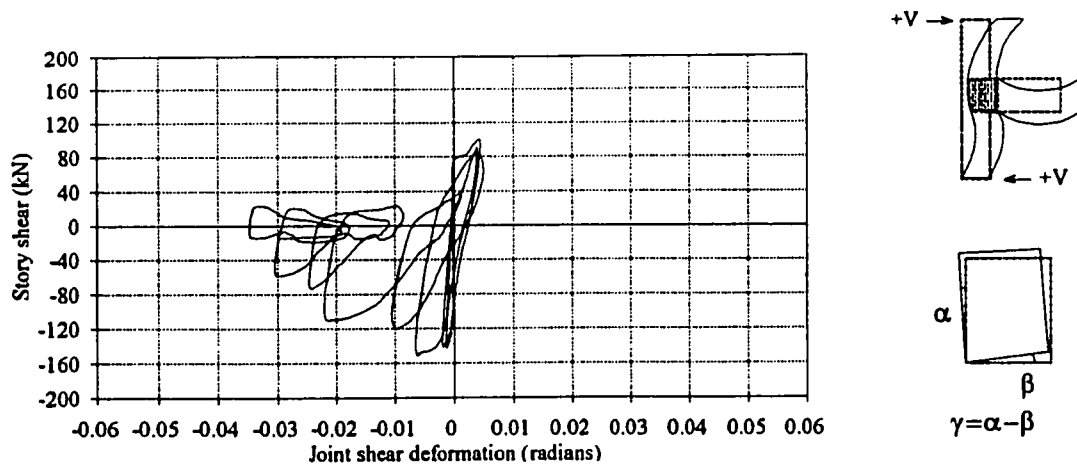


Figure 3.21d Story shear-joint shear deformation of specimen J4

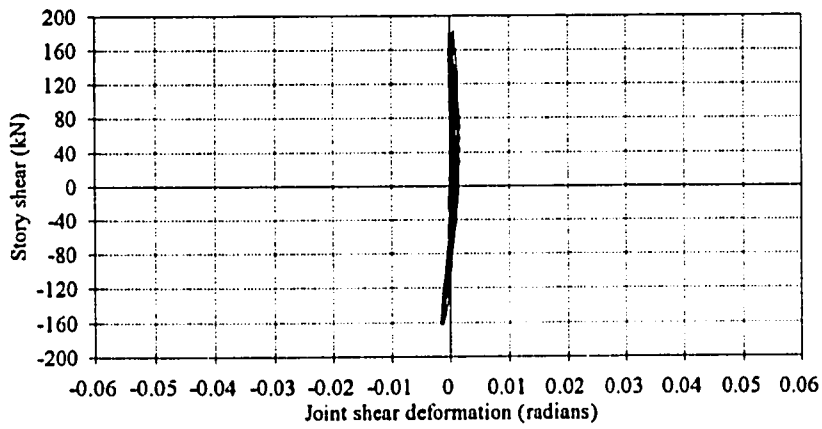


Figure 3.21e Story shear-joint shear deformation of specimen J5

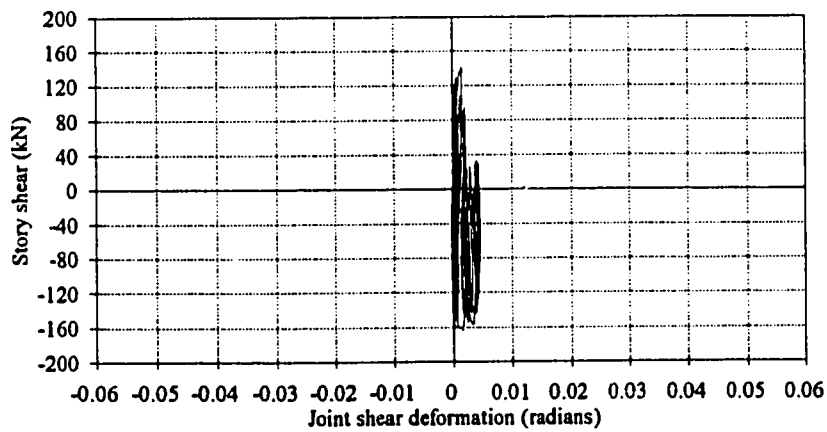


Figure 3.21f Story shear-joint shear deformation of specimen J6

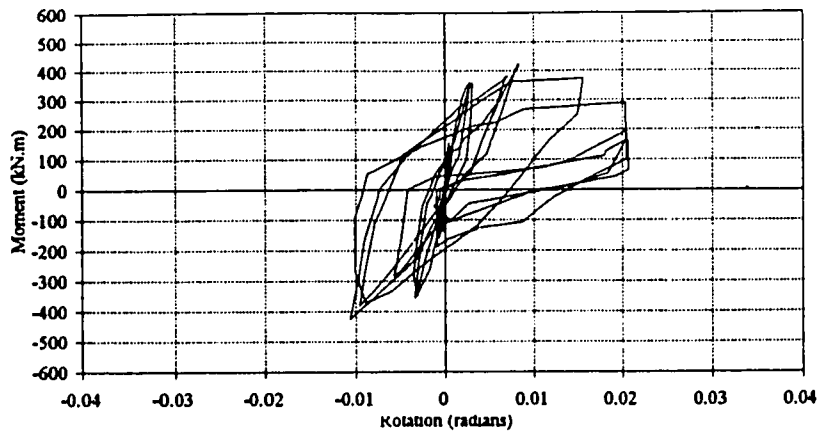


Figure 3.22a Beam moment-rotation at 80 mm from column face of specimen J1

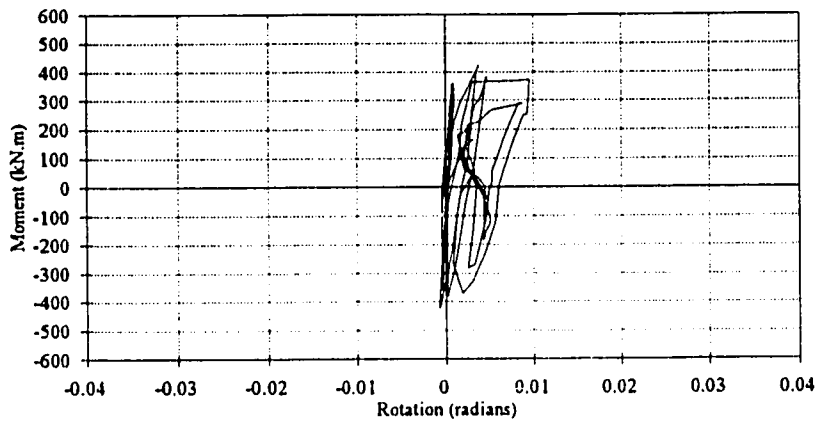


Figure 3.22b Beam moment-rotation at 330 mm from column face of specimen J1

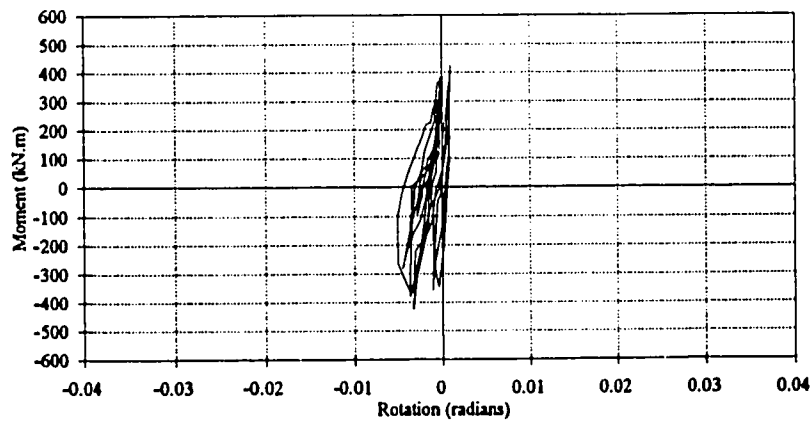


Figure 3.22c Beam moment-rotation at 580 mm from column face of specimen J1

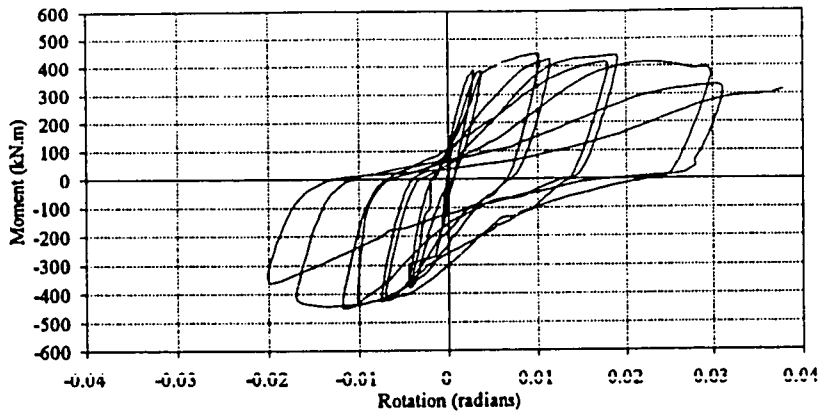


Figure 3.23a Beam moment-rotation at 80 mm from column face of specimen J2

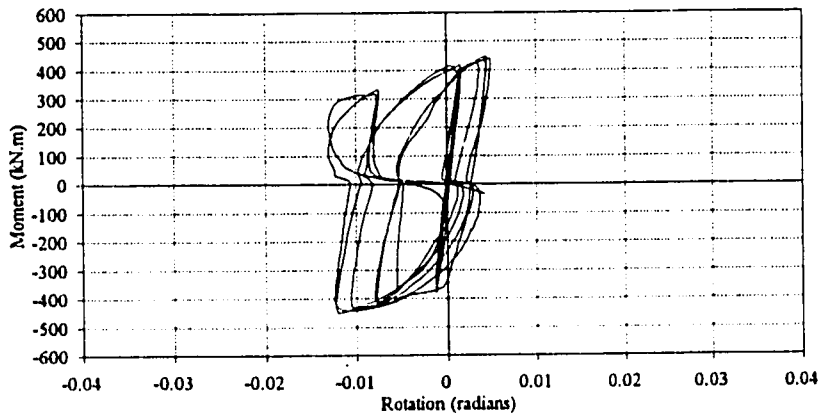


Figure 3.23b Beam moment-rotation at 330 mm from column face of specimen J2

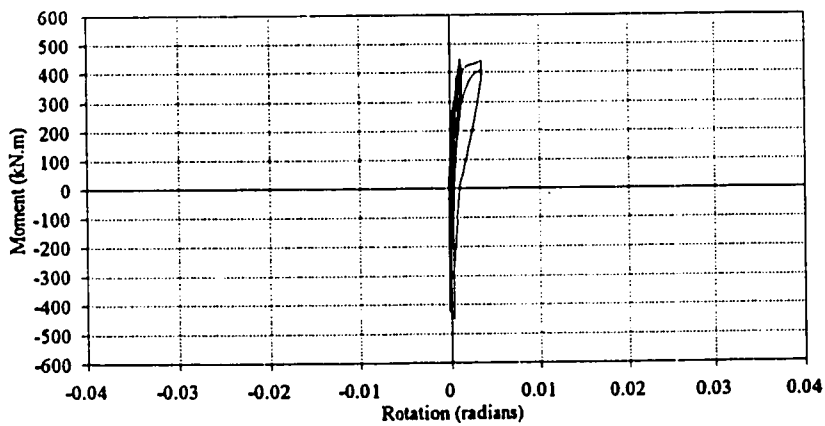


Figure 3.23c Beam moment-rotation at 580 mm from column face of specimen J2

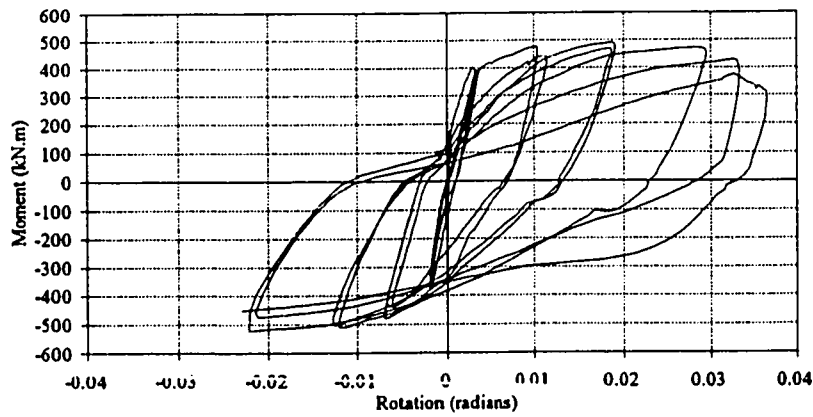


Figure 3.24a Beam moment-rotation at 80 mm from column face of specimen J3

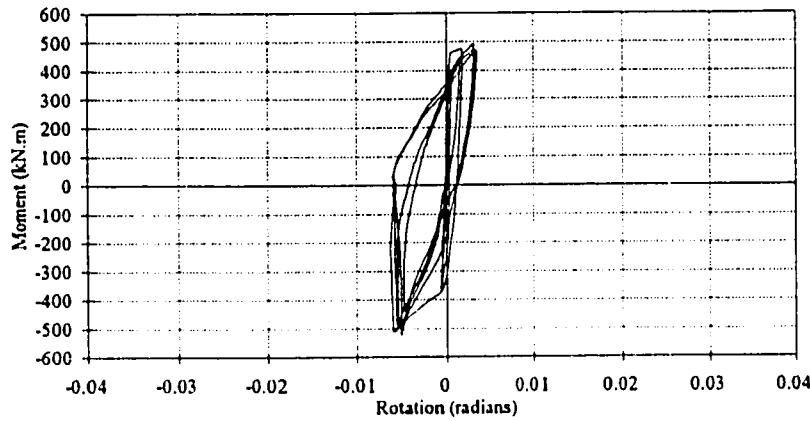


Figure 3.24b Beam moment-rotation at 330 mm from column face of specimen J3

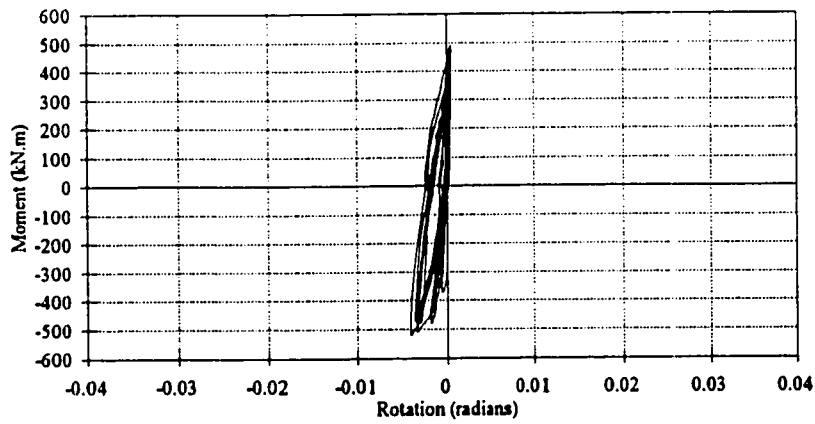


Figure 3.24c Beam moment-rotation at 580 mm from column face of specimen J3

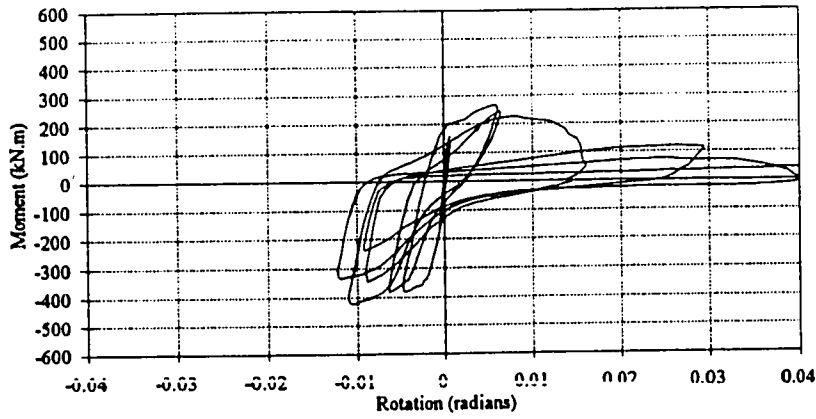


Figure 3.25a Beam moment-rotation at 80 mm from column face of specimen J4

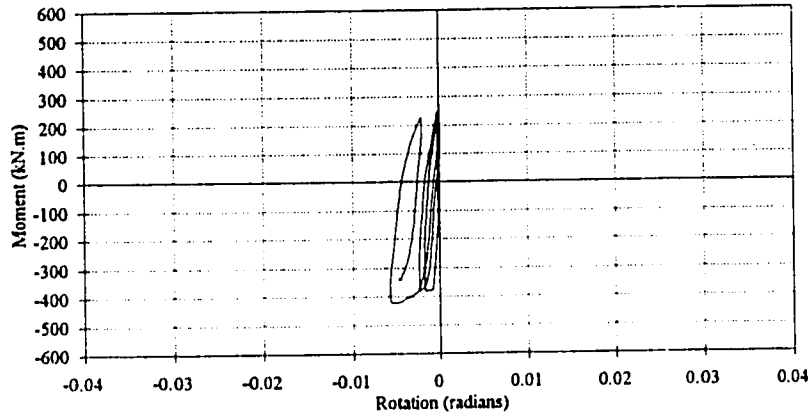


Figure 3.25b Beam moment-rotation at 330 mm from column face of specimen J4

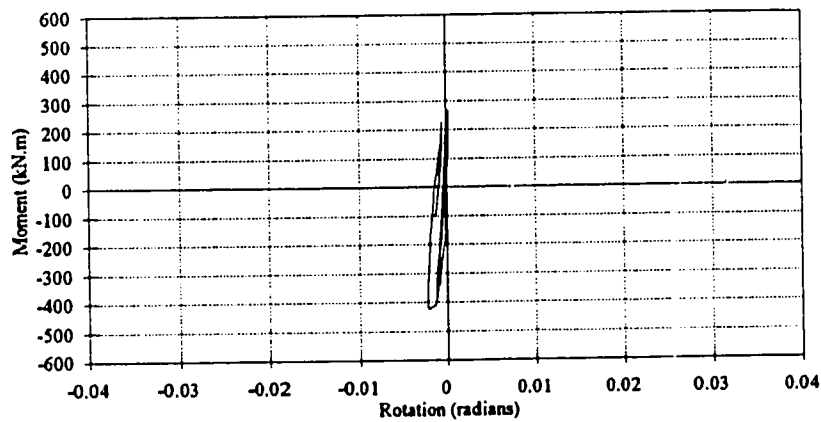


Figure 3.25c Beam moment-rotation at 580 mm from column face of specimen J4

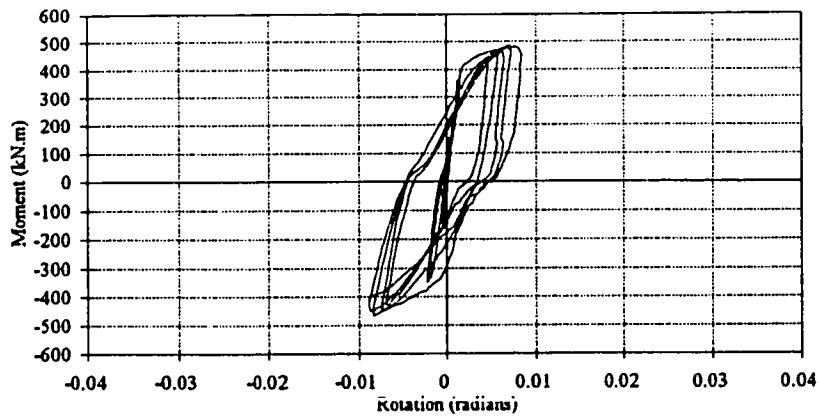


Figure 3.26a Beam moment-rotation at 80 mm from column face of specimen J5

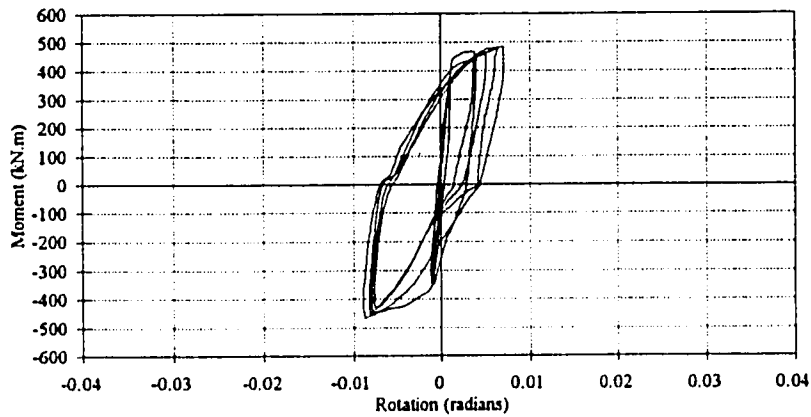


Figure 3.26b Beam moment-rotation at 330 mm from column face of specimen J5

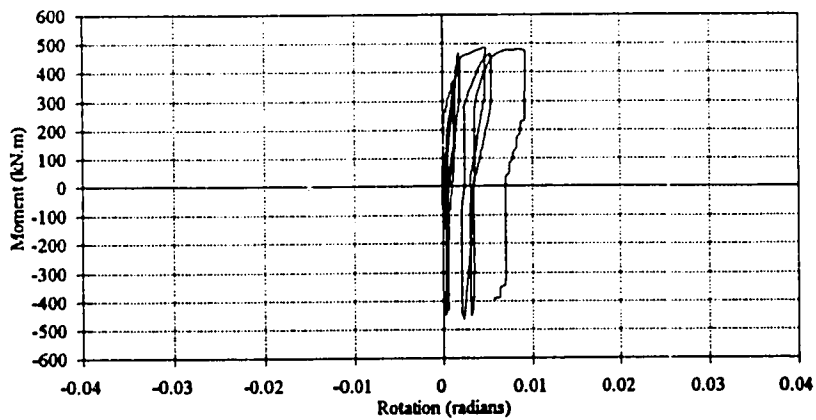


Figure 3.26c Beam moment-rotation at 580 mm from column face of specimen J5

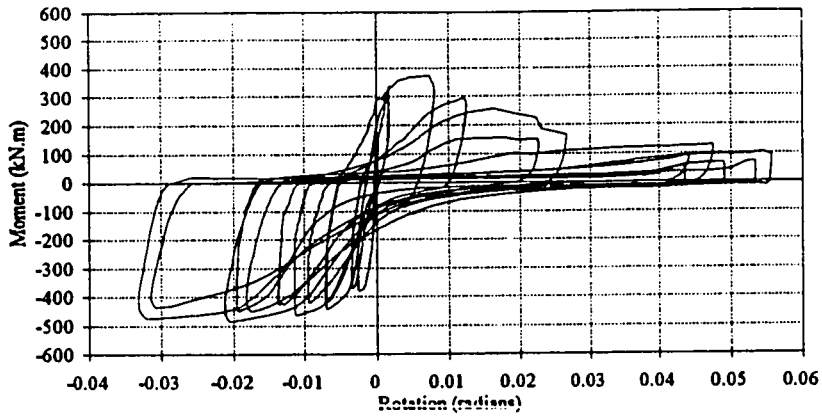


Figure 3.27a Beam moment-rotation at 80 mm from column face of specimen J6

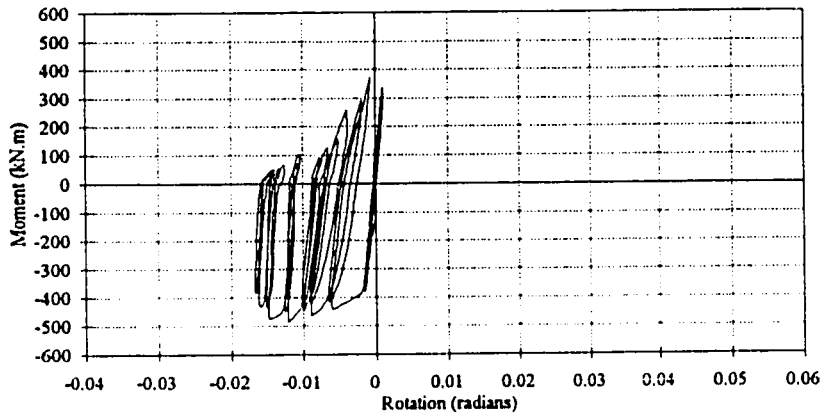


Figure 3.27b Beam moment-rotation at 330 mm from column face of specimen J6

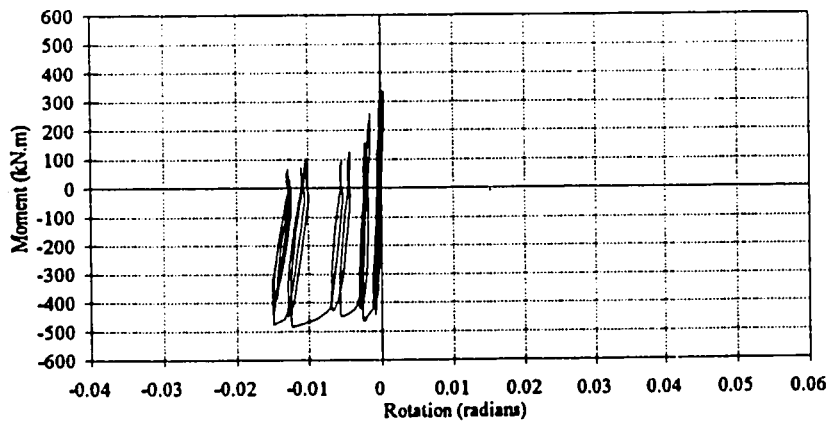


Figure 3.27c Beam moment-rotation at 580 mm from column face of specimen J6

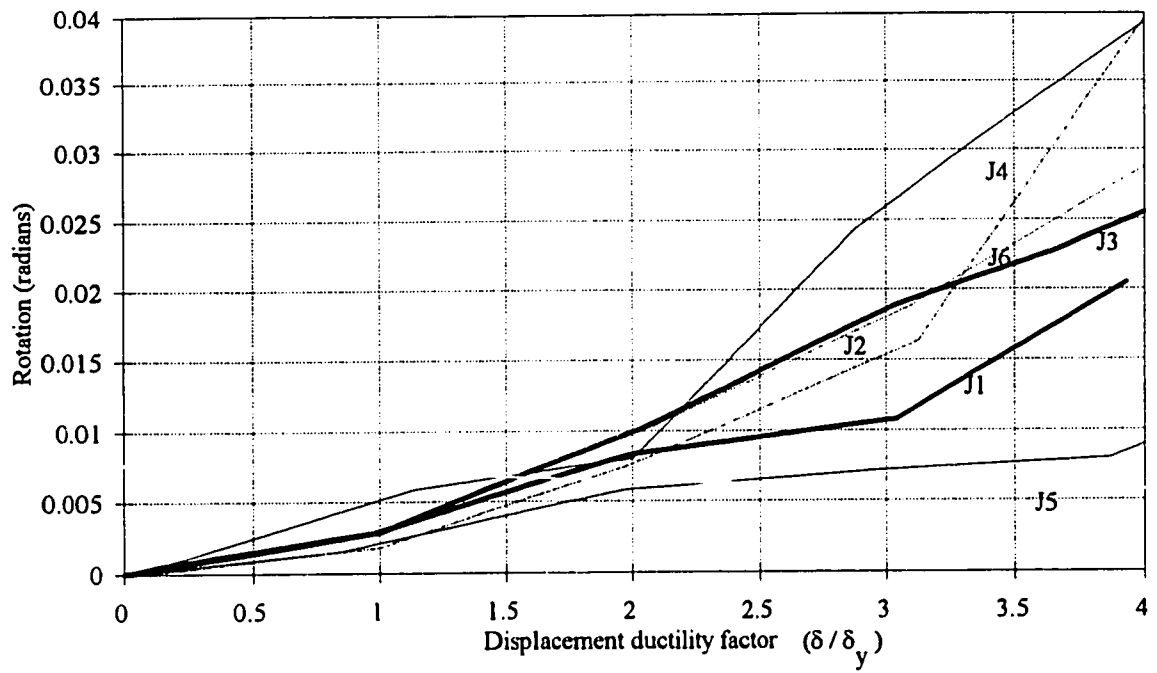


Figure 3.28a Positive rotation at 80 mm - displacement ductility factor

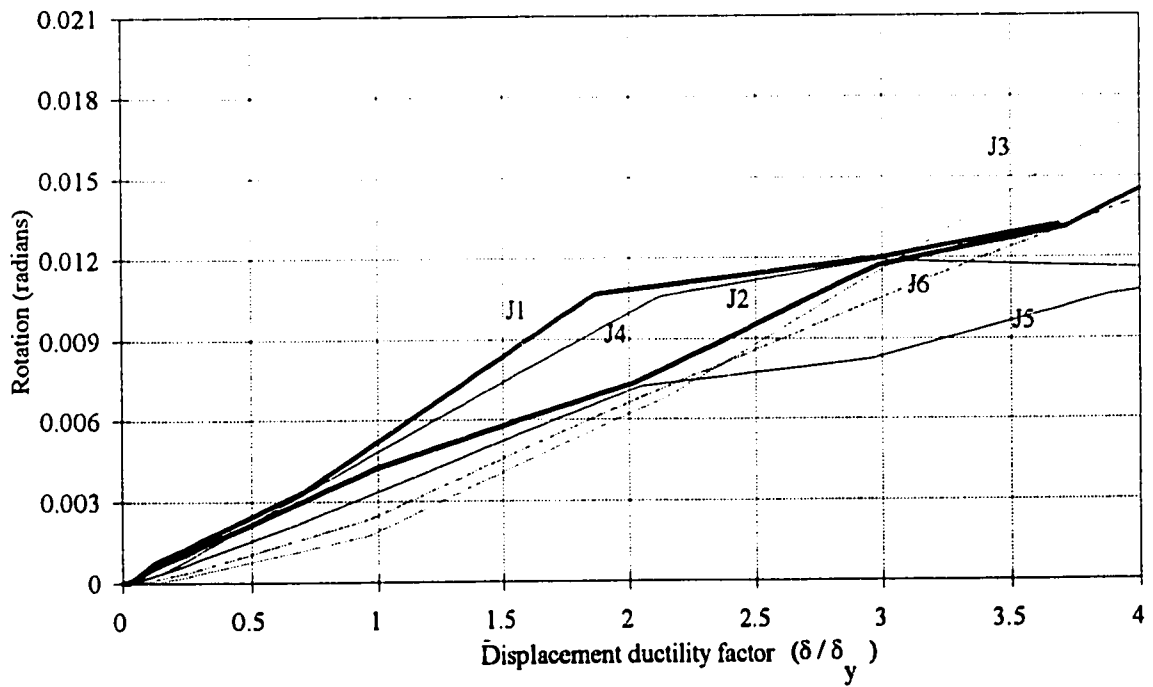


Figure 3.28b Negative rotation at 80 mm - displacement ductility factor

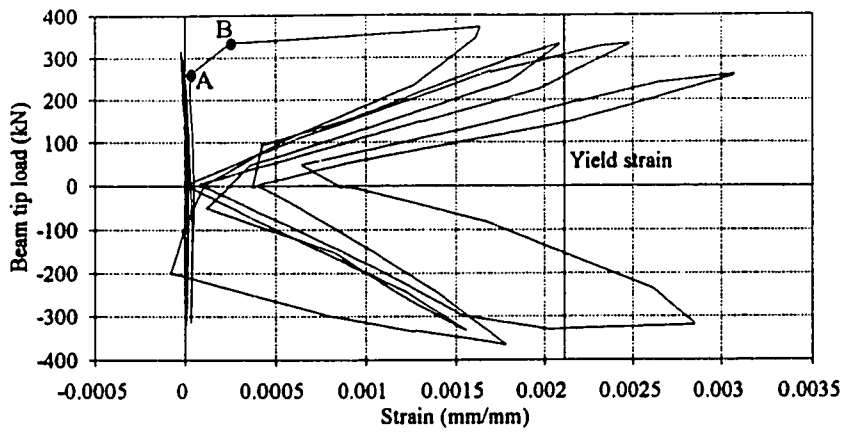


Figure 3.29 Beam tip load-strain at joint tie for specimen J1

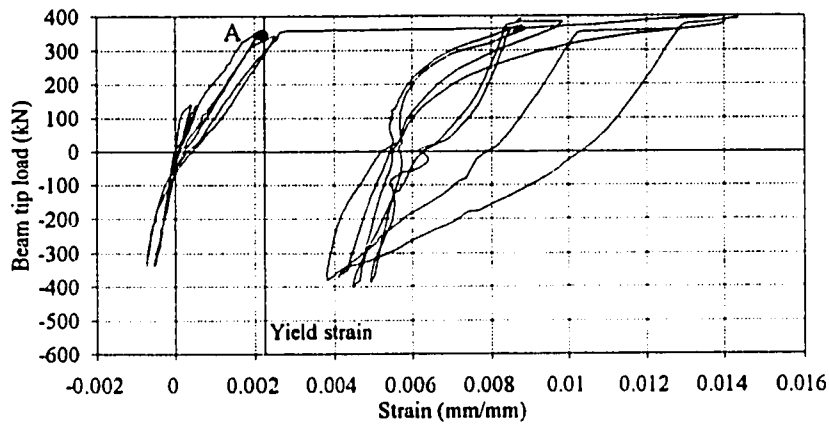


Figure 3.30 Beam tip load-strain at bottom steel of beam for specimen J2

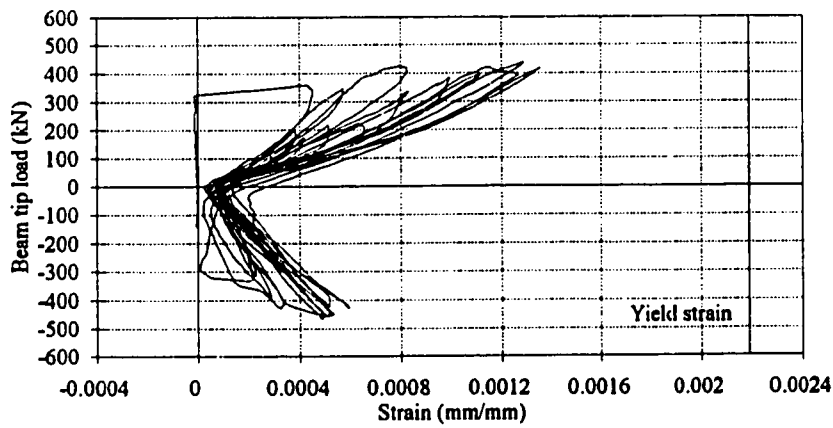


Figure 3.31 Beam tip load-strain at beam third stirrup for specimen J3

CHAPTER 4

ANALYSIS OF TEST RESULTS

4.1 INTRODUCTION

Analysis of the general behaviour of the specimens from observations and recorded data is presented in this chapter. The specimens are designated J1, J2, J3, J4, J5 and J6. Specimen J1 represents existing structure connection of 1970's code design. Specimen J2 represents current Canadian code designed connection. Specimen J3 is a rehabilitated connection using steel jacket on beam, column and joint. Specimen J4 represents 1960's code design. The rehabilitated connection using steel jacket on column and joint is J5. Specimen J6 is a rehabilitated connection of the 1960's design. The load-carrying capacity and story shear attained in each cycle were recorded. Analysis of the recorded data included the calculation of yield moment, shear in beams and shear in joints. The joint shear-shear deformation relationships are plotted. The member contributions to drift angle, useful in understanding the performance and mode of failure, are described. The stiffness of the specimens is evaluated using the peak to peak stiffness approach. The energy dissipation capacity of the subassemblages is assessed using the cumulative energy dissipated. An equivalent viscous damping factor for each specimen is calculated. Slippage between the

steel jacket and the grout is measured and plotted against the displacement ductility factor. The steel jacket confinement pressure at the joint region is plotted versus the displacement ductility factor.

4.2 LOAD-CARRYING CAPACITY

For all the specimens, the maximum beam tip load attained in each cycle was recorded and plotted versus the displacement ductility factor as shown in figure 4.1. Comparison between the behaviour of specimens J1 and J3 illustrates the effect of the rehabilitation technique on the load carrying capacity. Specimen J1 showed an increase in the load resistance during each additional cycle up to 25 mm displacement (displacement ductility factor of 2) resisting 380 kN, with a maximum resistance of 1.19 times that of the yield strength. Specimen J3 exhibited maximum load-carrying capacity of 466 kN (1.34 times that of the yield strength) at a displacement of 48 mm (displacement ductility factor of 4).

Comparison of the behaviour of specimens J1 and J2 illustrates the effect of the confinement provided to the joint by the transverse reinforcement. The joint ties provided to the code design specimen J2 increased the ductility of the specimen several times compared with the inadequate joint reinforcement of specimen J1. The effect of the joint ties was mainly to provide the adequate confinement of the concrete so that the lateral expansion of the concrete is resisted and the strength and ductility are increased. The joint being able to provide adequate anchorage of beam bars, the main horizontal member of the specimen was able to develop its full inelastic capacity. In addition to confinement, the ties provide the shear resistance in the joint.

The joint of specimen J1, with inadequate transverse reinforcement, was able to provide anchorage to beam steel to an extent that 98% of the theoretical ultimate capacity of the beam, which is 388 kN, was reached. However, the joint was unable to sustain the anchorage of beam steel in subsequent cycles. In specimens J2 and J3 where the joint has adequate transverse reinforcement and confinement, the anchorage was such that the beam was able to reach up to 103% and 120% of its theoretical ultimate capacity and maintain this capacity over a number of cycles.

The direction of the first cycle of loading for specimen J1 was positive while that for specimen J4 was negative. This is the reason why specimen J4 without ties in the joint appeared to carry more load in the first negative cycle than specimen J1 with a few ties in its joint (16% of the area required by the current Canadian code).

The steel jacket confinement and the steel angles used in specimen J5 caused the beam failure zone to move away from the column face. This resulted in higher shear forces than expected for specimen J5 with steel jacket on column only as compared to J3 with steel jacket on column and beam (figure 4.1). In the capacity design approach, underestimation of the beam section flexural capacity would result in underestimation of the design shear force and may result in a brittle shear failure. Therefore, the shear capacity of the beam should be checked and if it is critical, a steel jacket needs to be added to the beam in the critical region.

4.3 RESPONSE ENVELOPES AND STORY SHEAR BEHAVIOUR

The overall response of the specimens are compared using the story shear-drift angle envelope curves shown in figure 4.2. The strength of specimen J3 was 1.13 time greater at

2% drift and 2.2 times greater at 4% drift than the strength of specimen J1. At 1% drift, specimen J3 was 1.1 times stiffer than specimen J1. Comparison of J3 and J5 shows that by jacketing the column without the beam (J5), the strength at 2% drift and stiffness at 1% drift were 94% and 103% respectively of the values obtained for specimen J3 in which both the beam and column were jacketed. The strength of J5 at 4% drift angle was 78% of J3 strength.

The response of specimen J5 in the positive direction is different from that in the negative direction. This is because intersecting inclined cracks caused deterioration of the hinging zone by dividing the region into a matrix of prismatic blocks. The integrity of the region was influenced primarily by the ability of the reinforcement to decrease the mobility, and consequently degradation, of the individual blocks. As the transverse reinforcement of the beam of specimen J5 was insufficient, the intersecting inclined cracks which occurred in the negative direction of loading caused a reduction in the shear capacity as compared to the shear capacity in the positive direction.

4.4 DATA ANALYSIS

4.4.1 Yield moment

The experimental yield moments were obtained by multiplying the yield load by the moment arm to the critical section located at the column face. The yield moment values for all the specimens are listed in table 4.1. The theoretical yield moments were calculated by assuming a linear stress distribution in the concrete and were based on measured steel and concrete strengths. The calculated moments show good agreement with the experimental

measurements. The ratios of experimental to calculated yield moments range from 1.08 to 1.11 for the non-rehabilitated specimens and 1.07 to 1.23 for the rehabilitated specimens. The ratio is higher in case of rehabilitated specimens because of the confinement of the concrete which increases its resistance.

4.4.2 Shear in beams

The shear in the beam was assumed to be resisted by the concrete and the transverse reinforcement according to the expression:

$$V_t = V_c + V_s \quad (4.1)$$

where V_t is the total shear force in the beam, V_c is the shear force resisted by the concrete and V_s is the shear force resisted by the transverse reinforcement. Using the truss analogy, the shear resistance provided by the transverse reinforcement can be expressed as:

$$V_s = (A_v \cdot f_s \cdot d) / s \quad (4.2)$$

where s is the spacing of transverse reinforcement, A_v is the area of transverse reinforcement over a distance s , f_s is the stress in the transverse reinforcement and d is the distance from extreme compression fibre to tension reinforcement.

The strains measured in the stirrups were converted into stresses using the method described in section 3.6.1 of Chapter 3. The stresses were then introduced in equation 4.2 to calculate the shear resistance of the transverse reinforcement. The steel stress f_s was based on an average strain obtained from two strain gauge measurements. The total shear force in the beam from figure 4.1 minus the shear resisted by the transverse reinforcement equals the shear resisted by the concrete as plotted in figures 4.3 to 4.8. The concrete shear resistance, V_c , specified in the current concrete design code (CSA A23.3-94, 1994) is marked on the

figures. The concrete resistance V_c equals $0.2 \sqrt{f'_c} b_w d$ for nominal ductility members, equals $0.1 \sqrt{f'_c} b_w d$ for ductile members with axial compression greater than $0.1 A_g f'_c$ and equals zero for ductile members with axial compression less than $0.1 A_g f'_c$. The steel resistance $V_s = (A_v f_y d)/s$ is also plotted in the figures. Figure 4.3 for specimen J1 shows that the maximum concrete resistance occurred at displacement ductility of 1.0 with a value of $0.175 \sqrt{f'_c} b_w d$. At displacement ductility factor of 3.0, the transverse reinforcement resisted almost all the shear. Figure 4.4 for specimen J2 shows that the maximum concrete resistance occurred at displacement ductility of 2.0 with a value of $0.22 \sqrt{f'_c} b_w d$. At displacement ductility of 6.0 the concrete was still resisting some of the beam shear with a value of $0.05 \sqrt{f'_c} b_w d$. Figure 4.5 for specimen J3 shows that the maximum concrete shear resistance occurred at displacement ductility of 1.0 with value of $0.15 \sqrt{f'_c} b_w d$. After that, the casing started to carry shear. At displacement ductility of 4.0, the concrete carried only 12% of the shear, the stirrups carried 24% of the shear and the steel jacket carried 64% of the shear. Figure 4.6 for specimen J4 shows that the maximum concrete shear resistance occurred at displacement ductility factor of 1.0 with a value of $0.175 \sqrt{f'_c} b_w d$. Throughout the test, the concrete carried high percentage of shear because most of the damage was in the joint not in the beam. Figure 4.7 for specimen J5 shows that the maximum concrete resistance occurred at displacement ductility of +2.0 with a value of $0.21 \sqrt{f'_c} b_w d$ and at displacement ductility of -1.0 with a value of $0.175 \sqrt{f'_c} b_w d$. At displacement ductility of approximately 5.0, the transverse reinforcement resisted almost all the shear. Figure 4.8 for specimen J6 shows that the maximum concrete resistance occurred at displacement ductility of +1.0 with a value of $0.17 \sqrt{f'_c} b_w d$ and at displacement ductility of -3.0 with value of $0.186 \sqrt{f'_c} b_w d$. Because of

the steel plates resistance, the stirrups carried small percentage of shear. The actual compressive strength of the concrete f'_c determined by cylinder test on the day of experiment, was used in this calculation.

4.4.3 Shear in joints

The shear force in the joint is resisted by the concrete and the transverse reinforcement. To determine the shear force in the joint, the following expression was used

$$V_t = A_s f_s - V_{col} \quad (4.3)$$

where V_t is the total joint shear force, A_s is the area of the tensile reinforcement in the beam, f_s is the stress in the longitudinal tensile reinforcement in the beam and V_{col} is the column shear force. The shear force in the column can be obtained by static equilibrium using equation 2.3 including the P- Δ effect. The joint shear is plotted against the drift angles for the six specimens and is presented in figures 4.9 to 4.14. The shear force resisted by the transverse reinforcement was calculated as $V_s = A_v f_{st}$ where A_v is the total area of the transverse reinforcement in the joint and f_{st} is the stress in the joint transverse reinforcement calculated using the averaged strains measured by the strain gauges.

The results given in figure 4.9 for specimen J1 show that the concrete carried the total joint shear up to approximately 1% drift. At 3.5% drift, the total joint shear dropped below 100 kN. The joint ties carried part of the joint shear until they yielded. The strain gauges on the joint ties for specimen J2 did not work following the pouring of the concrete. For this reason, figure 4.10 shows only the total joint shear. The results given in figure 4.11 for specimen J3 show that the corrugated steel jacket confined the concrete such that at 4% drift the concrete carried approximately 50% of the joint shear.

Due to the absence of joint ties in specimen J4, the total joint shear was carried by the concrete as shown in figure 4.12. The ultimate joint shear carried by unreinforced joint (580 kN) averaged about 1.09 times the cracking shear (533 kN) given by the ACI 318-71 (1971):

$$v_c = 0.29 \sqrt{f'_c} \sqrt{1 + 0.29 \frac{P}{A_g}} \quad \text{MPa} \quad (4.4)$$

$$V_c = v_c b_j h_j$$

where P is the axial load on the column, A_g is the gross area of the column cross section, b_j is the joint width, h_j is the joint depth and f'_c is the concrete compressive strength. The ratio of experimental cracking shear force (490 kN) at first visible crack, to the theoretical cracking shear force (533 kN), averaged about 0.92. This indicates that equation 4.4 gives a reasonable estimate of the cracking shear. The results given in figure 4.13 for specimen J5 show that the concrete was confined by the corrugated steel jacket as it carried most of the joint shear up to 3% drift. The results given in figure 4.14 for specimen J6 show the effect of concrete confinement by the jacket particularly on the negative side compared with the result of specimen J4 in figure 4.12. In the positive direction of loading, specimen J6 suffered failure of the rehabilitation plate system attached to the beam.

4.4.4 Shear deformation of joints

Shear deformation in the joint provides a measure of joint stiffness. The two LVDTs placed diagonally across the corners of the joint panel measured the elongation and shortening of the diagonals with load. The average shear deformation of the joint panel was computed using the model suggested by Beckingsale et al. (1980) as shown in figure 4.15. The average

shear deformation γ_{average} is given by

$$\gamma_{\text{average}} = \frac{\Delta_1 + \Delta_2}{D \sin 2\theta} \quad (4.5)$$

where Δ_1 and Δ_2 are the change in the lengths of the diagonals, D is the length of the diagonal and θ is the angle between the diagonal and the horizontal member. The joint shear versus joint shear deformation for the different specimens are shown in figure 4.16. The joint shear deformation of specimen J3 with corrugated jacket is very low compared with that of J1. Bond slip of the beam bottom reinforcement of specimen J1 occurred in cycle #9 which reduced the joint shear deformation. The beam bottom bar pull out of specimen J4 reduced the shear deformation in the positive direction as compared with the other loading direction. The corrugated steel jacket reduced the shear deformation significantly in specimens J3, J5 and J6. The drift versus joint shear deformation plots of the specimens are shown in figures 4.17a and 4.17b. A comparison of the joint shear deformation for the same drift shows that the joint shear deformation is progressively reduced from specimen J1 to specimen J3 and that the corresponding shear stiffness is substantially improved in the same order. Specimen J4, which had no joint confining reinforcement, showed excessive shear deformation and stiffness degradation in the joint. After the pullout of the bottom reinforcement, the joint-shear deformation decreased to zero for the positive loading.

4.5 MEMBER CONTRIBUTION TO DRIFT ANGLE

The contribution of different members to specimen deformation gives a good indication of the behaviour of the specimen and helps in visualizing the possible mode of

failure. Joint distortion γ was calculated as the difference between the vertical joint angle α and the horizontal joint angle β as shown in figures 2.13a and 4.15.

The member contribution components to the drift angle R are R_b , R_c and R_j for beam, column and joint, respectively. The contributions were calculated as the ratio of the components of drift angle (R_b , R_c and R_j) over the imposed drift angle R using the procedure presented by Alcocer and Jirsa (1991):

$$R_b = R - \alpha + \gamma \frac{h_c}{L} \quad (4.6)$$

$$\gamma = \alpha - \beta \quad (4.7)$$

$$R_c = \frac{h_b}{H} \alpha + \beta - \frac{h_b}{H} \beta = \beta + \frac{h_b}{H} \gamma \quad (4.8)$$

$$R_j = \gamma \left(1 - \frac{h_c}{L} - \frac{h_b}{H} \right) \quad (4.9)$$

where H is the column height, h_c is the column depth and h_b is the beam depth. The summation of R_b , R_c and R_j equals the imposed drift angle R . Any of the drift components multiplied by the specimen height H gives the element's contribution to the interstory drift. For convenience in the presentation, the components of drift angle were multiplied by one hundred to give values in percent. The column contribution depended mainly on the magnitude of the horizontal joint angle β while the beam and joint contribution were governed by the vertical joint angle α . The angle α is always greater than β .

Member contributions to drift angle for the specimens J1 to J6 are presented in figures 4.18a to 4.18f, for positive drift and in figures 4.19a to 4.19f for negative drift. In general, at large deformation levels, an increase in the participation of the most damaged element was

accompanied with a severe loss of strength. For specimen J1 the column contribution which was large at the first stages of the test diminished by the end of the test when joint deformations contributed more to the total drift. After cycle #7 (2.7% drift), the joint contribution increased rapidly and accounted for 65% of the total drift by the end of the test (figure 4.19a). The specimen can be considered to have failed in cycle #9 (3.5% drift) due to severe joint distress. Comparison of contributions during tests J1 and J3 shows that the behaviour of specimen J1 was modified substantially. A joint failure system (specimen J1) was replaced by a weak beam-strong column system (specimen J3), in terms of strength, stiffness and ductility. In the case of specimen J3, the beam initially contributed 25% of the total deformation which steadily increased to 80%. Column contribution remained practically constant throughout the test whereas the joint contribution decreased with increasing story drift. The joint corrugated steel jacket proved to be effective in confining the concrete core thus preventing the brittle shear failure.

Comparing the differences between the specimens, the joint component of J1 increased remarkably with story drift and had already exceeded 50% of the total drift by the time 1% story drift was achieved (figures 4.18a and 4.19a). The contributions of the joint of specimens J2 and J3 to drift angle were approximately less than 25% and 30%, respectively as shown in figures 4.18a, 4.18b, 4.19a and 4.19b. There was little observed difference in the contribution of the joint of specimen J3 with jacket on column and beam and J5 with jacket on column only.

Member contributions to drift angle for all specimens are plotted in figure 4.20. Results are presented for the first positive cycle at a given ductility level, i.e. ductility factors

1, 2, 3 and 4. From this figure, it is clear that jacketing modified the behaviour of the existing structure so that all rehabilitated specimens behaved as "strong column - weak beam" systems, in which beam contributions were the largest throughout the test.

4.6 STIFFNESS

Satisfactory seismic design of structures requires designers to provide a balance of strength, stiffness, ductility and energy dissipation capacity. These parameters must be based on a number of factors, including the expected ground motion at the site, dynamic characteristics of the soil and the structure, structural system and materials, and intended use of the building. Ideally, the stiffness should not degrade with cyclic loading, must be large enough to control drift and should be consistent with deformation limits of nonstructural elements. Almost all reinforced concrete members experience stiffness degradation with loading. Stiffness degradation of reinforced concrete structures is attributable to concrete spalling, bond degradation, opening and closing of residual cracks, the Bauschinger effect in the reinforcing steel and decrease of the modulus of elasticity of the cracked concrete when subjected to alternating loads (Park and Paulay, 1975).

In this study, the stiffness of the specimens was evaluated using peak-to-peak stiffness (Secant stiffness) for both load versus displacement and story shear versus interstory drift relationships. The peak to peak stiffness is useful to represent the overall response of the specimen during a given cycle. The definition of peak-to-peak stiffness K_p is illustrated in figure 4.21 and is calculated as the slope relative to the abscissa of a line that joins load peaks in the same cycle.

The peak-to-peak stiffness for the specimens in each cycle are plotted versus the cycle number in figure 4.22. In the test two cycles of loading at the same displacement level were applied. The first of the two cycles at a given displacement level showed slightly higher stiffness than the second one because of some progressive decaying of the maximum values of the sustained load. The peak-to-peak stiffness versus the displacement ductility factor for the specimens are presented in figure 4.23.

The peak-to-peak stiffness values for the first cycle at a given displacement ductility factor level are given in table 4.2. A slower stiffness degradation was observed for the specimen J3 with corrugated jacket as compared to the specimen J1.

4.7 ENERGY DISSIPATION AND EQUIVALENT VISCOUS DAMPING FACTOR

4.7.1 Dissipated energy by the specimens

During major earthquakes a tremendous amount of energy is released. If the building is to withstand the earthquake without collapse, it must be capable of absorbing and dissipating energy through kinetic energy, viscous damping energy, recoverable elastic strain energy and irrecoverable inelastic (hysteretic) energy. The energy dissipated by a structure is important since the ability to dissipate energy has a strong influence on the response of the structure to dynamic loading. The foundation flexibility, soil internal damping and radiation damping may also be sources of energy dissipation. In a satisfactory design, the energy dissipation capacity of the structure should be larger than the energy demand.

The energy dissipated by a structure consists of: a) energy dissipated by steel reinforcement; b) energy dissipated by friction along existing cracks in concrete which occurs mostly when the displacements are relatively small and is attributed to opening and closing of cracks, slipping along shear cracks, and slippage of reinforcing bars; and c) energy dissipated during the formation of new cracks including the crushing of concrete which occurs when the displacements are sufficiently large to cause new damage. For each specimen, the energy dissipated in each cycle was obtained by calculating the area enclosed by the corresponding load-displacement hysteretic loop. The cumulative energy dissipated was obtained by summing the energy dissipated in consecutive loops throughout the test. Table 4.3 gives the energy dissipated at different ductility levels for each specimen. The results indicate that in any cycle, the energy dissipation values for specimen J3 with steel jacket were approximately 1.2 times that for specimen J1. The values for the cumulative energy dissipated for each specimen are calculated and plotted versus the cycle number and versus the displacement ductility factors as shown in figures 4.24 and 4.25, respectively. The results indicate that the specimen with corrugated steel jacket exhibited considerably higher values for cumulative energy dissipation as compared with specimen J1.

4.7.2 Equivalent viscous damping factor

Internal damping can be the product of several mechanisms, which include plastic deformation of metals and the friction between intergranular faces in most structural materials, such as aggregate interlock in structural concrete. These energy dissipation mechanisms vary with the frequency and are generally referred to as viscous damping. Coulomb damping, independent of frequency, is associated with the friction between

intergranular surfaces, and is sometimes called hysteretic damping. Therefore, Coulomb damping necessarily involves non-linear variation of displacement with static loads.

It is possible to determine the amount of equivalent damping that would make a linear system have the same response as a non-linear structure subjected to a given periodic excitation. Equating the energy dissipated per cycle in the non-linear structure to its linear equivalent, the equivalent damping can be computed. Although the equivalent damping is associated with the energy dissipated per cycle, i.e. related to the hysteretic damping, the equivalent damping is often referred to as equivalent viscous damping factor.

The definition of equivalent viscous damping factor ξ is shown in figure 4.26. It was taken as the ratio of the dissipated energy within a cycle to 2π times the strain energy measured at the peak of an equivalent linearly elastic system. The equivalent viscous damping factor was used to compare the energy dissipation capacity of the specimens. It also represents an indirect measure of pinching of hysteretic loops.

The variation of equivalent viscous damping factor ξ for each specimen with the displacement ductility factor is shown in figure 4.27. In general, damping ratios increased with increasing displacement ductility factor. The equivalent viscous damping factor of each cycle loop are listed in brackets in table 4.3. After yielding, damping of specimens J1 and J4 modelling the existing structure increased from approximately 5% pre-yield value to approximately 17% before failure. The change in specimen behaviour after rehabilitation was evident from the increase in the equivalent viscous damping of specimens J3, J5 and J6. The rehabilitated specimens J3, J5 and J6 and the code designed specimen J2 demonstrated stable energy dissipation, with the damping ratio increasing from approximately 5% pre-yield value

to approximately 25% at the displacement ductility level corresponding to the ultimate resistance of the specimens. The drop in specimen resistance at higher ductility levels produced a reduction in damping. Rehabilitated specimens have larger equivalent viscous damping factor than the unrehabilitated specimens and it was found to have superior energy absorption ability.

4.8 SLIPPAGE BETWEEN STEEL JACKET AND GROUT

To investigate relative displacement between the steel jacket and the grout in the transverse direction, two LVDTs were installed to measure the relative movement between the grout and the corrugated steel as shown in figure 4.28a. The slip versus displacement ductility factor for specimen J6 is shown in figure 4.28b. There is no slip until displacement ductility factor of 4.0. At low ductility levels, the perpendicular corrugated steel at the corner of the jacket prevent the horizontal slip between the grout and the corrugated steel.

4.9 LATERAL CONFINEMENT PRESSURE AT JOINT REGION

An attempt was made to measure the confinement pressure between the jacket and the concrete of specimen J6 (without joint ties). Two load cells were installed between the existing concrete and the grout as shown in figure 4.29a. The locations of the load cells are shown in figure 4.29b. The measured confinement stress versus displacement ductilities at the load cell locations are shown in figure 4.30. The corrugated steel jacket and the non-shrink grout confined concrete in the compression strut of the joint. The confinement pressure on the concrete reached 8 MPa (load cell #1) at displacement ductility factor of 6.0

which is about 35% f'_c . The confinement stress from load cell #1 increased rapidly after ductility of two which indicates increase in the compression stress of the compression strut in the joint. The confinement stress at the column region above the joint reached 6 MPa (load cell #2) at displacement ductility of 6.0. The measurements indicate that the jacket not only acts in shear but also acts in resisting the lateral pressure from the concrete. Difficulties were encountered due to the malfunction of the load cells. Due to the lack of sufficient data no attempt was made to analyse the state of stress and strain near the installed cells in the grout.

4.10 SUMMARY

The analysis of results confirmed that jacketing of frame elements improved the response of the existing structure. Member contribution to drift angle showed that rehabilitated specimens developed a strong column-weak beam response as opposed to the joint shear failure behaviour of the existing structure. Maximum strength of the existing specimen was achieved at 1.85% drift level while that for the rehabilitated specimen was achieved at 3.5% drift level. A slower stiffness degradation was observed for the rehabilitated specimens compared with the existing specimens. Specimens with corrugated steel jacket exhibited considerably higher values of cumulative energy dissipation.

Table 4.1 Comparison of beam yield moments

Specimen	Calculated yield moment M_{cal} (kN.m)	Experimental yield moment M_{exp} (kN.m)	M_{exp}/M_{cal}
J1	321	+358 -347	1.11 1.08
J2	325	+386 -380	1.19 1.17
J3	321	+390 -370	1.21 1.15
J4	300	No yield -358	NA 1.11
J5	325	+364 -347	1.12 1.07
J6	300	+340 -369	1.13 1.23

Table 4.2 Experimental peak-to-peak stiffness K_p (kN/mm)

Displacement Ductility Factor	Specimen					
	J1	J2	J3	J4	J5	J6
1	29	30	30.5	20.6	31	32.4
2	15.28	14.73	16.79	10.45	17.7	18.09
3	8.84	10.07	12.06	3.08	12.47	10.15
4	3.49	5.94	9.26	2.02	7.4	6.22
6	NA	2.61	5.31	NA	4.34	4.46

Table 4.3 Energy dissipated in each cycle (kN.m) and the equivalent damping factor

Specimen	factor =1		factor =2		factor =3		factor =4		factor =6		factor =8		factor =10	
	Cycle #1	Cycle #2	Ductility Cycle #1	Ductility Cycle #2	Ductility Cycle #1	Ductility Cycle #2	Ductility Cycle #1	Ductility Cycle #2	Ductility Cycle #1	Ductility Cycle #2	Ductility Cycle #1	Ductility Cycle #2	Ductility Cycle #1	Ductility Cycle #2
J1	3949.7 (12.3)	2887.2 (9.0)	12023.9 (17.6)	8541.6 (14.2)	19149.0 (18.1)	18734.5 (17.6)	11384.8 (15.5)	9332.1 (13.9)						
J2	4418.2 (12.6)	3364.2 (8.9)	13385.8 (20.6)	12514.9 (19.3)	21306.2 (22.7)	18948.9 (20.8)	29224.5 (25.2)	19700.0 (19.4)	29419.4 (21.5)	16208.6 (16.1)	21974.3 (15.7)	15486.7 (13.3)	18971 (13.2)	16249.1 (9.1)
J3	4056.4 (13.5)	2640.9 (9.3)	14098.4 (20.7)	11872.7 (19.0)	22012.1 (23.1)	20614.6 (22.0)	32477.7 (24.2)	29346.0 (24.0)	49316.5 (28.5)	29131.4 (23.6)	30235.5 (22.5)	26724.4 (21.2)	28122.2 (19.3)	23179.1 (18.6)
J4	4907.1 (11.4)	4136.9 (8.5)	10868.7 (16.2)	7531.7 (15.9)	9234.9 (17.0)	5767.3 (14.6)	7788.0 (15.0)	5952.8 (14.1)						
J5	2037.1 (10.5)	1220.9 (6.5)	11826.9 (19.9)	9560.7 (16.8)	17899.9 (19.7)	14834.7 (16.4)	22939.7 (20.5)	15588.4 (16.2)	29298.6 (22.6)	15370.4 (21.0)	12002.5 (17.9)	8446.4 (16.5)		
J6	2964.0 (12.9)	2077.3 (8.8)	8963.6 (19.5)	6683.9 (16.4)	13067.5 (20.3)	8554.1 (17.3)	11419.9 (18.6)	8510.0 (15.5)	18643.7 (19.0)	12030.4 (13.9)	18975.3 (15.4)	14349.2 (13.0)	16703.6 (12.3)	8613.1 (7.1)

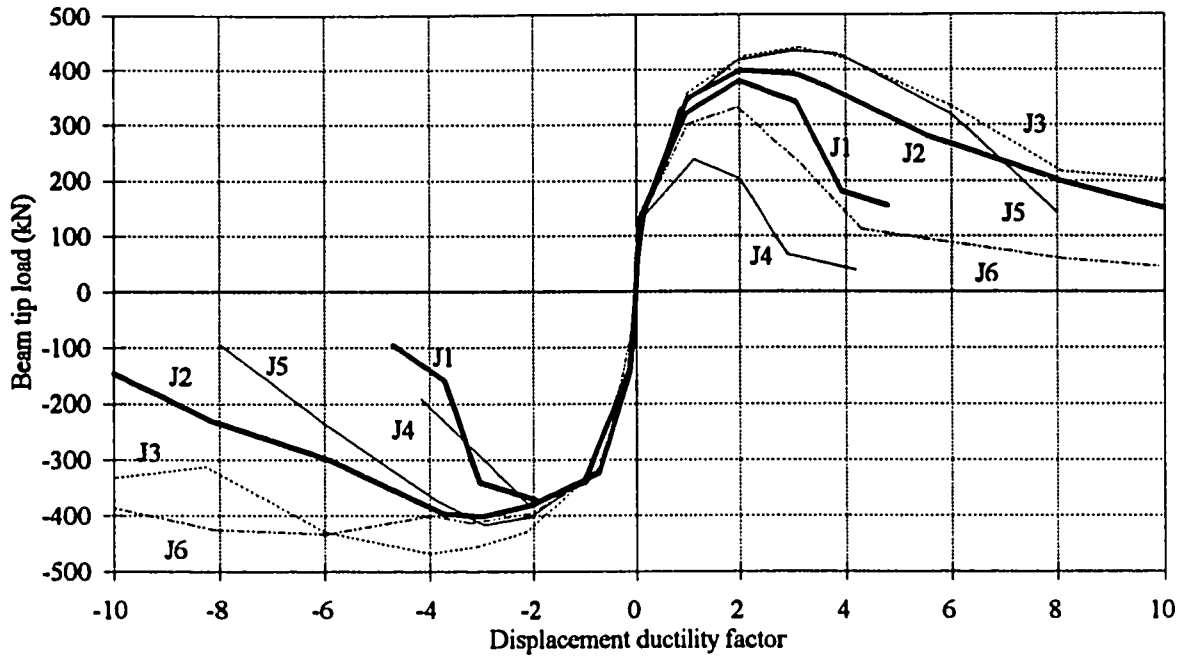


Figure 4.1 Comparison of load levels attained by specimens

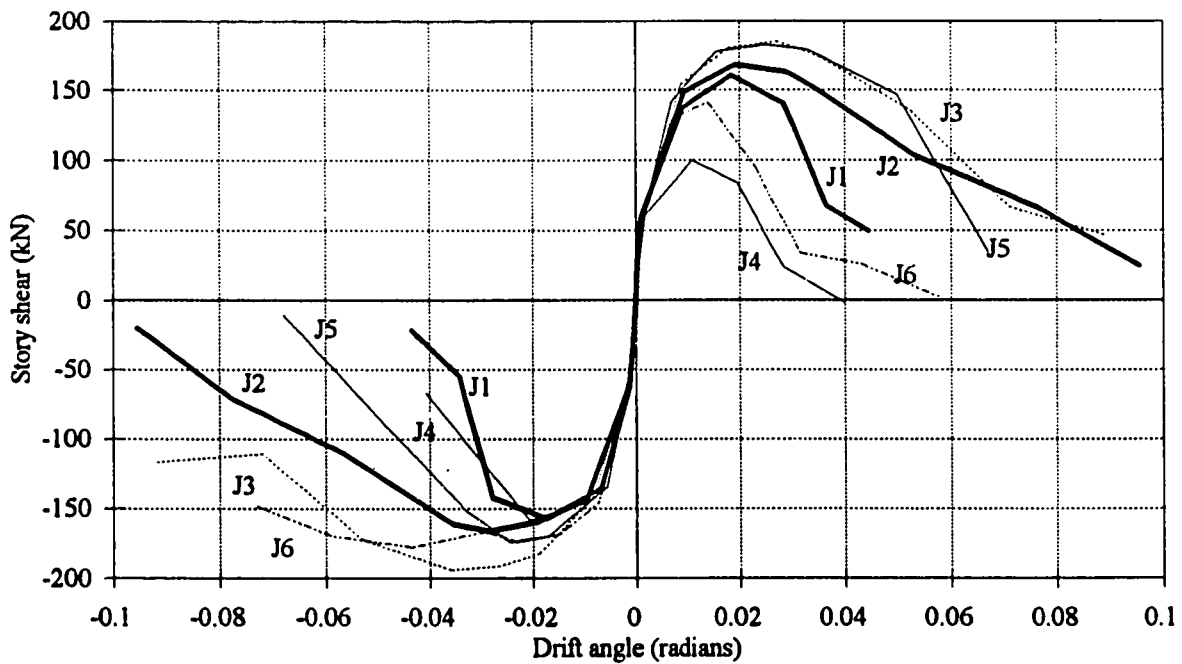


Figure 4.2 Comparison of story shear levels attained by specimens

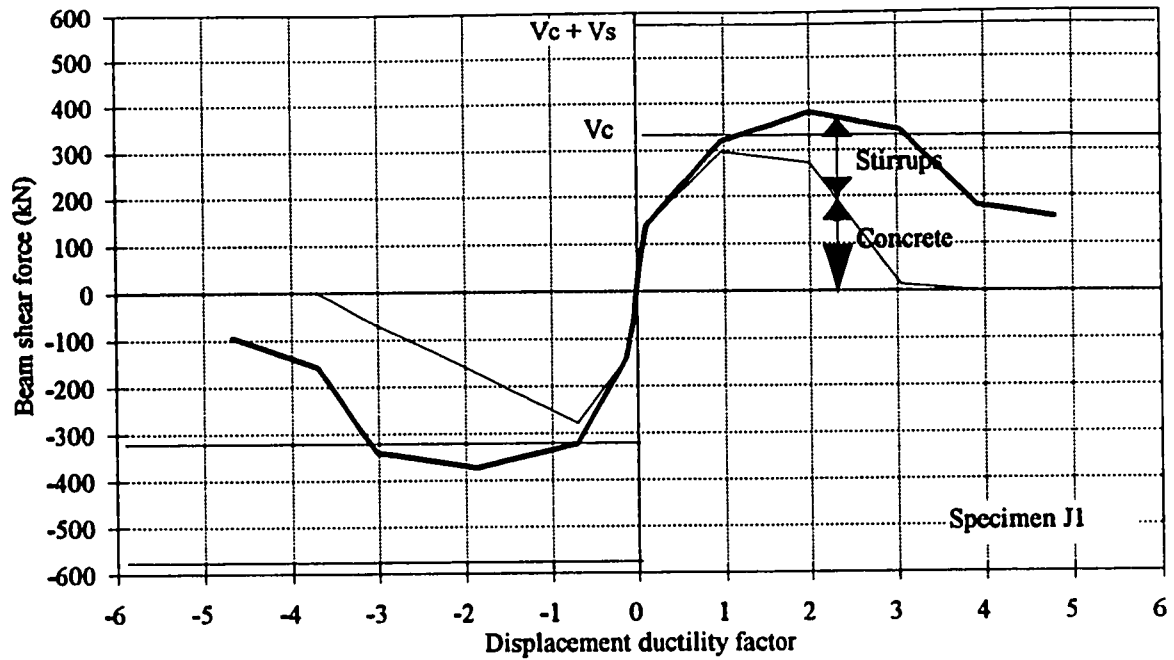


Figure 4.3 Beam shear force resisted by concrete and transverse reinforcement for J1

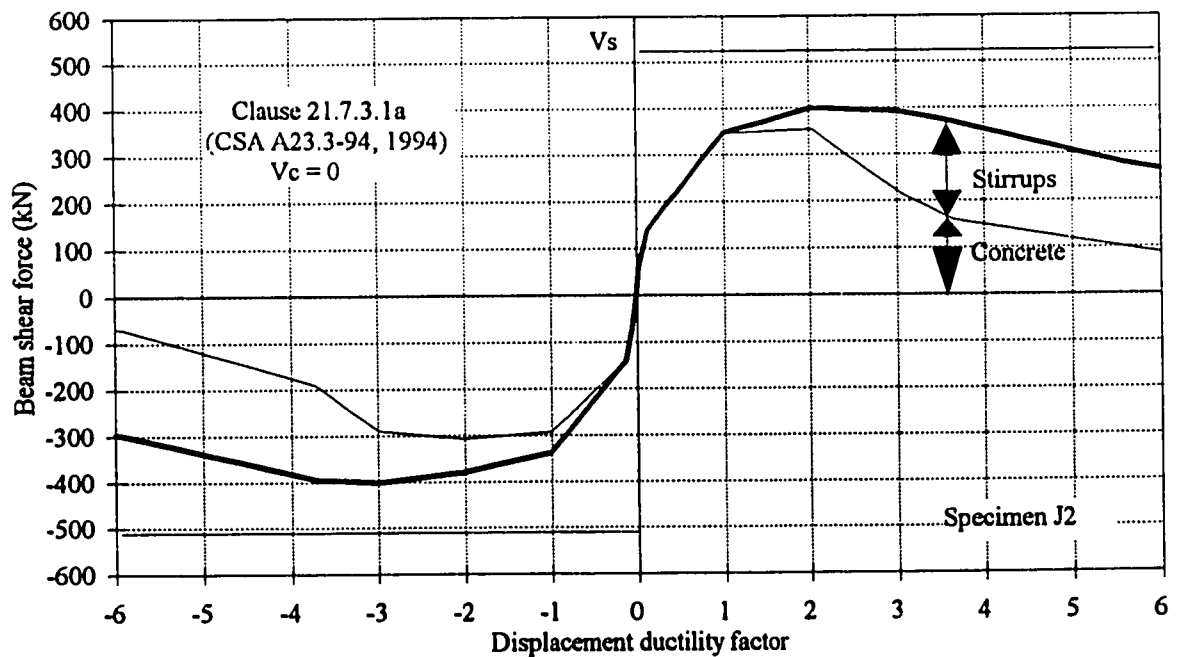


Figure 4.4 Beam shear force resisted by concrete and transverse reinforcement for J2

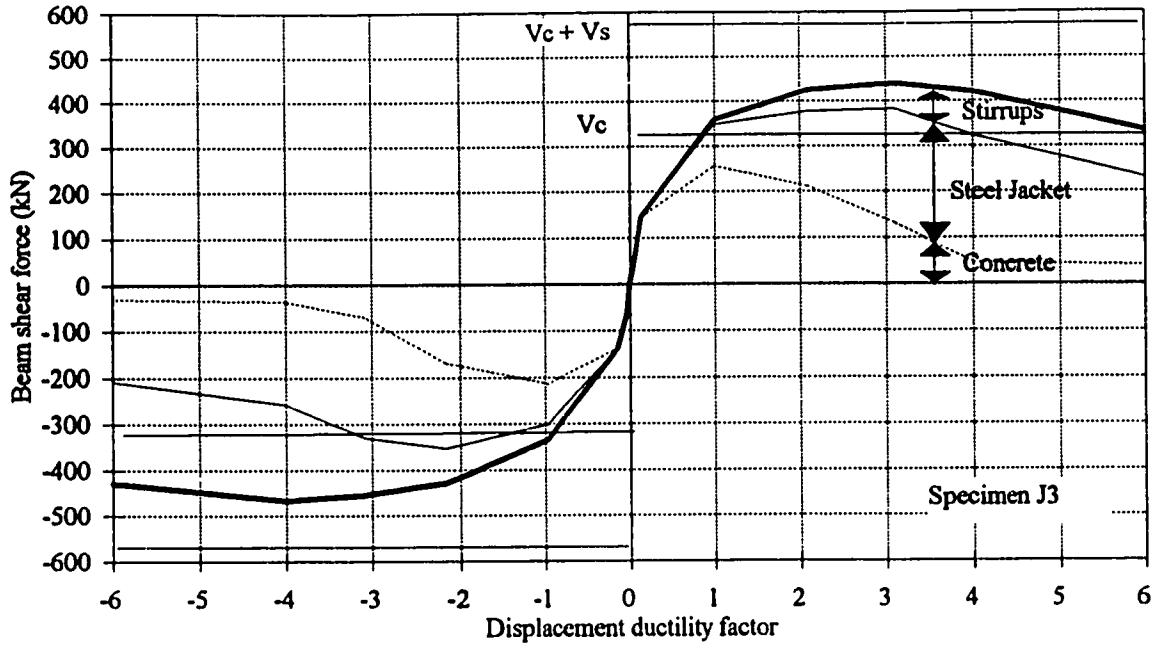


Figure 4.5 Beam shear force resisted by concrete and transverse reinforcement for J3

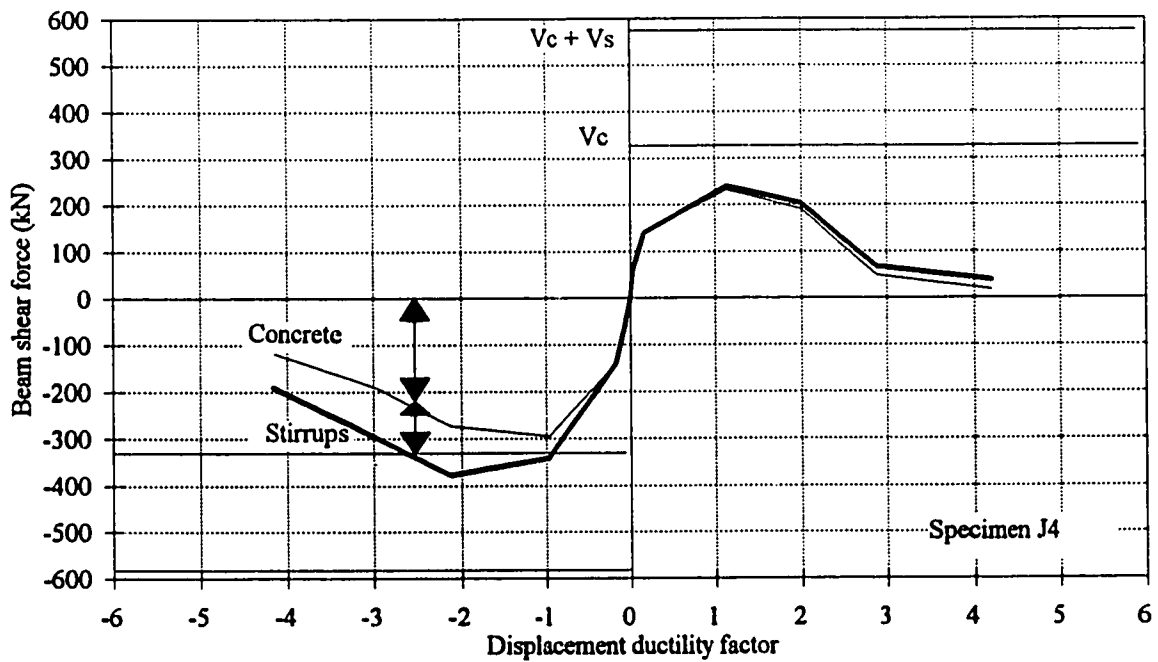


Figure 4.6 Beam shear force resisted by concrete and transverse reinforcement for J4

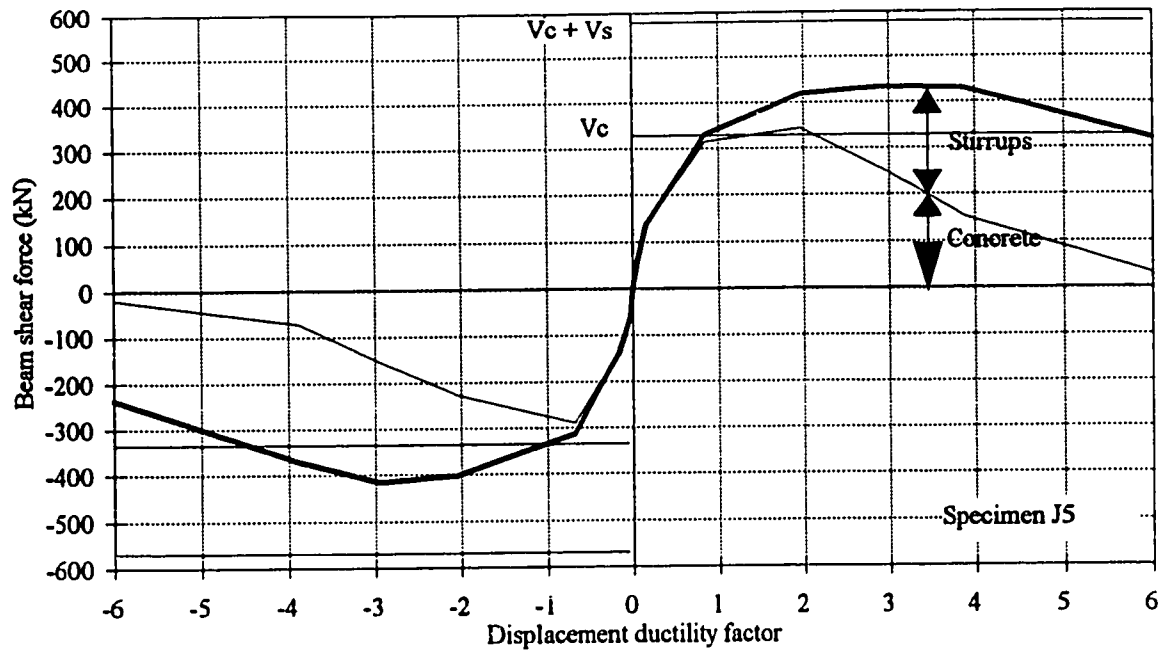


Figure 4.7 Beam shear force resisted by concrete and transverse reinforcement for J5

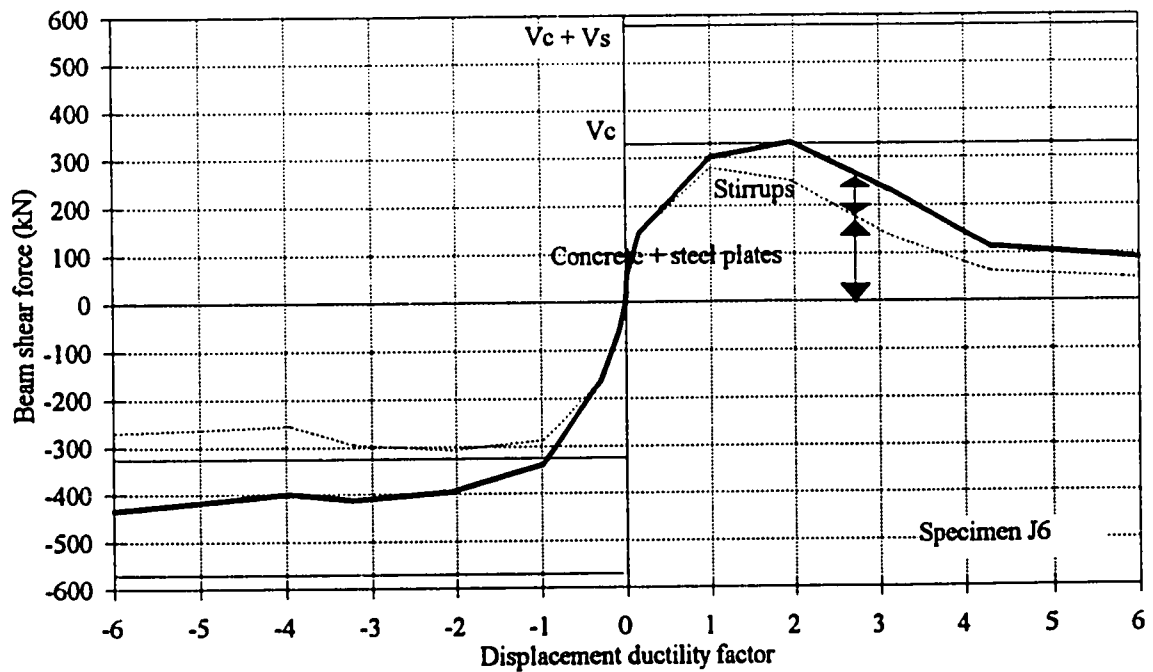


Figure 4.8 Beam shear force resisted by concrete and transverse reinforcement for J6

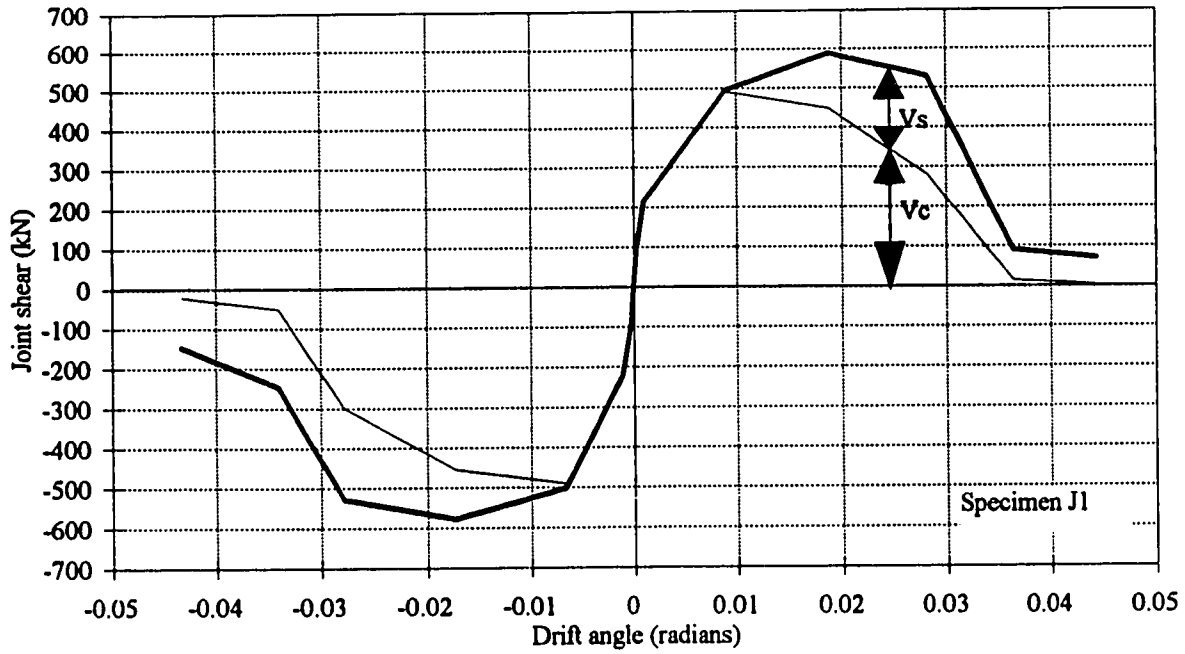


Figure 4.9 Joint shear resisted by concrete and transverse reinforcement for J1

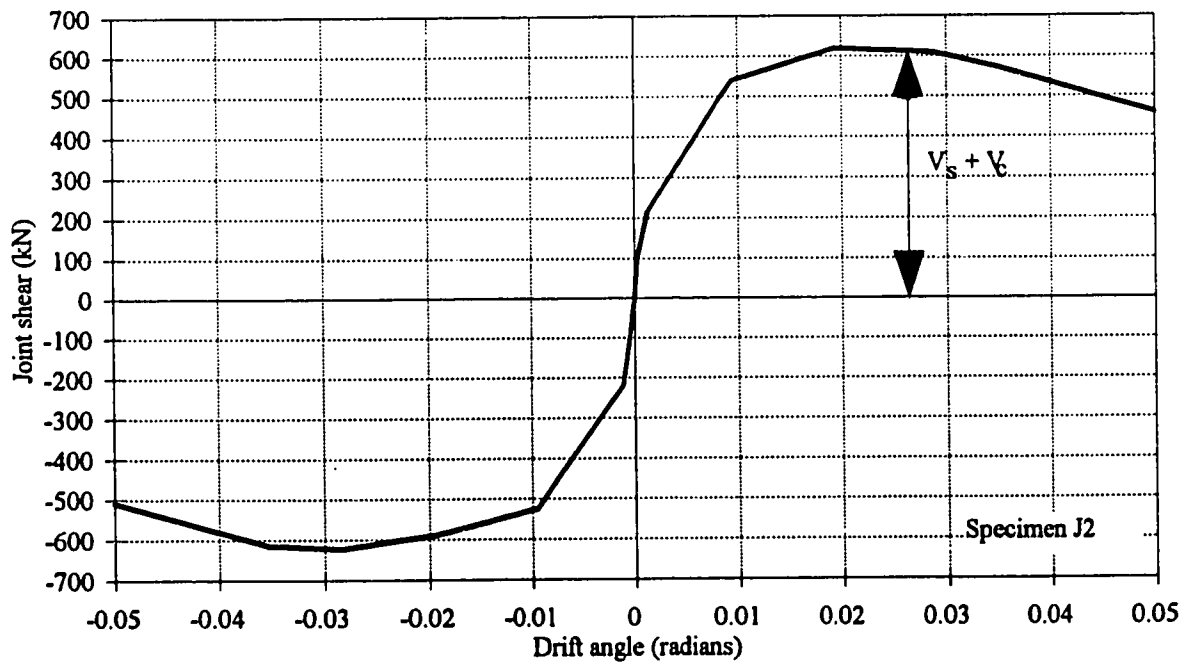


Figure 4.10 Joint shear resisted by concrete and transverse reinforcement for J2

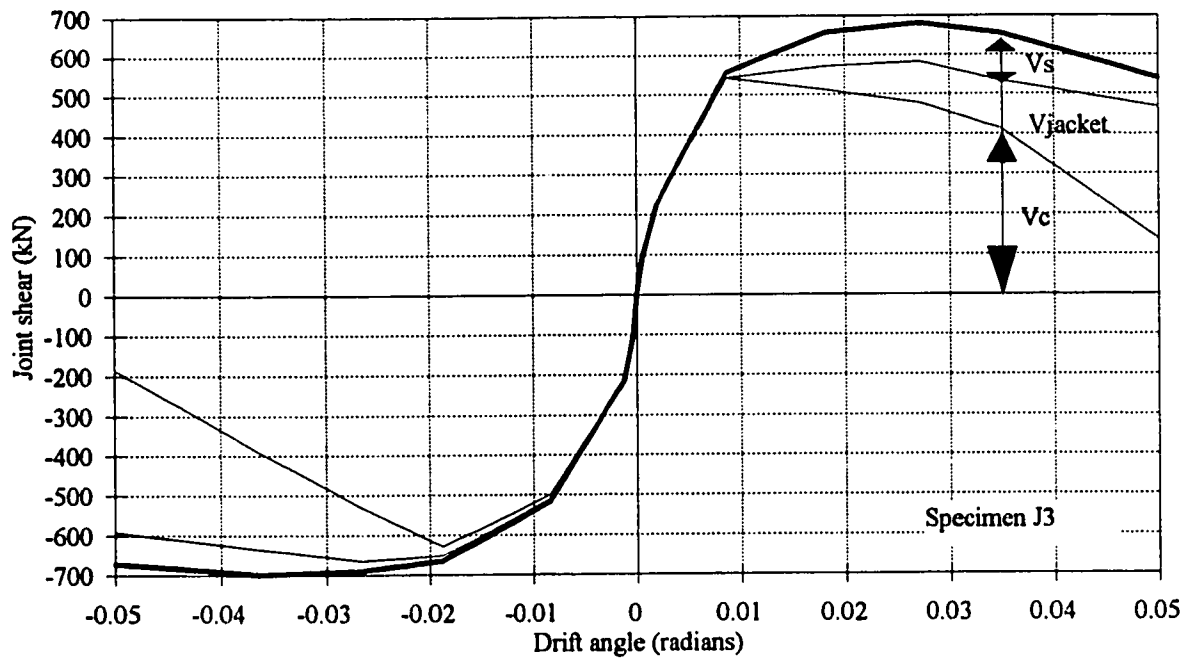


Figure 4.11 Joint shear resisted by concrete and transverse reinforcement for J3

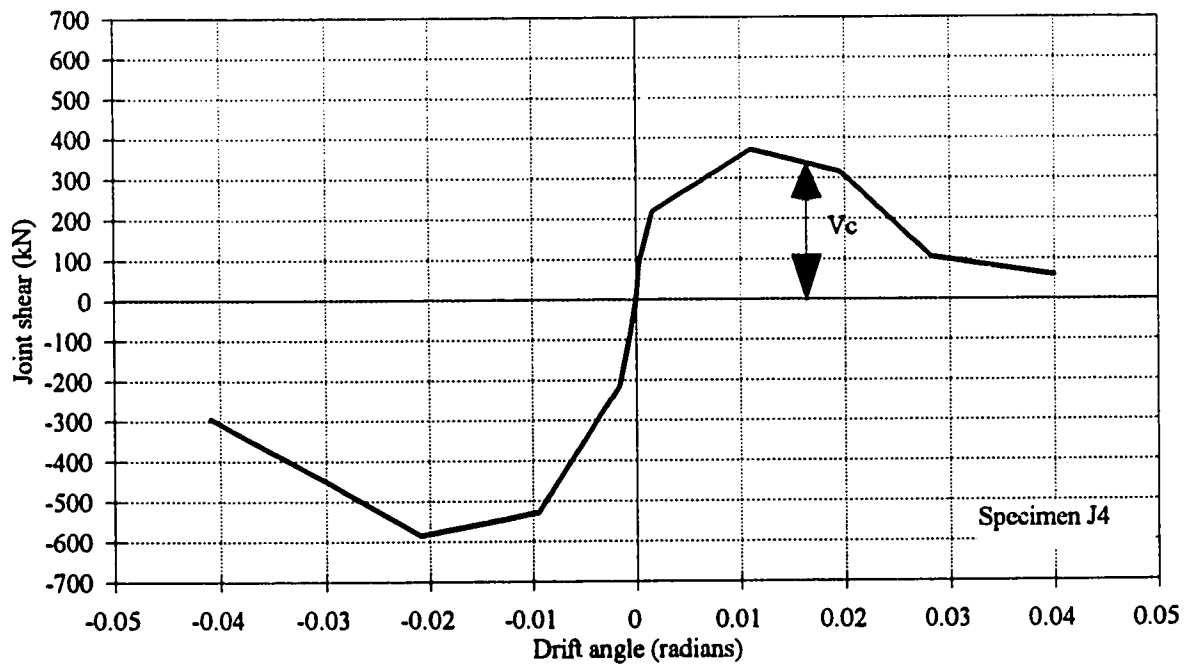


Figure 4.12 Joint shear resisted by concrete and transverse reinforcement for J4

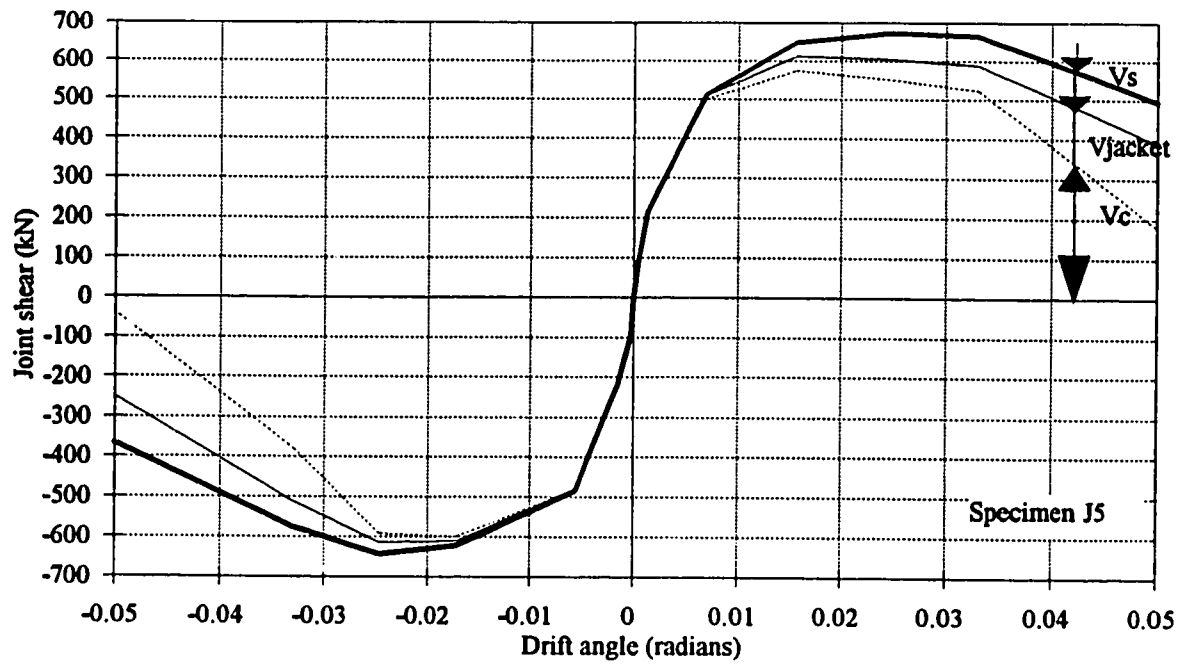


Figure 4.13 Joint shear resisted by concrete and transverse reinforcement for J5

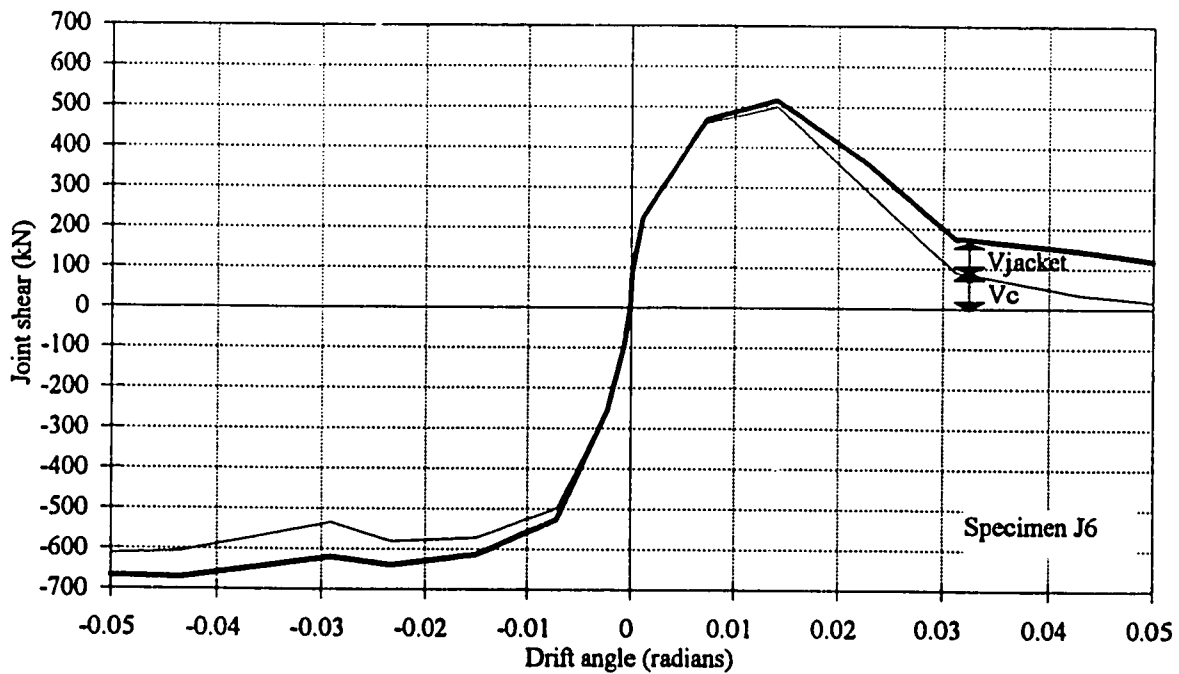


Figure 4.14 Joint shear resisted by concrete and transverse reinforcement for J6

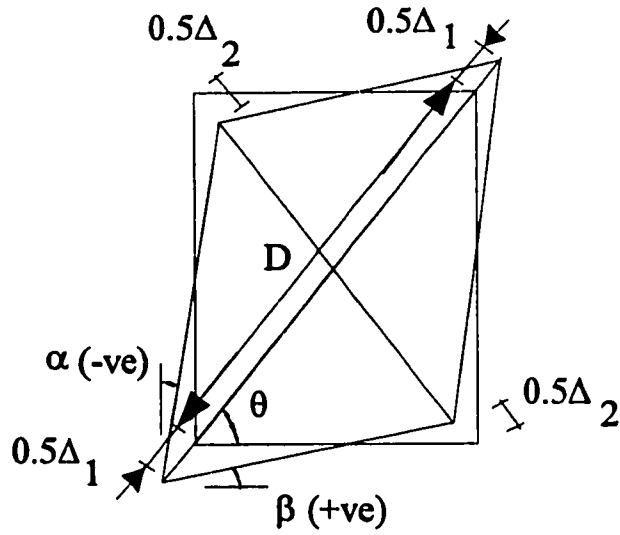


Figure 4.15 Joint shear deformation model

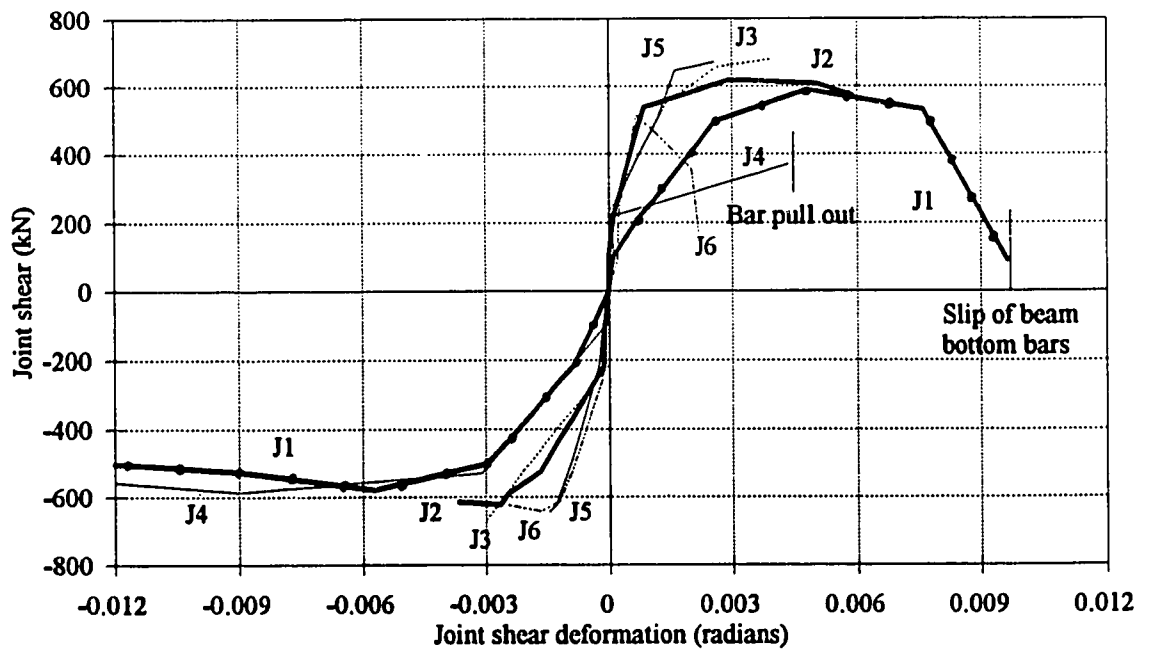


Figure 4.16 Joint shear-joint shear deformation

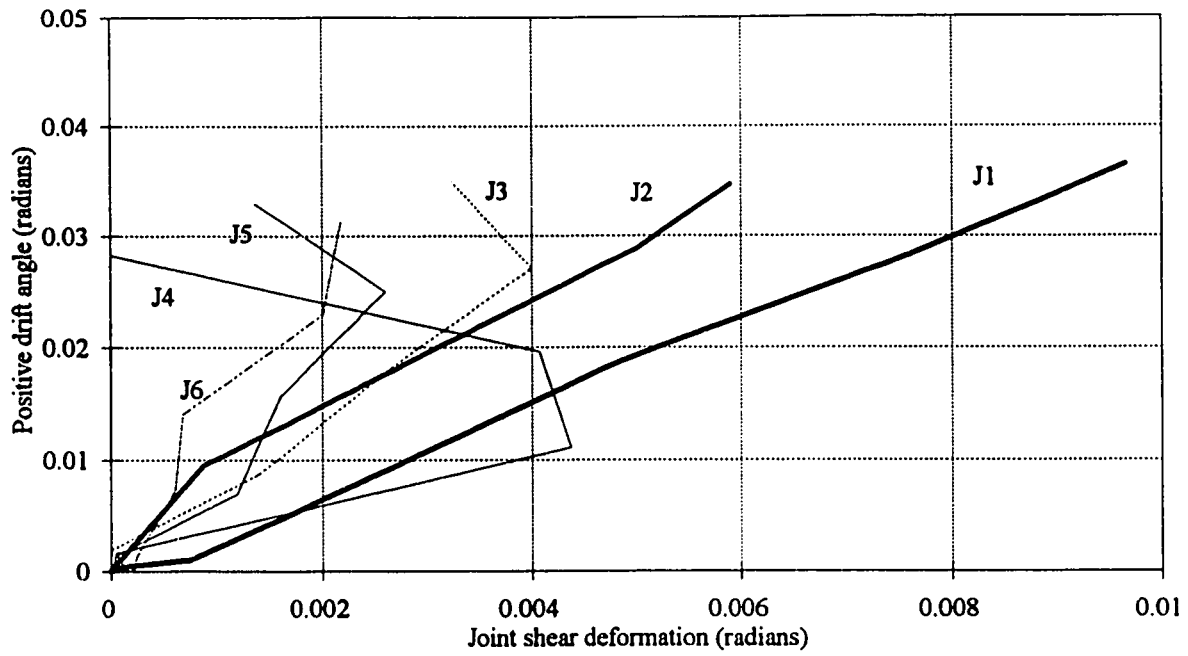


Figure 4.17a Positive drift angle-joint shear deformation

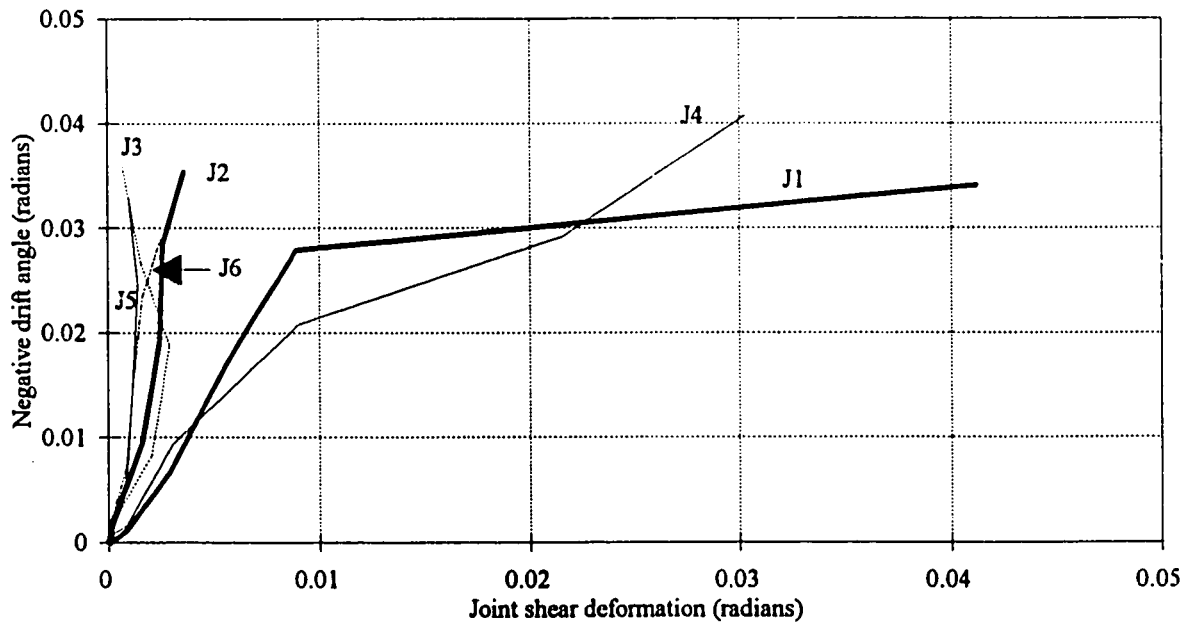


Figure 4.17b Negative drift angle-joint shear deformation

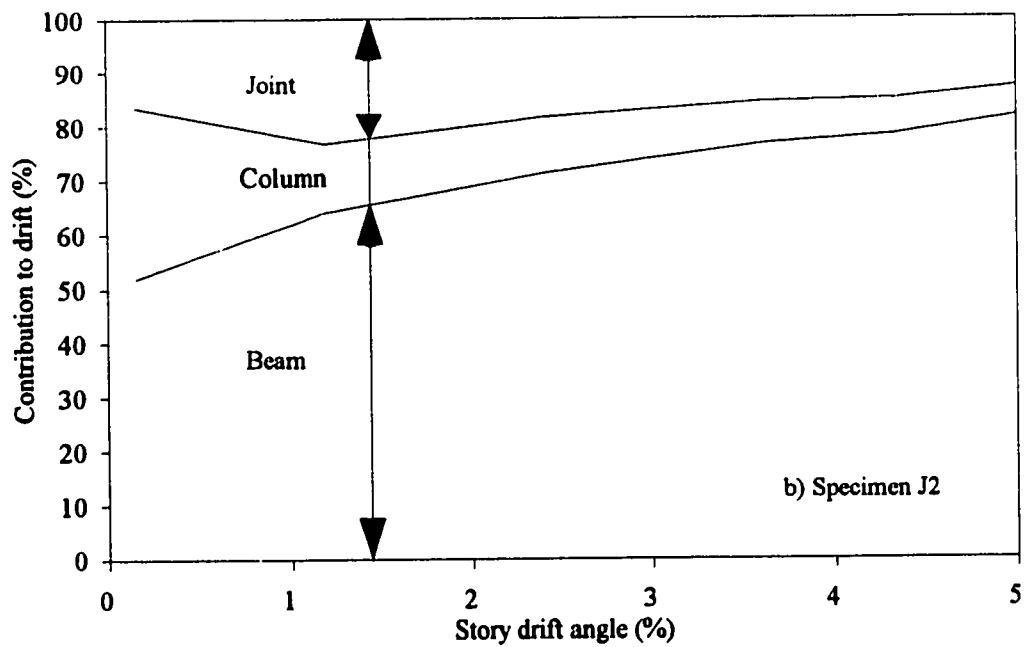
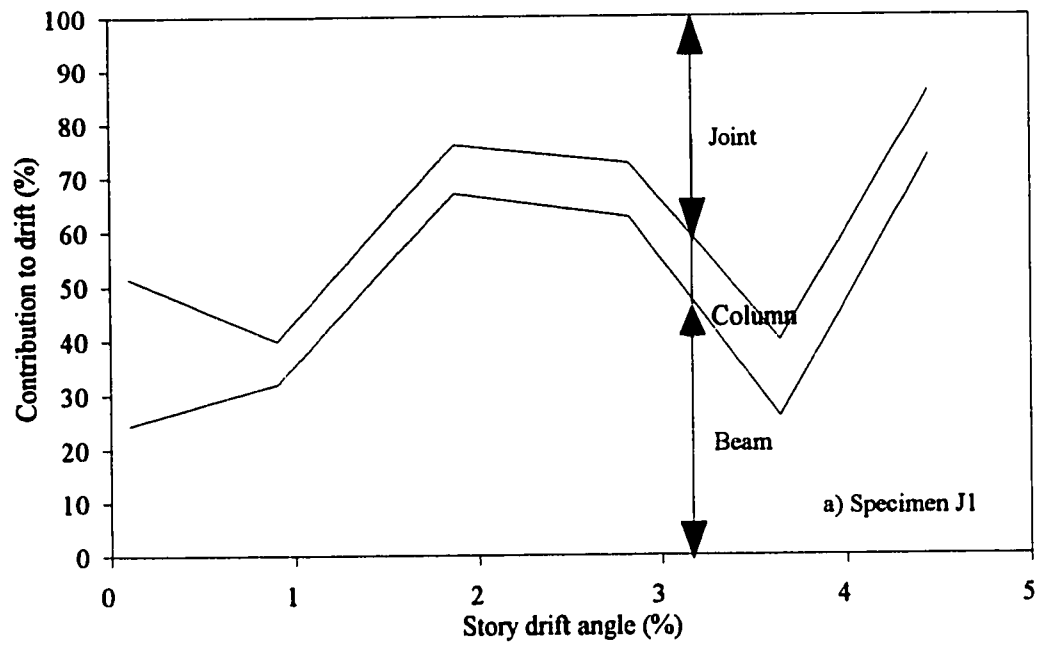


Figure 4.18a Contribution to story drift angle (positive drift) for specimens J1 and J2

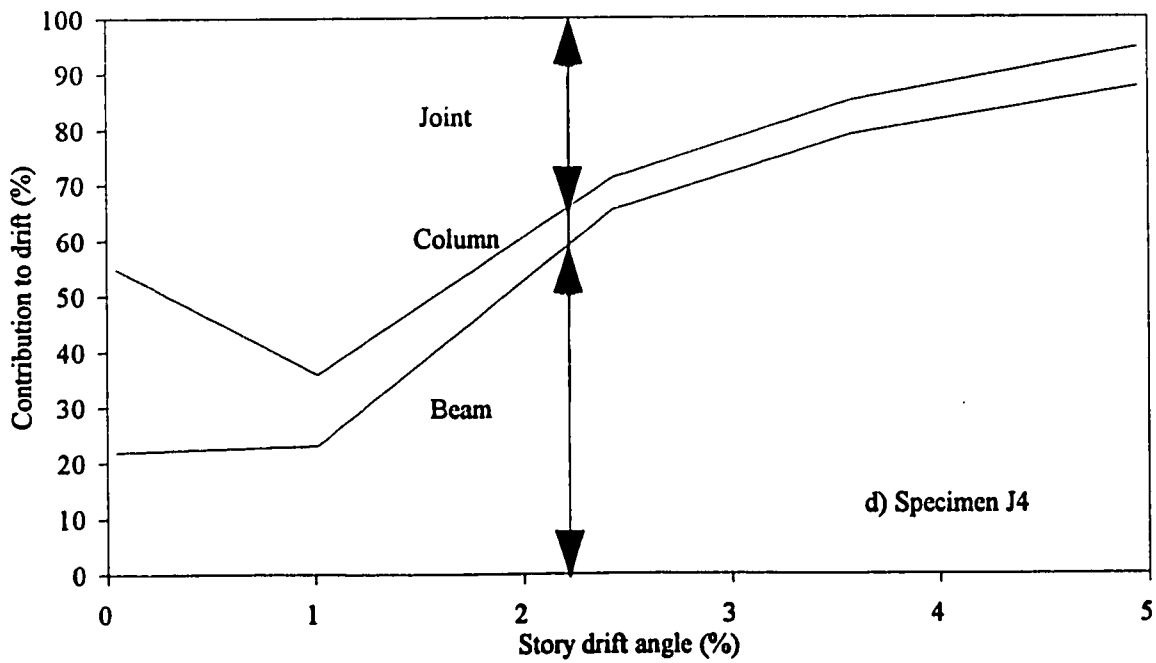
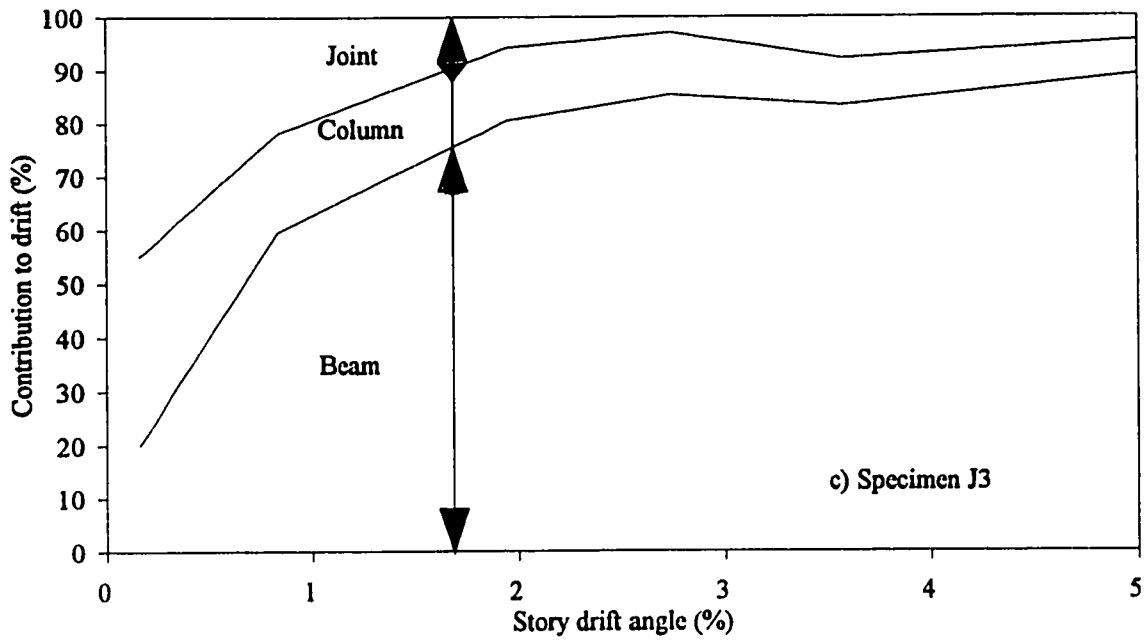


Figure 4.18b Contribution to story drift angle (positive drift) for specimens J3 and J4

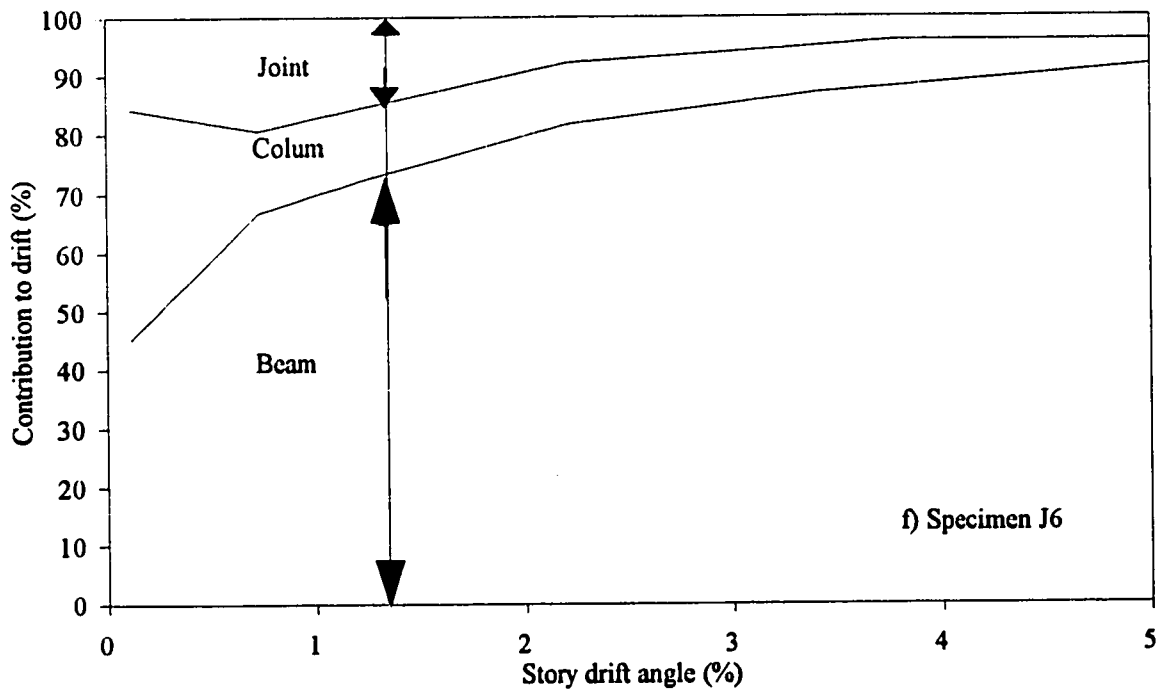
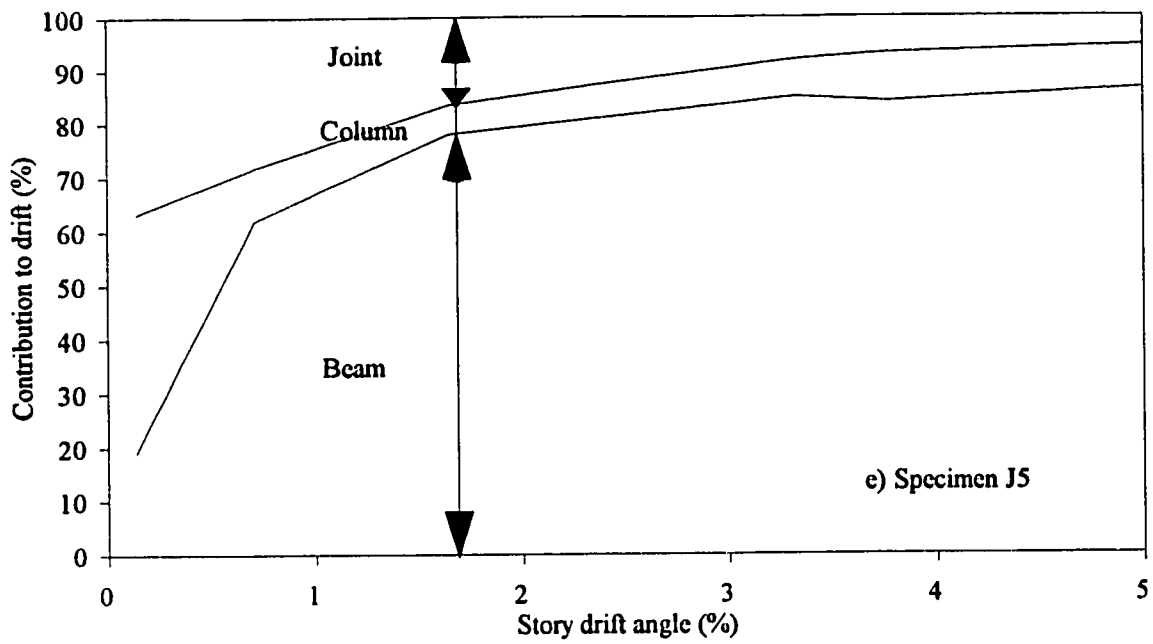


Figure 4.18c Contribution to story drift angle (positive drift) for specimens J5 and J6

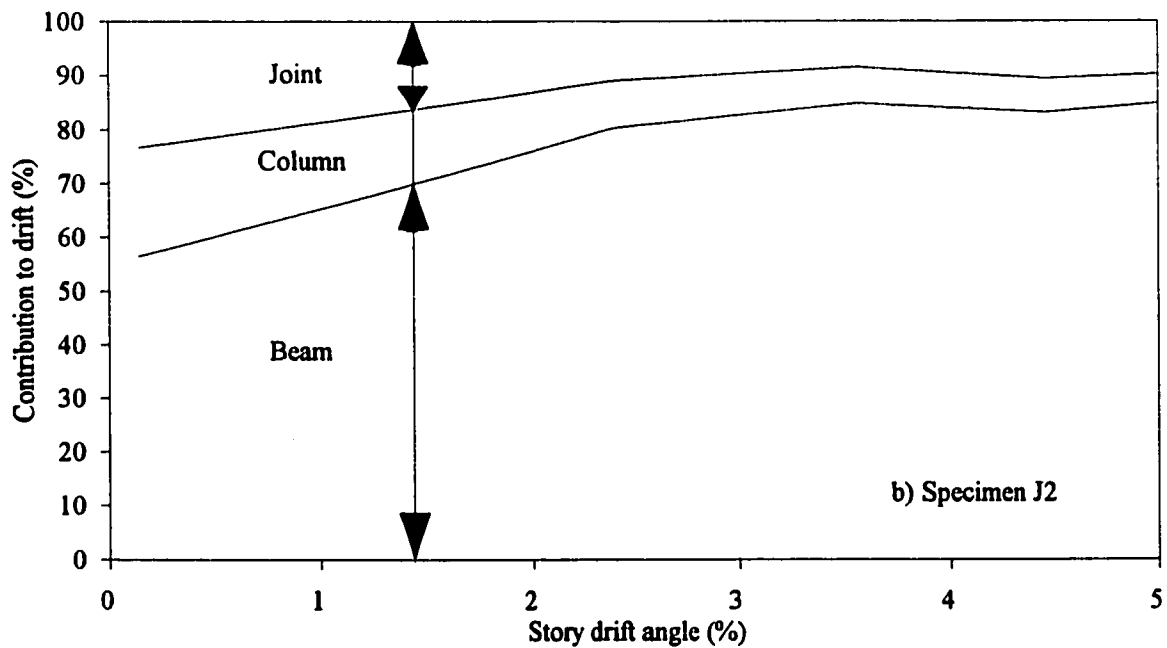
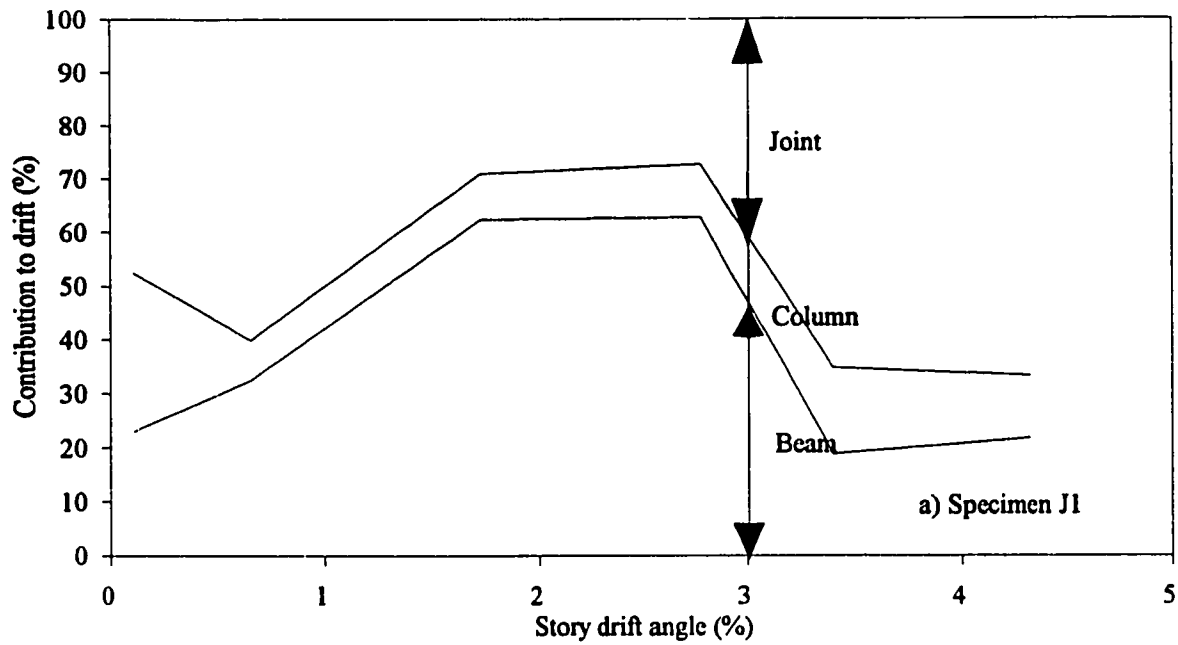


Figure 4.19a Contribution to story drift angle (negative drift) for specimens J1 and J2

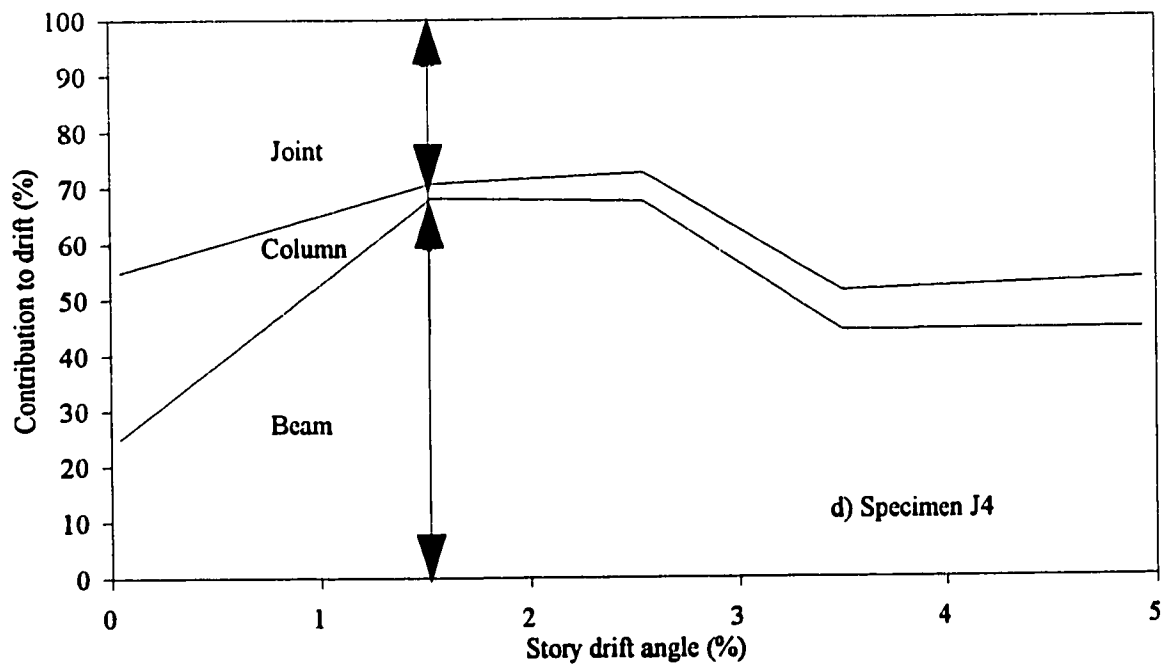
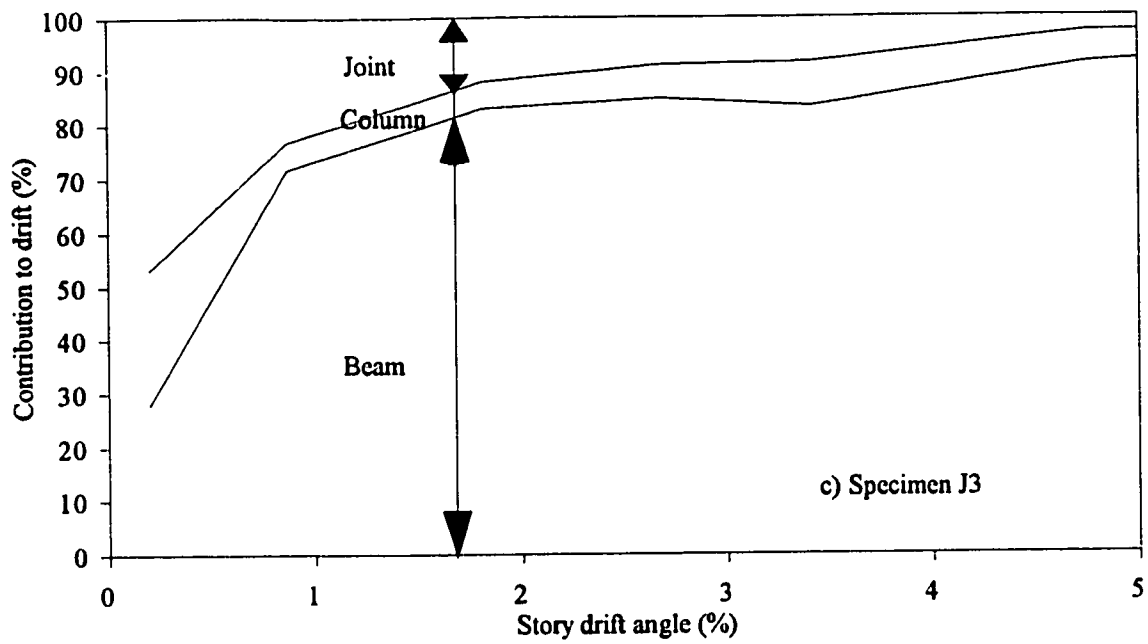


Figure 4.19b Contribution to story drift angle (negative drift) for specimens J3 and J4

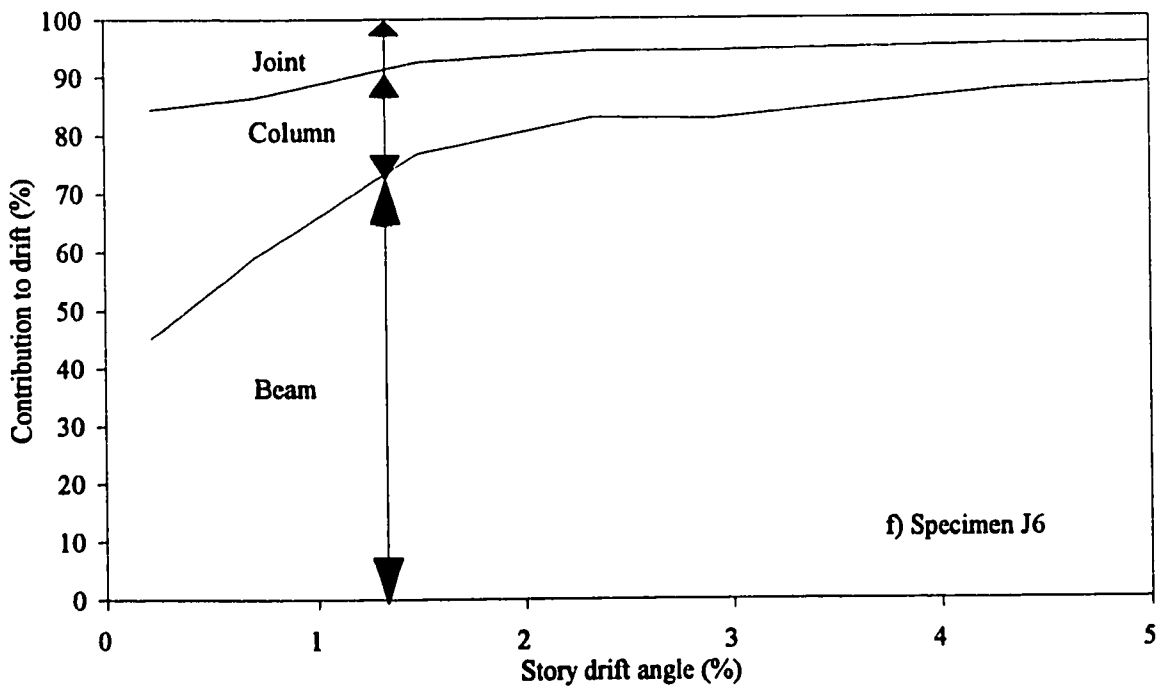
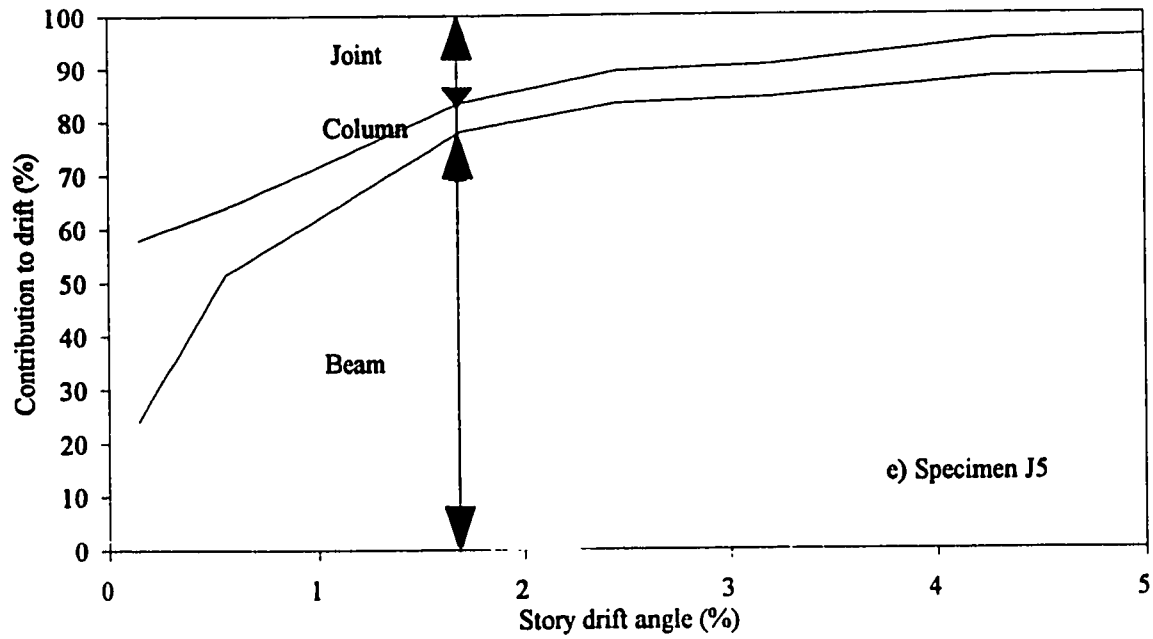


Figure 4.19c Contribution to story drift angle (negative drift) for specimens J5 and J6

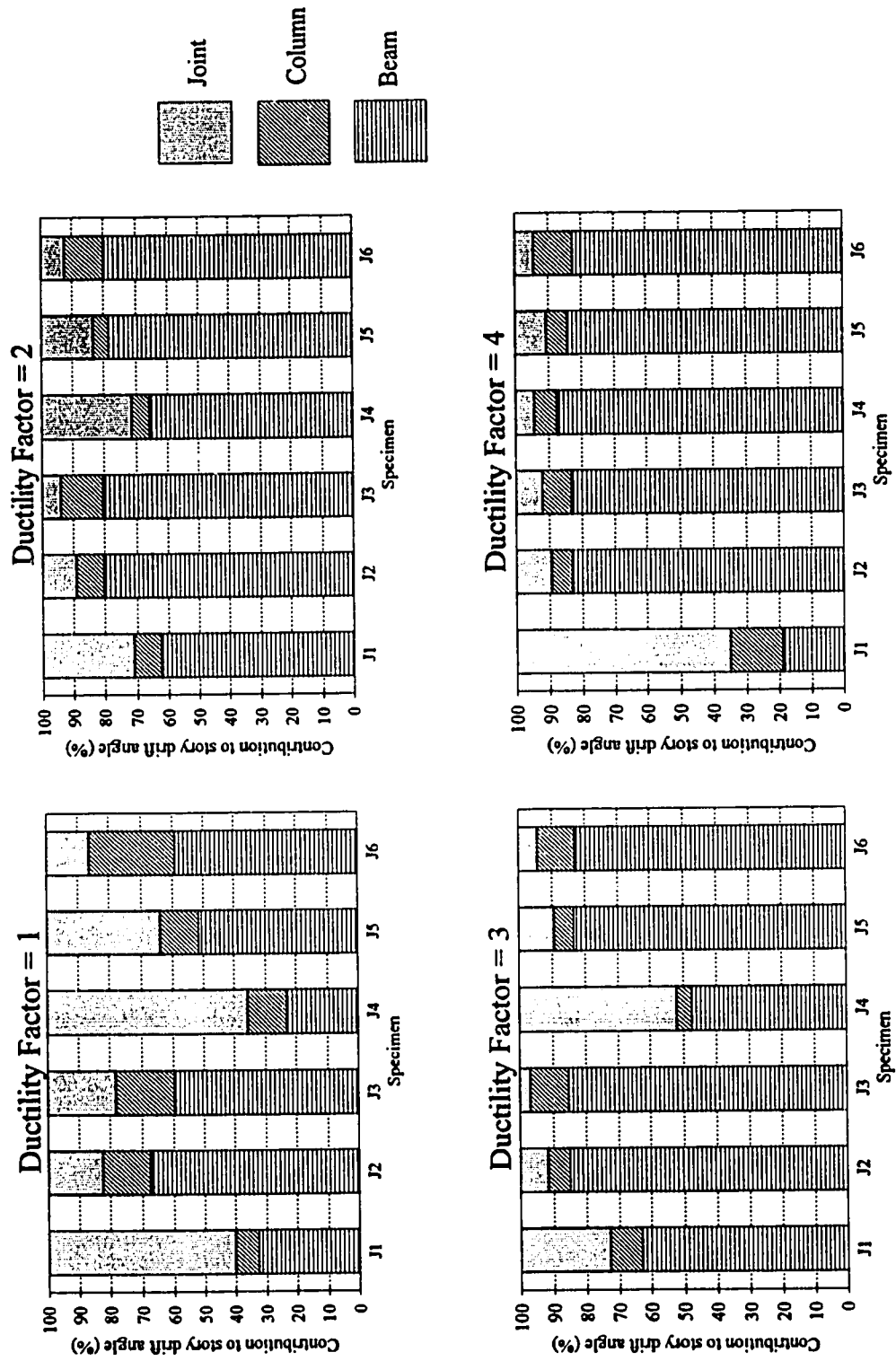


Figure 4.20 Member contributions to drift angle

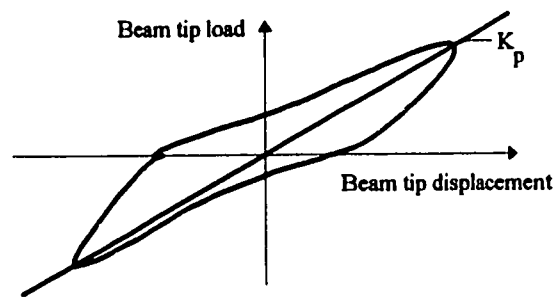


Figure 4.21 Definition of peak-to-peak stiffness

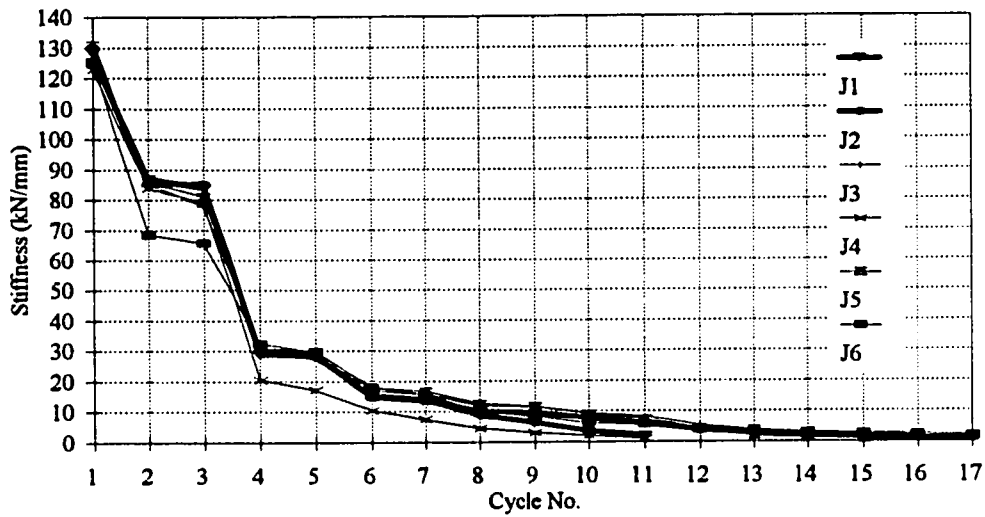


Figure 4.22 Comparison of peak-to-peak stiffness of specimens

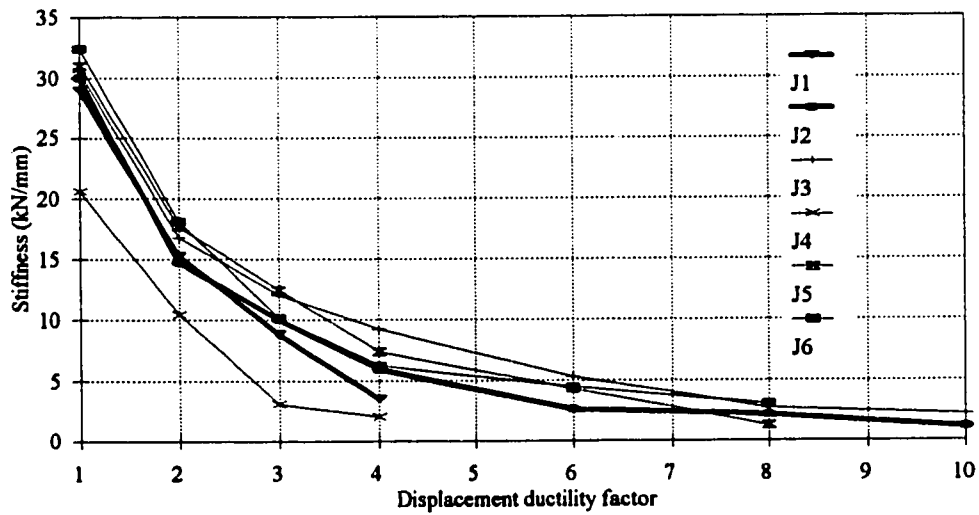


Figure 4.23 Stiffness-displacement ductility factor relationship

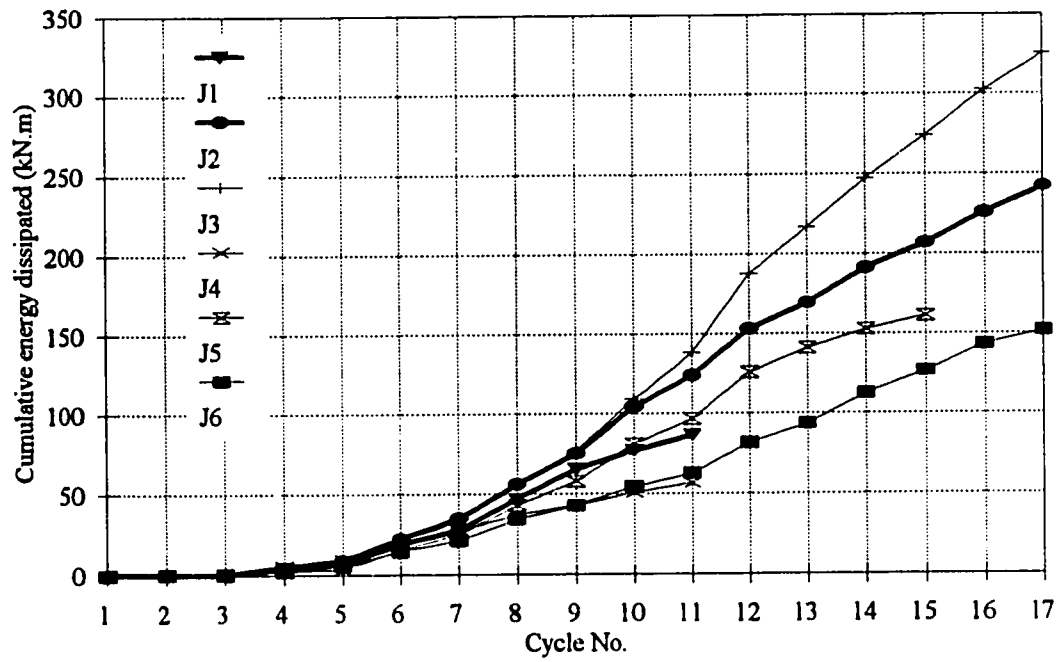


Figure 4.24 Cumulative energy dissipated-cycles number relationship

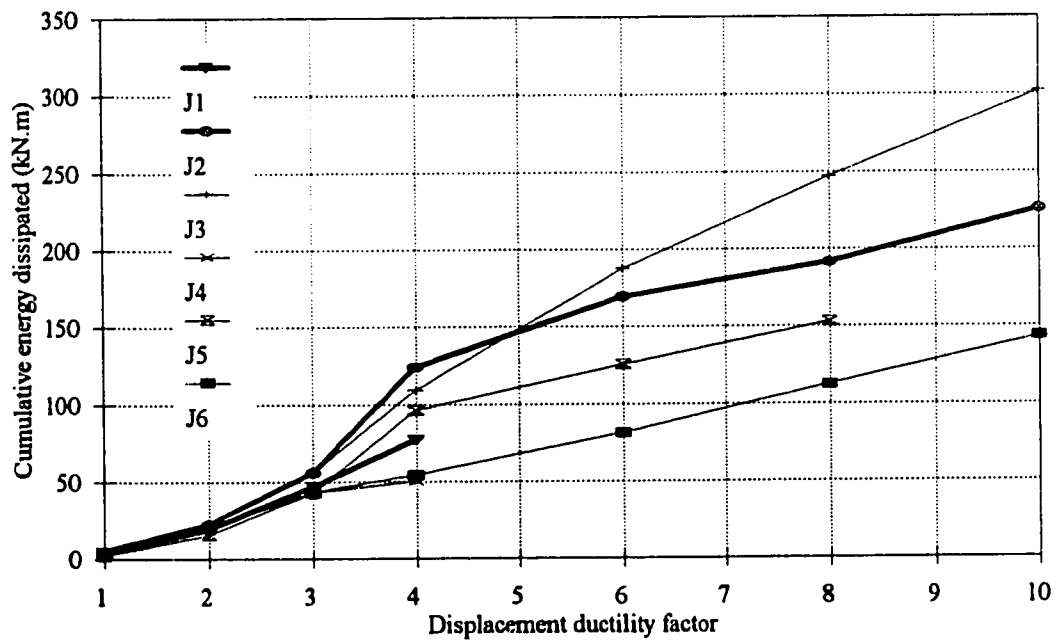


Figure 4.25 Cumulative energy dissipated-displacement ductility factor relationship

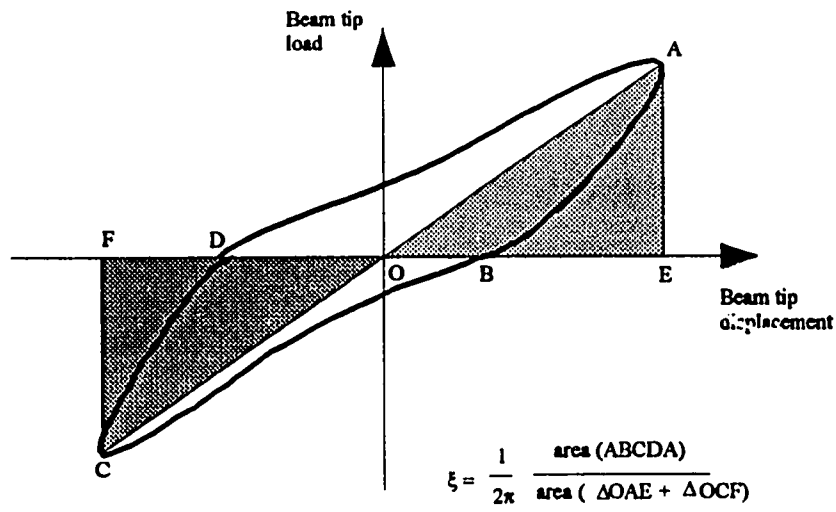


Figure 4.26 Definition of equivalent viscous damping factor

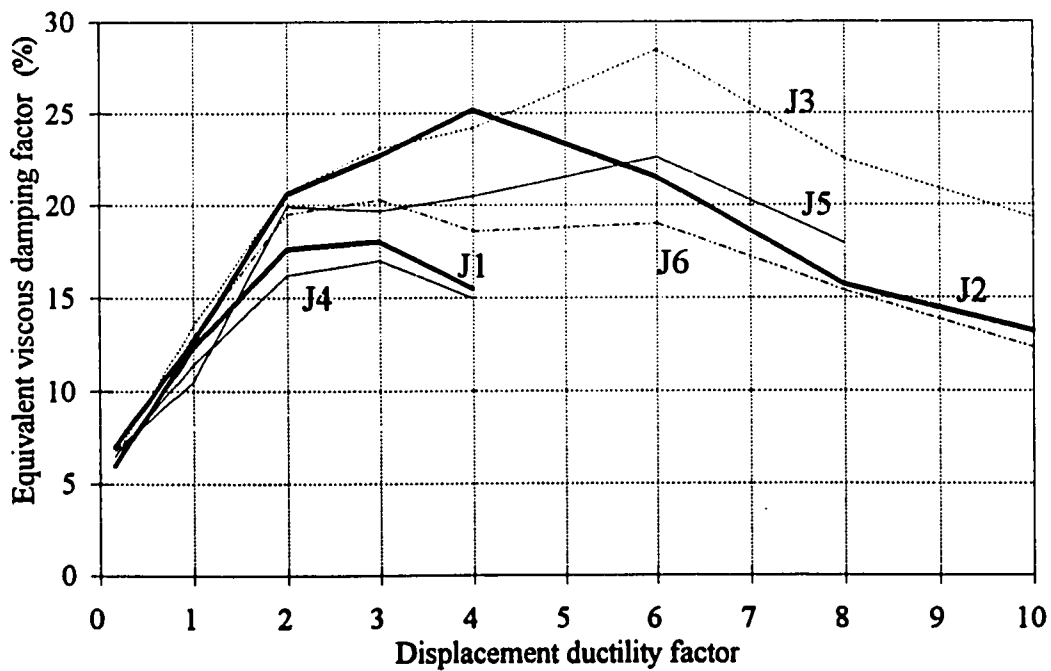


Figure 4.27 Equivalent viscous damping factor-displacement ductility factor relationship

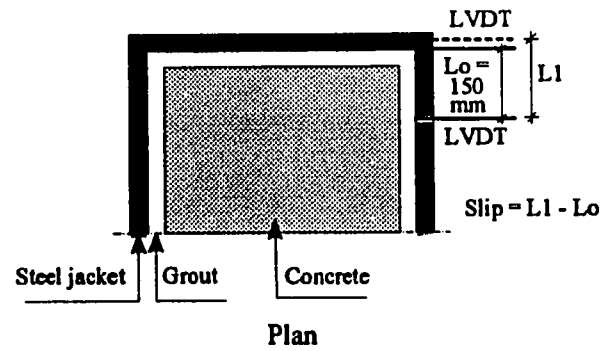


Figure 4.28a Slip between steel jacket and grout

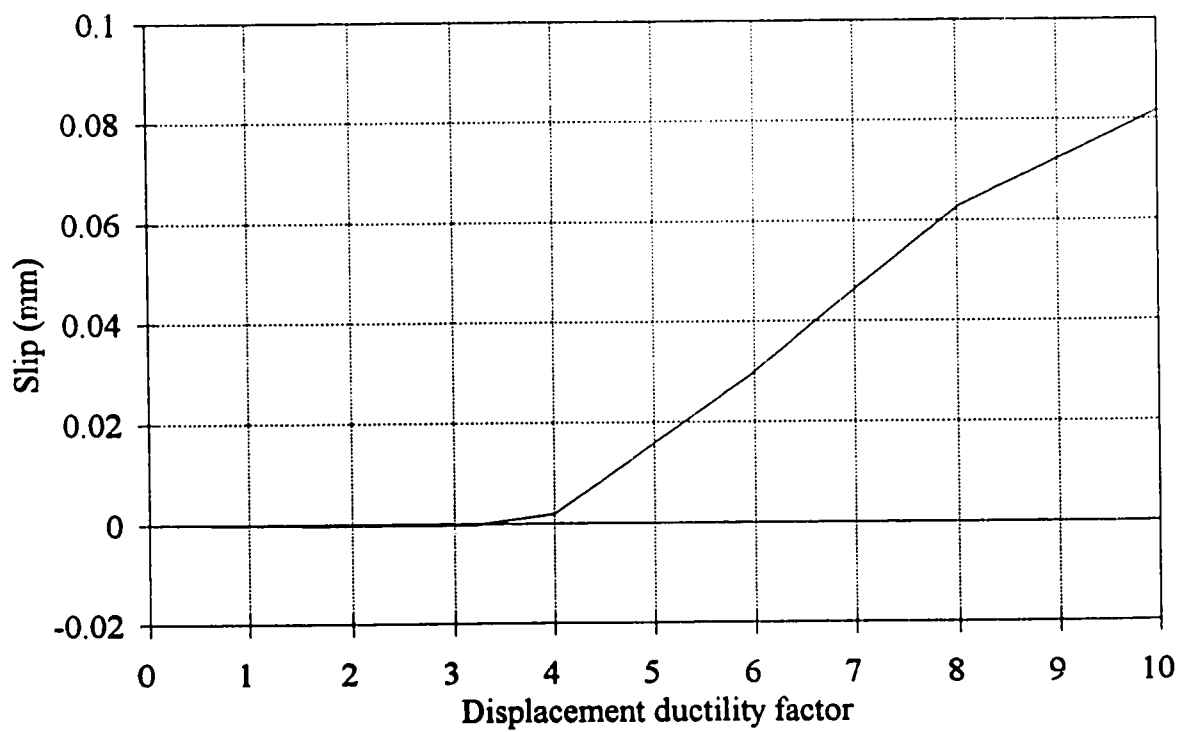
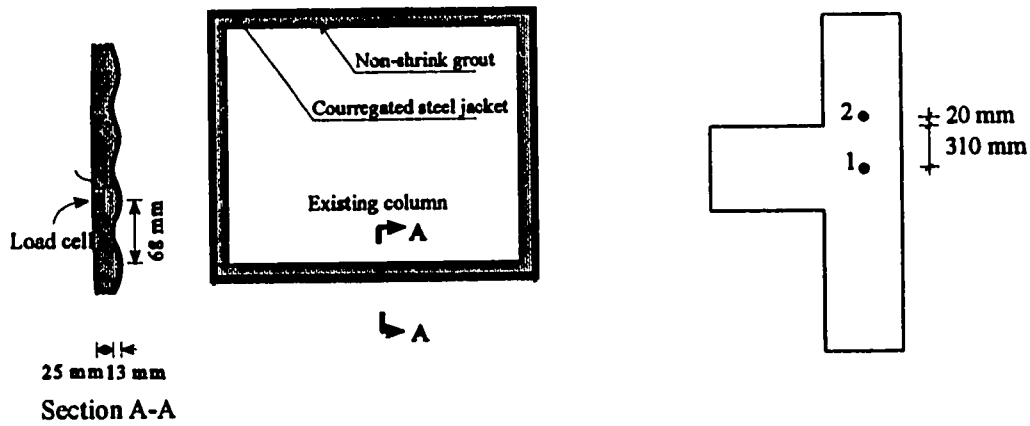


Figure 4.28b Slip between steel and grout-displacement ductility factor relationship



a) Installation of load cells

b) Location of load cells

Figure 4.29 Installation and location of load cells

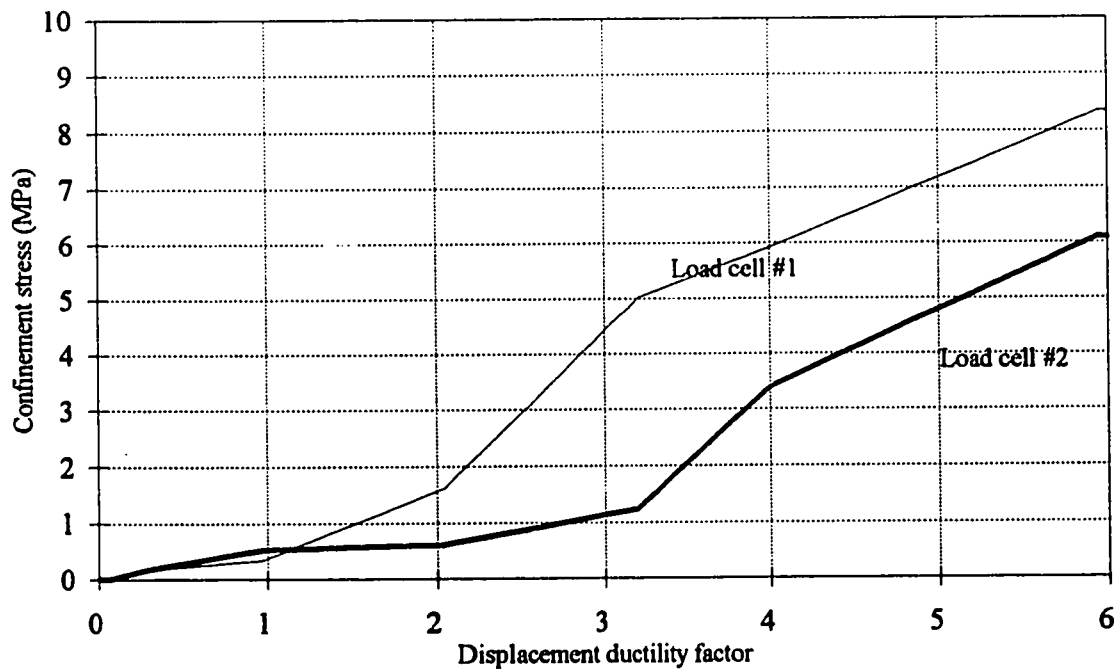


Figure 4.30 Confinement stress measured by the load-cells

CHAPTER 5

PROPOSED DESIGN AND CONSTRUCTION OF THE CORRUGATED STEEL JACKET

5.1 INTRODUCTION

According to the capacity design approach, the joint shear strength and bar bond strength must be sufficient to resist the effects of the most probable flexural resistance of the beams. One of the possible rehabilitation schemes for the joint is the reinforced concrete jacketing. However, reinforced concrete jackets are complex, labour intensive and costly. Therefore, corrugated steel jackets are proposed to achieve the necessary ductility at lower costs.

In this chapter, procedures for design and construction of corrugated steel jackets for rectangular columns and joints are proposed. The proposed design procedure is based upon a background taken from three sources. First, the design recommendation in the current concrete design code (CSA A23.3-94, 1994) is used in the estimation of transverse steel requirement. Second, the construction and observed performance of the tested specimens provide experience in using the corrugated steel jacket system. Third, the analysis of the test results of three large scale rehabilitated reinforced concrete frame connections using corrugated steel jacket provides performance prediction of the system.

The criteria for designing the corrugated steel jacket is to satisfy several requirements concerning the joint and column. As for the joint, it is required to provide the necessary confinement and shear strength. While for the column, it is required to provide the necessary confinement to satisfy the required curvature ductility and the necessary bond strength at the lap splices. The jacket may also be designed to enhance the column shear strength.

5.2 ADVANTAGES OF CORRUGATED STEEL

The corrugated steel shape is proposed in rehabilitation as it provides confining pressure by passive restraint to the concrete. Dilation of the flexural compression zone is restrained by the corrugated steel lateral stiffness. The poor behaviour of columns confined by flat plates can be illustrated by the results of the experiments carried out by Priestley et al. (1994) as shown in figure 5.1. In their investigation, a cyclic lateral load was applied to several rehabilitated columns and as a result outward bulging at midpoints of the flat plates was observed. When compared with ties or flat plates steel jackets, a corrugated steel jacket has high out-of-plane stiffness in the form of flexural rigidity which resists out-of-plane bulging.

The lateral confining compression on the concrete enhances its compressive strength and effective ultimate compressive strain. Restraint by the corrugated steel jacket of dilation on the flexural tension side of columns also provides an effective constraint against bond failure of longitudinal bar lap splices above joints. The lateral concrete confinement stress provided by the corrugated steel jacket is a function of the yield strength, thickness of the steel as well as the depth (amplitude) of the corrugation. The corrugated steel jacketing

system is an effective solution for joints and columns rehabilitation as the corrugated steel provides both lateral confinement and shear resistance to the rehabilitated area, thereby, adding strength and ductility.

5.3 PROPOSED DESIGN METHODOLOGY

Based on the observed performance and the analysis of the member contribution to the deformation of the tested specimens, corrugated steel jacketing of frame elements proved to be an effective technique for the rehabilitation of existing structures. Based on the recommendations in the current concrete design code (CSA A23.3-94, 1994) and on the observed performance of the specimens, a procedure for the design of corrugated steel jacket rehabilitation system is proposed.

5.3.1 Design of the steel jacket thickness

The steel jacket thickness should be designed such that: (a) the rehabilitated column or joint achieves the specified shear strength; (b) the rehabilitated column cross-section has the specified curvature ductility level; (c) the steel jacket provides the required confinement to the column or joint region; and (d) the yield strength of the lapped longitudinal reinforcement should be achieved prior to bond failure.

(a) shear strength enhancement:

The shear strength enhancement provided by the corrugated steel jackets can be conservatively estimated by considering the jacket to act as a series of independent hoops of cross-sectional area of $t_j \times t_j$ where t_j is the corrugated steel jacket thickness. The shear strength enhancement V_{sj} provided by a corrugated steel jacket can be written as:

$$V_{sj} = 2 f_{yj} h t_j \quad (5.1)$$

where h is the total depth of the member cross-section and f_{yj} is the yield strength of the corrugated jacket material.

(b) Curvature ductility requirement:

Recent theoretical and experimental research has shown that the amount of confining steel required for a given curvature ductility factor depends upon the axial force level (Zahn et al., 1986). Moreover, Sheikh (1994) proposed an effective procedure for predicting the required amount of confinement steel for rectangular columns considering the effect of curvature ductility and column axial load. The required confining steel jacket thickness t_j , for a rectangular column cross-section can be calculated using a modified form of the equation given by Sheikh (1994) as follows:

$$2 t_j \geq 0.12 \frac{f'_c h}{f_{yj}} \alpha \frac{\mu_\phi}{18} Y_p \quad (5.2)$$

where h is the larger cross-sectional dimension of the column; $Y_p = 6 (P_u/P_o) - 1.4 \geq 1.0$; $P_o = 0.85 A_g f'_c + A_s f_y$; P_u is the column axial load; μ_ϕ is the required curvature ductility; α is a factor depending on the transverse steel configuration and equals one in case of corrugated steel jacket; A_g is the gross cross-sectional area of the column; A_s is the longitudinal reinforcement area of the column and f_y is the yield strength of the longitudinal reinforcement. The modification to Sheikh's formula includes replacing the total required cross sectional area of transverse reinforcement spaced a distance S by $2t_j$.

(c) Confinement requirement:

The recommendations of the current concrete design code (CSA A23.3-94, 1994) are

used with modification to estimate the required confining steel jacket thickness. The jacket thickness is given for rectangular columns or joints by considering the jacket to act as a series of independent ties of cross-sectional area of $t_j \times t_j$ with spacing t_j . The thickness of the steel jacket can be given by the following relationship:

$$2 t_j \geq 0.09 \frac{f'_c h}{f_{yj}} \quad (5.3)$$

(d) Bond strength requirement for lap splices:

Based on Priestley and Seible's (1991) bond failure model, the lateral confining stress for full development of the yield strength of the lapped reinforcement can be expressed as:

$$f_L = \frac{A_b f_y}{p L_s} \quad (5.4)$$

where A_b is the area of the reinforcing bar; f_y is the yield strength of the lapped bars; L_s is the lap splice length and p is the perimeter of the rupture surface given as:

$$p = \frac{S_v}{2} + 2(d_{bv} + c) \leq 2\sqrt{2} (d_{bv} + c) \quad (5.5)$$

where S_v is the vertical bar spacing, d_{bv} is the vertical bar diameter and c is the thickness of the concrete cover. For rectangular sections confined by outside hoops only, the lateral confining stress varies along the column. However, confining the column by a corrugated steel jacket with inside grouting may give a more uniform lateral confining stress along the column. Assuming the confinement stress f_L / k_c is uniform along the width of the column and the resisting force is divided into two forces among the two sides of the jacket, the jacket thickness can be determined as follows:

$$t_j = \frac{f_L h}{2 f_{yj} k_e} \quad (5.6)$$

where k_e is the confinement effectiveness coefficient. Making use of the reported test results by Tomii (1993) and the suggested values of k_e for rectangular (0.75) and circular (0.95) ties by Priestley et al. (1996), the value of k_e is taken as 0.87.

5.3.2 Design of the depth of corrugation

An estimate of the stiffness of the corrugated steel section can be obtained by assuming that the lateral deformation of the corrugated steel sheet is equal to the lateral deformation of the ties designed according to the current concrete design code, accordingly:

$$\frac{h^4}{384 S I_{\text{corrugated/mm}}} = \frac{5 y^4}{384 I_{\text{tie}} \left[1 + \frac{5}{48} \frac{A_{\text{tie}} f_y y^2}{E_s I_{\text{tie}}} \right]} \quad (5.7)$$

which leads to:

$$I_{\text{corrugated/mm}} = \frac{h^4}{5 y^4 S} \left[I_{\text{tie}} + \frac{5}{48} \frac{A_{\text{tie}} f_y y^2}{E_s} \right] \quad (5.8)$$

where A_{tie} is the cross sectional area of a tie designed according to the current code with vertical spacing S and maximum horizontal spacing between legs of overlapping ties or cross ties y , I_{tie} is the moment of inertia of the tie and E_s is the Young's modulus of steel. The upper limit for y is assumed to be 300 mm. A simplified conservative version of equation 5.8 is as follows:

$$I_{\text{corrugated/mm}} = \frac{I_{\text{tie}}}{S} \frac{h^4}{y^4} \quad (5.9)$$

5.3.3 Design of column jacket height

For flexural rehabilitation of columns, it is not necessary that a steel jacket covers the full height of the column. Two criteria have been used to determine the height of the steel jacket: (1) to ensure that the plastic hinge is formed just above the column footing or just above the joint region (not in the region of column immediately above the steel jacket); and (2) to eliminate the possibility of shear failure above the steel jacket. In order to ensure that the plastic hinge is formed just above the column base, the moment demand immediately above the steel jacket should be smaller than the moment capacity of the original column section. In design practice, a safety factor $\alpha' = 0.85$ is typically introduced to ensure hinge formation in the rehabilitated region. The height of the steel jacket L_j can be calculated using the following expression:

$$L_j > (1 - \alpha' \frac{M_o}{M_r}) L - L_g \quad (5.10)$$

where M_o is the moment capacity of the original column section, M_r is the moment capacity of the rehabilitated column section, L is the column height or the distance from the plastic hinge to the point of contraflexure, and L_g is the gap between the end of the steel jacket and the top of the column base or the top of the beams connected to the joint region. This gap is to avoid any increase in the strength and stiffness of the jacketed member. The gap is recommended to be between 25 and 50 mm.

To prevent the column original cross-section above the jacket from shear failure, the nominal shear stress ($V/0.8 A_g$) is limited by $0.29 \sqrt{f'_c}$ MPa (Sun et al., 1993). If the nominal shear stress exceeds this limit, full column height jacket for rehabilitation is required.

According to current concrete design code (CSA A23.3-94, 1994), the length of concentration of transverse reinforcement (which reflects approximately the height of the jacket) should not be less than (a) the depth of the column, (b) 1/6 the clear column height, or (c) 450 mm.

5.4 NUMERICAL EXAMPLE

A design example for the rehabilitation of a reinforced concrete connection using corrugated steel jackets (for the column and the joint) is presented as shown in figure 5.2.

(a) Rehabilitation of column:

The column dimensions are taken to be 610 x 510 mm. The concrete compressive strength is 21 MPa. The column is reinforced by 12 longitudinal bars of 16 mm diameter, of yield strength of 400 MPa and spaced 165 mm. The concrete cover is 40 mm. The column axial force equals 505 kN. The lap splice length is 600 mm. It is assumed that no shear enhancement is required and that the required curvature ductility is 15. The corrugated steel used is of yield strength of 230 MPa. The steel jacket thickness can be determined according to the following procedure:

Equation 5.2 for the curvature ductility requirement gives:

$$t_j = \frac{0.12}{2} \frac{21 \times 610}{230} (1) \left(\frac{15}{18}\right) (1) = 2.78 \text{ mm} \quad (5.11)$$

The confinement requirement represented by equation 5.3 gives the jacket thickness to be:

$$t_j \geq \frac{0.09}{2} \frac{21 \times 610}{230} = 2.5 \text{ mm} \quad (5.12)$$

The lateral confinement stress for full development of the yield strength of the lapped reinforcement is calculated using equations 5.4 and 5.5 as follows:

$$f_L = \frac{200 \times 400}{158 \times 600} = 0.84 \text{ MPa} \quad (5.13)$$

where $P = (165 / 2) + 2 (16 + 40) = 194.5 \text{ mm} \leq 2 \sqrt{2} (16 + 40) = 158 \text{ mm}$.

The jacket thickness to provide the confinement necessary to inhibit bond failure is given by equation 5.6 as:

$$t_j = \frac{0.84 \times 610}{2 \times 230 \times 0.87} = 1.29 \text{ mm} \quad (5.14)$$

Using table 5.1, a corrugated steel sheets of thickness 2.8 mm with corrugation profile 68 x 13 mm is selected ($I_{\text{corrugated}} / \text{mm} = 54.57 \text{ mm}^4 / \text{mm}$)

Stiffness check:

According to the current concrete design code (CSA A23.3-94, 1994), the spacing between ties is the smallest of, a) 6 times the largest longitudinal bar diameter = $6 \times 16 \text{ mm} = 96 \text{ mm}$; b) 100 mm. The minimum spacing S is taken equal 96 mm. The total cross sectional area of transverse reinforcement spaced at a distance S is:

$$A_{sh} = 0.09 S y \frac{f'_c}{f_y} = 0.09 \times 96 \times 300 \times \frac{21}{400} = 136 \text{ mm}^2 \quad (5.15)$$

To satisfy the required cross sectional area of transverse reinforcement of 136 mm^2 , ties of 9.3 mm diameter ($I_{\text{tie}} = 367 \text{ mm}^4$) at spacing of 96 mm are selected. The inertia of the corrugated steel jacket given by equation 5.8 gives:

$$I_{\text{corrugated}} / \text{mm} = \frac{610^4}{5 \times (300)^4 \times 96} \left[367 + \frac{5}{48} \frac{68 \times 400 \times (300)^2}{210000} \right] \quad (5.16)$$

$$= 54.3 \text{ mm}^4/\text{mm} < 54.57 \text{ mm}^4/\text{mm}$$

In case that the shear strength enhancement of the column is required, the selected jacket thickness can be checked to satisfy the shear capacity given by the formula:

$$V_f \leq V_r = \phi_c V_c + \phi_s V_s + \phi_s V_{sj} \quad (5.17)$$

where V_f is the factored shear demand and V_r is the factored shear capacity.

The concrete and steel contributions to the shear capacity are:

$$V_c = 0.2 \sqrt{f'_c} b_w d \text{ MPa} \quad (5.18)$$

$$V_s = A_v f_{yh} d / S_e \quad (5.19)$$

where ϕ_c is the resistance factor for concrete (taken = 0.6), ϕ_s is the resisting factor for steel (taken = 0.85), b_w is the column width, d is the column effective depth, A_v is the existing tie area in column, f_{yh} is the yield strength of the existing transverse ties and S_e is the spacing between existing ties.

(b) Rehabilitation of joint:

The beam-column joint and its dimensions are shown in figure 5.2. The factored shear demand (i.e. V_f) is given as follows:

$$V_f = \frac{(1.25 \times 1400 \times 400 + 1.25 \times 200 \times 400)}{1000} - 110.98 = 689 \text{ kN} \quad (5.20)$$

$$V_r = 0.6 \left[\frac{0.2 \sqrt{21} \times 610 \times 465}{1000} \right] + \frac{0.85}{1000} \left[\frac{98 \times 400 \times 465}{150} + 2 \times 230 \times 510 t_j \right] = 689 \text{ kN} \quad (5.21)$$

equation 5.21 leads to $t_j = 2.2 \text{ mm}$. Following the design of the jacket thickness other checks

such as confinement are similar to the case of column jacket design.

Assuming four bolts connecting the steel jacket to the beam, the shear per bolt = $2 \times 2.8 \times (610 - 2 \times 40) \times 230 / 4 = 171 \text{ kN}$. Using table 5.2, four M20 Hilti bolt are selected.

5.5 PROPOSED CONSTRUCTION CONSIDERATIONS

5.5.1 Surface preparation

To achieve monolithic behaviour of jacketed elements, the concrete surface must be cleaned appropriately. Previous research on shear transfer between new and existing concrete interfaces (Bass et al., 1989) indicated that surface roughening preparation should be adequate for the transfer of shear forces. This involves removing the cover and the exterior concrete. In this program, the surface was cleaned using thick brush and vacuum cleaner and no bonding agent was applied to the surface. Some water for saturation of the concrete surface, was used just before placing the non-shrink grout.

5.5.2 Corrugated steel jacket construction

It is proposed to build up the corrugated steel jackets from premanufactured "U" shape sections to be welded at the site along the vertical seams as shown in figures 5.3 and 5.4. The section is slightly oversized for ease of installation and the gap between the concrete and the steel jacket is to be filled with grout to provide continuity between the jacket and the concrete. The welding is applicable to the column jacket but at the joint region two steel angles are proposed to resist the lateral pressure. These two angles are to be anchored to the concrete by anchor bolts as shown in figure 5.5. The anchor bolts are to be designed to take either tension or shear forces such that the tension or shear on each bolt is equal to $2 t_j (d-d')$

f_{yj}/n where d is the effective depth of beam, d' is the distance from the compression side of the beam to the centre of the compression steel of the beam, f_{yj} is the yield strength of the corrugated steel jacket and n is the number of bolts anchoring both angles.

If the shear strength enhancement is needed in the beam, a jacket will normally be required over a length equals to at least the depth of the beam. A gap is provided between the beam jacket and the column face, as shown in figure 5.4, to minimize flexural strength enhancement of the beam, which might cause excessive forces to develop in the connection.

5.5.3 Placing of non-shrink grout

The bottom of the column jacket and the near end of the beam jacket are sealed using foam or any sealing material. The non-shrink grout is delivered in bags, mixed with water in the field with a ratio of 6:1 or 5:1 by weight according to the required workability. The grout is placed between the column and the jacket from top. Based on the experience gained from the experimental program, it is recommended to use non-shrink grout of thickness not less than 25 mm to facilitate pouring the grout.

5.5.4 Proposed construction of different connections

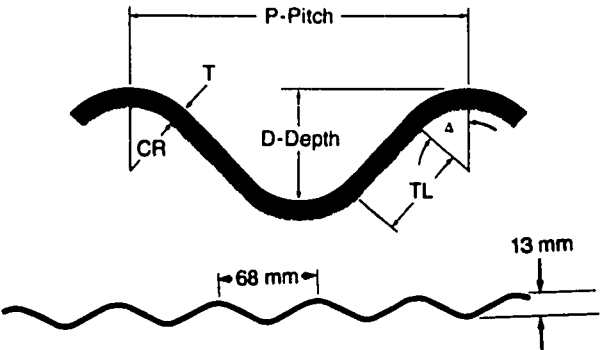
The proposed rehabilitation technique may be used in case of connections with floor slab and transverse beams. The column jacket can be installed in two parts: the first part is to be located on top of the slab and the second part may be installed just below the slab in case of connection with floor slab and no transverse beams. In case of connection with slab and one transverse beam, the second part of the column jacket can be installed just below the slab from one side and below the transverse beam from the other side. In other words, the jacket will be L-shape instead of U-shape at the joint level. Angles and anchor bolts can be

used to connect the L-shape to the concrete. If the connection has slab and two transverse beams, the second part of the column jacket may be installed just below the transverse beams. For jacketing the beam, U-shape jacket can be installed below the slab and connected to the slab with plates and anchor bolts. These described jacketing techniques assume that transverse beams provide adequate confinement to the joint. The rehabilitation techniques for different types of connections are illustrated in figures 5.6 and 5.7.

5.6 SUMMARY

The corrugated steel jackets have advantages as a rehabilitation technique when compared with flat steel jackets. Procedures for the design and construction of the corrugated steel jacket system for rectangular columns and joints are proposed. The corrugated steel jacket should be designed such that: (a) the rehabilitated column or joint achieves the specified shear strength; (b) the rehabilitated column cross-section has the specified curvature ductility level; (c) the steel jacket provides the required confinement to the column and joint region; and (d) the yield strength of the lapped longitudinal reinforcement should be achieved prior to bond failure. From testing experience, a corrugated steel jacket designed according to this procedure will perform satisfactorily without displaying undesirable modes of failure. The jacket design is based on the capacity design approach and the results obtained from the experimental program. The proposed rehabilitation technique may be used in case of connections with floor slab and transverse beams.

Table 5.1 Sectional design profiles for corrugated sheet (Handbook of steel, 1984)



Corrugation Profile: 68 × 13 mm
Corrugation Radius (CR): 17.46 mm

1	2	3	4	5	6	7	8	9
Wall Thickness		Area	Tangent Length	Tangent Angle	Moment Inertia	Section Modulus	Radius Gyration	Developed Width Factor
Specified	Design							
	T	A	TL	Δ	I	S	r	WF
	mm	mm ² /mm	mm	Degrees	mm ⁴ /mm	mm ³ /mm	mm	*
1.0	0.820	0.885	19.951	26.556	16.49	2.44	4.316	1.079
1.3	1.120	1.209	19.759	26.647	22.61	3.27	4.324	1.079
1.6	1.400	1.512	19.578	26.734	28.37	4.02	4.332	1.080
2.0	1.820	1.966	19.304	28.867	37.11	5.11	4.345	1.080
2.8	2.640	2.852	18.765	27.136	54.57	7.11	4.374	1.080
3.5	3.350	3.621	18.269	27.381	70.16	8.74	4.402	1.081
4.2	4.080	4.411	17.755	27.643	86.71	10.33	4.433	1.081

*WF measures flat sheet width to produce corrugated width.
Profile section properties calculated from design thickness.
(See definitions.)
NOTE: Dimensions are subject to manufacturing tolerances.

Table 5.2 Ultimate load capacity of Hilti bolts (Hilti, 1994)

HSL Ultimate Loads versus Concrete Strengths - Ultimate Loads = (x) kN									
Thread Diameter (mm)	Embed. Depth (mm)	Concrete Strength							
		21 MPa		28 MPa		35 MPa		40 MPa	
		Tension	Shear	Tension	Shear	Tension	Shear	Tension	Shear
M8	65	29.86	33.45	33.94	37.12	36.84	38.30	37.74	39.50
M10	75	42.12	55.51	49.15	58.80	56.10	62.09	60.02	65.39
M12	80	55.28	78.15	65.00	84.07	74.71	90.69	82.42	97.30
M16	105	100.91	137.40	116.83	149.63	132.77	161.86	139.67	174.09
M20	130	133.29	173.52	147.45	200.25	161.76	213.99	169.07	227.72
M24	155	167.38	246.02	198.86	278.51	230.35	305.98	255.83	333.44

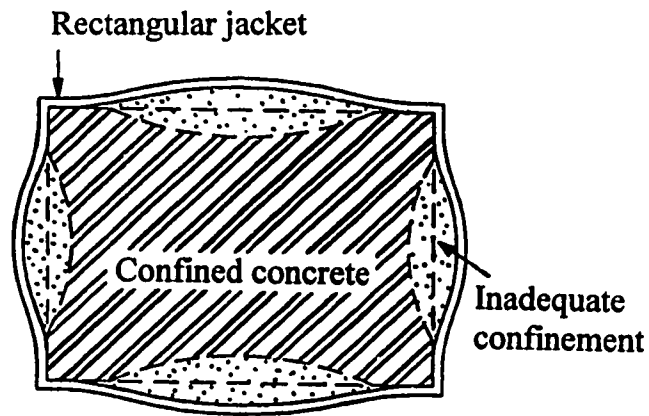


Figure 5.1 Behaviour of rehabilitated rectangular column using flat steel jacket (Priestley et al., 1994)

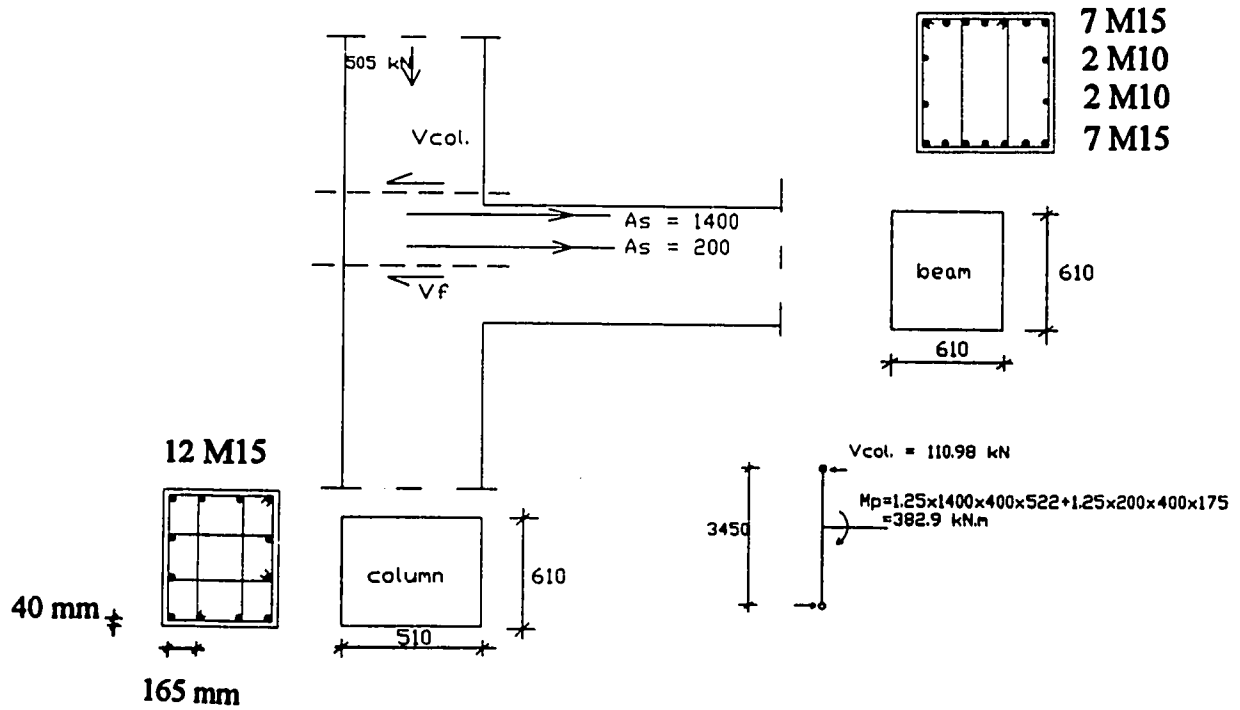


Figure 5.2 Column and joint dimensions

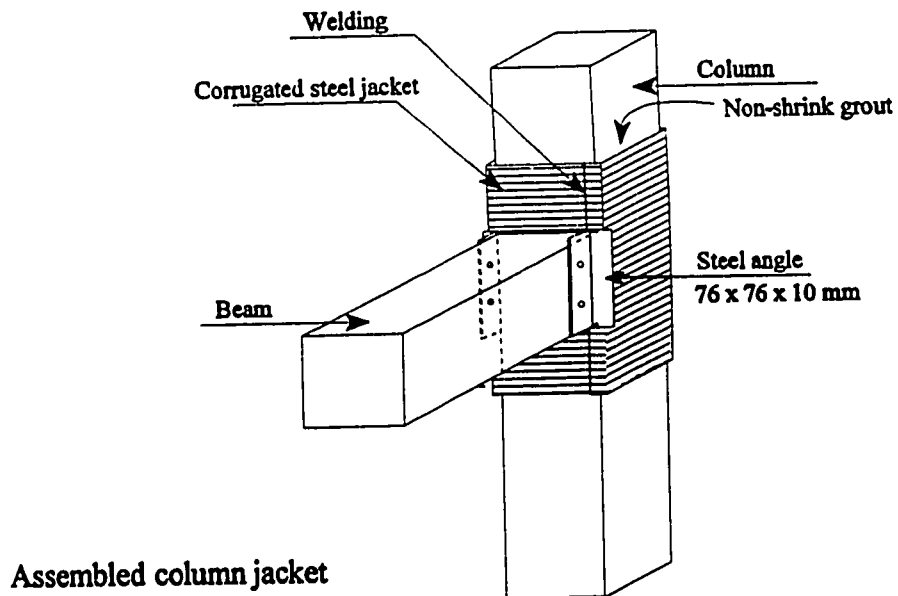
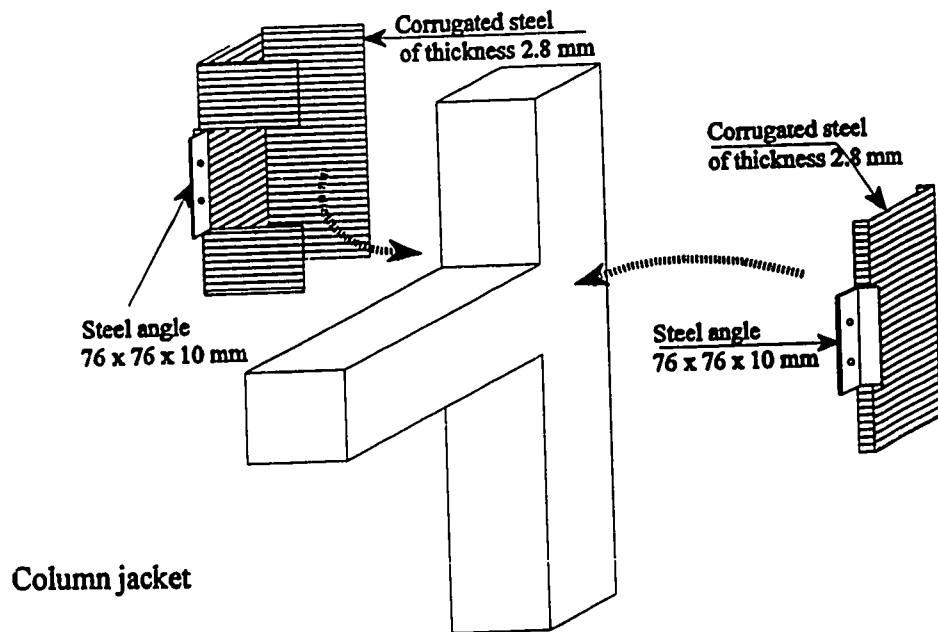


Figure 5.3 Proposed rehabilitation technique for columns and joints

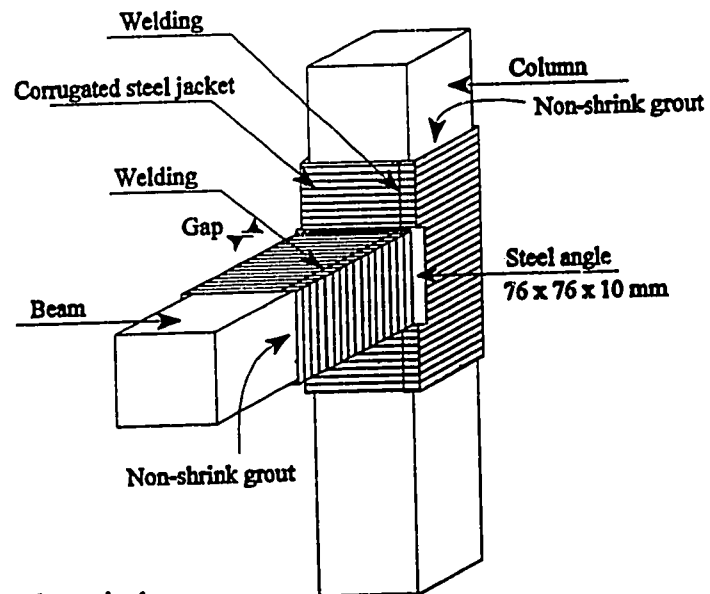
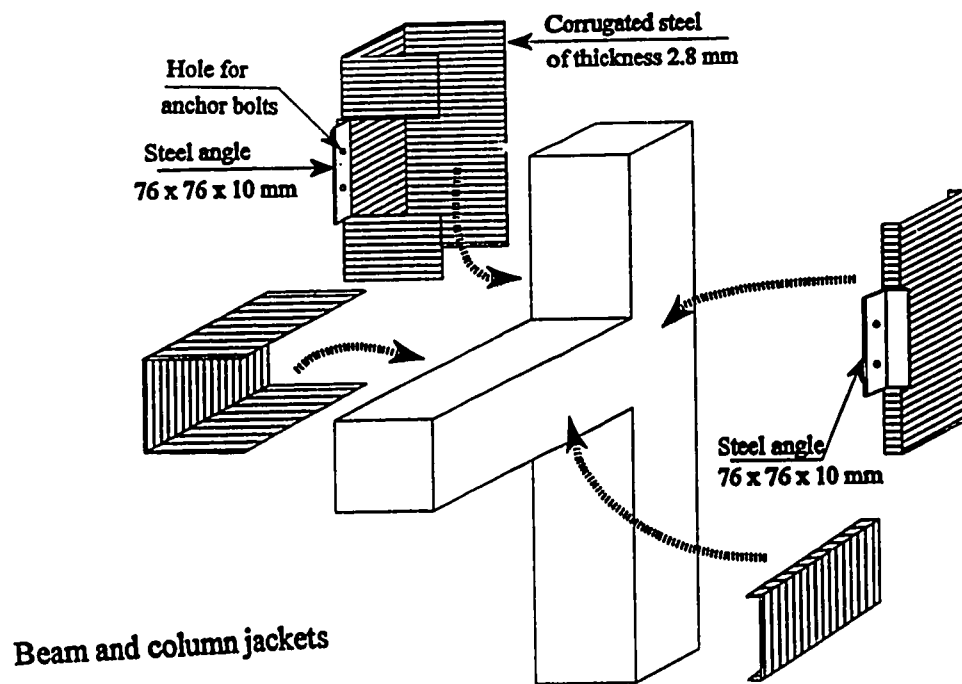


Figure 5.4 Installation technique for column, beam and joint jackets

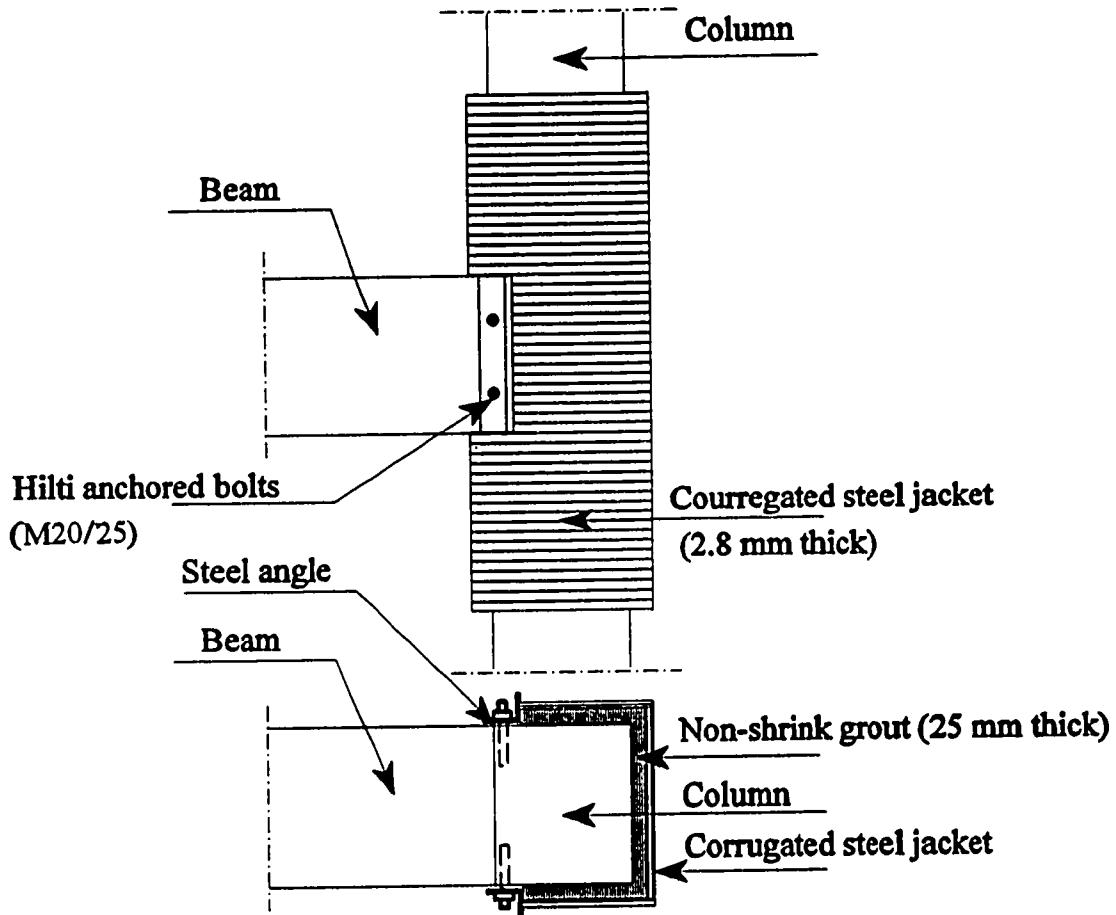
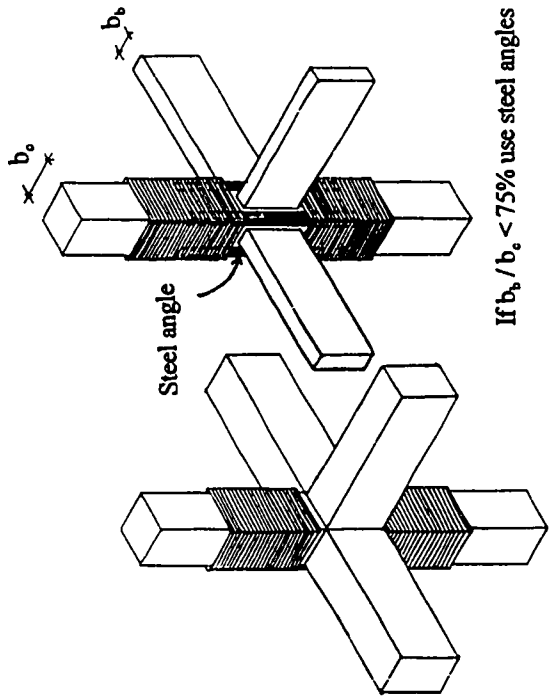
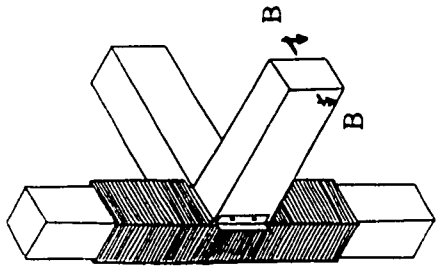


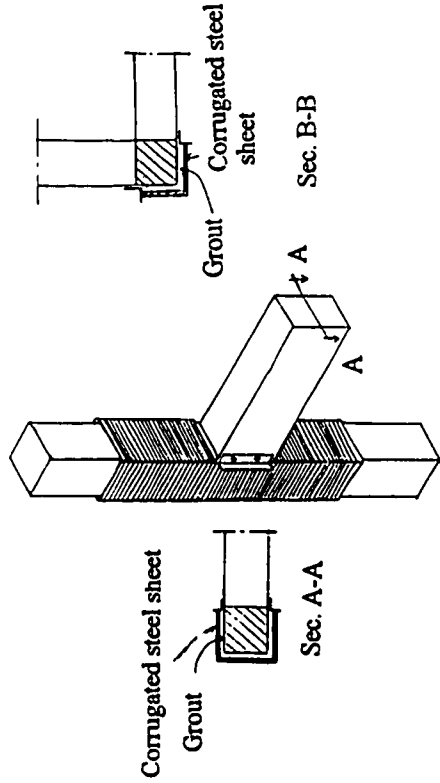
Figure 5.5 Installation of anchor bolts



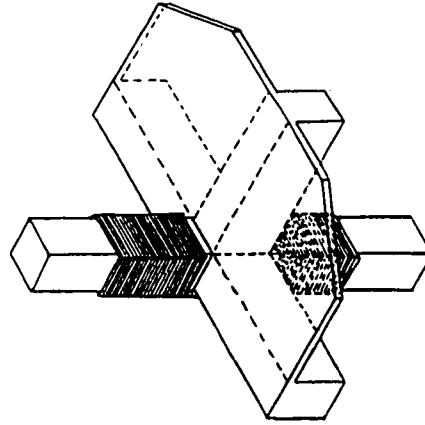
Two transverse beams - without slab



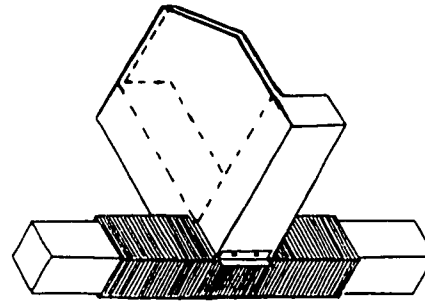
One transverse beam - without slab



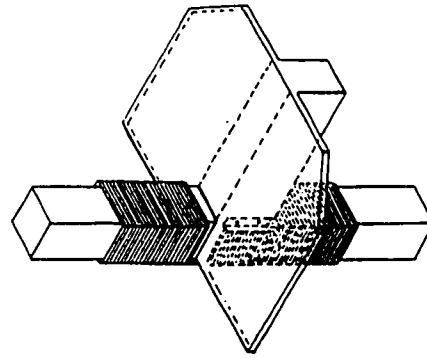
No transverse beam - without slab



Two transverse beams - with slab

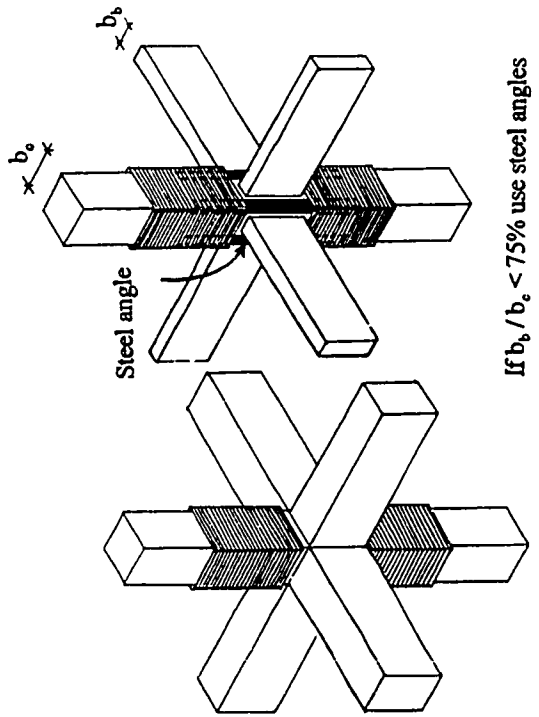


One transverse beam - with slab

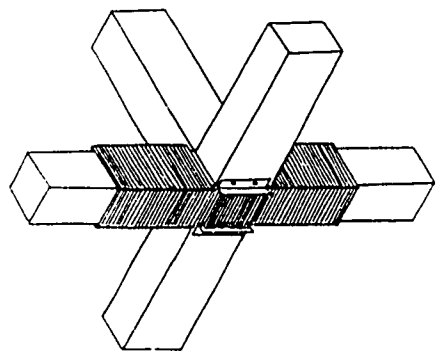


No transverse beam - with slab

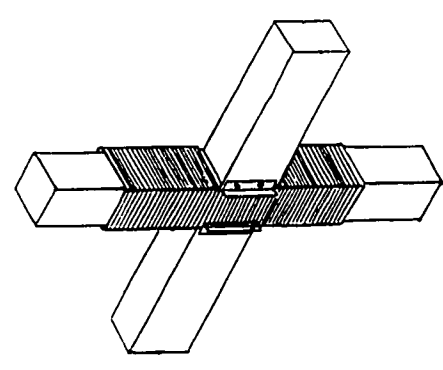
Figure 5.6 Proposed rehabilitation system for exterior connections with and without slabs and transverse beams



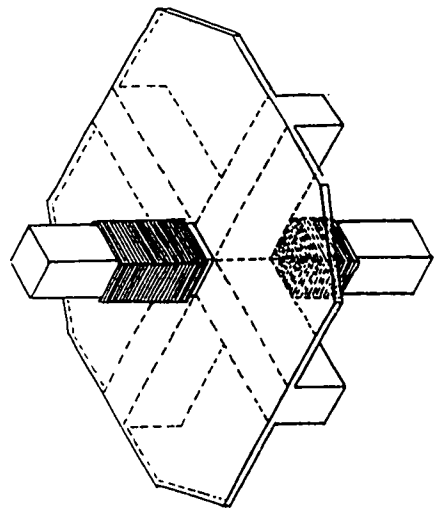
If $b_p / b_e < 75\%$ use steel angles



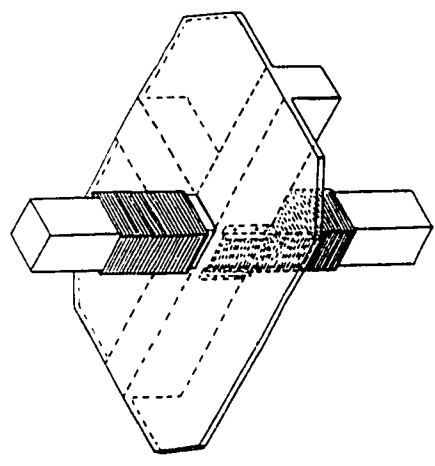
One transverse beam - without slab



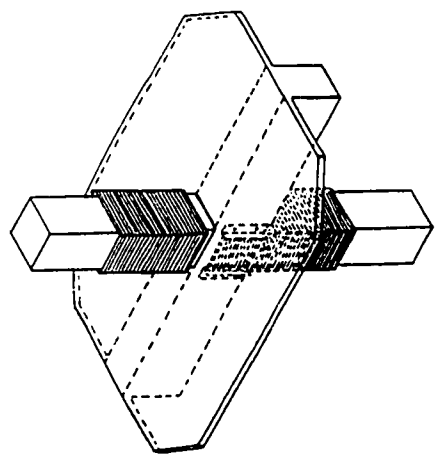
No transverse beam - without slab



Two transverse beams - with slab



One transverse beam - with slab



No transverse beam - with slab

Figure 5.7 Proposed rehabilitation system for interior connections with and without slabs and transverse beams

CHAPTER 6

DEVELOPMENT OF JOINT ELEMENT

6.1 INTRODUCTION

Reinforced concrete frames dissipate some of the ground motion energy input through inelastic deformations at critical regions. It is, therefore, important to develop models capable of simulating the hysteretic behaviour of the different critical regions of the frame in order to predict the distribution of forces and deformations in these structures accurately. To model the hysteretic behaviour of the different critical regions in reinforced concrete frames, shear deformation in joints and bar bond slip at beam-column interfaces need to be considered. The modelling should be simple yet sufficiently accurate. In addition, the modelling of girders and columns should account for inelastic deformation. Moreover, the girder element should include the effect of the slab. In this study, the attention is focused on the behaviour of frames. Shear wall or infill panel elements are not considered.

In the this Chapter, the computational tool is first described then followed by a proposed model that takes the slab contribution into account. A detailed model for the joint shear is presented using the softened truss model theory and is verified using experimental data. From the shear-deformation relationship, the moment-rotation relationship is calculated

using simple equilibrium to allow the joint shear to be represented by a rotational spring. The effects of transverse beams and slabs on the joint shear behaviour are also considered. A detailed model for the reinforcing bar bond slip at the beam-column interface is presented and verified using experimental data. Finally, the results of the complete model are compared with experimental measurements.

6.2 COMPUTATIONAL TOOL: SARCF

A modified version of the computer program Seismic Analysis of Reinforced Concrete Frames, SARCF (Meyer, 1994), was used in the dynamic analysis. The program is based on DRAIN-2D (Kanaan and Powell, 1973) with various enhancements. SARCF has an improved model for reinforced concrete elements which simulate the strength and stiffness degradation, possibility to interrupt the analysis to compute mode shapes and natural frequencies using the tangent stiffness method, as well as displacement control analysis. The original version of SARCF (Meyer, 1994) includes beam and column elements only. The program was modified to include joint elements simulating the shear deformations in joints and the reinforcing bars bond slip at the beam-column interface. A detailed description of the original program was presented by Chung et al. (1987).

6.3 MODELLING OF SLAB

Previous research indicated that monolithic floor-slabs may cause dramatic over-strength to the supporting beams in frame structures subjected to lateral loads (Durrani and Wight, 1982; Otani et al., 1984). The two important parameters affected by the slab

contribution are the initial stiffness and the negative moment flexural strength (French and Moehle, 1991). The effect of the initial stiffness may become less important after cracking. Experiments demonstrated that cracking under service loads caused reduction in stiffness by about 70% (Beres, 1994). On the other hand, the slab contribution to the flexural strength increases with increasing lateral displacements causing flexural over strength. This moment over-strength may be undesirable because it may increase the shear demand on the joint or alter the weak beam-strong column design of connection.

Slab contribution in a continuous structure differs from that in an isolated connection in several aspects that include locations of contraflexure points and the assumed free slab boundaries around the perimeter of the subassemblage. The restraint of the slab and beams in a continuous structure is larger than that of isolated connection tests (French and Moehle, 1991).

The most commonly used simple analytical model to represent the slab contribution is the effective slab width. To quantify the contribution of slab to the beam flexural resistance, analytically computed beam properties were compared to experimental results (Pantazopoulou, 1991). Various effective slab widths were assumed, equal to multiples of the beam depth, d . It was found that for negative moment, $3d + \text{beam width}$ at 2% drift, increased to $4d + \text{beam width}$ at 3% drift and finally to $5d + \text{beam width}$ at 6% drift. For positive moment, the effective slab width remained almost constant throughout the test at approximately $4d + \text{beam width}$. It is believed that the insensitivity of the effective width to the positive moment is probably a consequence of the limited amount of tension reinforcement at the bottom of the beam when the slab is in compression. As the amount of slab

reinforcement is usually small (relative to that in the beam), a high degree of accuracy in predicting the strength enhancement provided by the slab is normally not required and a simple estimation of the effective width of the tension flange is adequate.

In the present analysis, a slab width of 2 times the beam effective depth on each side of the beam is assumed for positive moments. This applies for both interior and exterior connections. For negative moments of interior connections, two times the beam effective depth on each side of the beam is assumed. For negative moments of exterior connections, a slab width equal to the transverse beam depth on each side of the column is assumed in case of a joint with transverse beams. In case of no transverse beams, a slab width equal to the column width on each side of the column is assumed as shown in figure 6.1.

6.4 MODELLING OF JOINT SHEAR

Experiments have shown that joint deformation is a strong indicator of beam-column joint performance. Satisfactory joint behaviour is associated with minimal contribution of joint distortion to the overall lateral drift of the structure. Ideally, joint contribution to drift should decrease with increasing total lateral drift as the adjacent beams develop plastic hinges and undergo the bulk of inelastic action. In cases of inadequate joint design, the contribution of joint distortion to the total drift increases with increasing total lateral drift, hence, joint failure may occur.

In the current study, the joint is represented by two rotational springs in series, one representing the joint shear deformation and the other representing the reinforcing bars bond-slip. The spring representing the shear deformation is influenced by the relative rotational

displacement between the nodes as shown in figure 6.2a. The moment transmitted by the element is the moment transferred from beams to the column. The deformation of the element represents the shear deformation of the joint (the change in the angle between the connected beams and columns). In this element, translational displacements of the nodes at both ends of the element are constrained to be identical. Also, the nodal coordinates were taken to be identical to satisfy equilibrium. The spring representing the reinforcing bars bond-slip is influenced by the relative rotational displacement between the nodes as shown in figure 6.2b. The deformation of the element represents the additional joint rotation due to bond-slip of the longitudinal bars of the beam.

6.4.1 Shear-deformation relationship

Analytical models range from purely empirical curve fitting of test data to extensive 3D finite element analysis. Although mathematical expressions fit closely virtually any shape of primary shear-deformation relationship, they suffer from the disadvantage that they can neither be extended outside the range of the calibration data nor can they be used for different dimensions or details of reinforcement. On the other hand, the finite element methods provide accurate representation of the behaviour for the beam-column connection. However, their modelling is a time consuming procedure, especially under cyclic and dynamic loading (Pantazopoulou and Bonacci, 1992). Recognition of the above limitations instigated the development of the so-called mechanical model using the softening truss model theory. This approach attempts to simulate the behaviour of beam-column joint. The actual shape of the shear-deformation primary relationship is obtained without the need to constrain it to follow predetermined patterns, thus no calibration to experimental results is needed. The joint

geometry is shown in figure 6.3.

The softened truss model is chosen to represent the joint behaviour as shown in figure 6.4. The softened truss model theory has been developed for the non-linear analysis of membrane elements by Hsu (1988). The theory's equations are derived on the basis of equilibrium of average stresses, compatibility of average strains, and the constitutive laws of concrete and reinforcement. An accurate prediction by the softened truss model depends strongly on the constitutive material laws for concrete and steel in the elements.

The reinforced concrete panel joint element is subjected to in-plane normal stresses and shear stresses. The definitions of stresses and co-ordinate systems are described in figure 6.4. The equations used in the softened truss model theory can be summarized as follows:

a) The equilibrium equations with generalization of the angle of inclination of the concrete struts as derived by Lampert and Thurlimann (1968) are employed. It is assumed that steel bars can resist only axial stresses. The three equilibrium equations satisfying Mohr's stress circle are as follows:

$$\begin{aligned}\sigma_x &= f_{c2} \cos^2 \theta + f_{c1} \sin^2 \theta + \rho_x f_{sx} \\ \sigma_y &= f_{c2} \sin^2 \theta + f_{c1} \cos^2 \theta + \rho_y f_{sy} \\ \tau_{xy} &= (-f_{c2} + f_{c1}) \sin \theta \cos \theta\end{aligned}\tag{6.1}$$

The three stress components σ_x , σ_y and τ_{xy} are the applied stresses on the reinforced concrete element (figure 6.4e). The stresses on the concrete strut itself are denoted as f_{cx} , f_{cy} and v_c , and are shown in figure 6.4f. The longitudinal and transverse steel provide the smeared stresses of $\rho_x f_{sx}$ and $\rho_y f_{sy}$ as shown in figure 6.4g, where f_{sx} and f_{sy} are the reinforcing steel stresses in x and y directions, respectively. The reinforcing steel ratio in x and y

directions, ρ_x and ρ_y are calculated by Pantazopoulou and Bonacci (1992). The average principal compressive and tensile stresses in concrete are denoted as f_{c2} and f_{t1} , respectively. The direction of the diagonal concrete struts are assumed to coincide with the direction of the principal compressive stress and strain in concrete which is inclined at an angle θ to the x-axis.

b) The compatibility equations of Collins (1978) are applied to determine the angle of inclination of the concrete struts, θ . The compatibility equations satisfying Mohr's strain circle are as follows:

$$\begin{aligned}\epsilon_x &= \epsilon_2 \cos^2 \theta + \epsilon_1 \sin^2 \theta \\ \epsilon_y &= \epsilon_2 \sin^2 \theta + \epsilon_1 \cos^2 \theta \\ \gamma_{xy} &= 2 (-\epsilon_2 + \epsilon_1) \sin \theta \cos \theta\end{aligned}\tag{6.2}$$

The three strain components ϵ_x , ϵ_y and γ_{xy} are the average longitudinal, transverse and shear strains. The average principal compressive and tensile strains are denoted as ϵ_2 and ϵ_1 , respectively.

c) The constitutive laws of materials are needed for the solution of the problem. To solve the above 6 equations (3 equilibrium and 3 compatibility equations) in 10 unknowns, given σ_x , σ_y , τ_{xy} , ρ_x and ρ_y , the stress-strain relationships for concrete in compression (f_{c2} , ϵ_2), concrete in tension (f_{t1} , ϵ_1), longitudinal steel (f_{sx} , ϵ_x) and transverse steel (f_{sy} , ϵ_y) are needed. The stress-strain relationship for concrete must reflect two characteristics. The first is the non-linear relationship between stress and strain. The second, and perhaps more important, is the softening of concrete in compression caused by cracking due to tension in the perpendicular direction as shown in figure 6.5a (Vecchio and Collins, 1986).

A confined-concrete model proposed by Saatcioglu and Razvi (1992) was modified and used in this analysis. The following expressions describe the modified model with reference to figure 6.5b:

$$f_{c2} = f_{c2max} \left[2 \frac{\epsilon_2}{\epsilon'_{cc}} - \left(\frac{\epsilon_2}{\epsilon'_{cc}} \right)^2 \right]^{1/(1+2K)} \leq f_{c2max} \quad (6.3)$$

where

$$f_{c2max} = \frac{f'_{cc}}{0.8 + 170 \epsilon_1} \leq f'_{cc} \quad (6.4)$$

$$f'_{cc} = f'_c + k_1 f_{le} ; \quad k_1 = 6.7 (f_{le})^{-0.17} ; \quad f_{le} = k_2 f_1 \quad (6.5)$$

$$k_2 = 0.26 \sqrt{\left(\frac{b_c}{S} \right) \left(\frac{b_c}{S_1} \right) \left(\frac{1}{f_1} \right)} \leq 1.0 \quad (6.6)$$

$$f_1 = \frac{\sum A_s f_{yt} \sin \alpha}{S b_c} \quad (6.7)$$

$$\epsilon'_{cc} = \epsilon_o (1 + 5K) ; \quad K = \frac{k_1 f_{le}}{f'_c} ; \quad \epsilon_o = 0.0004 \sqrt{f'_c} \quad (6.8)$$

$$\epsilon_{85} = 260 \rho \epsilon'_{cc} + \epsilon_{o85} ; \quad \rho = \frac{\sum A_s}{S(b_{cx} + b_{cy})} \quad (6.9)$$

where f'_c is the compressive strength of the unconfined concrete, f'_{cc} is the compressive strength of the confined concrete, ϵ_o is the unconfined concrete strain at maximum stress, ϵ'_{cc} is the confined concrete strain at maximum stress, S is the spacing of the transverse reinforcement in the longitudinal direction, S_1 is the spacing of longitudinal reinforcement

laterally supported by the corner of a hoop or the hook of a cross tie, b_c is the column core dimension measured center to center of perimeter hoop, b_{cx} and b_{cy} are the core dimensions in x and y directions, respectively, A_t is the area of one leg of transverse reinforcement, f_y is the yield strength of the transverse reinforcement and α is the angle between the leg of the transverse reinforcement and the column side.

The average principal tensile stress in the concrete, f_{cl} , was related to the principal tensile strain, ϵ_1 , and to the crack width, w . Prior to cracking, f_{cl} is given by the following:

$$f_{cl} = E_c \epsilon_1 \quad (6.10)$$

after cracking, f_{cl} is given by the following: (figure 6.5c)

$$f_{cl} = \frac{\alpha_1 \alpha_2 f_{cr}}{1 + \sqrt{500 \epsilon_1}} \quad (6.11)$$

where

$$f_{cr} = 0.33 \sqrt{f'_{cc}} \quad (6.12)$$

where α_1 , α_2 are factors accounting for the bond characteristics of reinforcement and type of loading, respectively. The value of α_1 is taken 1.0 for deformed reinforced bars, 0.7 for plain bars and 0.0 for unbonded reinforcement. The value of α_2 is taken 1.0 for monotonic loading and 0.7 for cyclic loading (Collins and Mitchell, 1991).

The described analysis considered average stresses and average strains while local variations were ignored. The stresses that occur at and near a crack location will differ from

the calculated average values. At cracks, there is no tensile stress in the concrete while the tensile stresses in the reinforcement are greater than their average values. The shear capacity of the joint may be limited by its ability to transmit forces across the crack (Collins and Mitchell, 1991). Figure 6.6 compares the average stresses that occur between the cracks (plane 1-1) with the local stresses that occur at a crack (plane 2-2). To maintain static equilibrium between the two sets of stresses shown in figure 6.6c and 6.6d, i.e. to have the same vertical and horizontal forces, it is required to limit the value of f_{c1} as follows:

$$f_{c1} \leq v_{ci} \tan\theta + \frac{A_{sy}}{S_x b} (f_{yy} - f_{sy})$$

$$f_{c1} \leq \frac{v_{ci}}{\tan\theta} + \frac{A_{sx}}{S_y b} (f_{yx} - f_{sx})$$
(6.13)

where A_{sx} and A_{sy} are the cross sectional area of the ties in x and y directions, S_x and S_y are the spacing between the ties in x and y directions as shown in figure 6.3, f_{yx} and f_{xy} are the yield strength of the reinforcing steel in x and y directions and v_{ci} is the local shear stress on the crack surface calculated as follows:

$$v_{ci} = \frac{0.18 \sqrt{f'_{cc}}}{0.3 + \frac{24w}{a + 16}} \quad \text{MPa}$$
(6.14)

where a is the maximum aggregate size (in mm) and the crack width, w (in mm) can be taken

$$w = \epsilon_1 S_{m0}$$
(6.15)

where S_{m0} is the spacing of the inclined cracks, which depends on the crack control characteristics of the reinforcement in both directions and the inclination of the cracks.

The following procedure is proposed for the calculation of $S_{m\theta}$ based on the element tests by Vecchio and Collins (1986) and the current concrete design code (CSA A23.3-94, 1994) approach. First, the minimum required cross sectional area of ties in the joint is calculated as follows:

$$A_{tie} = 0.06 \frac{\sqrt{f'_c}}{f_y} b_j S \quad (6.16)$$

where b_j is the joint width, S is the vertical spacing between the ties, and A_{tie} is the cross sectional area of the tie bars within a distance S . Second, the cross sectional area of the ties in the joint is compared to the specified minimum cross sectional area of the ties A_{tie} .

If the cross sectional area of the ties in the joint is less than the specified minimum cross sectional area of ties A_{tie} (CSA A23.3-94, 1994) then

$$S_{m\theta} = \frac{1}{\frac{\sin\theta}{S_{mx}} + \frac{\cos\theta}{S_{my}}} \quad (6.17)$$

where S_{mx} is the average crack spacing that would result if the element was subjected to a horizontal tension and S_{my} is the average crack spacing that would result if the element was subjected to a vertical tension as shown in figure 6.3. S_{my} depends on the distribution and cross sectional area of the horizontal reinforcement as shown in figure 6.3 such that: if the cross sectional area of the horizontal reinforcement is greater than or equal $0.004 b_j S_y$ then $S_{mx} = S_y$; otherwise $S_{mx} = 0.9$ the depth of the beam d_{beam} . Similarly approach is adopted in the case of the vertical reinforcement.

If the cross sectional area of the ties in the joint is greater than or equal to the specified minimum cross sectional area of ties A_{tie} (CSA A23.3-94, 1994) then $S_{m\theta} = 300$ mm.

The effective joint area

In the ACI code (1989) and the Architectural Institute of Japan, AIJ, guidelines (1988), the dominant shear resisting mechanism is assumed to be the diagonal strut action. Therefore, the entire column depth is assumed to be effective in an interior joint. However the horizontal projection of the 90-degree hook is used in an exterior joint because the compression strut is assumed to start at the corner of the bend by bearing against core concrete.

According to the ACI-ASCE committee 352 (1985), the joint width, b_j is equal to $(b_c + b_b)/2$ but not greater than the beam width b_b plus one-half of the column depth, h_c , on each side of the beam where b_c , b_b are the width of the column and beam, respectively, (figure 6.7a). The AIJ guidelines (1988) limit the effective joint width, b_j in an eccentric joint by $b_b + b_{a1} + b_{a2}$ where b_{a1} and b_{a2} are on either side of the beam and are the smaller of:

- (i) one-quarter of column depth (e.g. shaded area on bottom side in figure 6.7b); and
- (ii) one-half of distance between beam and column faces (e.g. shaded area on top side in figure 6.7b)

Criterion for shear failure

The failure of the joint element can be categorized as tensile failure or compressive failure. Compressive failure will occur when the compressive stress of concrete reaches the maximum strength of concrete. As the compressive strength of concrete deteriorates due to the existence of cracks, it is more appropriate to define the compressive failure by the maximum strain in the concrete. The failure criterion in compression is expressed by, $\epsilon_c \geq \epsilon_{cc}'$, where ϵ_c is the compressive strain of concrete and ϵ_{cc}' is the compressive strain corresponding

to the maximum strength. Tensile failure will occur when the reinforcing bar reaches the limit state. It is observed experimentally (Izumo, 1992) that the strain affects the maximum strength of the reinforced concrete panel less than the stress. Thus, the maximum strain of the reinforcing bar has been chosen to express the tensile failure for the reinforced concrete joints. Considering the experimental results, the maximum tensile strain in the reinforcing bar has been set at 0.03 for the tensile failure of the reinforced concrete joints.

6.4.2 Equilibrium of joint forces

The softening truss model is used to determine the shear stress-shear deformation relationship. This relationship can be changed to an equivalent moment-rotation relationship that defines the characteristics for the rotational spring to represent the shear deformation in the joint. Figure 6.8a shows a free body diagram of an interior beam-column assemblage between its points of contraflexure while figure 6.8b shows the equilibrium of an interior column between its points of contraflexure with equal and opposite axial forces substituted for the beam moment. Equilibrium of the forces in figure 6.8b in the horizontal direction gives:

$$V_{jh} = C_b + T_b - V_{col}$$

$$C_b = T_b = \frac{M_b}{jd} \quad (6.18)$$

where jd is the moment arm of the beam.

Summing the moments in figure 6.8a and expressing beam shear in terms of an equivalent beam moment results in:

$$V_{col} = V_b \frac{L_b}{L_c} = \frac{M_b L_b}{\frac{(L_b - h_c)}{2} L_c} = \frac{2 M_b}{L_c (1 - \frac{h_c}{L_b})} \quad (6.19)$$

Substituting equation 6.19 back in V_{jh} given by equation 6.18, then:

$$V_{jh} = \frac{2 M_b}{jd} - \frac{2 M_b}{L_c (1 - \frac{h_c}{L_b})} \quad (6.20)$$

Defining ΣM_b as the total beam moment to be transferred to the column by joint shear, the following expression can be obtained:

$$\Sigma M_b = 2 M_b = \frac{V_{jh}}{\frac{1}{jd} - \frac{1}{L_c (1 - \frac{h_c}{L_b})}} \quad (6.21)$$

Using the same procedure of calculating ΣM_b , as a function of the joint shear force, formulations for the ΣM_b can be made for interior top floor and exterior top floor beam-column connections including corner joints. Figures 6.9 and 6.10 show the equilibrium and shear diagram of an exterior middle floor and an interior top floor beam-column connections, respectively.

6.4.3 Development of computer program "SHEAR"

A computer program was developed to predict the response of reinforced concrete joints subjected to shear and axial force. A suitable solution algorithm using the above relationships to predict the moment-rotation relationship of the spring representing the joint is described in Appendix B. A listing of the program is also attached in Appendix B.

6.4.4 Model Verification

The calculated shear-deformation envelopes of the reinforced concrete joints have been compared to the test results of the six beam-column joints in the current experimental program, eight beam-column joints by Fujii and Morita (1991) and eighteen beam-column joints by Kaku and Asakusa (1991). The analytical results compare satisfactorily with experiments as shown in figures 6.11, 6.12 and 6.13. The proposed model for reinforced concrete joints has been shown to be effective for the analysis of the reinforced concrete joints under monotonic and reverse cyclic loading (envelope prediction).

6.4.5 Moment-rotation relationship under cyclic loading

The analytical model was extended to simulate the joint behaviour under cyclic loading conditions. The hysteretic model is shown in figure 6.14. This model was proposed by Sakata and Wada (1991) with the following features: a) as long as the joint shear remains below the cracking value, the joint behaves elastically with stiffness equal to the initial elastic stiffness (K_1); b) once the joint moment exceeds the cracking moment (M_1), the joint stiffness becomes equal to K_2 ; c) the joint unloads with stiffness equal to K_1 up to a moment equal to $2M_1$ subtracted from the maximum previously attained moment, then unloads with stiffness equal to K_2 ; and d) if the joint moment exceeds the yield moment M_2 , the joint stiffness becomes equal to K_3 .

From the described model, the entire joint response can be identified by five parameters, three stiffness values K_1 , K_2 , and K_3 and two limiting moments M_1 and M_2 .

6.4.6 Effect of transverse beams

The confining effect of transverse beams on the joint in indeterminate structures is

likely to be significant. From tests performed on interior beam-column joints with transverse beams, it has been established that even joints without ties can perform satisfactorily within realistic levels of lateral displacement (Kurose, Y., 1987). Kitayama et al. (1991) tested interior beam-column joints with and without transverse beams. It was observed that transverse beams, even when loaded in a cyclic way to flexural yielding, could enhance the joint shear strength by at least 1.2 times the shear in the case of no transverse beams. The increase in joint confinement is attributed to the longitudinal reinforcement in the transverse beams as shown in figure 6.15. The confining effect may be directly related to the amount of the longitudinal reinforcement in the transverse beams.

The Architectural Institute of Japan Standards (1988) increases the nominal shear strength of interior beam-column joints 1.3 times that in the case without transverse beams nor slab (i.e. from $0.25 f'_c$ to $0.33 f'_c$). This recommendation is based on the assumption that (a) transverse beams and slab are cracked, (b) beams frame into the four vertical faces of the joint and (c) at least two-thirds of each joint face is covered by framing beam. The Architectural Institute of Japan guidelines for earthquake resistant reinforced concrete buildings (1988) proposes that, in case of transverse beams, the shear resistance may be increased by a factor β such that

$$\beta = 1 + 0.3 \lambda \quad , \quad \lambda = \frac{\sum b_T D_T}{2(D_L D_c)} \quad \text{and} \quad D_T \leq D_L \quad (6.22)$$

where D_L , D_c , D_T and b_T are the total depth of the longitudinal beam, the total depth of the column, the total depth of the transverse beam and the width of the transverse beam, respectively. The effect of the transverse beam shall not be considered if the transverse beam

exists only on one side of the joint.

The shear resistance in this study is proposed to be increased by a factor β^* such that:

$$\begin{aligned} \beta^* &= 1.4 && \text{for the cracking shear stress} \\ \beta^* &= 1.0 + 10 \rho \lambda^* < 1.2 && \text{the ultimate shear strength for interior joints} \\ &< 1.4 && \text{the ultimate shear strength for exterior joints} \end{aligned}$$

where

$$\begin{aligned} \rho &= \frac{\sum \text{Longitudinal reinforcement in transverse beams}}{\text{average area of transverse beams}} \\ \lambda^* &= \frac{\sum b_T D_T}{D_c (D_{L \text{ [left]}} + D_{L \text{ [right]}})} \quad D_T \leq D_L \end{aligned} \quad (6.23)$$

6.4.7 Slab contribution

The influence of the floor slabs on the shear strength of interior joints is illustrated by figure 6.16. The average joint shear stress is compared for specimens with and without floor slabs. Joint shear strength was increased at least 1.1 times due to the floor slabs for interior connections (1.05 in case of exterior connection). The shear strength enhancement is attributed to the following reasons: a) the uniformly distributed shear stresses in the joint panel concrete; b) the relieving of the stress concentration from the joint diagonal compression strut; c) the shear from the slab concrete adjacent to the upper part of a joint in specimen A4 without transverse beams; d) the torsion of transverse beams framing into a joint such as specimen A3; and e) the slab confines the top part of the joint. In exterior joints, the increased tensile force provided by the slab reinforcement is introduced to the joint through

shear, weak-axis bending and twist of the transverse beam. These actions may require the use of additional shear reinforcement within the joint which is not accounted for in the current design philosophy for joints. It is also noted from figure 6.16 that the joint shear strength of specimen A3 with both transverse beams and floor slabs was more than 1.3 times larger than that of specimen A1 without transverse beams or floor slabs.

6.5 MODELLING OF BOND SLIP

Based on experimental results, several investigators (Kaku and Morita, 1978) indicated that additional rotations caused by the anchorage slip of the reinforcing bars from the beam-column joints contribute significantly to the total inelastic deformations of reinforced concrete multistory frames subjected to strong earthquake motions. Analytical approaches to determine the load-displacement relationship of reinforced concrete beam-column subassemblages or frames are developed considering these additional rotations (Ichinose, 1983). More complex bond-slip models have also been proposed (Hawkins and Lin, 1979, Filippou et al., 1986, Filippou, 1986 and Alsiwat and Saatcioglu, 1992).

When bond-slip occurs, the joint shear is reduced and the contribution of bond-slip to story drift is accompanied by reduction in the contribution of joint distortion to drift. Therefore, beam hinging and bond-slip indicate stiff joint panel behaviour. Beam bars with favourable bond conditions induce more joint shear distortion to the joint panel and require larger amount of joint hoop reinforcement. However, in connections with poor bond conditions along the beam bars, the joint rotates as a rigid body to accommodate the excessive pull-out of the reinforcement. The resulting increased connection flexibility could

not be counteracted by higher axial loads or by increased transverse reinforcement. This is probably the reason why tests done in north America are different from those conducted in New Zealand. North American specimens are characterized by poor bond condition and high joint rotation as rigid body and the behaviour is not affected by axial load and amount of transverse steel ties (Pantazopoulou and Bonacci, 1994). New Zealand specimens are characterized by favourable bond condition and high joint shear distortion and the behaviour is affected by the axial load and required large amount of joint hoop reinforcement.

6.5.1 Moment-rotation relationship

In the current study, a simple moment-rotation relationship is proposed. The moment-rotation relationship due to bond-slip is defined by the critical points of cracking (M_{cr}), yielding (M_y, θ_y) and ultimate (M_u, θ_u) conditions. A bi-linear idealization is assumed as shown in figure 6.17. The advantage of this simple relationship is its easy application and introduction into the non-linear frame analysis. The various constants used in this formulation are determined based on analytical calculations and experimental data.

Neglecting the concrete strain along the bar in the joint, the slippage Δ_s at the beam-column interface is given by the integration of the steel strain distribution over a length L_s as follows:

$$\Delta_s = \int_0^{L_s} \epsilon_s \, dx \quad (6.24)$$

where L_s represents the distance from the beam-column interface to the point at which the bar begins to slip as shown in figure 6.18a.

Before bar yielding ($\epsilon_s \leq \epsilon_y$), it is assumed that (a) the steel stress and strain

distributions are linear, (b) the concrete bond stress is uniform and (c) its magnitude is proportional to the tensile strain ϵ_s at the beam-column interface and the square root of the concrete strength, hence,

$$f_b = \eta^* \epsilon_s \sqrt{f'_c} \quad \text{MPa} \quad \text{where } \eta^* = 600 \quad (6.25)$$

where f'_c is the concrete compressive strength in MPa. The constant value η^* was determined from experimental test results of Morita and Kaku (1972). This value also gives a good agreement between the bond stress and that calculated by the ACI committee 408 (1979).

From the equilibrium of the bar axial force,

$$L_s = \frac{f_s A_s}{\sum \text{perimeter} \cdot f_b} = \frac{E_s d_b}{4 \eta^* \sqrt{f'_c}} \quad (6.26)$$

where A_s is the area of the beam reinforcing bar in square mm, d_b is the diameter of the bar in mm, E_s is the modulus of elasticity of steel in MPa, f_b is the average bond stress in MPa, f_s is the beam reinforcing bar stress in MPa.

The bar slippage from the joint in mm is given by:

$$\Delta_s = \frac{L_s \epsilon_s}{2} = \frac{f_s d_b}{4800 \sqrt{f'_c}} \quad (6.27)$$

After the yielding of the steel bar, ($\epsilon_s > \epsilon_y$), it is assumed that the bar stress-strain relationship includes no plastic flow and that the strain hardening immediately follows. The stress and strain distributions in the joint may be assumed bilinear as shown in figure 6.18b.

After yielding the slope of the bilinear $M-\theta$ relationship depends on the strain-hardening characteristics of the reinforcing bars, the thickness of the concrete cover relative to the dimensions of the cross section confined by the transverse steel, the amount of transverse steel, the size of the yielding region, the penetration of yielding into the beam-column connection as well as other factors. The upper limit length of slip region is denoted L_{\max} and is defined in figure 6.19 for interior and exterior joints. The yield development length is denoted L_y (figure 6.18b) and was determined from the strain measurements of bars in the joints of the beam-column subassemblages tested by Morita and Kaku (1984) as follows:

$$\chi = \frac{f_s}{f_y} \leq \frac{f_{ult}}{f_y} \quad (6.28)$$

$$\text{for } 1 < \chi \leq 1.05 \quad L_y = 2000 \chi - 2000 \text{ mm}$$

$$\chi > 1.05 \quad L_y = 500 \chi - 425 \text{ mm}$$

Therefore, the value of bar slippage from the joint can be calculated as:

$$\Delta_s = \frac{L_s \epsilon_y + L_y (\epsilon_y + \epsilon_s)}{2} \quad (6.29)$$

$$= \left[\frac{(L_s + 2 L_y)}{E_s} + (\chi - 1) \frac{L_y}{E_{sh}} \right] \frac{f_y}{2}$$

where E_{sh} is the strain hardening modulus of elasticity of steel and f_{ult} is the ultimate strength of the reinforcing bars. The yield development length L_y , should not exceed the maximum limit ($L_{y\max}$) which is defined in figure 6.19 for interior and exterior joints (Morita and Kaku, 1984). If $L_s + L_y > L_{\max}$ or $L_y > L_{y\max}$, L_{\max} or $L_{y\max}$ are substituted for $(L_s + L_y)$ or L_y in the above equations, respectively.

The situation is either yielding of the reinforcement before slippage ($L_s \leq L_{max}$) or pull-out before yielding ($L_s > L_{max}$). In the first case of yielding then slippage, the stiffness before yielding K_1 as shown in figure 6.17 is calculated as:

$$\begin{aligned} K_1 &= \frac{M_y}{\theta_y} = \frac{n A_s f_y}{\Delta_y} (d-d')^2 \\ &= 1200 \pi n d_b (d-d')^2 \sqrt{f'_c} \quad \text{N.mm} \end{aligned} \quad (6.30)$$

where θ_y and Δ_y are the rotation and bar slippage at yielding, $(d-d')$ is the effective depth of the beam and d_b is the beam tensile reinforcing bar diameter and n is the number of tensile reinforcing bars in the beam.

After yielding, the stiffness is not constant and it is assumed to be a function of χ . Consider a point on the moment-rotation relationship (figure 6.17) with coordinates (θ_2, M_2) identified by $L_y = L_{ymax}$. The factor χ at this point (denoted χ_2). The stiffness K_2 can be calculated as follows:

$$\chi_2 = \frac{f_{s2}}{f_y} = \frac{M_2}{M_y} \leq \frac{f_{ult}}{f_y} \quad (6.31)$$

$$K_2 = \frac{M_2 - M_y}{\theta_2 - \theta_y} = \frac{(\chi_2 - 1) n A_s f_y (d-d')^2}{\Delta_2 - \Delta_y} \quad (6.32)$$

$$K_2 = \frac{2 (\chi_2 - 1) n A_s (d-d')^2 E_s}{2 L_{ymax} + \left(\frac{\chi_2 - 1}{\zeta}\right) L_{ymax}} \quad (6.33)$$

where $\zeta = E_{st}/E_s$

If $L_s + L_{y\max} > L_{\max}$ then $L_y = L_{\max} - L_s$

$$K_2 = \frac{2 (\chi_2 - 1) n A_s (d-d')^2 E_s}{(L_{\max} - L_s) [2 + (\frac{\chi_2 - 1}{\zeta})]} \quad (6.34)$$

In the second case of bar pull-out before yielding in which $L_s > L_{\max}$ and $K_2 = 0$, the moment M_1 and the stiffness K_1 can be calculated as follows:

$$M_1 = n A_s f_y (d - d') \frac{L_{\max}}{L_s} \quad (6.35)$$

$$K_1 = \frac{2 n A_s E_s (d-d')^2}{L_{\max}} \quad (6.36)$$

6.5.2 Moment-rotation relationship under cyclic loading

The model developed by Chung et al. (1987) is adopted to represent the hysteretic behaviour of the rotation spring representing the bond slip. The model is capable of including the effects of stiffness degradation, strength deterioration and pinching. An input parameter governs the strength deterioration ranges between 0.0 and 0.1, where a value of 0.0 signifies no strength deterioration. In the present study, it is selected to be 0.1.

The bond deterioration zone is limited to the neighbourhood of column face if the bars have full development length. Only top and bottom bars are assumed to resist the external moment without contribution from the concrete. This phenomenon is characterized as a stable spindle type in the load deflection curve. On the other hand, in the case of a bar with

short development length, the complete bar slippage from the joint will occur at low load level following a number of high load cycles. This phenomenon is characterized as a pinching type in load-deflection curve (Morita and Kaku, 1984). The pinching effect is introduced in the loops by an input parameter α^* as shown in figure 6.20. The parameter α^* ranges between 0.0 and 1.0. A value of 1.0 signifies no pinching. The value of α^* depends on several parameters such as the development length of the beam bars in the joint, the degree of shear reinforcement in the joint, the existence of transverse beam and number of loading cycles. The parameter α^* can be calculated after making use of the reported test results by Morita and Kaku (1984) as:

For interior columns:

$$\begin{aligned} L_s &\leq h_c & \alpha^* &= 1.0 \quad (\text{no pinching}) \\ h_c &< L_s \leq L_{\max} & \alpha^* &= 1.0 - 0.5 [(L_s - h_c)/(L_{\max} - h_c)] \\ L_s &> L_{\max} & \alpha^* &= 0.5 \end{aligned}$$

For exterior column:

$$\begin{aligned} L_s &\leq h_c & \alpha^* &= 1.0 \quad (\text{no pinching}) \\ h_c &< L_s \leq L_{\max} & \alpha^* &= 1.0 - 0.25 [(L_s - h_c)/(L_{\max} - h_c)] \\ L_s &> L_{\max} & \alpha^* &= 0.75 \end{aligned}$$

where h_c represents the column depth.

6.6 MODELLING OF LAP-SPLICES IN COLUMN BARS

Lap splices in column bars designed prior to 1970 were typically about 20 bar diameters, and were often located in the potential plastic hinge regions. Strength of such lap

splices can be determined by postulating the full pattern of cracking that should be developed to enable each bar to slide relative to the adjacent bars with which they are lapped (Priestley, 1996). Generally, this involves a plane of cracking in the plane of the spliced bars and two perpendicular cracks per pair of lapped bars, as shown in figure 6.21. For rectangular columns, examination of the mechanics of the splice failure leads to the following expression for the maximum tensile force that can be developed in a single longitudinal bar:

$$T_b = f_t p L_d \quad (6.37)$$

$$p = \frac{S}{2} + 2(d_b + c) \leq 2\sqrt{2}(d_b + c) \quad (6.38)$$

where f_t is the tensile strength of concrete taken as $0.33 \sqrt{f'_c}$ MPa, L_d is the lap length and p is the perimeter of the crack surface depending on local bar spacing S , concrete cover c and bar diameter d_b which are schematically shown in figure 6.21.

Due to the insufficient experimental data available and the difficulties of numerically modelling the extremely complicated bond-slip conditions of such unconfined columns, a simplified elastic perfectly plastic behaviour mode is assumed as shown in figure 6.17 with stiffness $K_2 = 0$ and moment M_y calculated as:

$$M_1 = M_y = n T_b (d - d') \quad (6.39)$$

where n is the number of longitudinal bars in the column, d is the depth of the column and d' is the depth of the compression reinforcement of the column.

Assuming that the steel elongation contributes to the crack opening at the face of the column, then the opening of the crack at the level of the steel (δ) is given by the integration of the steel strain distribution over the lap splice length L_d as follows:

$$\delta = \frac{L_{sl}}{2} \epsilon_s = \frac{L_{sl} T_b}{2 A_s E_s} \quad (6.40)$$

The concentrated rotation of the column at the column face due to bond-slip is calculated as $\delta / (d - d')$. Therefore, the stiffness K_1 is given as:

$$K_1 = \frac{M_1}{\delta} (d - d') = \frac{2 n A_s E_s (d - d')^2}{L_{sl}} \quad (6.41)$$

where A_s is the cross sectional area of one of the longitudinal bars of the column.

6.7 CORRELATION WITH TEST RESULTS

The developed reinforced concrete joint shear element and bar bond slip element were implemented in the SARCF computer program for the non-linear static and dynamic response of reinforced concrete frames. To establish the validity and accuracy of the proposed models, the program is used in the simulation of the hysteretic behaviour of beam-column subassemblages. The analytical model used to simulate the behaviour of the specimens consists of a girder element, two column elements, joint shear element and bond slip element. The properties of the constituent elements are derived from the material and geometric properties of the specimens. Using the measured stress-strain relationships of concrete and reinforcing steel, the section geometry and the reinforcement layout of the girder, the monotonic moment-curvature relationship of a typical girder section can be established. The parameters of the joint shear elements and the bar bond slip elements are summarized in table

6.1. Figure 6.22 shows the analytical and experimental load-displacement relationship of the specimens. Figure 6.23 shows the analytical and experimental load-displacement envelopes of the specimens. From the results presented in figures 6.22 and 6.23, the following observations are made:

- a) in spite of the simplicity of the hysteretic model used in the different elements, good agreement between the predicted local behaviour of beam-column subassemblages and the experimental evidence is found.
- b) the analytical model is capable of correctly representing the strength and stiffness of the subassemblage. This is important in the case of the post-yield stiffness where slight discrepancies can lead to substantial deviations between observed and predicted forces. The strength degradation in the model agrees with the experimental measurements.
- c) the pinching of the hysteretic behaviour of the girder caused by the interaction of shear forces with the opening and closing of the cracks is predicted by the analytical model. This effect is particularly important in short span members.
- d) a limitation of the hysteretic models appears to be the value of the unloading stiffness which is consistently lower than observed in experiments. There is, however, as yet no rational model for predicting the unloading stiffness in the inelastic girder regions.

6.8 SUMMARY

In typical reinforced concrete construction, a floor slab is cast monolithically with the beams and lower column. The effect of a monolithic slab can not be ignored in design since

the additional moment capacity will affect the behaviour of the joint in two ways. First, the presence of the slab will increase the total joint shear, and second, it will decrease the column-to-beam moment ratio. An analytical model to take the floor effects into account was suggested. A bi-linear moment-rotation analytical model representing beam reinforcing bar bond-slip was selected for the case of monotonic loading and to establish the envelope of reversed cyclic loading. A tri-linear moment-rotation analytical model representing joint shear was developed for the case of monotonic loading and to establish the envelope of reversed cyclic loading. The model sensitivity was assessed by comparing its results to experimental measured results of reinforced concrete joints. The developed model was found to be capable of accurately predicting the behaviour of reinforced concrete joints subjected to in-plane stresses. A reasonable analytical prediction of the hysteretic behaviour of the tested specimens was accomplished.

Table 6.1 Parameters of joint shear and bar bond slip elements

Specimens	Shear element					Bond slip element					
	M_1 (kN.m)	M_2 (kN.m)	K_1 (kN.m/rad)	K_2 (kN.m/rad)	K_3 (kN.m/rad)	M_1 (kN.m)	K_1 (kN.m/rad)	K_2 (kN.m/rad)	L_s (mm)	L_{max} (mm)	L_{ymax} (mm)
J1	327	401	1758064	21301	3348	320	598730	11803	255	507	394
J2	327	691	1758064	77380	28926	320	670600	9793	227	503	390
J3	327	728	1758064	84000	21066	320	645849	9937	236	507	394
J4	327	327	1758064	0	0	290	605696	0	278	250	250
J5	327	728	1758064	84000	21066	320	645849	9937	236	507	394
J6	327	754	1758064	92544	0	320	645849	0	236	510	510

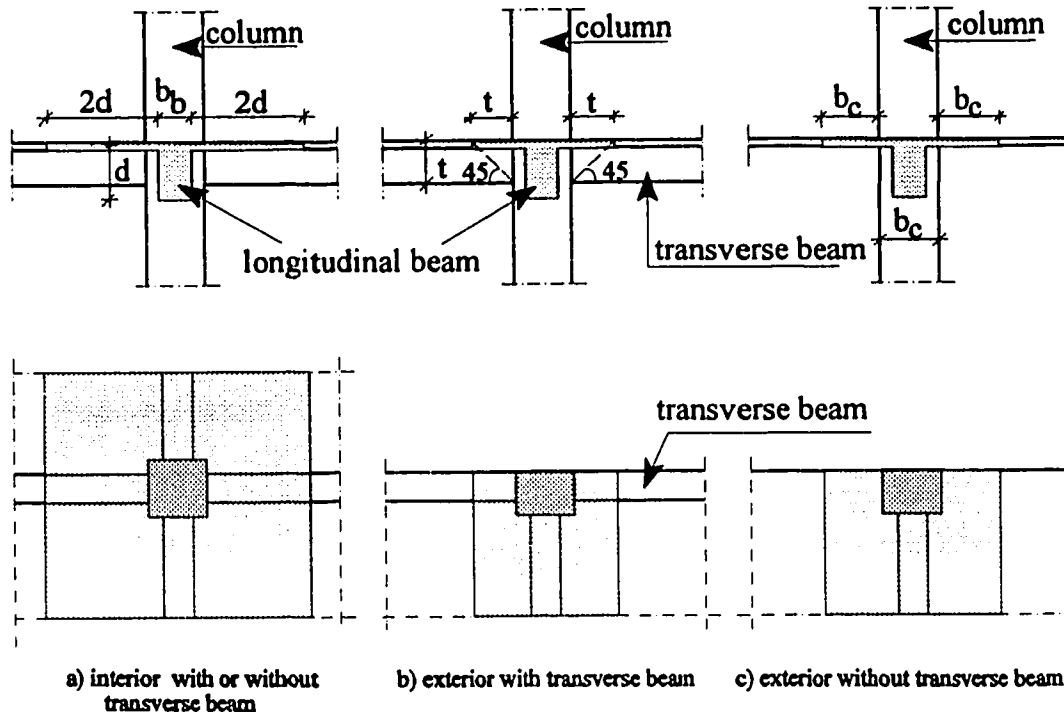


Figure 6.1 Proposed effective slab width for negative moments

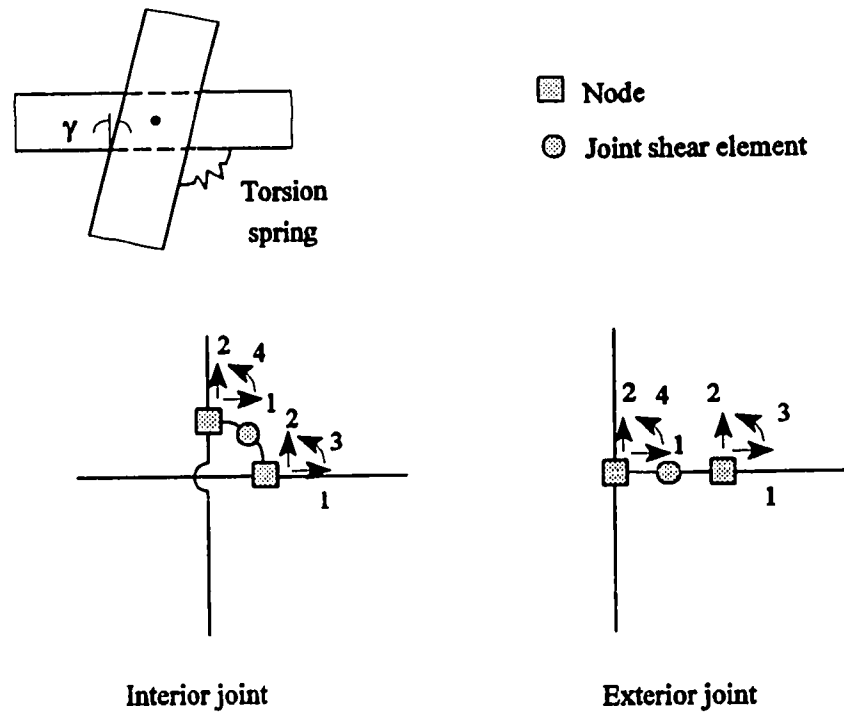


Figure 6.2a Idealization of the joint shear element in frame analysis

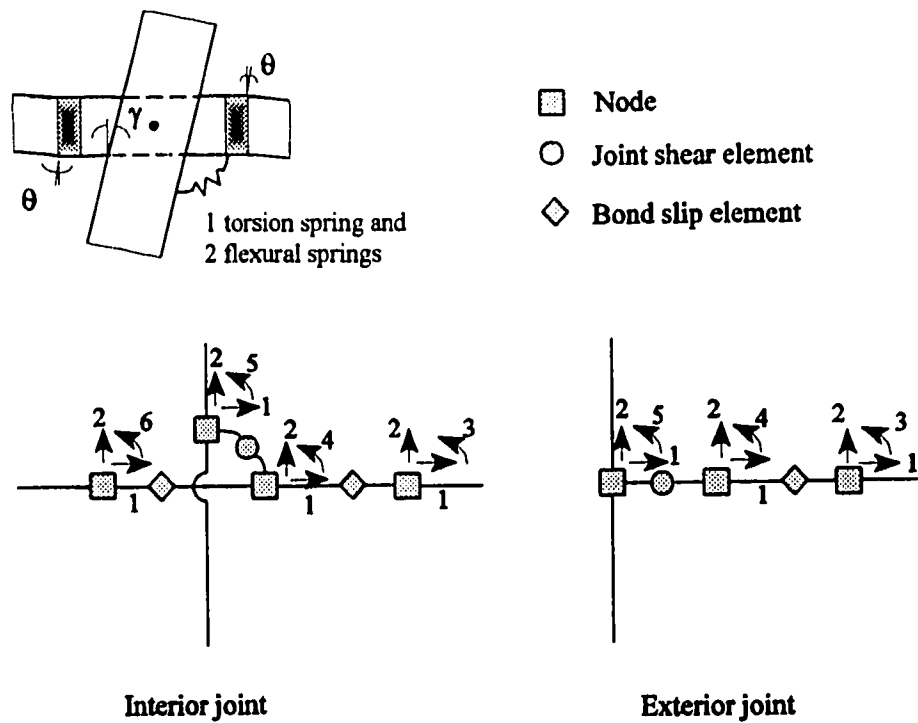
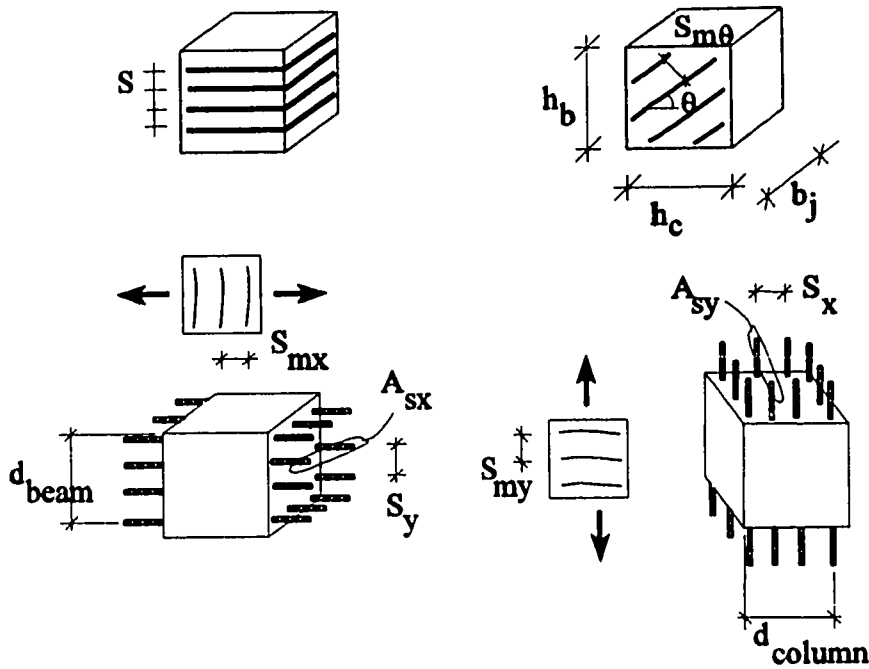


Figure 6.2b Idealization of the joint shear and bond slip elements in frame analysis



If $A_{sx} < 0.004 b_j S_y$
 then $S_{mx} = 0.9 d_{beam}$
 If $A_{sx} \geq 0.004 b_j S_y$
 then $S_{mx} = S_y$

If $A_{sy} < 0.004 b_j S_x$
 then $S_{my} = 0.9 d_{column}$
 If $A_{sy} \geq 0.004 b_j S_x$
 then $S_{my} = S_x$

where $S_{m\theta}$ = the average crack spacing
 S_{mx} = the average crack spacing that would result if the element was subjected to horizontal tension
 S_{my} = the average crack spacing that would result if the element was subjected to vertical tension

Figure 6.3 Joint geometry

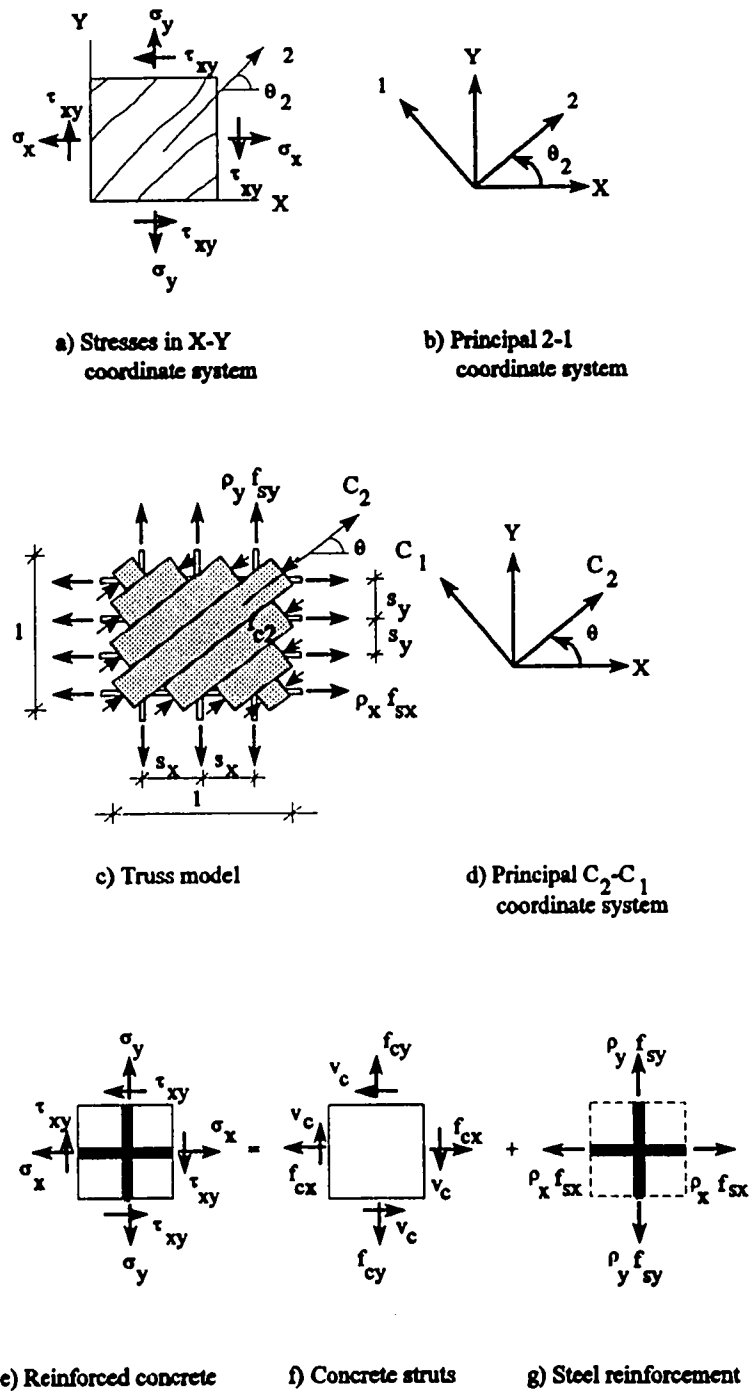
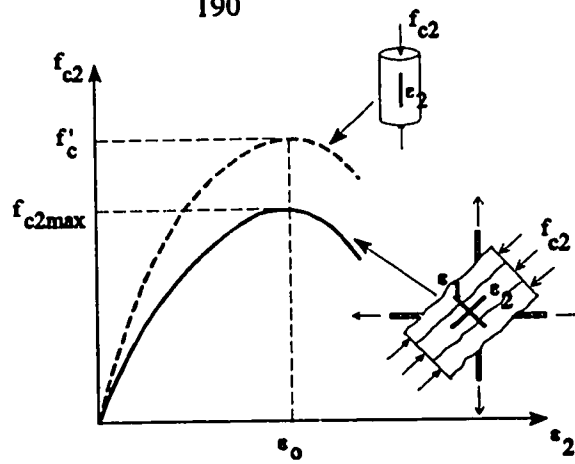
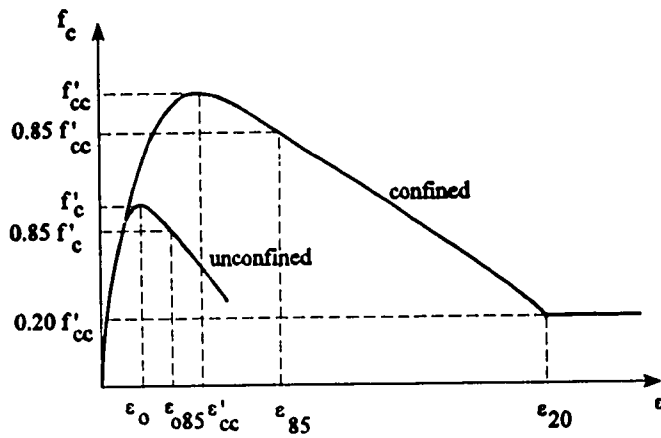


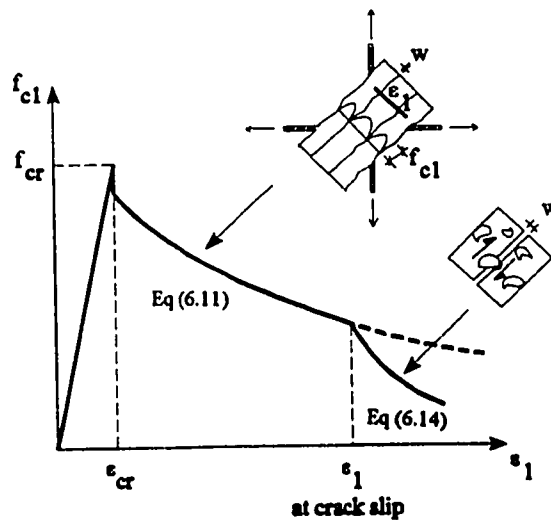
Figure 6.4 Definitions of stresses and coordinate systems



a) stress-strain relationship for cracked concrete in compression



b) confined concrete model



c) average stress-strain relationship for cracked concrete in tension

Figure 6.5 Stress-strain relationships for concrete

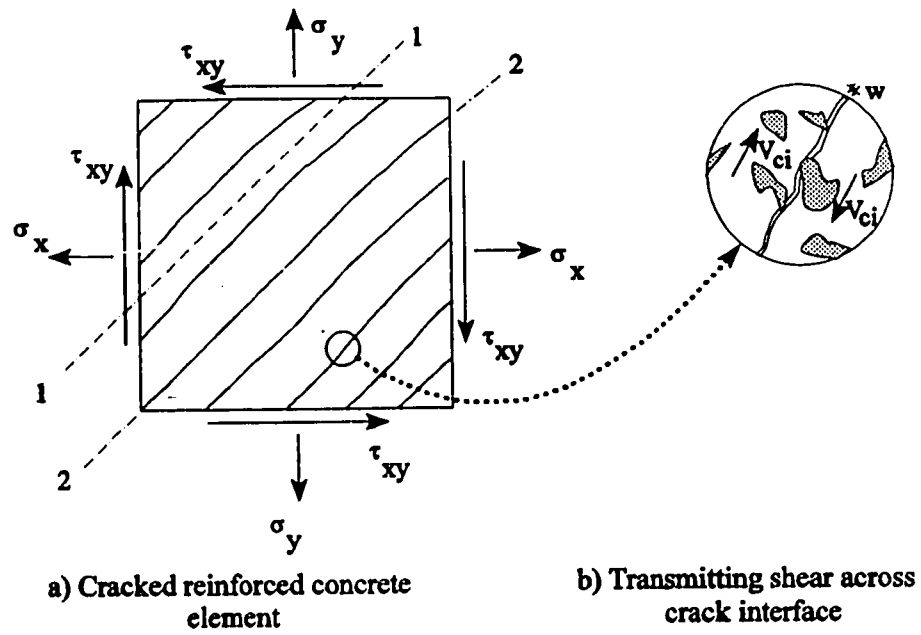
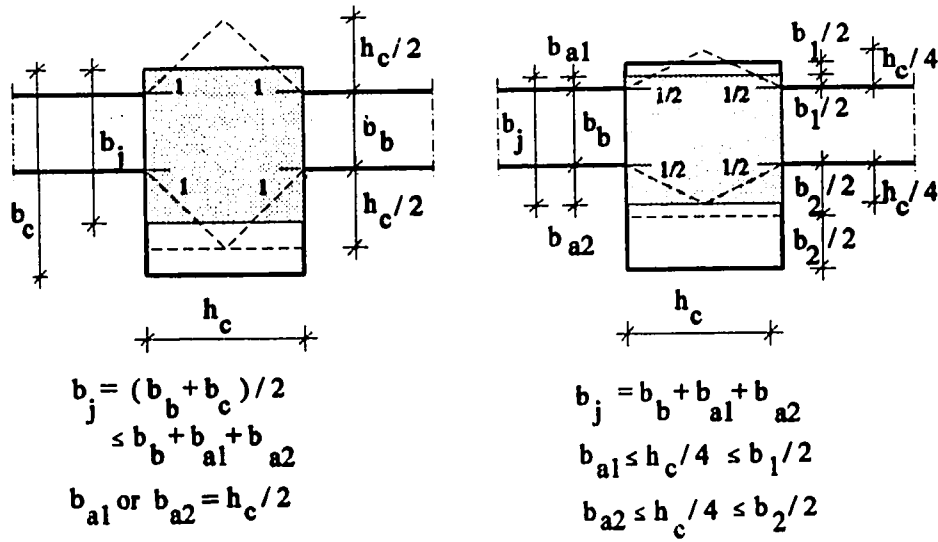


Figure 6.6 Local stresses at a crack



a) ACI 352 committee, 1985

b) AIJ guidelines, 1988

Figure 6.7 Effective joint width

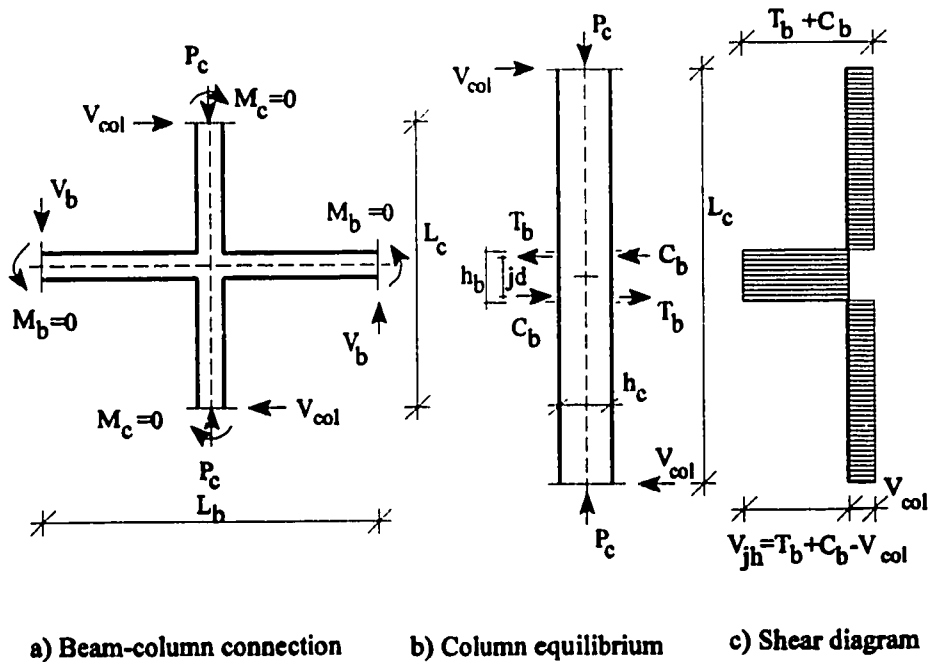


Figure 6.8 Equilibrium of interior beam-column joint

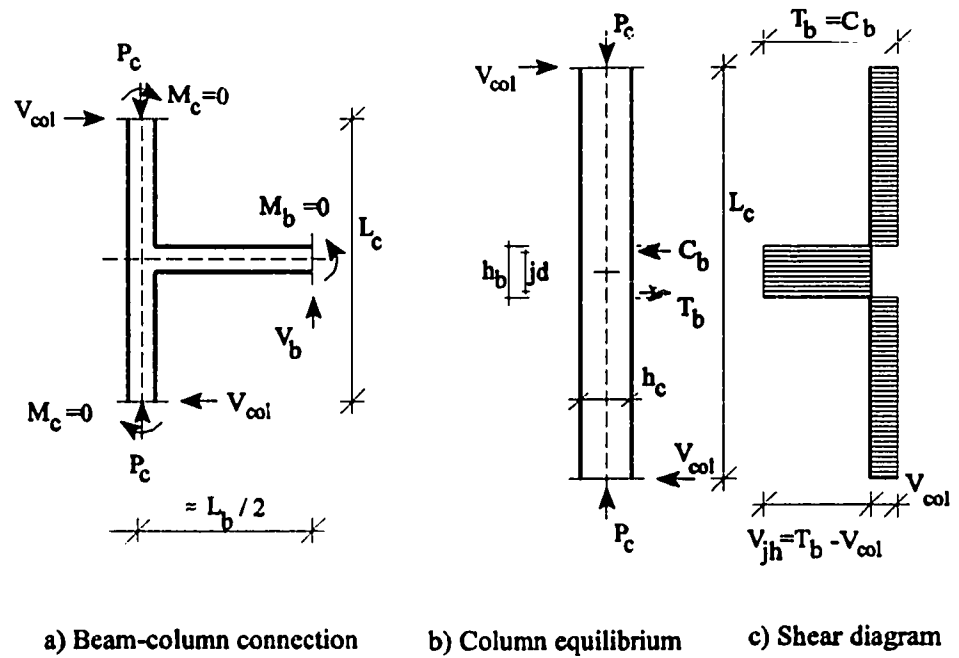


Figure 6.9 Equilibrium of exterior beam-column joint

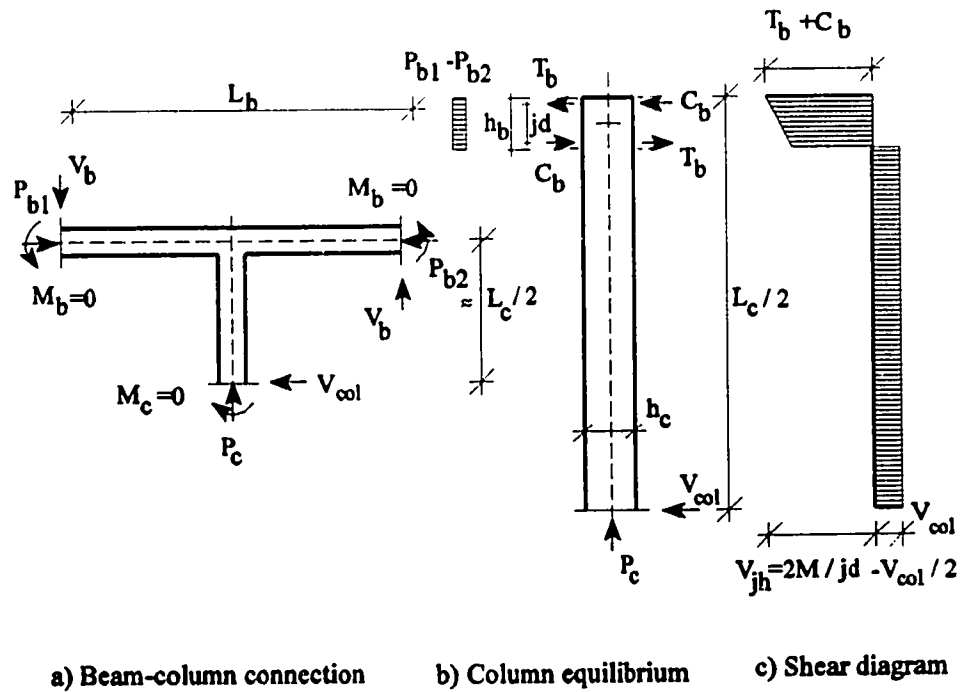


Figure 6.10 Equilibrium of top floor interior beam-column joint

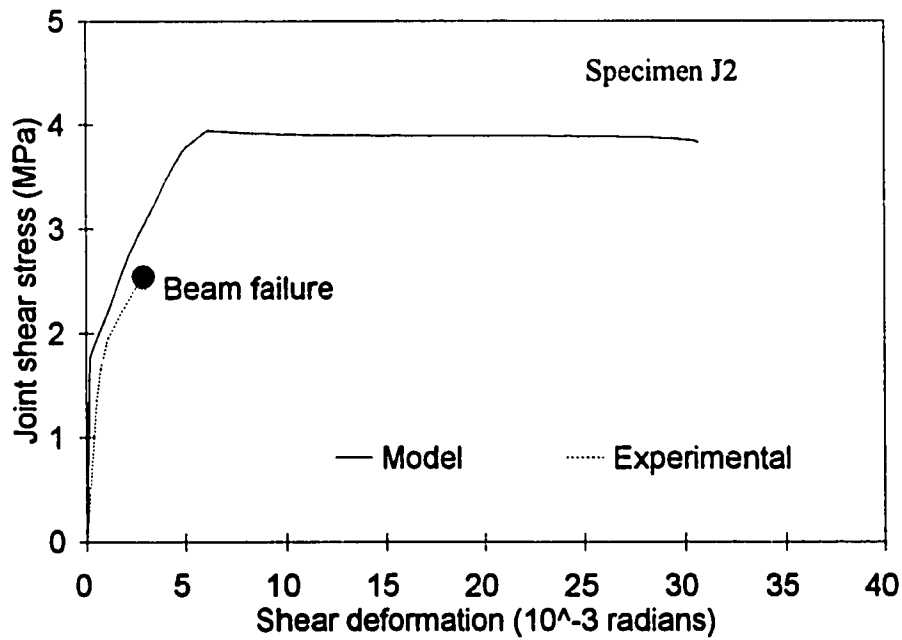
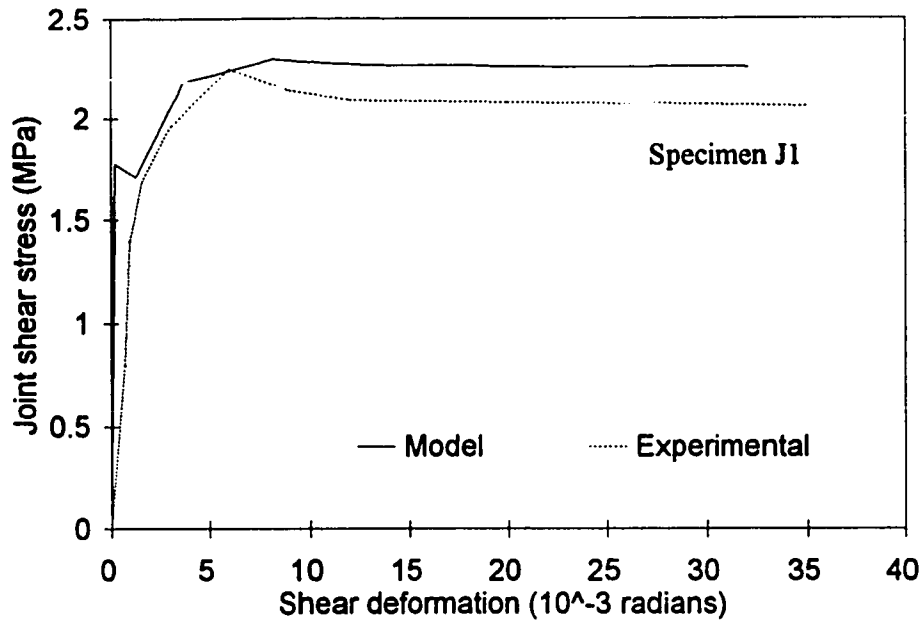


Figure 6.11 Analytical results compared to current experimental program results

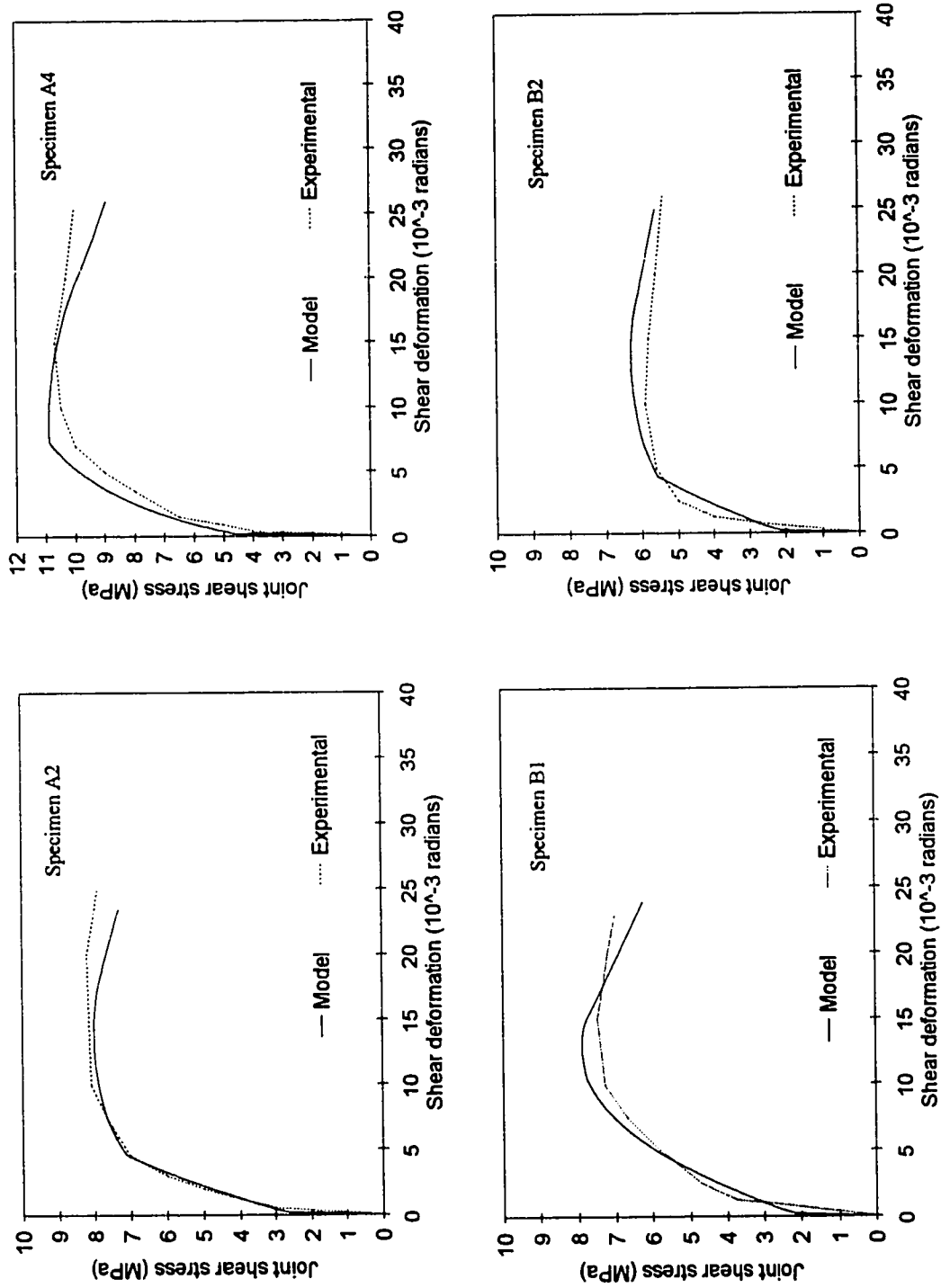


Figure 6.12 Analytical results compared with the experimental results of Morita and Fujii (1991)

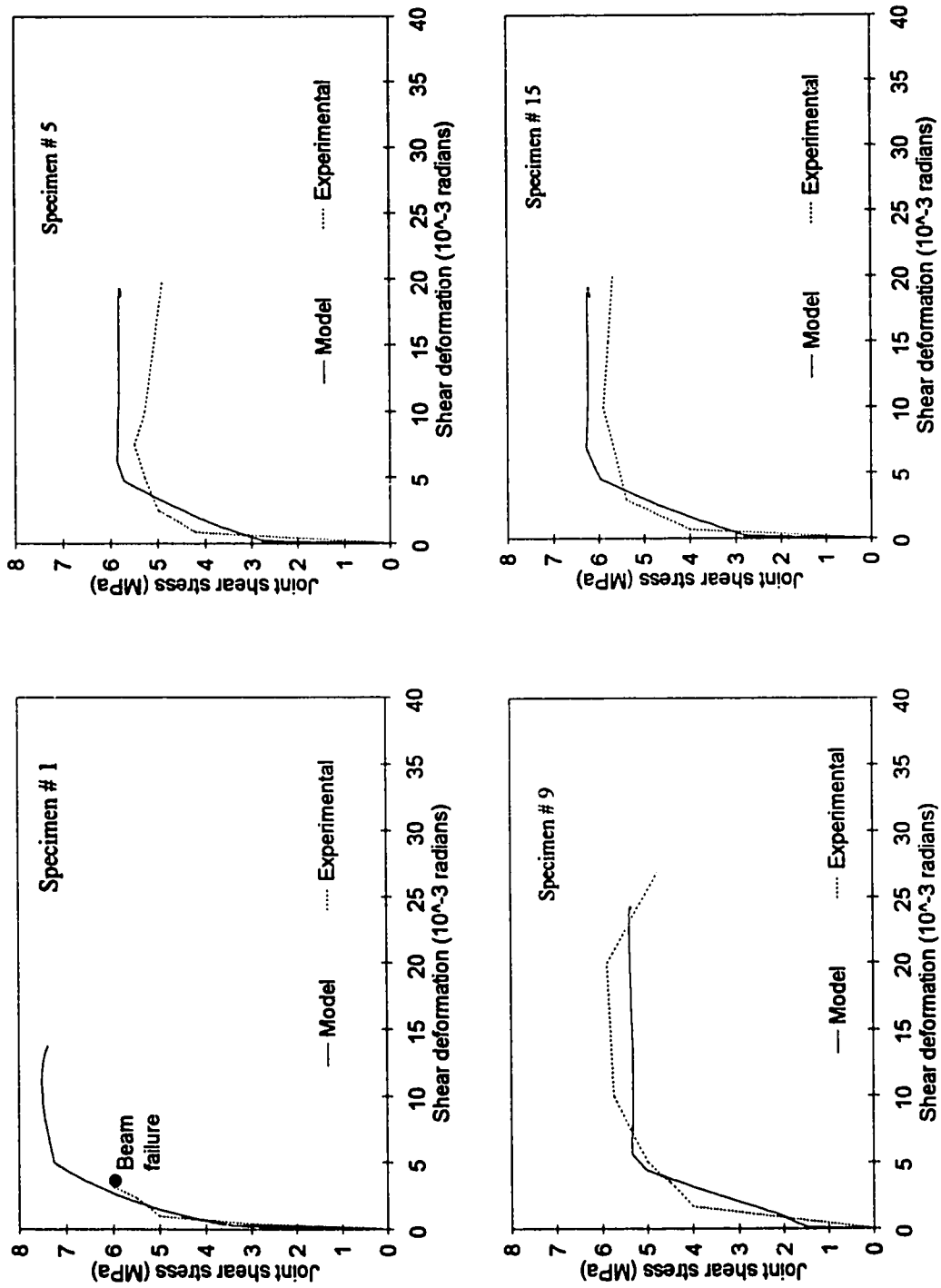


Figure 6.13 Analytical results compared with the experimental results of Kaku and Asakusa (1991)

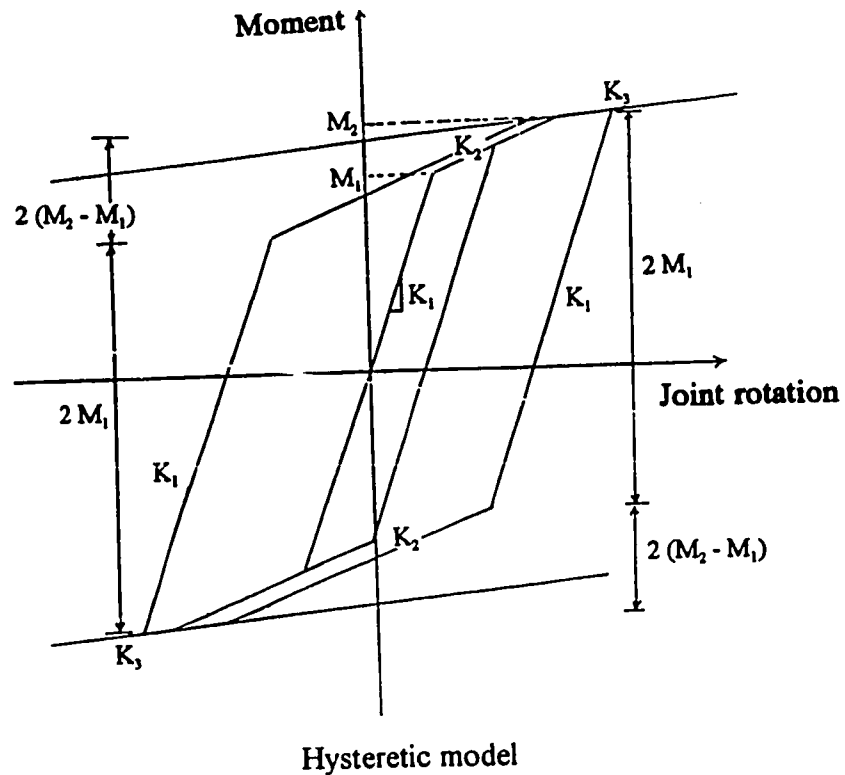


Figure 6.14 Typical moment-rotation relationship for the shear spring

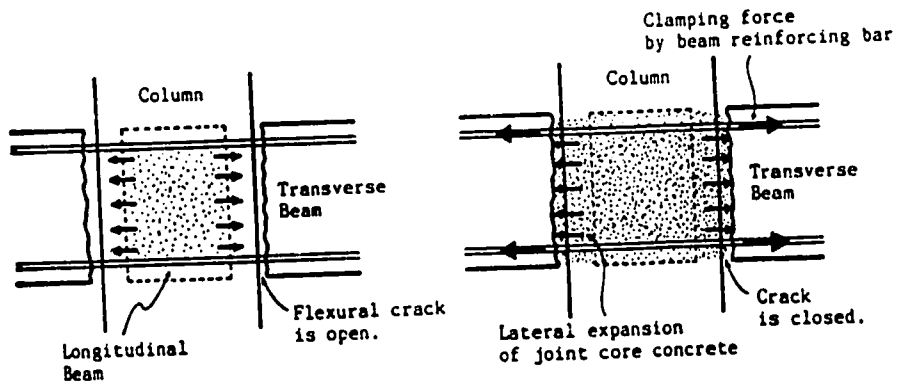


Figure 6.15 Confinement action due to cracked transverse beams (Kitayama, 1991)

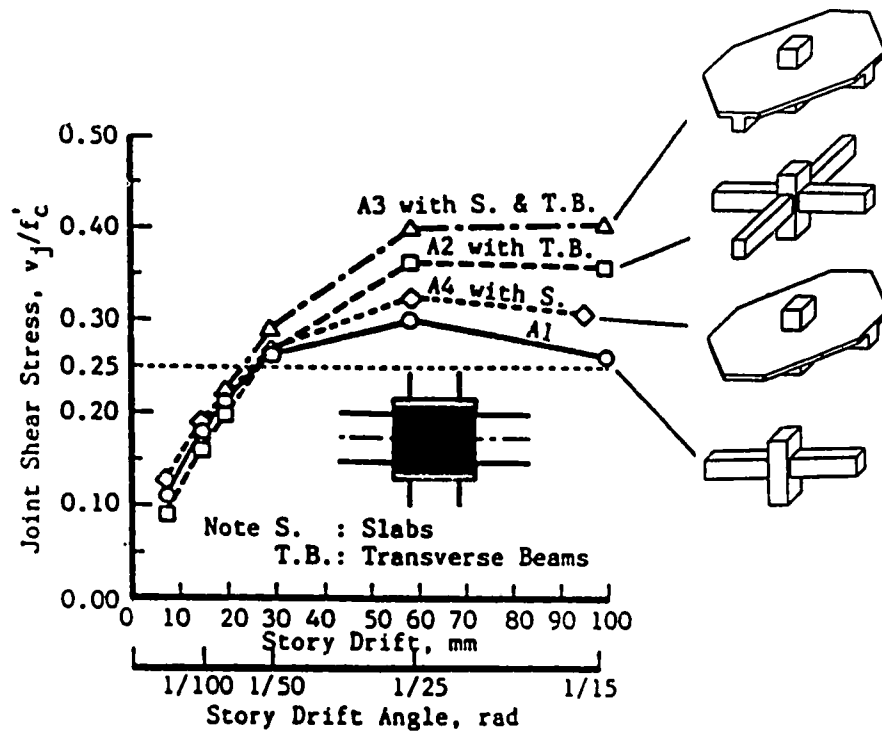


Figure 6.16 Story drift-joint shear stress relationships (Kitayama, 1991)

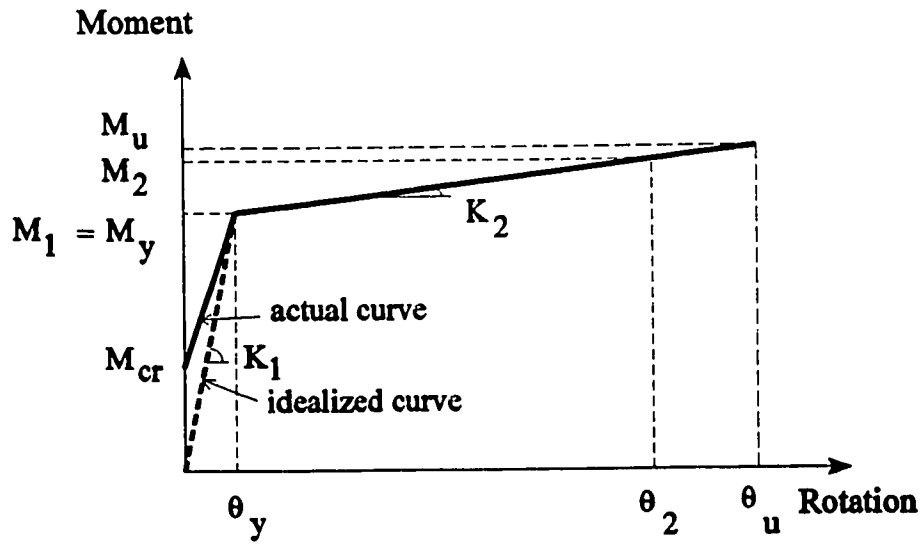


Figure 6.17 Proposed moment-rotation relationship due to bond slip

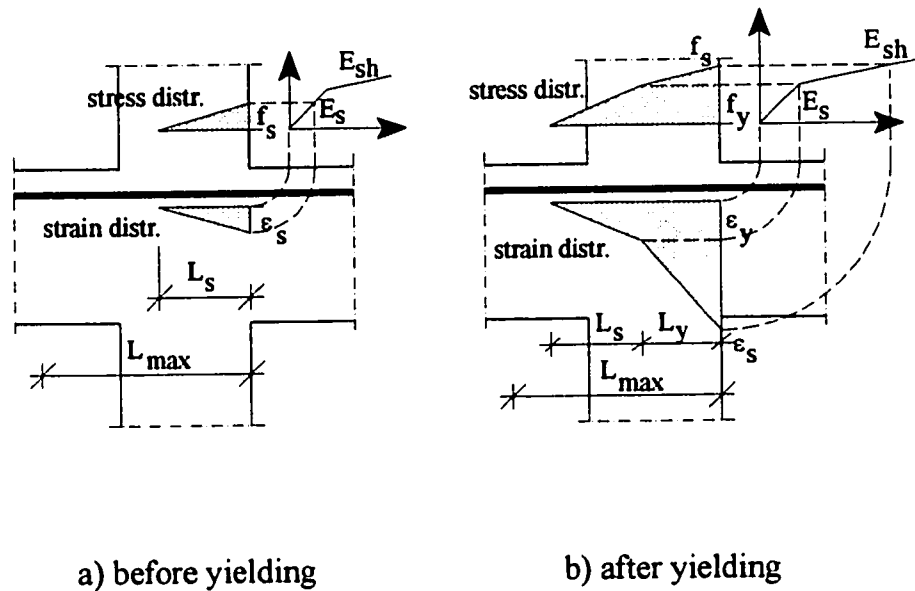


Figure 6.18 Stress and strain distribution assumption in the joint

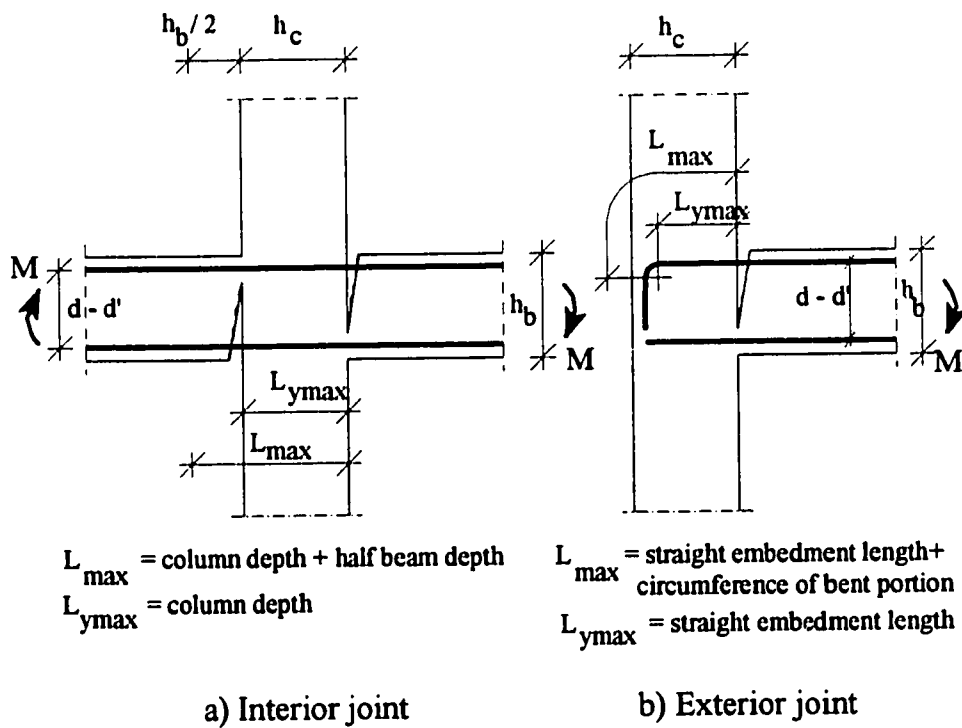
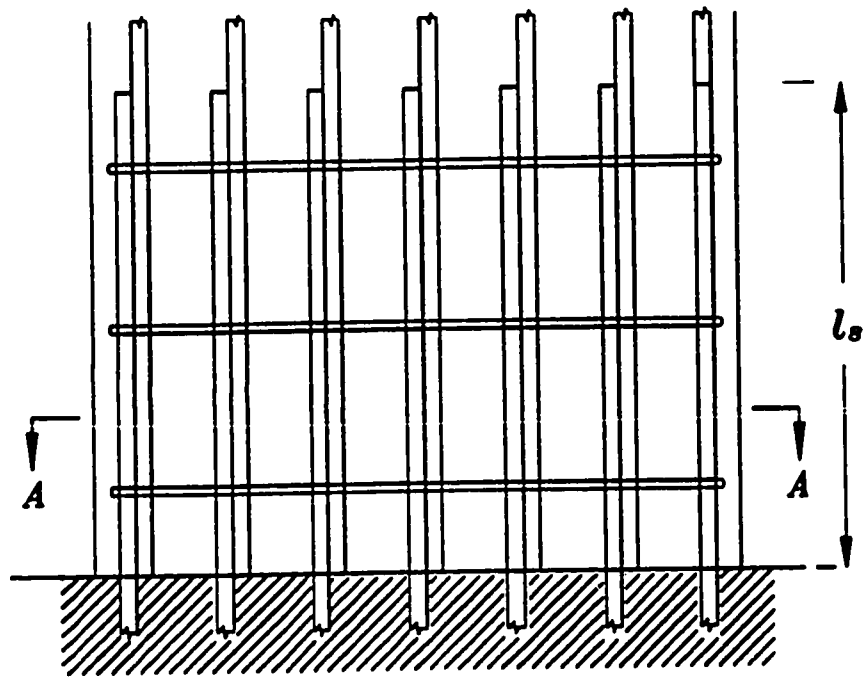
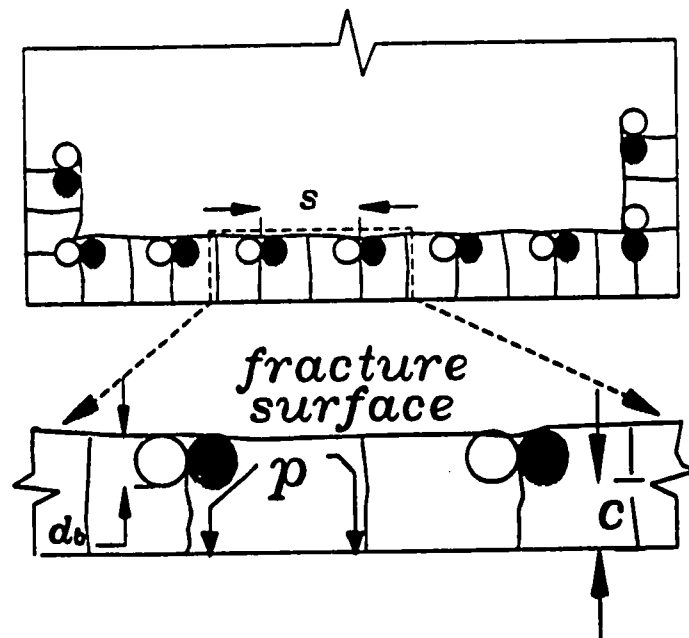


Figure 6.19 Definition of L_{max} and $L_{y_{max}}$

Figure 6.20 Computational procedure for pinching effect



(a) Elevation



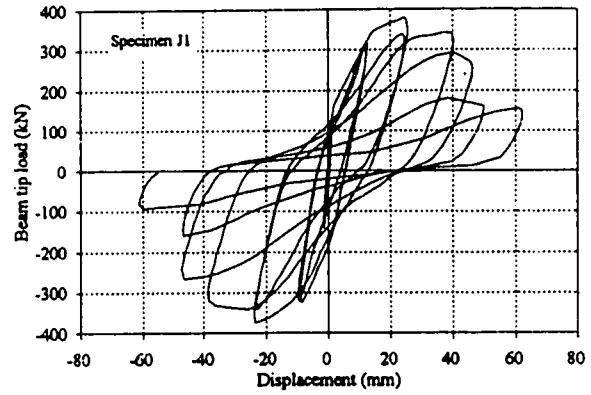
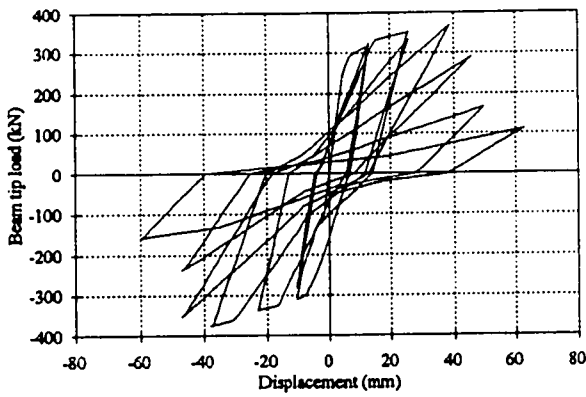
(b) Section A-A and enlargement

Figure 6.21 Bond failure of lapped reinforcement (Priestley and Seible, 1991)

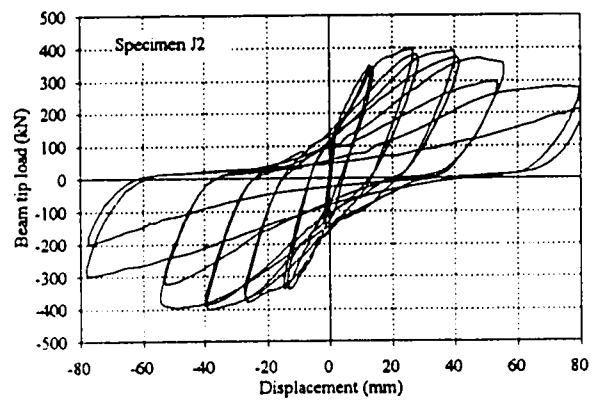
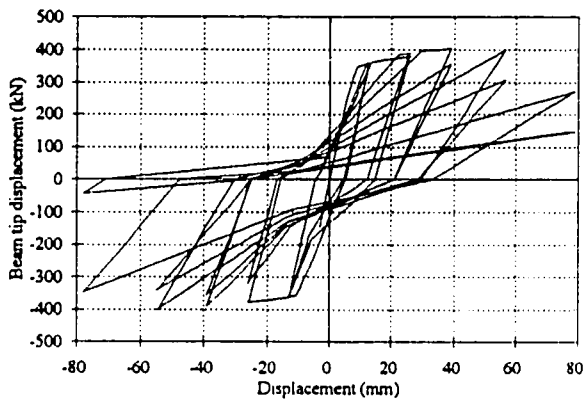
Analytical

Experimental

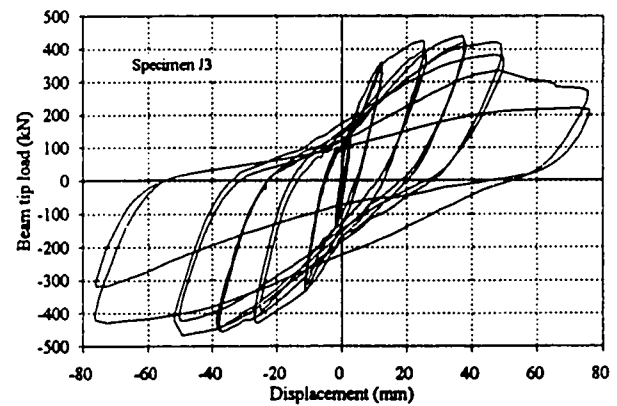
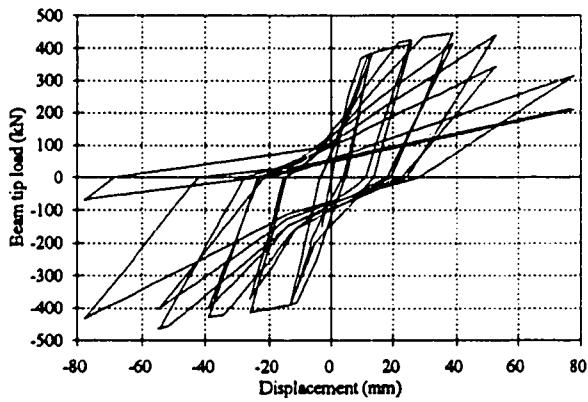
a) Specimen J1



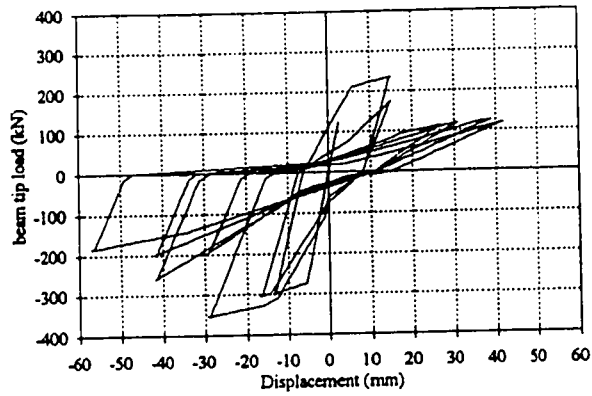
b) Specimen J2



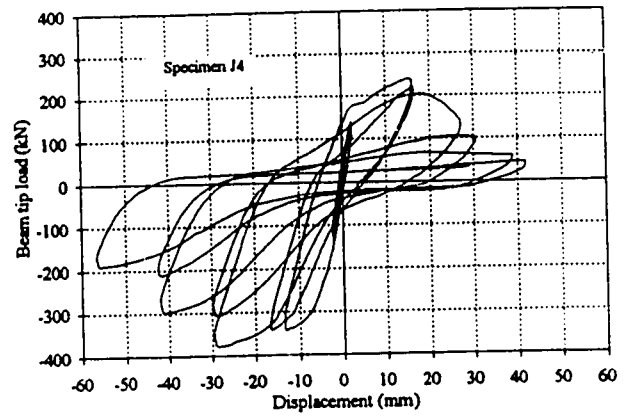
c) Specimen J3



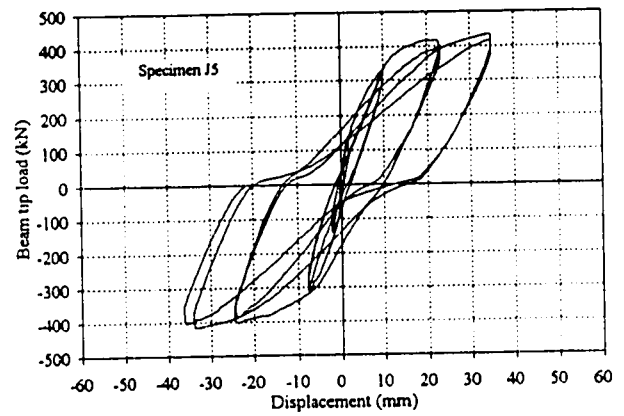
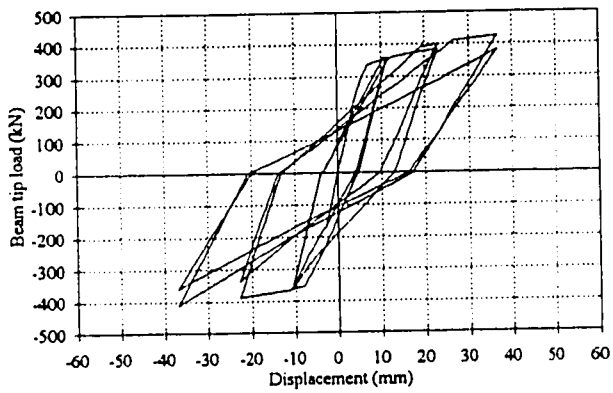
Analytical
d) Specimen J4



Experimental



e) Specimen J5



f) Specimen J6

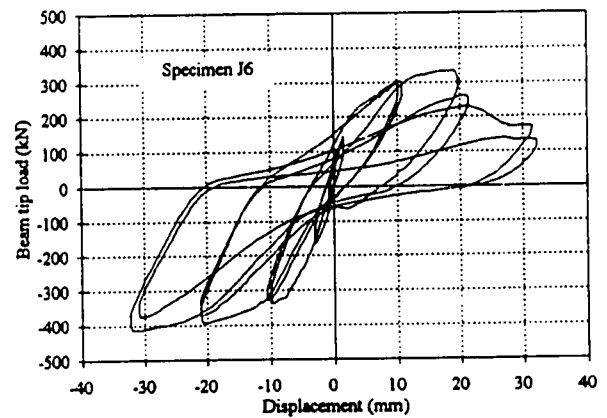
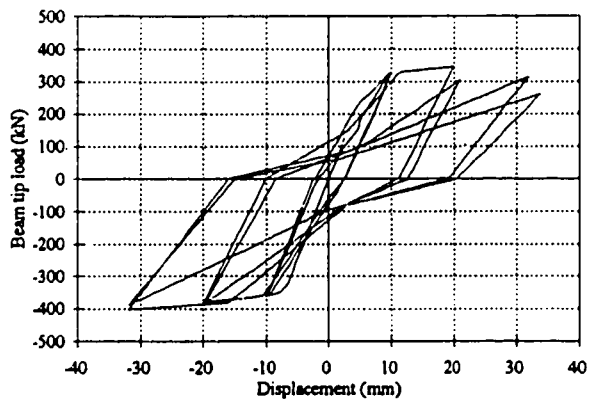


Figure 6.22 Comparison between experimental and analytical load-deflection curves of the tested specimens

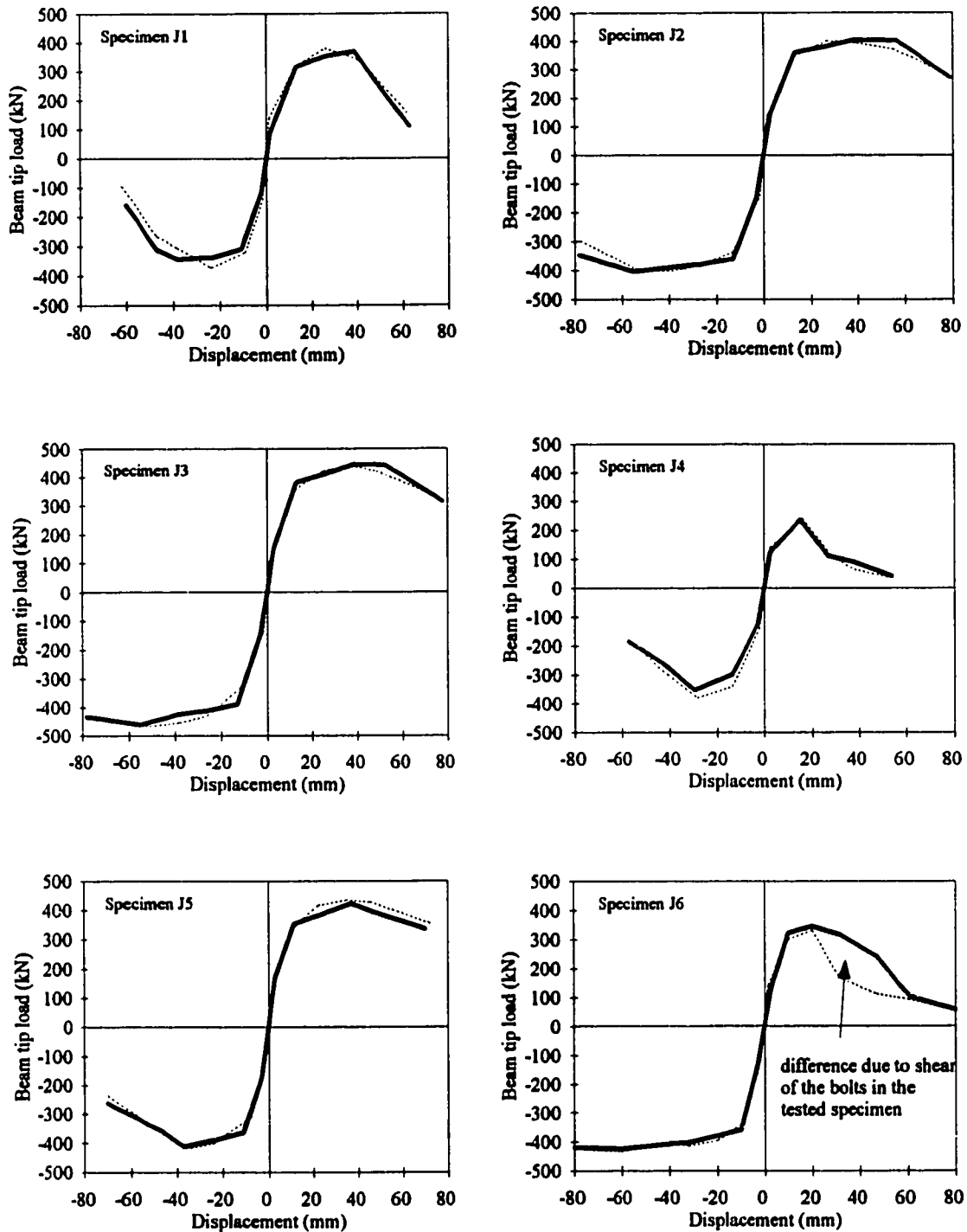


Figure 6.23 Comparison between experimental and analytical load-deflection envelopes of the tested specimens

CHAPTER 7

DYNAMIC ANALYSIS OF MULTI-STORY FRAMES

7.1 INTRODUCTION

The conventional rigid joint assumption in modelling existing reinforced concrete frames constructed prior to 1970 is questionable. The principal characteristics of these frames are their high flexibility due to the slender columns, weak joints and the potential slipping of the beam bottom bars which are discontinuous at the joint. At higher loads, distress may develop in the joints which may contain few or no ties. As a result, high overall and story drift will occur. In order to model the frame's behaviour properly, slippage of beam bottom reinforcement and joint flexibility should be taken into consideration.

In the past decade a variety of techniques for strengthening existing reinforced concrete frames have been experimentally investigated, among them are steel jacketing of beam-column connections (Ghobarah et al., 1996a, b and c), concrete jacketing of beam-column connections (Alcocer and Jirsa, 1993) and addition of structural walls (Shah, 1989). Most of these studies have been conducted on subassemblages representing critical zones of a building. Some of these retrofit systems were shown to be a practical way for improving the strength and ductility of the tested subassemblages. However, few studies have been performed to include the experimentally determined element performance into the behaviour

of the complete structural systems (Tena-Colunga et al., 1996). Three-story and 9-story buildings intended to be representative of existing low-rise and medium-rise buildings were designed according to North America's codes in the early 60's. These frames were analysed with flexible joints and the responses were compared with the responses of the frames using the rigid joint assumption. The frames were rehabilitated using corrugated steel jacketing of columns and joints and analysed to compare their behaviour with that of the existing unretrofitted frames. The main emphasis in rehabilitation is to develop a ductile system that allows energy dissipation at the plastic hinge zones. In general a flexible system attracts less forces than a stiff system. If the system displacements are kept within the allowable drift limits, moderate damage will be restricted to the flexural hinging zones.

7.2 DESIGN OF THE EXISTING FRAME STRUCTURES

For the purpose of this analytical study, 3-story and 9-story reinforced concrete buildings measuring 18 m by 30 m in plan, with a bay spacing of 6 m (3 bays by 5 bays) were selected to represent typical office buildings that may be found in many cities in North America. Floor to floor height is taken to be 3.6 m. The structure was designed in sufficient detail to provide input for the dynamic analysis program. The buildings shown in figure 7.1 were designed following the provisions of the 1964 Uniform Building Code (UBC-64, 1964), and the American Concrete Institute building code (ACI 318-63, 1963). The buildings are intended to represent a typical moment resisting frame designed in North America in the late 50's or early 60's.

Table 7.1 summarizes the design loads. The design concrete compressive strength used was 21 MPa and the yield strength of the steel reinforcement was specified at 300 MPa. The fundamental periods of the 3- and 9-story frames were computed to be 0.45 and 1.01 seconds, respectively according to the NBCC (1995) code. With the lateral load level specified by the Uniform Building Code (UBC-64, 1964), the load combination that included only gravity loads controlled the design. This resulted in the columns being designed as compression members with the minimum eccentricity requirement of 0.1 times the column depth. A splice length of 20 times the maximum longitudinal bar diameter was specified for the column longitudinal reinforcement. Small shear demands in the column resulted in minimal shear reinforcement. For shear reinforcement, #3 ties (3/8 in. diameter) were spaced according to the American Concrete Institute building code (ACI 318-63, 1963). No extra confinement reinforcement was required at the column ends. Column cross-sections were designed every three story levels. The cross-section dimensions of the beams and columns are shown in figure 7.2.

The beams and columns longitudinal and transverse reinforcement are shown in figure 7.3. The design of the beams was controlled by gravity-load combinations, and therefore, no moment reversals due to lateral loads were anticipated. This resulted in non-continuous beam bottom reinforcement through the joints. A 150 mm anchorage length for bottom longitudinal reinforcement was provided as suggested by the American Concrete Institute building code (ACI 318-63, 1963). The reinforcement details for the beams were identical for all story levels. Figure 7.4 shows the details of the reinforcement steel along with the corresponding beam cross-sections at the critical design locations.

For simplicity, it is assumed that factored snow loads and roof dead loads were of the same order as the factored floor loads. The ratio of sum of column moment capacities to sum of beam moment capacities varied according to the story level and the type of connection (exterior or interior). A summary of these ratios is shown in table 7.2. Joint reinforcement was not required by the American Concrete Institute building code (ACI 318-63, 1963), and was not provided. The roof and floor slabs were two way 150 mm thick slabs designed according to the ACI 318-63 code. Straight bars were used.

7.3 DESIGN OF REHABILITATED FRAME STRUCTURES

If it is desired to rehabilitate the existing building to current code provisions, it would be necessary to perform modifications on all the structural elements. This alternative is impractical and probably quite expensive. A deficient structure can be rehabilitated by upgrading some of its structural elements. The design of the retrofitting system can be such that the interference with the normal operations of the building during construction are reduced. The main concern when rehabilitating selected elements of a given structure is that the damage to unstrengthened elements must be limited. A criterion involving maximum force or deformation demands on these elements must be established. The lack of strength and ductility were identified as the principal deficiencies in existing buildings. Jacketing of columns and joints are considered.

Dimensions of the jacketed elements were determined to satisfy strength and ductility rather than satisfying stiffness. Table 7.3 shows the thickness and dimensions of the corrugated steel jackets designed for the rehabilitated buildings. Figure 5.3 in Chapter 5 gives

further details of this rehabilitation technique. To rehabilitate the discontinuity of the beam bottom reinforcement, the procedure proposed by Estrada (1990) is used as shown in figure 7.5.

7.4 COMPUTER MODELLING

In the analytical model, the slab is considered as a rigid diaphragm in its own plane. The building was idealized as a series of planar frames linked at the floor levels. This idealization resulted in only one lateral degree of freedom per floor level. In modelling the beams and columns of the frame, one dimensional beam-column elements were used. The beam's shear deformation was neglected. The joints shear and bond slip were represented by springs using tri-linear and bi-linear springs, respectively. The stiffness of the springs were calculated as described in Chapter 6.

Damping proportional to both the mass and the initial stiffness was used. A damping of 5% of critical was assigned to the first two modes. The damping coefficients were determined using the methodology of Clough and Penzien (1975). It is believed that the error in estimating the damping in the system is within an acceptable range of accuracy implicit in the analysis. Soil-structure interaction effects were ignored.

The frames were subjected to gravity loads that included specified dead and live loads. Gravity loads applied to the beams were modelled by specifying fixed end forces at the beam ends. Masses of the tributary floor areas, wall units and partitions were all assumed to be lumped at the column-beam joints.

To account for the age effects on the concrete compressive strength, expressions for

the time-dependent concrete compressive strength $(f_c)_t$ as a function of the 28-days concrete compressive strength f'_c are used (Branson, 1977). The expression for normal weight concrete takes the following form:

$$(f_c)_t = \frac{t}{4.0 + 0.85t} (f'_c) \quad (7.1)$$

where t is the concrete age in days. After 30 years the compressive strength increases 18%. However, environmental stressors may attack the integrity of the concrete in concert with or independent of operating, environmental and accidental loads (Mori and Ellingwood, 1993), causing the strength to degrade over time. For concrete strength, the most significant stressors are freeze-thaw cycles, sulphate attack, alkali-silicate reactions within the concrete and temperature and irradiation effects. Mori and Ellingwood (1993) suggested a linear degradation rate corresponding to a residual strength after 40 years ranging between 0.7 and 0.9 of the original strength. In this analysis, a linear degradation function is used with low degradation rate corresponding to a residual strength equal to 90% of the original strength after 40 years. Assuming that the building is 30 years old, the strength of the building is taken equal to 0.93 of its original strength. Therefore, the combined effect of strength increase and deterioration is $1.18 \times 0.93 f'_c$ which leads to $1.1 f'_c$.

The dynamic analysis of the frames was performed using the SARCF computer program. The dynamic analysis in this program is designed to perform a time history inelastic response analysis of a plane structure subjected to an earthquake ground excitation. The frame response to the input ground motion is determined by solving the equation of motion by numerical step-by-step integration procedure. The Newmark integration method is used

in the analysis with an integration factor of 0.5, which corresponds to the constant average acceleration method. The post-yield strength matrix of the structure is assumed to remain constant within each time step. If the stiffness of an element is changed during the time step, the post-yield stiffness matrix is updated by adding the changes in the element stiffness into the current structure stiffness, avoiding the process of reassembling a complete new stiffness matrix. An equilibrium imbalance may exist at the end of the time interval due to the changes in the stiffness of one or more elements that may occur during a time step. Unbalanced loads resulting from errors in the assumed linear behaviour within the step are corrected by applying corrective loads in the subsequent time step. The time step used in this frame analysis was selected to be 0.005 seconds to reduce the computer process unit (CPU) time consumed. The dynamic frame response results were essentially unchanged when using time steps of 0.005 and 0.001 seconds.

7.5 INPUT GROUND MOTION

The intensity, duration of strong shaking and frequency content of an earthquake record depends on a number of factors such as the magnitude of the earthquake, the epicentral distance, the local geology and the site conditions. The differences among records can lead to significant differences in the structural response. One important factor that has significant effect on structural response is the frequency content of the record. To account for the frequency content, the ratio of peak ground acceleration PGA, "A" (expressed in units of gravitational acceleration "g") to peak ground velocity, "v" (expressed in units of m/s) has been used as an indicator. Records can be broadly divided into three categories, namely high

A/v ratio ($A/v > 1.2$), intermediate A/v ratios ($1.2 > A/v > 0.8$) and low A/v ratio ($A/v < 0.8$). Statistically, records with high A/v ratios are normally associated with stiff and rock sites at short epicentral distances, while records with low A/v ratios are normally associated with soft sites at long epicentral distances.

For the purpose of defining input motion in the present study, three real earthquake ground motions were used, one from each category in addition to one artificial earthquake that was generated to fit the NBCC (1995) design spectrum. It is of interest to examine levels of story shear and drift obtained from the generated accelerogram record that is compatible with the NBCC (1995) design spectrum. The artificial earthquake was constructed using the computer program SYNTH (Naumoski, 1985). This program utilizes input of spectral acceleration for various periods to construct a ground motion time history that would produce such a response spectrum. Using the response spectra given in the commentary of the NBCC (1995) as a target spectrum with the $Z_u > Z_v$ corresponding to the Ottawa region, a ground motion time history was generated. Figure 7.6 shows the artificial earthquake motion and its elastic spectrum compared with the NBCC (1995) spectrum. The inelastic response spectra of the artificial earthquake are also shown in figure 7.6. The ground motions selected for this study as shown in figures 7.7a and 7.7b cover a wide range of spectral response, from the very high frequency content of the Nahanni 1985 earthquake to the longer period Mexico 1985 earthquake. Nahanni 1985 earthquake can be considered as a typical earthquake in the north-east region of North America (Papageorgiou, 1987). The properties of the three earthquakes are summarized in table 7.4.

The ground motion records were scaled to different maximum PGA (0.1g, 0.2g and

0.3g) in order to produce "minor", "moderate" and "severe" effects on the frame. The moderate maximum acceleration corresponds approximately to the peak horizontal acceleration at Ottawa having probability of exceedance of 10% in 50 years (approximately 475-year return period). The minor earthquakes were assumed to have probability of exceedance of about 40% in 50 years (100-year return period). This minor earthquake is used to study the response of the structures under small earthquakes having large probabilities of occurrence during the life of the structure. The severe maximum accelerations were assumed to be 1.5 times the moderate maximum acceleration with a probability of exceedance of about 5% in 50 years (1000-year return period).

7.6 DYNAMIC ANALYSIS

Inclusion of the joint element in the dynamic analysis of a frame is expected to affect its dynamic characteristics and its response. Frame F3flex (3-story existing frame with flexible joints which is considered a realistic model) is studied under dynamic loading and compared with frames F3rigid (3-story existing frame with the conventional rigid joint assumption) and F3rehab (rehabilitated 3-story frame with flexible joints). Similarly, Frame F9flex (9-story existing frame with realistic modelling of joints) is studied under dynamic loading and compared with frames F9rigid (9-story existing frame with the conventional rigid joint assumption) and F9rehab (rehabilitated 9-story frame with flexible joints).

7.6.1 Dynamic characteristics of the frames

Incorporating the joint element in the frame analysis reduces the stiffness and lengthens the vibration periods of the frame. The computer program SARCF was used to

determine the periods of free vibration of the frames. The fundamental period of each of the 3-story frames is 0.96, 0.86 and 0.87 for F3flex, F3rigid and F3rehab, respectively. The fundamental period of each of the 9-story frames is 2.03, 1.8 and 1.8, for F9flex, F9rigid and F9rehab, respectively. The fundamental period of frames F3flex and F9flex including joint elements is about 1.12 times that of frames F3rigid and F9rigid. The fundamental periods of the frames were plotted on figure 7.7b to show the location of the period on the response spectra of the selected earthquakes.

7.6.2 Roof displacement time histories

Figures 7.8 to 7.13 show the roof displacement time histories for the frames when subjected to the selected earthquakes scaled to PGA of 0.3g. Table 7.5 summarizes the results in the form of the maximum predicted roof displacements. From the table, it is observed that even with significant inelastic action occurring at the highest level of ground acceleration the resulting displacements for the different input motion records are approximately proportional to the levels of acceleration. The exception is for the frame F9flex at high level of ground acceleration due to the formation of soft story at the seventh floor.

Examination of the response of the 3-and 9-story frames has shown that collapse is likely only at maximum ground acceleration levels of about 0.3g or slightly higher. For El Centro earthquake scaled to 0.2g, the existing frames with flexible joint assumption underwent larger maximum roof displacement (62.1 mm for F3flex) than that of the existing frames with rigid joint assumption (55.6 mm for F3rigid). This is mainly due to the increased deformations in the joints caused by bond slip and joint shear distortion. For Mexico 1985

earthquake record scaled to 0.2g, the existing frame F3flex was displaced to a maximum value of 109.6 mm at about 19 seconds into the record. The rehabilitated frame F3rehab was displaced to a maximum value of 58.8 mm at about 18 seconds into the record. The frame response was elastic throughout the duration of the input of ground motion and sustained no residual displacement at the end of the record. For the Mexico 1985 earthquake record scaled to 0.3g, the existing frame F3flex formed a collapse mechanism after 19 seconds into the record. The mechanism consisted of joint failure at the top and plastic hinges at the bottom of the first-story columns. This resulted in inelastic response of the frame, and caused residual permanent displacement of the frame. The rehabilitated frame F3rehab showed high inelastic deformation that caused some residual displacement at the end of the record. Frame F9flex with joint elements exhibited 18% and 46% increase in roof displacement as compared to frame F9rigid with rigid joint assumption for the Mexico earthquake scaled to PGA of 0.1g and 0.3g, respectively.

The response of the existing frames as well as the rehabilitated frames were found to be almost elastic during the Nahanni earthquake scaled to PGA of 0.1g and 0.2g. The earthquake record is rich in high frequencies and does not impart much energy to flexible structures as shown in figure 7.7b. For this reason, the earthquake had little effect on the 3- and 9-story frames. The Nahanni earthquake scaled to PGA of 0.3g caused plastic hinges to form only in the first two floor beams of frames F3rigid and F3rehab. Beam reinforcement pull out occurred in the frame F3flex. The reason for the formation of plastic hinges is the fact that rigid connections attract higher moments.

The low level of response of the existing 9-story frames when subjected to the

generated (artificial) earthquake can be explained by examining the effect of ground motion frequency characteristic on the inelastic response of frames of different periods. According to Tso et al. (1992), the low A/v ground motions of long duration are more damaging to frames with long period than the high or intermediate A/v ground motions. However, the standard design spectra are generally representative of the ground motion at moderate distances from the seismic source, and can hardly account for ground motions from a distant causative fault. Therefore, the frame response when subjected to the generated (artificial) earthquake can not reflect the damaging effect of long duration ground motion on the long period structures. The design spectra may reflect the response of rigid frames but may underestimate the responses of flexible frames.

7.6.3 Fundamental period variation with time

A decrease in the stiffness of some elements of the frame will result in a decrease of the global stiffness of the frame and an increase of its fundamental period. The variation of the fundamental period with time for the frames when subjected to the selected earthquakes are plotted in figures 7.14 to 7.19. The instantaneous fundamental period can be easily computed from the first eigenvalue of the instantaneous tangent stiffness matrix of the frame. The initial fundamental period T_{initial} and the final fundamental period T_{final} for the 3- and 9-story frames and the state of damage to the frames are shown in figures 7.20 to 7.39. As can be seen from the figures, there is a significant change in the period of the frames especially for the case of input ground motion of PGA of 0.3g which reflects the influence of joint deformation and bar bond-slip. The fundamental period computed for each time step of the dynamic analysis presents considerable variability. The maximum values are usually reached

when some members yield and the slope of the hysteretic loop is small before the next load reversal occurs. In the design approaches of the codes, a constant period is assumed. Since the stiffness of the flexible frames is always smaller than that of the rigid frames and the differences in masses between the two types of frames is minor, the fundamental period of the flexible frames is larger than that of the rigid frames.

7.6.4 Damage index

The evaluation of seismic capacity of existing structures and the prediction of the damage to reinforced concrete buildings during earthquakes have become important subjects. A global damage index , D.I., for the entire structure can give an idea of the level of damage (light, repairable, irreparable or collapse). The current practice of seismic evaluation of buildings is largely based on the ductilities demanded by the different elements of a structure. The use of ductility as a performance index has been questioned (Ayala and Xianguo, 1995) especially when shear distortion in joints and beam bottom bars pull out are anticipated. Hence, the need for more general indices to characterize structural performance is essential. An interesting and relatively simple damage index is based on measures of change in the fundamental period of the structure due to changes in stiffness relative to the initial condition (Dipassquale and Cakmak, 1987). It is referred to as the final softening and is defined as a function of the initial fundamental period $T_{initial}$ and the final period T_{final} , consequently:

$$D.I. = 1 - \left(\frac{T_{initial}}{T_{final}} \right)^2 \quad (7.2)$$

The damage index varies from 0.0 for no damage to 1.0 for collapse. At damage

index of 0.7, the frame is considered to be on the verge of collapse (collapse prevention level). This limit is derived after manipulating the results given by Rodriguez-Gomez and Cakmak (1990). After the collapse prevention limit, few new hinges are formed and larger deformations occur at different levels. The failure mechanism differs depending on the ground motion record selected in the analysis.

The damage index for each frame when subjected to the different earthquakes is shown in figures 7.20 to 7.39 for the 3- and 9-story frames. For the relatively low-level earthquakes (PGA of 0.1g) that may occur several times during the life of the structure, little structural damage is predicted except for frame F3flex when subjected to the El Centro and Mexico earthquakes which shows D.I. of 0.58 and 0.53, respectively. For earthquakes time histories with high peak ground accelerations and low probability of occurrence during the life of the structure, the ductility capacity of columns, bar bond-slip as well as the joint shear capacity have significant effects on the predicted damage levels. From the figures, the inclusion of the joint element in the dynamic analysis of the frame shows more damage as compared with the frames with rigid joint assumption. For example when subjected to the Artificial earthquake scaled to PGA of 0.3g, frames F3flex and F3rigid show D.I. of 0.78 and 0.14, respectively. Similarly, when subjected to El Centro earthquake scaled to PGA of 0.3g, frames F9flex and F9rigid show D.I. of 0.87 and 0.17, respectively.

The rehabilitation technique reduced the damage from D.I. of 0.88 for the existing frame F3flex in the case of the El Centro earthquake scaled to PGA of 0.3g to D.I. of 0.47 for the rehabilitated frame F3rehab. Similarly, rehabilitation reduced the damage from D.I. of 0.92 for existing frame F9flex due to the Mexico earthquake of PGA of 0.3g to D.I. of

0.53 for the rehabilitated frame F9rehab. The rehabilitated frames are predicted to sustain non-repairable structural damage without collapse for high-level earthquakes (PGA of 0.3g).

7.6.5 Location and type of hinges

The aggregate of all inelastic actions in the components of the frames is illustrated by a number of symbols to show cracking or yielding of joints, flexural yielding of beams and columns, bar bond-slip and column splice failure. Figures 7.20 to 7.29 show the locations of plastic hinges in the 3-story frames while figures 7.30 to 7.39 show the locations of plastic hinges in the 9-story frames. From the figures, several points are observed which can be illustrated as shown in figure 7.40:

- a) At the three top floors of the frame, failure is anticipated either in the column or in the joint. If the failure is in the column, it is either column splice failure or flexural hinge. The column flexural hinging occurs because the beams are stronger than the columns at these floors as shown in table 7.2. Column splice failure occurred at the levels where the column dimensions were changed. At these levels, the column splices were subjected to moments which sometimes exceed the splice capacity.
- b) At the intermediate floors of the frame, failure is anticipated at the joints. It is either yielding of the joint transverse reinforcement, if any, or joint failure. The joints are subjected to high forces as the beams approach or reach their maximum bending resistance. The low level of axial load in the columns at these floors compared with the load on the columns at lower floors and the small dimensions of the joints, reduce the joint shear strength.
- c) At the lower floors of the frame, failure is anticipated in the beams by either bar

pullout and/or flexural yielding. At these floors the flexural capacity of the columns is several times that of the beams as shown in table 7.2. In addition, joint dimensions and high column axial loads increase the joint shear strength in these lower stories. At negative yielding, the full moment of beam is mobilized. At positive moment, bar pullout is expected to reduce the force on the joint that otherwise would have been imposed. However, as observed in the experiments, bar pullout of embedded reinforcement may disrupt the integrity of the joint concrete, and this may reduce joint shear capacity.

7.6.6 Envelopes of lateral displacements

The envelopes of lateral displacements for the frames studied are presented in figures 7.41 to 7.48. It is evident that the maximum response depends strongly on the input ground motion since a wide range of envelopes is predicted for each level of ground motion. Examining the figures supports the conclusion that flexible joint elements increase the frame's lateral deflection. A large difference between the envelopes of lateral displacements can be observed from the figures at the levels where joint failure and beam bottom bars pull out occurred.

As can be interpreted from figure 7.7b, the longer the natural period of a frame, the smaller the inertia force induced by the seismic load. From this point of view, a flexible frame may have less lateral deflection than the rigid frame. However, the global stiffness of a flexible frame may be considerably smaller than that of a rigid frame of the same configuration. In this case, the deflection of the flexible frame tend to be larger than that of the rigid frame provided the load conditions are the same. Therefore, a flexible frame has

both the advantage of less inertia force when subjected to seismic load and the disadvantage of low stiffness. If the effects of reduced seismic load and reduced stiffness are nearly equal, the deflection of a flexible frame will not differ significantly from the deflection of the rigid frame. In the case of the 3-story frame subjected to the El Centro, Mexico and Artificial earthquakes, the lateral deflections of the flexible frame are 7% to 58% higher than those of the rigid frame. In the case of the 9-story frame, the deflections of the flexible frame are 15% to 87% higher than those of the rigid frame. On the other hand, for the 9-story frame subjected to the Nahanni earthquake, the lateral deflections of the flexible frame are 11% to 14% less than those of the rigid frame. Therefore, under seismic load the deflections of the flexible frame are not necessarily greater than those of the rigid frame.

7.6.7 Interstory drift

Figures 7.41 to 7.48 show the envelopes of the interstory drift (ratio of the maximum story drift to the story height) for the studied frames. The interstory drift limit of 2% is recommended in the supplement to the 1995 National Building Code of Canada, NBCC (1995) to control damage and avoid structural instability. Interstory drifts are normally less than 2%. Frame F3rehab displays a maximum inter-story drift ratio of about 0.80% while frames F3flex and F3rigid have drift ratios greater than 2% when subjected to the Mexico earthquake scaled to PGA of 0.2g. For the Mexico earthquake scaled to PGA of 0.3g, all the 3-story frames exceed the 2% limit recommended by the NBCC (1995). The interstory drift exceeded the 2% when El Centro of PGA of 0.3g and Mexico earthquake of PGA of 0.3g are applied to the frame F9flex. Frame F9flex displays large interstory drift in the middle stories due to the significant contribution of joint shear distortions and bond slip to the response.

Table 7.6 summarizes the maximum interstory drift for the 3-story frames and 9-story frames when subjected to different ground motions.

The rehabilitation system reduced the interstory drift by 12% and 69% for the 3- and 9-story frames, respectively when subjected to El Centro earthquake scaled to PGA of 0.2g. Rehabilitation reduced the interstory drift by 175% and 11% for the 3- and 9-story frames, respectively, when subjected to the Mexico earthquake scaled to PGA of 0.2g. As expected, there is considerable variation in the interstory drift depending on the characteristics of the ground motions.

For the 9-story frames, the interstory drift increases from the roof to the sixth floor then decreases when the frames were subjected to the El Centro and Nahanni earthquakes. It increases from the second to fourth floor then decreases when the frames were subjected to the Mexico earthquake. This can be explained by the change in column dimensions at the third and sixth floor levels. High interstory drifts are obtained at the sixth floor when the frames are subjected to the El Centro earthquake scaled to PGA of 0.3g. In this case, the drift exceeded the NBCC (1995) limit because of the soft story mechanism developed at this floor. When subjected to the Mexico earthquake scaled to PGA of 0.3g, the existing frame F3flex suffered large first story drift. This is a result of the formation of plastic hinges in the lower first story columns and in the first story beams.

7.6.8 Curvature ductilities

The predicted curvature ductilities for the beams and columns of the different frames are plotted in figures 7.49 to 7.54. The predicted curvature ductility demands on the beams of the 3-story frames indicate that significant yielding has taken place in the beams of the

bottom story and that some beams in the second story reached yielding. The predicted curvature ductility demands for the columns of the 3-story frame F3flex are quite different from that of the frame F3rigid, which emphasize the importance of modelling the flexible joints in the analysis of existing frames. In general, ductility demand for F3flex decreases significantly due to the introduction of an additional energy absorption source. The rehabilitation technique increases the curvature ductility demand on beams and decreases it on columns. For the 9-story frames subjected to the Mexico earthquake, the curvature ductility demands on the beams of F9flex at the lower floors are less than those on the beams of F9rigid or F9rehab. This is because most of the deformation is due to the beam bar pull out at the lower floors.

7.6.9 Shear strength envelopes

Figures 7.49 to 7.54 show the predicted story shear due to the different earthquakes. The figures compare the story shear for 3 different levels (severe, moderate and minor) of earthquakes. Due to the joint distortion and bar bond slip, frames F3flex and F9flex attracted less forces as compared with frames F3rigid and F9rigid as shown in table 7.7. On the one hand, the maximum base shears of frame F3flex during the El Centro, Mexico, Artificial and Nahanni earthquakes (scaled to PGA of 0.2g) were found to be 94%, 107%, 74% and 53% of the base shear calculated according to the NBCC (1995) with $R=1$, respectively. On the other hand, the maximum base shears for the frame F9flex were found to be 84%, 94%, 46% and 24% of the base shear calculated according to the NBCC (1995) $R=1$, respectively.

The shear capacities of both the interior and exterior columns as well as the beams were found to be greater than the shear demand predicted for all the studied frames. The

shear capacities were determined using the equation of the current concrete design code (CSA A23.3-94, 1994).

7.7 APPLICATION OF NBCC 1995 TO EVALUATE EXISTING BUILDINGS

Comparing the elastic base shear to the inelastic base shear provides the average modified base shear factor (F1). The average modified base shear factor, F1, obtained from the Artificial earthquake equals 1.1 for moderate excitation (PGA of 0.2g) and 1.45 for severe excitation (PGA of 0.3g). According to NBCC (1995), the ductility reduction factor for systems other than the ductile or nominally ductile systems, is 1.5. Therefore, for gravity designed frames during severe earthquakes the ductility reduction factor is similar to the NBCC (1995) code which expects the frame to suffer overstress during the design earthquake.

The factor F2 is defined as the ratio between the maximum interstory drift in both elastic and inelastic cases. Table 7.8 lists the average modified response factors F1 and F2 obtained from the Artificial earthquake. From table 7.8, F2 factor confirms the observation by several researchers that drift in the elastic and inelastic systems are close because of the energy dissipation.

From table 7.8, increasing the peak ground acceleration increases F1 and decreases F2. This is because increasing the peak ground acceleration causes more inelastic deformations which decrease the stiffness and reduce F2. Decreasing the stiffness attracts less forces which increases F1. Frame F9flex shows high reduction in F2 and significant increase in F1 because of the high inelastic deformations due to beam bar pull out and joint shear

deformation.

The upper bound for the two factors as an accepted limit is recommended by Youssef and Hilmy (1990) to be equal 2.0. The response modification factors F_1 and F_2 have the physical meaning and are easy to understand and to employ in design using elastic response spectra.

7.8 SUMMARY

Joint elements are incorporated in the dynamic analysis of two existing buildings of 3- and 9-stories. The frame response with joint elements, when subjected to dynamic loading, was compared with the response of a rigid joint assumption frame and the response of a rehabilitated frame. On the basis of the results obtained from the analysis, the following conclusions are arrived at:

- 1) The overall displacement response increases when joint shear deformation and beam reinforcing bar bond slip are included in the analysis. However, ductility demand decreases due to the introduction of an additional energy absorption source.
- 2) The existing frame representing buildings of non-ductile detailing displayed high levels of interstory drift. These high drifts were mainly due to the significant shear deformations of the joint regions and bar pull out in some beams in the lower stories. The large predicted interstory drift, together with the "poor" construction quality classification assigned to these buildings, result in severe structural damage during strong earthquakes.
- 3) The rigid joint assumption is inappropriate when assessing the behaviour of existing

structures. Realistic modelling of the joint is essential for dynamic analysis of existing frame structures to show the deficiencies in the structures.

4) Introducing joint elements in the frame analysis lengthens the initial fundamental period of the frame by about 12%. This is associated with slight reduction in base shear as compared to conventional rigid joint assumption frames.

5) Joint failure occurs mainly in the middle and top floors while beam bar pull out occurs in the bottom floors. Column splice failure occurs at the levels where the column cross-section dimensions change.

6) The proposed corrugated steel jacket rehabilitation technique develops favourable behaviour with low ductility demands on the columns. The curvature ductilities for the beams were within acceptable limits, with a uniform distribution of the rotations over the entire frame. The uniform distribution of rotations confirms that the system has good energy dissipation characteristics which is a desirable feature in the seismic resistant structures.

7) The jacketing scheme can be used to limit inelastic behaviour in existing structures to acceptable levels.

Table 7.1 Summary of design loads for the existing building

Load	Value
Dead loads	<ul style="list-style-type: none"> - Structure self-weight (density of concrete = 24 kN/m^3) - 0.75 kN/m^2 for floor covering, utilities, etc. - 7.0 kN/m for exterior wall each floor at perimeter
Live loads	<ul style="list-style-type: none"> - 2.4 kN/m^2 for occupancy - 1.0 kN/m^2 for moveable partitions

Table 7.2 Ratio of sum of column moment capacities to sum of beam moment capacities at connections

Floors	3-story frames		9-story frames	
	Exterior connections	Interior connections	Exterior connections	Interior connections
Top floor	1.27	0.83	1.27	0.83
First floor	2.30	1.39	6.50	3.60

Table 7.3 Thickness and dimensions of the steel jackets

Column size	Jacket thickness (mm)	Amplitude of corrugation (mm)	Jacket height below and above the joint (mm)	Pitch of corrugation (mm)
300 x 300	1.3	13	450	68
400 x 400	1.6	13	450	68
500 x 500	2.0	13	500	68
600 x 600	2.8	13	600	68

Table 7.4 Characteristics of the selected ground motions

Station Name	Geology	Earthquake data	Magnitude	Epicentral distance (km)	Direction	PGA (g's)	PGV (m/sec.)	A/v ratio
Nahanni Iverson (site 1)	Rock	Canada Dec. 23, 1985	6.9	7.5	N10	1.101	0.462	2.38
El Centro	Alluvium	Imperial vally May 18, 1940	6.6	8	S00E	0.348	0.334	1.04
Mexico Zihuatenejo Guerrero Array	Rock	Mexico Sept. 19, 1985	8.1	135	S00E	0.103	0.159	0.65

Table 7.5 Maximum predicted roof displacement

PGA scale of ground motion	Roof displacement (mm)					
	3-story frames			9-story frames		
	F3flex	F3rigid	F3rehab	F9flex	F9rigid	F9rehab
El Centro 0.1g	38.2	36.4	38.9	70.3	55.2	55.9
El Centro 0.2g	62.1	55.6	58.6	160.6	104.0	104.2
El Centro 0.3g	82.0	73.5	77.5	230.0	142.7	150.7
Mexico 0.1g	45.2	28.6	27.9	162.6	138.1	144.0
Mexico 0.2g	109.6	93.5	58.8	318.7	285.0	289.0
Mexico 0.3g	178.0	157.4	133.2	645.5	441.0	462.5
Artificial 0.1g	20.5	19.1	20.4	41.9	36.6	36.6
Artificial 0.2g	43	38.2	40.8	130.0	73.0	73.0
Artificial 0.3g	66.0	54.5	63.0	183.0	97.8	104.5
Nahanni 0.1g	12.4	12.6	12.5	15.3	17.0	16.7
Nahanni 0.2g	24.8	25.1	25.0	30.6	34.0	33.5
Nahanni 0.3g	37.4	37.7	37.6	45.0	51.0	50.1
Nahanni 1.0g	120.6	121.0	119.3	191.9	133.0	134.0

Table 7.6 Maximum predicted story drift

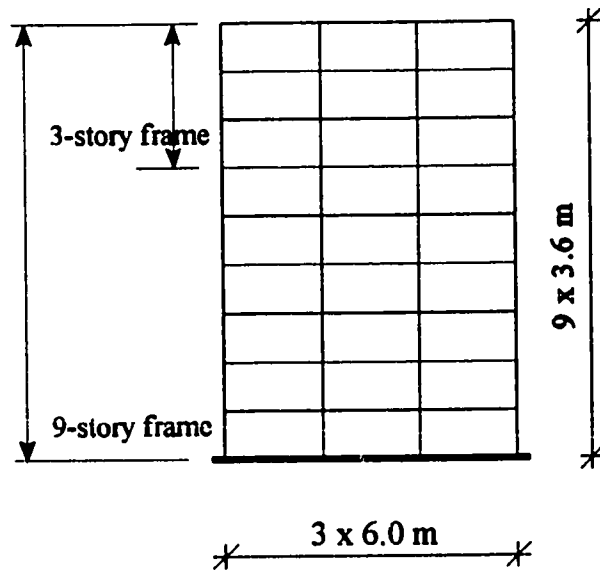
PGA scale of ground motion	Maximum story drift (% of story height)					
	3-story frames			9-story frames		
	F3flex	F3rigid	F3rehab	F9flex	F9rigid	F9rehab
El Centro 0.1g	0.52	0.44	0.46	0.33	0.30	0.28
El Centro 0.2g	0.90	0.90	0.76	1.05	0.74	0.62
El Centro 0.3g	1.20	1.10	1.10	3.95	1.28	1.00
Mexico 0.1g	0.58	0.35	0.32	0.83	0.86	0.85
Mexico 0.2g	2.20	2.10	0.80	1.74	1.75	1.57
Mexico 0.3g	3.82	3.92	2.49	3.40	2.48	2.40
Artificial 0.1g	0.25	0.22	0.24	0.19	0.20	0.18
Artificial 0.2g	0.52	0.45	0.50	0.59	0.38	0.37
Artificial 0.3g	0.93	0.80	0.90	1.02	0.65	0.64
Nahanni 0.1g	0.16	0.15	0.16	0.10	0.10	0.10
Nahanni 0.2g	0.31	0.30	0.31	0.22	0.20	0.20
Nahanni 0.3g	0.46	0.45	0.45	0.30	0.30	0.30
Nahanni 1.0g	2.00	2.67	1.75	1.02	1.00	0.92

Table 7.7 Maximum base shear

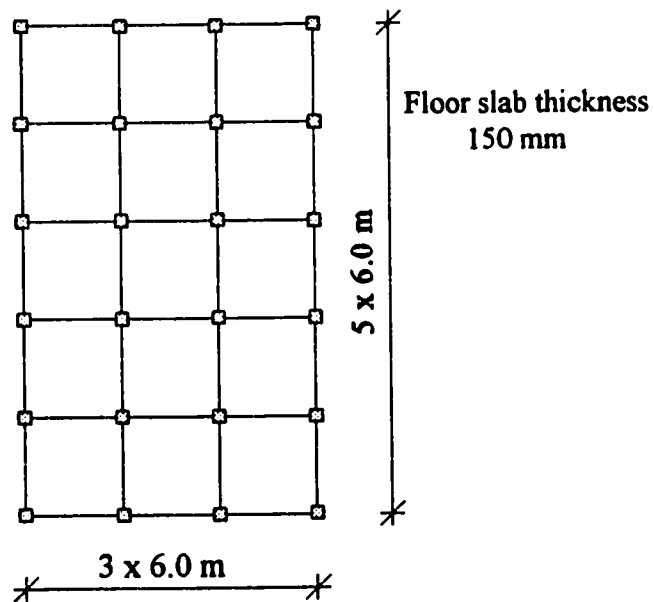
PGA scale of ground motion	Maximum base shear (% of weight)					
	3-story frames			9-story frames		
	F3flex	F3rigid	F3rehab	F9flex	F9rigid	F9rehab
El Centro 0.1g	12.1	13.2	14.7	4.4	4.9	4.9
El Centro 0.2g	14.2	15.9	18.7	7.5	9.5	9.2
El Centro 0.3g	15.6	16.4	19.7	7.7	11.4	11.9
Mexico 0.1g	12.6	11.6	11.6	6.4	7.6	8.0
Mexico 0.2g	16.2	17.6	18.7	8.3	11.4	12.3
Mexico 0.3g	17.8	19.1	19.8	12.5	15.0	15.9
Artificial 0.1g	6.1	7.5	8.5	2.7	3.2	3.1
Artificial 0.2g	11.2	13.7	15.8	4.5	6.0	6.0
Artificial 0.3g	13.2	15.3	18.3	5.1	6.7	6.7
Nahanni 0.1g	4.1	4.9	5.6	1.1	1.3	1.3
Nahanni 0.2g	8.0	9.8	11.3	2.1	2.6	2.6
Nahanni 0.3g	11.2	13.5	15.9	3.2	3.9	4.0
Nahanni 1.0g	16.0	17.7	20.0	8.6	8.9	7.9

Table 7.8 Modified response factors (elastic/inelastic)

Frames	PGA = 0.2 g		PGA = 0.3 g	
	Base shear factor F1	Drift factor F2	Base shear factor F1	Drift factor F2
F3flex	1.09	0.96	1.39	0.81
F3rigid	1.09	0.98	1.47	0.83
F3rehab	1.08	0.96	1.39	0.80
F9flex	1.20	0.64	1.59	0.56
F9rigid	1.07	1.05	1.43	0.92
F9rehab	1.03	0.97	1.39	0.84



Typical frame elevation for the 3- and 9-story frames



Typical floor plan

Figure 7.1 Plan and elevation for the 3- and 9- story buildings

			250 x 600	
300 x 300	400 x 400		250 x 600	
300 x 300	400 x 400		250 x 600	
300 x 300	400 x 400		250 x 600	
400 x 400	500 x 500		250 x 600	
400 x 400	500 x 500		250 x 600	
400 x 400	500 x 500		250 x 600	
500 x 500	600 x 600		250 x 600	
500 x 500	600 x 600		250 x 600	
500 x 500	600 x 600			
Column dimensions		Beam dimensions		

3-story frame

Figure 7.2 Member dimensions (mm) for the 3- and 9-story frames

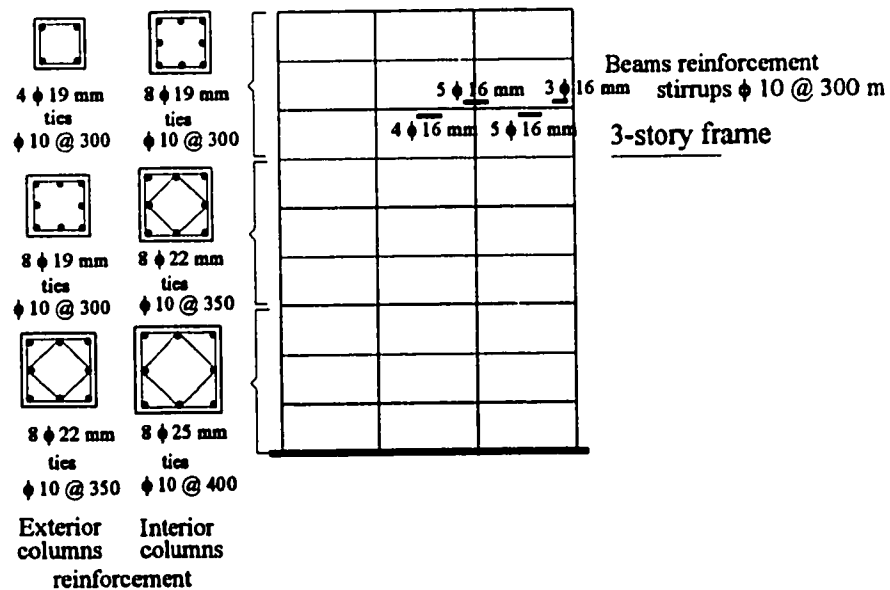


Figure 7.3 Reinforcement details for the 3- and 9-story frames

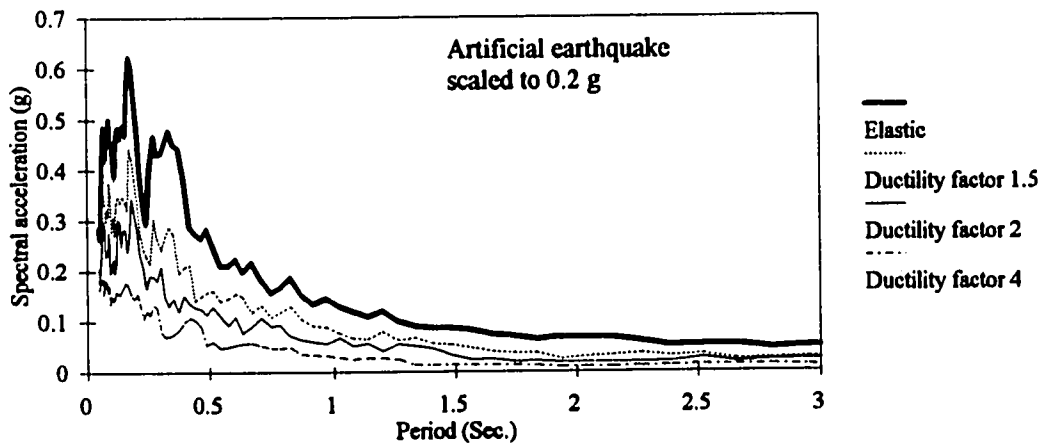
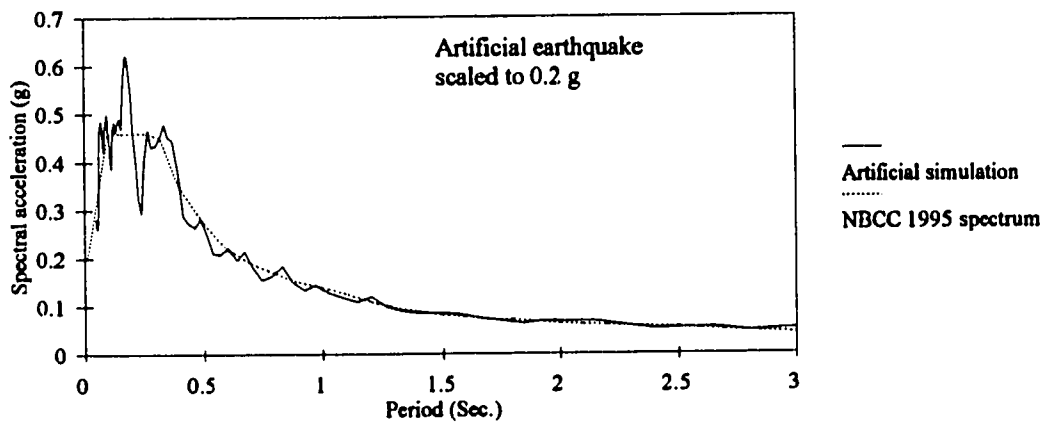
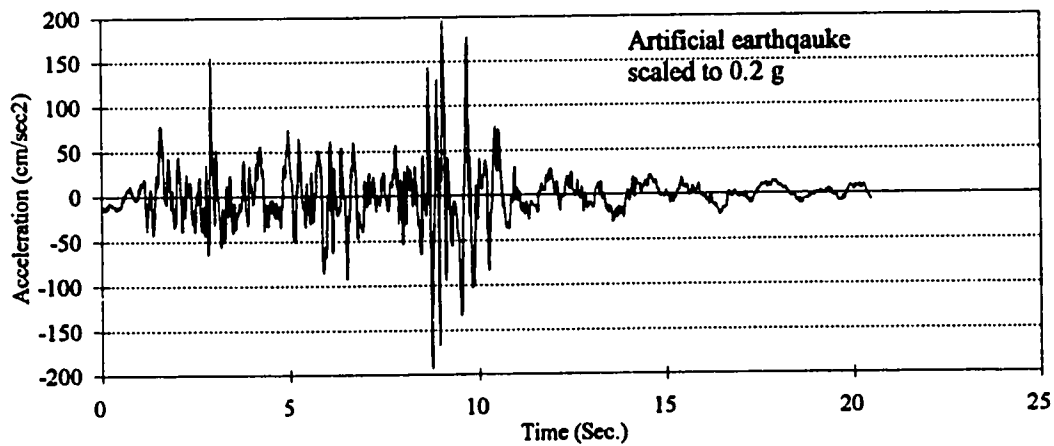


Figure 7.6 Acceleration time history and response spectra for the Artificial earthquake scaled to PGA of 0.2 g

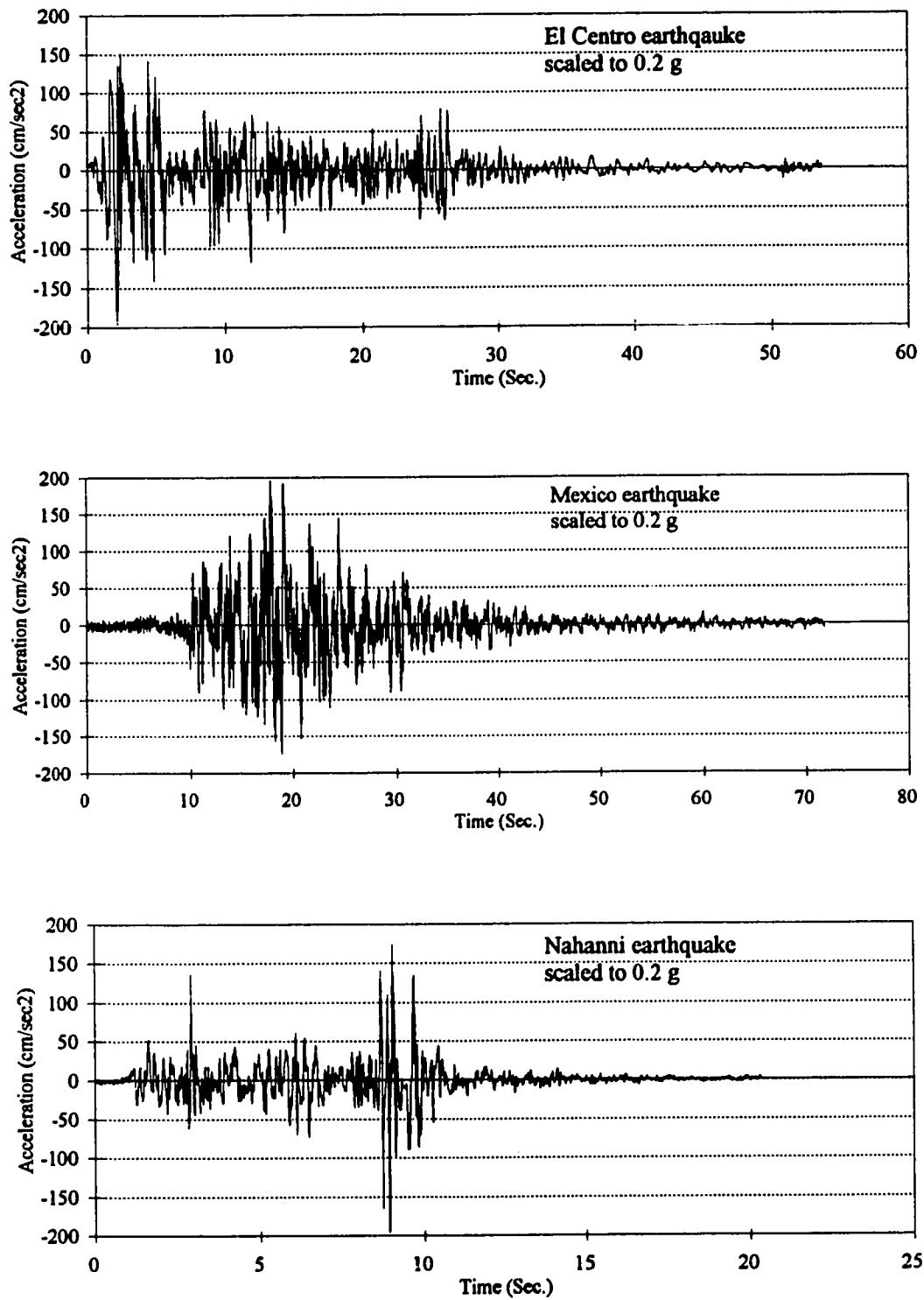


Figure 7.7a Acceleration time histories for the selected earthquake records

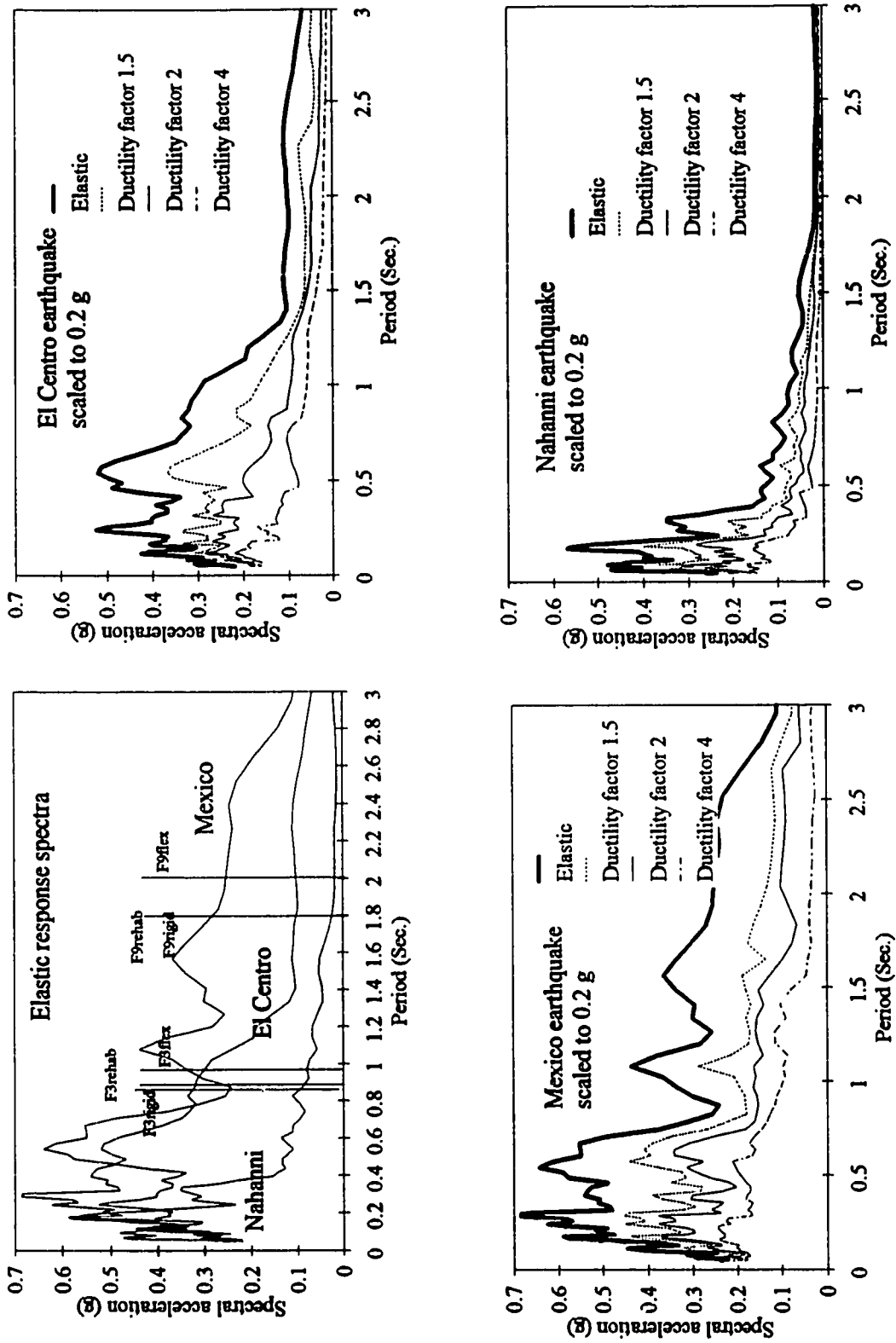


Figure 7.7b Response spectra for the selected earthquake records

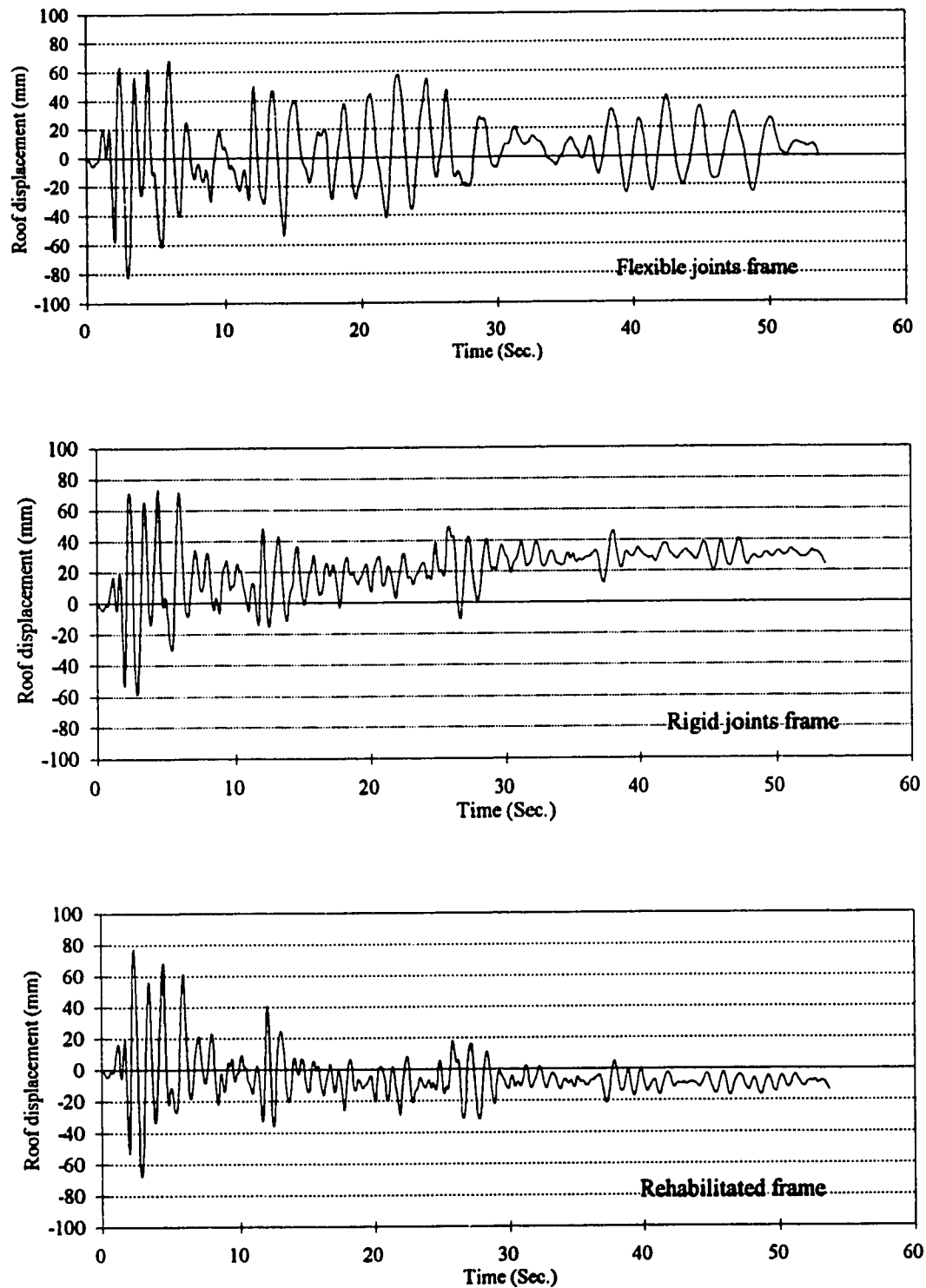


Figure 7.8 Roof displacement time histories for the 3-story frames due to the El Centro earthquake scaled to PGA of 0.3g

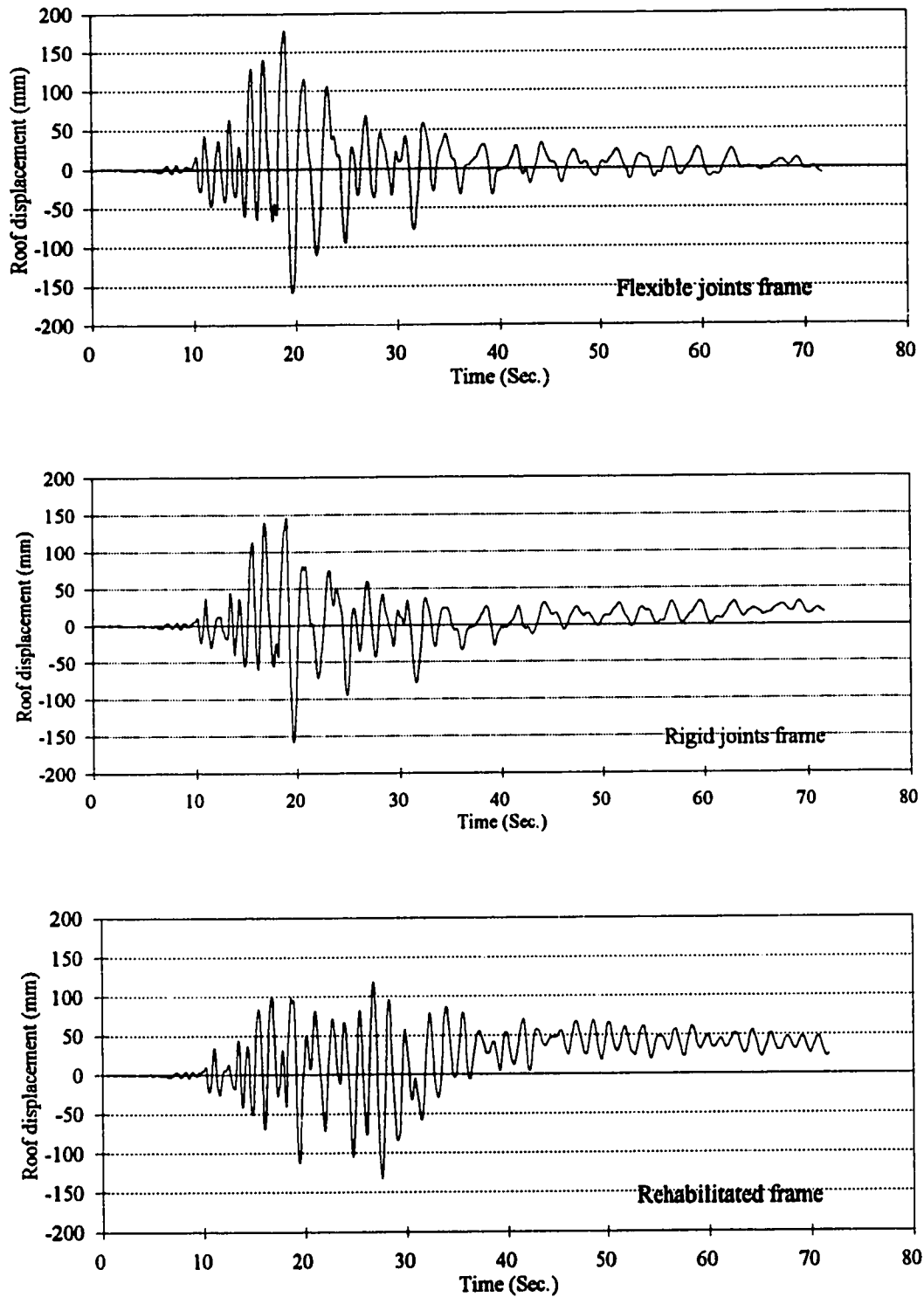


Figure 7.9 Roof displacement time histories for the 3-story frames due to the Mexico earthquake scaled to PGA of 0.3g

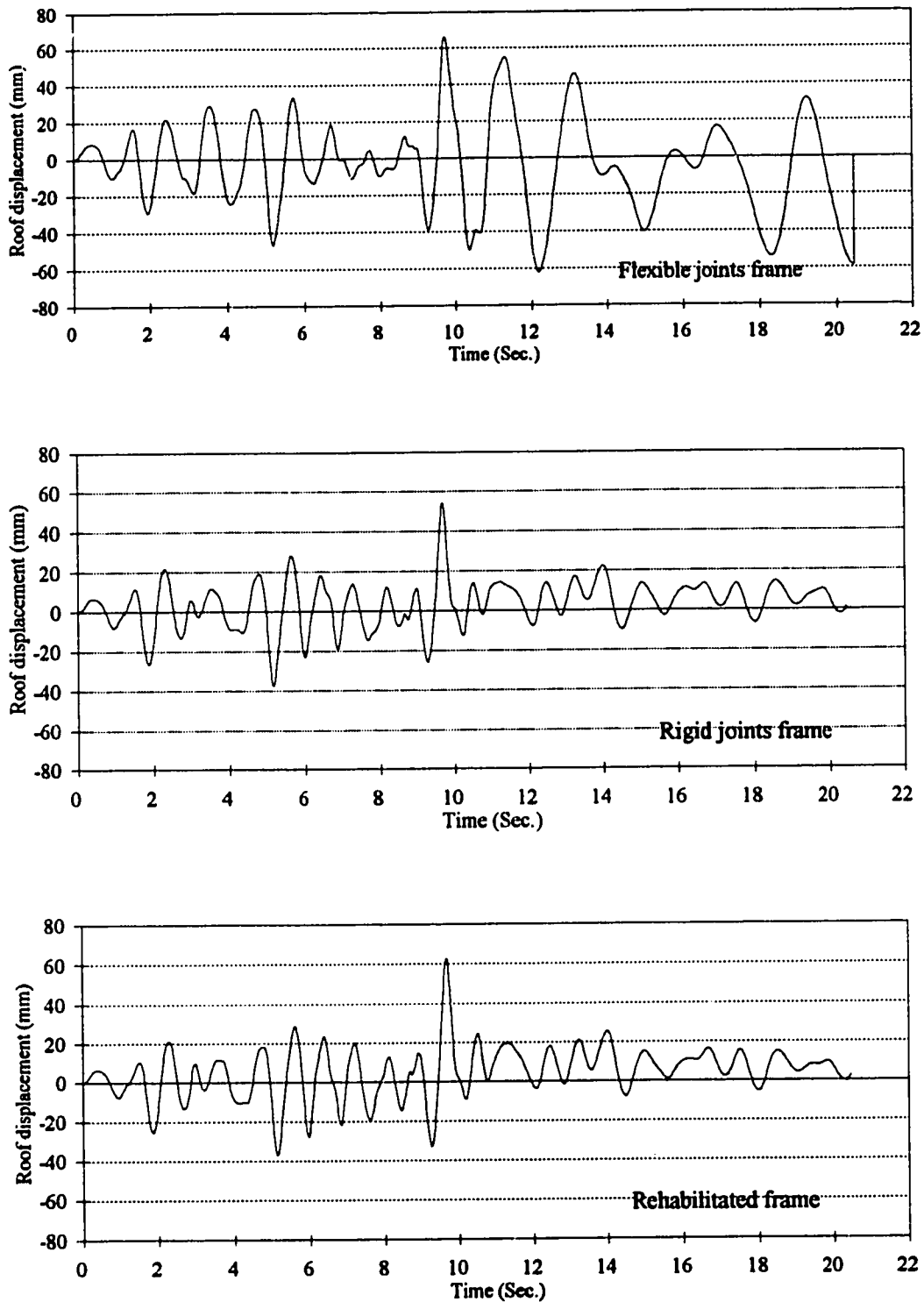


Figure 7.10 Roof displacement time histories for the 3-story frames due to the Artificial earthquake scaled to PGA of 0.3g

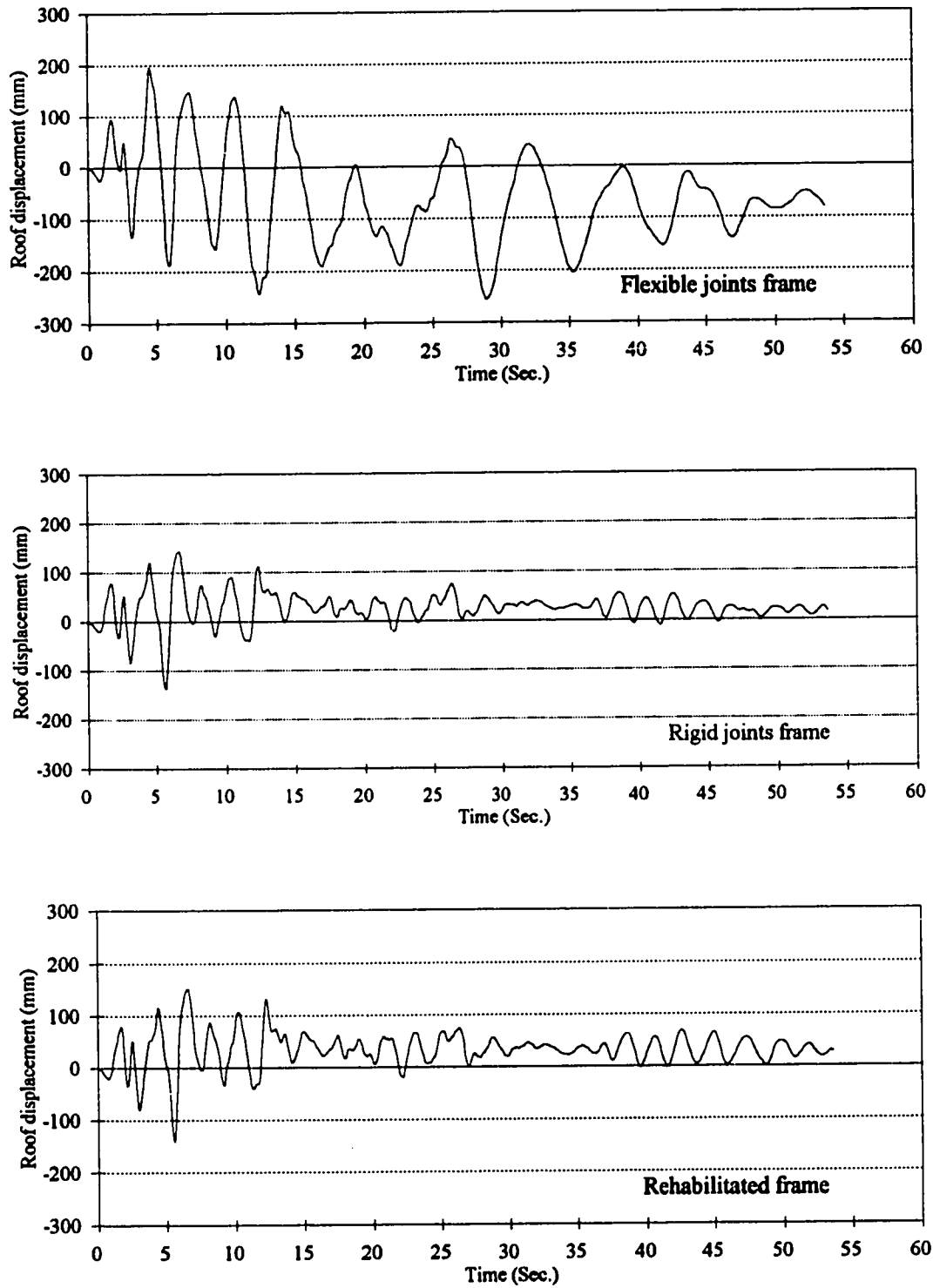


Figure 7.11 Roof displacement time histories for the 9-story frames due to the El Centro earthquake scaled to PGA of 0.3g

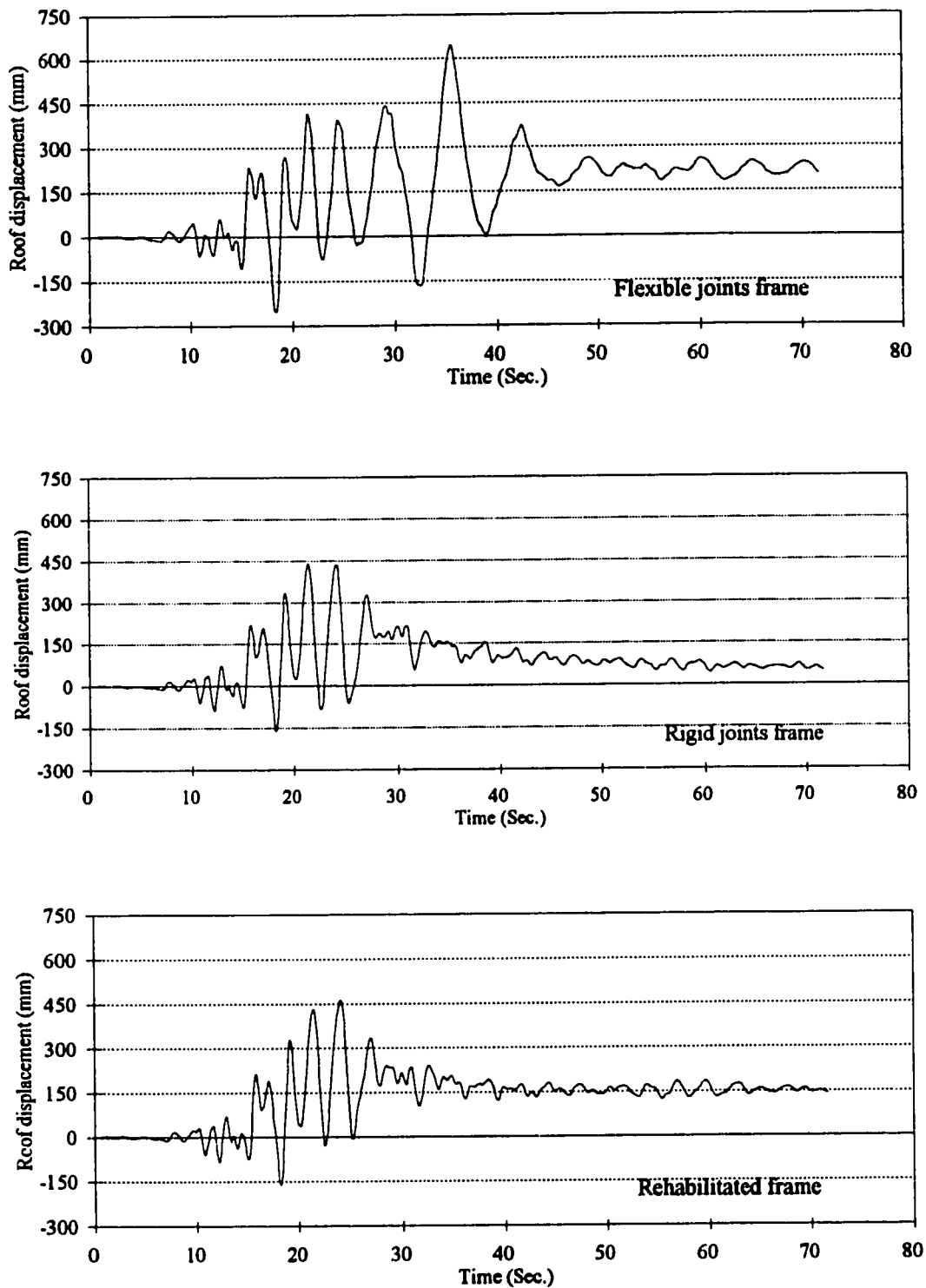


Figure 7.12 Roof displacement time histories for the 9-story frames due to the Mexico earthquake scaled to PGA of 0.3g

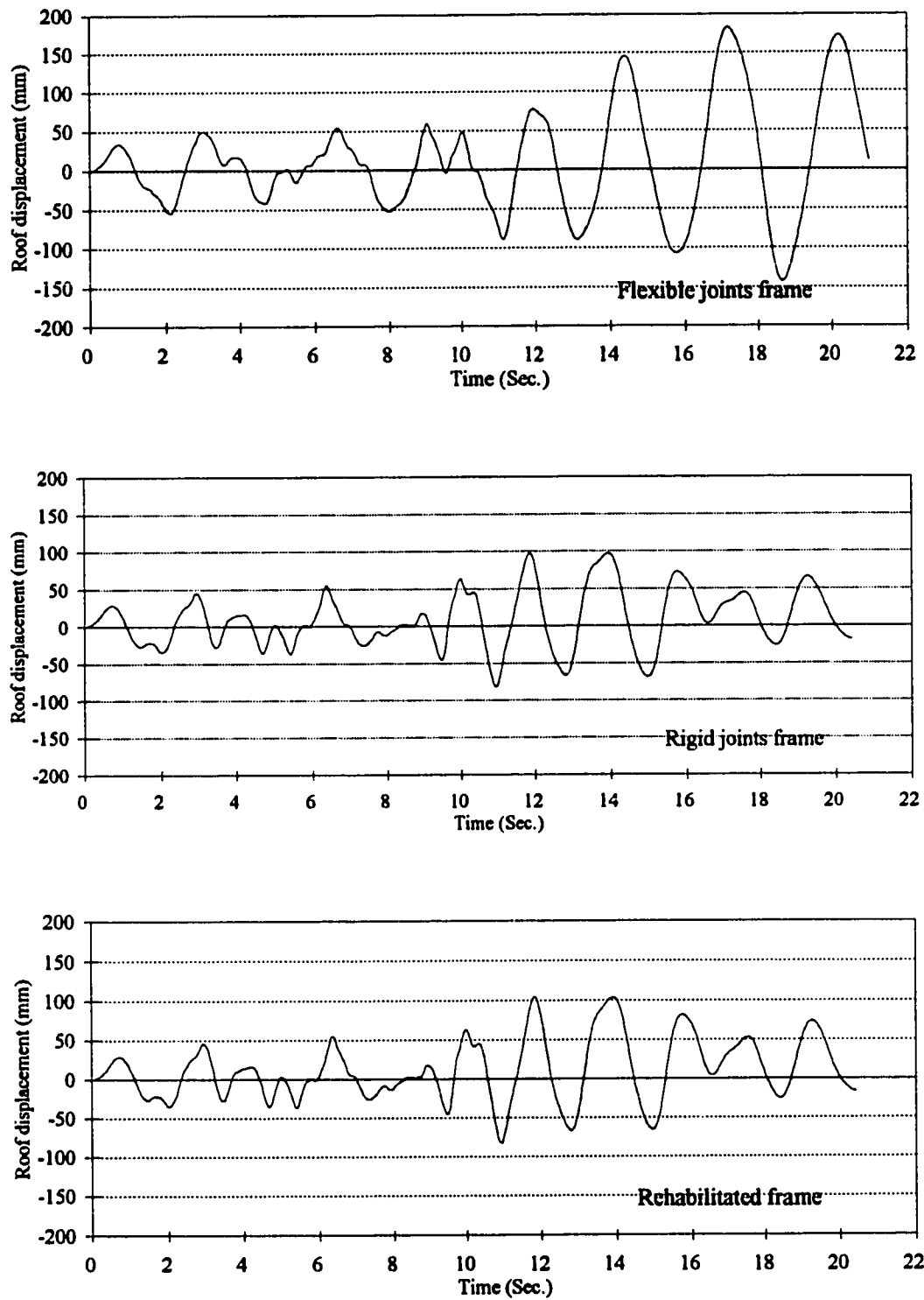


Figure 7.13 Roof displacement time histories for the 9-story frames due to the Artificial earthquake scaled to PGA of 0.3g

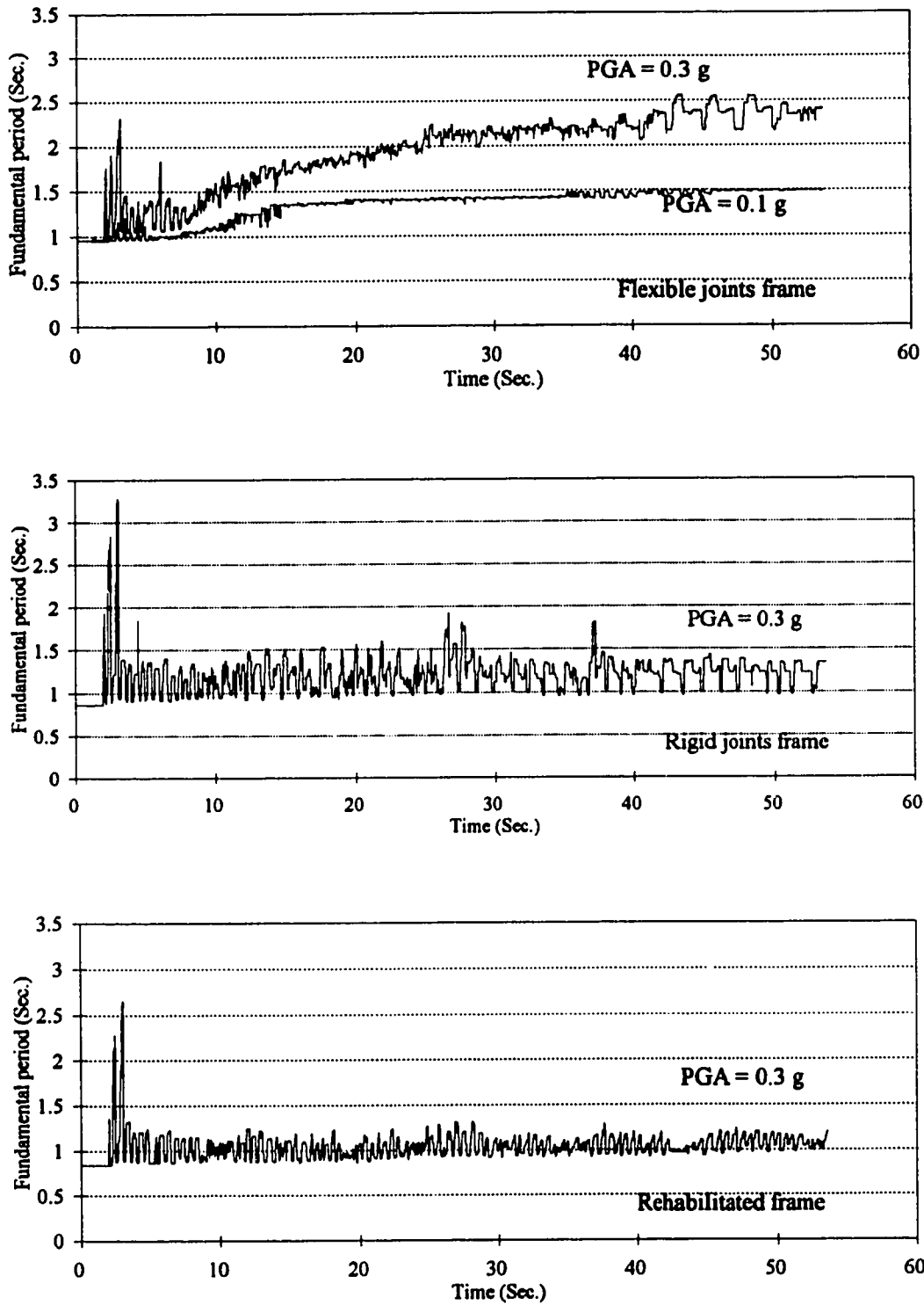


Figure 7.14 Variation of the fundamental period with time for the 3-story frames when subjected to the El Centro earthquake

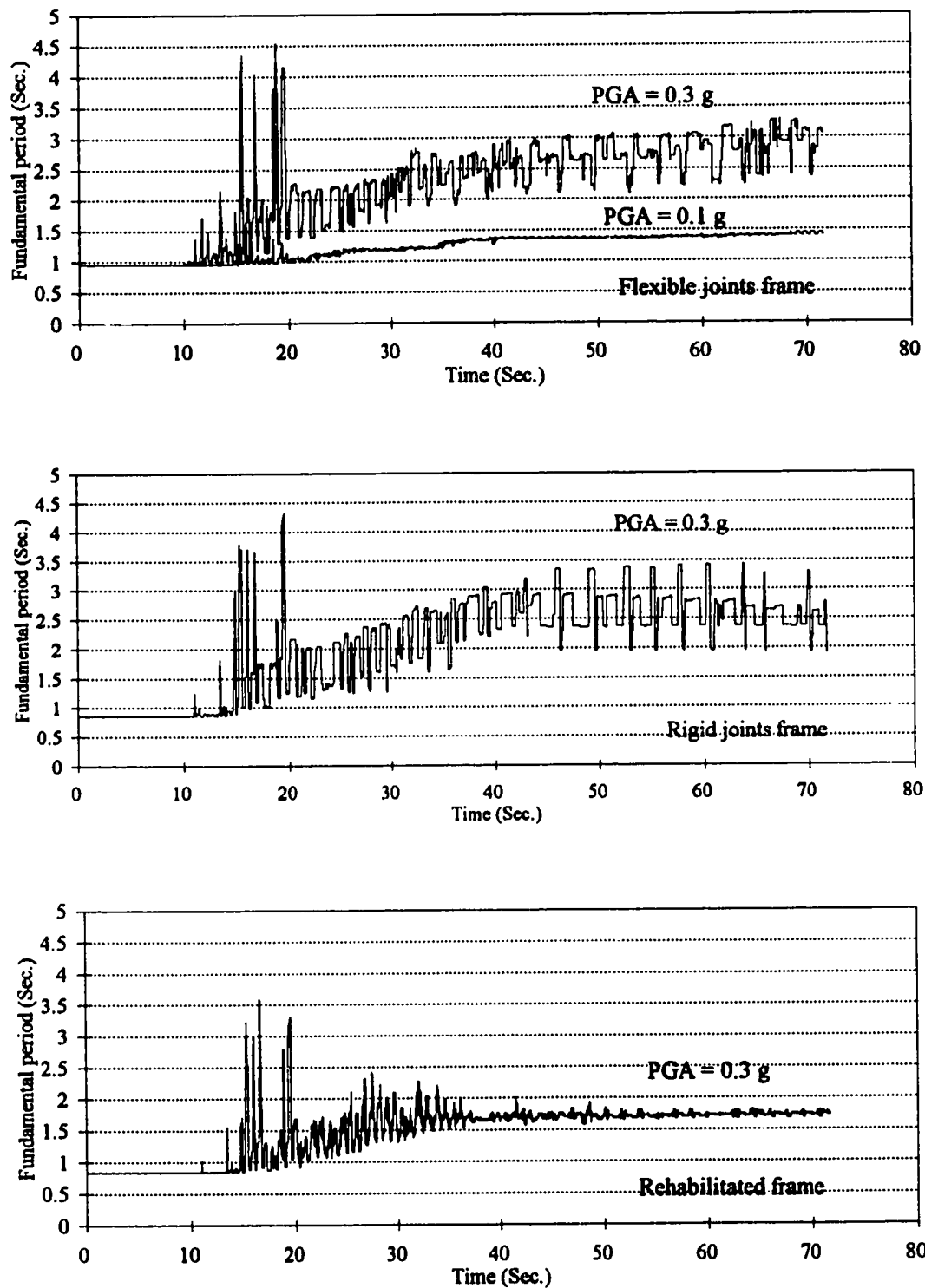


Figure 7.15 Variation of the fundamental period with time for the 3-story frames when subjected to the Mexico earthquake

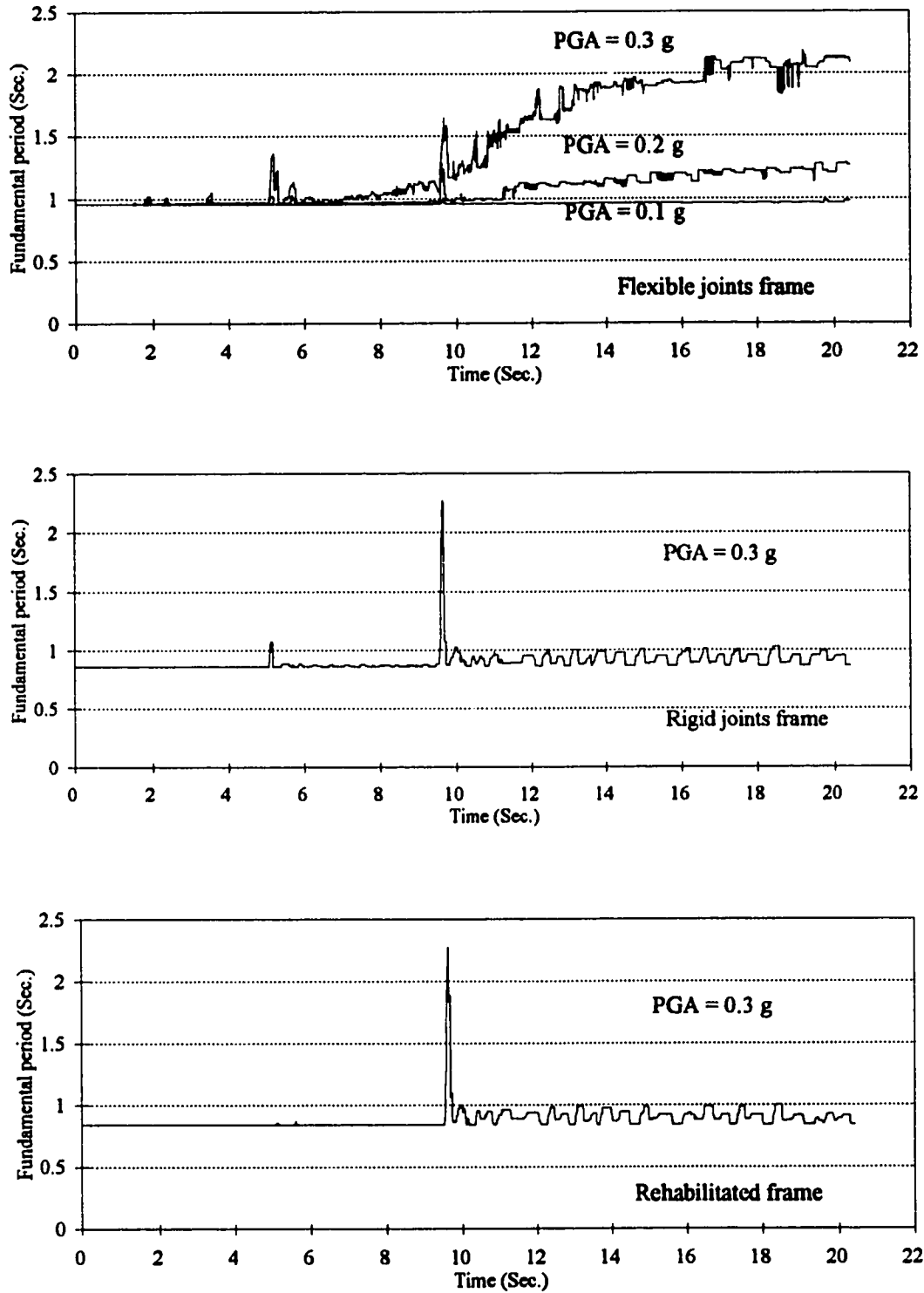


Figure 7.16 Variation of the fundamental period with time for the 3-story frames when subjected to the Artificial earthquake

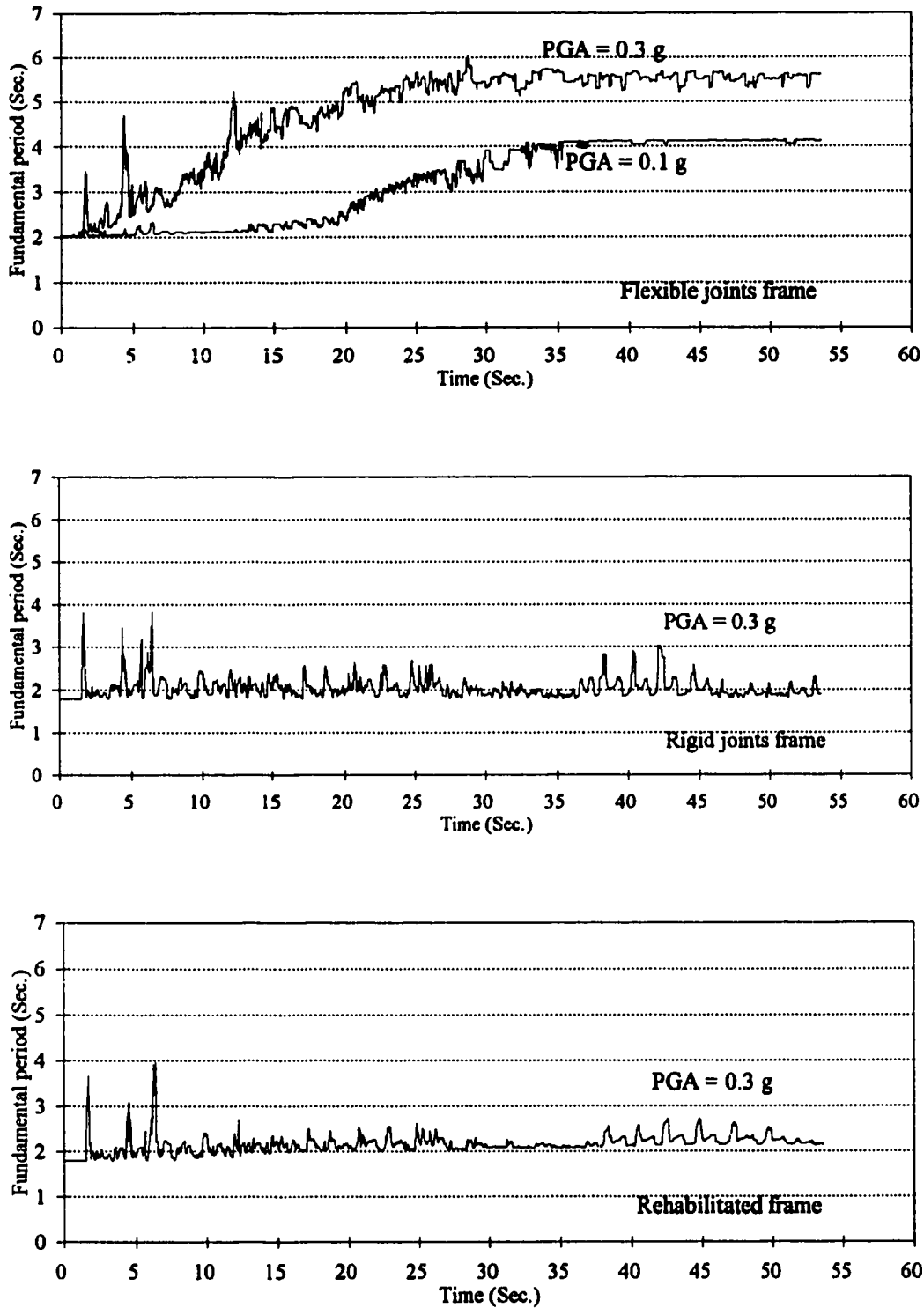


Figure 7.17 Variation of the fundamental period with time for the 9-story frames when subjected to the El Centro earthquake

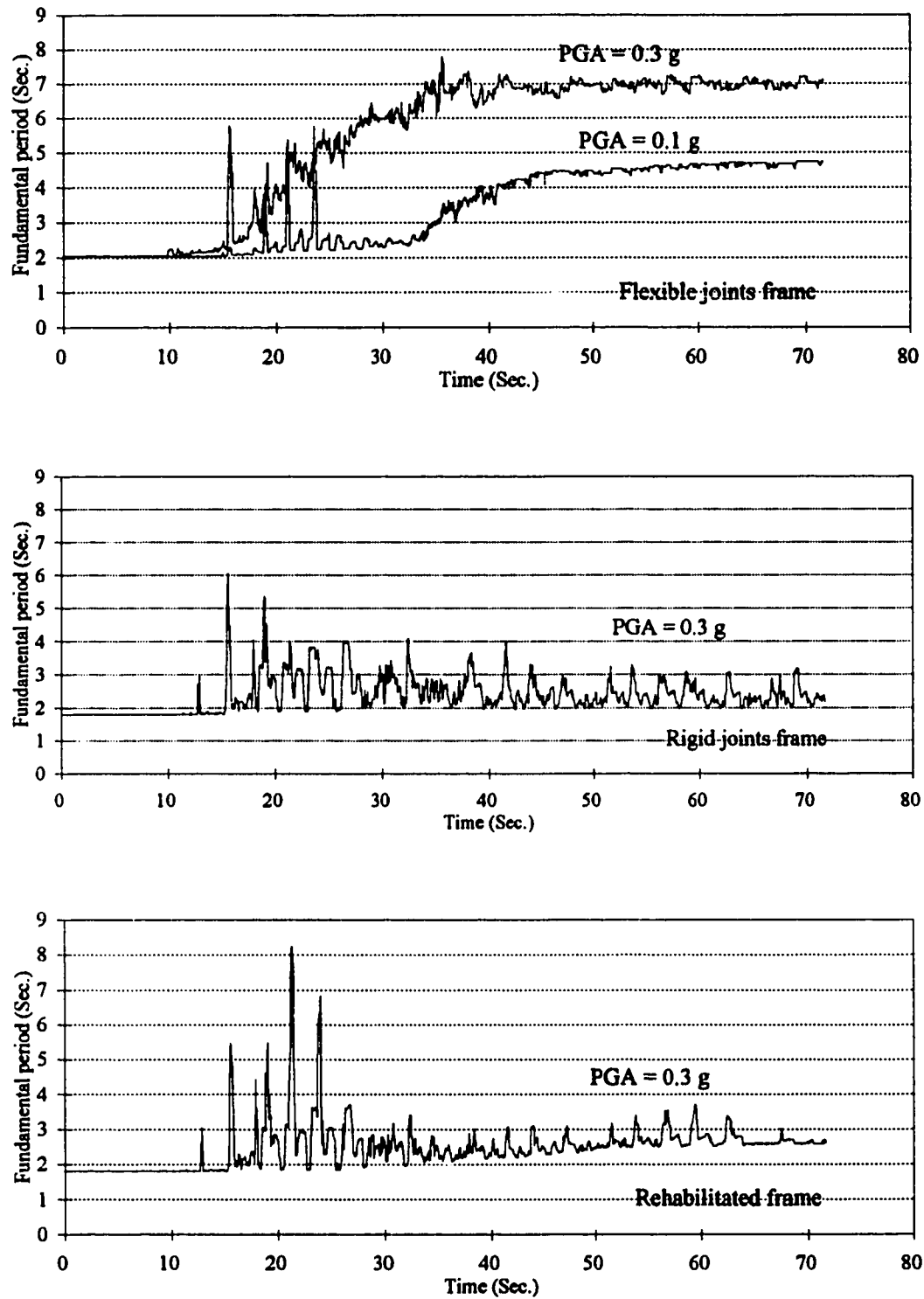


Figure 7.18 Variation of the fundamental period with time for the 9-story frames when subjected to the Mexico earthquake

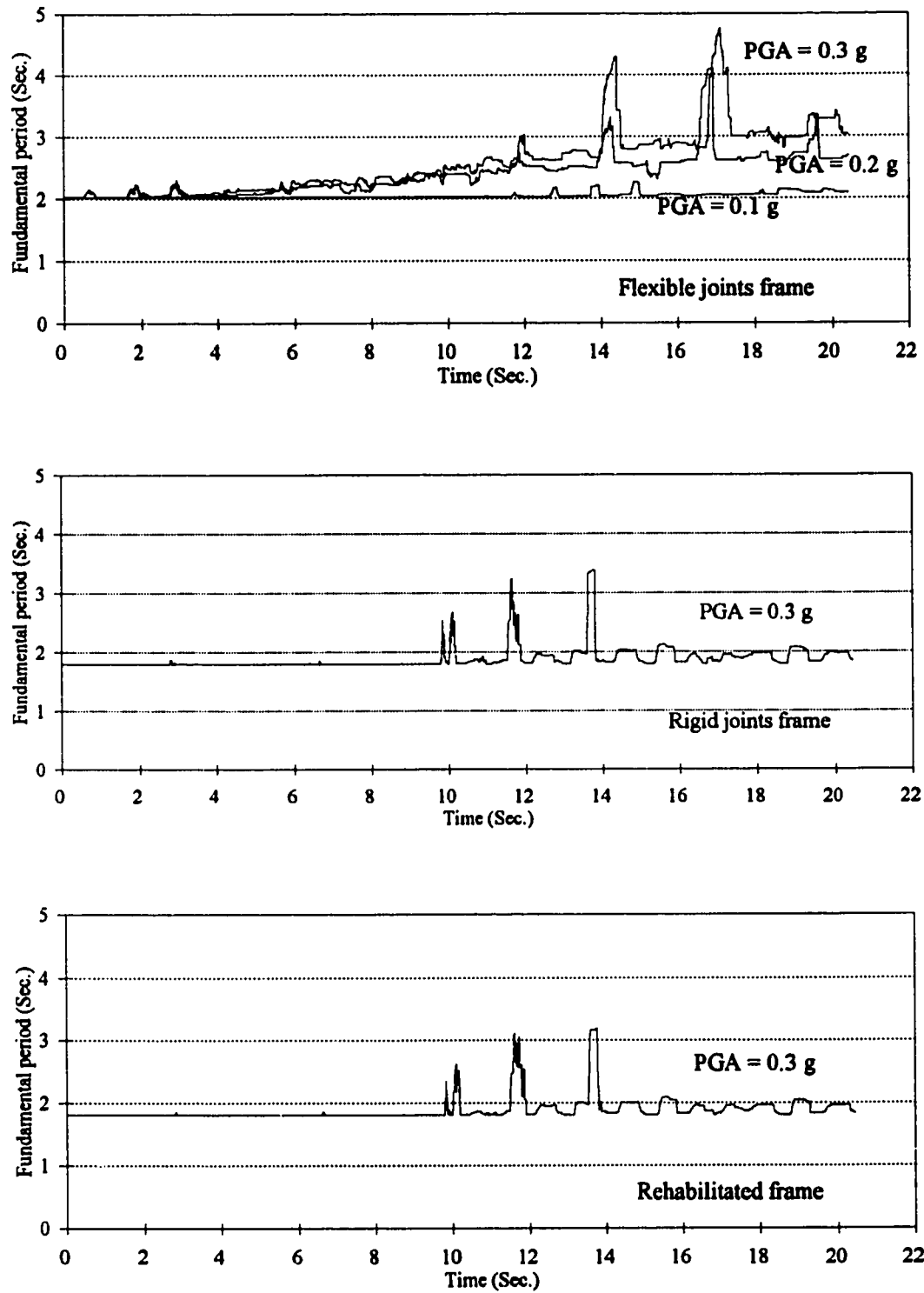


Figure 7.19 Variation of the fundamental period with time for the 9-story frames when subjected to the Artificial earthquake

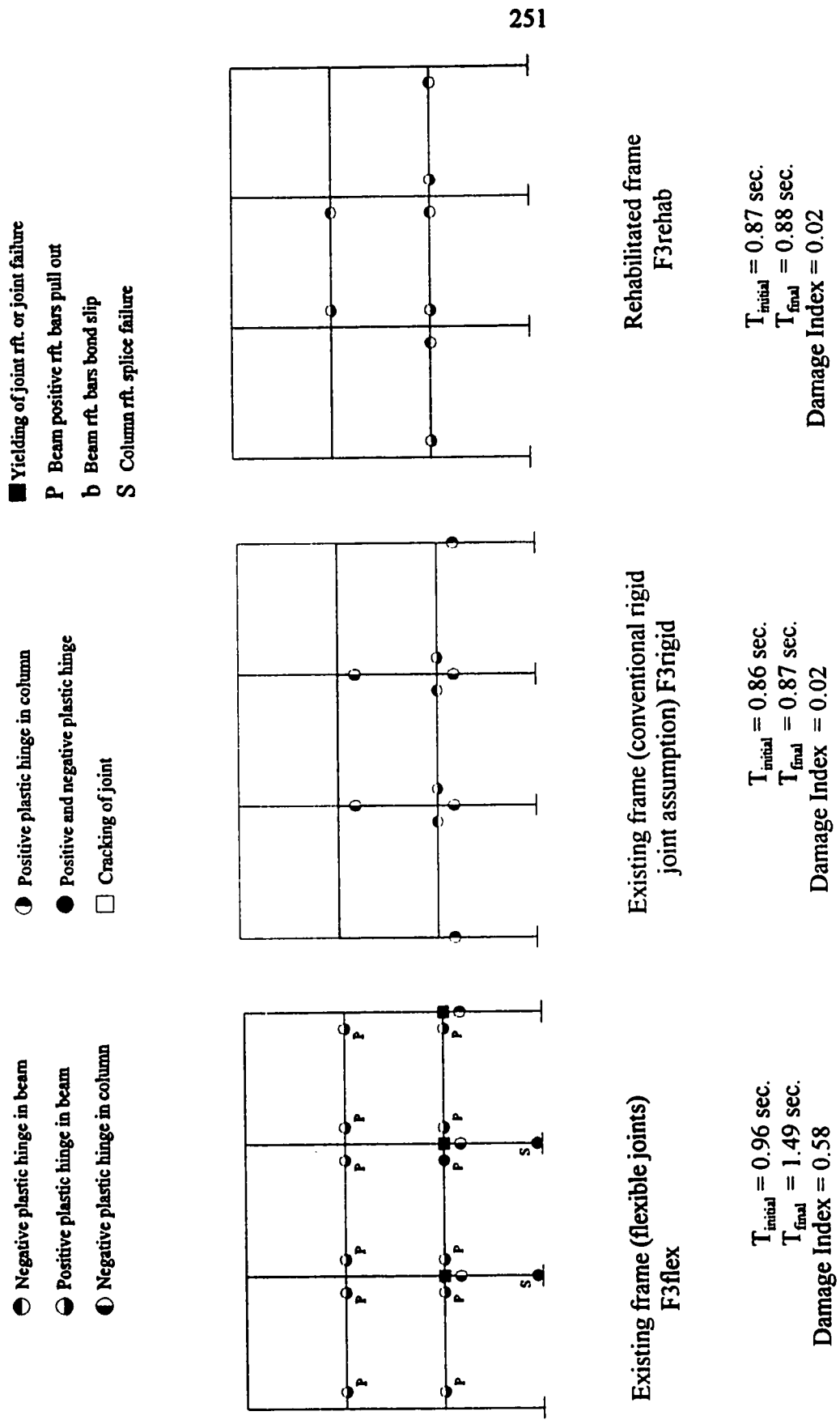
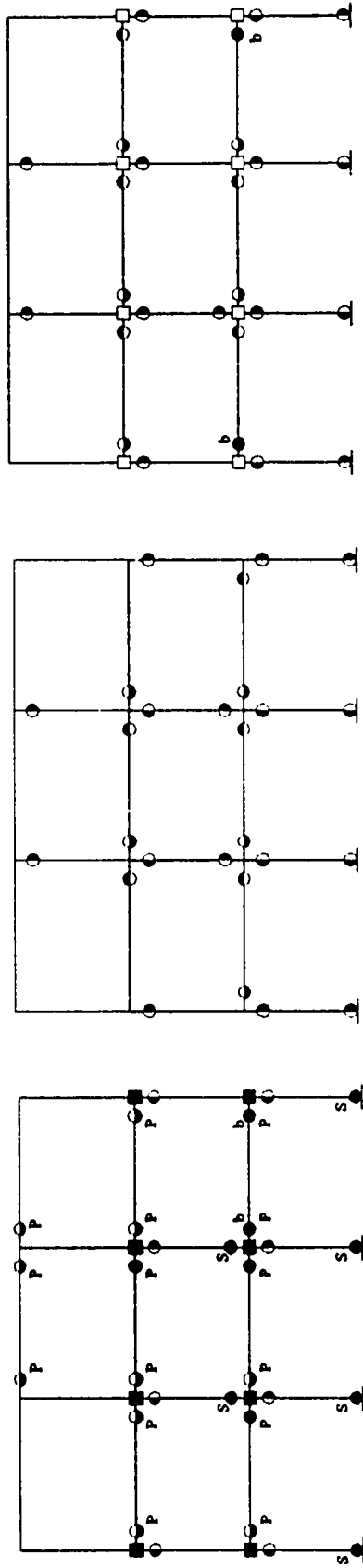


Figure 7.20 Summary of hinge type and location for the 3-story frames due to the El Centro earthquake scaled to PGA of 0.1g

- Negative plastic hinge in beam
- Positive plastic hinge in beam
- Negative plastic hinge in column
- Positive plastic hinge in column
- Positive and negative plastic hinge
- Cracking of joint
- Yielding of joint rft. or joint failure
- P Beam positive rft. bars pull out
- b Beam rft. bars bond slip
- S Column rft. splice failure



Existing frame (flexible joints)
F3flex

$T_{\text{initial}} = 0.96 \text{ sec.}$
 $T_{\text{final}} = 2.29 \text{ sec.}$
Damage Index = 0.82

Existing frame (conventional rigid
joint assumption) F3rigid

$T_{\text{initial}} = 0.86 \text{ sec.}$
 $T_{\text{final}} = 1.37 \text{ sec.}$
Damage Index = 0.60

Rehabilitated frame
F3rehab

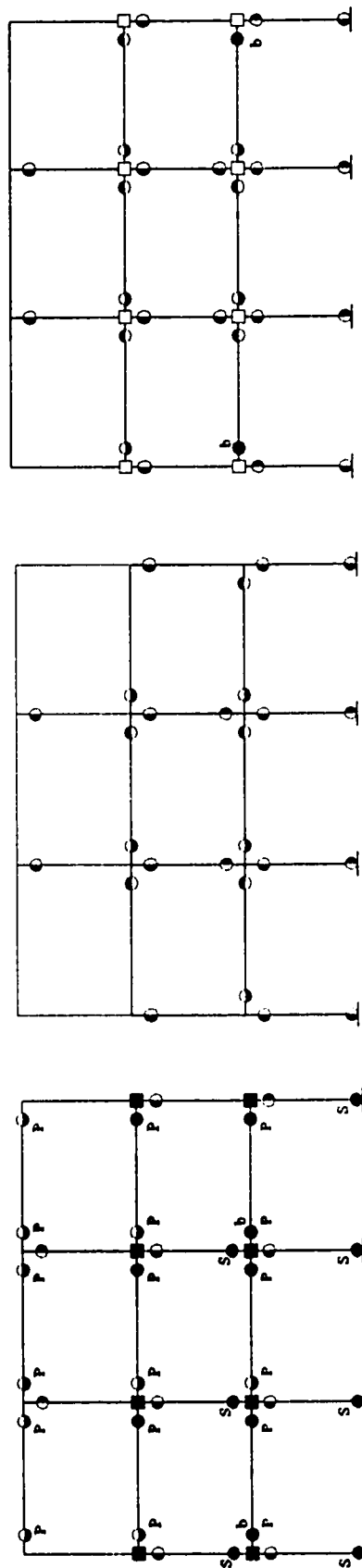
$T_{\text{initial}} = 0.87 \text{ sec.}$
 $T_{\text{final}} = 0.92 \text{ sec.}$
Damage Index = 0.11

Figure 7.21 Summary of hinge type and location for the 3-story frames due to El Centro earthquake scaled to PGA of 0.2g

- Yielding of joint rft. or joint failure
- P Beam positive rft. bars pull out
- b Beam rft. bars bond slip
- S Column rft. splice failure

- Positive plastic hinge in column
- Positive and negative plastic hinge
- Cracking of joint

- Negative plastic hinge in beam
- Positive plastic hinge in beam
- Negative plastic hinge in column



Existing frame (flexible joints)
F3flex

$T_{\text{initial}} = 0.96 \text{ sec.}$
 $T_{\text{final}} = 2.77 \text{ sec.}$
Damage Index = 0.88

Existing frame (conventional rigid
joint assumption) F3rigid

$T_{\text{initial}} = 0.86 \text{ sec.}$
 $T_{\text{final}} = 1.43 \text{ sec.}$
Damage Index = 0.64

Rehabilitated frame
F3rehab

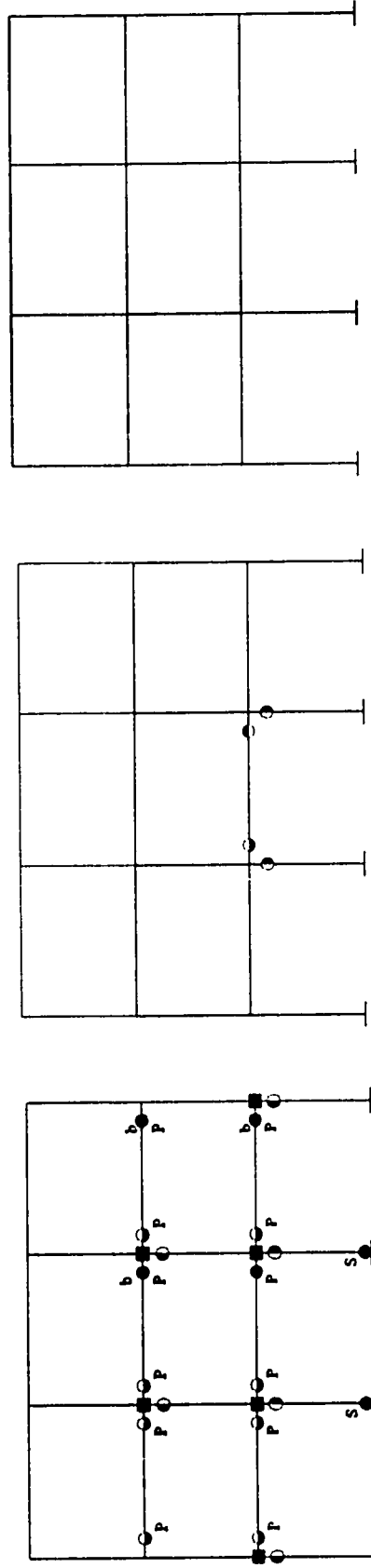
$T_{\text{initial}} = 0.87 \text{ sec.}$
 $T_{\text{final}} = 1.2 \text{ sec.}$
Damage Index = 0.47

Figure 7.22 Summary of hinge type and location for the 3-story frames due to the El Centro earthquake scaled to PGA of 0.3g

- Yielding of joint rft. or joint failure
- P Beam positive rft. bars pull out
- b Beam rft. bars bond slip
- S Column rft. splice failure

- Positive plastic hinge in column
- Positive and negative plastic hinge
- Cracking of joint

- Negative plastic hinge in beam
- Positive plastic hinge in beam
- Negative plastic hinge in column



Rehabilitated frame
F3rehab

$T_{\text{initial}} = 0.87 \text{ sec.}$
 $T_{\text{final}} = 0.87 \text{ sec.}$
 Damage Index = 0.0

Existing frame (conventional rigid
joint assumption) F3rigid

$T_{\text{initial}} = 0.86 \text{ sec.}$
 $T_{\text{final}} = 0.86 \text{ sec.}$
 Damage Index = 0.0

Existing frame (flexible joints)
F3flex

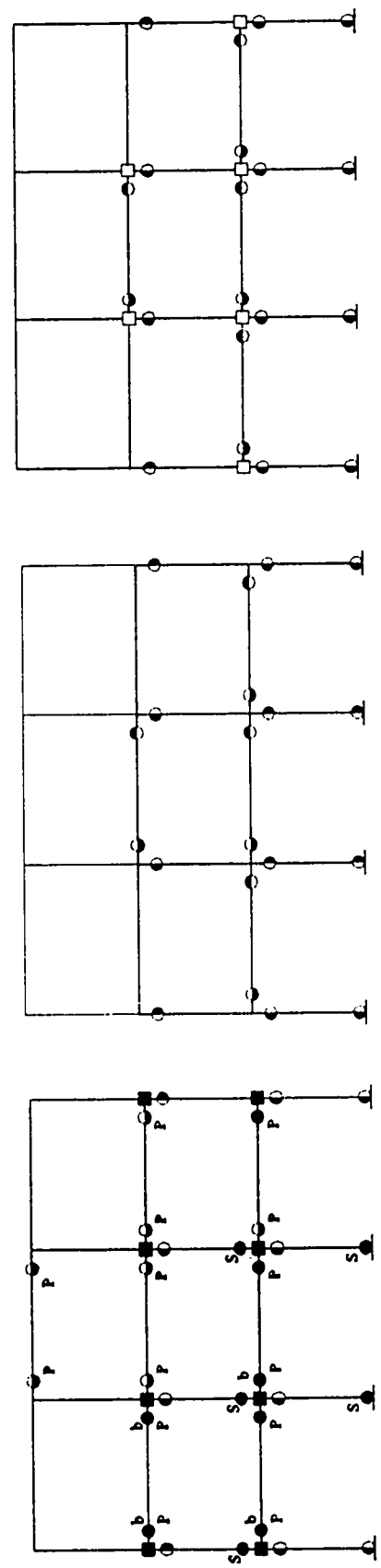
$T_{\text{initial}} = 0.96 \text{ sec.}$
 $T_{\text{final}} = 1.41 \text{ sec.}$
 Damage Index = 0.53

Figure 7.23 Summary of hinge type and location for the 3-story frames due to the Mexico earthquake scaled to PGA of 0.1g

- Yielding of joint rft. or joint failure
- P Beam positive rft. bars pull out
- b Beam rft. bars bond slip
- S Column rft. splice failure

- Positive plastic hinge in column
- Positive and negative plastic hinge
- Cracking of joint

- Negative plastic hinge in beam
- Positive plastic hinge in beam
- Negative plastic hinge in column



Existing frame (flexible joints)
F3flex

$T_{initial} = 0.96 \text{ sec.}$
 $T_{final} = 2.25 \text{ sec.}$
Damage Index = 0.82

Existing frame (conventional rigid joint assumption) F3rigid

$T_{initial} = 0.86 \text{ sec.}$
 $T_{final} = 1.55 \text{ sec.}$
Damage Index = 0.69

Rehabilitated frame
F3rehab

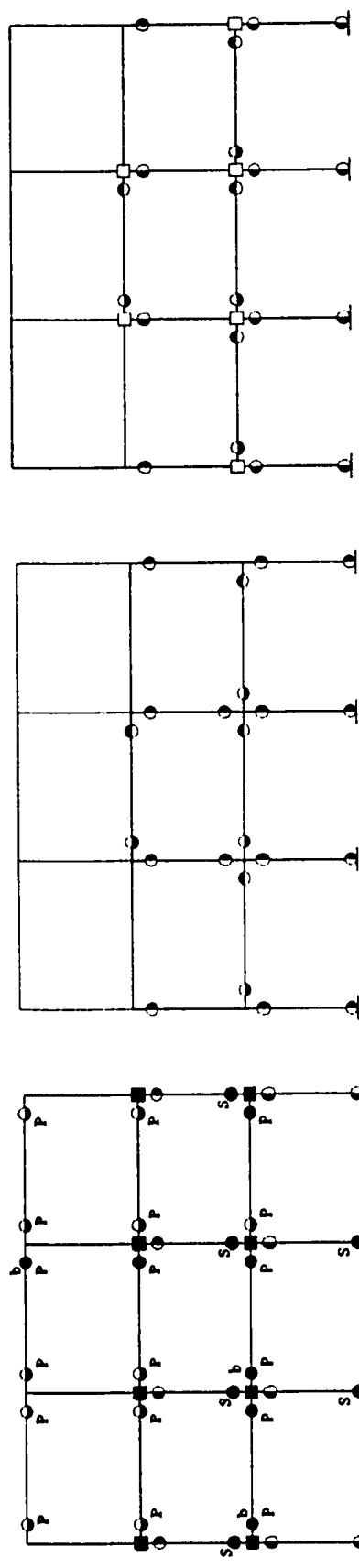
$T_{initial} = 0.87 \text{ sec.}$
 $T_{final} = 0.94 \text{ sec.}$
Damage Index = 0.14

Figure 7.24 Summary of hinge type and location for the 3-story frames due to the Mexico earthquake scaled to PGA of 0.2g

- Yielding of joint rft. or joint failure
- P Beam positive rft. bars pull out
- b Beam rft. bars bond slip
- S Column rft. splice failure

- Positive plastic hinge in column
- Positive and negative plastic hinge
- Cracking of joint

- Negative plastic hinge in beam
- Positive plastic hinge in beam
- Negative plastic hinge in column



Existing frame (flexible joints)
F3flex

$T_{initial} = 0.96 \text{ sec.}$
 $T_{final} = 3.08 \text{ sec.}$
Damage Index = 0.90

Existing frame (conventional rigid joint assumption) F3rigid

$T_{initial} = 0.86 \text{ sec.}$
 $T_{final} = 1.90 \text{ sec.}$
Damage Index = 0.80

Rehabilitated frame
F3rehab

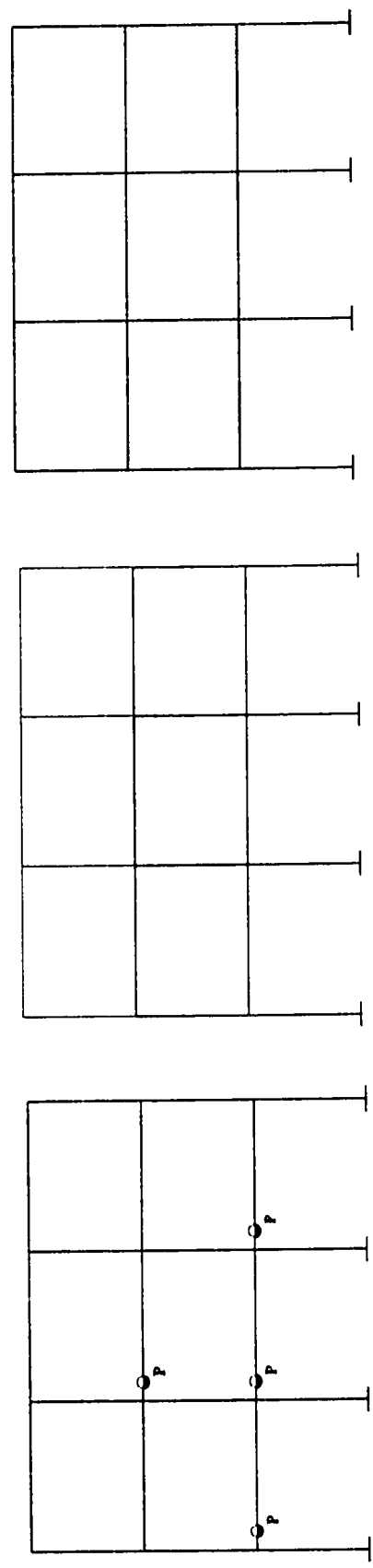
$T_{initial} = 0.87 \text{ sec.}$
 $T_{final} = 1.70 \text{ sec.}$
Damage Index = 0.74

Figure 7.25 Summary of hinge type and location for the 3-story frames due to the Mexico earthquake scaled to PGA of 0.3g

- Yielding of joint rft. or joint failure
- P Beam positive rft. bars pull out
- b Beam rft. bars bond slip
- S Column rft. splice failure

- Positive plastic hinge in column
- Positive and negative plastic hinge
- Cracking of joint

- Negative plastic hinge in beam
- Positive plastic hinge in beam
- Negative plastic hinge in column



Existing frame (flexible joints)
F3flex

Existing frame (conventional rigid
joint assumption) F3rigid

Rehabilitated frame
F3rehab

$T_{initial} = 0.96 \text{ sec.}$
 $T_{final} = 0.98 \text{ sec.}$
Damage Index = 0.04

$T_{initial} = 0.86 \text{ sec.}$
 $T_{final} = 0.86 \text{ sec.}$
Damage Index = 0.0

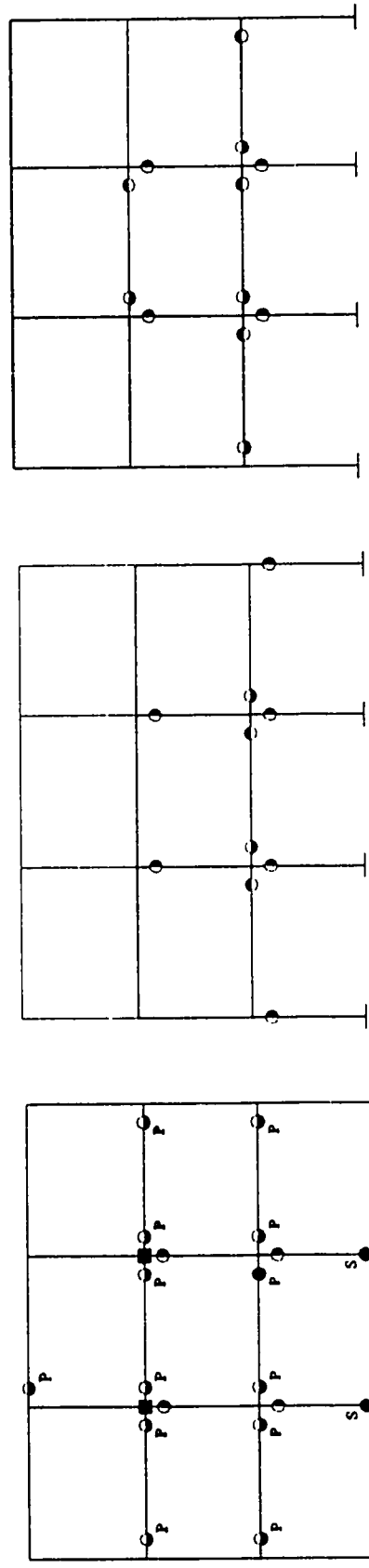
$T_{initial} = 0.87 \text{ sec.}$
 $T_{final} = 0.87 \text{ sec.}$
Damage Index = 0.0

Figure 7.26 Summary of hinge type and location for the 3-story frames due to the Artificial earthquake scaled to PGA of 0.1g

- Yielding of joint rft. or joint failure
- P Beam positive rft. bars pull out
- b Beam rft. bars bond slip
- S Column rft. splice failure

- Positive plastic hinge in column
- Positive and negative plastic hinge
- Cracking of joint

- Negative plastic hinge in beam
- Positive plastic hinge in beam
- Negative plastic hinge in column



Existing frame (flexible joints)
F3flex

$T_{initial} = 0.96$ sec.
 $T_{final} = 1.27$ sec.
Damage Index = 0.43

Existing frame (conventional rigid joint assumption) F3rigid

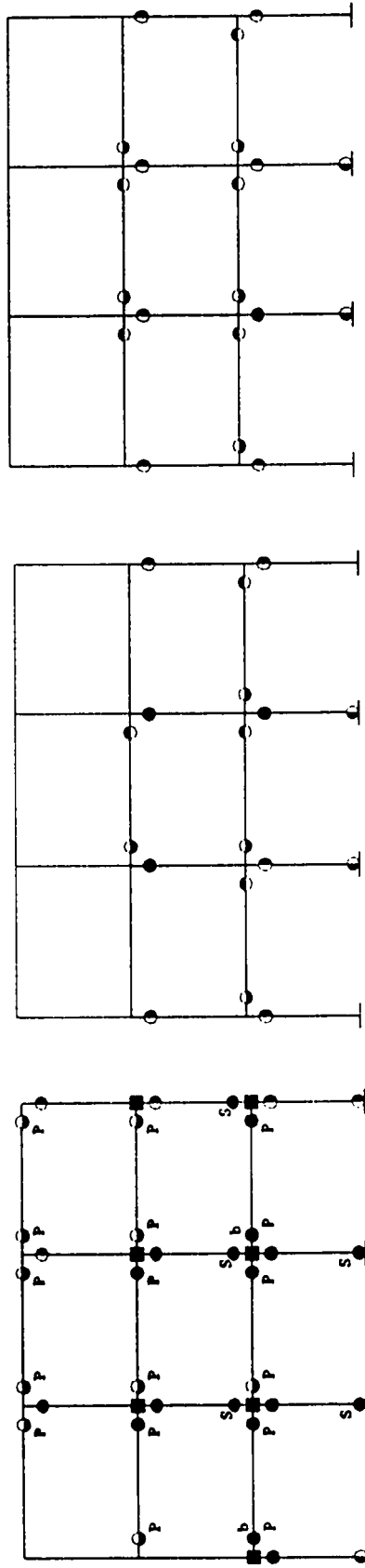
$T_{initial} = 0.86$ sec.
 $T_{final} = 0.87$ sec.
Damage Index = 0.02

Rehabilitated frame
F3rehab

$T_{initial} = 0.87$ sec.
 $T_{final} = 0.88$ sec.
Damage Index = 0.02

Figure 7.27 Summary of hinge type and location for the 3-story frames due to the Artificial earthquake scaled to PGA of 0.2g

- Negative plastic hinge in beam
- Positive plastic hinge in beam
- Negative plastic hinge in column
- Positive plastic hinge in column
- Positive and negative plastic hinge
- Cracking of joint
- Yielding of joint rft. or joint failure
- P Beam positive rft. bars pull out
- b Beam rft. bars bond slip
- S Column rft. splice failure



Existing frame (flexible joints)
F3flex

$T_{\text{initial}} = 0.96 \text{ sec.}$
 $T_{\text{final}} = 2.04 \text{ sec.}$
Damage Index = 0.78

Existing frame (conventional rigid
joint assumption) F3rigid

$T_{\text{initial}} = 0.86 \text{ sec.}$
 $T_{\text{final}} = 0.93 \text{ sec.}$
Damage Index = 0.14

Rehabilitated frame
F3rehab

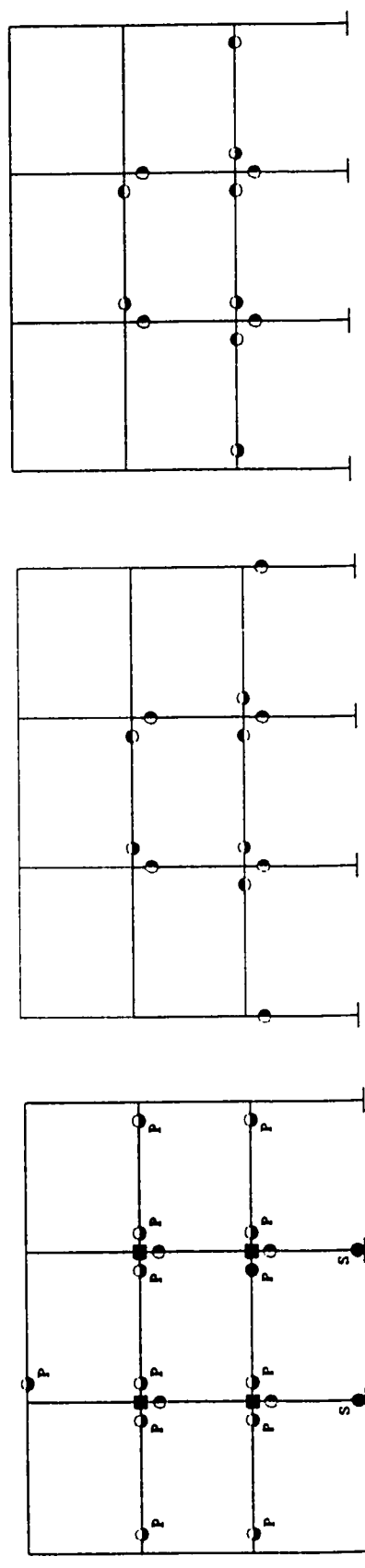
$T_{\text{initial}} = 0.87 \text{ sec.}$
 $T_{\text{final}} = 0.92 \text{ sec.}$
Damage Index = 0.11

Figure 7.28 Summary of hinge type and location for the 3-story frames due to the Artificial earthquake scaled to PGA of 0.3g

- Yielding of joint rft. or joint failure
- P Beam positive rft. bars pull out
- b Beam rft. bars bond slip
- S Column rft. splice failure

- Positive plastic hinge in column
- Positive and negative plastic hinge
- Cracking of joint

- Negative plastic hinge in beam
- Positive plastic hinge in beam
- Negative plastic hinge in column



Existing frame (flexible joints)
F3flex

$T_{\text{initial}} = 0.96 \text{ sec.}$
 $T_{\text{final}} = 2.11 \text{ sec.}$
Damage Index = 0.79

Existing frame (conventional rigid joint assumption) F3rigid

$T_{\text{initial}} = 0.86 \text{ sec.}$
 $T_{\text{final}} = 0.88 \text{ sec.}$
Damage Index = 0.05

Rehabilitated frame
F3rehab

$T_{\text{initial}} = 0.87 \text{ sec.}$
 $T_{\text{final}} = 0.88 \text{ sec.}$
Damage Index = 0.02

Figure 7.29 Summary of hinge type and location for the 3-story frames due to the Nahanni earthquake scaled to PGA of 0.3g

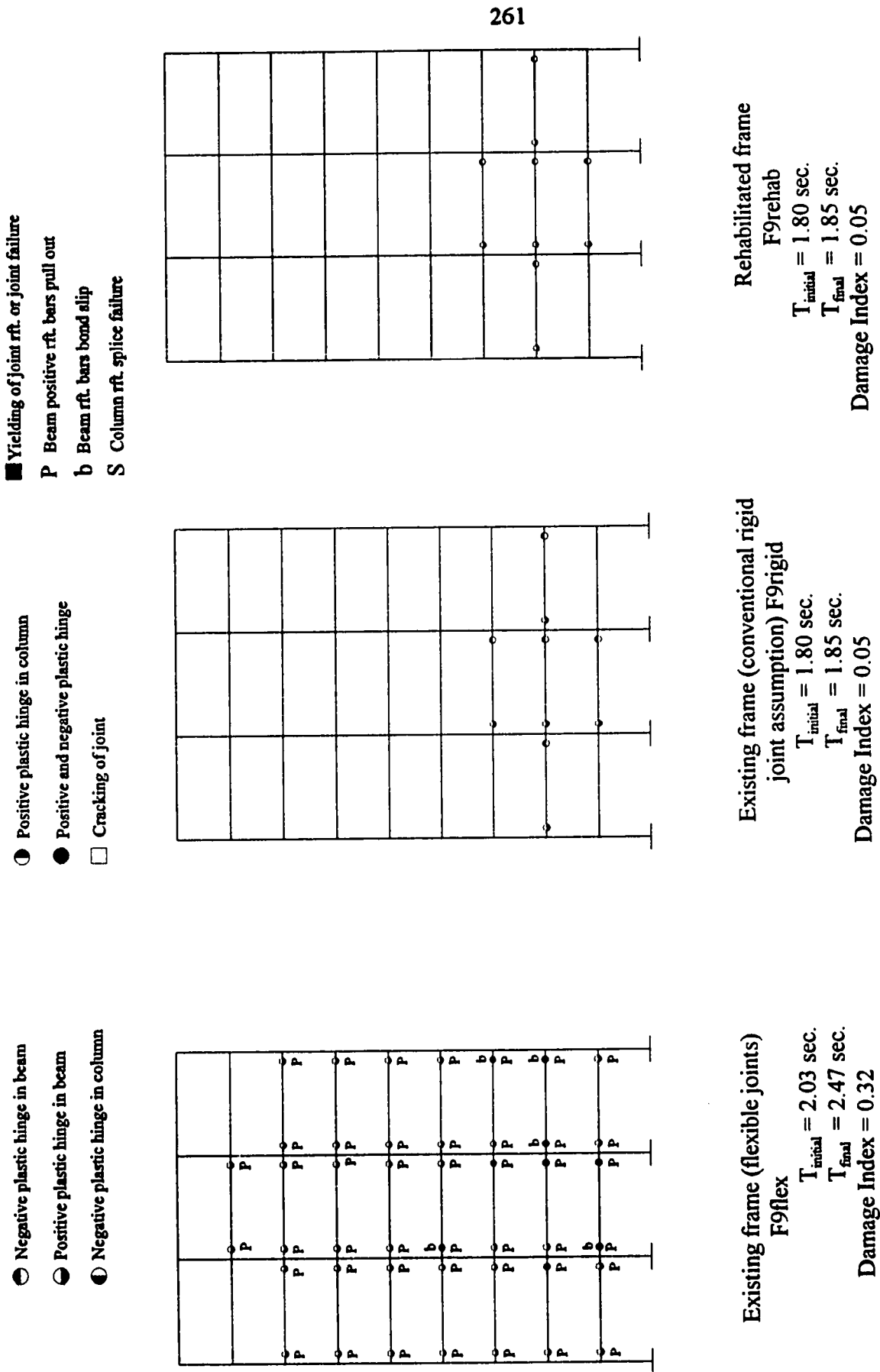
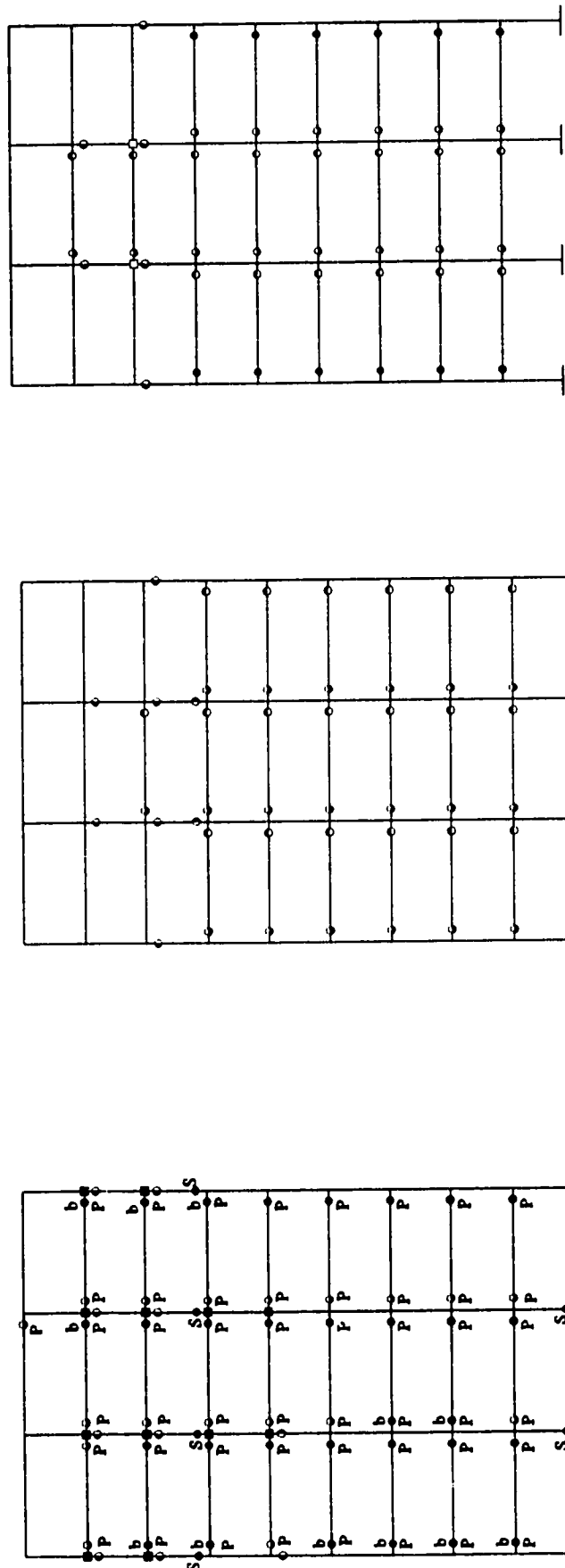


Figure 7.30 Summary of hinge type and location for the 9-story frames due to the El Centro earthquake scaled to PGA of 0.1g

- Yielding of joint rft. or joint failure
- P Beam positive rft. bars pull out
- b Beam rft. bars bond slip
- S Column rft. splice failure

- Positive plastic hinge in column
- Positive and negative plastic hinge
- Cracking of joint

- Negative plastic hinge in beam
- Positive plastic hinge in beam
- Negative plastic hinge in column



Existing frame (flexible joints)
F9flex
 $T_{\text{initial}} = 2.03 \text{ sec.}$
 $T_{\text{final}} = 4.16 \text{ sec.}$
 Damage Index = 0.76

Existing frame (conventional rigid
joint assumption) F9rigid
 $T_{\text{initial}} = 1.80 \text{ sec.}$
 $T_{\text{final}} = 1.88 \text{ sec.}$
 Damage Index = 0.08

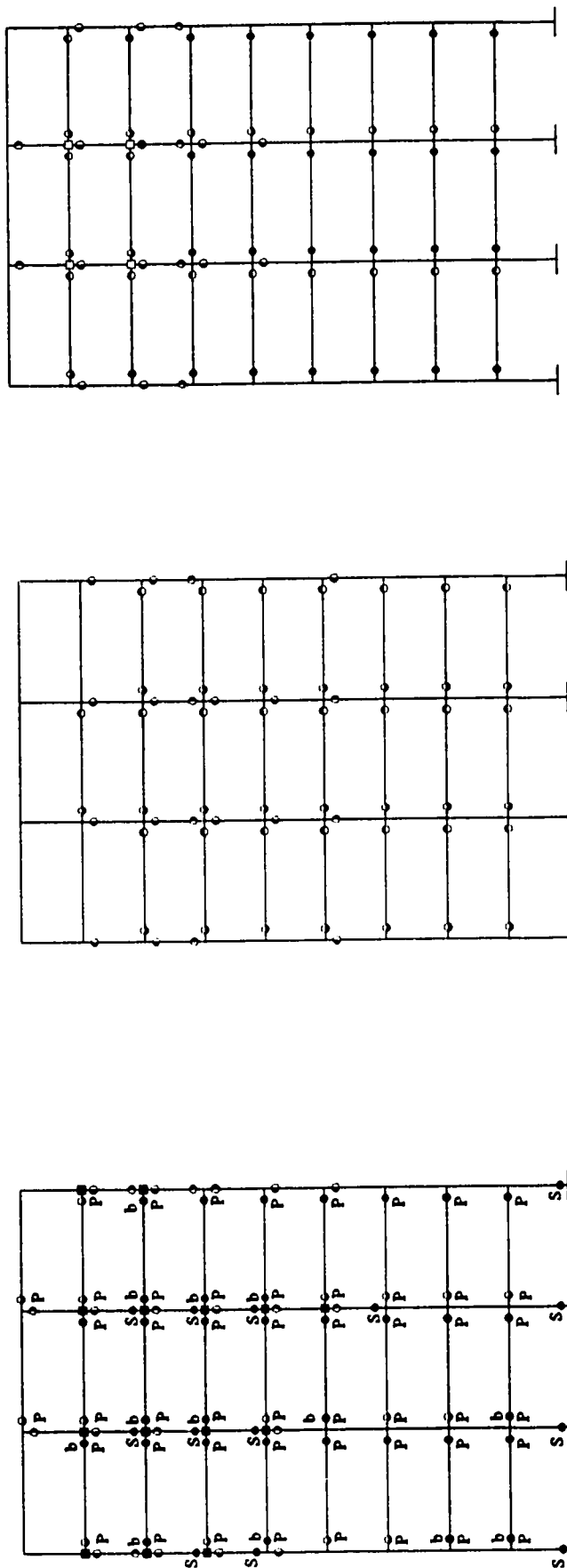
Rehabilitated frame
F9rehab
 $T_{\text{initial}} = 1.80 \text{ sec.}$
 $T_{\text{final}} = 1.97 \text{ sec.}$
 Damage Index = 0.16

Figure 7.31 Summary of hinge type and location for the 9-story frames due to the El Centro earthquake scaled to PGA of 0.2g

- Yielding of joint rft. or joint failure
- P Beam positive rft. bars pull out
- b Beam rft. bars bond slip
- S Column rft. splice failure

- Positive plastic hinge in column
- Positive and negative plastic hinge
- Cracking of joint

- Negative plastic hinge in beam
- Positive plastic hinge in beam
- Negative plastic hinge in column



Existing frame (flexible joints)
F9flex
 $T_{initial} = 2.03 \text{ sec.}$
 $T_{final} = 5.60 \text{ sec.}$
Damage Index = 0.87

Existing frame (conventional rigid joint assumption) F9rigid
 $T_{initial} = 1.80 \text{ sec.}$
 $T_{final} = 1.97 \text{ sec.}$
Damage Index = 0.17

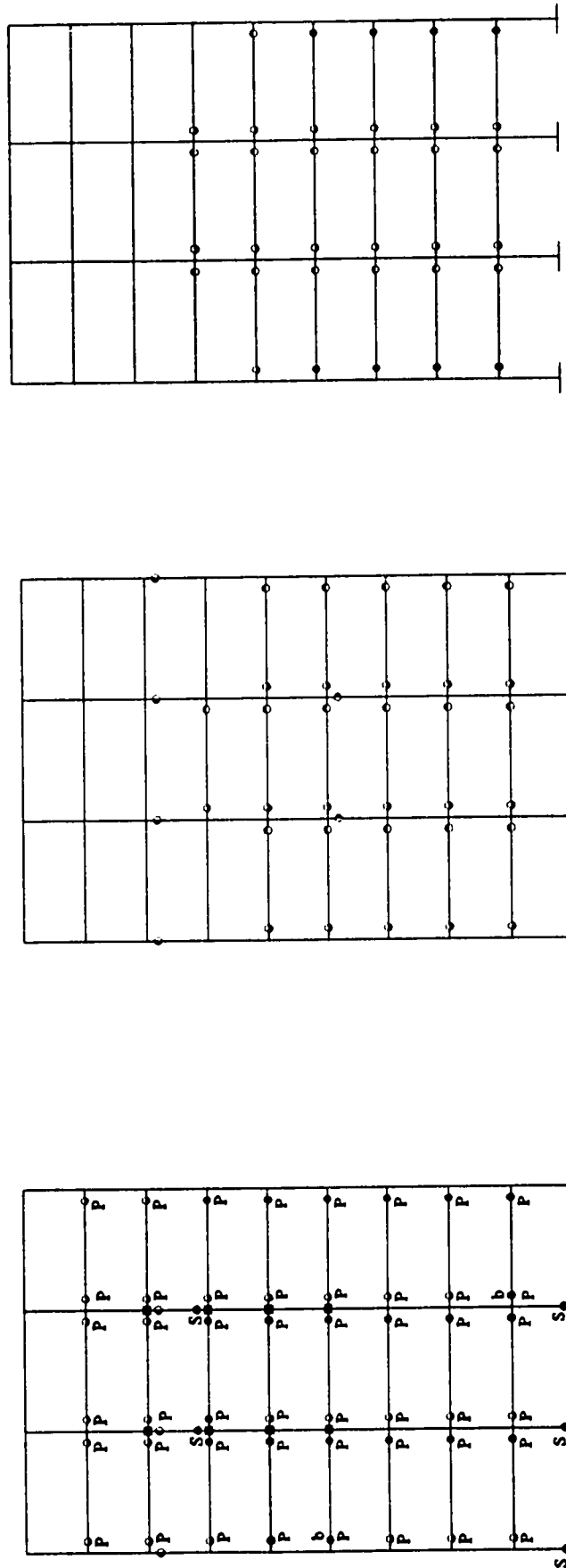
Rehabilitated frame
F9rehab
 $T_{initial} = 1.80 \text{ sec.}$
 $T_{final} = 2.15 \text{ sec.}$
Damage Index = 0.30

Figure 7.32 Summary of hinge type and location for the 9-story frames due to the El Centro earthquake scaled to PGA of 0.3g

- Yielding of joint rft. or joint failure
- P Beam positive rft. bars pull out
- b Beam rft. bars bond slip
- S Column rft. splice failure

- Positive plastic hinge in column
- Positive and negative plastic hinge
- Cracking of joint

- Negative plastic hinge in beam
- Positive plastic hinge in beam
- Negative plastic hinge in column



Existing frame (flexible joints)
F9flex
 $T_{\text{initial}} = 2.03 \text{ sec.}$
 $T_{\text{final}} = 4.71 \text{ sec.}$
 Damage Index = 0.81

Existing frame (conventional rigid
joint assumption) F9rigid
 $T_{\text{initial}} = 1.80 \text{ sec.}$
 $T_{\text{final}} = 1.85 \text{ sec.}$
 Damage Index = 0.05

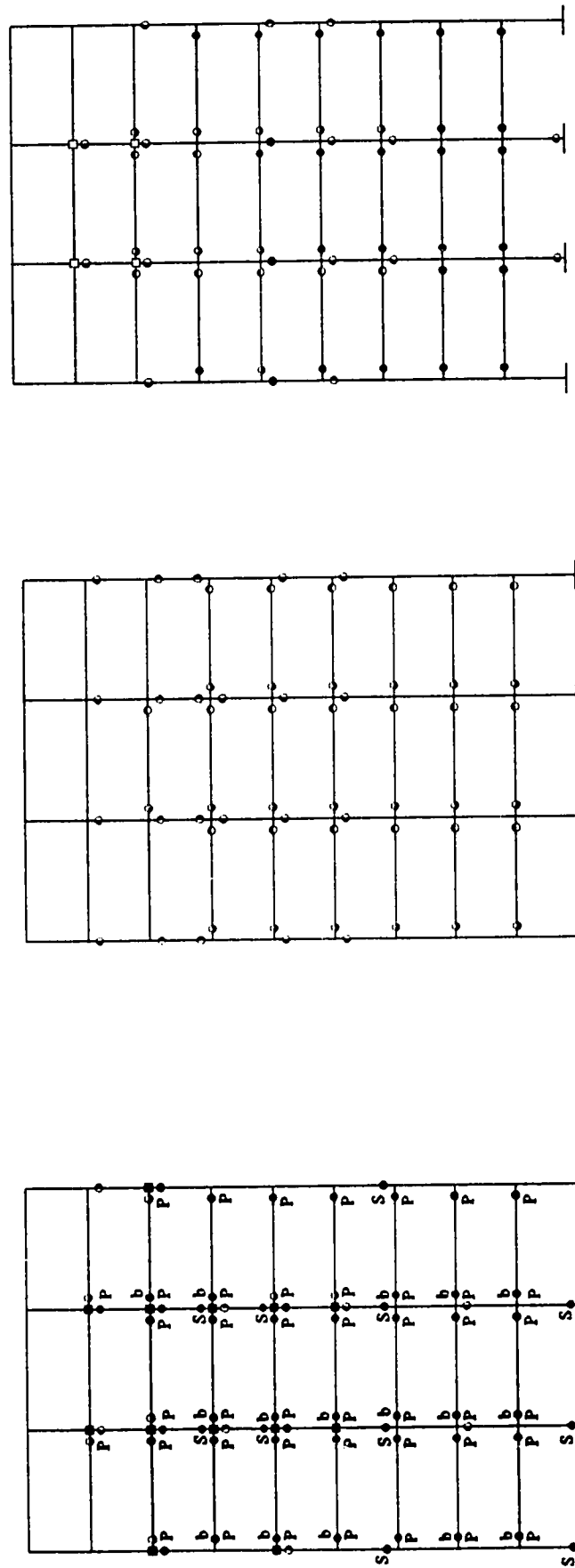
Rehabilitated frame
F9rehab
 $T_{\text{initial}} = 1.80 \text{ sec.}$
 $T_{\text{final}} = 1.93 \text{ sec.}$
 Damage Index = 0.13

Figure 7.33 Summary of hinge type and location for the 9-story frames due to the Mexico earthquake scaled to PGA of 0.1g

- Yielding of joint rft. or joint failure
- P Beam positive rft. bars pull out
- b Beam rft. bars bond slip
- S Column rft. splice failure

- Positive plastic hinge in column
- Positive and negative plastic hinge
- Cracking of joint

- Negative plastic hinge in beam
- Positive plastic hinge in beam
- Negative plastic hinge in column



Existing frame (flexible joints)
F9flex
 $T_{\text{initial}} = 2.03 \text{ sec.}$
 $T_{\text{final}} = 5.10 \text{ sec.}$
 Damage Index = 0.84

Existing frame (conventional rigid joint assumption) F9rigid
 $T_{\text{initial}} = 1.80 \text{ sec.}$
 $T_{\text{final}} = 1.98 \text{ sec.}$
 Damage Index = 0.17

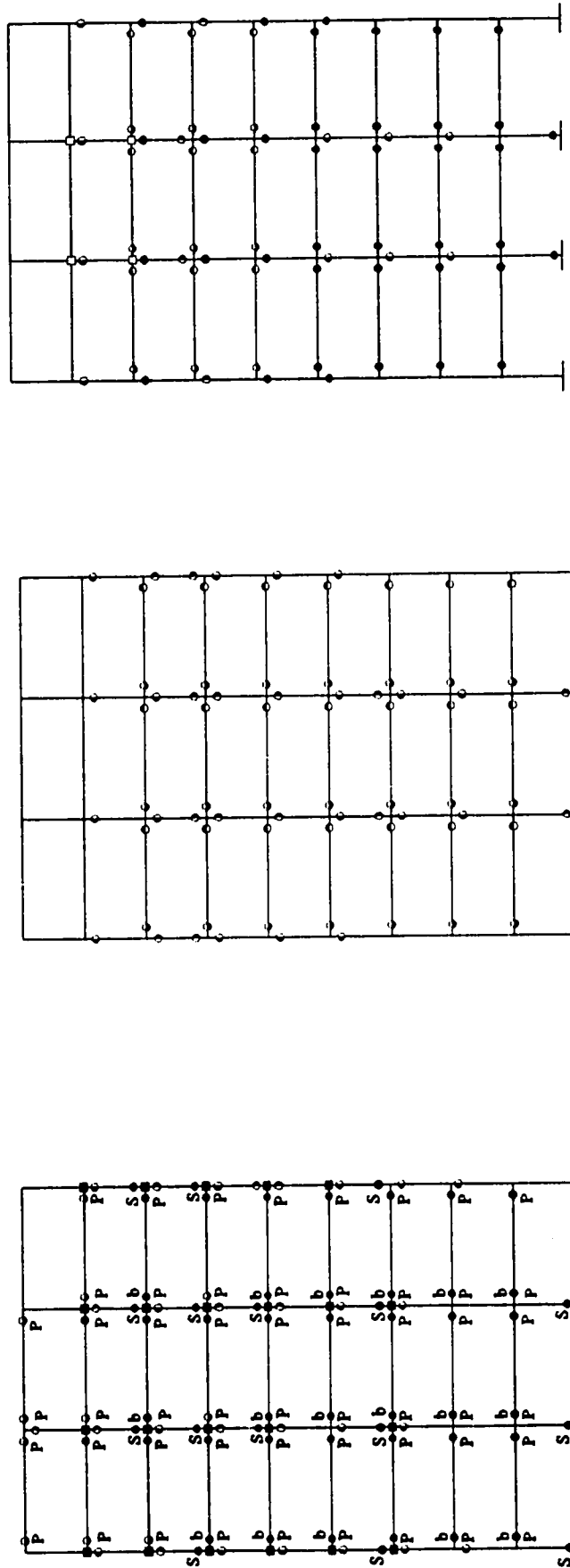
Rehabilitated frame
F9rehab
 $T_{\text{initial}} = 1.80 \text{ sec.}$
 $T_{\text{final}} = 2.21 \text{ sec.}$
 Damage Index = 0.34

Figure 7.34 Summary of hinge type and location for the 9-story frames due to the Mexico earthquake scaled to PGA of 0.2g

- Yielding of joint rft. or joint failure
- P Beam positive rft. bars pull out
- b Beam rft. bars bond slip
- S Column rft. splice failure

- Positive plastic hinge in column
- Positive and negative plastic hinge
- Cracking of joint

- Negative plastic hinge in beam
- Positive plastic hinge in beam
- Negative plastic hinge in column



Existing frame (flexible joints)
F9flex

$T_{\text{initial}} = 2.03 \text{ sec.}$
 $T_{\text{final}} = 7.11 \text{ sec.}$
 Damage Index = 0.92

Existing frame (conventional rigid
joint assumption) F9rigid

$T_{\text{initial}} = 1.80 \text{ sec.}$
 $T_{\text{final}} = 2.28 \text{ sec.}$
 Damage Index = 0.38

Rehabilitated frame
F9rehab

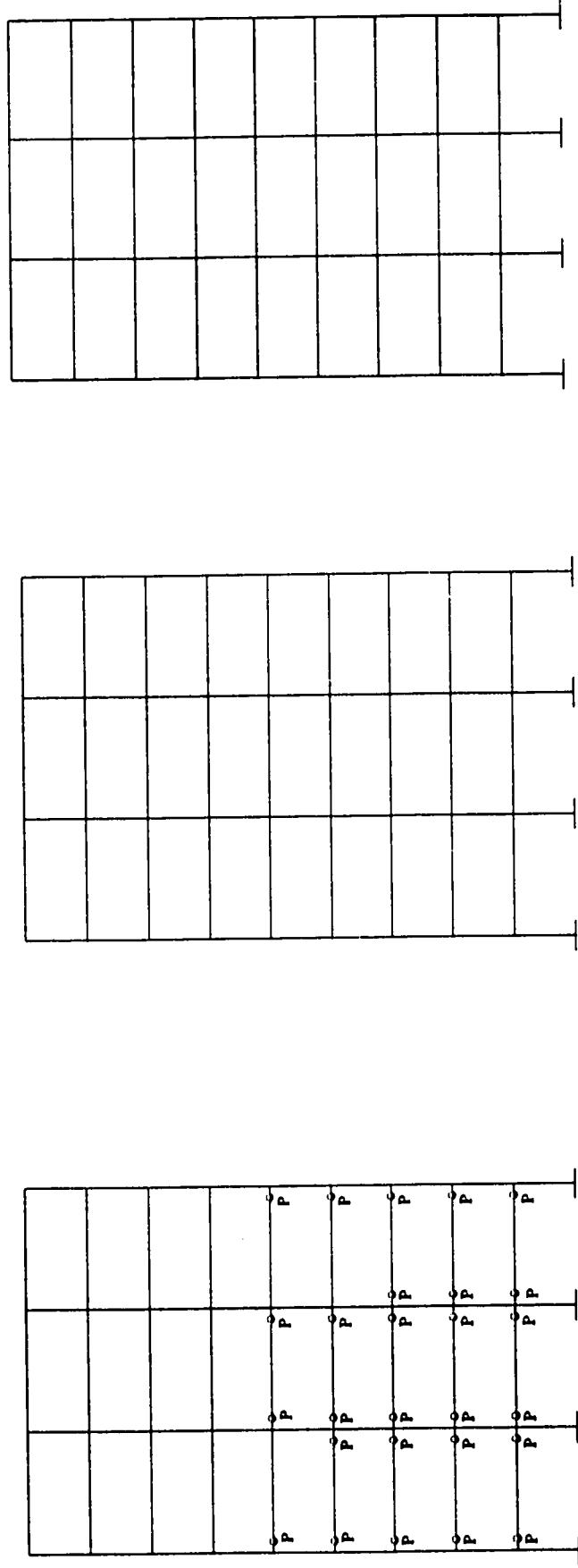
$T_{\text{initial}} = 1.80 \text{ sec.}$
 $T_{\text{final}} = 2.62 \text{ sec.}$
 Damage Index = 0.53

Figure 7.35 Summary of hinge type and location for the 9-story frames due to the Mexico earthquake scaled to PGA of 0.3g

- Yielding of joint rft. or joint failure
- P Beam positive rft. bars pull out
- b Beam rft. bars bond slip
- S Column rft. splice failure

- Positive plastic hinge in column
- Positive and negative plastic hinge
- Cracking of joint

- Negative plastic hinge in beam
- Positive plastic hinge in beam
- Negative plastic hinge in column



Existing frame (flexible joints)
F9flex
 $T_{initial} = 2.03 \text{ sec.}$
 $T_{final} = 2.12 \text{ sec.}$
Damage Index = 0.08

Existing frame (conventional rigid
joint assumption) F9rigid
 $T_{initial} = 1.80 \text{ sec.}$
 $T_{final} = 1.80 \text{ sec.}$
Damage Index = 0.0

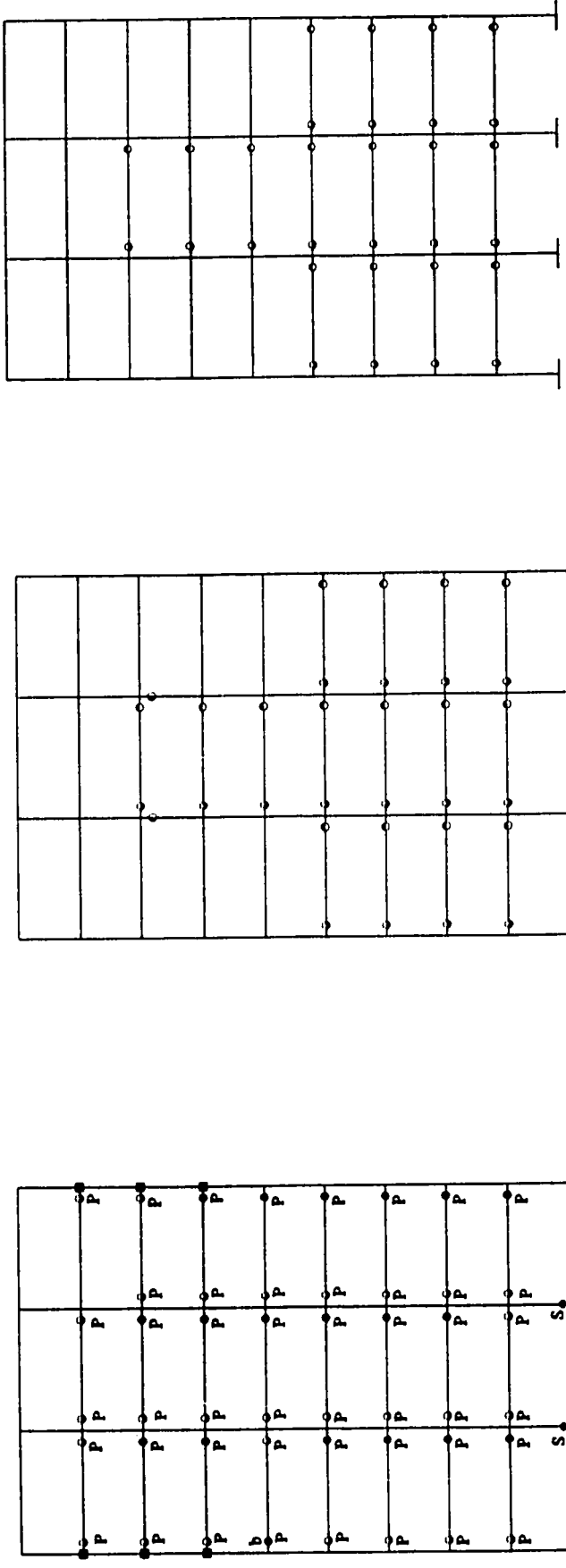
Rehabilitated frame
F9rehab
 $T_{initial} = 1.80 \text{ sec.}$
 $T_{final} = 1.80 \text{ sec.}$
Damage Index = 0.0

Figure 7.36 Summary of hinge type and location for the 9-story frames due to the Artificial earthquake scaled to PGA of 0.1g

- Yielding of joint rft. or joint failure
- P Beam positive rft. bars pull out
- b Beam rft. bars bond slip
- S Column rft. splice failure

- Positive plastic hinge in column
- Positive and negative plastic hinge
- Cracking of joint

- Negative plastic hinge in beam
- Positive plastic hinge in beam
- Negative plastic hinge in column



Existing frame (flexible joints)
F9flex
 $T_{initial} = 2.03 \text{ sec.}$
 $T_{final} = 2.71 \text{ sec.}$
Damage Index = 0.44

Existing frame (conventional rigid joint assumption) F9rigid
 $T_{initial} = 1.80 \text{ sec.}$
 $T_{final} = 1.90 \text{ sec.}$
Damage Index = 0.10

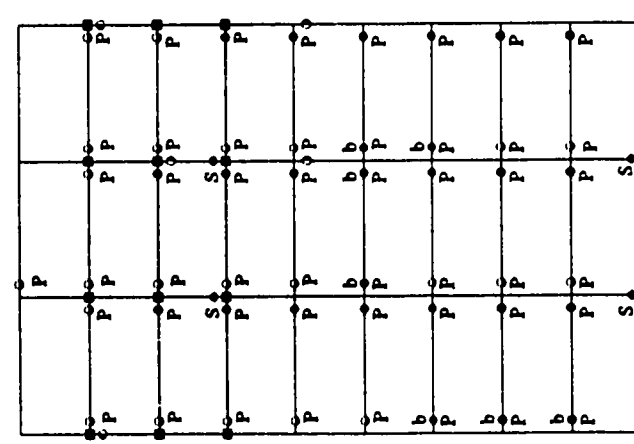
Rehabilitated frame
F9rehab
 $T_{initial} = 1.80 \text{ sec.}$
 $T_{final} = 1.88 \text{ sec.}$
Damage Index = 0.08

Figure 7.37 Summary of hinge type and location for the 9-story frames due to the Artificial earthquake scaled to PGA of 0.2g

- Yielding of joint rft. or joint failure
- P Beam positive rft. bars pull out
- b Beam rft. bars bond slip
- S Column rft. splice failure

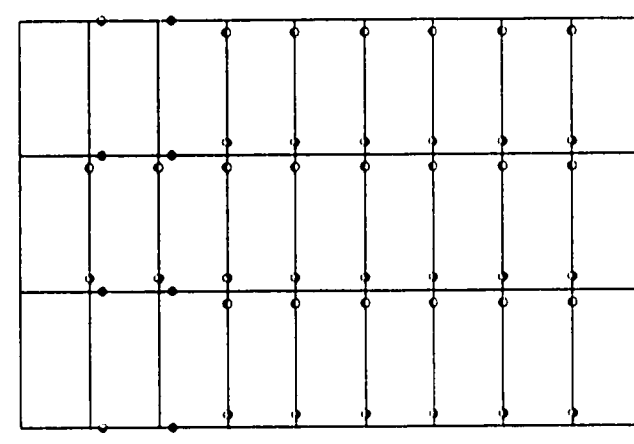
- Positive plastic hinge in column
- Positive and negative plastic hinge
- Cracking of joint

- Negative plastic hinge in beam
- Positive plastic hinge in beam
- Negative plastic hinge in column



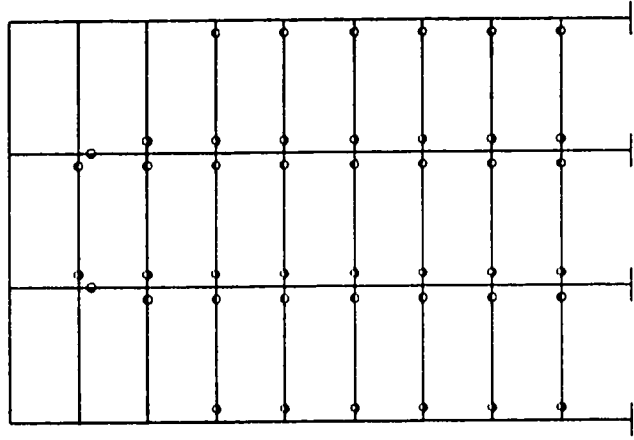
Existing frame (flexible joints)
F9flex

$T_{\text{initial}} = 2.03 \text{ sec.}$
 $T_{\text{final}} = 3.03 \text{ sec.}$
 Damage Index = 0.55



Existing frame (conventional rigid
joint assumption) F9rigid

$T_{\text{initial}} = 1.80 \text{ sec.}$
 $T_{\text{final}} = 2.00 \text{ sec.}$
 Damage Index = 0.19



Rehabilitated frame
F9rehab

$T_{\text{initial}} = 1.80 \text{ sec.}$
 $T_{\text{final}} = 1.93 \text{ sec.}$
 Damage Index = 0.13

Figure 7.38 Summary of hinge type and location for the 9-story frames due to the Artificial earthquake scaled to PGA of 0.3g

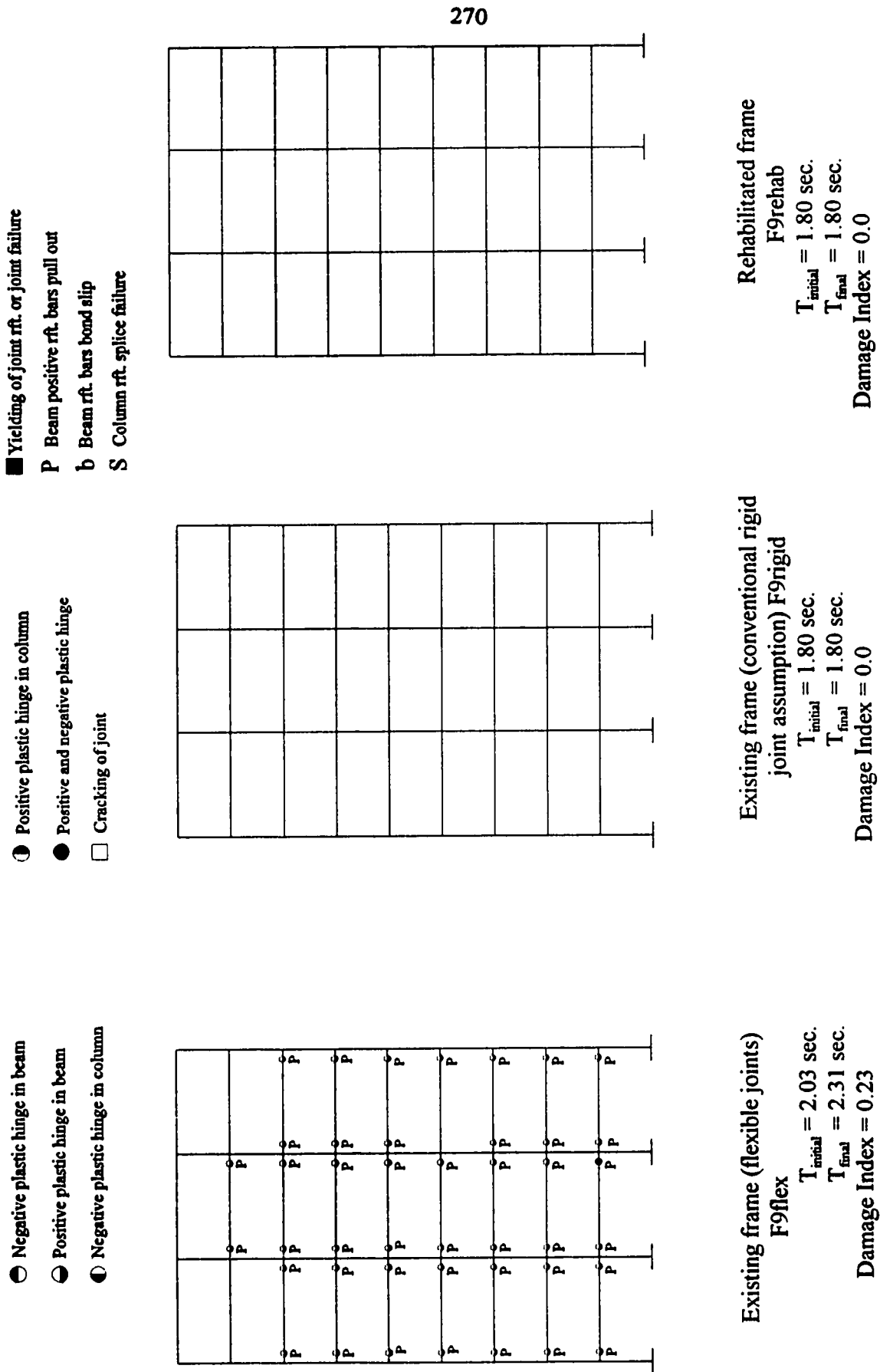


Figure 7.39 Summary of hinge type and location for the 9-story frames due to the Nahanni earthquake scaled to PGA of 0.3g

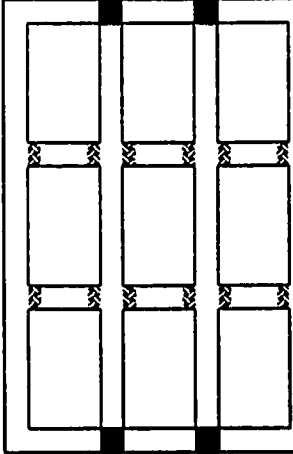
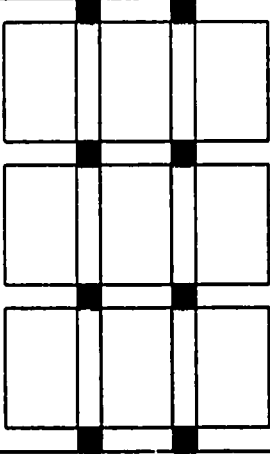
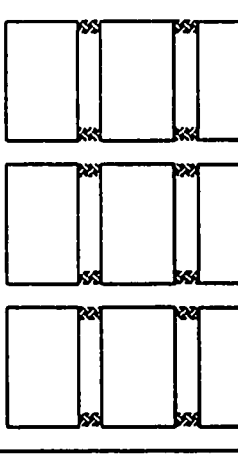

Damage	Rehabilitation strategy
 <p>Joints and columns</p>	<ul style="list-style-type: none"> - Enhance the lap splice performance of columns. - Increase concrete confinement at columns critical regions and joints. - Increase shear strength of joints.
 <p>Joints</p>	<ul style="list-style-type: none"> - Increase concrete confinement and shear strength of joints.
 <p>Beams (either flexural or pull out)</p>	<ul style="list-style-type: none"> - Rehabilitate the anchorage of the bottom reinforcement bars of the beams. - Check the columns shear capacities. - Check the beams ductility capacities.
 <p>Column base (either flexural or splice failure)</p>	<ul style="list-style-type: none"> - Check the rotational ductility, the lap splice design and the confinement at the column base.

Figure 7.40 The damaged areas in existing frames and a proposed rehabilitation strategy

.... Existing (rigid joint assumption)
 Existing (realistic assumption)
 Rehabilitated (realistic assumption)

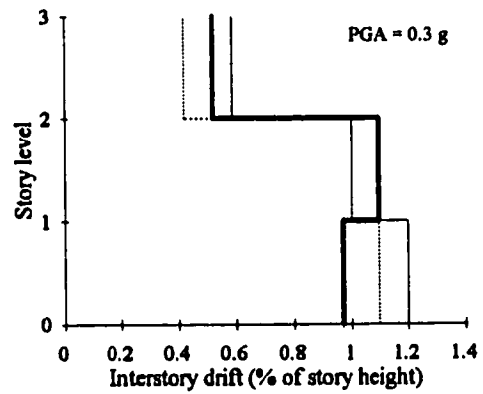
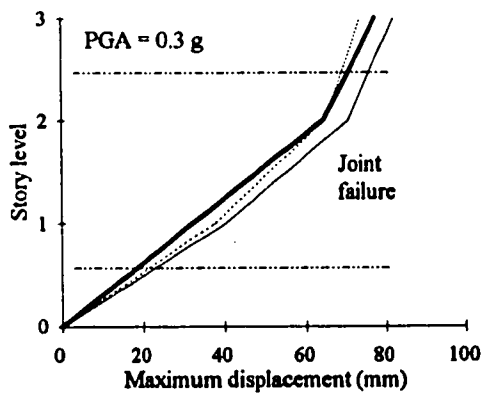
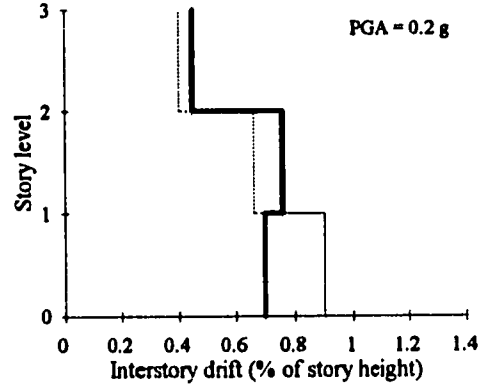
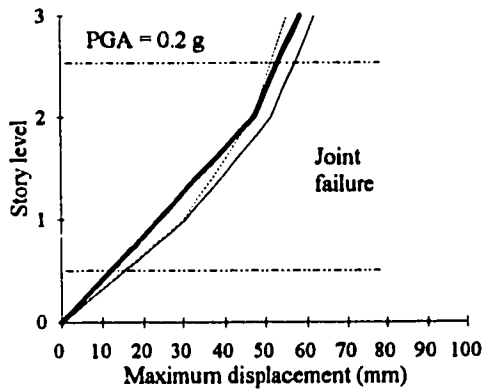
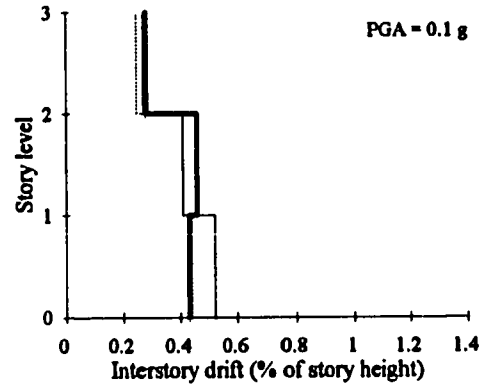
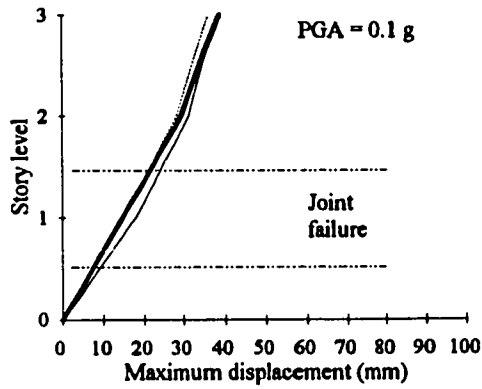


Figure 7.41 Maximum displacement and interstory drift for the 3-story frames due to the El Centro earthquake

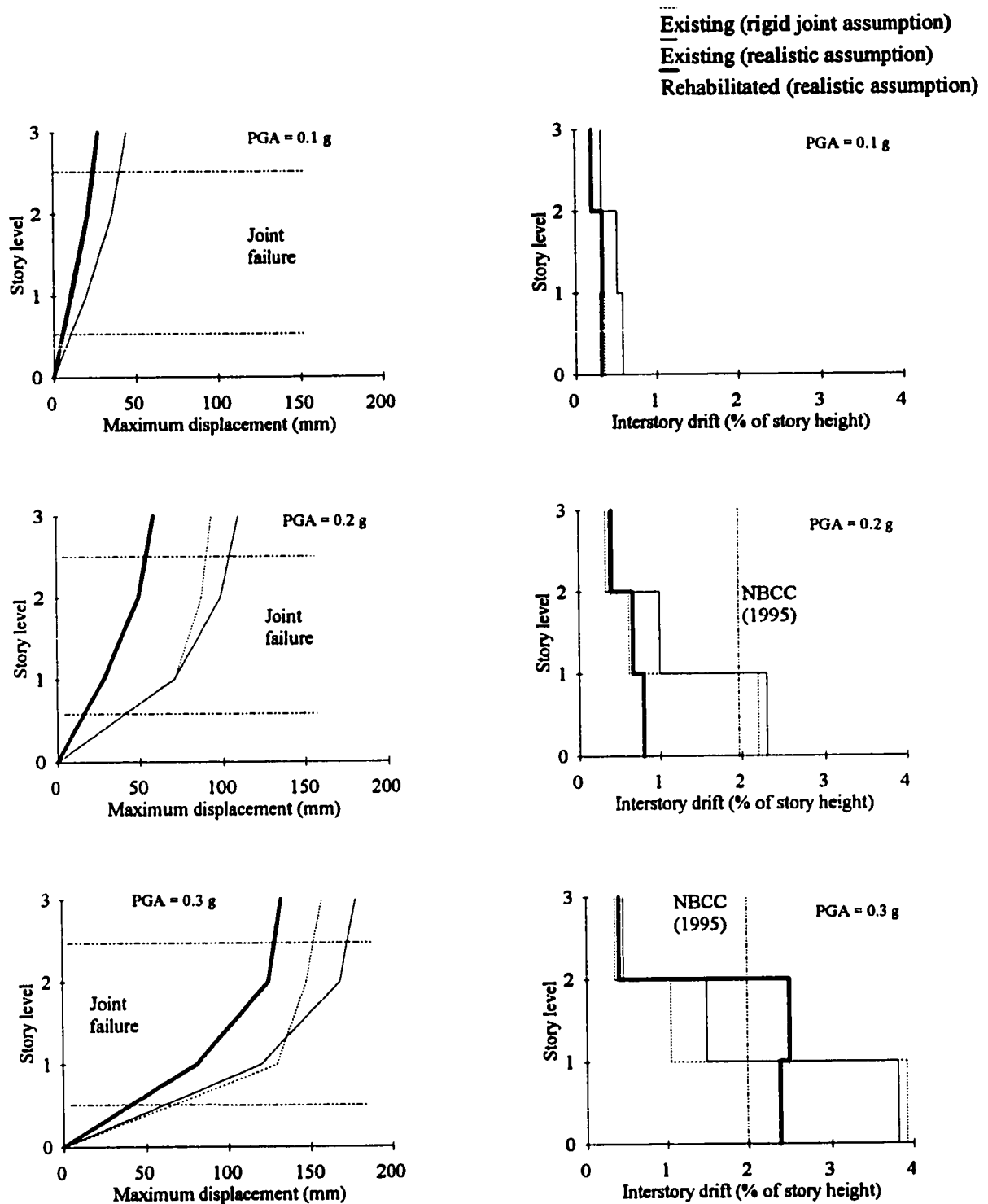


Figure 7.42 Maximum displacement and interstory drift for the 3-story frames due to the Mexico earthquake

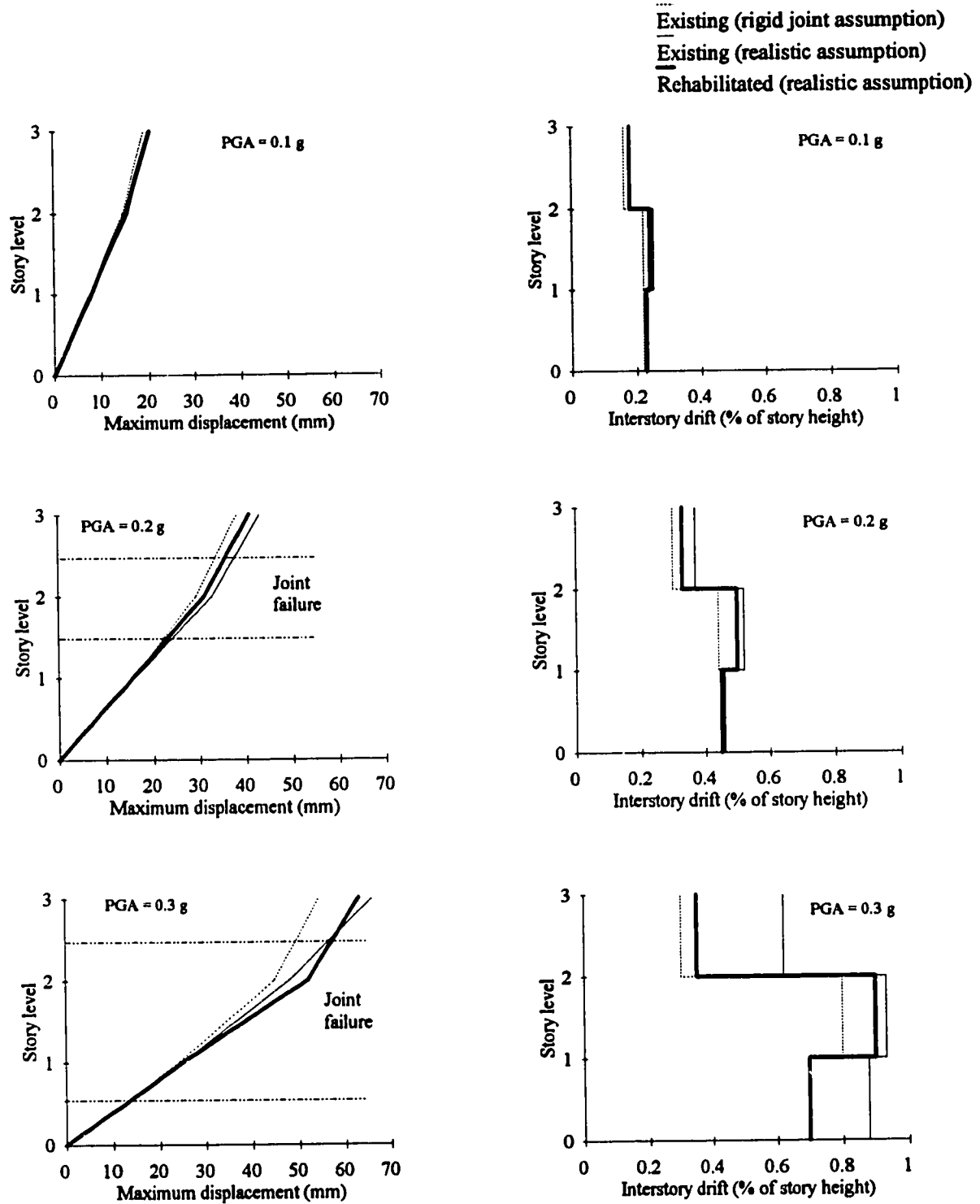


Figure 7.43 Maximum displacement and interstory drift for the 3-story frames due to the Artificial earthquake

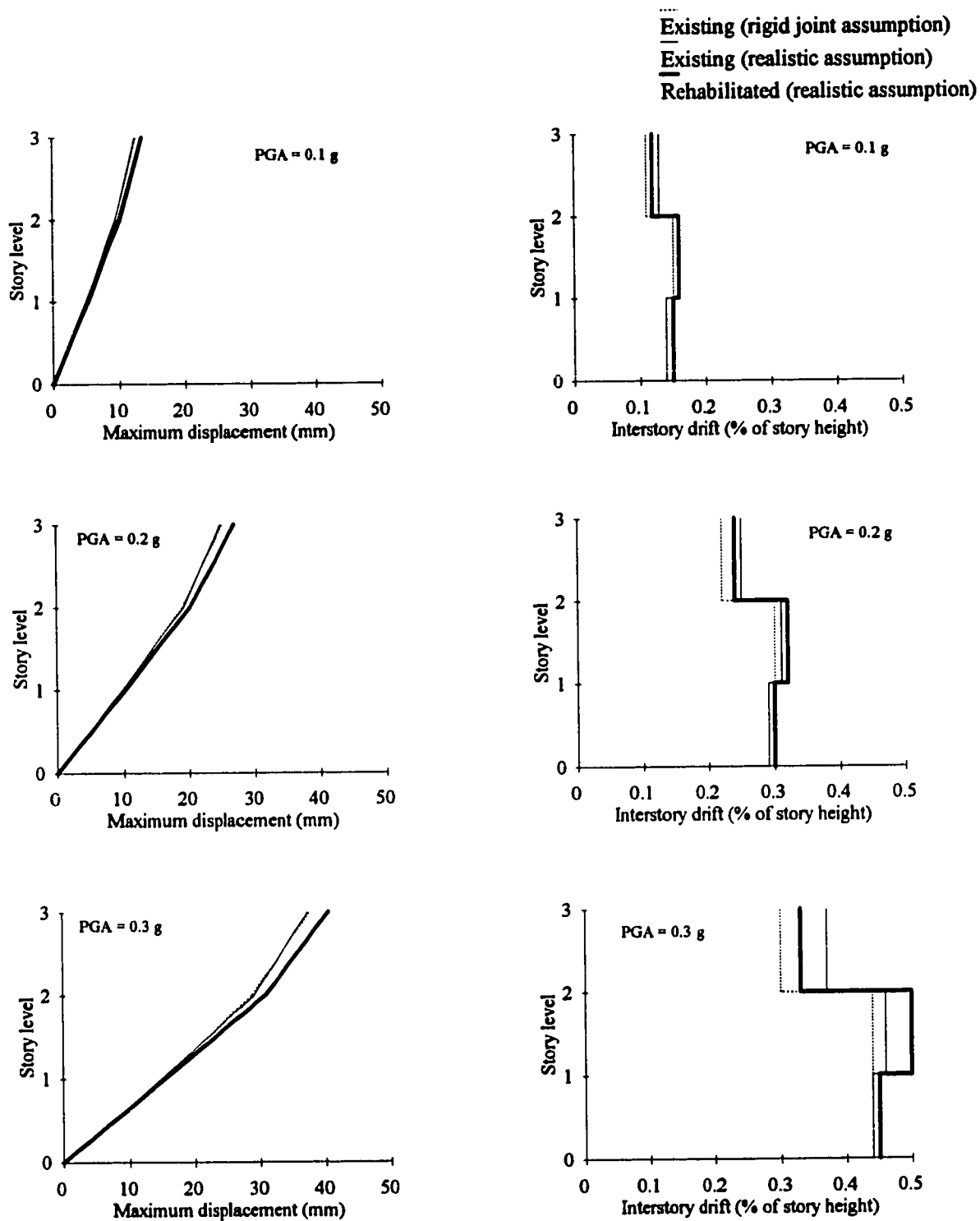


Figure 7.44 Maximum displacement and interstory drifts for the 3-story frames due to the Nahanni earthquake

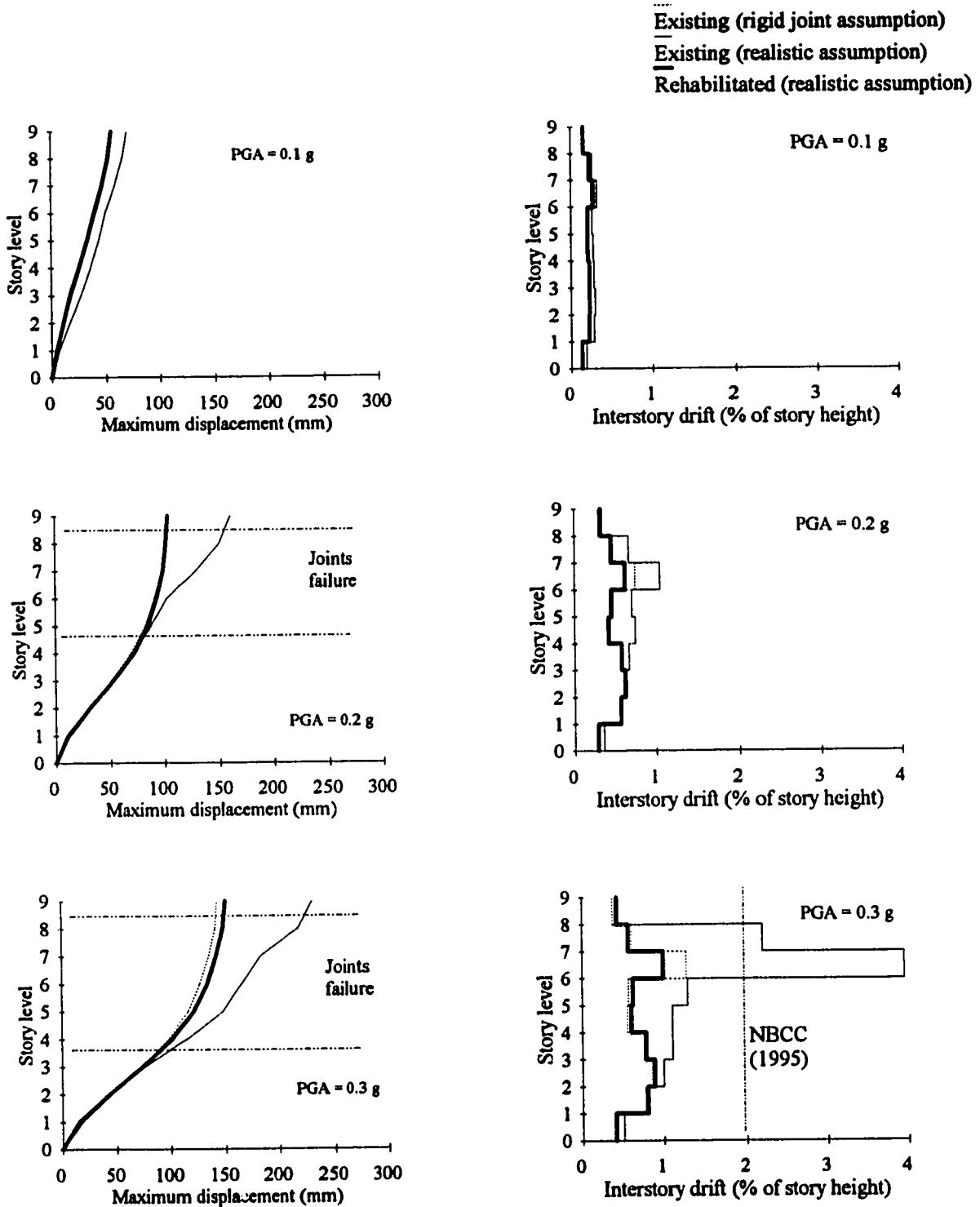


Figure 7.45 Maximum displacement and interstory drifts for the 9-story frames due to the El Centro earthquake

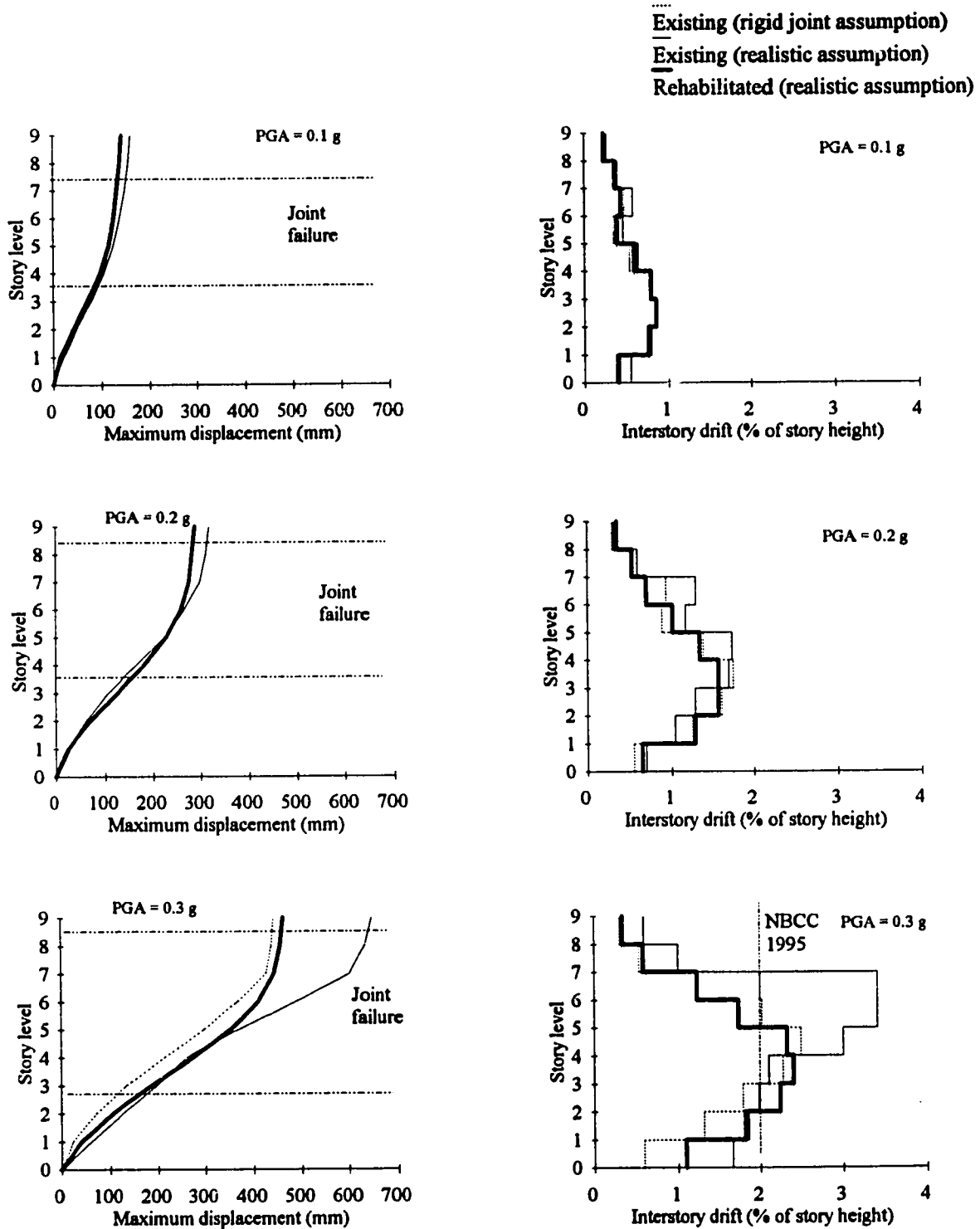


Figure 7.46 Maximum displacement and interstory drift for the 9-story frames due to the Mexico earthquake

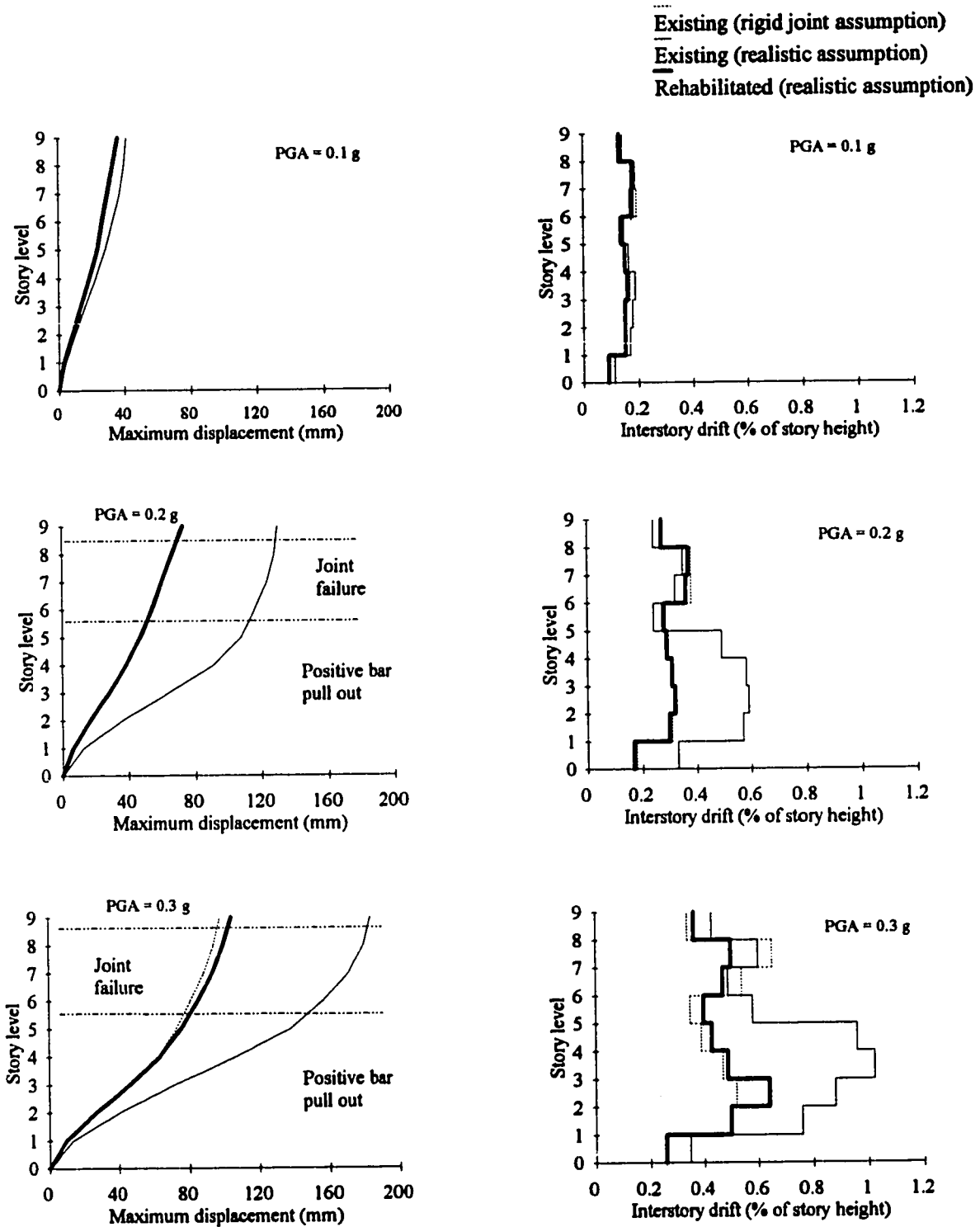


Figure 7.47 Maximum displacement and interstory drift for the 9-story frames due to the Artificial earthquake

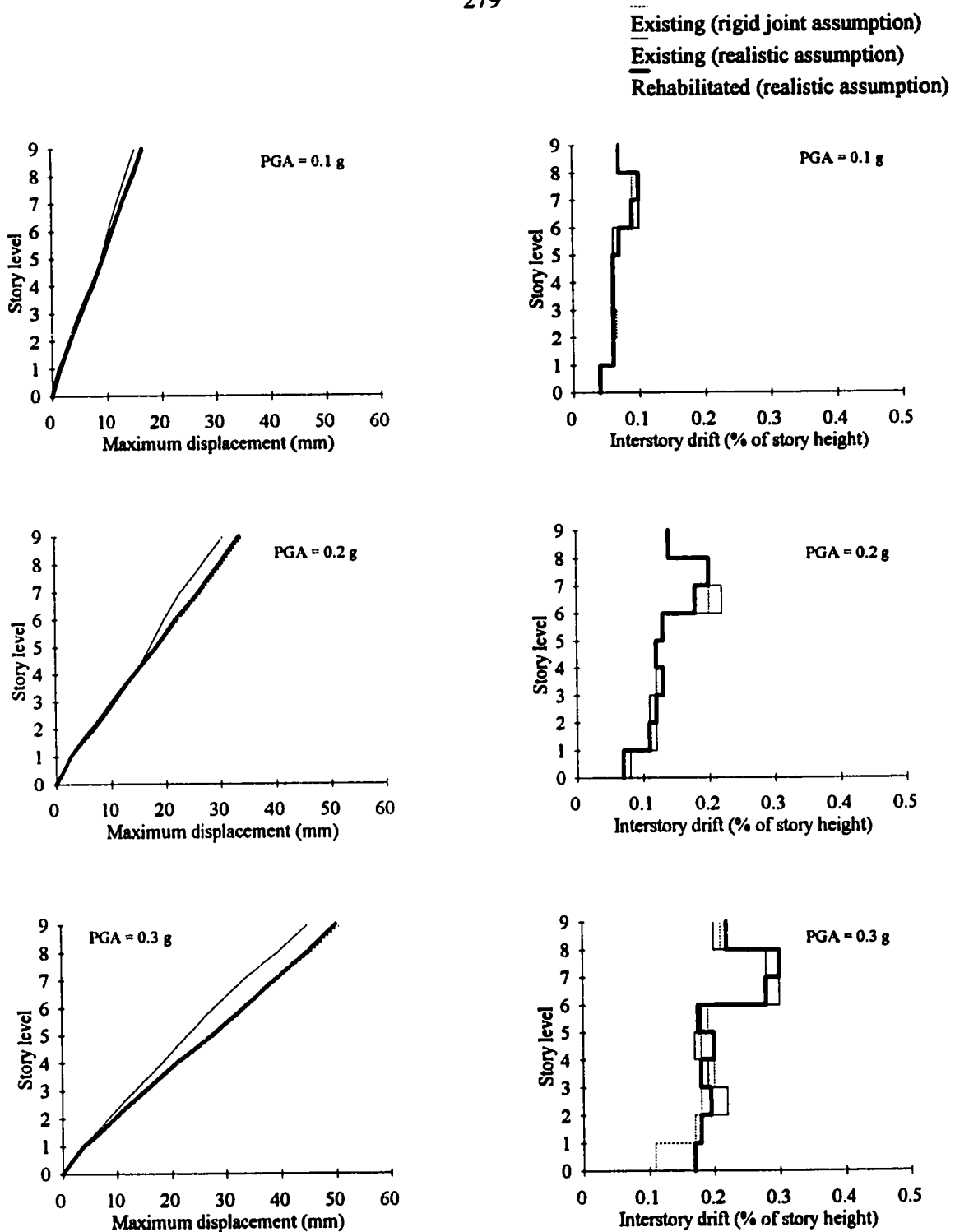


Figure 7.48 Maximum displacement and interstory drift for the 9-story frames due to the Nahanni earthquake

.... Existing (rigid joint assumption)
 — Existing (realistic assumption)
 — Rehabilitated (realistic assumption)

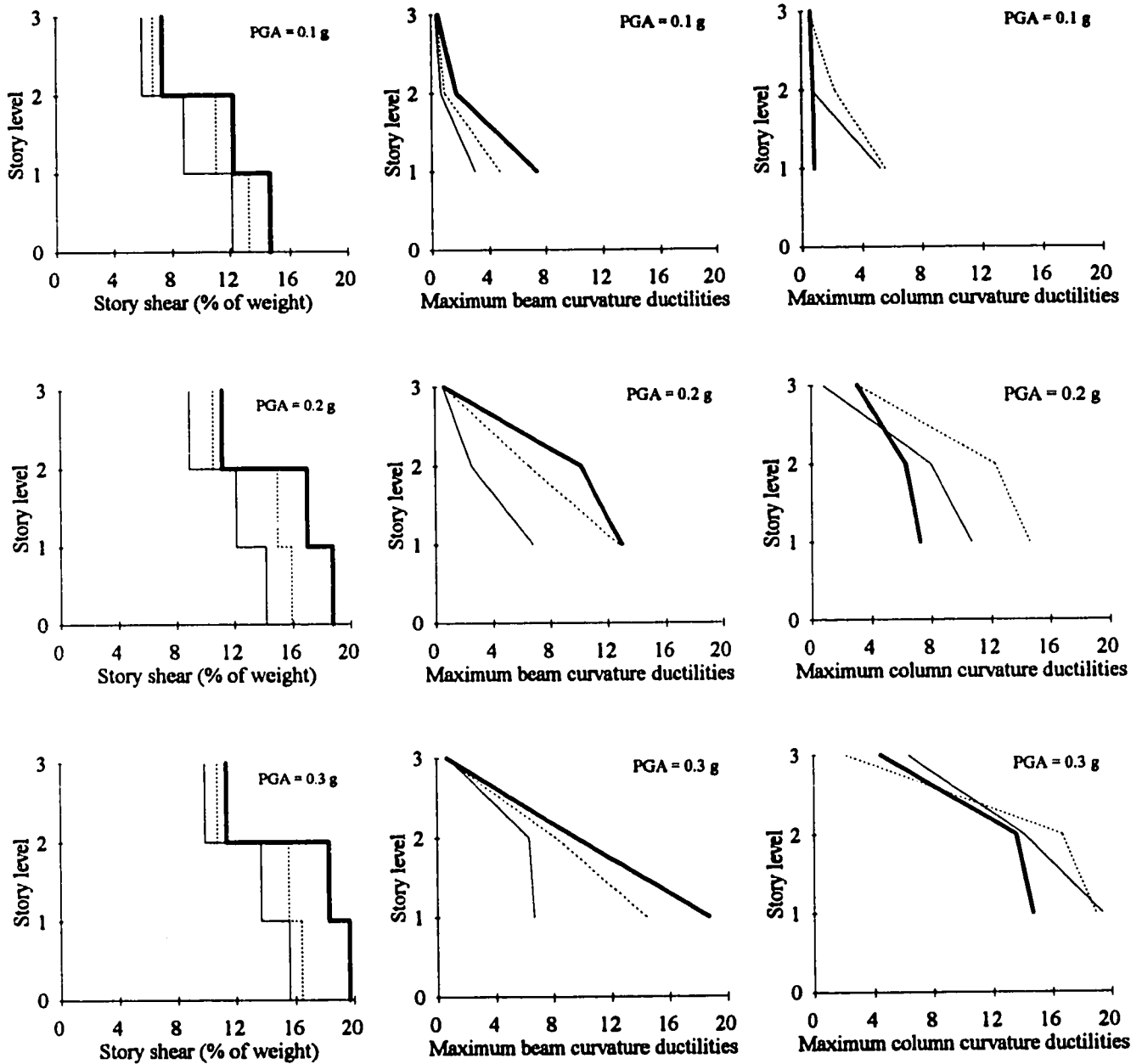


Figure 7.49 Maximum story shear, beam and column ductilities for the 3-story frames when subjected to El Centro earthquake

..... Existing (rigid joint assumption)
 — Existing (realistic assumption)
 — Rehabilitated (realistic assumption)

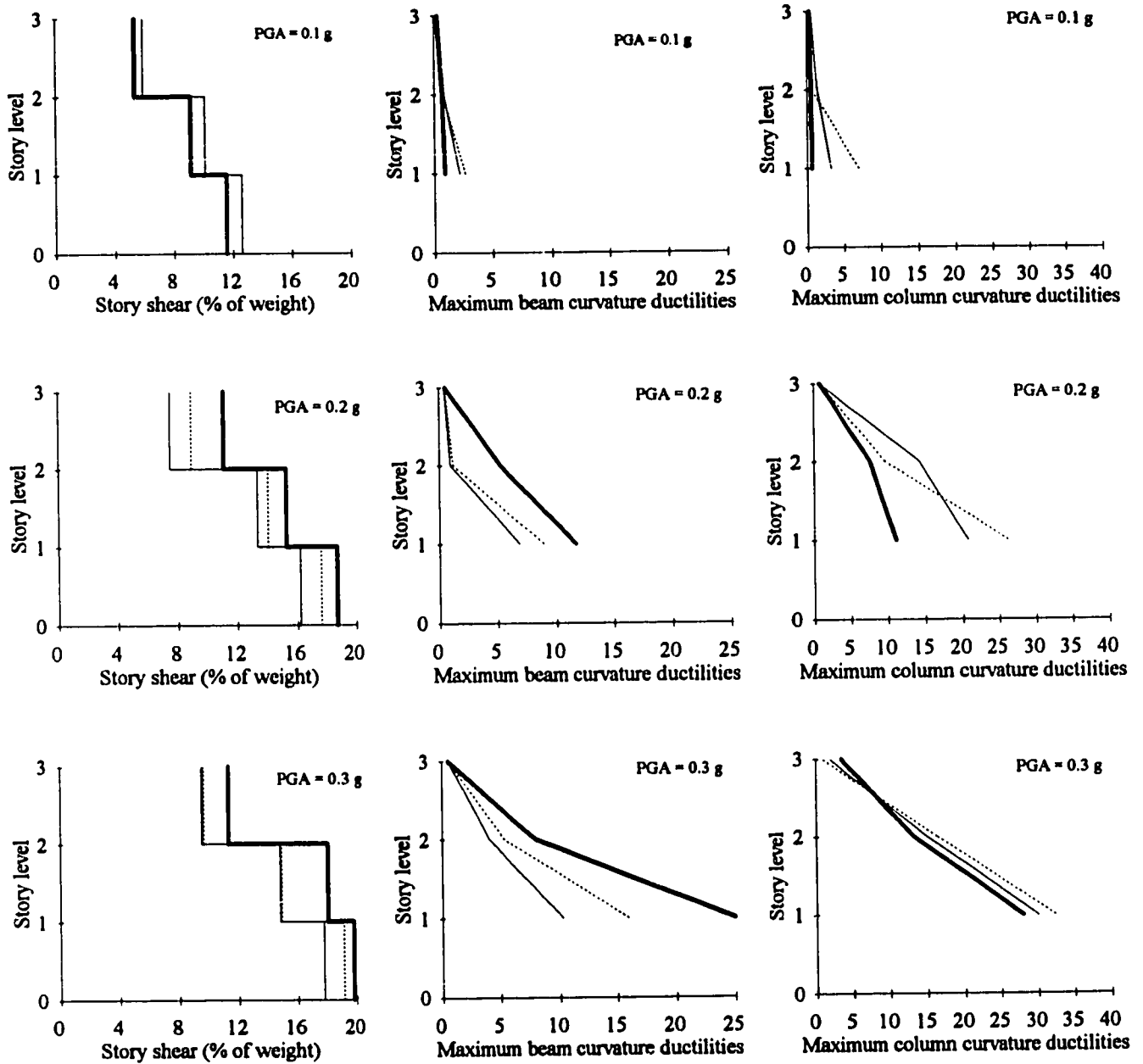


Figure 7.50 Maximum story shear, beam and column ductilities for the 3-story frames when subjected to the Mexico earthquake

..... Existing (rigid joint assumption)
 — Existing (realistic assumption)
 — Rehabilitated (realistic assumption)

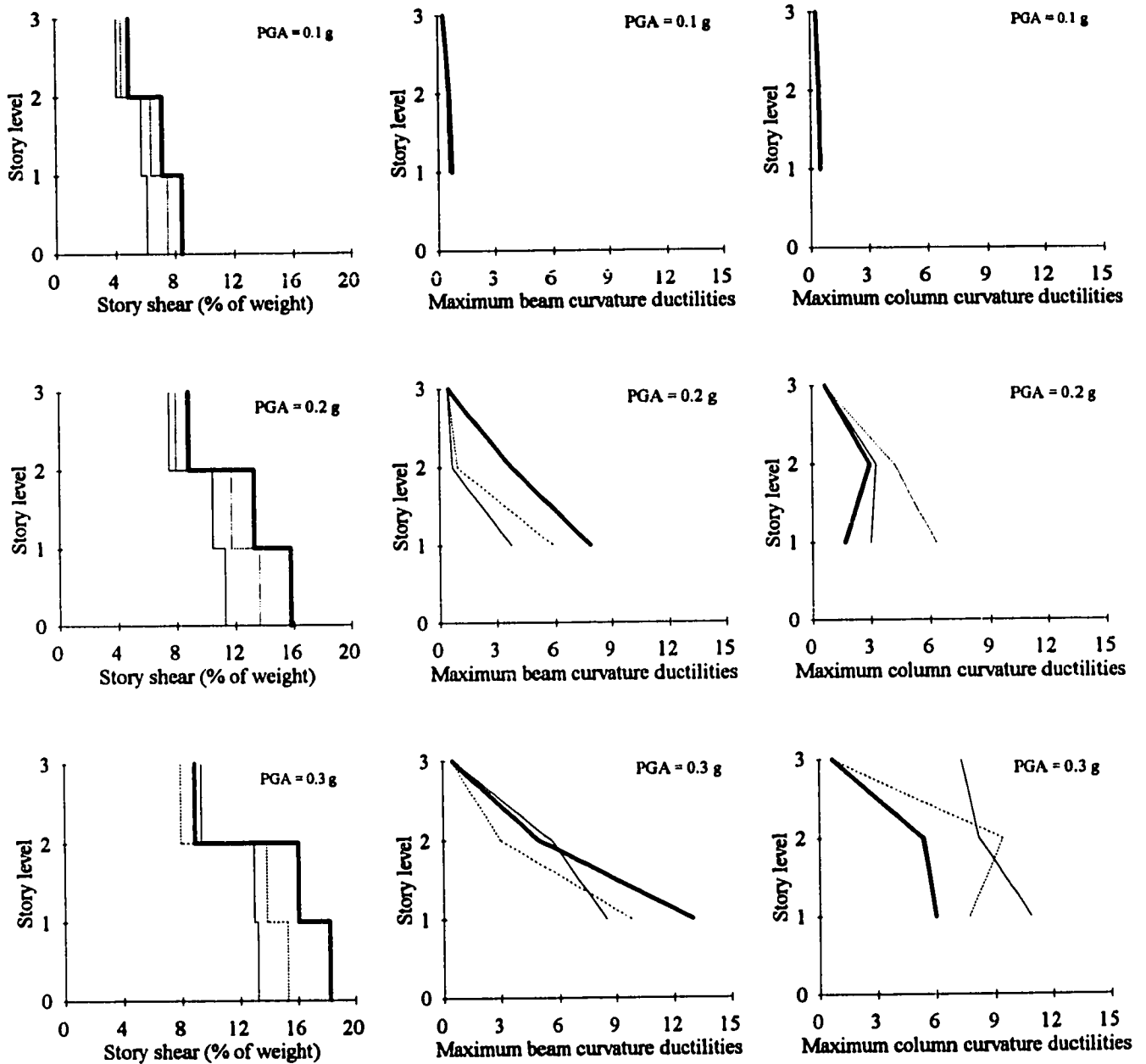


Figure 7.51 Maximum story shear, beam and column ductilities for the 3-story frames when subjected to the Artificial earthquake

..... Existing (rigid joint assumption)
 — Existing (realistic assumption)
 — Rehabilitated (realistic assumption)

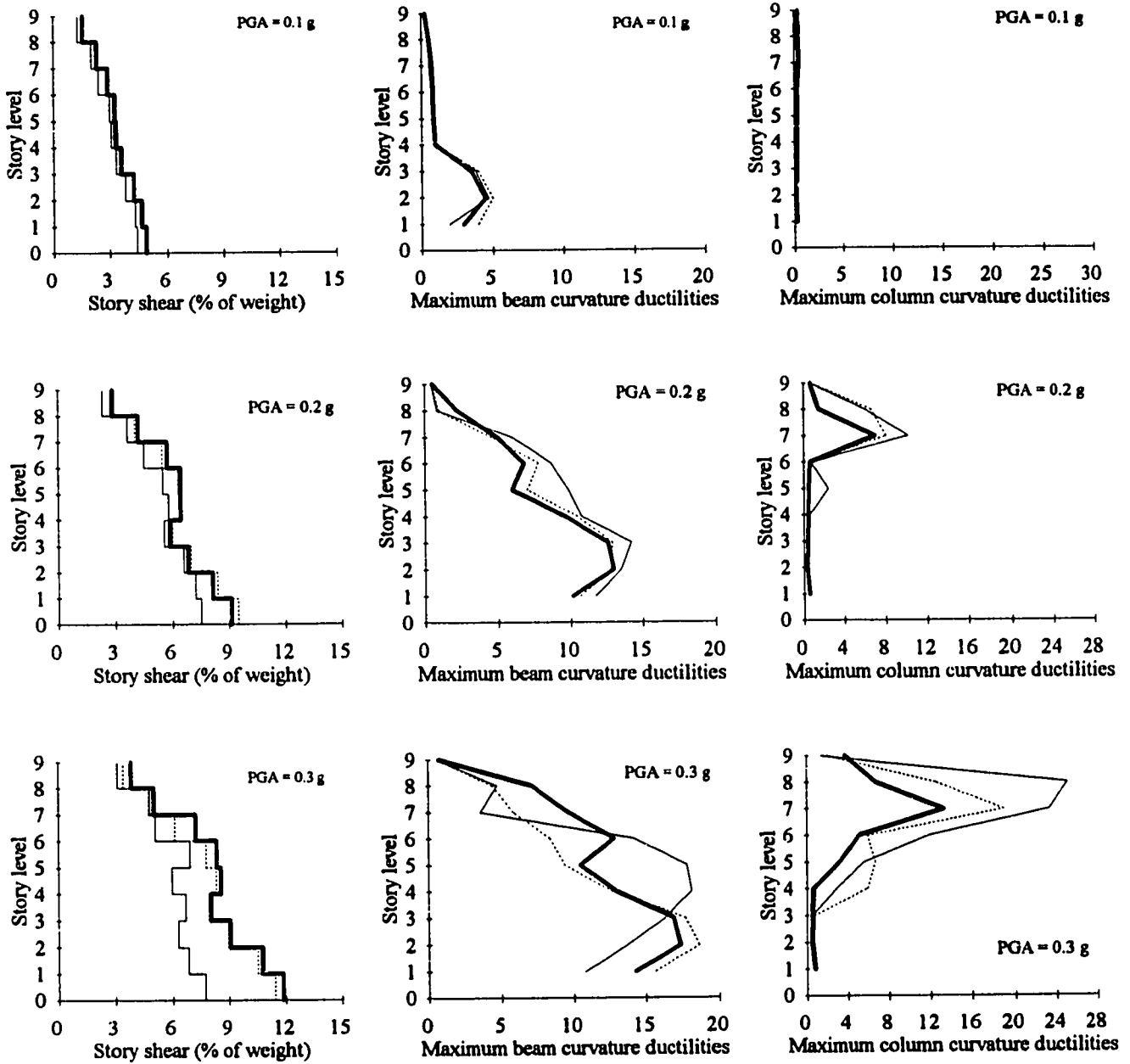


Figure 7.52 Maximum story shear, beam and column ductilities for the 9-story frames when subjected to the El Centro earthquake

..... Existing (rigid joint assumption)
 — Existing (realistic assumption)
 — Rehabilitated (realistic assumption)

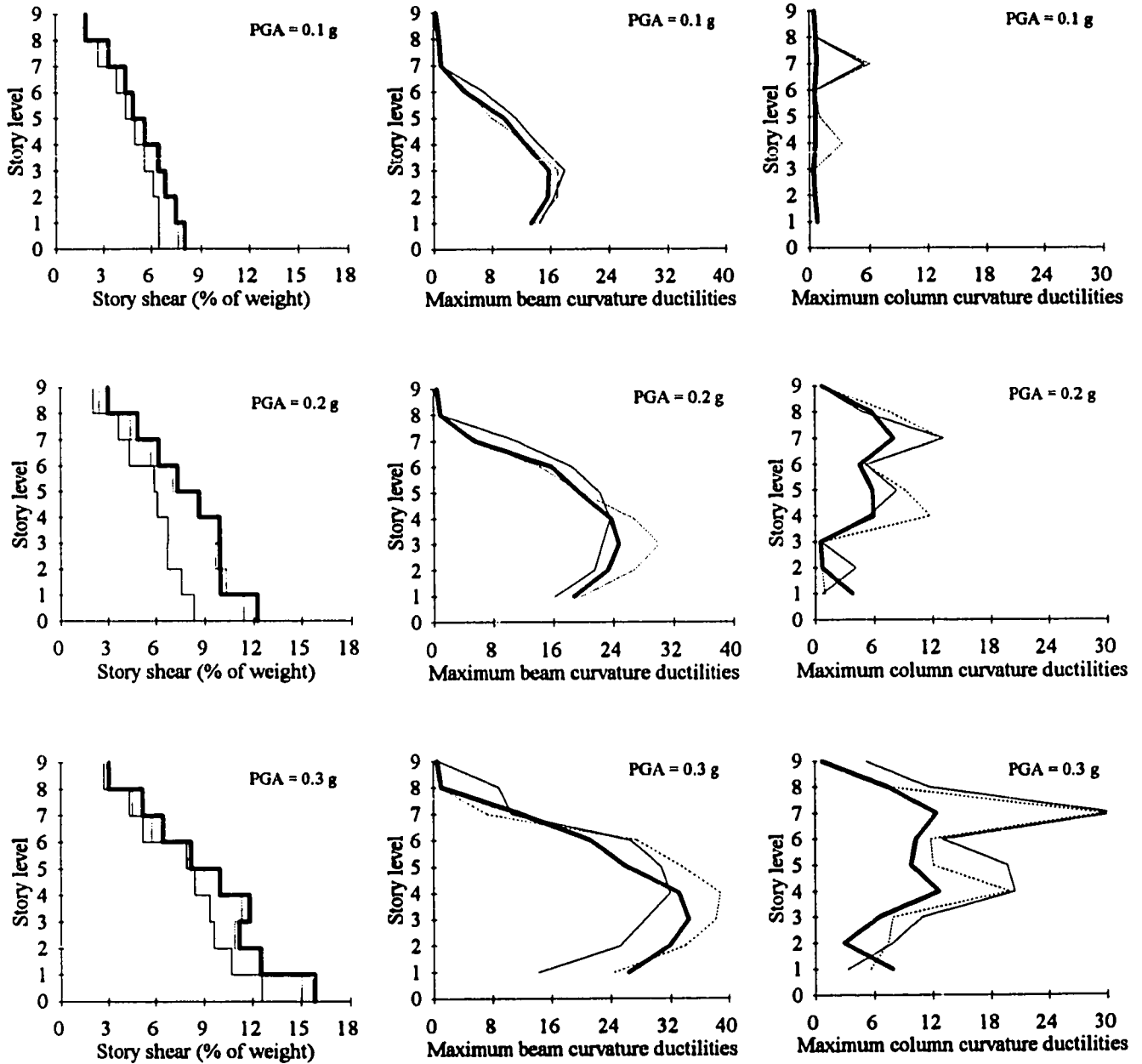


Figure 7.53 Maximum story shear, beam and column ductilities for the 9-story frames when subjected to the Mexico earthquake

..... Existing (rigid joint assumption)
 — Existing (realistic assumption)
 — Rehabilitated (realistic assumption)

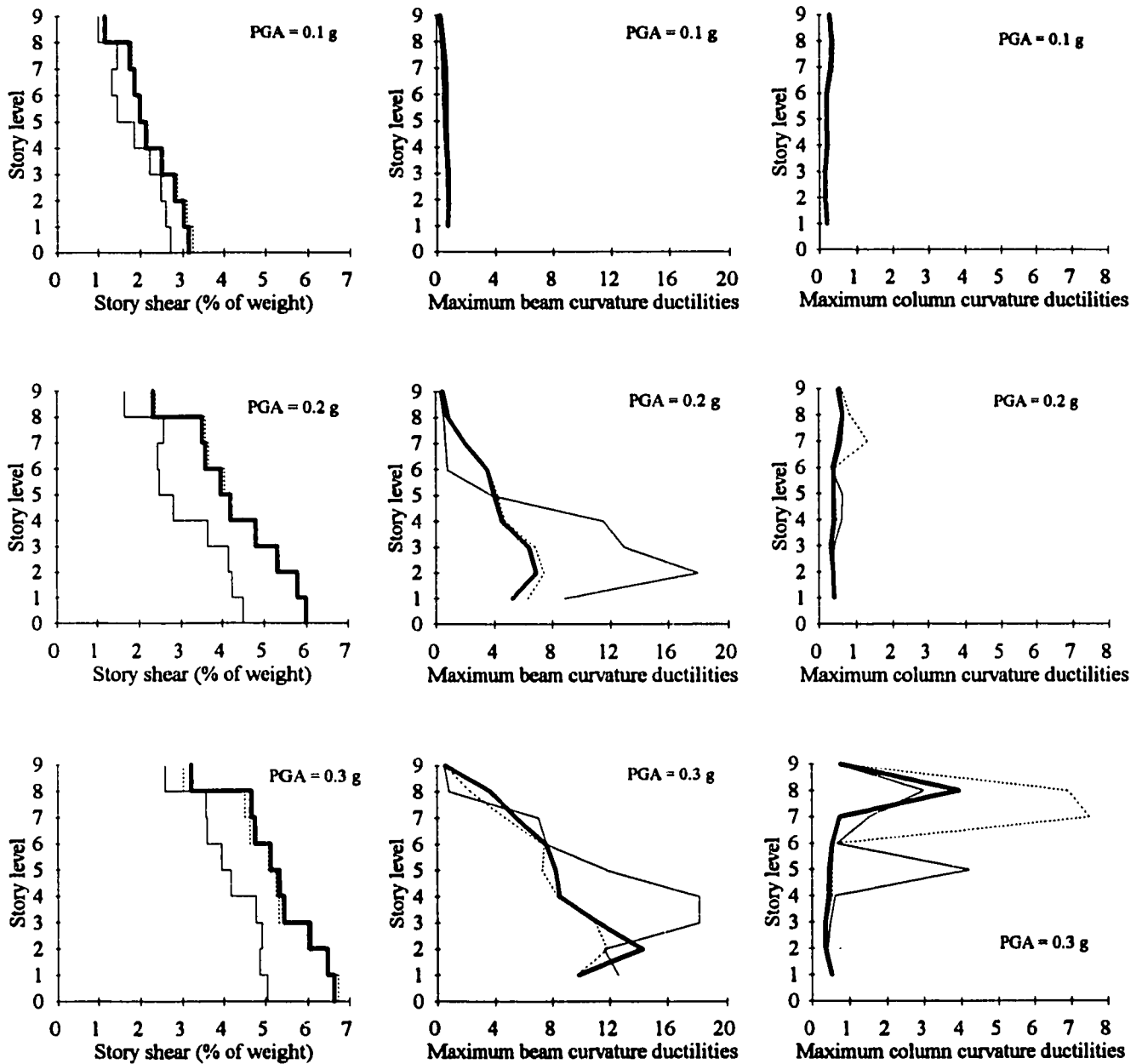


Figure 7.54 Maximum story shear, beam and column ductilities for the 9-story frames when subjected to the Artificial earthquake

CHAPTER 8

CONCLUSIONS

8.1 SUMMARY

The research program on the seismic behaviour of existing and rehabilitated joints is divided into two parts: experimental investigation and analytical study. First, the experimental investigation was to develop an effective, inexpensive and non-disruptive rehabilitation system for existing deficient joints in non-ductile reinforced concrete frames. It was also intended to develop an economical jacket design procedure. Second, the analytical study was aimed at evaluating the behaviour of existing frames during earthquakes by developing a flexible joint model that takes into account joint failure modes.

Six large scale beam-column connections were constructed as test specimens. Two of them represented existing structures, another one was designed according to the current seismic design codes and the other three were rehabilitated connections. The test results showed satisfactory performance for the connections rehabilitated using corrugated steel jackets. Design and construction recommendations are proposed for the steel jacket rehabilitation system.

A joint model, capable of predicting the dynamic behaviour and the failure modes of the joints, was developed and incorporated into a non-linear inelastic dynamic analysis

program to represent properly the behaviour of reinforced concrete frames that include joints of various details. The performance of the proposed model was assessed by comparing the model's predicted response with the experimental results. Taking into account the effect of the joint behaviour, the behaviour of two existing frames was assessed and compared with the results obtained when assuming rigid joints. The proposed joint model is accurate, simple and practical.

Finally, the performance of the two frames after applying the proposed rehabilitation technique is assessed in order to evaluate the effectiveness of such technique in improving the dynamic performance of the frames.

8.2 CONCLUSIONS

The following conclusions were reached from the results of the experimental and analytical investigations:

- 1- The connection representing existing joints exhibited rapid degradation in stiffness and strength once the ultimate load was reached. This was attributed to the brittle shear failure of the joint.
- 2- The current code designed connection sustained a higher applied displacement as compared with existing connection due to the ductile flexural hinging in the beam as compared to brittle joint shear failure in existing connection.
- 3- The code designed connection was detailed according to the provisions of current concrete design code, however, high shear at the flexural hinge caused rapid deterioration and disintegration of the concrete in the hinge zone. This is because of

the high depth to length ratio of the beam. The current code provisions should be experimentally checked in case of beams with high depth to length ratio.

- 4- The existing connection without adequate joint confinement was unable to continue the anchorage of the beam reinforcement during high loading cycles even if the anchorage length satisfied the current concrete design code requirements. On the other hand, in the code designed and the rehabilitated specimens, the anchorage was such that the beam was able to reach the theoretical ultimate moment capacity and maintain this capacity over a number of cycles.
- 5- An effective rehabilitation system was proposed and evaluated experimentally for deficient beam-column connections in existing reinforced concrete frames. The corrugated steel jackets enhance existing reinforced concrete connections that may fail by joint shear and change its behaviour to flexural ductile one.
- 6- All the rehabilitated specimens showed more favourable energy dissipation mechanisms than those exhibited by the specimens modelling existing structures.
- 7- A design methodology for calculating the required thickness of the corrugated steel jackets needed to increase the shear strength and ductility of rectangular columns and beam-column connections was proposed and verified with a limited number of tests.
- 8- In the design of structures rehabilitated using steel jacketing, the change in the mode of failure and redistribution of forces should be considered. The rehabilitation scheme enhances the joint shear strength which may force the beam flexural hinging to occur first (weak beam behaviour). Beam shear capacity must be sufficient to develop beam flexural hinging. Beam jacketing prevented the shear failure in the beam and instead

flexural failure occurred. If beam jacketing is required, a gap should be provided at the column face to minimize flexural strength enhancement for beams.

- 9- An analytical model to take the floor slab effects into account was proposed. Moreover, a bi-linear moment-rotation analytical model representing beam reinforcing bar bond slip was selected for the case of monotonic loading and to establish the envelope of reversed cyclic loading.
- 10- A tri-linear moment-rotation analytical model representing joint shear was developed for the case of monotonic loading and to establish the envelope of reversed cyclic loading. The model sensitivity was assessed by comparing its results to experimental measurements. The developed model was found to be capable of accurately predicting the behaviour of reinforced concrete joints subjected to in-plane stresses.
- 11- A reasonable analytical prediction of the hysteretic behaviour of the tested specimens was accomplished. The maximum lateral strength as well as the hysteretic characteristics (initial stiffness, strength and stiffness degradation) were successfully predicted.
- 12- The rigid joint assumption is inappropriate when assessing the behaviour of existing structures. Realistic modelling for the joint is essential for dynamic analysis of existing frame structures to model the deficiencies in the structures.
- 13- Joint failure occurs mainly in the middle and top floors while beam bar pull out occurs in the bottom floors. Column splice failure occurs at the levels where the column cross-section dimensions change.
- 14- The proposed corrugated steel jacket rehabilitation technique develops favourable

behaviour with low ductility demands on the columns. The curvature ductilities for the beams were within acceptable limits, with a uniform distribution of the rotations over the entire frame. The uniform distribution of rotations confirms that the system has good energy dissipation characteristics which is a desirable feature in the seismic resistant structures.

8.3 RECOMMENDATIONS FOR FUTURE RESEARCH

Further research is needed in the following areas:

- 1- Analytical and experimental investigation may be conducted to study the behaviour of beam-column connections with slabs and transverse beams rehabilitated with corrugated steel jackets. The purpose would be to develop the system, methods of construction and locations of anchors. Comparison can be made with other retrofit systems.
- 2- An experimental research program is needed to test beam-column joints with various corrugated steel jacket thickness, corrugation depths and heights to refine the proposed method of the design of corrugated steel jackets. Code type formulas can be developed for use by the practising professionals.
- 3- An attempt was made in the experimental program to measure the pressure between the steel jacket and the concrete. Difficulties were encountered due to the malfunction of the load cells. Further experimental work is required to improve the system's reliability and analyse the readings from the load cells in order to calibrate these readings in terms of confinement stress.

APPENDIX A

STRAIN GAUGE DATA

In this Appendix, some of the strain gauge data measurements for the six specimens are compiled and plotted. The strain measurements are used to explain and confirm visual observations of the specimen behaviour during the loading test.

A.1 SPECIMEN J1

Specimen J1 experienced deterioration of bond along the main reinforcement between the face of the column and the beginning of the bar hook inside the joint. Beam load versus strain in the bottom longitudinal reinforcement of specimen J1 at the beginning of the hook and in the beam at 150 mm from the face of the column are shown in figures A.1 and A.2 respectively. These plots indicate that deterioration of bond along the lower main reinforcement spreads from the column face into the beam-column joint. Strains near the bar hook became larger in each consecutive load cycle. Concrete cover of the reinforcement in this area swelled sideways and eventually spalled off between the face of the column and the main bar hooks. However, the damage was superficial because the bar at the hook was able to develop the yield stress in the bottom reinforcement. The beam load versus strain in the top longitudinal reinforcement of the beam of specimen J1 at the face of the column, at the beginning of the hook and at 150 mm from the face of the column are shown in figures A.3,

A.4, and A.5 respectively. The plots indicate that no bond deterioration took place along the top reinforcement of the beam.

In specimen J1, due to the insufficient joint reinforcement, most of the damage was concentrated at the joint which prevented the development of large flexural-shear cracking over a wide region of the beam, as occurred in specimen J5. Instead, the shear deformation is concentrated along the beam-column interface cracks. Most of the shear force along the beam was carried by the nearly-uncracked concrete section. The forces transmitted to the shear reinforcement were small, resulting in low elastic strains as shown in figure A.6. On the other hand, large shear forces in the beam developed in specimen. The shear stress of $0.27\sqrt{f'_c}$ MPa caused the shear reinforcement to resist a substantial proportion of the load which resulted in extensive flexural-shear cracking. The forces in the shear reinforcement were large enough to yield the stirrups as shown in figure A.7.

A.2 SPECIMEN J2

The beam stirrups were sufficient to resist the shear and develop flexural plastic hinge. The stirrups did not reach yield until cycle #9, (displacement ductility factor of 3), as shown in figure A.8.

A.3 SPECIMEN J3

Data from strain gauges attached to the main reinforcement of the beam did not indicate any slippage of bars in the joint. Strain gauges on the column bars indicate elastic behaviour. In figure A.9, the column bar was under compression and tension depending on the direction of loading. The bar was able to sustain the increase in the applied load indicating no deterioration of bond along the column bars.

Figure A.10 illustrates the behaviour of the joint hoop reinforcement. The hoops did not yield during the test, indicating no loss of confinement due to the effect of the steel jacket on the joint behaviour.

Figure A.11 illustrates the behaviour of beam stirrups. The stirrup did yield after 10% drift, indicating the effect of the steel jacket on the beam behaviour.

Data from strain gauges attached to the corrugated steel jacket showed the effect of confinement of the jacket on the specimen. Figures A.12 and A.13 show the beam load versus strain of the beam jacket at different locations which show the contribution of the jacket in resisting shear and confining the concrete of the beam. Figures A.14 and A.15 show the load versus strain at the middle of the joint jacket which show the contribution of the jacket to the joint shear resistance and confinement.

Even though the steel jacket was not heavily stressed in the test, the absence of shear cracks inside the joint and the beam hinge region leads to the conclusion that the jacket provided good confinement and performed well in increasing the shear capacity of the joint and the beam.

A.4 SPECIMEN J4

Specimen J4 experienced deterioration of bond along the main reinforcement in the beam. The bottom reinforcing bars of the beam were pulled out during cycle #6. The load versus bottom beam reinforcement strain at the face of the column is shown in figure A.16. The figure shows that the bar was pulled out before yielding of the steel was reached.

The lower section of the column showed some vertical cracking which caused yielding of the bottom column ties as shown in figure A.17. The column ties are not sufficient.

Approximately 16% of the required area by the current Canadian code was provided. The upper section of the column showed few vertical cracks but the ties did not yield as shown in figure A.18.

Due to the absence of joint reinforcement in specimen J4, most of the damage was concentrated at the joint which prevented the development of large flexural-shear cracking over a very wide region of the beam, as was the case in specimen J5. The shear deformation was concentrated along the beam-column interface cracks. Most of the shear force along the beam was carried by the nearly-uncracked concrete section and the forces transmitted to the shear reinforcement were small. The stirrup strains remained in the elastic range as shown in figure A.19.

A.5 SPECIMEN J5

The beam longitudinal bars did not show any slippage. Figure A.20 and A.21 show the strain history of the beam bottom bar at the column face and at the beginning of the hook, respectively. The bar was strained as much as eight times the yield strain, causing wide flexural-shear cracks in the beam region adjacent to the column.

The strain gauges attached to the longitudinal bars of the column indicated elastic behaviour identical to the column of specimen J3. The column bars remained elastic during all the loading cycles. Figures A.22, A.23 and A.24 show the strain history of the edge bar of the joint at top column, middle of joint and bottom column, respectively. In figure A.23, during the first five cycles of loading, the column bar at the middle of the joint was under almost no strain regardless of the direction of loading. After the fifth cycle, the column bar acted to balance the vertical component of the joint concrete compression strut as shown in

figure A.25. To develop the tensile force in the column bar, it has to be anchored in the column beyond the joint core by bond forces. Idealized distribution of stress necessary to sustain the vertical component of the compression strut together with flexural stresses are shown in figure A.26. The resulting combined stress pattern is similar to that measured during the test.

Typical load versus strain plots for the joint hoops are shown in figure A.27 and A.28. No yield of transverse reinforcement was recorded throughout the test.

Data from strain gauges attached to the corrugated steel jacket showed the effect of confinement of the jacket on the specimen. Figure A.29 shows the beam load versus strain at the middle of the jacket confining the joint.

A.6 SPECIMEN J6

The beam top reinforcement yielded at the face of the column during cycle #4. The beam bottom reinforcement at the column face yielded during cycle #6 as shown in Figure A.30. The column bars remained elastic during all the loading cycles. Figures A.31 and A.32 show the strain history of the edge bar of the joint at top column and at bottom column respectively. The top column tie behaved in an elastic manner as shown in figure A.33.

Figure A.34 illustrates the behaviour of beam stirrups. The instrumented stirrup did not yield indicating the effect of the steel plates on the beam behaviour.

Data from strain gauges attached to the corrugated steel jacket indicated that the jacket remained in the elastic range.

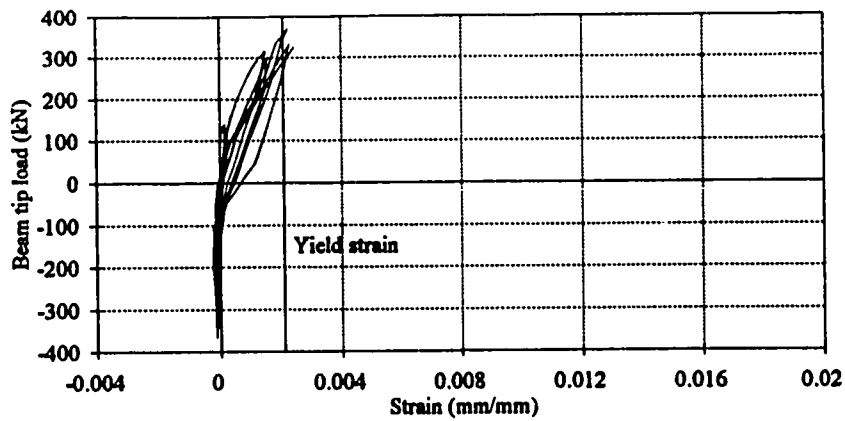


Figure A.1 Beam tip load-strain at bottom steel of beam of specimen J1

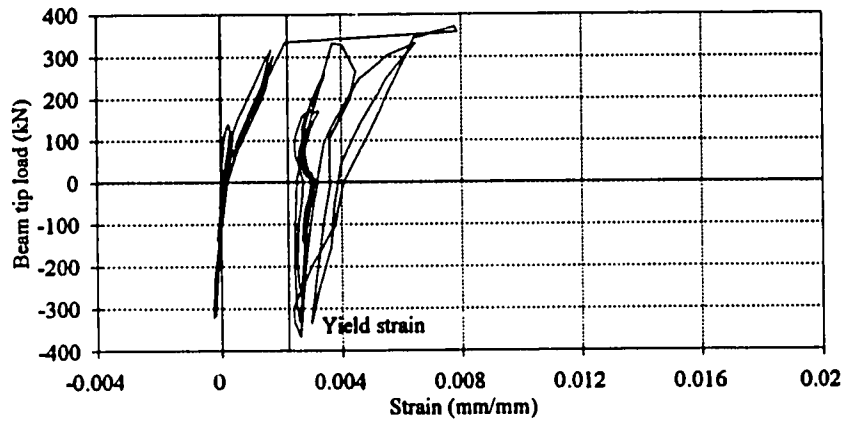


Figure A.2 Beam tip load-strain at bottom steel of beam of specimen J1

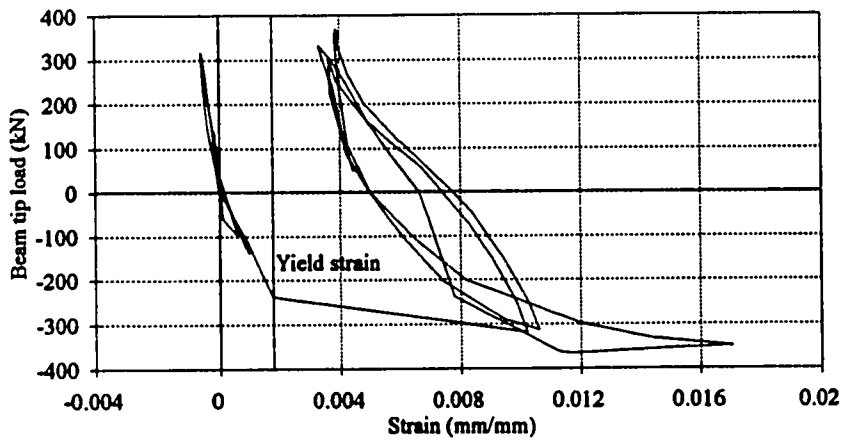


Figure A.3 Beam tip load-strain at top steel of beam of specimen J1

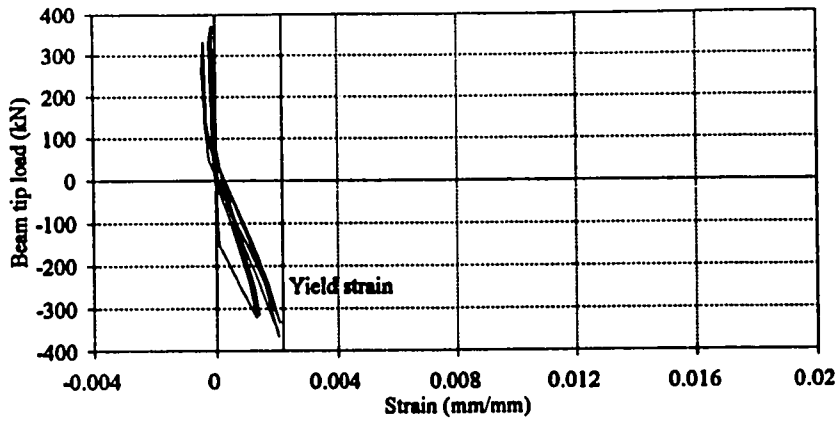


Figure A.4 Beam tip load-strain at top steel of beam of specimen J1

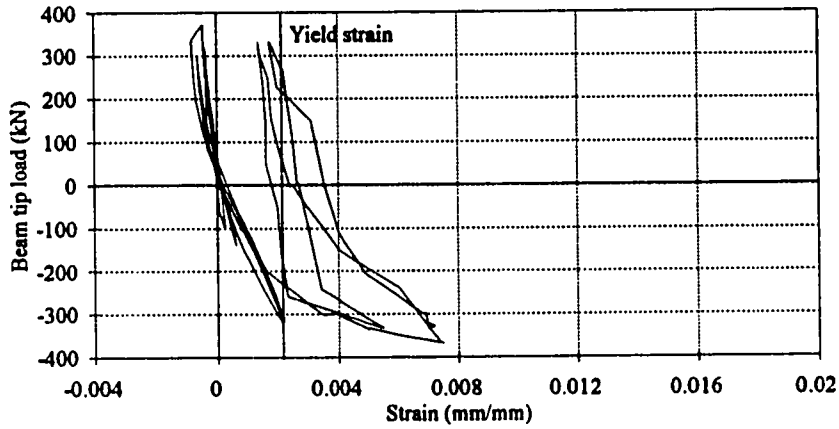


Figure A.5 Beam tip load-strain at top steel of beam of specimen J1

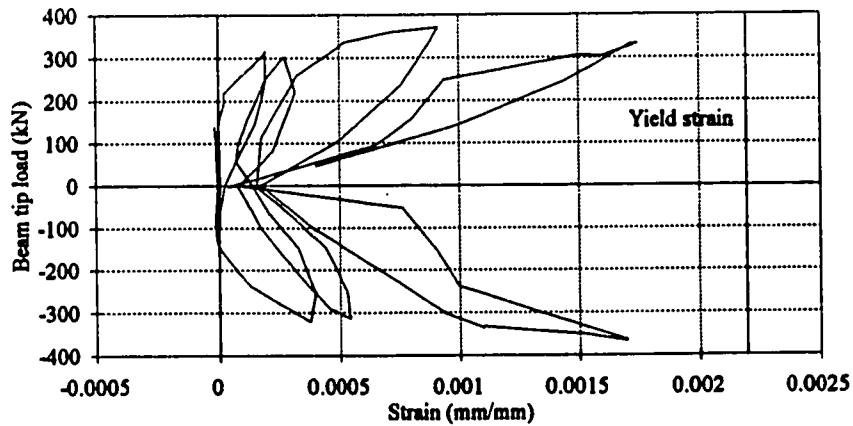


Figure A.6 Beam tip load-strain at beam second stirrup of specimen J1

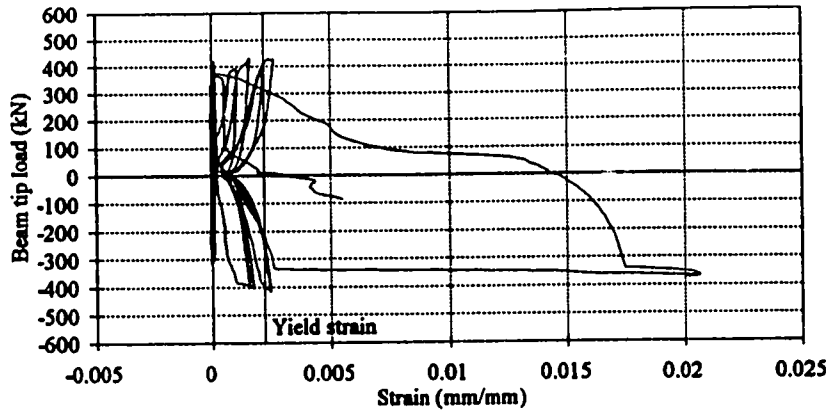


Figure A.7 Beam tip load-strain at beam second stirrup of specimen J5

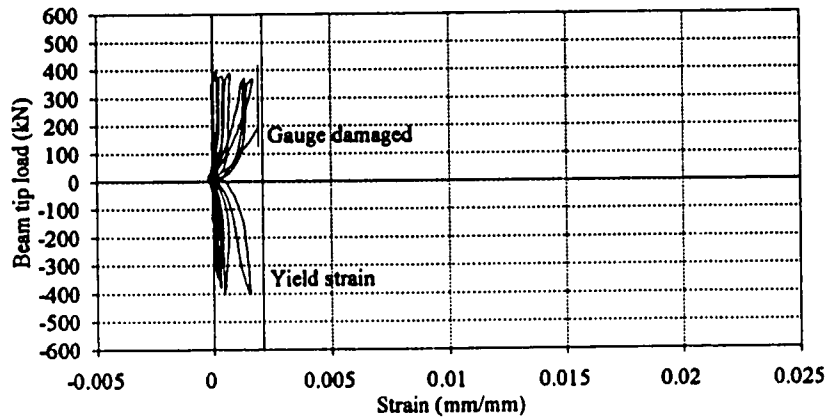


Figure A.8 Beam tip load-strain at beam second stirrup of specimen J2

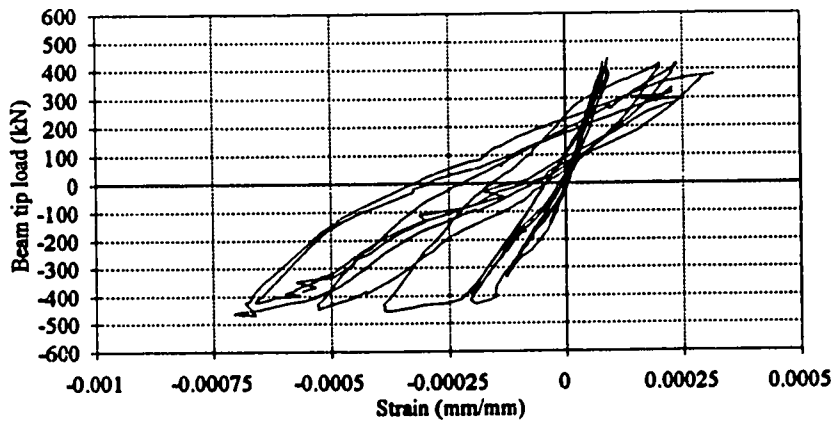


Figure A.9 Beam tip load-strain at column main steel above joint of specimen J3

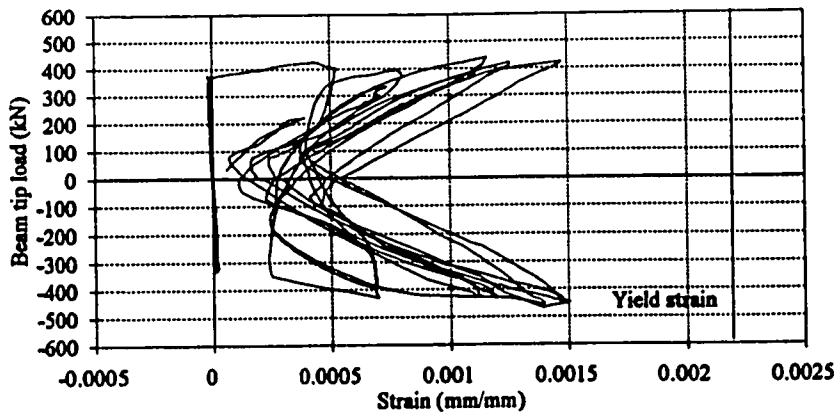


Figure A.10 Beam tip load-strain at joint tie of specimen J3

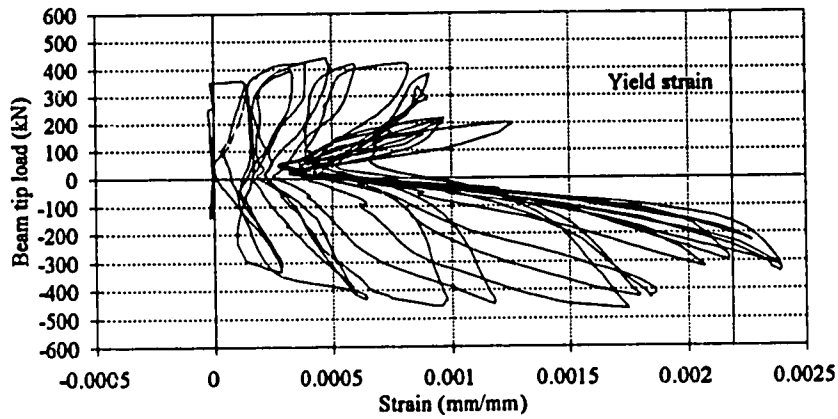


Figure A.11 Beam tip load-strain at beam second stirrup of specimen J3

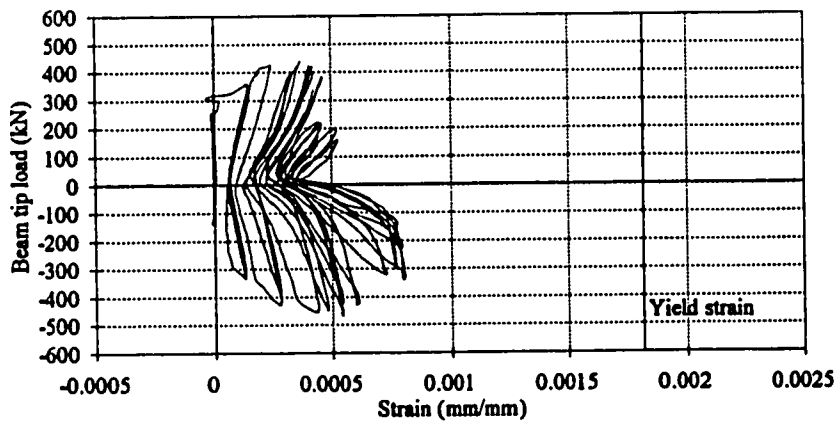


Figure A.12 Beam tip load-strain at beam steel jacket (mid point) of specimen J3

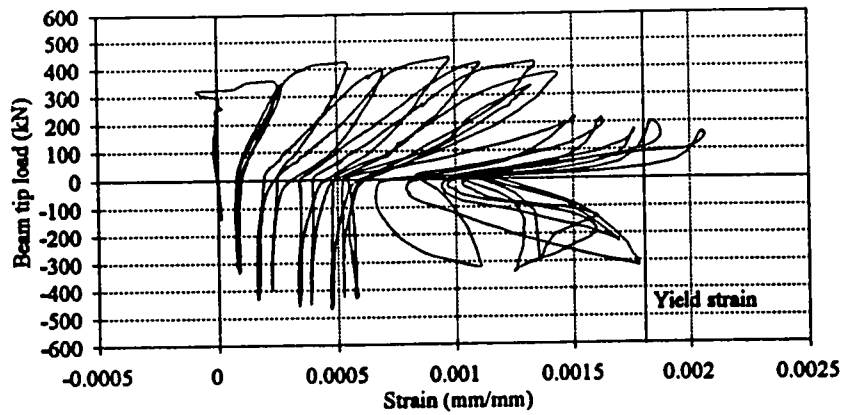


Figure A.13 Beam tip load-strain at beam steel jacket (bottom side) of specimen J3

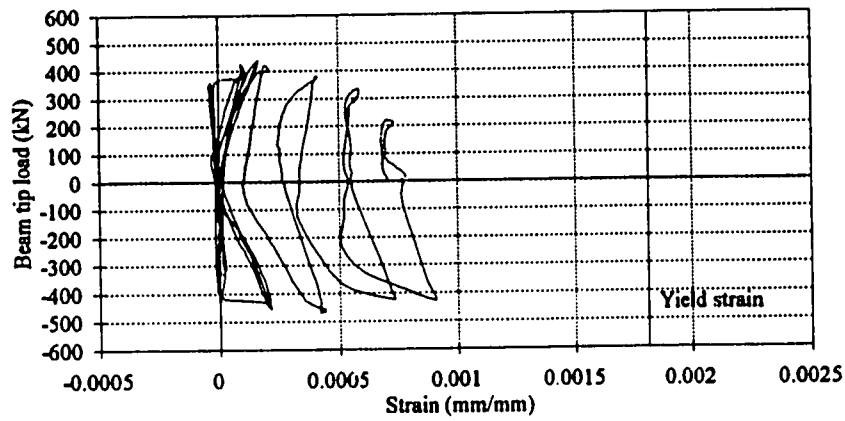


Figure A.14 Beam tip load-strain at steel jacket at joint of specimen J3

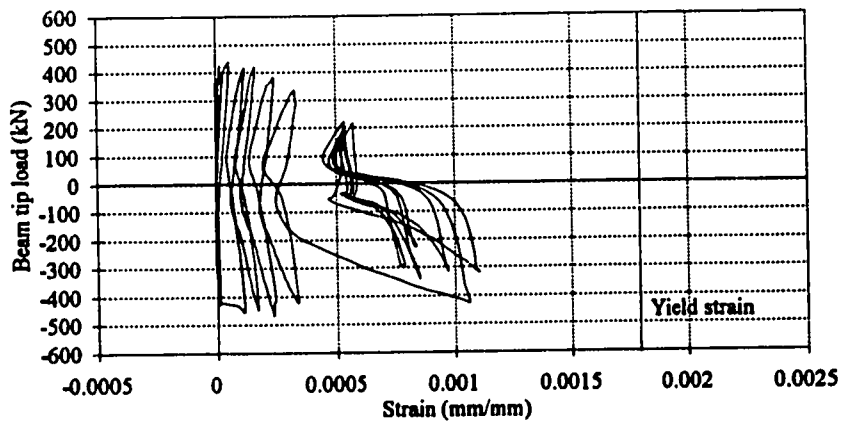


Figure A.15 Beam tip load-strain at steel jacket (joint confinement) of specimen J3

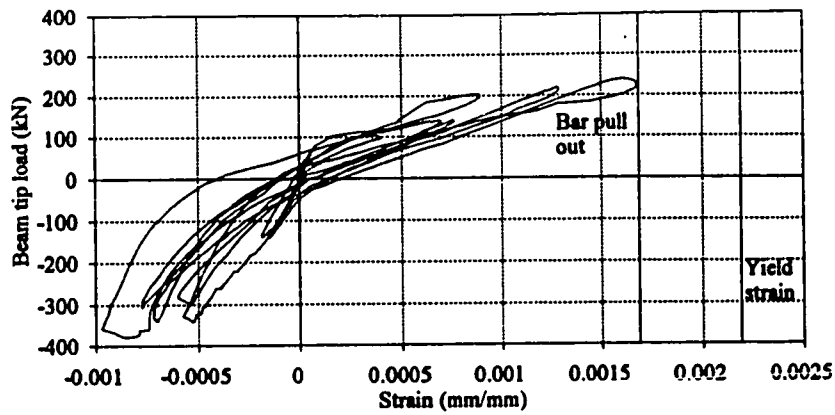


Figure A.16 Beam tip load-strain at bottom steel of beam of specimen J4

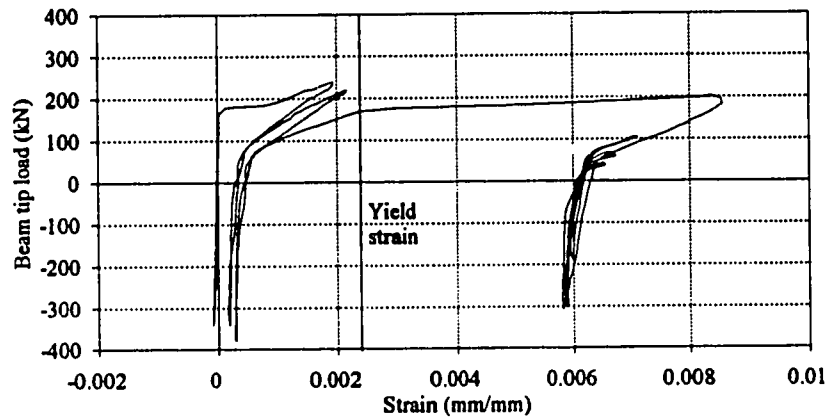


Figure A.17 Beam tip load-strain at column tie below joint of specimen J4

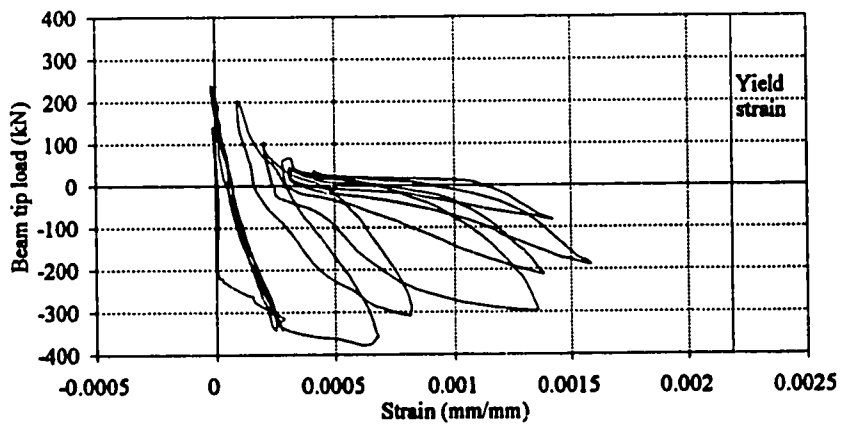


Figure A.18 Beam tip load-strain at column tie above joint of specimen J4

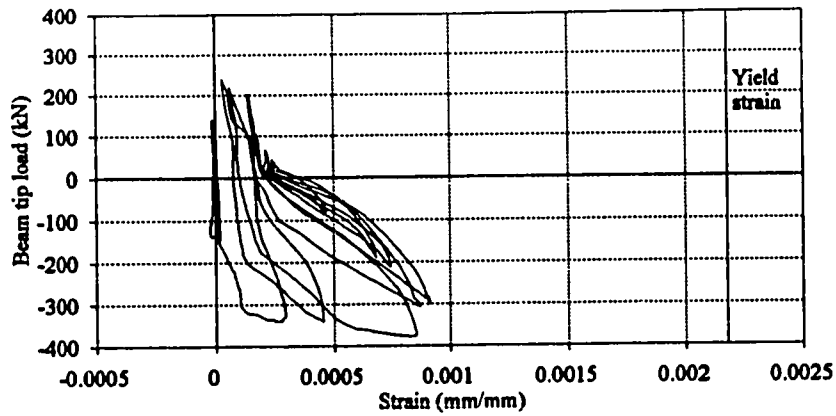


Figure A.19 Beam tip load-strain at beam second stirrup of specimen J4

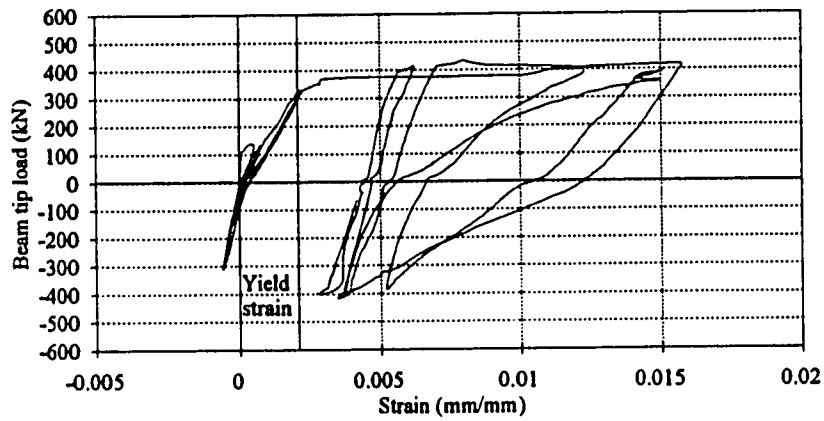


Figure A.20 Beam tip load-strain at bottom steel of beam of specimen J5

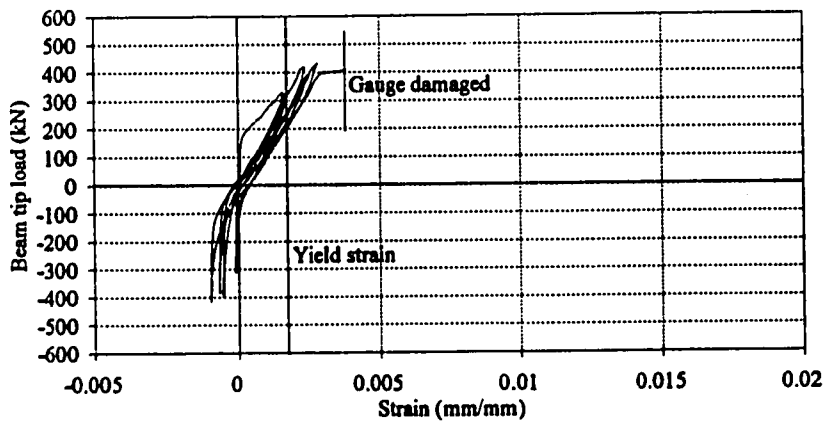


Figure A.21 Beam tip load-strain at bottom steel of beam of specimen J5

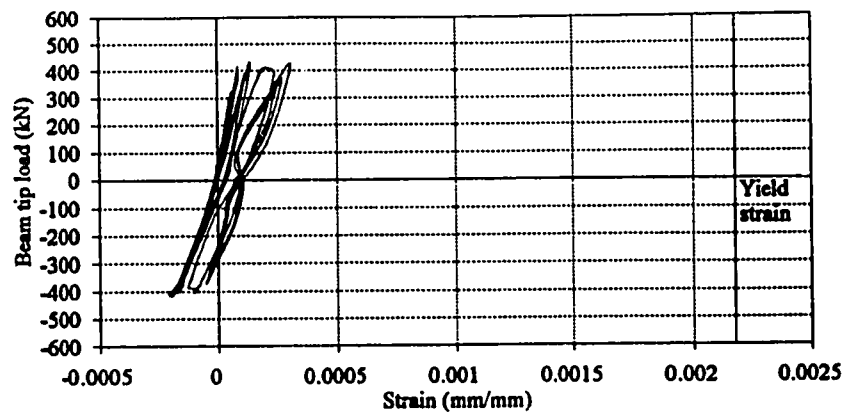


Figure A.22 Beam tip load-strain at column main steel above joint of specimen J5

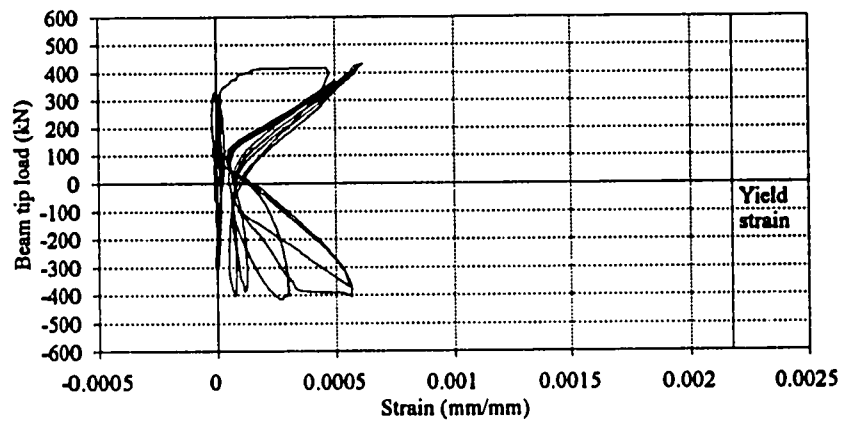


Figure A.23 Beam tip load-strain at column main steel in the joint of specimen J5

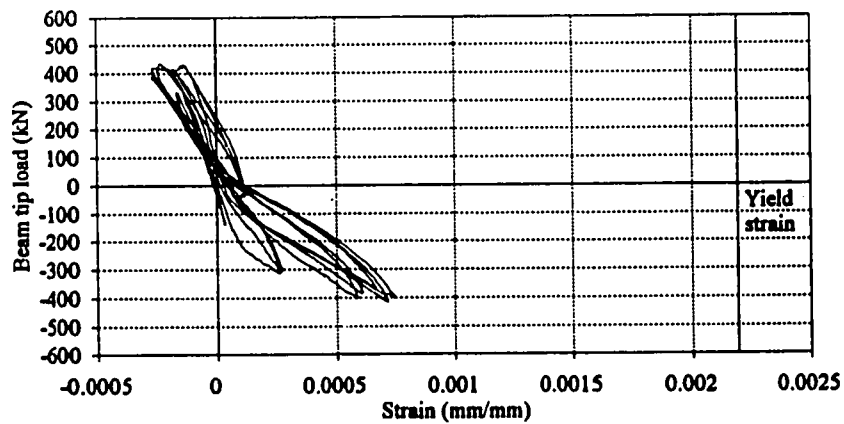


Figure A.24 Beam tip load-strain at column main steel below joint of specimen J5

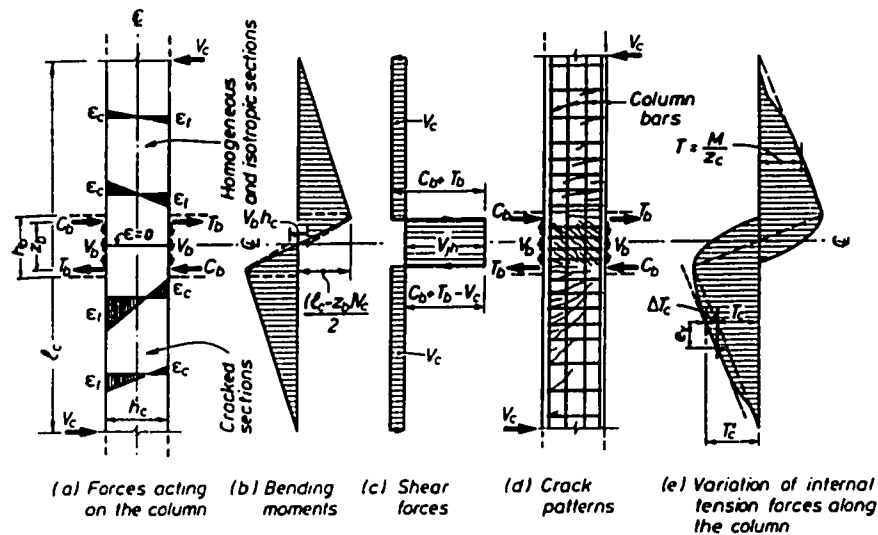


Figure A.25 Features of column and joint behaviour (Paulay and Priestley, 1992).

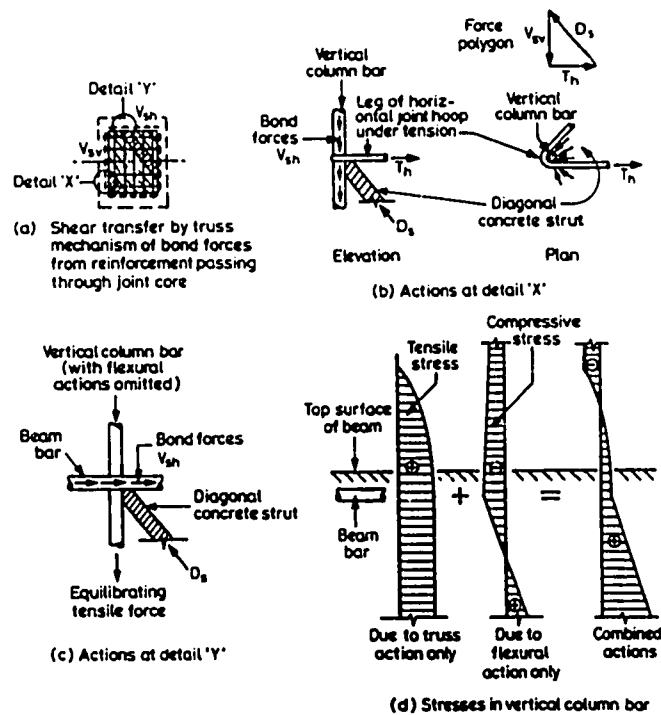


Figure A.26 Development of tensile strians in column bars participating in truss mechanism of joint shear resistance (Cheung et al., 1993).

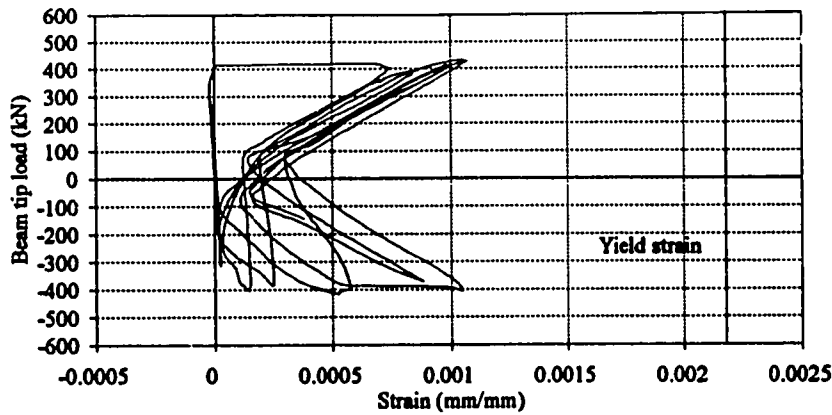


Figure A.27 Beam tip load-strain at joint tie of specimen J5

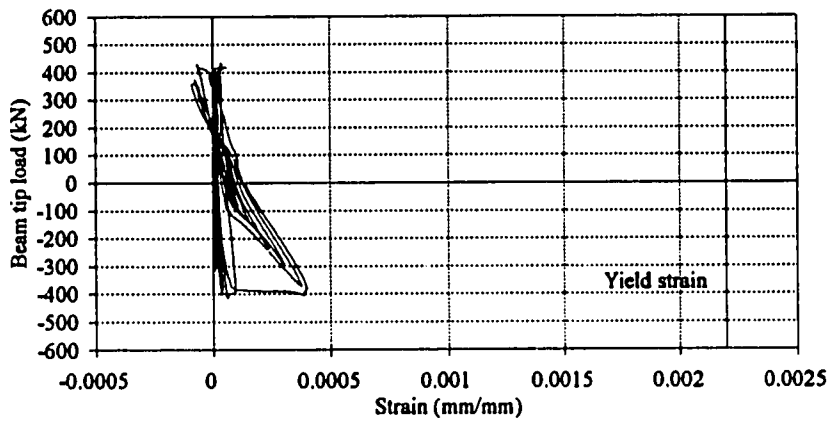


Figure A.28 Beam tip load-strain at joint tie (joint confinement) of specimen J5

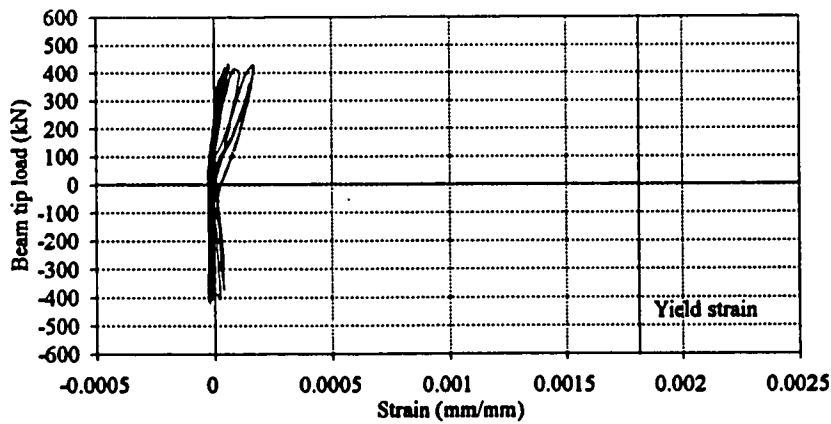


Figure A.29 Beam tip load-strain at joint steel jacket of specimen J5

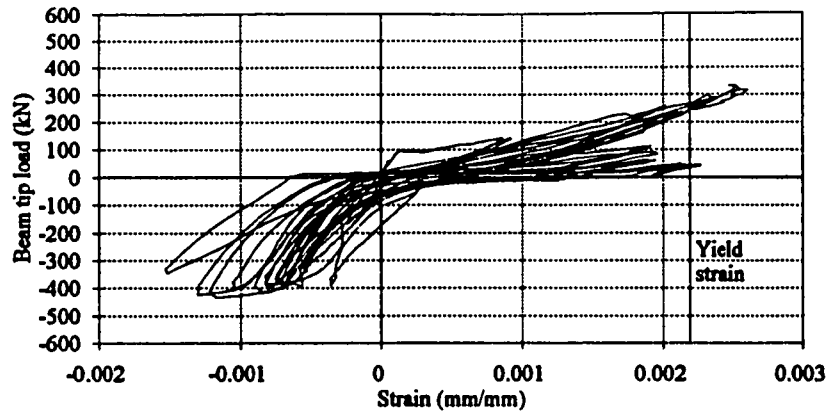


Figure A.30 Beam tip load-strain at bottom steel of beam of specimen J6

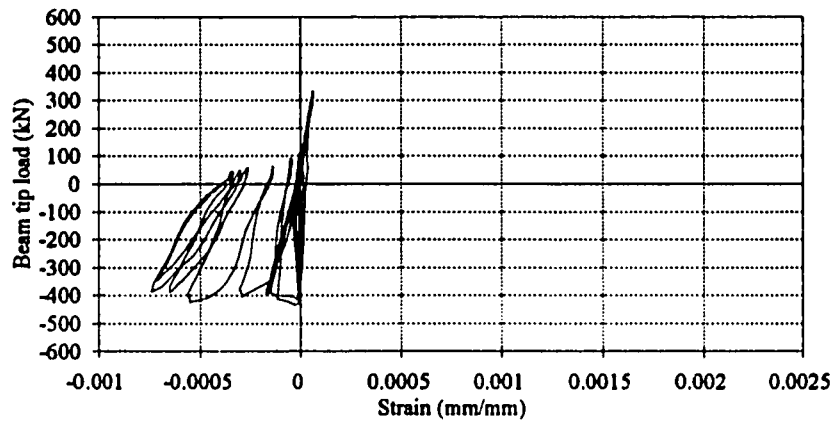


Figure A.31 Beam tip load-strain at column main steel above joint of specimen J6

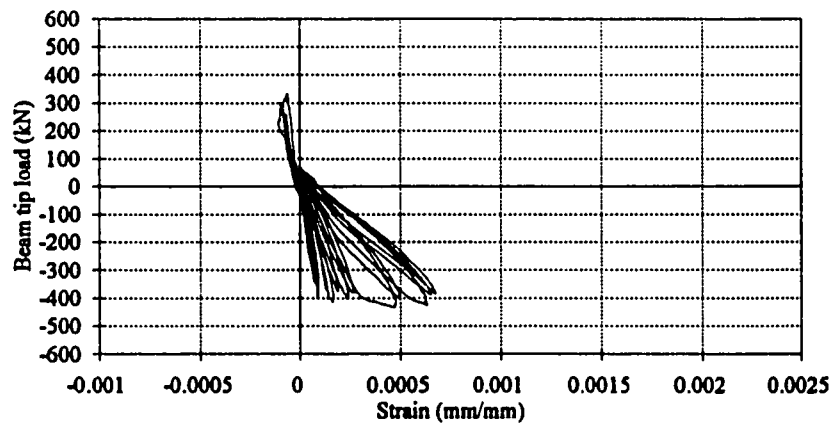


Figure A.32 Beam tip load-strain at column main steel below joint of specimen J6

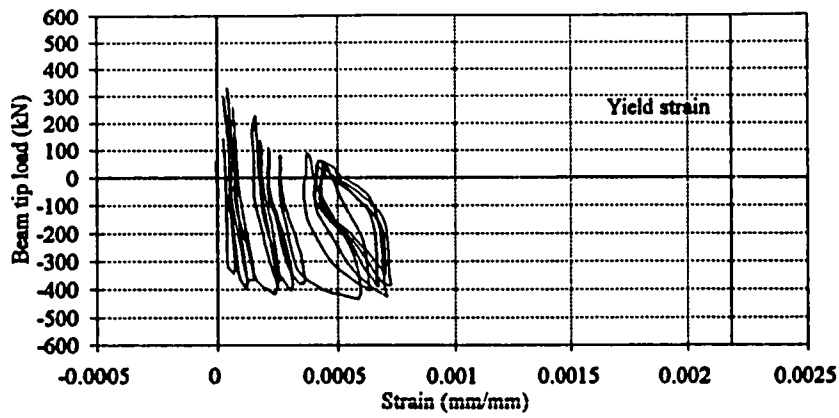


Figure A.33 Beam tip load-strain at column tie above joint of specimen J6

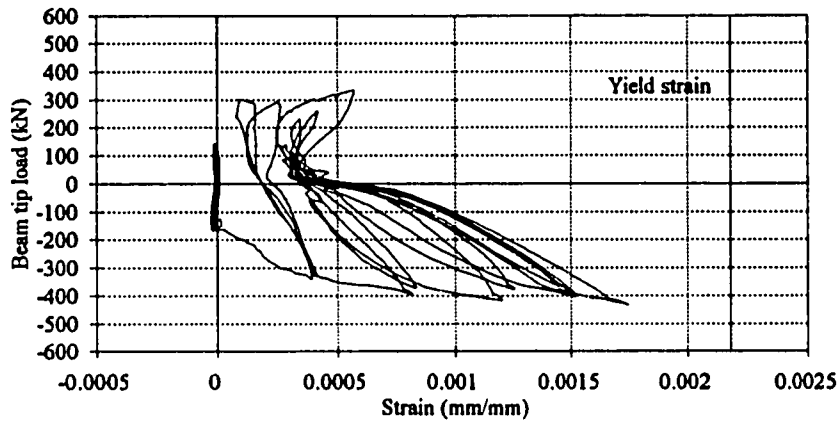


Figure A.34 Beam tip load-strain at beam second stirrup of specimen J6

APPENDIX B

COMPUTER PROGRAM 'SHEAR'

In this Appendix, a suitable solution algorithm using the relationships presented in chapter 6 to predict the moment-rotation relationship of the spring representing the joint is described. A listing of the program "SHEAR" developed to predict this moment-rotation relationship is presented.

B.1 SOLUTION ALGORITHM

The solution algorithm is given as follows:

First, at cracking:

Step 1: Calculate the angle θ as follows:

$$\cos^2 \theta = \frac{\frac{\sigma_x}{1 + \rho_x m} - f_{cl}}{\frac{\sigma_y}{1 + \rho_y m} + \frac{\sigma_x}{1 + \rho_x m} - 2f_{cl}} \quad (B.1)$$

where σ_x and σ_y are the average stress acting on the joint in the x and y directions, ρ_x and ρ_y are the percentage of reinforcement in the joint in x and y directions, $m = E_s / E_c - 1$, E_s is the steel Young's modulus, E_c is the concrete Young's modulus and f_{cl} is the concrete principal

tensile stress.

Step 2: Calculate the concrete principal compressive stress f_{c2} as follows:

$$f_{c2} = \frac{\frac{\sigma_y}{1 + \rho_y m} - f_{c1} \cos^2 \theta}{\sin^2 \theta} \quad (\text{B.2})$$

Step 3: Calculate the concrete shear stress v_c as follows:

$$v_c = (f_{c1} - f_{c2}) \sin \theta \cos \theta \quad (\text{B.3})$$

Step 4: Calculate the shear deformation γ as follows:

$$\begin{aligned} \epsilon_1 &= \frac{1}{E_c} (f_{c1} - \mu f_{c2}) \\ \epsilon_2 &= \frac{1}{E_c} (f_{c2} - \mu f_{c1}) \\ \gamma &= 2(\epsilon_1 - \epsilon_2) \sin \theta \cos \theta \end{aligned} \quad (\text{B.4})$$

where μ is the concrete Poisson's ratio.

Step 5: Calculate the total beam moment to be transferred to the column by joint shear using equation 6.21.

Second, after cracking:

Step 6: Assume a value of ϵ_2 at which to perform the calculations (starting with $\epsilon_2 = -0.0001$)

Step 7: Estimate a value of ϵ_1 (say $+0.0001$)

Step 8: Calculate the crack width w using equation 6.15.

Step 9: Calculate f_{c1} and f_{c2} using equations 6.3 to 6.14.

Step 10: Calculate the strain in x direction ϵ_x as follows:

$$\epsilon_x = \epsilon_1 + \frac{\epsilon_1 - \epsilon_2}{f_{c1} - f_{c2}} (\sigma_x - f_{c1} - \rho_x f_{sx}) \quad (B.5)$$

Step 11: Calculate the strain in y direction ϵ_y as follows:

$$\epsilon_y = \epsilon_1 + \frac{\epsilon_1 - \epsilon_2}{f_{c1} - f_{c2}} (\sigma_y - f_{c1} - \rho_y f_{sy}) \quad (B.6)$$

where f_{sx} and f_{sy} are the steel stresses in x and y directions.

Step 12: Check $\epsilon_1 + \epsilon_2 = \epsilon_x + \epsilon_y$. If $\epsilon_1 > \epsilon_x + \epsilon_y - \epsilon_2$, choose larger ϵ_1 and go to step 8.

If $\epsilon_1 < \epsilon_x + \epsilon_y - \epsilon_2$, choose smaller ϵ_1 and go to step 8.

Step 13: Calculate the angle θ as follows:

$$\tan^2 \theta = \frac{\epsilon_x - \epsilon_2}{\epsilon_y - \epsilon_2} \quad (B.7)$$

Step 14: Calculate the concrete shear stress v_c using equation B.3.

Step 15: Calculate the shear deformation γ as follows:

$$\gamma = 2(\epsilon_1 - \epsilon_2) \sin \theta \cos \theta \quad (B.8)$$

Step 16: Calculate the total beam moment to be transferred to the column by joint shear using equation 6.21.

Step 17: If $\epsilon_2 < \epsilon_{85}$ in equation 6.9 then stop, if $\gamma > 0.05$ then stop and if ϵ_x or $\epsilon_y \geq 0.03$ then stop.

Step 18: Choose $\epsilon_2 = \epsilon_2 - 0.000005$ and go to step 7.

B.2 LISTING OF THE PROGRAM

The listing of the computer program "SHEAR" for predicting the moment-rotation relationship of the spring representing the joints is as follows:

```
*****
PROGRAM SHEAR
CONFINED CONCRETE
*****
```

```
c  UNITS MM, KN, MPA
    IMPLICIT DOUBLE PRECISION (A-H,O-Z)
    OPEN(5,FILE='DATA',STATUS='OLD')
    OPEN(6,FILE='OUT',STATUS='NEW')
    OPEN(8,FILE='OUT1',STATUS='NEW')
    OPEN(9,FILE='OUT2',STATUS='NEW')
    READ(5,*) VN,HN,BJ,HC,HB,D,D1
    WRITE(8,2) VN,HN,BJ,HC,HB,D,D1
    READ(5,*) FC,FYINX,FYINY,HL,BL,ASV,ASH
    READ(5,*) S,SSX,SSY,AGG,AV,DBX,DBY
    READ(5,*) BCX,BCY,S1X,S1Y,SUMASX,SUMASY
c*****
c  AGG=MAX. AGGREGATE SIZE
c  SSX=SPACING BETWEEN VERTICAL REINFORCEMENT
c  SSY=SPACING BETWEEN HORIZONTAL REINFORCEMENT
c  DBX=DIAMETER OF THE HORIZONTAL INTERMEDIATE REINFORCEMENT
c  DBY=DIAMETER OF THE VERTICAL INTERMEDIATE REINFORCEMENT
c  S=SPACING BETWEEN HORIZONTAL STIRRUPS IN JOINT
c  AV=AREA OF ONE STIRRUP INCLUDING ALL BRANCHES
c  BCX,BCY=COLUMN CORE DIMENSION IN X AND Y DIRECTIONS,
c  RESPECTIVELY
c  S1X,S1Y=SPACING OF LONGITUDINAL REINFORCEMENT, LATERALLY
```

c SUPPORTED BY
 c THE CORNER OF A HOOP OR THE HOOK OF A CROSS TIE IN X AND Y
 c DIRECTIONS, RESPECTIVELY
 c SUMASX,SUMASY=AREA OF ALL BRANCHES OF ONE TIE IN THE X AND Y
 c DIRECTIONS, RESPECTIVELY MULTIPLIED BY THE CORRESPONDING
 c YIELD STRESS

c*****

```

WRITE(8,3) FC,FYINX,FYINY,HL,BL,ASV,ASH
2 FORMAT (5X,'VERTICAL LOAD IN kN           =' ,E15.7,
+       /,5X,'HORIZONTAL LOAD IN kN        =' ,E15.7,
+       /,5X,'JOINT EFFECTIVE WIDTH IN mm   =' ,E15.7,
+       /,5X,'COLUMN DEPTH EFFECTIVE FOR JOINT IN mm   =' ,E15.7,
+       /,5X,'BEAM DEPTH EFFECTIVE FOR JOINT IN mm   =' ,E15.7,
+       /,5X,'BEAM DEPTH (CONCRETE TO TENSION STEEL) (mm)=' ,E15.7,
+       /,5X,'BEAM DEPTH (CONCRETE TO COMP. STEEL) (mm) =' ,E15.7)
3 FORMAT (5X,'CONCRETE STRENGTH IN MPa      =' ,E15.7,
+       /,5X,'STEEL YIELD STRENGTH IN X DIRECTION IN MPa =' ,E15.7,
+       /,5X,'STEEL YIELD STRENGTH IN Y DIRECTION IN MPa =' ,E15.7,
+       /,5X,'FLOOR HEIGHT IN mm           =' ,E15.7,
+       /,5X,'AVERAGE BEAM CLEAR SPAN IN mm       =' ,E15.7,
+       /,5X,'INTERIOR STEEL IN COLUMN IN mm^2      =' ,E15.7,
+       /,5X,'INT. STEEL IN BEAM WELL CON.+ STIR. (mm^2) =' ,E15.7)
SEGX=HN*1000.0/(BJ*HB)
SEGY=VN*1000.0/(BJ*HC)
ROX=ASH/(BJ*HB)
ROY=ASV/(BJ*HC)
ES=200000.0

```

c***** CALCULATION OF CONCRETE YOUNG'S MODULUS *****

```

EC=2.*FC/0.002
DJ=D-D1
DDD=0.9*D
IF(DJ.LT.DDD) DJ=DDD

```

c***** BEFORE CRACKING *****

```

c CALCULATE CRACKING MOMENT & THE ACCOMPANIED DISTORTION
c REPETED LOAD; ALPHA2=0.7
FCCC1=0.7*0.33*SQRT(FC)
SSM=(ES/EC)-1.
ROOX=1.+ROX*SSM

```

```

ROOY=1.+ROY*SSM
SSGX=SEGX/ROOX
SSGY=SEGY/ROOY
CCTA=(SSGX-FCCC1)/(SSGY+SSGX-(2.0*FCCC1))
SCTA=SQRT(CCTA)
THET=ACOS(SCTA)
FCCC2=(SSGY-FCCC1*(COS(THET))**2)/(SIN(THET))**2
c CALCULATION OF SHEAR STRESS AT CRACKING TTO
TTO=(FCCC1-FCCC2)*SIN(THET)*COS(THET)
CREPS1=(FCCC1-0.2*FCCC2)/EC
CREPS2=(FCCC2-0.2*FCCC1)/EC
c *****
c CALCULATION OF SHEAR DEFORMATION AT CRACKING CRGAMA
CRGAMA=2*(CREPS1-CREPS2)*SIN(THET)*COS(THET)
c CALCULATION OF BEAM MOMENT AT CRACKING OF JOINT CRM
CRM=TTO*BJ*HC/(1000000.*((1/(DJ))-(1/(HL*(1-(HC/
*BL))))))
c *****
WRITE(8,9)
WRITE(6,7) 0.,0.
WRITE(9,7) 0.,0.
WRITE(8,18) 0.,0.,0.
89 WRITE(6,7) CRM,CRGAMA
WRITE(9,7) TTO,CRGAMA
WRITE(8,28)
WRITE(8,18) TTO,CRM,CRGAMA
7 FORMAT (1E14.7,3X,1E14.7)
9 FORMAT ('SHEAR STRESS',2X,'MOMENT (KN.m)',2X,'JOINT SHEAR DEFORM
*',2X)
28 FORMAT (1X,'***** CRACKING *****',1X)
c***** AFTER CRACKING *****
c***** CONFINED PART *****
FLX=SUMASX/(BCY*S)
AK2X=0.26*SQRT(BCY**2/(S*S1Y*FLX))
IF(AK2X.GT.1.) AK2X=1.0
FLEX=AK2X*FLX
FLY=SUMASY/(BCX*S)
AK2Y=0.26*SQRT(BCX**2/(S*S1X*FLY))

```

```

IF(AK2Y.GT.1.) AK2Y=1.0
FLEY=AK2Y*FLY
FLE=(FLEX*BCY+FLEY*BCX)/(BCX+BCY)
AK1=6.7*(FLE)**(-.17)
AK=AK1*FLE/FC
FCC=FC+AK1*FLE
FFF1=-0.00044*SQRT(FC)*(1.+5.*AK)
ROO=(SUMASX+SUMASY)/(FYINY*S*(BCY+BCX))
FOLD85=-1.387*0.00044*SQRT(FC)
FFF85=260.*ROO*FFF1+FOLD85
c  WRITE(*,*) FCC,FFF1
c*** FFF1 IS THE STRAIN AT MAXIMUM STRESS FCC
c*****
      VVV=0.
      HHH=0.
10 FCR=0.33*SQRT(FCC)
      EPSCR=FCR/EC
      EPS2=-0.0001
400 EPS1=0.0001
      IF(EPS1.LT.EPSCR) EPS1=EPSCR
      NITER=0
200 BBETA=(1./(0.8+170.*EPS1))
      F2=-BBETA*FCC*((2.*EPS2/FFF1)-(EPS2/FFF1)**2)**(1./(1.+2.*AK))
c  ASSUME WE HAVE DEFORMED BARS; ALPHA1=1.0, AND REPETED LOAD;
      ALPHA2=0.7
700 IF(EPS1.LT.0.0) F1=0.7*FCR
      IF(EPS1.LT.0.0) GO TO 701
      F1=0.7*FCR/(1.0+SQRT(500*EPS1))
701 IF(F1.EQ.F2) F1=0.0
      XX=(EPS1-EPS2)/(F1-F2)
      EPSY=(EPS1+XX*(SEGY-F1))/(1.+XX*(ROY*ES))
      EYINX=FYINX/ES
      EYINY=FYINY/ES
      EYY=0.03
c  ASSUMING THE FAILURE OF THE JOINT IF THE STEEL STRAIN EXCEEDED
      0.03
      IF(EPSY.GT.EYINY) EPSY=(EPS1+XX*(SEGY-F1-ROY*FYINY+ROY*EYINY*
*0.025*ES))/(1.+XX*ROY*0.025*ES)

```

```

IF(EPSY.GT.EYY) EPSY=(EPS1+XX*(SEGY-F1))
EPSX=(EPS1+XX*(SEGX-F1))/(1.+XX*(ROX*ES))
IF(EPSX.GT.EYINX) EPSX=(EPS1+XX*(SEGX-F1-ROX*FYINX+ROX*EYINX*
*0.025*ES))/(1.+XX*ROX*0.025*ES)
IF(EPSX.GT.EYY) EPSX=(EPS1+XX*(SEGX-F1))
EPS11=EPSX+EPSY-EPS2
EEE=ABS(EPS11-EPS1)
EE=0.00001
IF(EEE.LT.EE) GO TO 985
EPS1=EPS11
If (NITER.GT.50) GO TO 260
NITER=NITER+1
GO TO 200
985 IF(EPSX.LE.EPS2) GO TO 333
IF(EPSY.LE.EPS2) GO TO 333
SOS=ABS((EPSX-EPS2)/(EPSY-EPS2))
YY=SQRT(SOS)
THETA=ATAN(YY)
AMIN=(0.06*SQRT(FC)/FYINY)*BJ*S
IF(AV.GE.AMIN) SMTH=300.0
IF(AV.GE.AMIN) GO TO 66
AMINV=0.004*BJ*SSX
AMINH=0.004*BJ*SSY
ASVONE=2.*((22./7.)*(DBY)**2)/4.
ASHONE=2.*((22./7.)*(DBX)**2)/4.
SMX=0.9*HC
IF(ASVONE.GT.AMINV) SMX=SSX
SMY=0.9*HB
IF(ASHONE.GT.AMINH) SMY=SSY
SMTH=1./((SIN(THETA)/SMX)+(COS(THETA)/SMY))
66 WW=EPS1*SMTH
VCI=0.18*(SQRT(FCC))/(0.3+((24.*WW)/(AGG+16.)))
FFFF2=VCI*TAN(THETA)+(ASV/(HC*BJ))*(FYINY-EPSY*ES)
IF(FYINY.LE.(EPSY*ES)) FFFF2=VCI*TAN(THETA)
FFFF3=(VCI/TAN(THETA))+(ASH/(HB*BJ))*(FYINX-EPSX*ES)
IF(FYINX.LE.(EPSX*ES)) FFFF3=VCI/TAN(THETA)
IF(FFFF2.LT.FFFF3) FFFF1=FFFF2
IF(FFFF2.LT.FFFF3) GO TO 44

```



```

      FFFF1=FFFF3
44 IF(F1.GT.FFFF1) F1=FFFF1
      IF (F1.GT.FFFF1) GO TO 701
      V=(F1-F2)*SIN(THETA)*COS(THETA)
c *****
      SMM=V*BJ*HC/(1000000.*((1/(DJ))-(1/(HL*(1-(HC/
      *BL))))))
      GAMA=2.*(EPS1-EPS2)*SIN(THETA)*COS(THETA)
c *****
      IF(VVV.EQ.1.) GO TO 99
      IF(EPSY.GT.EYINY) VVV=1.
      IF(EPSY.GT.EYINY) WRITE(8,38)
99 IF(HHH.EQ.1.) GO TO 999
      IF(EPSX.GT.EYINX) HHH=1.
      IF(EPSX.GT.EYINX) WRITE(8,58)
999 IF(EPSY.GE.EYY) WRITE(8,48)
      IF(EPSY.GE.EYY) GO TO 260
      IF(EPSX.GE.EYY) WRITE(8,68)
      IF(EPSX.GE.EYY) GO TO 260
333 WRITE(6,8) SMM,GAMA
      WRITE(9,8) V,GAMA
      WRITE(8,18) V,SMM,GAMA
      IF(EPS2.LE.FFF85) WRITE(8,78)
      8 FORMAT (1E14.7,3X,1E14.7)
      18 FORMAT (1E14.7,3X,1E14.7,3X,1E14.7)
      38 FORMAT (1X,'***** YIELDING OF VERTICAL RFT. *****',1X)
      48 FORMAT (1X,'***** ULTIMATE OF VERTICAL RFT. *****',1X)
      58 FORMAT (1X,'***** YIELDING OF HORIZONTAL RFT. *****',1X)
      68 FORMAT (1X,'***** ULTIMATE OF HORIZONTAL RFT. *****',1X)
      78 FORMAT (1X,'***** CONCRETE CRUSHING *****',1X)
      IF(EPS2.LE.FFF85) GO TO 260
      IF(GAMA.GT.0.05) GO TO 260
      EPS2=EPS2-0.000005
      GO TO 400
260 WRITE(8,100)
100 FORMAT (/,'***** END *****')
      STOP
      END

```

REFERENCES

Abrams, D.P., 1987, "Scale relations for reinforced concrete beam-column joints", American Concrete Institute, ACI, Structural Journal, Vol. 84, No. 6, pp. 502-512.

ACI-ASCE committee 352, 1985, "Recommendations for design of beam-column joints in monolithic reinforced concrete structures", ACI Structural Journal, Vol. 82, No. 3, pp. 266-283.

ACI-318, 1963, 1971, 1989, "Building code requirements for reinforced concrete", American Concrete Institute, Detroit, Michigan.

ACI-408, 1979, "Suggestion for development, splices, and standard hook provisions for deformed bars in tension", American concrete institute, Detroit, Michigan.

Alcocer, S. M., and Jirsa, J. O., 1991, "Reinforced concrete frame connections rehabilitated by jacketing", PMFSEL report No. 91-1, Phil M. Ferguson Structural Engineering Laboratory, the University of Texas at Austin, 221 pages.

Alcocer, S.M., and Jirsa, J.O., 1993, "Strength of reinforced concrete frame connections rehabilitated by jacketing", ACI Structural Journal, Vol. 90, No. 3, PP. 249-261.

Al-Haddad, M. and Wight, J.K., 1988, "Relocating beam plastic hinging zones for earthquake resistant design of reinforced concrete buildings", ACI Structural Journal, Vol. 85, No. 2, pp. 123-133.

Allahabadi, R., 1987, "DRAIN-2DX, Seismic response and damage assessment for 2D structures, Ph. D. dissertation, University of California, Berkeley, CA.

Alsiwat, J.M. and Saatcioglu, M., 1992, "Modelling anchorage slip for dynamic analysis", Tenth World Conference on Earthquake Engineering, Madrid, pp. 2627-2632.

Architectural Institute of Japan (AIJ) Guidelines, 1988, "Design guidelines for earthquake resistant reinforced concrete buildings based on ultimate strength concept and commentary", 337 pages.

Architectural Institute of Japan (AIJ) Standards, 1988, "AIJ Standard for structural calculation of reinforced concrete structures".

Ayala, G. and Xianguo, Y., 1995, "Analytical evaluation of the structural seismic damage of reinforced concrete frames", Seventh Canadian Conference on Earthquake Engineering, Montreal, Canada, pp. 389-396.

Aycardi, L. E., Mander, J. B. and Reinhorn, A. M., 1992, "Seismic resistance of R/C frame structures designed only for gravity loads, Part II: Experimental performance of subassemblages", NCEER technical report No. 92-0028, National Center for Earthquake Engineering Research, State University of New York at Buffalo, N.Y.

Aziz, T.S., Ghobarah, A. and Biddah, A., 1995, "Seismic Assessment of Existing Reinforced Concrete Frame Connections", Al-Azhar Engineering Fourth International Conference, Vol. 3, pp. 268-276.

Bass, R.A., Carrasquillo, R.L. and Jirsa, J.O., 1989, "Shear transfer across new and existing concrete interfaces", ACI Structural Journal, Vol. 86, No. 4, pp. 383-393.

Beckingsale, A., Park, R. and Paulay, T., 1980, "Post elastic behaviour of reinforced concrete beam-column joints", research report 80-20, Department of Civil Engineering, University of Canterbury, Christchurch, New Zealand.

Beres, A., El-Borgi, S., White, R. N. and Gergely, P., 1992, "Experimental results of repaired and retrofitted beam-column joint tests in lightly reinforced concrete frame buildings", NCEER technical report No. 92-0025, National Center for Earthquake Engineering Research, State University of New York at Buffalo, N.Y.

Beres, A.B., 1994, "Experimental and Analytical Study of the Performance of Reinforced Concrete Frames with Non-Ductile Details", Ph. D. thesis, Department of Civil Engineering, Cornell University.

Biddah, A., Ghobarah, A. and Aziz, T.S., 1995, "Assessment of the Capacity of existing Beam-Column Connections", Seventh Canadian Conference on Earthquake Engineering, Montreal, pp. 421-428.

Biddah, A. and Ghobarah, A. and Aziz, T.S., 1997, "Upgrading of non-ductile reinforced concrete frame connections", Journal of Structural Engineering, ASCE, Vol. 123, No. 8.

Biddah, A., Ghobarah, A., 1997, Rehabilitation strategy for medium-rise reinforced concrete buildings", Al-Azhar Engineering Fifth International Conference, Cairo, Vol. 3.

Biddah, A. and Ghobarah, A., 1998, "Inelastic shear deformation modelling in existing and retrofitted concrete frames", Sixth U.S. National Conference on Earthquake Engineering on Seismic Design and Mitigation for the Third Millennium, Seattle, Washington, USA.

Blume, J. A., Newmark, N. M., and Corning, L. H., 1961, "Design of multi-storey concrete buildings for earthquake motions", Portland Cement Association, Skokie, Illinois.

Branson, D.E., 1977, "Deformation of concrete structures", McGraw-Hill, New York.

CSA A23.3-94, 1994, "Design of concrete structures", Canadian Standards Association, Rexdale, Ontario, Canada, 209 pages.

CSA CAN3-G401-M81, 1981, "Corrugated steel pipe products: The national standard of Canada for material and fabrication of CSP and SPCSP products.", Canadian Standards Association, Rexdale, Ontario, Canada, 137 pages.

Cheung, P.C., Paulay, T. and Park, R., 1993, "Behaviour of beam-column joints in seismically loaded reinforced concrete frames", Journal of Structural Engineering, ASCE, Vol. 71, No. 8, pp. 129-138.

Choudhuri, D., Mander, J. B. and Reinhorn, A.M., 1992, "Evaluation of seismic retrofit of reinforced concrete frame structures: Part I - Experimental performance of retrofitted subassemblages", NCEER technical report No. 92-0030, National Center for Earthquake Engineering Research, State University of New York at Buffalo, N.Y.

Chung, Y.S., Meyer, C., and Shinozuka, M., 1987, "Seismic damage assessment of reinforced concrete members", report No. NCEER-87-0022, National Center for Earthquake Engineering Research, State University of New York at Buffalo, NY.

Clough, R.W., 1966, "Effect of stiffness degradation on earthquake ductility requirements", structural and materials research report No. 66-16, University of California, Berkeley, CA.

Clough, R.W. and Penzien, J., 1975, "Dynamics of structures", McGraw-Hill, New York, 652 pages.

Collins, M.P., 1978, "Towards a rational theory for reinforced concrete members in shear", Journal of the Structural Division, ASCE, Vol. 104, pp. 649-666.

Collins, M.P. and Mitchell, D., 1991, "Prestressed concrete structures", Prentice-Hall, Inc., New Jersey, 766 pages.

Corazao, M. and Durrani, A. J., 1989, "Repair and strengthening of beam-to-column connections subjected to earthquake loading", NCEER technical report No. 89-0013, National Center for Earthquake Engineering Research, State University of New York at Buffalo, N.Y., 93 pages.

Dipasquale, E. and Cakmak, A.S., 1987, "Detection and assessment of seismic structural damage", NCEER 87-0015, National Center for Earthquake Research Center, State University of New York at Buffalo, N.Y.

Durrani, A. J. and Wight, J. K., 1982, "Experimental and analytical study of internal beam-to-column connections subjected to reversed cyclic loading", research report No. UMEE 82R3, Department of Civil Engineering, University of Michigan, Ann Arbor, 275 pages.

Ehsani, M.R. and Alameddine, A., 1989, "Behaviour of ductile high strength concrete connections", report No. CEEM-89-105, Department of Civil Engineering, University of Arizona.

Estrada, J.I., 1990, "Use of steel elements to strengthen a reinforced concrete building", M.Sc. thesis, University of Texas at Austin, 66 pages.

Filippou, F.C., 1986, "A Simplified model for reinforcing bar anchorages under cyclic excitations", Journal of the Structural Division, ASCE, Vol. 112, No. ST7, pp. 1639-1659.

Filippou, F.C., Popov, E.P. and Bertero, V.V., 1986, "Analytical studies of hysteretic behaviour of reinforced concrete joints", Journal of the Structural Division, ASCE, Vol. 112, No. ST7, pp. 1605-1623.

Filippou, F. and Issa, A., 1988, "Nonlinear analysis of reinforced concrete frames under cyclic load reversals", report No. UCB/EERC-88/12, University of California, Berkeley, California.

French, C.W. and Moehle, J.P., 1991, "Effect of floor slab on behaviour of slab-beam-column connections", ACI-SP 123, Design of Beam-Column Joints for Seismic Resistance, Detroit, MI, pp. 225-258.

Fujii, S. and Morita, S., 1991, "Comparison between interior and exterior reinforced concrete beam-column joint behaviour", ACI-SP 123, Design of Beam-Column Joints for Seismic Resistance, Detroit, MI, pp. 145-165.

Gavrilovic, P., Velkov, M., Jurukovski, D. and Mamucevski, D., 1980, "Behaviour of reinforced concrete beam-column joints under cyclic loading", proceeding of Seventh World Conference on Earthquake Engineering, Vol. 7, pp. 289-296.

Ghobarah, A., Biddah, A. and Pilette, C., 1995, "Seismic assessment of safety-related structure: Laboratory testing of the PRD frame at Pickering NPP", 13th International Conference on Structural Mechanics in Reactor Technology (SMiRT), Porto Alegre RS, Brazil, pp. 223-228.

Ghobarah, A., Aziz, T.S. and Biddah, A., 1995, "Evaluation of the seismic response of existing reinforced concrete structures", Second Cairo Earthquake Engineering Symposium on Seismic Design Codes, Cairo, Egypt, pp. 67-77.

Ghobarah, A., Aziz, T.S. and Biddah, A., 1996a, "Seismic behaviour of rehabilitated reinforced concrete connections", Cairo First International Conference on Concrete Structures, Vol. 1, session I, Cairo, Egypt, pp. 11-21.

Ghobarah, A., Aziz, T.S. and Biddah, A., 1996b, "Rehabilitation of reinforced concrete beam-column joints", Eleventh World Conference on Earthquake Engineering, Acapulco, Mexico, paper no. 1394, 8 pages.

Ghobarah A., Aziz T.S. and Biddah A., 1996c, "Seismic rehabilitation of reinforced concrete beam-column connections", *Earthquake Spectra*, Repair and Rehabilitation Issue, Vol. 12, No. 4, pp. 761-780.

Ghobarah, A., Aziz, T.S. and Biddah, A., 1997, "Rehabilitation of reinforced concrete connections using corrugated steel jacketing", *ACI, American concrete institute Structural Journal*, Vol. 94, No. 3.

Ghobarah, A., Biddah, A. and Mahgoub, M., 1997, "Seismic retrofit of reinforced concrete columns using steel jackets", *European Journal of Earthquake Engineering*, No. 1.

Ghobarah, A., Biddah, A. and Pilette, C., 1997, "Seismic assessment of safety-related structures: response of the PRD frame at Pickering NPP", Fourteenth International Conference on Structural Mechanics in Reactor Technology (SmiRT), Lyon, France, Division "K", paper 303, pp. 1-8.

Gobarah, A., Biddah, A. And Mahgoub, M., 1998, "Rehabilitation of reinforced concrete columns using corrugated steel jacketing", to appear in the *Journal of Earthquake Engineering*.

Handbook of steel drainage and highway construction products, 1984, published by the American Iron and Steel Institute, Washington, DC 20005-2701, 413 pages.

Hanson, N. M., and Conner, H. W., 1967, "Seismic resistance of reinforced concrete beam-column joints" *Journal of the Structural Division*, proceedings of ASCE, Vol. 93, pp. 533-560.

Hawkins, N.M. and Lin, I.J., 1979, "Bond characteristics of reinforced bars for seismic loading", Third Canadian Conference on Earthquake Engineering, Montreal, Que., Vol. II, pp. 1225-1252.

Hilti, 1994, "Systems and solutions manual", 6325 Dixie Road, Unit #4, Mississauga, Ontario, L5T 2E5.

Hoffmann, G.W., Kunnath, S.K., Reinhorn, A.M. and Mander, J.B., 1992, "Gravity-load designed reinforced concrete buildings" technical report, NCEER-92-0016, National Center for Earthquake Engineering Research, State University of New York at Buffalo, N.Y.

Hoffschild T.E., Prion H.G.L. and Cherry S., 1993, "Seismic retrofit of beam-to-column joints with grouted steel tubes", proceedings of the Tom Paulay Symposium on Recent Developments in Lateral Force Transfer in Buildings, University of California, San Diego, La jolla, CA. pp. 403-431.

Hsu, T.T.C., 1988, "Softened truss model theory for shear and torsion", *ACI Structural Journal*, Vol. 85, No. 6, pp. 624-634.

Ichinose, T., 1983, "Methods of inelastic analysis of reinforced concrete frames with bond slip", Transaction of the Architectural Institute of Japan, AIJ, No. 328, pp. 26-35.

Izumo, J., 1992, "A parametric study of the reinforced concrete panel ductility by using the analytical model", Concrete Shear in Earthquake, Elsevier Science Publishers Ltd., pp. 365-374.

Kaku, T. and Asakusa, H., 1991, "Ductility estimation of exterior beam-column subassemblages in reinforced concrete frames", ACI-SP 123, Design of Beam-Column Joints for Seismic Resistance, Detroit, MI, pp. 167-185.

Kaku T. and Morita, S., 1978, "Bond behaviour of beam bars in the joint of reinforced concrete frame", Annual Meeting of the Architectural Institute of Japan, AIJ, pp. 1777-1778.

Kanaan, A.E. and Powell, G.H., 1973, "DRAIN-2D, A general purpose computer program for dynamic analysis of planner structures", UBC/EERC report 73-6, University of California, Berkeley, CA.

Kanada, K., Fujii, S. and Morita, S., 1985, "Effects of joint shear reinforcement on behaviours of exterior beam-column joints", Transaction of the Japan Concrete Institute, Vol. 7, pp. 559.

Kitayama, K., Kurusu, K., Otani, S. and Aoyama, H., 1985, "Behaviour of beam-column connections with improved beam reinforcement bond", Transaction of the Japan Concrete Institute, Vol. 7, pp. 551.

Kitayama, K., Otani, S. and Aoyama, H., 1987, "Earthquake resistant design criteria for reinforced concrete interior beam-column joints", proceedings, Pacific Conference on Earthquake Engineering, New Zealand, Vol. 1, pp. 315-326

Kitayama, K., Otani, S. and Aoyama, H., 1991, "Development of design criteria for reinforced concrete interior beam-column joints", ACI-SP 123, Design of Beam-Column Joints for Seismic Resistance, Detroit, MI, pp. 97-123.

Kurose, Y., 1987, "Recent studies on reinforced concrete beam-column joints in Japan", PMFSEL report No. 87-8, Phil M. Ferguson Structural Engineering Laboratory, Department of Civil Engineering, University of Texas at Austin, 163 pages.

Kurose, Y., Guimaraes, G. N., Liu, Z., Kreger, M. E. and Jirsa, J. O., 1988, "Study of reinforced concrete beam-column joints under uniaxial and biaxial loading", PMFSEL report No. 88-2, Phil M. Ferguson Structural Engineering Laboratory, the University of Texas at Austin, 146 pages.

Lampert P. and Thurlimann B., 1968, "Torsion tests of reinforced concrete beams", Bericht No. 6506-2, Institut für Baustatik, ETH, Zürich, 101 pages and "Torsion-bending tests on reinforced concrete beams", Bericht No. 6506-3, Institut für Baustatik, ETH, Zürich, 116 pages.

- Liu, S. C. and Lagoria, H. J., 1991, "U.S. National program on seismic repair and retrofit of structures", Sixth Canadian Conference on Earthquake Engineering, Toronto, pp. 783-790.
- Meyer, C., 1994, "Seismic analysis of reinforced concrete frames, SARCF, computer program", private communication.
- Migliacci, A., Antonucci, R., Maio, N. A., Napoli, P., Ferretti, A. S. and Via, G., 1983, "Repair techniques of reinforced concrete beam-column joints", final report, IABSE Symposium on Strengthening of Building Structures - diagnosis and therapy, Venice, pp. 355-362.
- Mori, Y. and Ellingwood, B.R., 1993, "Reliability based service life assessment of aging concrete structures" *Journal of Structural Engineering*, ASCE, Vol. 119, No. 5, pp. 1600-1621.
- Morita, S. and Kaku, T., 1972, "Pull-out of the beam bar from the joint of reinforced concrete beam-column subassemblages", Annual Meeting of the Architectural Institute of Japan, AIJ, pp. 1099-1100.
- Morita, S. and Kaku, T., 1984, "Slippage of reinforcement in beam-column joint of reinforced concrete frame", Eighth World Conference, San Francisco, pp. 477-484.
- NBCC, 1995, "National building code of Canada", the National Research Council of Canada, Ottawa, Ontario, Canada.
- Naumoski, N., 1985, "McMaster earthquake engineering software library, documentation for IBM system", Department of Civil Engineering, Hamilton, Ontario, Canada.
- Otani, S., 1974, "Inelastic analysis of reinforced concrete frame structures", *Journal of the Structural Division*, ASCE, Vol. 100, No. ST-7, pp. 1433-1449.
- Otani, S., Kabeyasawa, T., Shiohara, H. and Aoyama, H., 1984, "Analysis of the full-scale seven-story reinforced concrete test structure - earthquake effects on reinforced concrete structures", U.S.-Japan research, ACI-SP 84, Detroit.
- Pantazopoulou, S., 1991, "The effect of floor slabs on the behaviour of beam-column connections under seismic loads", Sixth Canadian Conference of Earthquake Engineering, Toronto, pp. 591-599.
- Pantazopoulou, S. and Bonacci, J., 1992, "Consideration of questions about beam-column joints", *ACI Structural Journal*, Vol. 89, No. 1, pp. 27-36.
- Pantazopoulou, S. and Bonacci, J., 1994, "On earthquake-resistant reinforced concrete frame connections", *Canadian Journal of Civil Engineering*, Vol. 21, pp. 307-328.

Papageorgiou, A.S., 1987, "Estimation of earthquake strong ground motion in eastern North America: preliminary estimates Vis-A-Vis existing data", Proceedings, Symposium on Seismic Hazards, Ground Motions, Soil Liquefaction and Engineering Practice in eastern North America, State University of New York at Buffalo, N.Y., pp. 282-299.

Park, R., 1989, "Evaluation of ductility of structures and structural assemblages from laboratory testing", Bulletin of the New Zealand National Society for Earthquake Engineering, Vol. 22, No. 3, pp. 155-166.

Park, R. and Paulay, T., 1975, "Reinforced concrete structures", John Wiley and Sons, New York.

Park, Y. J., Reinhorn, A. M., and Kunnath, S. K., 1987, "IDARC: Inelastic Damage Analysis of Reinforced Concrete frame-shear wall structures", NCEER technical report No. 87-0007, National Center for Earthquake Engineering Research, State University of New York at Buffalo, N.Y.

Paulay, T., Park, R. and Priestley, M.J.N., 1978, "Reinforced concrete beam-column joints under seismic actions", ACI Structural Journal, Vol. 75, No. 11, pp. 585-599.

Paulay, T. and Priestley, M.J.N., 1992, "Seismic Design of Reinforced Concrete and Masonry Buildings," John Wiley and Sons, Inc., 744 pages.

Pessiki, S.P., Conley, C.H., Gergely, P. and White R.N., 1990, "Seismic behaviour of lightly-reinforced concrete column and beam-column joint details", NCEER technical report No. 90-0014, National Center for Earthquake Engineering Research, State University of New York at Buffalo, N.Y.

Phan, L.T., Todd, D.R. and Lew, H.S., 1994, "Strengthening methodology for lightly reinforced concrete frames - I", NISTIR 5128, National Institute of Standards and Technology, Gaithersburg, Maryland.

Powell, G.H. and Prakash, V., 1992, "DRAIN-2DX Version 1.00 User manual", Earthquake Engineering Research Center, EERC, University of California, Berkeley, California..

Priestley, M.J.N. and Seible, F., 1991, "Seismic assessment and retrofit of bridges" report No. SSRP-91/3, Department of Applied Mechanics and Engineering Sciences, AMES, University of California, San Diego.

Priestley, M.J.N., Seible, F., Xiao, Y. and Verma, R., 1994, "Steel jacket retrofitting of reinforced concrete bridge columns for enhanced shear strength - Part 1: Theoretical considerations and test design," ACI structural journal, Vol. 91, No. 4, pp. 394-405.

Priestley, M.J.N., 1996, "Assessment and retrofit of concrete columns for seismic performance", Proceedings of the International Conference on Retrofitting of Structures, Columbia University, pp. 248-263.

- Priestley, M.J.N., Seible, F. and Calvi, G.M., 1996, "Seismic design and retrofit of bridges", John Wiley and Sons, Inc., 686 pages.
- Rodriguez-Gomez, S. and Cakmak, A.S., 1990, "Evaluation of seismic damage indices for reinforced concrete structures", NCEER 90-0022, National Center for Earthquake Research Center, State University of New York at Buffalo, N.Y.
- Roufaiel, M. and Meyer, C., 1987, "Analytical modelling of hysteretic behaviour of reinforced concrete frames", *Journal of Structural Engineering*, ASCE, Vol. 113, No. 3, pp. 429-444.
- Ruitong, D. and Park, R., 1987, "A comparison of the behaviour of reinforced concrete beam-column joints designed for ductility and limited ductility", research report 87-4, Department of Civil Engineering, University of Canterbury, Christchurch, New Zealand.
- Saatcioglu, M. and Razvi, S.R., 1992, "Strength and ductility of confined concrete", *Journal of Structural Engineering*, ASCE, Vol. 118, No. 6, pp. 1590-1607.
- Sakata, H. And Wada, A., 1991, "A study on elasto-plastic behaviour of one-twentieth scale reinforced concrete frames", Sixth Canadian Conference on Earthquake Engineering, Toronto, pp. 671-679.
- Shah, S.N., 1989, "Evaluation of infill wall strengthening schemes for non-ductile reinforced concrete buildings", Master thesis, University of Texas at Austin.
- Shahrooz, B. M. and Muvdi, R., 1991, "Seismic performance of R.C. structures in the eastern U.S.A.", proceedings of the Sixth Canadian Conference of Earthquake Engineering, Toronto, Canada, pp. 269-276.
- Sheikh, S.A., 1994, "Design of confinement steel for reinforced concrete columns", Fifth U.S. National Conference on Earthquake Engineering, Chicago, Illinois, pp. 609-618.
- Sheikh, S.A. and Uzumeri, S.M., 1980, "Strength and ductility of tied concrete columns", *Journal of the Structural Division*, ASCE, Vol. 106, No. ST5, pp. 1079-1102.
- Sugano, S., Nagashima, T., Kimura, H. and Ichikawa, A., 1990, "An experimental study on behaviour of reinforced concrete interior beam-column joints of high strength concrete", proceedings of the Fourth U.S. National Conference on Earthquake Engineering, Palm Springs, California, Vol. 2, pp. 727 - 736.
- Sun, Z., Seible, F. and Priestley, M.J.N., 1993, "Diagnostics and retrofit of rectangular bridge columns for seismic loads" Technical Report No. SSRP-93-07, Department of Applied Mechanics and Engineering Sciences, University of California, San Diego, La Jolla, California, 263 pages.
- Takeda, T., Sozen, M. and Nielsen, N., 1970, "Reinforced Concrete Response to Simulated Earthquakes", *Journal of the Structural Division*, ASCE, Vol. 96, No. ST-12, pp. 2557-2573.

Tena-Colunga, A., Valle, E.D. and Perez-Moreno, D., 1996, "Issues on the seismic retrofit of a building near resonant response and structural pounding", *Earthquake Spectra*, Vol. 12, No. 3, pp. 567-597.

Tomii, M., 1993, "Non-hooped reinforced concrete columns and beam-column connections laterally confined in bellows square steel tube", proceedings of the Tom Paulay Symposium on Recent Developments in Lateral Force Transfer in Buildings, University of California, San Diego, La Jolla, California, pp. 383-402.

Tso, W.K., Zhu, T.J. and Heidebrecht, A.C., 1992, "Engineering implication of ground motion A/V ratio", *Soil Dynamics and earthquake Engineering*, Vol. 11, pp. 133-144.

UBC-64, 1964, Uniform Building Code, International Conference of Building Officials, Whittier, Ca.

Uzumeri, S.M. and Seckin, M., 1974, "Behaviour of reinforced concrete beam-column joints subjected to slow load reversals", report No. 74-05, Department of Civil Engineering, University of Toronto, 72 pages.

Valles, R.E. Reinhorn, A.M., Kunnath, S.K., Li, C. and Madan, A., 1996, "IDARC2D - ver. 4.0: A computer program for the inelastic analysis of buildings", technical report NCEER-96-0010, National Center for Earthquake Engineering Research, State University of New York at Buffalo, N.Y.

Vecchio, F.J. and Collins, M.P., 1986, "The modified compression field theory for reinforced concrete elements subjected to shear", *ACI Structural Journal*, Vol. 83, No. 2, pp. 219-231.

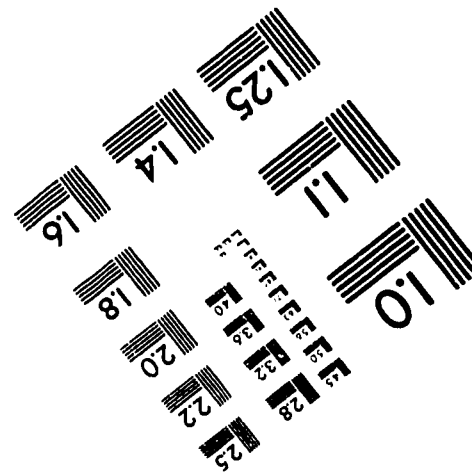
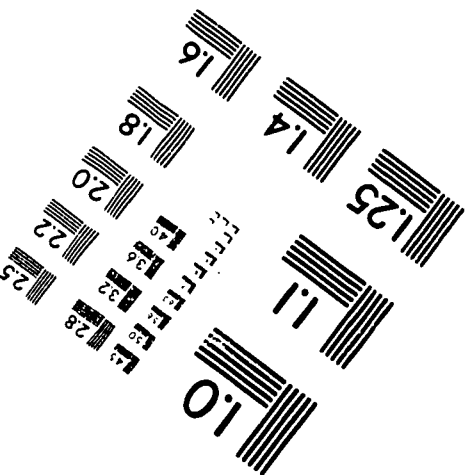
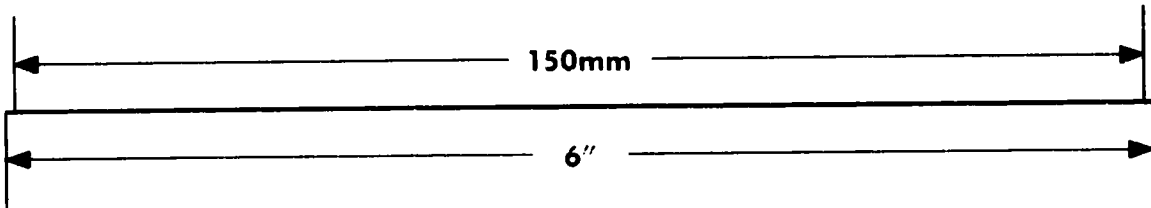
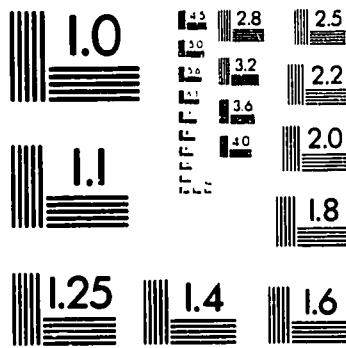
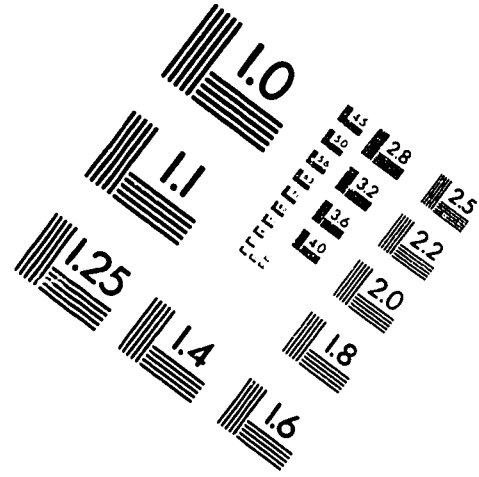
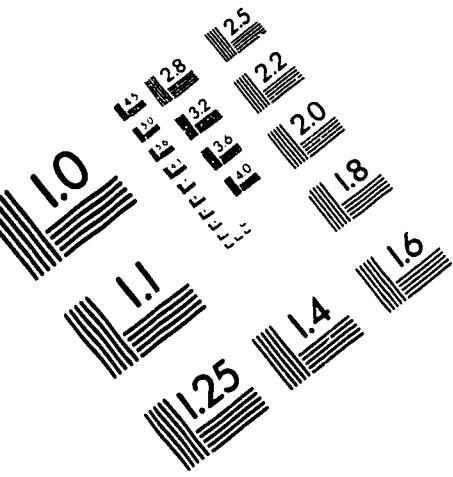
Winters, C. W., Hoffmann, G. W., Symans, M. D. and Wood, T. L., 1991, "An experimental study of four beam-column joint assemblages", special study report, Department of Civil Engineering, State University of New York at Buffalo, N.Y.

Wight, J. K., and Sozen, M. A., 1973, "Shear strength decay in reinforced concrete columns subjected to large deformation reversals", report No. SRS 403, Department of Civil Engineering, University of Illinois, Urbana.

Youssef, N.F.G. and Hilmy S.I., 1990, "Design and analytical considerations of supplementary ductility approach for seismic retrofit of reinforced concrete framed structures", Proceedings of Fourth U.S. National Conference on Earthquake Engineering, Vol. 3, Palm Springs, California, EERI, pp. 413-422.

Zahn, F.A. Park, R. Priestley, M.J.N. and Chapman, H.E., 1986, "Development of design procedures for the flexural strength and ductility of reinforced concrete bridge columns," *Bulletin of the New Zealand National Society for Earthquake Engineering*, Vol. 19, No. 3, pp. 200-212.

IMAGE EVALUATION TEST TARGET (QA-3)



APPLIED IMAGE, Inc
1653 East Main Street
Rochester, NY 14609 USA
Phone: 716/482-0300
Fax: 716/288-5989

© 1993, Applied Image, Inc., All Rights Reserved